This Page is Inserted by IFW Indexing and Scanning Operations and is not part of the Official Record

BEST AVAILABLE IMAGES

Defective images within this document are accurate representations of the original documents submitted by the applicant.

Defects in the images include but are not limited to the items checked:

- ☐ BLACK BORDERS
- ☐ IMAGE CUT OFF AT TOP, BOTTOM OR SIDES
- ☐ FADED TEXT OR DRAWING
- ☐ BLURRED OR ILLEGIBLE TEXT OR DRAWING
- ☐ SKEWED/SLANTED IMAGES
- ☐ COLOR OR BLACK AND WHITE PHOTOGRAPHS
- ☐ GRAY SCALE DOCUMENTS
- ☐ LINES OR MARKS ON ORIGINAL DOCUMENT
- ☐ REFERENCE(S) OR EXHIBIT(S) SUBMITTED ARE POOR QUALITY
- ☐ OTHER: _____

IMAGES ARE BEST AVAILABLE COPY.
As rescanning these documents will not correct the image problems checked, please do not report these problems to the IFW Image Problem Mailbox.

ARCHIVES OF BIOCHEMISTRY AND BIOPHYSICS 181, 363–370 (1977)

Crystal and Molecular Structure of a 1:1 Molecular Complex of Adenine and Riboflavin

SATOSHI FUJII, KAZUKO KAWASAKI, ATSUKO SATO, TAKAJI FUJIWARA, AND KEN-ICHI TOMITA

Faculty of Pharmaceutical Sciences, Osaka University, Yamada-kami, Suita, Osaka 565, Japan

Received May 25, 1976

As a model compound of flavin-adenine dinucleotide, the crystal and molecular structure of a 1:1 molecular complex of adenine and riboflavin has been determined by an X-ray diffraction method. There are two independent 1:1 complexes in an asymmetric unit, and, in both complexes, adenine and riboflavin molecules were connected by similar reversed Hoogsteen-type hydrogen bonds. In addition, nearly coplanar adenine and isoalloxazine rings interact with each other to form an infinite alternate stacking. Riboflavin molecules were found to have two rotational isomers about the glycosyl bond and the orientations of carbon atoms in the ribityl chain are nonplanar to avoid intramolecular nonbonding short contacts. These two conformations are significant to considerations of plausible flavin-adenine dinucleotide models consistent with the results of nuclear magnetic resonance studies.

Riboflavin is well known as an important biological substance, not only as vitamin B_2, but also as a component of coenzyme, FAD[1] or FMN, in oxidation–reduction systems. Recently, it was shown that adenine accelerated the photochemical inactivation of riboflavin-sensitized dehydrogenase (1), and it was of interest to examine the interaction between riboflavin and the other chromophore. Several studies have been reported of the interactions, using such physicochemical methods as fluorescence quenching, ultraviolet, infrared, and other spectroscopic measurements (2–5). In the FAD molecule, particularly, the mode of interaction between the isoalloxazine and adenine rings is an interesting problem relating to its biological role as a coenzyme. Several interaction mechanisms have been postulated, including (9) the stacking between two chromophoric rings by charge transfer or π–π interaction (6) and (b) characteristic hydrogen bonding between the pyrimidine (uracil) skeleton in the isoalloxazine ring and the adenine ring similar to the base pairing found in polynucleotides or crystalline purine–pyrimidine base-paired complexes (7, 8).

Therefore, we attempted to solve the crystal and molecular structure of a 1:1 molecular complex of adenine and riboflavin as a model compound of FAD. In this paper, we deal with the detailed structure analysis and also consider a new FAD molecular conformation, assuming that the two rotational isomers in the ribityl group found in this crystal are maintained in solution. The chemical structures of riboflavin and adenine are shown in Fig. 1 with the atomic numbering scheme.

EXPERIMENTAL PROCEDURE

Materials and methods. Adenine and riboflavin were purchased from Nakarai Chemicals, Ltd. Equimolar amounts of adenine and riboflavin were dissolved in warm dimethyl sulfoxide. The solution was equlibrated with water in a sealed container, and, within a few days, small, dark yellowish plate-

[1] Abbreviations used: FAD, flavin-adenine dinucleotide; FMN, riboflavin 5′-phosphate; RF1 and RF2, first and second riboflavins, respectively; A1 and A2, first and second adenines, respectively; Brads:Rf, the crystal structure of a 1:1 complex of 5′-bromo-5′-deoxyadenosine with riboflavin; *P* conformation, $\chi_f = +90°$; *M* conformation, $\chi_f = -90°$; CPK model, Corey–Pauling Koltun model.

Copyright © 1977 by Academic Press, Inc.
All rights of reproduction in any form reserved.

ISSN 0003-9861

UM00013729
NOVARTIS EXHIBIT 1017
Novartis v. Regents, IPR2023-01346
Page 2475 of 4460

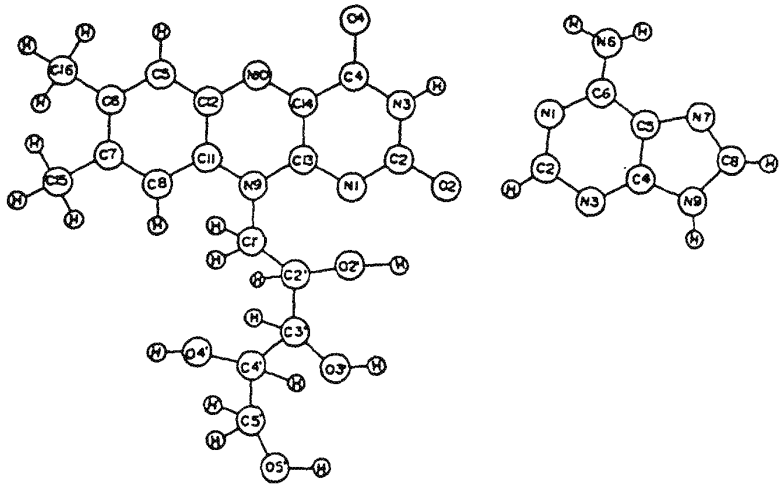


FIG. 1. Numbering of atoms adopted in the text.

like crystals were obtained. The crystallographic data are shown in Table I. The space group was determined to be $P2_1$ in the monoclinic system by systematic absence on $(0k0)$ reflections with $k = 2n + 1$. The calculated density containing four formula units in a unit cell, 1.479 g/cm³, is in good agreement with the experimental value of 1.472 g/cm³, measured by the floatation method.

The intensities of a total of 1512 independent reflections up to a limit of 2θ, 76° were measured on a Rigaku-Denki computer-controlled four-circle diffractometer with Ni-filtered Cu$K\alpha$ radiation. The ω–2θ scanning technique was employed at a rate of ¼°/min. The intensities of three standard reflections measured for every 30 reflections of the data set indicated that there was no structural damage during the run. Lorentz-polarization corrections were applied to the measured intensities, but no absorption correction was considered because of the small size of the crystal (0.20 × 0.20 × 0.01 mm³).

Structure determination and refinement. From the requirement of the space group $P2_1$ and the number of molecules in a unit cell calculated from the density measurement, it was found that two units of the complex containing one adenine, one riboflavin, and three water molecules should occur in one asymmetric unit. With reference to the crystal structure of a 1:1 complex of 5′-bromo-5′-deoxyadenosine with riboflavin (hereafter abbreviated as Br-ads:Rf) determined by Voet and Rich (9), an interesting correlation between the unit cell dimensions of the two crystals was found. The values, for comparison, are $a = 7.873$ ($b = 7.88$), $b = 8.601$ ($a = 8.53$), $c = 48.493$ (37.82) Å, and $\alpha = \beta = \gamma = 90°$ ($\beta = 97.83°$); the values in parentheses are those found in this work. The significant difference in the c-axis dimension (10.67 Å) might be due to the additional ribose group in the 5′-bromo-5′-deoxyadenosine molecule. Moreover, the space group $P2_1$ in this crystal is different from that found in the other, $P2_12_12_1$, but it seems likely that the molecular arrangement related by the twofold screw axis along the a-axis in the crystal structure of the Br-ads:Rf complex might be similar to that related by the twofold screw axis along the b-axis in this crystal. These facts seem to indicate that the molecular conformation and packing in these crystals resemble each other rather closely.

The structure determination was continued by a combination of Patterson vector search and Fourier techniques. A total of 80 nonhydrogen atoms was determined. The rigid-body vector set was calculated from 29 atoms where isoalloxazine and adenine rings were connected by hydrogen bonds as found in the crystal of Br-ads:Rf. Rotation and translation of the vector set against the Patterson function properly located the above 29 atoms. At this stage, the R index ($R = \sum||F_o| - |F_c||/\sum|F_o|$) was 0.48, and careful inspection of the Fourier map with phases based on 29 atoms made it possible to locate another pair of isoalloxazine and adenine rings. After 10 cycles of successive Fourier synthesis, the positions of all of the remaining nonhydrogen atoms were determined and the R index was lowered to 0.35. Further refinement of positional and isotropic temperature parameters was carried out by a block-

UM00013730

NOVARTIS EXHIBIT 1017
Novartis v. Regents, IPR2023-01346
Page 2476 of 4460

TABLE I

CRYSTAL DATA OF THE ADENINE–RIBOFLAVIN COMPLEX

Chemical formula	$C_{22}H_{23}N_9O_6 3H_2O$
Molecular weight	565.5
a (Å)	8.53 ± 0.01
b (Å)	7.88 ± 0.01
c (Å)	37.82 ± 0.04
β (°)	97.83
Crystal system	Monoclinic
Space group	$P2_1$
Z	4
Dm (g·cm^{-3})	1.472 ± 0.04
Dx (g·cm^{-3})	1.479

diagonal least-squares method with unit weight, and the final R index was decreased to 0.22, which is relatively high, probably due to the small size of the crystal and/or the disorder attendant on dehydration similar to that found in the crystal structure of Br-ads:Rf. For all computations, the UNICS system program was used (10).

RESULTS AND DISCUSSION

The positional parameters for all nonhydrogen atoms are listed in Table II, in which the two independent riboflavin molecules are designated as RF1 and RF2, and the two adenine molecules are designated as A1 and A2. Figure 2 shows the bond lengths and angles in the two independent complexes. Owing to the low accuracy of the final structural parameters, the quoted bond lengths and the bond angles are slightly inexact, but these values are within standard deviations (ca. 0.05 Å in distance and 2° in angle).

As shown in Figs. 3 and 4, each riboflavin molecule is associated with a particular adenine molecule by two hydrogen bonds (the reversed Hoogsteen type), one between the amino N(6) of adenine and the isoalloxazine O(2) of riboflavin, and the other between N(7) of adenine and N(3) of riboflavin, similar to those found in some molecular complexes containing adenine and uracil (8) or in the Br-ads:Rf complex. Raszka and Kaplan (11) have examined the conformational specificity of FAD by intramolecular hydrogen bond formation, and, according to them, this intramolecular hydrogen bonding, which is energetically less favored, could exist in aqueous solution. Their proposed FAD model has Hoogsteen-type intramolecular hydrogen bonds between O(4) and N(3) of the riboflavin and the amino N(6) and N(7) of the adenine moiety, respectively, which differ from those found in this work. Using either of these two types of hydrogen bonding, it is possible to construct FAD molecular models with the space-filling CPK models.

Voet and Rich (12) suggested that the hydrogen-bonded FAD molecule fits into a pocket of the enzyme molecule having a large hydrophobic surface and that the specificity arising from the intramolecular hydrogen-bonded FAD conformation is a protection against any genetic modification of the adenine group or the pyrimidine ring of the isoalloxazine group. Such hydrogen bond formation could be involved in the acceleration of photochemical inactivation of riboflavin-sensitized dehydrogenase by adenine (13).

The adenine ring and isoalloxazine ring of riboflavin in each complex molecule interact with each other to form an infinite alternate stacking. It is interesting to compare the mode of stacking in each complex molecule. The riboflavin, RF1 (Fig. 3), which forms the hydrogen-bonded dimer with the neighboring adenine (A1) molecule, stacks between two adjacent adenine rings, of which the upper one associates with large overlap and an interplanar spacing of 3.4 Å while the lower one overlaps slightly with a 3.5-Å separation. On the other hand, the second riboflavin molecule, RF2 (Fig. 4), also involved in a hydrogen-bonded dimer with adenine (A2), has a large overlap with the lower adenine (spacing: 3.4 Å) and a small overlap with the upper one (spacing: 3.5 Å). Even though the separation in the highly overlapping stack, 3.4 Å, is somewhat too great to be regarded as a charge-transfer interaction, a similar mode of overlapping was observed in the crystal structure of the Br-ads:Rf complex. However, the small overlapping association found in this crystal differs considerably from that observed in the Br-ads:Rf complex, and it indicates that this weak stacking may be easily changed by packing forces.

The observed strong stacking between

NOVARTIS EXHIBIT 1017

TABLE II

ATOMIC POSITIONS IN FRACTIONS OF A UNIT CELL EDGE OF THE CRYSTAL STRUCTURE OF THE ADENINE-RIBOFLAVIN COMPLEX

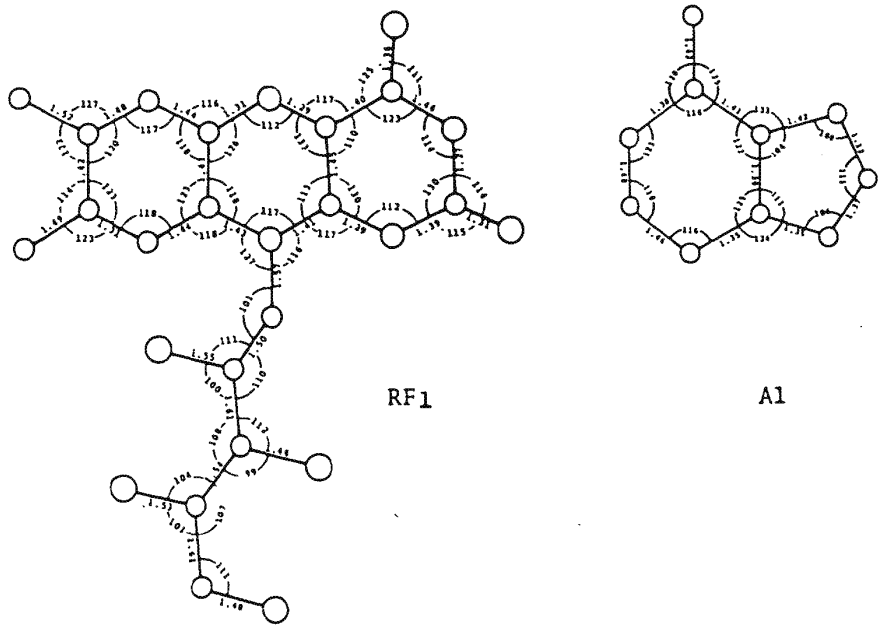
Atom	*X*	*Y*	*Z*	Atom	*X*	*Y*	*Z*
RF1				RF2			
N1	0.6255	0.2200	0.1116	N1	0.3623	0.4449	0.3920
C2	0.7769	0.1833	0.1285	C2	0.2203	0.4816	0.3807
N3	0.8380	0.2061	0.1608	N3	0.1583	0.4666	0.3447
C4	0.7381	0.3021	0.1820	C4	0.2186	0.3660	0.3205
C5	0.2733	0.5772	0.1977	C5	0.7083	0.1035	0.3050
C6	0.1144	0.6324	0.1808	C6	0.8708	0.0758	0.3115
C7	0.0566	0.5825	0.1454	C7	0.9336	0.0947	0.3522
C8	0.1399	0.4932	0.1254	C8	0.8476	0.2003	0.3765
N9	0.3880	0.3497	0.1176	N9	0.6044	0.3242	0.3818
N10	0.5108	0.4447	0.1900	N10	0.4792	0.2540	0.3134
C11	0.3001	0.4508	0.1393	C11	0.7011	0.2391	0.3618
C12	0.3686	0.4866	0.1752	C12	0.6356	0.2190	0.3254
C13	0.5447	0.3072	0.1318	C13	0.4439	0.3522	0.3685
C14	0.5851	0.3581	0.1686	C14	0.3834	0.3358	0.3323
C15	−0.1060	0.6438	0.1329	C15	1.1129	0.0360	0.3670
C16	0.0121	0.7288	0.2041	C16	0.9571	−0.0426	0.2858
O2	0.8643	0.0943	0.1094	O2	0.1276	0.5623	0.3965
O4	0.8114	0.3287	0.2156	O4	0.1658	0.3550	0.2894
C1′	0.3352	0.2967	0.0778	C1′	0.6764	0.3876	0.4192
C2′	0.3515	0.4622	0.0590	C2′	0.6276	0.2550	0.4461
O2′	0.5280	0.5101	0.0599	O2′	0.7300	0.0933	0.4443
C3′	0.3026	0.4393	0.0165	C3′	0.6672	0.3327	0.4858
O3′	0.3872	0.2976	0.0027	O3′	0.6175	0.1904	0.5072
C4′	0.1343	0.3656	0.0100	C4′	0.8485	0.3457	0.4999
O4′	0.0350	0.4933	0.0280	O4′	0.8806	0.5042	0.4745
C5′	0.0674	0.3979	−0.0315	C5′	0.8873	0.4205	0.5398
O5′	−0.0899	0.3187	−0.0412	O5′	0.7579	0.5771	0.5423
A1				A2			
N1	1.4611	−0.1153	0.1537	N1	−0.4578	0.7873	0.3483
C2	1.5769	−0.1120	0.1866	C2	−0.5648	0.7917	0.3210
N3	1.5360	−0.0162	0.2170	N3	−0.5385	0.7130	0.2928
C4	1.3903	0.0541	0.2128	C4	−0.3908	0.6453	0.2921
C5	1.2794	0.0424	0.1823	C5	−0.2759	0.6445	0.3220
C6	1.3141	−0.0400	0.1512	C6	−0.3115	0.7220	0.3520
N6	1.2082	−0.0519	0.1188	N6	−0.2217	0.7237	0.3847
N7	1.1513	0.1439	0.1900	N7	−0.1447	0.5569	0.3163
C8	1.1864	0.2023	0.2230	C8	−0.1796	0.5201	0.2824
N9	1.3323	0.1475	0.2381	N9	−0.3353	0.5586	0.2660
Water				Water			
O1	0.7805	0.3106	0.0452	O4	0.5693	0.3997	0.5886
O2	0.3867	0.9784	0.0260	O5	0.3237	0.2952	0.5379
O3	0.5571	0.8080	0.0888	O6	0.1865	0.4374	0.4668

the isoalloxazine and adenine rings of the FAD molecule in aqueous solution may play an important role in maintaining its conformational rigidity and many models involving such stacking have been postulated. However, the proposed models based on circular dichroism by Miles and Urry (14), and on nuclear magnetic resonance spectra by Sarma *et al.* (15) and Kainosho and Kyogoku (16), differ considerably from our model based on X-ray analysis of the adenine–riboflavin com-

UM00013732
NOVARTIS EXHIBIT 1017
Novartis v. Regents, IPR2023-01346
Page 2478 of 4460

ADENINE-

Z
0.3920
0.3807
0.3447
0.3205
0.3050
0.3115
0.3522
0.3765
0.3818
0.3134
0.3618
0.3254
0.3685
0.3323
0.3670
0.2858
0.3965
0.2894
0.4192
0.4461
0.4443
0.4858
[illegible]072
[illegible]4999
0.4745
0.5398
0.5423
0.3483
0.3210
0.2928
0.2921
0.3220
0.3520
0.3847
0.3163
0.2824
0.2660
0.5886
0.5379
0.4668



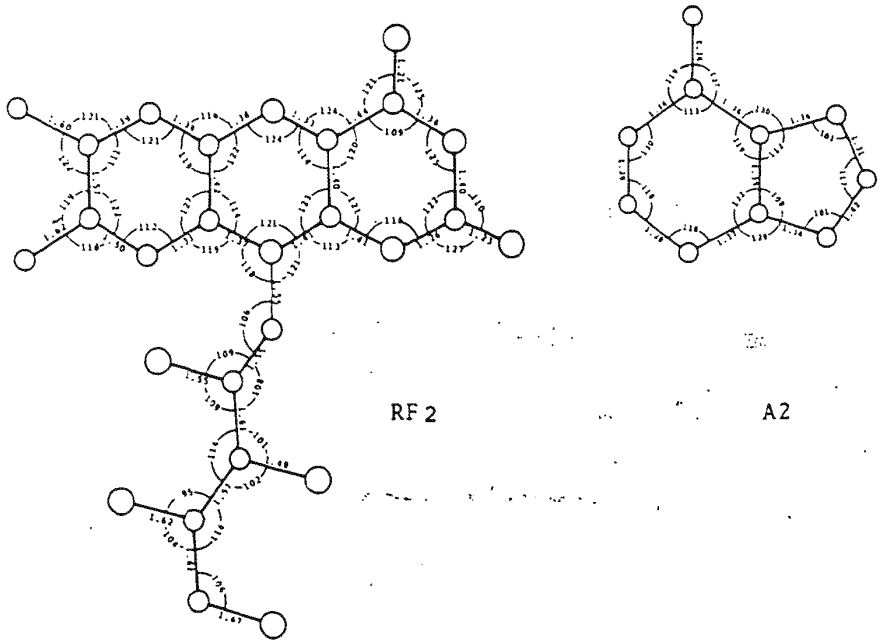


FIG. 2. Bond distances (in Ångstrom units) and bond angles (in degrees) in the adenine-riboflavin complex.

iles and
tic reso-
15) and
· consid-
a X-ray
in com-

UM00013733
NOVARTIS EXHIBIT 1017
Novartis v. Regents, IPR2023-01346
Page 2479 of 4460

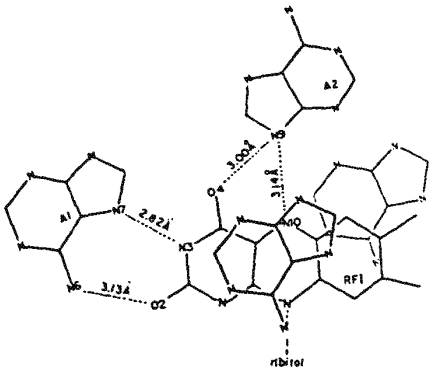


FIG. 3. A projection of the first intermolecular complex onto the plane of the isoalloxazine ring of riboflavin RF1. The hydrogen-bonded (dashed lines) and stacking relationships among the adenine and the isoalloxazine rings are shown.

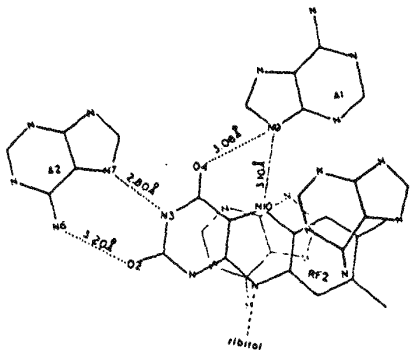


FIG. 4. A projection of the second intermolecular complex onto the plane of the isoalloxazine ring of riboflavin RF2. The hydrogen-bonded (dashed lines) and stacking relationships among the adenine and the isoalloxazine rings are shown.

plex. It is possible to build a stacking space-filling CPK model based on this work, but there are still some difficulties in building a model having sugar and pyrophosphate groups consistent with the results of solution studies, especially by nuclear magnetic resonance. Therefore, the intermolecular stacking mode detected in the adenine–riboflavin complex does not seem to be the same as the intramolecular stacking mode of the FAD molecule. But the large overlapping stack is plausible in intermolecular interactions between the riboflavin moiety and the adenine moiety of adjacent FAD molecules, which was noted by Sarma *et al.* (15). This could also be considered as an alternative explanation of the acceleration of photochemical inactivation in riboflavin-sensitized dehydrogenase by adenine.

It is of interest that two independent rotational isomers around the glycosyl bond were found in this crystal. The torsion angle about the glycosyl N(9)–C(1′) bond is denoted by the symbol χ_f. The sequence of atoms chosen to define this angle is C(13)–N(9)–C(1′)–C(2′). The use of the symbols, *P* and *M*, corresponding to $\chi_f = +90°$ and $-90°$ conformations, respectively, is found to be advantageous in describing the conformational differences of the ribityl moieties. It makes a distinction between two ribityl conformations, that is, the *P* conformation for the RF1 molecule and the *M* conformation for the RF2 molecule. The conformations of the ribityl group in riboflavin found in seven crystal structures are listed in Table III. The *P* conformation is commonly observed in the crystal structures, but the *M* conformation is found in only two crystals. Courrière and Pullman (21) suggest that riboflavin has one global minimum at $\chi_f = +90°$ ($\tau_{1f} = 180°$) and an energetically close local minimum at $\chi_f = -90°$ ($\tau_{1f} = 180°$). The riboflavin insolution and in the enzyme (as FMN and FAD) could be considered to have the *M* conformation as well as the *P* conformation. The P-t-g^--t conformation (corresponding to the χ_f–τ_{1f}–τ_{2f}–τ_{3f} torsion angles in Table III) including riboflavin RF1 of this crystal is commonly observed. On the other hand, the M-t-g^+-t conformation (riboflavin RF2 of this crystal) is observed here for the first time. The plus or minus gauche conformation at τ_{2f}, with the aid of the *trans* conformation of adjacent bonds at each side, avoids intramolecular short contact, especially between hydroxy substituents, and it means that the carbon atoms in ribityl backbones take nonplanar conformations. By energy calculations, we found that these two nonplanar conformations are the preferred ones among the many cases in Table III (unpublished work).

From nuclear magnetic resonance studies, Kainosho and Kyogoku (16) have predicted interchangeable forms (two folded

UM00013734

NOVARTIS EXHIBIT 1017
Novartis v. Regents, IPR2023-01346
Page 2480 of 4460

TABLE III

CONFORMATIONAL CHARACTER IN THE RIBITOL OF RIBOFLAVIN[a]

Crystal[b]		Torsion angles (°)					References
		χ_f	τ_{1f}	τ_{2f}	τ_{3f}	τ_{4f}	
Rf·HBr·H_2O		97 (*P*)	175 (*t*)	298 (g^-)	193 (*t*)	310 (g^-)	17
Br-Ads:Rf·$3H_2O$		95 (*P*)	186 (*t*)	303 (g^-)	192 (*t*)	188 (*t*)	9
2Rf·2Cu(ClO_4)$_2$·$12H_2O$	Mol-I	284 (*M*)	157 (*t*)	298 (g^-)	201 (*t*)	179 (*t*)	18
2Rf·2Cu(ClO_4)$_2$·$12H_2O$	Mol-II	103 (*P*)	177 (*t*)	288 (g^-)	183 (*t*)	56 (g^+)	18
Rf[c]·$AgClO_4$·$1/2H_2O$		96 (*P*)	166 (*t*)	168 (*t*)	56 (g^+)	62 (g^+)	19
2Rf·2quinol·4HBr·$4H_2O$	Mol-I	98 (*P*)	193 (*t*)	169 (*t*)	296 (g^-)	297 (g^-)	20
2Rf·2quinol·4HBr·$4H_2O$	Mol-II	96 (*P*)	191 (*t*)	186 (*t*)	281 (g^-)	191 (*t*)	20
2Rf·2Ade·$6H_2O$	RF1	105 (*P*)	180 (*t*)	306 (g^-)	202 (*t*)	190 (*t*)	This work
2Rf·2Ade·$6H_2O$	RF2	279 (M)	169 (*t*)	75 (g^+)	186 (*t*)	37 (g^+)	This work

[a] Conformational characters, χ_f, τ_{1f}, τ_{2f}, τ_{3f}, and τ_{4f}, correspond to the rotations around the bonds of N(9)–C(1′), C(1′)–C(2′), C(2′)–C(3′), C(3′)–C(4′), and C(4′)–C(5′), respectively. The definition of the symbols, P and M, is described in Footnote 1. The other symbols, *t*, g^+, and g^-, correspond to *trans*, plus gauche, and minus gauche conformations in each bond, respectively.

[b] Rf, riboflavin; Br-Ads, 5′-bromo-5′-deoxyadenosine; Ade, adenine.

[c] Formylated (45%) on the 5′ position by the formic acid solvent.

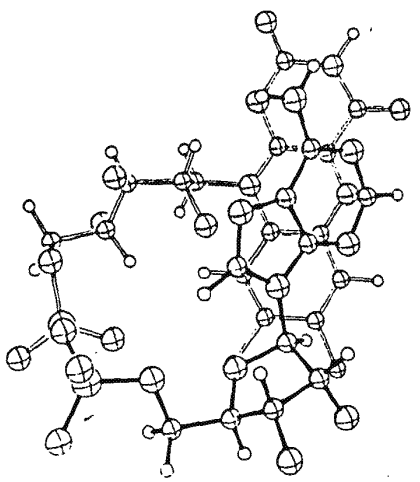


FIG. 5. A model of a FAD molecule having the stacked form in which the conformation of the ribityl moiety, M–t–g^-–t, corresponds to one of the observed conformations in this work.

forms and a flexible open form) as the most plausible models of the FAD molecule, which bear the P–t–g^-–t conformation in the ribityl residue. However, the M–t–g^+–t conformation found in the RF2 molecule could not be excluded as a possible backbone conformation of the FAD model, because it is also consistent with the nuclear magnetic resonance results. In fact, it is possible to build a new FAD molecule with CPK models, in which the planar isoalloxazine and adenine rings are highly stacked (Fig. 5), and it should be reexamined by nuclear magnetic resonance as a possible folded form.

The molecular arrangement of this crystal is similar to that of the Br-ads:Rf complex. The molecular conformation and arrangement of the riboflavin (RF1) and the adenine (A1) are very similar, which is to be expected from the correlation between the unit cell dimensions of two crystals. The second riboflavin (RF2) and adenine (A2) molecules are also very similar, except for the ribityl moiety. This fact shows that the difference between adenine and adenosine derivatives has little effect on molecular packing.

Both independent ribityl groups arranged around the dyad-screw axis and the water molecules interact primarily with the ribityl group to occupy the space in the lattice (Fig. 6). All of the hydroxy oxygen atoms in the ribityl group are hydrogen bonded to other hydroxy or water oxygen atoms of the neighboring molecule with distances of 2.6–3.1 Å. The atom N(1) of the riboflavin (RF2) is not involved in hydrogen bonding, contrary to the case of the riboflavin complex with copper (II) perchlorate, which also has the ribityl backbone in the M conformation (18).

Two independent coplanar complexes form a coplanar association with each other by a bifurcated hydrogen bonding between N(9) of adenine and N(10) or O(4) of the isoalloxazine ring of the adjacent

UM00013735
NOVARTIS EXHIBIT 1017
Novartis v. Regents, IPR2023-01346
Page 2481 of 4460

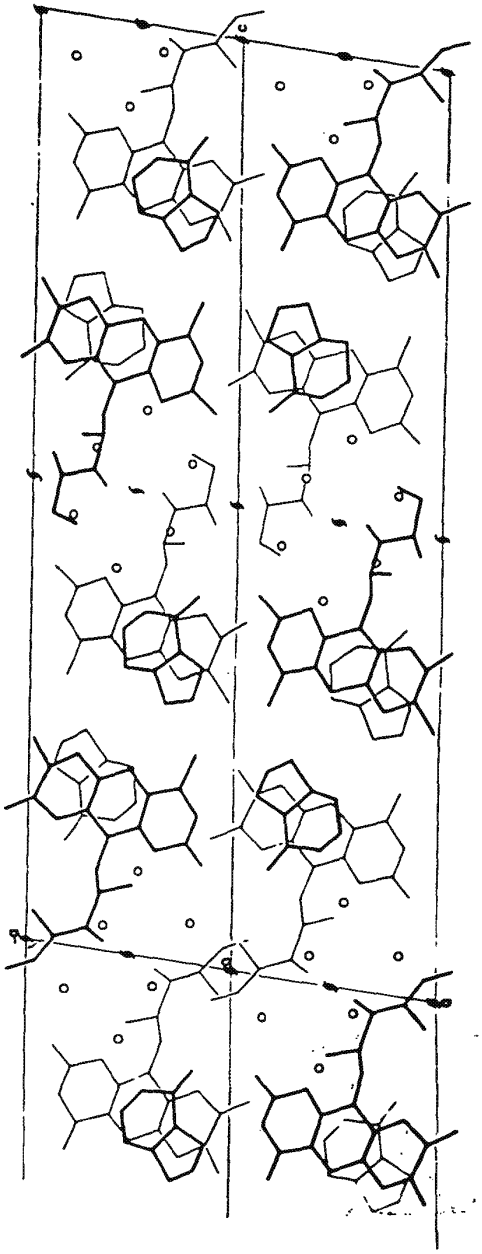


FIG. 6. A projection of the crystal structure along the *b*-axis. The water molecules are represented as open circles.

riboflavin molecule (Figs. 3 and 4). There exists an approximate center of symmetry at the middle of two independent complex molecules, excluding the ribityl group, which has three asymmetric carbon atoms, as shown in Fig. 6. This sort of tetramer interacts with itself to form the infinite molecular array in the crystal.

ACKNOWLEDGMENTS

We are grateful to Professor K. Uehara for encouragement and advice and to Professor Y. Kyogoku for many helpful discussions.

REFERENCES

1. UEHARA, K., YONEZAWA, M., HOSOMI, S., AND HAYASHI, R. (1966) *J. Biochem. (Tokyo)* 60, 721–722.
2. WEBER, G. (1950) *Biochem. J.* 47, 114–221.
3. WRIGHT, L. D., AND MCCORMICK, D. B. (1964) *Experientia* 20, 501–502.
4. KYOGOKU, Y., AND YU, B. S. (1969) *Bull. Chem. Soc. Japan* 42, 1387–1393.
5. SLIFKIN, M. A. (1971) Charge Transfer Interaction of Biomolecules, p. 132, Academic Press, New York.
6. TSIBRIS, J. C. M., MCCORMICK, D. B., AND WRIGHT, L. D. (1965) *Biochemistry* 4, 504–510.
7. TOMITA, K., AND RICH, A. (1964) *Nature (London)* 201, 1160–1163.
8. VOET, D., AND RICH, A. (1970) *Prog. Nucl. Acid Res. Mol. Biol.* 10, 183–210.
9. VOET, D., AND RICH, A. (1971) *Proc. Nat. Acad. Sci. USA* 68, 1151–1156.
10. ASHIDA, T. (1973) The Universal Crystallographic Computing System–Osaka, The Computation Center, Osaka University.
11. RASZKA, M., AND KAPLAN, N. O. (1974) *Proc. Nat. Acad. Sci. USA* 71, 4546–4550.
12. VOET, D., AND RICH, A. (1971) *in* Flavins and Flavoproteins (Kamen, H., ed.), Vol. 3, pp. 23–27, University Park Press, State College, Penn.
13. UEHARA, K., MIZOGUCHI, T., HOSOMI, S., FUJIWARA, T., AND TOMITA, K. (1968) *J. Biochem. (Tokyo)* 64, 589–593.
14. MILES, D. W., AND URRY, D. W. (1968) *Biochemistry* 7, 2791–2798.
15. SARMA, R., DANNIES, P., AND KAPLAN, N. O. (1968) *Biochemistry* 7, 4359–4367.
16. KAINOSHO, M., AND KYOGOKU, Y. (1972) *Biochemistry* 11, 741–752.
17. TANAKA, N., ASHIDA, T., SASADA, Y., AND KAKUDO, M. (1969) *Bull. Chem. Soc. Japan* 42, 1546–1554.
18. GARLAND, W. T., AND FRITCHIE, C. J. (1974) *J. Biol. Chem.* 249, 2228–2234.
19. WADE, T. D., AND FRITCHIE, C. J. (1973) *J. Biol. Chem.* 248, 2337–2343.
20. BEAR, C. A., WATERS, T. N., AND WATERS, J. M. (1973) *J. Chem. Soc. Perkin* II, 1266–1270.
21. COURRIÈRE, P., AND PULLMAN, B. (1971) *C. R. Acad. Sci. (Paris)* 273, 2674–2676.

UM00013736

NOVARTIS EXHIBIT 1017
Novartis v. Regents, IPR2023-01346
Page 2482 of 4460

This Page is Inserted by IFW Indexing and Scanning Operations and is not part of the Official Record

BEST AVAILABLE IMAGES

Defective images within this document are accurate representations of the original documents submitted by the applicant.

Defects in the images include but are not limited to the items checked:

- ☐ BLACK BORDERS
- ☐ IMAGE CUT OFF AT TOP, BOTTOM OR SIDES
- ☐ FADED TEXT OR DRAWING
- ☐ BLURRED OR ILLEGIBLE TEXT OR DRAWING
- ☐ SKEWED/SLANTED IMAGES
- ☐ COLOR OR BLACK AND WHITE PHOTOGRAPHS
- ☐ GRAY SCALE DOCUMENTS
- ☐ LINES OR MARKS ON ORIGINAL DOCUMENT
- ☐ REFERENCE(S) OR EXHIBIT(S) SUBMITTED ARE POOR QUALITY
- ☐ OTHER: _____

IMAGES ARE BEST AVAILABLE COPY.
As rescanning these documents will not correct the image problems checked, please do not report these problems to the IFW Image Problem Mailbox.

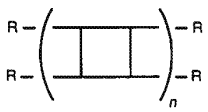
Ladderanes

Supramolecular Construction of Molecular Ladders in the Solid State**

*Xiuchun Gao,† Tomislav Friščić, and Leonard R. MacGillivray**

In memory of Xiuchun Gao

An [*n*]ladderane is a molecule that consists of *n* edge-sharing cyclobutane rings (where $n \geq 2$) that define a molecular equivalent of a macroscopic ladder.[1] Ladderanes are considered promising building blocks in optoelectronics[2] and, very recently, have been identified in biological systems ($n = 3$ and 5), in the form of ladderane lipids,[3,4] which are integral components in the microbiological conversion of ammonium and nitrite ions to dinitrogen gas.[3,4] In the simplest case, a *cis*-fused [*n*]ladderane ($n = 3, 5, 7\ldots$) can be constructed by photochemical dimerization of two all-*trans*-poly-*m*-enes ($m = 2, 3, 4\ldots$). Despite the apparent simplicity of this intermolecular process, however, such a transformation generally fails.[1] This can be attributed to the lack of a method that overcomes the energetic cost, due to solvent[5] and entropy[1,5] effects, of organizing two polyene molecules in a suitable geometry in the liquid phase for photoreaction, although a covalent linker that holds two polyene chains in a parallel orientation for a high-yield, intramolecular photoaddition to give a [*n*]ladderane ($n = 3$ and 5) has been reported.[6]



[*n*]ladderane

We believe that a supramolecular approach to covalent synthesis[7,8] in the organized, solvent-free environment of the solid state[8] can provide a solution to the problem of organizing two polyenes for an intermolecular reaction to give a ladderane. Specifically, by taking an approach to control reactivity in solids[9] by using molecules that serve as linear templates,[10–13] we have anticipated that the cocrystallization of resorcinol (1,3-benzenediol), or a derivative, with an all-*trans*-bis(4-pyridyl)poly-*m*-ene (4-pyr-poly-*m*-ene) would produce a four-component molecular assembly, 2(resorcinol)·2(4-pyr-poly-*m*-ene), in which each resorcinol preorganizes, through two O–H···N hydrogen-bonding interactions, two poly-*m*-enes for [2+2] photoaddition.[14] In this design, the two polyenes (Scheme 1) would be positioned by

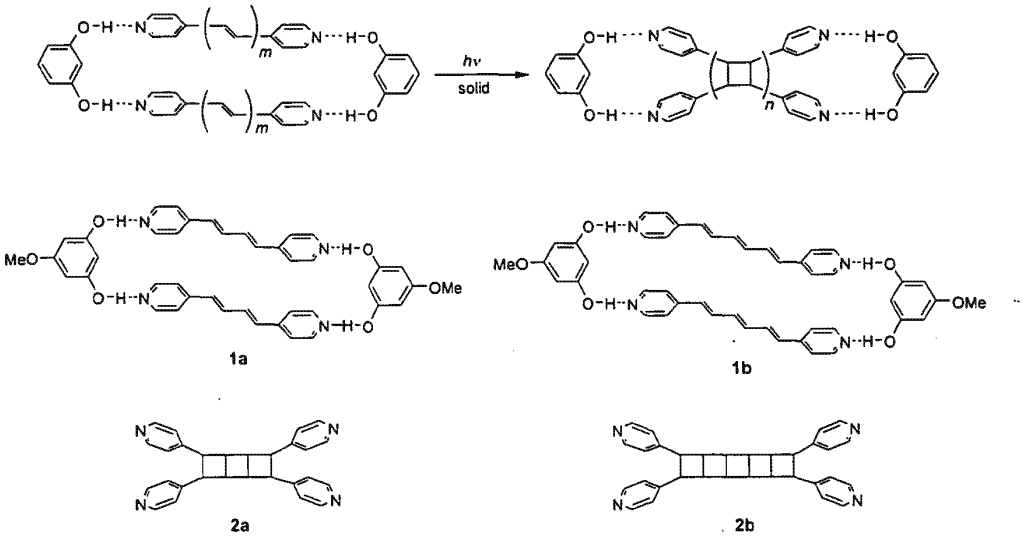
[*] T. Friščić, Prof. L. R. MacGillivray
Department of Chemistry, University of Iowa
Iowa City, IA 52242-1294 (USA)
Fax: (+1) 319-335-1270
E-mail: len-macgillivray@uiowa.edu

[†] Deceased

[**] We are grateful to the National Science Foundation (CAREER Award, L.R.M., DMR-0133138) for funding. Acknowledgment is also made to the Research Corporation (Research Innovation Award) for financial support.

 © 2004 Wiley-VCH Verlag GmbH & Co. KGaA, Weinheim DOI: 10.1002/anie.200352713

UM00013738
NOVARTIS EXHIBIT 1017
Novartis v. Regents, IPR2023-01346
Page 2484 of 4460



Scheme 1.

the templates such that the C=C bonds of the olefins lie parallel and separated by <4.2 Å, a position suitable for the photoreaction. UV irradiation of the solid would produce the targeted [*n*]ladderane, with the C=C bonds reacting to form the fused cyclobutane framework. Herein, we report the application of 2(5-OMe-res)·2(4-pyr-poly-*m*-ene) (where: $m=2$ (**1a**) and 3 (**1b**); 5-OMe-res = 5-methoxyresorcinol) to construct [*n*]ladderanes (where $n=3$ (**2a**) and 5 (**2b**)) in the solid state. The remarkable efficiency of this intermolecular process is exemplified by the fact that the polyenes are converted to the ladderanes stereospecifically, in gram quantities, and in 100% yield.[11]

In a typical experiment, one equivalent of 5-OMe-res[11] was co-crystallized with an equimolar amount of a 4-pyr-poly-*m*-ene[15] in methanol. Single crystals of **1a** and **1b** suitable for X-ray analysis formed in the methanolic solution within a period of approximately one day.

Single-crystal X-ray structure analyses of **1a** and **1b** reveal that the linear templates preorganize each polyene into a position for intermolecular photoaddition that is favorable for ladderane formation.[6]

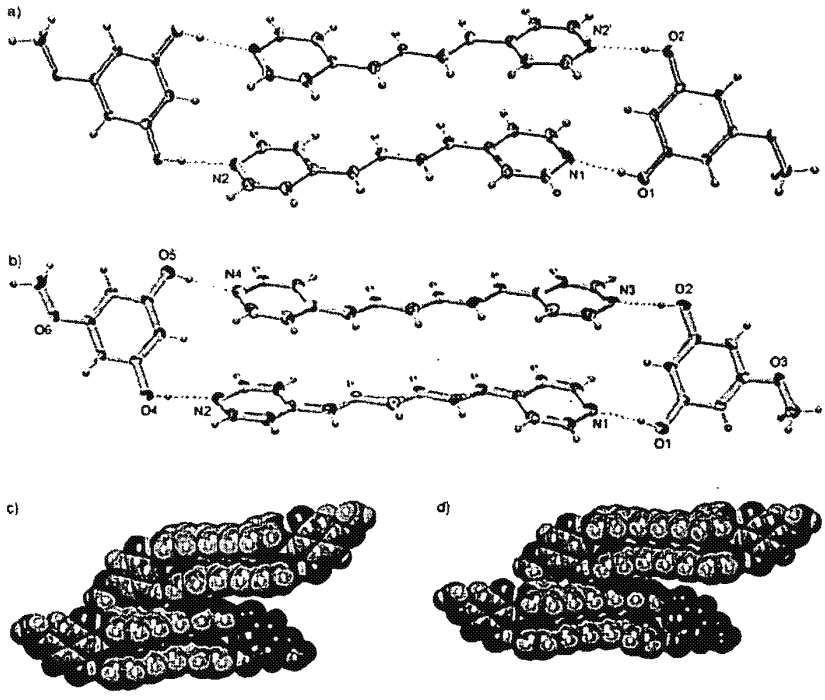


Figure 1. X-ray crystal structures of **1a** and **1b**: a) ORTEP view of **1a**, b) ORTEP view of **1b**, c) space-filling view of the packing of **1a**, and d) space-filling view of the packing of **1b**. Selected interatomic distances [Å] and angles [°]: a) O1···N1 2.761(3), O2···N2^{i} 2.736(3), O1-H1O···N1 175.5(2), O2-H2O···N2^{i} 171.4(2); b) O1···N1 2.792(5), O2···N3 2.777(6), O4···N2 2.782(6), O5···N4 2.756(6), O1-H1O···N1 173.6(3), O2-H2O···N3 173.4(3), O4-H4O···N2 176.6(3), O5-H5O···N4 175.1(3). Symmetry operator i: $-x+1, -y, -z+2$. The asymmetric unit of 2(5-OMe-res)·2(4-pyr-poly-2-ene) consists of one half assembly, which resides around a crystallographic center of inversion, whereas that of 2(5-OMe-res)·2(4-pyr-poly-3-ene) involves two full assemblies, which are virtually identical.

 © 2004 Wiley-VCH Verlag GmbH & Co. KGaA, Weinheim

UM00013739
NOVARTIS EXHIBIT 1017
Novartis v. Regents, IPR2023-01346
Page 2485 of 4460

In each case, the linear templates and polyenes form discrete, four-component molecular assemblies that are held together by four O–H···N hydrogen bonds (Figure 1a,b), wherein the templates orient the polyenes in a parallel arrangement. The separation between the stacked C=C bonds ranges from 3.78 to 3.82 Å and 3.69 to 3.97 Å in **1a** and **1b**, respectively. Nearest-neighbor assemblies of each solid pack in an antiparallel fashion so that the olefins of the hydrogen-bonded assemblies are the sole C=C bonds organized to undergo reaction (Figure 1c,d).

To evaluate the reactivity of the solid-state molecular assemblies, powdered crystalline samples of **1a** and **1b** were subjected to UV irradiation (broadband Hg lamp) for periods of approximately 120 and 72 h, respectively. As evidenced by ^{1}H NMR spectroscopy (in [D$_6$]DMSO), **2a** and **2b** formed stereospecifically and in 100% yield (Figure 2). Each ladderane is characterized by the complete disappearance of the olefinic protons and the emergence of cyclobutane protons in the $\delta = 3.0$–4.3 ppm range.[6,16] The three fused cyclobutane rings of **2a** produced two broad signals at $\delta = 3.49$ and 4.30 ppm (1:1 ratio), while the five fused cyclobutane rings of **2b** produced three broad signals at $\delta = 3.12$, 3.27, and 4.27 ppm (1:1:1 ratio).

To confirm the structures of the ladderanes, the reactions were repeated in gram quantities. The linear templates were then separated from each photoproduct by solvent extraction. Single-crystals of **2a** and **2b**·2(benzene) were grown, over a period of approximately three days, by way of slow solvent evaporation from ethanol and benzene, respectively.

Single-crystal X-ray structure analyses confirm the structures of **2a** and **2b** (Figure 3). Each photoproduct consists of a *cis*-fused cyclobutane framework with ends that are functionalized with four 4-pyridyl groups. The C–C bond lengths and C-C-C bond angles of the fused cyclobutane units compare well to both calculated and experimentally related structures.[6,16]

The ladderanes **2a** and **2b** appear to form within **1a** and **1b** through stepwise [2+2] photodimerizations. ^{1}H NMR spectra obtained 24 and 48 h into each reaction reveal that lower-order [*n*]ladderanes form during the generation of each

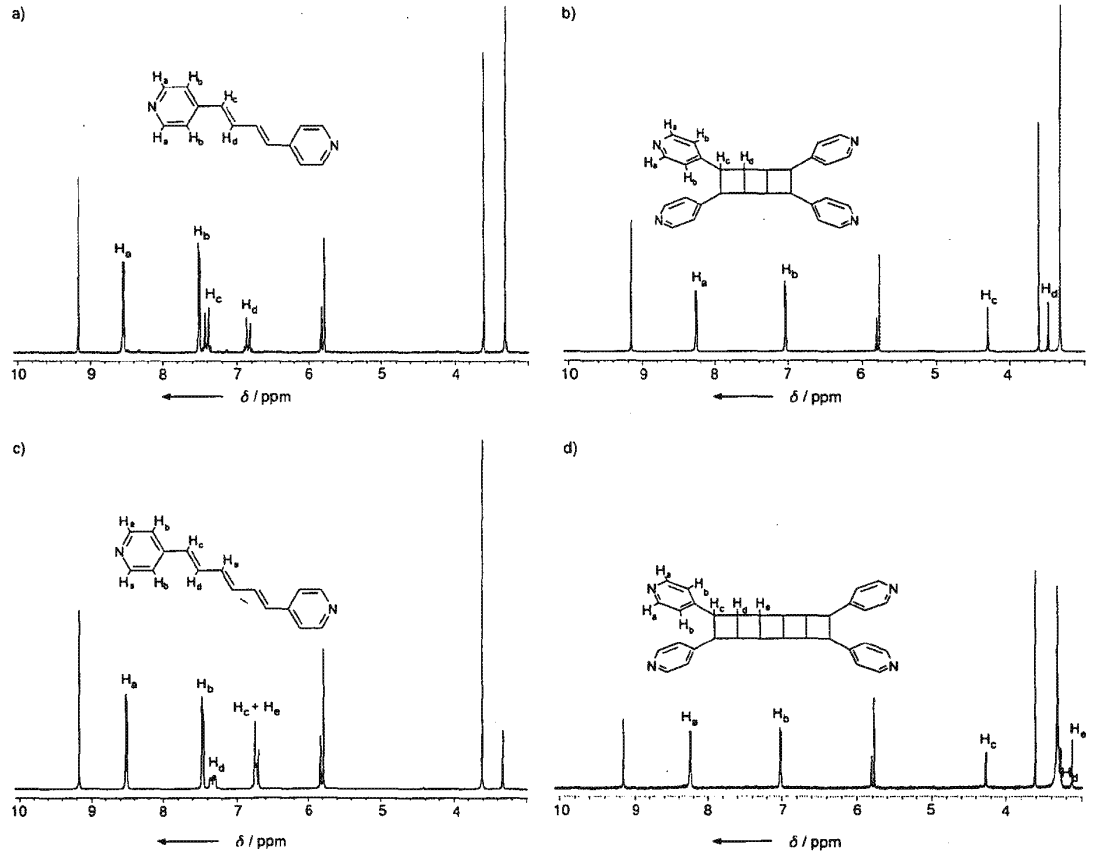


Figure 2. ^{1}H NMR spectra of the solid-state assemblies before and after photoreaction: a) **1a** (before), b) **1a** (after), c) **1b** (before), and d) **1b** (after).

 © 2004 Wiley-VCH Verlag GmbH & Co. KGaA, Weinheim

UM00013740
NOVARTIS EXHIBIT 1017
Novartis v. Regents, IPR2023-01346
Page 2486 of 4460

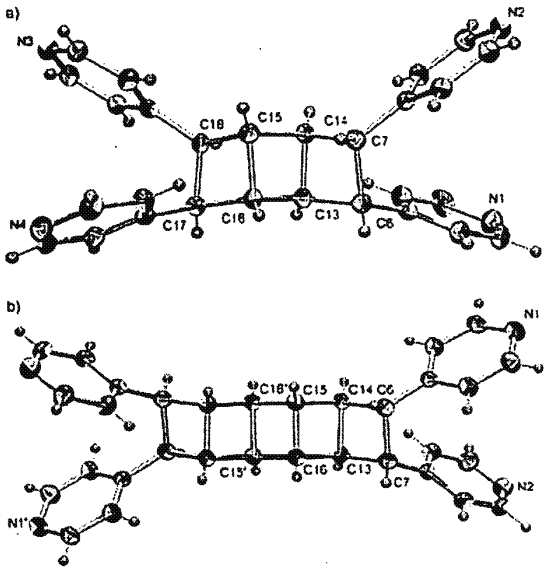


Figure 3. ORTEP perspectives of the ladderanes: a) **2a** and b) **2b**. Selected interatomic distances [Å] and angles [°]: C6-C7 1.593(5), C13-C14 1.566(5), C15-C16 1.575(5); b) C6-C7 1.585(3), C13-C14 1.567(3), C15-C16 1.585(3), C16-C15^{ii} 1.526(3). Symmetry operator ii: $-x+2$, $-y$, $-z+1$. The asymmetric unit of **2a** contains two full ladderanes, which are virtually identical, while that of **2b**·2(benzene) contains one half ladderane, which resides around a crystallographic center of inversion, and an included benzene molecule, respectively.

final product. Thus, a product consistent with a single cycloaddition (i.e., "[1]ladderane") precedes **2a** while products consistent with single and double cycloadditions (e.g., [3]ladderane) precede **2b**. Such observations contrast reactivity experiments involving 1,4-butadienes,[14,17] which exhibit similar packing in the solid state and react, via a single photodimerization, to produce *cis*-vinyl cyclobutanes and rearrange thermally, via a Cope rearrangement,[18] into *cis–cis* cyclooctadienes.[19] Here, the relatively strong O–H···N hydrogen bonds between the templates and reactants may serve to force divinyl groups from a first photoaddition into a conformation suitable for a second and third photoaddition, thus leading to each ladderane product.[20] In the case of **2b**, such stepwise transformations may occur either randomly or by way of a "zipper" process in the solid.[6] Experiments are underway to determine the structures of the lower-order ladderanes and the sequence by which the photocycloadditions occur.[21]

In this report, we have demonstrated that a linear template may be used to position two polyenes for an intermolecular reaction to produce [*n*]ladderanes ($n = 3$ or 5). The template preorganizes the polyenes, through hydrogen-bonding interactions, for [2+2] photodimerizations in the solid state. By using the organized, solvent-free environment of the solid state[9] for reaction, the ladderanes can be formed in gram quantities and in 100% yield. We believe that these results illuminate the utility of applying concepts of supramolecular chemistry and self-assembly to address a problem of covalent synthesis[7,8] and we are now exploring whether such template molecules can be used to construct ladderanes of increasing size and complexity in the solid state.[8]

Experimental Section

1a and **1b**: 4-pyr-poly-2-ene and 4-pyr-poly-3-ene were prepared according to a literature procedure.[22] 5-OMe-res was commercially available. Cocrystals of **1a** were obtained by evaporation of a solution of 4-pyr-poly-2-ene (0.058 g, 0.28 mmol) and 5-OMe-res (0.039 g, 0.28 mmol) in hot methanol (3.0 mL). Co-crystals of **1b** were obtained in a similar manner using 4-pyr-poly-3-ene (0.030 g, 0.13 mmol) and 5-OMe-res (0.018 g, 0.13 mmol).

Solid-state photoreactions and isolation of **2a** and **2b**: UV irradiation of powdered crystalline **1a** (500 W Hg lamp) over a period of 120 h resulted in 100% conversion of poly-2-ene to [3]ladderane. In the case of **1b**, the quantitative formation of the [5]ladderane was achieved after 72 h. In both cases, the irradiation experiments were performed by placing finely ground samples of either **1a** or **1b** between two pyrex plates and turning each sample in eight-hour intervals to ensure uniform irradiation. The irradiated solids were stirred with 1M KOH solution, then extraction with methylene chloride and evaporation of the organic phase yielded the appropriate ladderane as a white solid in 85% yield. All procedures were readily scaled up to give the ladderanes in gram quantities. Single crystals of **2a** were grown from ethanol, while single crystals of **2b** were grown from benzene yielding a 1:2 benzene solvate. ^{1}H NMR of **1a** before irradiation (300 MHz, [D$_6$]DMSO): $\delta = 9.15$ (br s, 2H), 8.54 (dd, 4H), 7.50 (dd, 4H), 7.40 (dd, 4H), (dd, 4H), 5.82 (br t, 1H), 5.78 (br d, 2H), 3.61 ppm (s, 3H). ^{1}H NMR of irradiated **1a** (300 MHz, [D$_6$]DMSO): $\delta = 9.16$ (br s, 4H), 8.26 (dd, 8H), 7.04 (dd, 8H), (br t, 2H), 5.78 (br d, 4H), 4.30 (br s, 4H), 3.61 (s, 6H), 3.49 ppm (br s, 4H). ^{1}H NMR of **1b** before irradiation (300 MHz, [D$_6$]DMSO): $\delta = 9.16$ (br s, 2H), 8.52 (dd, 4H), 7.46 (dd, 4H), 7.33 (m, 2H), 6.72 (m, 4H), 5.82 (br t, 1H), 5.79 (br d, 2H), 3.61 ppm (s, 3H). ^{1}H NMR of irradiated **1b** (300 MHz, [D$_6$]DMSO): $\delta = 9.15$ (br s, 4H), 8.25 (dd, 8H), 7.02 (dd, 8H), (br t, 2H), 5.78 (br d, 4H), 4.27 (br s, 4H), 3.61 (s, 6H), 3.27 (br s, 4H), 3.12 ppm (br s, 4H).

Crystal data for **1a**: monoclinic, $P2_1/c$, $a = 9.182(5)$, $b = 13.381(5)$, $c = 15.122(5)$ Å, $\beta = 106.712(5)°$, $V = 1779.5(13)$ Å^3, $Z = 4$, $\rho_{calcd} = 1.300$ g cm^{-3}, $R_1 = 0.0441$ for 2324 reflections with $I > 2\sigma(I)$. Crystal data for **1b**: triclinic, $P\bar{1}$, $a = 9.081(3)$, $b = 21.143(4)$, $c = 21.308(18)$ Å, $\alpha = 87.92(4)$, $\beta = 79.47(6)$, $\gamma = 78.91(2)°$, $V = 3947(4)$ Å^3, $Z = 2$, $\rho_{calcd} = 1.260$ g cm^{-3}, $R_1 = 0.0891$ for 6150 reflections with $I > 2\sigma(I)$. Crystal data for the **2a**: triclinic, $P\bar{1}$, $a = 12.534(5)$, $b = 12.583(5)$, $c = 14.787(5)$ Å, $\alpha = 100.388(5)$, $\beta = 106.555(5)$, $\gamma = 89.945(5)°$, $V = 2195.7(14)$ Å^3, $Z = 2$, $\rho_{calcd} = 1.260$ g cm^{-3}, $R_1 = 0.0647$ for 4018 reflections with $I > 2\sigma(I)$. Crystal data for **2b**·2(benzene): monoclinic, $P2_1/c$, $a = 9.475(2)$, $b = 15.048(3)$, $c = 12.235(2)$ Å, $\beta = 95.95(3)°$, $V = 1735.0(6)$ Å^3, $Z = 4$, $\rho_{calcd} = 1.196$ g cm^{-3}, $R_1 = 0.0438$ for 1625 reflections with $I > 2\sigma(I)$. All crystal data were measured on a Nonius Kappa CCD single-crystal X-ray diffractometer at 77 K. After anisotropic refinement of all non-hydrogen atoms, aromatic, methine, and hydroxyl hydrogen atoms were placed in idealized positions and allowed to ride on the atom to which they were attached. The structure of **1b** was determined to be a rotational twin, the twinning law being a twofold rotation about the (011) reciprocal lattice direction. All crystallographic calculations were conducted using SHELXL-97.[23] CCDC-218101 (**1a**), CCDC-218102 (**1b**), CCDC-218103 (**2a**), and CCDC-218104 (**2b**) contain the supplementary crystallographic data for this paper. These data can be obtained free of charge via www.ccdc.cam.ac.uk/conts/retrieving.html (or from the Cambridge Crystallographic Data Centre, 12, Union Road, Cam-

 © 2004 Wiley-VCH Verlag GmbH & Co. KGaA, Weinheim

UM00013741
NOVARTIS EXHIBIT 1017
Novartis v. Regents, IPR2023-01346
Page 2487 of 4460

bridge CB2 1EZ, UK; fax: (+44) 1223-336-033; or deposit@ccdc.cam.ac.uk).

Received: August 25, 2003 [Z52713]
Published Online: November 5, 2003

Keywords: dimerization · ladderanes · self-assembly · supramolecular chemistry · topochemistry

[1] For a recent highlight on ladderanes, see: H. Hopf, *Angew. Chem.* **2003**, *115*, 2928–2931; *Angew. Chem. Int. Ed.* **2003**, *42*, 2822–2825.
[2] W. Li, M. A. Fox, *J. Am. Chem. Soc.* **1996**, *118*, 11752–11758.
[3] a) J. S. S. Damste, M. Strous, W. I. C. Rijpstra, E. C. Hopmans, J. A. J. Geenevasen, A. C. T. van Duin, L. A. van Niftrik, M. S. M. Jetten, *Nature* **2002**, *419*, 708–712; b) E. F. DeLong, *Nature* **2002**, *419*, 676–677.
[4] M. M. M. Kuypers, A. O. Sliekers, G. Lavik, M. Schmidt, B. B. Jørgensen, J. G. Kuenen, J. S. S. Damste, M. Strous, M. S. M. Jetten, *Nature* **2003**, *422*, 608–611.
[5] For discussions on organizing molecules in solution, see: a) D. H. Williams, E. Stephens, M. Zhou, *Chem. Commun.* **2003**, 1973–1976; b) M. Rekharsky, Y. Inoue, S. L. Tobey, A. Metzger, E. V. Anslyn, *J. Am. Chem. Soc.* **2002**, *124*, 14959–14967.
[6] H. Hopf, H. Greiving, P. G. Jones, P. Bubenitschek, *Angew. Chem.* **1995**, *107*, 742–744; *Angew. Chem. Int. Ed. Engl.* **1995**, *34*, 685–687.
[7] M. C. T. Fyfe, J. F. Stoddart, *Acc. Chem. Res.* **1997**, *30*, 393–401.
[8] a) J. Xiao, M. Yang, J. W. Lauher, F. W. Fowler, *Angew. Chem.* **2000**, *112*, 2216–2219; *Angew. Chem. Int. Ed.* **2000**, *39*, 2132–2135; b) J. J. Kane, R.-F. Liao, J. W. Lauher, F. W. Fowler, *J. Am. Chem. Soc.* **1995**, *117*, 12003–12005.
[9] a) K. Tanaka, F. Toda, *Chem. Rev.* **2000**, *100*, 1025–1074; b) V. Ramamurthy, K. Venkatesan, *Chem. Rev.* **1987**, *87*, 433–481.
[10] a) L. R. MacGillivray, *CrystEngComm* **2002**, *4*, 37–42; b) D. B. Varshney, G. S. Papaefstathiou, L. R. MacGillivray, *Chem. Commun.* **2002**, 1964–1965; c) L. R. MacGillivray, J. L. Reid, J. A. Ripmeester, G. S. Papaefstathiou, *Ind. Eng. Chem. Res.* **2002**, *41*, 4494–4497; d) G. S. Papaefstathiou, A. J. Kipp, L. R. MacGillivray, *Chem. Commun.* **2001**, 2432–2433; e) L. R. MacGillivray, J. L. Reid, J. A. Ripmeester, *J. Am. Chem. Soc.* **2000**, *122*, 7817–7818.
[11] We used "template switching" to identify a template that affords each [*n*]ladderane in 100% yield. See: T. Friščić, L. R. MacGillivray, *Chem. Commun.* **2003**, 1306–1307.
[12] For use of linear templates in the solid state, see also: a) Y. Ito, B. Borecka, J. Trotter, J. R. Scheffer *Tetrahedron Lett.* **1995**, *36*, 6083–6086; b) D. G. Amirakis, M. A. Garcia-Garibay, S. J. Rowan, J. F. Stoddart, A. J. P. White, D. J. Williams, *Angew. Chem.* **2001**, *113*, 4386–4391; *Angew. Chem. Int. Ed.* **2001**, *40*, 4256–4261; c) S. Phba, H. Hosomi, Y. Ito *J. Am. Chem. Soc.* **2001**, *123*, 6349–6352; d) D. G. Amirsakis, A. M. Elizarov, M. A. Garcia-Garibay, P. T. Glink, J. F. Stoddart, A. J. P. White, D. J. Williams, *Angew. Chem.* **2003**, *115*, 1158–1164; *Angew. Chem. Int. Ed.* **2003**, *42*, 1126–1132; e) N. Shan, W. Jones, *Tetrahedron Lett.* **2003**, *44*, 3687–3689.
[13] For use of linear templates in the liquid phase, see: a) T. R. Kelly, C. Zhao, G. J. Bridger, *J. Am. Chem. Soc.* **1989**, *111*, 3744–3745; b) R. J. Pieters, I. Huc, J. Rebek *Tetrahedron* **1995**, *51*, 485–498; c) D. M. Bassani, V. Darcos, S. Mahony, J.-P. Desvergne, *J. Am. Chem. Soc.* **2000**, *122*, 8795–8796; c) D. M. Bassani, X. Sallenave, V. Darcos, J.-P. Desvergne, *Chem. Commun.* **2001**, 1446–1447; d) H. Zitt, I. Dix, H. Hopf, P. G. Jones, *Eur. J. Org. Chem.* **2002**, 2298–2307.
[14] G. M. J. Schmidt, *Pure Appl. Chem.* **1971**, *27*, 647–678.
[15] S. Woitellier, J. P. Launay, C. W. Spangler, *Inorg. Chem.* **1989**, *28*, 758–762.
[16] a) G. Mehta, M. B. Viswanath, A. C. Kunwar, *J. Org. Chem.* **1994**, *59*, 6131–6132; b) R. N. Warrener, G. Abbenante, C. H. L. Kennard, *J. Am. Chem. Soc.* **1994**, *116*, 3645–3646; c) M. A. Miller, J. M. Schulman, *J. Mol. Struct.* **1988**, *163*, 133–141.
[17] a) A. Elgavi, B. S. Green, G. M. J. Schmidt, **1973**, *95*, 2058–2059; b) M. D. Cohen, A. Elgavi, B. S. Green, Z. Ludmer, G. M. J. Schmidt, *J. Am. Chem. Soc.* **1972**, *94*, 6776–6779.
[18] For a theoretical treatment of the Cope rearrangement in ladderanes, see: D. J. Tantillo, R. Hoffmann, *Angew. Chem.* **2002**, *114*, 1075–1078; *Angew. Chem. Int. Ed.* **2002**, *41*, 1033–1036.
[19] For oligomerizations and polymerizations of cyclobutanes in the solid state, see: a) L. Addadi, M Lahav, *J. Am. Chem. Soc.* **1978**, *100*, 2838–2844; b) M. Hasegawa, *Chem. Rev.* **1983**, *83*, 507–518.
[20] For movement in crystals, see: a) G. R. Desiraju, *Nature* **2003**, *423*, 485; b) I. C. Paul, D. Y. Curtin, *Acc. Chem. Res.* **1973**, *6*, 217–225.
[21] V. Enkelmann, G. Wegner, K. Novak, K. B. Wagener, *J. Am. Chem. Soc.* **1993**, *115*, 10390–10391.
[22] P. Carsky, S. Hünig, I. Stemmler, D. Scheutzow, *Liebigs Ann. Chem.* **1980**, 291–304.
[23] G. M. Sheldrick, SHELXL-97, Program for Refinement of Crystal Structure, University of Göttingen, Göttingen (Germany), **1997**.

 © 2004 Wiley-VCH Verlag GmbH & Co. KGaA, Weinheim

UM00013742
NOVARTIS EXHIBIT 1017
Novartis v. Regents, IPR2023-01346
Page 2488 of 4460

Acta Cryst. (1974). B30, 980

Hydrogen Bonding NH···O=C of Barbiturates: The (1:1) Crystal Complex of Urea and 5,5-Diethylbarbituric Acid (Barbital)

BY G. L. GARTLAND* AND B. M. CRAVEN

Department of Crystallography, Univeristy of Pittsburgh, Pittsburgh, Pennsylvania 15260, *U.S.A.*

(*Received* 12 *October* 1973; *accepted* 10 *December* 1973)

The 1:1 complex of urea and barbital ($CH_4N_2O.C_8H_{12}N_2O_3$), m.p. 146–150°C, is orthorhombic with space group $P2_12_12_1$. Lattice translations are $a=10{\cdot}302$ (5), $b=10{\cdot}181$ (2), and $c=11{\cdot}627$ (3) Å. The crystal density ($D_m=1{\cdot}320$ g cm^{-3}) agrees with the calculated density ($D_x=1{\cdot}330$ g cm^{-3}) for four molecules of each component in the unit cell. The crystal structure has been determined from 1144 integrated intensities measured on a computer-controlled four-circle diffractometer with nickel-filtered Cu $K\alpha$ radiation (absorption coefficient, 9·05 cm^{-1}). The final R index is 0·037. In the crystal structure, barbital molecules hydrogen bond exclusively with urea molecules and *vice versa*. The NH···O=C hydrogen bonds in which barbital (NH) is donor are stronger (N···O distances 2·78 and 2·80 Å) than those in which it is acceptor (N···O distances 2·95, 3·16 Å). The minor role of urea as the hydrogen-bonding donor in this complex is confirmed by the isomorphous replacement of urea by acetamide. Thus we consider that the association in this complex is essentially that of a hydrogen-bonding acid (barbital) with a hydrogen-bonding base (urea).

Introduction

We have undertaken a series of crystal-structure determinations of molecular complexes of drug-active barbiturates such as barbital (Fig. 1) with other molecules which also contain the –NH–CO– amide grouping. Our particular interests are in the modes of NH···O=C hydrogen bonding, and the hydrogen-bonding distances in the crystal structures of the molecular complexes and of the component molecules. These crystal structures provide opportunities for NH···O=C hydrogen bonding of the types $A_d\cdots A_a$, $B_d\cdots B_a$, $A_d\cdots B_a$ and $B_d\cdots A_a$, where A and B are the component amide and barbiturate molecules respectively, and subscripts d and a refer to donor (NH) and acceptor (O=C) functions. We wish to determine whether any one of these is a preferred mode of hydrogen bonding, and whether there is any correlation between the N···O hydrogen-bonding distances and the mode of hydrogen bonding.

The results of nine crystal-structure determinations of barbiturate complexes, including those for the 1:1 barbital/urea complex which are presently reported, suggest that such relationships may exist. The barbiturate drugs appear to be more effective hydrogen-bonding donors than acceptors.

Experimental

The crystal complex was obtained as transparent prisms,† m.p. 146–150°C, from a solution of barbital (600 mg) and urea (300 mg) in an equal volume mixture of n-propanol and ethanol. The crystals are orthorhombic with space group $P2_12_12_1$ and lattice translations $a=10{\cdot}302$ (5), $b=10{\cdot}181$ (2) and $c=11{\cdot}627$ (3) Å. The crystal density (1·320 g cm^{-3}), which was determined by flotation in a mixture of ethyl acetate and tribromomethane, agrees with the calculated value (1·330 g cm^{-3}), assuming four molecules of each component in the unit cell. The lattice translations and X-ray intensity data were measured on a four-circle automatic diffractometer using nickel-filtered Cu $K\alpha$ radiation ($\lambda=1{\cdot}5418$ Å, $\mu=9{\cdot}05$ cm^{-1}). Integrated intensities were measured for 1144 symmetry-independent reflections in the range $\sin\theta/\lambda\leq 0{\cdot}59$ Å^{-1} ($\theta\leq 65°$) with the prism axis of the crystal (a) along the φ axis of the goniostat. The crystal dimensions were approximately $0{\cdot}5\times 0{\cdot}3\times 0{\cdot}3$ mm. Reflections were scanned in the θ:2θ mode at a rate of 2° min^{-1} with 20 s background counts being taken at each of the scan limits. The 2θ scan width was based on 1·4° and was varied to allow for spectral dispersion. There were 44 reflections for which the integrated intensity, I, was less than 1·2 $\sigma(I)$ as calculated from the counting statistics. These reflections were arbitrarily assigned intensities of $\sigma(I)/2$. No corrections were applied for X-ray absorption or extinction.

The crystal structure was determined by direct methods as reported in detail by Gartland (1971). Atomic parameters (Table 1) were refined by a block-diagonal least-squares procedure. The function minimized was $\sum_H w_H\Delta_H^2$, where $\Delta_H=|F_H^{obs}|-|F_H^{calc}|$. The weights were $w_H=1/\sigma^2(F_H)$, with $\sigma^2(F_H)=0{\cdot}16-0{\cdot}015\,|F_H|+0{\cdot}0024\,|F_H|^2$. The atomic scattering factors were those of Cromer & Waber (1965) for C, N, O and Stewart, Davidson & Simpson (1965) for H. All

* Present address: The University of Alabama Medical Center, Birmingham, Alabama 35233, U.S.A.

† Sekiguchi, Himuro, Horikoshi, Tsukuda, Okamoto & Yotsuyanagi (1969) describe the crystallization of this complex from n-propanol.

UM00013743
NOVARTIS EXHIBIT 1017
Novartis v. Regents, IPR2023-01346
Page 2489 of 4460

hydrogen-atom positions were obtained from difference Fourier syntheses which were calculated after refinement of anisotropic thermal parameters had been introduced for the non-hydrogen atoms. Hydrogen-atom positional parameters were subsequently included as variables in the refinement, but hydrogen-atom temperature parameters were fixed with values the same as those of the atoms to which they are covalently bonded. Before the last two cycles of least-squares refinement, 12 strong reflections for which $|F^{calc}| > |F^{obs}|$ were given zero weight. The calculated and observed structure amplitudes are listed in Table 2. The final overall R^* index was 0·037. The r.m.s. displacements of atoms along the principal axes of their thermal ellipsoids are given in Table 1. In the barbital molecule, the largest atomic r.m.s. thermal displacements, excluding atoms of the ethyl groups, are approximately normal to the ring plane. Except for C(4) and C(5), which appear to have isotropic motion, the greatest deviations from this direction are about 20–25° for the carbonyl oxygen atoms. In the urea molecule, the largest thermal amplitudes are within 15° of being normal to the molecular plane, except for N(4), where the deviation from perpendicularity is 32°.

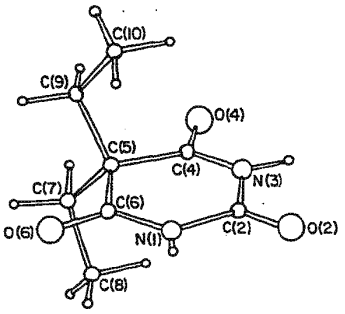


Fig. 1. Molecular structure of 5,5-diethylbarbituric acid (barbital).

* $R = \sum_H |\Delta_H| / \sum_H |F_H^{obs}|$.

Table 1. *Atomic parameters and their e.s.d.'s*

Positional parameters are given as fractions of the unit-cell translations. Thermal parameters are given according to the expression: $T = \exp(-\sum_i \sum_j \beta_{ij} h_i h_j)$. The quantity U_k is the r.m.s. displacement (Å), derived from the components β_{ij}, along the direction of the kth principal axis of the thermal ellipsoid. The e.s.d.'s given in parentheses refer to the least significant figures in the parameter values. Non-hydrogen positional parameters and all thermal parameters are $\times 10^4$, hydrogen positional parameters are $\times 10^3$ and U_k parameters are $\times 10^2$.

(i) The barbital molecule

	x	y	z	β_{11}	β_{22}	β_{33}	β_{12}	β_{13}	β_{23}	U_1	U_2	U_3
N(1)	5754 (2)	4037 (2)	4891 (2)	93 (2)	70 (2)	60 (1)	3 (2)	25 (1)	3 (1)	17	19	25
H(1)	530 (2)	397 (2)	549 (2)									
C(2)	6588 (2)	3014 (2)	4688 (2)	108 (2)	62 (2)	52 (2)	0 (2)	9 (2)	2 (2)	18	19	24
O(2)	6704 (2)	2096 (2)	5348 (2)	185 (3)	87 (2)	71 (1)	25 (2)	32 (2)	27 (1)	18	23	33
N(3)	7285 (2)	3059 (2)	3684 (2)	101 (2)	65 (2)	48 (1)	21 (2)	10 (1)	6 (1)	17	18	25
H(3)	782 (3)	242 (2)	355 (2)									
C(4)	7199 (2)	4030 (2)	2864 (2)	66 (2)	85 (2)	55 (2)	2 (2)	−2 (1)	3 (2)	19	19	21
O(4)	7778 (2)	3896 (2)	1961 (1)	99 (2)	127 (2)	49 (1)	24 (2)	14 (1)	12 (1)	17	22	28
C(5)	6429 (2)	5255 (2)	3138 (2)	76 (2)	65 (2)	61 (2)	−1 (2)	1 (2)	8 (2)	18	20	21
C(6)	5626 (2)	5145 (2)	4232 (2)	86 (2)	71 (2)	71 (2)	1 (2)	13 (2)	−6 (2)	19	20	24
O(6)	4891 (2)	6006 (2)	4520 (2)	143 (2)	95 (2)	115 (2)	48 (2)	47 (2)	2 (2)	17	25	34
C(7)	5524 (3)	5591 (2)	2125 (2)	101 (3)	81 (2)	79 (2)	8 (2)	−18 (2)	7 (2)	19	22	26
H(71)	518 (3)	639 (2)	233 (2)									
H(72)	614 (3)	575 (3)	145 (2)									
C(8)	4563 (3)	4504 (3)	1814 (3)	92 (3)	131 (3)	102 (2)	1 (3)	−16 (2)	−12 (3)	21	25	28
H(81)	410 (3)	429 (3)	254 (2)									
H(82)	506 (3)	368 (3)	154 (3)									
H(83)	392 (3)	484 (3)	122 (2)									
C(9)	7427 (3)	6382 (2)	3301 (2)	109 (3)	84 (2)	76 (2)	−24 (2)	−3 (2)	10 (2)	19	23	26
H(91)	689 (3)	722 (3)	335 (2)									
H(92)	789 (3)	654 (2)	254 (2)									
C(10)	8372 (3)	6199 (3)	4282 (2)	108 (3)	130 (3)	75 (2)	−22 (3)	−2 (2)	−10 (2)	22	23	28
H(101)	786 (3)	605 (3)	500 (2)									
H(102)	894 (3)	539 (3)	419 (2)									
H(103)	902 (3)	696 (3)	423 (2)									

(ii) The urea molecule

C	3894 (2)	4614 (2)	7596 (2)	67 (2)	92 (2)	60 (2)	−3 (2)	1 (2)	−11 (2)	19	19	23
O	4178 (2)	3786 (2)	6845 (1)	113 (2)	87 (2)	67 (1)	−31 (2)	30 (1)	−23 (1)	18	19	29
N(2)	4294 (2)	5858 (2)	7532 (2)	129 (2)	81 (2)	84 (2)	−3 (2)	18 (2)	−16 (2)	19	23	28
H(21)	470 (3)	596 (2)	698 (2)									
H(22)	425 (3)	644 (3)	816 (2)									
N(4)	3164 (2)	4292 (3)	8499 (2)	116 (2)	134 (3)	66 (2)	−13 (2)	23 (2)	−13 (2)	19	25	28
H(41)	300 (3)	356 (3)	856 (2)									
H(42)	295 (3)	488 (3)	904 (2)									

UM00013744
NOVARTIS EXHIBIT 1017
Novartis v. Regents, IPR2023-01346
Page 2490 of 4460

The molecular structures

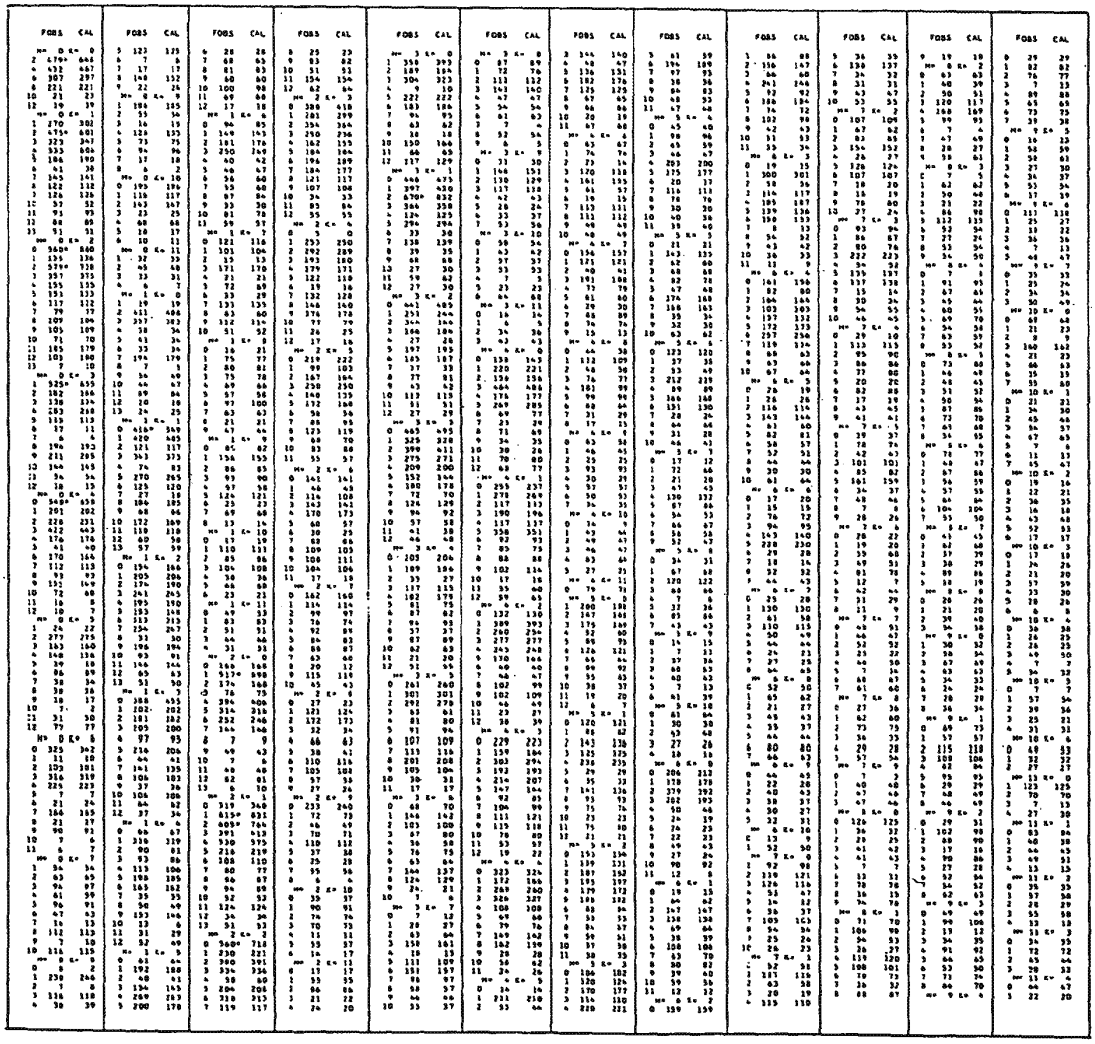
(i) *Barbital*

The oxopyrimidine ring is almost planar, with C(5) and ethyl carbon atoms forming the spine of a hydrocarbon chain which extends nearly perpendicular to the ring. The slight twist conformation of the ring has already been shown and compared with similar conformations found in other barbiturate crystal structures (Craven, Cusatis, Gartland & Vizzini, 1973). Torsion angles C(8)–C(7) → C(5)–C(9) and C(10)–C(9) → C(5)–C(7) are 184·6 and 180·9° respectively, indicating that the extended hydrocarbon spine C(8)–C(7)–C(5)–C(9)–C(10) deviates slightly from two-fold symmetry about the axis C(5)···C(2). All carbon atoms of the hydrocarbon spine are coplanar to within 0·03 Å, and the best least-squares planes through these atoms and through atoms of the pyrimidine ring form a dihedral angle of 89·3°.

The bond lengths and angles (Table 3) are similar to those found in other barbiturates (Craven *et al.*, 1973). Within experimental error, the C=O and C–N bond lengths are symmetrical about the C(5)···C(2) molecular axis. There is thus no evidence of the small (0·01 Å) C–N and C=O bond-length differences which consistently appear in barbiturate crystal structures

Table 2. *Observed and calculated structure amplitudes*

Successive columns are l, $10|F_H^{obs}|$, $10|F_H^{calc}|$. Reflections marked (*) were given zero weight in the final refinement cycles.



UM00013745
NOVARTIS EXHIBIT 1017
Novartis v. Regents, IPR2023-01346
Page 2491 of 4460

where the O(4) oxygen atom is hydrogen bonded but O(6) is not. In barbital/urea, the barbital O(4) and O(6) oxygen atoms are both at most weakly hydrogen bonded.

(ii) *Urea*

The urea molecule is planar except possibly for the hydrogen atom H(22) which is 0·19 Å (6σ) from the plane. The bond lengths and angles (Table 3) are in good agreement with those found in the crystal structures of urea itself (Caron & Donohue, 1964; Pryor & Sanger, 1970) and the 1:1 glucose/urea complex (Snyder & Rosenstein, 1971). The bonds N(2)–H(22) and N(4)–H(42), which are *trans* to the urea oxygen atom, may be significantly longer (0·94 and 0·89 Å) than the other two urea N–H bonds (0·77 Å). The longer bonds involve the hydrogen atoms which are weakly hydrogen bonded to barbital oxygen atom O(2).

Table 3. *Bond lengths and angles for the barbital and urea molecules*

These values have not been corrected for the effects of anisotropic thermal motion. The e.s.d.'s are given in parentheses and refer to the least significant digits in the tabulated quantities.

(*a*) Bond lengths

(i) Barbital

C(6)–N(1)	1·370 (3) Å	N(1)—H(1)	0·84 (2) Å
N(1)–C(2)	1·370 (3)	N(3)—H(3)	0·87 (2)
C(2)–N(3)	1·371 (3)	C(7)—H(71)	0·92 (2)
N(3)–C(4)	1·376 (3)	C(7)—H(72)	1·02 (3)
C(6)–O(6)	1·205 (3)	C(9)—H(91)	1·02 (3)
C(2)–O(2)	1·215 (3)	C(9)—H(92)	1·01 (2)
C(4)–O(4)	1·215 (3)	C(8)—H(81)	0·99 (3)
C(5)–C(4)	1·511 (3)	C(8)—H(82)	1·04 (3)
C(5)–C(6)	1·522 (3)	C(8)—H(83)	1·02 (3)
C(5)–C(7)	1·540 (3)	C(10)–H(101)	1·00 (3)
C(5)–C(9)	1·552 (3)	C(10)–H(102)	1·02 (3)
C(7)–C(8)	1·528 (4)	C(10)–H(103)	1·03 (3)
C(9)–C(10)	1·511 (4)		

(ii) Urea

C——O	1·238 (3)	N(2)—H(21)	0·77 (2)
C——N(2)	1·344 (3)	N(2)—H(22)	0·94 (3)
C——N(4)	1·332 (3)	N(4)—H(41)	0·77 (3)
		N(4)—H(42)	0·89 (3)

(*b*) Bond angles

(i) Barbital

N(1)–C(2)–O(2)	122·5 (2)°
N(1)–C(2)–N(3)	116·7 (2)
N(3)–C(2)–O(2)	120·8 (2)
C(2)–N(3)–C(4)	125·5 (2)
N(3)–C(4)–O(4)	119·1 (2)
N(3)–C(4)–C(5)	118·7 (2)
C(5)–C(4)–O(4)	122·1 (2)
C(4)–C(5)–C(6)	113·6 (2)
C(5)–C(6)–O(6)	121·3 (2)
C(5)–C(6)–N(1)	118·4 (2)
N(1)–C(6)–O(6)	120·2 (2)
C(6)–N(1)–C(2)	126·1 (2)
C(4)–C(5)–C(7)	109·8 (2)
C(4)–C(5)–C(9)	106·8 (2)
C(6)–C(5)–C(9)	108·2 (2)
C(6)–C(5)–C(7)	109·1 (2)
C(7)——C(5)—C(9)	109·3 (2)°
C(5)——C(7)—C(8)	114·3 (2)
C(5)——C(9)—C(10)	115·4 (2)
C(6)——N(1)—H(1)	119 (1)
C(2)——N(1)—H(1)	115 (1)
C(4)——N(3)—H(3)	117 (2)
C(2)——N(3)—H(3)	117 (2)
H(71)—C(7)—H(72)	107 (2)
H(81)—C(8)—H(82)	109 (2)
H(81)—C(8)—H(83)	110 (2)
H(82)—C(8)—H(83)	113 (2)
H(91)—C(9)—H(92)	100 (2)
H(101)–C(10)–H(102)	106 (2)
H(101)–C(10)–H(103)	121 (2)
H(102)–C(10)–H(103)	103 (2)

(ii) Urea

N(2)–C——O	122·0 (2)°
O——C——N(4)	121·2 (2)
N(4)–C——N(2)	116·9 (2)
C——N(2)–H(21)	110 (2)
C——N(2)–H(22)	123 (2)
H(21)—N(2)—H(22)	126 (3)
C———N(4)—H(41)	116 (2)
C———N(4)—H(42)	121 (2)
H(41)—N(4)—H(42)	122 (3)

The hydrogen bonding

In the crystal structure of the 1:1 barbital/urea complex, the most important intermolecular interactions are the NH···O=C hydrogen bonds, which link the molecules to form a three-dimensional network (Fig. 2). The hydrogen-bonding environments of barbital and urea are shown separately in Figs. 3 and 4. Barbital molecules are hydrogen bonded exclusively to urea molecules and *vice versa*, *i.e.*, there are only $B_d\cdots A_a$ and $A_d\cdots B_a$ hydrogen bonds. The two barbital NH groups both form hydrogen bonds with the urea oxygen atom with N···O distances of 2·78 and 2·80 Å. Only two of the four urea hydrogen atoms form hydrogen bonds, and both of these involve the same barbital oxygen atom, O(2). The N···O distances (2·95 and 3·16 Å) are significantly longer for the $(NH)_{urea}\cdots O(2)_{barb}$ hydrogen bonds than for the $(NH)_{barb}\cdots O_{urea}$ hydrogen bonds, and in the former, the NH···O angles are more severely bent (Table 4). The NH···O=

Table 4. *Hydrogen-bonding distances and angles*

Parameters for atoms not in the crystal chemical unit (as listed in Table 1) may be derived by operations specified by the subscripts *i*, *j*, where *i* is $(\frac{1}{2}+x,\frac{1}{2}-y,1-z)$ and *j* is $(1-x,\frac{1}{2}+y,\frac{1}{2}-z)$. The e.s.d.'s given in parentheses refer to the least significant figures in tabulated values.

N(1)····O	2·803 (3) Å	N(1)···O———C	129·9 (2)°
H(1)····O	1·96 (2)	N(1)—H(1)····O	177 (2)
N(3)····O_i	2·777 (3)	N(3)···O_i———C_i	116·6 (1)
H(3)····O_i	1·92 (2)	N(3)—H(3)····O_i	171 (2)
N(2)····$O(2)_j$	2·953 (3)	N(2)···$O(2)_j$——$C(2)_j$	145·2 (2)
H(22)···$O(2)_j$	2·10 (3)	N(2)—H(22)···$O(2)_j$	150 (2)
N(4)····$O(2)_j$	3·157 (3)	N(4)···$O(2)_j$——$C(2)_j$	165·5 (2)
H(42)···$O(2)_j$	2·39 (3)	N(4)—H(42)···$O(2)_j$	144 (2)

UM00013746
NOVARTIS EXHIBIT 1017
Novartis v. Regents, IPR2023-01346
Page 2492 of 4460

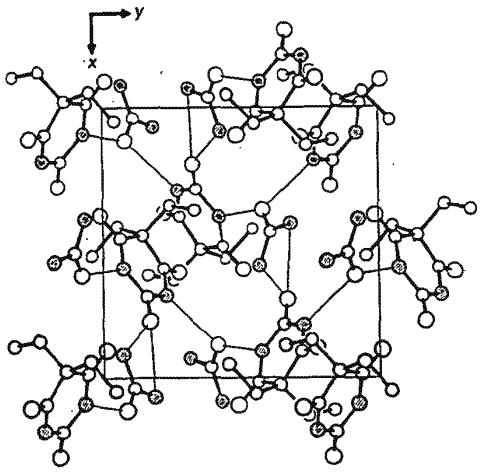


Fig. 2. The crystal structure viewed down c. Circles of decreasing size represent oxygen, nitrogen and carbon atoms respectively. Nitrogen atoms are also cross-hatched. Hydrogen bonds are shown as thin lines.

C hydrogen bonds in which urea is donor ($A_d\cdots B_a$) are thus considerably weaker than those in which barbiturate is donor ($B_d\cdots A_a$). This conclusion is supported by a comparison with the structure of the 1:1 barbital/acetamide complex (Hsu & Craven, 1974*a*), which is isomorphous with the 1:1 barbital/urea complex. The CH_3 group of acetamide, which does not hydrogen bond, replaces one of the NH_2 groups of urea, with only minor perturbation of the crystal structure.

The existence of both strong and weak NH···O=C hydrogen bonds in the barbital/urea crystal structure may be the result of the overall packing requirements of more or less rigid molecules. However, the N···O distance* may also depend to some extent, on the electronic structures of the molecules which provide the particular NH donor group and carbonyl oxygen acceptor atom. A similar effect has been noted in the hydrogen bonding of ammonium ions with oxyanions in the crystal structures of inorganic salts. Baur & Khan (1970) find that the N···O distances in such NH···O hydrogen bonds increase with the coordination number of the oxygen acceptor atom.

Table 5 lists the N···O distances determined from crystal structures with NH···O=C hydrogen bonds in which a barbiturate provides either the NH donor, the carbonyl acceptor or both. A remarkable feature is the narrow range (2·82 to 2·92 Å) of the $B_d\cdots B_a$ hydrogen bond N···O distances in the crystal structures of the barbituric acids themselves [Table 5(*a*)]. The barbiturate ring (Fig. 1) has one carbonyl group C(2)–O(2) covalently bonded to two NH groups and two equivalent carbonyl groups C(4)–O(4) and C(6)–O(6) bonded to one NH group. The N···O distances for hydrogen bonds between barbiturate NH donors and these two kinds of barbiturate oxygen atoms have very similar distributions. The average values are 2·88 Å and 2·89 Å for distances involving O(4) and O(2), respectively. It should be noted that in many cases, the oxygen atoms accept a second hydrogen bond, The

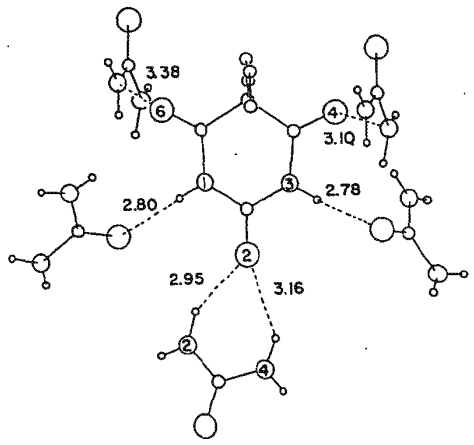


Fig. 3. The environment of the barbital molecule viewed normal to the plane of the pyrimidine ring. Distances N···O are shown in Å.

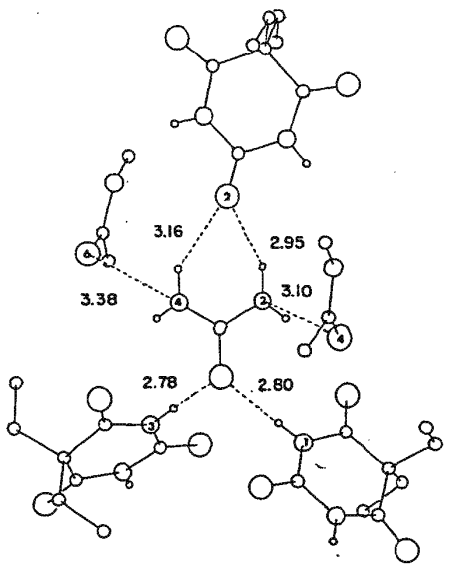


Fig. 4. The environment of the urea molecule viewed normal to the plane of the molecule. Distances N···O are shown in Å.

* The N···O distance gives a convenient, although not a definitive measure of hydrogen-bond strength. Nakamoto, Margoshes & Rundle (1955) have correlated NH infrared stretching frequencies with N···O distances in NH···O hydrogen bonds.

UM00013747
NOVARTIS EXHIBIT 1017
Novartis v. Regents, IPR2023-01346
Page 2493 of 4460

angles N–H···O range between 155 and 177°, with an average value of 170°. The N···O=C angles are grouped in the ranges 124–131° and 160–177°. There is no obvious correlation between either of these angles and the N···O distance.

The N···O distances for $B_d \cdots B_a$ hydrogen bonds in crystal structures of 1-methylbarbituric acids [Table 5(*b*)], barbiturate anions [Table 5(*c*)] and barbiturate molecular complexes [Table 5(*d*)] fall within the same range as found in Table 5(*a*) (2·82 to 2·92 Å) except for one slightly shorter distance of 2·78 Å in calcium barbital trihydrate, and three slightly longer distances of 2·93, 2·94 and 2·98 Å in 2:1 barbital/caffeine. Thus changes in barbiturate structure, electronic charge and molecular environment appear to have at most a small effect on the observed N···O distances in NH···O=C hydrogen bonds which involve barbiturates as both donor and acceptor. These hydrogen bonds may be considered to have a distance N···O of 2·9 Å subject to variations of ±0·1 Å.*

* Table 5 lists hydrogen-bonding data for barbiturates with non-polar C(5) substituents. Voet & Rich (1970) list data for barbituric acid, its dihydrate and other non drug-active barbiturates with polar C(5) substituents. The N···O distances in these crystal structures range from 2·79 to 3·07 Å. The long N···O distances of 3·00 and 3·07 Å in perdeuterated violuric acid monohydrate have been explained (Craven & Takei, 1964) in terms of an unusual kind of intermolecular packing.

Table 5. *Distances* N···O *in* NH···O=C *hydrogen bonds involving barbiturate derivatives with nonpolar* C(5) *substituents*

Crystal structure	$(NH)_{barb}\cdots O(4)=C_{barb}$	$(NH)_{barb}\cdots O(2)=C_{barb}$
(*a*) Barbituric acids		
5,5-Diethylbarbituric acid (barbital), form I (Craven, Vizzini & Rodrigues, 1969)	2·87 Å	2·89 Å
Barbital, form II (Craven, Vizzini & Rodrigues, 1969)	2·87	–
Barbital, form IV (Craven & Vizzini, 1971)	2·90, 2·87, 2·91, 2·91, 2·92, 2·91, 2·92, 2·85	–
5-Ethyl-5-isoamylbarbituric acid (amobarbital), form I (Craven & Vizzini, 1969)	2·89	2·92
Amobarbital, form II (Craven & Vizzini, 1969)	2·91, 2·86	2·92, 2·88
5-Ethyl-5-(3,3-dimethylbutyl)barbituric acid (Gartland & Craven, 1971)	2·82	2·88
5-Ethyl-5-(1-methylbutenyl)barbituric acid (Craven & Cusatis, 1969)	2·87, 2·92	–
5-Ethyl-5-butylbarbituric acid (Bideau, 1971)	2·86	2·87
5-Ethyl-5-(1-cyclohexen-1-yl)barbituric acid (Bideau & Artaud, 1970)	2·87	2·90
5-Ethyl-5-(1-cyclohepten-1-yl)barbituric acid (Bideau, Leroy & Housty, 1969)	2·89, 2·87	–
5-Ethyl-5-phenylbarbituric acid, form III (Williams, 1974)	2·89, 2·91	–
5-Methyl-5-phenylbarbituric acid (Bravic, Housty & Bideau, 1968)	2·90	2·89
5-Ethylbarbituric acid (Gatehouse & Craven, 1971)	2·85	2·89
(*b*) 1-Methylbarbituric acids		
1-Methyl-5,5-diethylbarbituric acid (Wunderlich, 1973)	2·84	–
1-Methyl-5-ethyl-5-(1-cyclohexen-1-yl)barbituric acid (Bideau, Leroy & Housty, 1970)	2·88	–
1-Methyl-5-ethyl-5-phenylbarbituric acid (Bideau, Marly & Housty, 1969)	2·89	–
(*c*) Barbiturate anions		
Sodium barbital (Berking & Craven, 1971)	2·84	–
Calcium barbital trihydrate (Berking, 1972)	–	2·82, 2·78, 2·86, 2·85
Guanidinium barbital dihydrate (McClure & Craven, 1973)	–	2·85

(*d*) Barbiturate molecular complexes

Crystal structure	$(NH)_{barb}\cdots(O=C)_{barb}$	$(NH)_{barb}\cdots(O=C)_{other}$	$(NH)_{other}\cdots(O=C)_{barb}$
5-Ethyl-5-phenylbarbituric acid/8-bromo-9-ethyladenine (1:2) (Kim & Rich, 1968)	–	–	2·97, 3·19 Å
5-Isopropyl-5-bromoallylbarbituric acid/9-ethyladenine (1:1) (Voet & Rich, 1972)	–	–	3·34, 3·12
5,5-Diethylbarbituric acid/9-ethyladenine (1:1) (Voet, 1972)	–	–	3·22, 3·39
5,5-Diethylbarbituric acid/caffeine (2:1) (Craven & Gartland, 1970)	2·98, 2·94, 2·93	–	–
5,5-Diethylbarbituric acid/aminopyrine (1:1) (Kiryu, 1971)	2·82	2·75	–
5,5-Diethylbarbituric acid/urea (1:1) (This paper)	–	2·78, 2·80	2·95, 3·16
5,5-Diethylbarbituric acid/acetamide) (1:1) (Hsu & Craven, 1974*a*)	–	2·82, 2·82	2·95, 3·08
5-Ethyl-5-isoamylbarbituric acid/salicylamide (1:1) (Hsu & Craven, 1974*b*)	2·92	–	3·00
5,5-Diethylbarbituric acid/imidazole (1:1) (Hsu & Craven, 1974*c*)	2·91	–	3·21

UM00013748
NOVARTIS EXHIBIT 1017
Novartis v. Regents, IPR2023-01346
Page 2494 of 4460

The observed range of N···O distances in all NH···O=C hydrogen bonds is considerably greater. The shortest reported distances which we could find were 2·55 Å in cysteylglycine sodium iodide (Dyer, 1951) and 2·62 Å in guanine hydrochloride monohydrate (Broomhead, 1951). Since these structure determinations were based only on zonal X-ray intensity data, a more reliable lower limit for N···O distances might be 2·67 Å which occurs in the urea/parabanic acid complex (Colman & Medlin, 1970; Table 6). At the other extreme, there are N···O distances in NH···O=C interactions which are doubtfully described as hydrogen bonds. In the 1:1 complex of barbital with 9-ethyladenine (Voet, 1972), there is an NH···O=C interaction in which the NH···O atoms are collinear, with an N···O distance of 3·39 Å [Table 3(*d*)]. However, the H···O distance (2·47 Å) is too long for hydrogen bonding according to Hamilton & Ibers (1968), who state that the H···O distance should be shorter than the van der Waals distance (2·6 Å) by at least 0·2 Å.

It is possible that additional N···O distances in $B_d\cdots B_a$ barbiturate hydrogen bonds will be found which will make their range conform more closely to the range of all N···O distances in NH···O=C hydrogen bonds. This would imply that there is little value in characterizing an N···O distance on the basis of the particular donor and acceptor groups which are involved. However, the available evidence is to the contrary. The five N···O distances in Table 5(*d*) for $B_d\cdots A_a$ hydrogen bonds are all between 2·75 and 2·82 Å which is at the short limit of the range for $B_d\cdots B_a$ hydrogen bonds. The 12 distances for $A_d\cdots B_a$ hydrogen bonds are between 2·95 and 3·39 Å which is at and beyond the long limit of the range for $B_d\cdots B_a$ hydrogen bonds. These data are consistent with the drug-active barbiturates being more effective as donors than as acceptors in NH···O=C hydrogen bonds.

The N···O distances for hydrogen bonds in which urea is both donor and acceptor have an average value of 2·98 Å and range between 2·84 and 3·13 Å (Table 6). In urea complexes, 21 hydrogen bonds have N···O distances for which urea is donor and other molecules are acceptor, but only eight of these involve a carbonyl oxygen acceptor atom. The latter have an average value of 3·07 Å and range from 2·91 to 3·24 Å. There are four NH···O=C hydrogen bonds in which urea is acceptor and all are short, ranging from 2·67 to 2·80 Å. The available data for the NH···O=C hydrogen bonding of urea are fewer than for the barbiturates, but they are suggestive of a trend which is complementary to that of the barbiturates, namely for urea to be more effective as an acceptor than as a donor.

Thus, while barbital and urea both have hydrogen-bonding donor and acceptor capability, their association in the 1:1 crystal complex may be considered to be essentially that of a hydrogen-bonding acid (barbital) with a hydrogen-bonding base (urea). The association of barbiturates with adenine derivatives in the complexes listed in Table 5(*d*) would appear to be of a similar nature, with barbital as the hydrogen-bonding acid and adenine as the hydrogen-bonding base. The strong hydrogen bonds in these complexes are of the type NH···N involving barbiturate as donor. The N···N distances in these and other NH···N barbiturate hydrogen bonds are discussed in our report of the crystal structure determinations of the 1:1 complexes of barbital with imidazole and with 2-aminopyridine (Hsu & Craven, 1974*c*,*d*).

This work was supported by the U. S. Public Health Service, National Institutes of Health, Grant No. NS-

Table 6. *Distances* N···O *in* NH···O *hydrogen bonds involving urea and the uronium ion*

Crystal structure	$(NH)_{urea}\cdots(O=C)_{urea}$	$(NH)_{urea}\cdots O_{other}$	$(NH)_{other}\cdots(O=C)_{urea}$
Urea (Pryor & Sanger, 1970)	2·98, 3·04 Å	–	–
Barbital/urea (1:1) (This paper)	–	2·95*, 3·16* Å	2·78, 2·80 Å
Parabanic acid/urea (1:1) (Colman & Medlin, 1970)	3·01	3·07*, 3·20*, 3·24*	2·67
5-Nitro-2-furaldehyde-oxime/urea (1:1) (Mathew & Palenik, 1972)	2·84	2·94, 3·07	–
L-Cysteine ethyl ester hydrochloride/urea (1:1) (Haas, 1965)	2·88	3·06*	2·70
Hydrogen peroxide/urea (1:1) (Lu, Hughes & Giguère, 1941)	2·94	–	–
2,6-Lutidine/urea (1:1) (Lee & Wallwork, 1965)	3·05	–	–
Estradiol/urea (1:1) (Duax, 1972)	2·85	3·03, 3·15, 3·04	–
Oxalic acid/urea (1:1) (Harkema, Bats, Weyenberg & Feil, 1972)	2·94	3·00*, 3·12, 2·91*, 2·94	–
Phosphoric acid/urea (1:1)† (Mootz & Albrand, 1972; Kostansek & Busing, 1972)	3·10, 3·13	2·98, 3·16	–
Uronium nitrate (Worsham & Busing, 1969)	–	2·98, 2·97, 2·90, 2·92	–
Range	2·84–3·13	2·90–3·24	2·67–2·80

* This hydrogen bond involves a carbonyl oxygen atom as acceptor.

† This crystalline compound is intermediate in character between an adduct and a salt, because of the very strong more or less centered O–H···O hydrogen bond between the two components.

UM00013749
NOVARTIS EXHIBIT 1017
Novartis v. Regents, IPR2023-01346
Page 2495 of 4460

02763. We thank Dr R. Shiono for the computer programs which we used.

References

BAUR, W. H. & KHAN, A. A. (1970). *Acta Cryst.* B26, 1584–1596.

BERKING, B. (1972). *Acta Cryst.* B28, 98–113.

BERKING, B. & CRAVEN, B. M. (1971). *Acta Cryst.* B27, 1107–1115.

BIDEAU, J. P. (1971). *C. R. Acad. Sci. Paris*, 272, 757–760.

BIDEAU, J. P. & ARTAUD, M. (1970). *C. R. Acad. Sci. Paris*, 271, 806–809.

BIDEAU, J. P., LEROY, F. & HOUSTY, J. (1969). *C. R. Acad. Sci. Paris*, 268, 1590–1592.

BIDEAU, J. P., LEROY, F. & HOUSTY, J. (1970). *C. R. Acad. Sci. Paris*, 271, 500–502.

BIDEAU, J. P., MARLY, L. & HOUSTY, J. (1969). *C. R. Acad. Sci. Paris*, 269, 549–551.

BRAVIC, G., HOUSTY, J. & BIDEAU, J. P. (1968). *C. R. Acad. Sci. Paris*, 266, 969–971.

BROOMHEAD, J. M. (1951). *Acta Cryst.* 4, 92–100.

CARON, A. & DONOHUE, J. (1964). *Acta Cryst.* 17, 544–546.

COLMAN, P. M. & MEDLIN, E. H. (1970). *Acta Cryst.* B26, 1547–1553.

CRAVEN, B. M. & CUSATIS, C. (1969). *Acta Cryst.* B25, 2291–2298.

CRAVEN, B. M., CUSATIS, C., GARTLAND, G. L. & VIZZINI, E. A. (1973). *J. Mol. Struct.* 16, 331–342.

CRAVEN, B. M. & GARTLAND, G. L. (1970). *J. Pharm. Sci.* 59, 1666–1670.

CRAVEN, B. M. & TAKEI, W. J. (1964). *Acta Cryst.* 17, 415–420.

CRAVEN, B. M. & VIZZINI, E. A. (1969). *Acta Cryst.* B25, 1993–2009.

CRAVEN, B. M. & VIZZINI, E. A. (1971). *Acta Cryst.* B27, 1917–1924.

CRAVEN, B. M., VIZZINI, E. A. & RODRIGUES, M. M. (1969). *Acta Cryst.* B25, 1978–1993.

CROMER, D. T. & WABER, J. T. (1965). *Acta Cryst.* 18, 104–109.

DUAX, W. L. (1972). *Acta Cryst.* B28, 1864–1871.

DYER, H. B. (1951). *Acta Cryst.* 4, 42–50.

GARTLAND, G. L. (1971). Ph. D. Dissertation, Univ. of Pittsburgh, Pittsburgh, Pa.

GARTLAND, G. L. & CRAVEN, B. M. (1971). *Acta Cryst.* B27, 1909–1916.

GATEHOUSE, B. M. & CRAVEN, B. M. (1971). *Acta Cryst.* B27, 1337–1344.

HAAS, D. J. (1965). *Acta Cryst.* 19, 860–861.

HAMILTON, W. C. & IBERS, J. A. (1968). *Hydrogen Bonding in Solids*. New York: Benjamin.

HARKEMA, S., BATS, J. W., WEYENBERG, A. M. & FEIL, D. (1972). *Acta Cryst.* B28, 1646–1648.

HSU, I-N. & CRAVEN, B. M. (1974*a*). *Acta Cryst.* B30, 974–979.

HSU, I-N. & CRAVEN, B. M. (1974*b*). *Acta Cryst.* B30, 843–846.

HSU, I-N. & CRAVEN, B. M. (1974*c*). *Acta Cryst.* B30, 988–993.

HSU, I-N. & CRAVEN, B. M. (1974*d*) *Acta Cryst.* B30, 994–997.

KIM, S. H. & RICH, A. (1968). *Proc. Natl. Acad. Sci. U.S.* 60, 402–408.

KIRYU, S. (1971). *J. Pharm. Sci.* 60, 699–703.

KOSTANSEK, E. C. & BUSING, W. R. (1972). *Acta Cryst.* B28, 2454–2459.

LEE, J. D. & WALLWORK, S. C. (1965). *Acta Cryst.* 19, 311–315.

LU, C. S., HUGHES, W. & GIGUÈRE, P. A. (1941). *J. Amer. Chem. Soc.* 63, 1507–1513.

MCCLURE, R. J. & CRAVEN, B. M. (1973). *Acta Cryst.* B29, 1860–1864.

MATHEW, M. & PALENIK, G. J. (1972). *J. Chem. Soc. Perkin II*, pp. 1033–1036.

MOOTZ, D. & ALBRAND, K.-R. (1972). *Acta Cryst.* B28, 2459–2463.

NAKAMOTO, K., MARGOSHES, M. & RUNDLE, R. E. (1955). *J. Amer. Chem. Soc.* 77, 6480–6486.

PRYOR, A. W. & SANGER, P. L. (1970). *Acta Cryst.* A26, 543–558.

SEKIGUCHI, K., HIMURO, I., HORIKOSHI, I., TSUKADA, T., OKAMOTO, T. & YOTSUYANAGI, T. (1969). *Chem. Pharm. Bull. (Japan)*, 17, 191–199.

SNYDER, R. L. & ROSENSTEIN, R. D. (1971). *Acta Cryst.* B27, 1969–1975.

STEWART, R. F., DAVIDSON, E. R. & SIMPSON, W. T. (1965). *J. Chem. Phys.* 42, 3175–3187.

VOET, D. (1972). *J. Amer. Chem. Soc.* 94, 8213–8222.

VOET, D. & RICH, A. (1970). In *Progress in Nucleic Acid Research and Molecular Biology*, Vol. 10, pp. 183–264. Edited by J. N. DAVIDSON and W. E. COHN. New York and London: Academic Press.

VOET, D. & RICH, A. (1972). *J. Amer. Chem. Soc.* 94, 5888–5891.

WILLIAMS, P. P. (1974). *Acta Cryst.* B30, 12–17.

WORSHAM, J. E. & BUSING, W. R. (1969). *Acta Cryst.* B25, 572–578.

WUNDERLICH, H. (1973). *Acta Cryst.* B29, 168–173.

UM00013750
NOVARTIS EXHIBIT 1017
Novartis v. Regents, IPR2023-01346
Page 2496 of 4460

This Page is Inserted by IFW Indexing and Scanning Operations and is not part of the Official Record

BEST AVAILABLE IMAGES

Defective images within this document are accurate representations of the original documents submitted by the applicant.

Defects in the images include but are not limited to the items checked:

- ☐ BLACK BORDERS
- ☐ IMAGE CUT OFF AT TOP, BOTTOM OR SIDES
- ☐ FADED TEXT OR DRAWING
- ☐ BLURRED OR ILLEGIBLE TEXT OR DRAWING
- ☐ SKEWED/SLANTED IMAGES
- ☐ COLOR OR BLACK AND WHITE PHOTOGRAPHS
- ☐ GRAY SCALE DOCUMENTS
- ☐ LINES OR MARKS ON ORIGINAL DOCUMENT
- ☐ REFERENCE(S) OR EXHIBIT(S) SUBMITTED ARE POOR QUALITY
- ☐ OTHER: _____

IMAGES ARE BEST AVAILABLE COPY.
As rescanning these documents will not correct the image problems checked, please do not report these problems to the IFW Image Problem Mailbox.

KAMAEV, F. G., BARAM, N. I., ISMAILOV, A. I., LEONTEV, V. B. & SADYKOV, S. A. (1979). *Izv. Akad. Nauk SSSR Ser. Khim.* pp. 1003–1010.

MAIN, P., FISKE, S. J., HULL, S. E., LESSINGER, L., GERMAIN, G., DECLERQ, J.-P. & WOOLFSON, M. M. (1980). *MULTAN80. A System of Computer Programs for the Automatic Solution of Crystal Structures from X-ray Diffraction Data.* Univs. of York, England, and Louvain, Belgium.

MOTHERWELL, W. D. S. & CLEGG, W. (1978). *PLUTO.* Program for plotting molecular and crystal structures. Univ. of Cambridge, England.

REYES, J., WYRICK, S. D., BORRIERO, L. & BENAS, D. J. (1986). *Biochem. Biophys. Acta*, **863**, 101–109.

SHELDRICK, G. M. (1976). *SHELX76.* Program for crystal structure determination. Univ. of Cambridge, England.

WEBER, E. & JOSEL, H.-P. (1983). *J. Inclusion Phenom.* **1**, 79–85.

Acta Cryst. (1991). C**47**, 577–580

Structure and Conformation of the 1:1 Molecular Complex Sulfaproxyline–Caffeine

BY M. GHOSH,* A. K. BASAK AND S. K. MAZUMDAR

Crystallography and Molecular Biology Division, Saha Institute of Nuclear Physics, Sector 1, Block AF, Bidhannagar, Calcutta 700 064, India

AND B. SHELDRICK

The Astbury Department of Biophysics, University of Leeds, Leeds LS2 9JT, England

(*Received* 22 *January* 1990; *accepted* 7 *June* 1990)

Abstract. *p*-Isopropoxy-*N*-sulfanilylbenzamide–3,7-dihydro-1,3,7-trimethyl-1*H*-purine-2,6-dione (1/1), $C_{16}H_{18}N_2O_4S.C_8H_{10}N_4O_2$, $M_r = 528{\cdot}58$, monoclinic, $P2_1/c$, $Z = 8$, $a = 12{\cdot}197$ (1), $b = 34{\cdot}109$ (5), $c = 12{\cdot}878$ (1) Å, $\beta = 108{\cdot}68$ (1)°, $V = 5075{\cdot}4$ (1·0) Å^3, $D_x = 1{\cdot}38$ g cm^{-3}, Cu $K\alpha$, $\lambda = 1{\cdot}5418$ Å, $\mu = 15{\cdot}32$ cm^{-1}, $F(000) = 2224$, $T = 293$ K, final $R = 0{\cdot}046$ for 5997 observed reflections with $F \geq 3\sigma(F)$. The asymmetric unit contains two sulfaproxyline and two caffeine molecules. In the crystal the flat caffeine molecule is packed parallel to another caffeine molecule. Hydrogen bonds, where present, are weak ($D\cdots A$ lengths > 3·0 Å), showing that the packing is dominated by the non-bonded interactions.

Introduction. Sulfonamides form molecular complexes with different small molecules. Trimethoprim–sulfamethoxazole (Nakai, Takasuka & Shiro, 1984), sulfathiazole–xanthine (Higuchi & Lach, 1954), sulfathiazole–theophylline (Shefter & Sackman, 1971) *etc.* are such molecular complexes. The molecular basis for complex formation in such a simple system helps in the understanding of the interaction of small molecules with a bioreceptor and of the resulting antibacterial activity.

Here crystallographic studies on such a sulfonamide complex (1:1 sulfaproxyline–caffeine) have been carried out to determine the nature of the interaction between the compounds, hydrogen bonding and change in structural features, if any, due to this complex formation. Sulfaproxyline is widely used in synergestic combination with sulfamerazine, as the metabolites are readily soluble in acid urine preventing the formation of crystalluria even at acidic pH. Caffeine, a xanthine derivative, stimulates the central nervous system, cardiac muscle, cortex and respiratory system.

Experimental. Needle-shaped light-yellowish crystals were obtained by slow evaporation of an acetone solution of a 1:1 mixture of sulfaproxyline and caffeine. Weissenberg photographs showed the crystals to be monoclinic and systematic absence conditions determined the space group as $P2_1/c$. The lattice parameters a, b, c and β were also found using oscillation as well as Weissenberg photographs.

A crystal of dimensions 0·26 × 0·08 × 0·05 mm was used for intensity data collection on an Enraf–Nonius CAD-4F diffractometer using Cu $K\alpha$ radiation. The cell parameters were determined by least-squares refinement of 48 reflections with $19 < \theta < 42°$. ω–2θ scans. The data were measured for values of 2θ up to 120° with $-13 \leq h \leq 13$, $0 \leq k \leq 38$ and $-14 \leq l \leq 14$. The reflection $\bar{3}57$ was measured at regular intervals as an intensity check with an average count of 449·5 and σ (calculated from distribution) = 7·2 (1·6%). The data were corrected for Lorentz and polarization factors but not for absorption. 11 447 values were recorded and merged using *SHELX76* (Sheldrick, 1976) to give 6454 unique reflections (merging $R = 0{\cdot}02$). The structure was solved by direct methods using *MULTAN78* (Main,

* To whom all correspondence should be addressed.

0108-2701/91/030577-04$03.00

© 1991 International Union of Crystallography

NOVARTIS EXHIBIT 1017
Novartis v. Regents, IPR2023-01346
Page 2498 of 4460

Hull, Lessinger, Germain, Declercq & Woolfson, 1978) and refined isotropically by full-matrix least squares based on F using *SHELX*76 with 5997 observed [$F \geq 3\sigma(F)$] reflections. Owing to the limitation of the total number of parameters in *SHELX*76 each pair of molecules forming half of the asymmetric unit was refined anisotropically in turn. H atoms were located from a difference Fourier synthesis and put into the atom list with the equivalent isotropic thermal parameter of the attached atom.

Further refinement gave $R = 0{\cdot}046$, $wR = 0{\cdot}051$ with $w = 1{\cdot}7237/(\sigma^2 F_o + 0{\cdot}001297|F_o|^2)$. In the final refinement cycle, the average shift to e.s.d. ratio was 0·1; maximum and minimum electron densities in the final ΔF map were 0·295 and $-0{\cdot}290$ e Å^{-3}, respectively. Scattering factors were taken from *International Tables for X-ray Crystallography* (1974, Vol. IV).

Discussion. The final atomic parameters are listed in Table 1* and bond distances, angles and selected torsion angles are given in Table 2. Two complex molecules are present in each asymmetric unit. Fig. 1 shows the molecular diagram with the atomic numbering scheme.

Sulfaproxyline possesses various conformations about the C(1)—S, S—N(1) and N(1)—C(7) bonds. The torsion angles $|\varepsilon_1|$ [C(X)—C(1)—S—N(1), where $X = 2$ or 6] and $|\varepsilon_2|$ [C(1)—S—N(1)—C(7)], defining the conformation of the sulfonamide group, lie in the range 70–120 and 60–90°, respectively, found in related molecules (Kálmán, Czugler & Argay, 1981). But the values are different in the free sulfaproxyline molecule (Basak, Mazumdar & Chaudhuri, 1984) where $\varepsilon_1 = -84{\cdot}1$ (3), 103·8 (3)° and $\varepsilon_2 = 75{\cdot}6$ (2)°. The torsion angles S—N(1)—C(7)—C(8) for molecules A and B of present structure are greater than the value of 161·4 (2)° in the free molecule. The conformations of sulfaproxyline in the free molecule and in the present structure about the S—N(1) bond are shown in Fig. 2, in which Newman projections along the same bond are compared.

The two planar rings are almost perpendicular to each other, the dihedral angle between them being 82·9 (1) and 82·0 (1)° for molecules A and B, respectively. However, this dihedral angle in the free molecule is 51·9 (1)°, which is significantly smaller than those in the present structure and the values observed in most of the sulfonamides.

* Lists of structure factors, anisotropic thermal parameters, H-atom parameters, bond lengths and angles involving H atoms, and least-squares-planes data have been deposited with the British Library Document Supply Centre as Supplementary Publication No. SUP 53270 (42 pp.). Copies may be obtained through The Technical Editor, International Union of Crystallography, 5 Abbey Square, Chester CH1 2HU, England.

Table 1. *Fractional atomic coordinates and U_{eq} values (Å^2) for non-H atoms with e.s.d.'s in parentheses*

$$U_{eq} = \tfrac{1}{3}\Sigma_i\Sigma_j a_i^* a_j^* \mathbf{a}_i.\mathbf{a}_j.$$

	x	y	z	U_{eq}
Molecule *A*				
S	0·2404 (1)	0·3129 (0)	0·5784 (1)	0·0412 (2)
N(1)	0·3147 (2)	0·3089 (1)	0·7116 (2)	0·0417 (8)
N(2)	0·0056 (2)	0·3557 (1)	0·2801 (2)	0·0522 (9)
N(3)	0·1536 (2)	0·3355 (1)	0·2095 (2)	0·0635 (10)
N(4)	0·3844 (2)	0·4633 (1)	0·4378 (2)	0·0603 (10)
N(5)	0·1213 (2)	0·4430 (1)	0·2170 (2)	0·0636 (10)
N(6)	−0·0172 (2)	0·4256 (1)	0·2916 (2)	0·0500 (9)
O(1)	0·2729 (2)	0·2813 (1)	0·5223 (1)	0·0534 (8)
O(2)	0·1228 (1)	0·3159 (1)	0·5773 (2)	0·0513 (8)
O(3)	0·4921 (1)	0·3046 (1)	0·6896 (1)	0·0500 (8)
O(4)	0·6527 (2)	0·2939 (1)	1·2074 (1)	0·0549 (7)
O(5)	0·2614 (2)	0·3800 (1)	0·1491 (2)	0·0881 (13)
O(6)	0·0393 (2)	0·2910 (1)	0·2599 (2)	0·0878 (12)
C(1)	0·2812 (2)	0·3572 (1)	0·5342 (2)	0·0401 (9)
C(2)	0·2210 (2)	0·3915 (1)	0·5375 (2)	0·0430 (9)
C(3)	0·2541 (2)	0·4265 (1)	0·5056 (2)	0·0470 (11)
C(4)	0·3500 (2)	0·4286 (1)	0·4687 (2)	0·0442 (10)
C(5)	0·4095 (2)	0·3941 (1)	0·4638 (2)	0·0505 (11)
C(6)	0·3760 (2)	0·3589 (1)	0·4964 (2)	0·0463 (10)
C(7)	0·4336 (2)	0·3048 (1)	0·7512 (2)	0·0396 (9)
C(8)	0·4866 (2)	0·3013 (1)	0·8719 (2)	0·0399 (9)
C(9)	0·4295 (2)	0·2846 (1)	0·9388 (2)	0·0489 (10)
C(10)	0·4818 (2)	0·2817 (1)	1·0501 (2)	0·0525 (11)
C(11)	0·5929 (2)	0·2961 (1)	1·0975 (2)	0·0443 (9)
C(12)	0·6528 (2)	0·3117 (1)	1·0319 (2)	0·0490 (11)
C(13)	0·6000 (2)	0·3140 (1)	0·9204 (2)	0·0457 (10)
C(14)	0·5889 (2)	0·2978 (1)	1·2842 (2)	0·0526 (11)
C(15)	0·6716 (3)	0·2872 (1)	1·3939 (3)	0·0786 (15)
C(16)	0·5437 (4)	0·3389 (1)	1·2790 (4)	0·1052 (19)
C(17)	0·0646 (3)	0·3251 (1)	0·2505 (2)	0·0629 (14)
C(18)	0·1848 (3)	0·3739 (1)	0·1888 (2)	0·0597 (13)
C(19)	0·1172 (2)	0·4026 (1)	0·2196 (2)	0·0487 (10)
C(20)	0·0330 (2)	0·3939 (1)	0·2653 (2)	0·0460 (10)
C(21)	0·0392 (3)	0·4555 (1)	0·2613 (3)	0·0658 (14)
C(22)	0·2205 (3)	0·3028 (1)	0·1863 (4)	0·0957 (19)
C(23)	−0·0907 (3)	0·3463 (1)	0·3191 (3)	0·0735 (14)
C(24)	0·1941 (3)	0·4677 (1)	0·1750 (3)	0·0852 (17)
Molecule *B*				
S	0·8758 (1)	0·0558 (0)	1·0618 (1)	0·0459 (3)
N(1)	0·8222 (2)	0·0538 (1)	0·9261 (2)	0·0460 (8)
N(2)	1·1177 (2)	0·1081 (1)	1·3663 (2)	0·0435 (8)
N(3)	0·9633 (2)	0·0973 (1)	1·4358 (2)	0·0490 (9)
N(4)	0·7476 (2)	0·2096 (1)	1·1947 (2)	0·0693 (11)
N(5)	1·0295 (2)	0·2019 (1)	1·4166 (2)	0·0527 (9)
N(6)	1·1630 (2)	0·1765 (1)	1·3485 (2)	0·0496 (9)
O(1)	0·8191 (2)	0·0258 (1)	1·1029 (2)	0·0628 (8)
O(2)	0·9983 (2)	0·0540 (1)	1·0836 (2)	0·0592 (8)
O(3)	0·6320 (2)	0·0541 (1)	0·9126 (2)	0·0607 (7)
O(4)	0·6160 (2)	0·0301 (1)	0·4152 (1)	0·0512 (7)
O(5)	0·8714 (2)	0·1477 (1)	1·4917 (2)	0·0777 (10)
O(6)	1·0559 (2)	0·0462 (1)	1·3843 (2)	0·0663 (9)
C(1)	0·8384 (2)	0·1013 (1)	1·1016 (2)	0·0407 (10)
C(2)	0·7351 (2)	0·1060 (1)	1·1239 (2)	0·0515 (10)
C(3)	0·7058 (2)	0·1417 (1)	1·1543 (2)	0·0541 (11)
C(4)	0·7780 (2)	0·1740 (1)	1·1635 (2)	0·0475 (9)
C(5)	0·8821 (2)	0·1690 (1)	1·1416 (2)	0·0493 (11)
C(6)	0·9113 (2)	0·1331 (1)	1·1108 (2)	0·0444 (10)
C(7)	0·7059 (2)	0·0511 (1)	0·8679 (2)	0·0465 (9)
C(8)	0·6792 (2)	0·0444 (1)	0·7489 (2)	0·0446 (10)
C(9)	0·5778 (2)	0·0593 (1)	0·6761 (2)	0·0511 (01)
C(10)	0·5519 (2)	0·0550 (1)	0·5645 (2)	0·0507 (10)
C(11)	0·6279 (2)	0·0351 (1)	0·5231 (2)	0·0435 (9)
C(12)	0·7263 (2)	0·0176 (1)	0·5953 (2)	0·0433 (10)
C(13)	0·7517 (2)	0·0227 (1)	0·7063 (2)	0·0434 (9)
C(14)	0·5185 (2)	0·0475 (1)	0·3314 (2)	0·0505 (10)
C(15)	0·5302 (3)	0·0911 (1)	0·3272 (3)	0·0784 (16)
C(16)	0·5212 (3)	0·0278 (1)	0·2268 (2)	0·0670 (13)
C(17)	1·0462 (2)	0·0817 (1)	1·3946 (2)	0·0481 (11)
C(18)	0·9453 (2)	0·1369 (1)	1·4525 (2)	0·0489 (10)
C(19)	1·0220 (2)	0·1616 (1)	1·4195 (2)	0·0421 (10)
C(20)	1·1037 (2)	0·1476 (1)	1·3775 (2)	0·0400 (9)
C(21)	1·1144 (3)	0·2091 (1)	1·3733 (3)	0·0583 (12)
C(22)	0·8868 (3)	0·0688 (1)	1·4646 (3)	0·0723 (16)
C(23)	1·2113 (3)	0·0929 (1)	1·3301 (3)	0·0698 (15)
C(24)	0·9623 (3)	0·2314 (1)	1·4534 (3)	0·0703 (14)

UM00013753
NOVARTIS EXHIBIT 1017
Novartis v. Regents, IPR2023-01346
Page 2499 of 4460

Table 2. *Bond distances* (Å), *angles* (°) *and selected torsion angles* (°)

	Molecule *A*	Molecule *B*
Distances in sulfaproxyline		
S—N(1)	1·669 (2)	1·660 (3)
S—O(1)	1·423 (3)	1·428 (3)
N(1)—C(7)	1·382 (3)	1·379 (3)
C(7)—O(3)	1·225 (3)	1·219 (4)
C(14)—O(4)	1·447 (4)	1·452 (3)
C(14)—C(16)	1·500 (5)	1·515 (4)
C(1)—C(2)	1·389 (4)	1·388 (4)
C(3)—C(4)	1·398 (4)	1·392 (4)
C(5)—C(6)	1·376 (5)	1·369 (5)
C(8)—C(9)	1·391 (4)	1·387 (3)
C(10)—C(11)	1·386 (3)	1·386 (4)
C(12)—C(13)	1·375 (3)	1·373 (4)
S—C(1)	1·742 (3)	1·740 (3)
S—O(2)	1·433 (2)	1·430 (3)
N(4)—C(4)	1·357 (5)	1·367 (5)
C(11)—O(4)	1·371 (3)	1·361 (3)
C(14)—C(15)	1·494 (4)	1·497 (5)
C(7)—C(8)	1·485 (3)	1·479 (4)
C(2)—C(3)	1·365 (5)	1·361 (5)
C(4)—C(5)	1·394 (4)	1·396 (4)
C(6)—C(1)	1·392 (4)	1·383 (4)
C(9)—C(10)	1·373 (3)	1·377 (4)
C(11)—C(12)	1·388 (4)	1·395 (3)
C(13)—C(8)	1·392 (3)	1·393 (4)
Distances in caffeine		
N(3)—C(17)	1·396 (5)	1·389 (4)
N(3)—C(22)	1·468 (5)	1·475 (5)
N(2)—C(20)	1·373 (5)	1·371 (5)
N(5)—C(19)	1·380 (5)	1·379 (5)
N(5)—C(24)	1·449 (5)	1·469 (5)
N(6)—C(21)	1·356 (5)	1·346 (5)
C(17)—O(6)	1·219 (5)	1·228 (5)
N(3)—C(18)	1·413 (5)	1·396 (5)
N(2)—C(17)	1·389 (5)	1·381 (4)
N(2)—C(23)	1·453 (5)	1·460 (5)
N(5)—C(21)	1·370 (5)	1·347 (5)
N(6)—C(20)	1·338 (5)	1·344 (4)
C(18)—O(5)	1·218 (5)	1·222 (4)
C(19)—C(20)	1·370 (4)	1·363 (4)
C(18)—C(19)	1·416 (5)	1·421 (4)
Bond angles in sulfaproxyline		
O(1)—S—C(1)	109·6 (1)	109·0 (2)
O(1)—S—O(2)	119·3 (1)	119·7 (2)
O(1)—S—N(1)	108·2 (2)	106·6 (2)
S—N(1)—C(7)	123·2 (2)	124·4 (2)
O(3)—C(7)—C(8)	121·9 (2)	123·5 (3)
N(4)—C(4)—C(3)	121·0 (3)	120·3 (3)
C(2)—C(1)—C(6)	118·8 (3)	119·5 (3)
C(2)—C(3)—C(4)	120·5 (3)	121·0 (3)
C(4)—C(5)—C(6)	120·8 (3)	120·4 (3)
S—C(1)—C(2)	120·7 (2)	120·3 (3)
C(7)—C(8)—C(9)	123·0 (2)	119·8 (2)
C(9)—C(8)—C(13)	118·2 (2)	118·0 (2)
C(9)—C(10)—C(11)	119·7 (2)	119·7 (2)
C(11)—C(12)—C(13)	119·7 (3)	119·9 (3)
O(4)—C(11)—C(10)	123·9 (2)	126·0 (2)
O(4)—C(14)—C(15)	106·0 (2)	111·6 (2)
C(11)—O(4)—C(14)	118·4 (2)	120·1 (2)
O(2)—S—C(1)	108·9 (2)	109·6 (2)
C(1)—S—N(1)	106·8 (2)	107·1 (2)
O(2)—S—N(1)	103·2 (1)	103·8 (2)
O(3)—C(7)—N(1)	121·4 (2)	121·7 (2)
N(1)—C(7)—C(8)	116·6 (2)	114·9 (2)
N(4)—C(4)—C(5)	120·5 (3)	121·2 (3)
C(1)—C(2)—C(3)	121·1 (3)	120·1 (3)
C(3)—C(4)—C(5)	118·4 (3)	118·5 (3)
C(5)—C(6)—C(1)	120·3 (3)	120·4 (3)
S—C(1)—C(6)	120·4 (3)	120·2 (2)
C(7)—C(8)—C(13)	118·8 (2)	122·2 (2)
C(8)—C(9)—C(10)	121·2 (3)	121·5 (3)
C(10)—C(11)—C(12)	119·9 (2)	119·5 (2)
C(8)—C(13)—C(12)	121·1 (3)	121·1 (3)
O(4)—C(11)—C(12)	116·1 (2)	114·5 (2)
O(4)—C(14)—C(16)	109·0 (2)	103·5 (2)
O(15)—C(14)—C(16)	113·3 (3)	112·3 (3)
Bond angles in caffeine		
C(17)—N(3)—C(18)	126·6 (3)	126·8 (3)
C(18)—N(3)—C(22)	117·7 (3)	117·1 (3)
C(17)—N(2)—C(23)	118·4 (3)	118·5 (3)
C(19)—N(5)—C(21)	105·3 (3)	105·0 (3)

Table 2 (*cont.*)

	Molecule *A*	Molecule *B*
C(21)—N(5)—C(24)	126·3 (3)	126·2 (3)
N(5)—C(21)—N(6)	113·1 (3)	113·8 (3)
O(6)—C(17)—N(2)	121·3 (3)	121·6 (3)
O(5)—C(18)—C(19)	126·4 (3)	126·0 (3)
N(6)—C(20)—C(19)	113·6 (3)	112·3 (3)
C(18)—C(19)—C(20)	123·7 (3)	123·1 (3)
N(2)—C(20)—N(6)	125·4 (3)	126·5 (3)
C(20)—C(19)—N(5)	105·3 (3)	106·0 (3)
C(17)—N(3)—C(22)	115·7 (3)	116·1 (3)
C(17)—N(2)—C(20)	120·3 (3)	120·1 (3)
C(20)—N(2)—C(23)	121·1 (3)	121·3 (3)
C(19)—N(5)—C(24)	128·4 (3)	128·7 (3)
C(20)—N(6)—C(21)	102·7 (3)	102·9 (3)
O(6)—C(17)—N(3)	122·1 (3)	121·7 (3)
O(5)—C(18)—N(3)	121·8 (3)	121·9 (3)
N(2)—C(17)—N(3)	116·5 (3)	116·7 (3)
N(3)—C(18)—C(19)	111·8 (3)	112·1 (3)
C(19)—C(20)—N(2)	120·9 (3)	121·1 (3)
C(18)—C(19)—N(5)	130·9 (3)	130·9 (3)
Torsion angles in sulfaproxyline		
C(2)—C(1)—S—N(1)	−90·6 (3)	89·7 (3)
C(2)—C(1)—S—O(1)	152·5 (2)	−25·3 (3)
C(2)—C(1)—S—O(2)	20·2 (3)	−158·2 (2)
C(1)—S—N(1)—C(7)	−66·0 (3)	−70·1 (3)
O(2)—S—N(1)—C(7)	179·2 (3)	173·8 (3)
S—N(1)—C(7)—O(3)	1·4 (4)	7·8 (5)
C(6)—C(1)—S—N(1)	88·5 (3)	−90·0 (3)
C(6)—C(1)—S—O(1)	−28·5 (3)	154·9 (3)
C(6)—C(1)—S—O(2)	−160·7 (2)	22·1 (3)
O(1)—S—N(1)—C(7)	51·9 (3)	46·5 (3)
S—N(1)—C(7)—C(8)	−179·5 (2)	−172·2 (2)

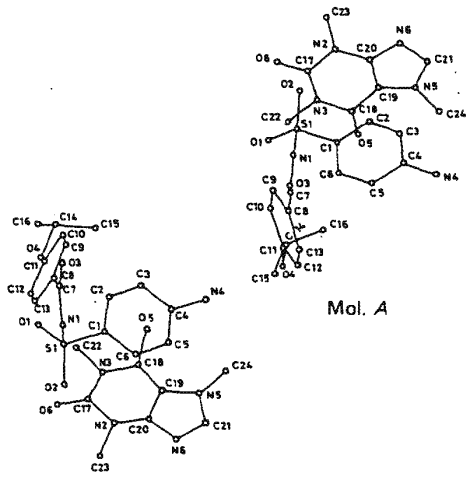


Fig. 1. Molecular diagram.

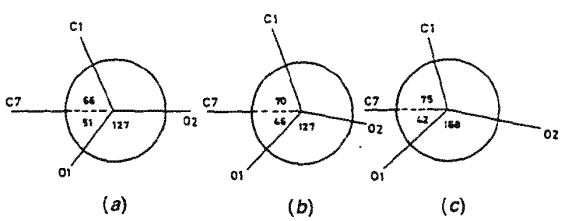


Fig. 2. Newman projection showing characteristic features of sulfaproxyline along the S—N(1) bond. (*a*) Molecule *A* and (*b*) molecule *B* in the present structure. (*c*) Free molecule.

UM00013754
NOVARTIS EXHIBIT 1017
Novartis v. Regents, IPR2023-01346
Page 2500 of 4460

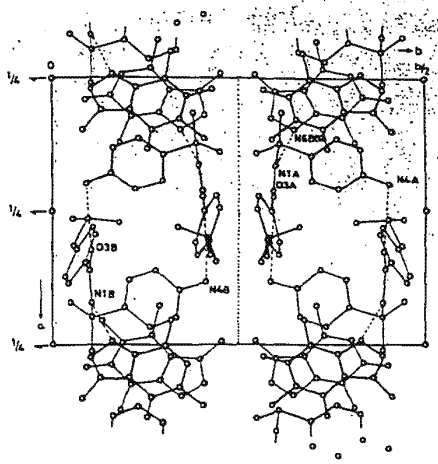


Fig. 3. Molecular packing diagram viewed along the *c* axis.

The pyrimidine and imidazole rings of the caffeine molecule are planar and the dihedral angle between them is 1·6 (1) and 2·6 (1)° for molecules *A* and *B*, respectively; the dihedral angle between them is 67·0 (2)° in the free molecule (Sutor, 1958).

Intermolecular bonds and molecular packing. Molecular packing in the crystal is shown in Fig. 3. Three hydrogens are available for hydrogen bonding in each molecule, two from the aryl amino nitrogen and one from the sulfonamido nitrogen. But H(42)*A* and H(41)*B* do not participate in hydrogen bonding.

Table 3. *Hydrogen-bond geometry* (Å, °)

D—H···*A*	*D*—H	*D*···*A*	H···*A*	*D*—H···*A*
N(4)*B*—H(42)*B*···O(3^{i})*A*	0·79 (3)	3·134 (3)	2·38 (3)	160·7 (2·6)
N(4)*A*—H(41)*A*···O(3^{ii})*B*	0·79 (3)	3·195 (4)	2·45 (3)	159·3 (2·6)
N(1)*B*—H(1)*B*···N(6^{iii})*A*	0·80 (3)	3·083 (3)	2·29 (3)	171·4 (2·3)
N(1)*A*—H(1)*A*···N(6^{iv})*B*	0·81 (3)	2·978 (4)	2·17 (3)	172·0 (2·1)

Symmetry code: (i) $x, -y+\frac{1}{2}, z+\frac{1}{2}$; (ii) $x, -y+\frac{1}{2}, z-\frac{1}{2}$; (iii) x, y, z; (iv) $x-1, -y+\frac{1}{2}, z-\frac{1}{2}$.

The hydrogen-bonding geometry (Table 3) shows weak hydrogen bonds having *D*···*A* lengths > 3·0 Å. The predominant intermolecular forces responsible for complex formation are therefore non-bonded interactions. The flat caffeine molecules are packed parallel to each other.

References

BASAK, A. K., MAZUMDAR, S. K. & CHAUDHURI, S. (1984). *Acta Cryst.* C**40**, 419–422.

HIGUCHI, T. & LACH, J. L. (1954). *J. Am. Pharm. Assoc. Sci. Ed.* **43**, 349–354.

KÁLMÁN, A., CZUGLER, M. & ARGAY, G. (1981). *Acta Cryst.* B37, 868–877.

MAIN, P., HULL, S. E., LESSINGER, L., GERMAIN, G., DECLERCQ, J.-P. & WOOLFSON, M. M. (1978). *MULTAN*78. *A System of Computer Programs for the Automatic Solution of Crystal Structures from X-ray Diffraction Data.* Univs. of York, England, and Louvain, Belgium.

NAKAI, H., TAKASUKA, M. & SHIRO, M. (1984). *J. Chem. Soc. Perkin Trans.* 2, pp. 1459–1464.

SHEFTER, E. & SACKMAN, P. (1971). *J. Pharm. Sci.* **60**, 282–286.

SHELDRICK, G. M. (1976). *SHELX*76. Program for crystal structure determination. Univ. of Cambridge, England.

SUTOR, D. J. (1958). *Acta Cryst.* **11**, 453–458.

Acta Cryst. (1991). C**47**, 580–584

Structure of an Adenine Tetrafluoroborate Salt

BY AIDEEN C. M. YOUNG AND JOHN C. DEWAN*

Department of Chemistry, New York University, New York, NY 10003, *USA*

AND ANTHONY J. EDWARDS

*Department of Chemistry, University of Birmingham, Edgbaston, Birmingham B*15 2*TT, England*

(*Received* 26 *January* 1990; *accepted* 2 *May* 1990)

Abstract. Adenine–adeninium tetrafluoroborate–water (1/1/2), $C_5H_5N_5.C_5H_6N_5^+.BF_4^-.2H_2O$, M_r = 394·10, monoclinic, $P2_1/m$, a = 5·358 (1), b = 19·468 (7), c = 7·905 (2) Å, β = 104·75 (2)°, V = 797·4 (7) Å^3, Z = 2, D_x = 1·641 g cm^{-3}, λ(Mo $K\alpha$) = 0·71069 Å, μ = 1·42 cm^{-1}, $F(000)$ = 404, T = 298 K. Final R = 0·062 for 1597 unique observed reflections with $I_o > 2\sigma(I_o)$. After consideration of various factors the structure was assigned as adenine and adeninium moieties in a 1:1 ratio, disordered over the one site. The BF_4^- anion and the two water molecules of crystallization lie on mirror planes. H atoms on C(2), N(6), C(8) and N(9) of adenine were located in difference-Fourier maps and were refined, but those

* Author to whom correspondence should be addressed.

0108-2701/91/030580-05$03.00

© 1991 International Union of Crystallography

UM00013755

NOVARTIS EXHIBIT 1017
Novartis v. Regents, IPR2023-01346
Page 2501 of 4460

This Page is Inserted by IFW Indexing and Scanning Operations and is not part of the Official Record

BEST AVAILABLE IMAGES

Defective images within this document are accurate representations of the original documents submitted by the applicant.

Defects in the images include but are not limited to the items checked:

- ☐ BLACK BORDERS
- ☐ IMAGE CUT OFF AT TOP, BOTTOM OR SIDES
- ☐ FADED TEXT OR DRAWING
- ☐ BLURRED OR ILLEGIBLE TEXT OR DRAWING
- ☐ SKEWED/SLANTED IMAGES
- ☐ COLOR OR BLACK AND WHITE PHOTOGRAPHS
- ☐ GRAY SCALE DOCUMENTS
- ☐ LINES OR MARKS ON ORIGINAL DOCUMENT
- ☐ REFERENCE(S) OR EXHIBIT(S) SUBMITTED ARE POOR QUALITY
- ☐ OTHER: _____

IMAGES ARE BEST AVAILABLE COPY.
As rescanning these documents will not correct the image problems checked, please do not report these problems to the IFW Image Problem Mailbox.

(1980)

THE CRYSTAL STRUCTURE OF A SULFAMETHOXAZOLE-TRIMETHOPRIM 1:1 MOLECULAR COMPOUND (*)

G. GIUSEPPETTI - C. TADINI

CENTRO DI CRISTALLOGRAFIA STRUTTURALE - CNR
ISTITUTO DI MINERALOGIA - UNIVERSITÀ DI PAVIA (ITALY)

G.P. BETTINETTI - F. GIORDANO - A. LA MANNA

DIPARTIMENTO DI CHIMICA FARMACEUTICA - UNIVERSITÀ DI PAVIA (ITALY)

SUMMARY. — *The crystal structure of a sulfamethoxazole (SMZ)-trimethoprim (TMP) 1:1 molecular compound (TSC) was determined from three-dimensional X-ray diffraction data. In TSC the association between SMZ and TMP molecules is achieved through two N.....N hydrogen bonds. The packing of TSC molecules in the crystal is stabilized mainly by a system of N.....O hydrogen bridges.*

RIASSUNTO. — *È stata determinata con l'analisi diffrattometrica a raggi X la struttura cristallina di un composto di associazione molecolare 1:1 (TSC) tra sulfametossazolo (SMZ) e trimethoprim (TMP). Nel TSC l'associazione tra le molecole di SMZ e TMP avviene attraverso due legami a idrogeno di tipo N.....N. L'impaccamento delle molecole di complesso nel reticolo cristallino è dovuto principalmente a ponti d'idrogeno di tipo N.....O.*

In a previous paper the physico-chemical properties of a sulfamethoxazole-trimethoprim 1:1 molecular compound (TSC) were investigated and the possible nature of bonding between components was briefly discussed on the basis of I.R. spectra (1).

The present work deals with crystal and molecular structure of the title complex by the X-ray diffraction method.

(*) This work has been partially supported by CNR.

UM00013757
NOVARTIS EXHIBIT 1017
Novartis v. Regents, IPR2023-01346
Page 2503 of 4460

Experimental

Transparent single crystals of TSC were obtained by sublimation (0.1 mm, 170-75°) of fragile, needle-shaped crystals prepared by recrystallization of equimolecular amounts of components (m.p. 178-79°). The identity of the crystals was confirmed by I.R. spectrum and X-ray diffraction pattern.

Single crystal data, CuK_α, $\lambda = 1.5418$ Å, are: sulfamethoxazole (3-sulfanilamido-5-methylisoxazole, SMZ) - trimethoprim [2,4-diamino-5-(3,4,5-trimethoxybenzyl)pyrimidine, TMP] 1 : 1 molecular compound, $C_{10}H_{11}N_3O_3S \cdot C_{14}H_{18}N_4O_3$ (TSC); system orthorhombic, space group *Pbca*, $a = 12.055(0)$ Å, $b = 24.476(1)$ Å, $c = 17.423(1)$ Å, $V = 5141$ Å^3, $Z = 8$, $D_c = 1.406$ g cm^{-3}, $D_{m\ (\text{Hellium pycnometer})} = 1.40$ g cm^{-3}.

Intensity data, structure determination and refinement

The intensities were collected on a Philips four circle computer controlled diffractometer PW 1100, by using CuK_α radiation monochromatized with a graphite chystal and $\vartheta - 2\vartheta$ scan mode, from a 0.4 x 0.2 x 0.1 mm specimen. The intensities of independent reflections were inspected ($\vartheta_{max} = 60°$): reflections with $I < 3\sigma(I)$ were considered as unobserved. No absorption correction was applied.

The crystal structure was solved by direct methods using the MULTAN program (2) and refined by full matrix least-squares techniques (3) with anisotropic thermal parameters for the non-hydrogen atoms.

All hydrogen atoms were localized geometrically and checked on a difference Fourier synthesis. Scattering factors are from H a n s o n *et al.* (4).

Out of a total of 2072 independent reflections collected, 1464 were used in the present work. Final conventional R factor is 0.054.

The structural parameters of TSC are reported in the following Tables and Figures.

Comments

In the SMZ molecule the intramolecular bond lengths and angles agree well with their equivalents in other compounds concerning both sulfanilamide (5-8) and isoxazole (9) portions. The benzene and isoxazole rings are essentially planar and make an angle with each other of 61.4°.

(one hydrogen atom, H1(N1), is displaced by —0.750 Å from the phenyl ring plane) as observed in β-sulfanilamide (10). The hydrogen bonding ring plane] as observed in β-sulfanilamide (10). The hydrogen bonding about this functional group (see later) is no doubt responsible to a great extent for the distortion from trigonal symmetry.

The stereochemistry about the sulphur atom is a slightly distorted tetrahedron and the deviation of the angle O(1)-S-O(2) [116.3(2)°] from the ideal tetrahedral conformation is expectedly large (10). The two

UM00013758
NOVARTIS EXHIBIT 1017
Novartis v. Regents, IPR2023-01346
Page 2504 of 4460

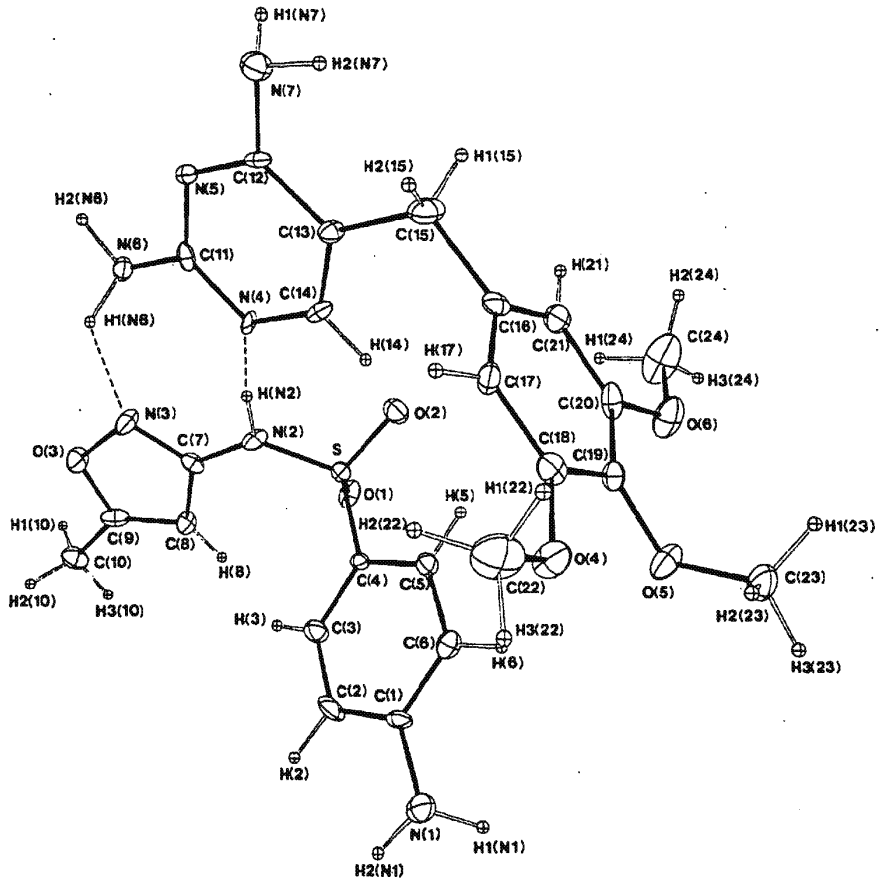


Fig. 1

A computer generated drawing of TSC showing the molecular conformation and the ellipsoids of thermal vibration. The ellipsoid surfaces are drawn at the 25% probability level. The hydrogen bondings between SMZ and TMP are shown by broken lines.

S-O bonds [1.459(4) and 1.448(4) Å] differ by 0.011 Å: this may be related to the different hydrogen bond characteristics of each oxygen atom, O(1) having two intermolecular links while O(2) has only one (see later).

The amido tautomer (hydrogen atom linked to N(2)) seems the stable form in the solid state but the C(7)-N(2) bond distance [1.367(7) Å] is shorter respect to other amido tautomers (1.390-1.400 Å) (11, 12).

Comparable N(sulfonamide)-C(heterocyclic ring) bond distances [1.36(2) and 1.37(2) Å] were found for two polymorphs of silver

UM00013759
NOVARTIS EXHIBIT 1017
Novartis v. Regents, IPR2023-01346
Page 2505 of 4460

TABLE I

Final atomic coordinates and thermal parameters (*) (x 10^4) for non-hydrogen atoms.

atom	x/a	y/b	z/c	b_{11}	b_{22}	b_{33}	b_{12}	b_{13}	b_{23}
				Sulfamethoxazole					
S	6832(1)	3788(1)	4490(1)	32(2)	8(0)	14(1)	—1(1)	0(1)	0(1)
O(1)	6699(3)	3938(2)	3685(2)	42(4)	17(1)	16(2)	8(2)	—3(2)	—2(1)
O(2)	6071(3)	3380(2)	4783(2)	46(4)	11(1)	28(2)	—5(2)	0(2)	—1(1)
O(3)	10723(3)	3707(2)	3964(2)	34(4)	14(1)	31(2)	1(2)	13(3)	7(1)
N(1)	5853(4)	5788(2)	6309(3)	45(6)	12(1)	30(3)	4(2)	—12(3)	—4(2)
N(2)	8050(4)	3575(2)	4663(3)	53(6)	9(1)	17(2)	6(2)	—4(3)	7(1)
N(3)	9893(4)	3452(2)	4420(3)	42(5)	13(2)	27(3)	10(2)	2(4)	6(2)
C(1)	6085(5)	5322(2)	5872(4)	42(7)	5(2)	21(3)	—1(3)	—13(4)	—3(2)
C(2)	6948(5)	5316(2)	5334(4)	52(7)	9(2)	33(4)	—13(3)	6(4)	2(2)
C(3)	7170(5)	4853(2)	4920(4)	47(7)	10(2)	30(4)	—5(3)	11(4)	—7(2)
C(4)	6567(5)	4386(2)	5046(3)	28(6)	5(1)	21(3)	0(3)	—10(4)	—1(2)
C(5)	5722(5)	4384(2)	5586(4)	32(6)	8(2)	20(3)	—1(3)	—1(4)	2(2)
C(6)	5496(5)	4854(3)	5997(3)	40(7)	12(2)	15(3)	3(3)	5(4)	—2(2)
C(7)	8978(5)	3730(2)	4268(3)	44(7)	8(2)	13(3)	—6(3)	4(4)	0(2)
C(8)	9160(5)	4157(2)	3714(4)	34(7)	12(2)	17(3)	2(3)	7(4)	2(2)
C(9)	10255(6)	4126(2)	3555(4)	76(8)	7(2)	12(3)	1(3)	5(4)	—2(2)
C(10)	11006(5)	4440(2)	3065(4)	66(7)	11(2)	26(4)	—7(3)	10(4)	2(2)

UM00013760

NOVARTIS EXHIBIT 1017
Novartis v. Regents, IPR2023-01346
Page 2506 of 4460

(follows Table I)

atom	x/a	y/b	z/c	b_{11}	b_{22}	b_{33}	b_{12}	b_{13}	b_{23}
				Trimethoprim					
O(4)	4721(3)	4261(2)	8228(3)	55(5)	14(1)	29(2)	6(2)	—15(3)	—6(1)
O(5)	3183(3)	4309(2)	7124(2)	55(5)	16(1)	29(2)	12(2)	11(3)	—1(1)
O(6)	2827(3)	3471(2)	6197(2)	54(5)	24(1)	28(2)	8(2)	—2(3)	—13(1)
N(4)	8016(4)	2895(2)	5914(3)	13(5)	9(1)	22(2)	6(2)	11(3)	2(1)
N(5)	8714(4)	2086(2)	6484(3)	28(5)	5(1)	21(3)	1(2)	3(3)	3(2)
N(6)	9694(4)	2532(2)	5542(3)	28(5)	8(1)	23(3)	2(2)	—6(3)	—3(2)
N(7)	7794(4)	1666(2)	7457(3)	50(5)	9(1)	26(3)	0(2)	9(3)	1(2)
C(11)	8794(4)	2508(3)	5998(3)	20(6)	11(2)	12(3)	—4(3)	0(4)	—5(2)
C(12)	7814(5)	2076(2)	6935(3)	45(7)	3(2)	14(3)	—1(3)	—9(4)	2(2)
C(13)	6950(5)	2470(2)	6896(3)	41(6)	7(2)	14(3)	3(3)	6(4)	2(2)
C(14)	7100(5)	2867(2)	6370(4)	43(7)	6(2)	22(3)	8(3)	—2(4)	0(2)
C(15)	5909(5)	2422(2)	7391(4)	70(7)	9(2)	28(4)	4(3)	14(4)	6(2)
C(16)	5139(5)	2914(2)	7336(4)	47(7)	6(2)	22(4)	—2(3)	20(4)	1(2)
C(17)	5298(5)	3346(2)	7834(4)	23(6)	12(2)	27(4)	3(3)	3(4)	4(2)
C(18)	4621(5)	3806(3)	7778(4)	46(7)	12(2)	16(3)	—4(3)	7(4)	—3(2)
C(19)	3803(5)	3836(3)	7220(4)	32(6)	11(2)	19(3)	0(3)	11(4)	0(2)
C(20)	3673(5)	3400(3)	6726(4)	26(7)	18(2)	17(3)	—3(3)	4(4)	—5(2)
C(21)	4329(5)	2935(2)	6767(4)	45(7)	10(2)	28(4)	0(3)	14(4)	—3(2)
C(22)	5384(6)	4226(3)	8890(4)	109(9)	18(2)	32(4)	0(4)	7(5)	—8(2)
C(23)	2367(5)	4392(3)	7710(4)	32(6)	15(2)	46(4)	0(3)	—2(5)	—11(2)
C(24)	2707(6)	3079(3)	5622(4)	83(9)	37(3)	43(4)	15(4)	—16(5)	—18(3)

(*) Anisotropic temperature factors (x 10^4) defined by: $\exp [-(b_{11}h^2 + b_{22}k^2 + b_{33}l^2 + b_{12}2hk + b_{13}2hl + b_{23}2kl)]$.

UM00013761

NOVARTIS EXHIBIT 1017
Novartis v. Regents, IPR2023-01346
Page 2507 of 4460

TABLE II

Atomic coordinates (x 10^3) *for hydrogen atoms* (*).

atom	x/a	y/b	z/c
	Sulfamethoxazole		
H(N2)	812	330	509
H1(N1)	511	591	623
H2(N1)	635	608	614
H(2)	744	564	523
H(3)	773	484	453
H(5)	531	405	565
H(6)	491	484	638
H(8)	865	441	350
H1(10)	1133	420	264
H2(10)	1161	462	334
H3(10)	1054	473	281
	Trimethoprim		
H1(N6)	1008	287	566
H2(N6)	1020	224	566
H1(N7)	777	133	722
H2(N7)	708	171	776
H(14)	653	315	633
H1(15)	551	209	724
H2(15)	614	237	793
H(17)	589	333	821
H(21)	421	262	644
H1(22)	503	393	925
H2(22)	614	411	877
H3(22)	538	458	919
H1(23)	181	408	772
H2(23)	272	442	823
H3(23)	194	475	762
H1(24)	340	304	524
H2(24)	255	269	577
H3(24)	208	317	520

(*) The thermal parameters were given a fixed B = 5.0 Å^2.

C(24)	2707(6)	3079(3)	5622(4)	83(9)	37(3)	43(4)	15(4)	—16(5)	—18(3)

(*) Anisotropic temperature factors (x 10^4) defined by: $\exp[-(b_{11}h^2 + b_{22}k^2 + b_{33}l^2 + b_{12}2hk + b_{13}2hl + b_{23}2kl)]$.

UM00013762
NOVARTIS EXHIBIT 1017
Novartis v. Regents, IPR2023-01346
Page 2508 of 4460

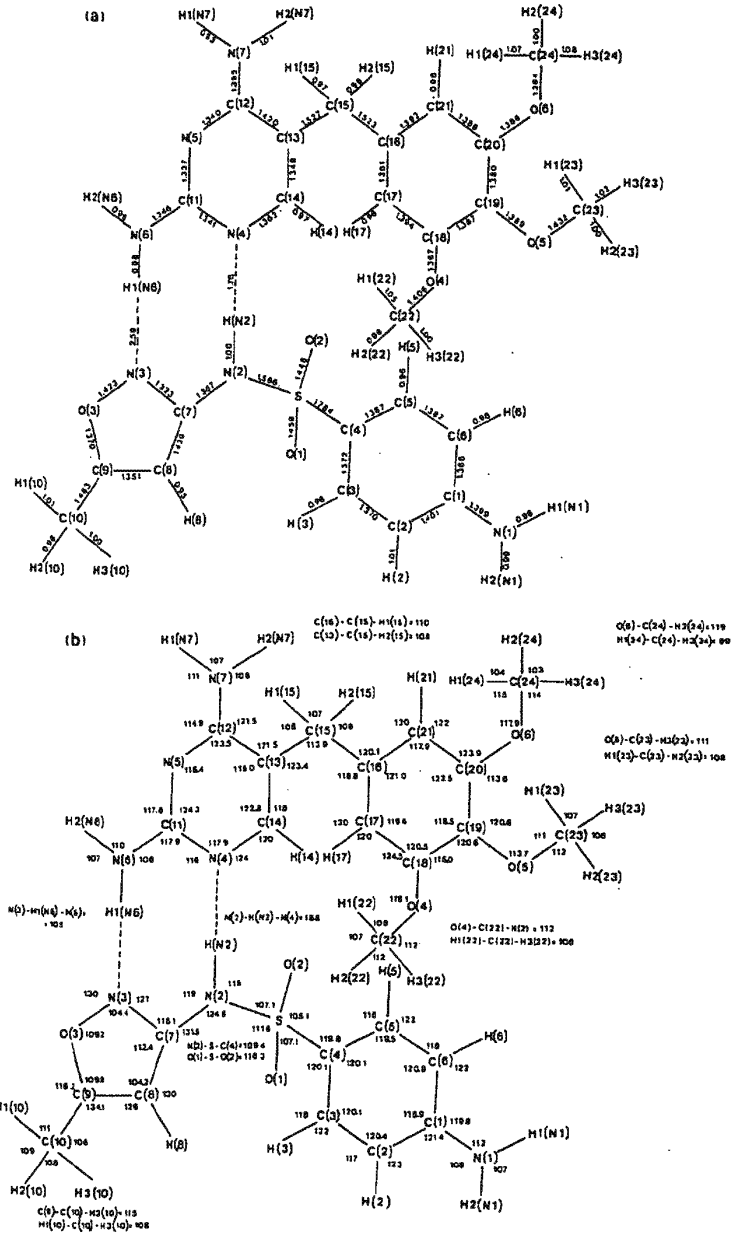


Fig. 2

(a) *bond lengths (Å),* (b) *valency angles (°) of TSC. The hydrogen bridges between SMZ and TMP molecules are shown by broken lines. The σ values for bonds and angles not involving hydrogen atoms range between* 0.004-0.007 *Å and* 0.3-0.6°, *respectively.*

UM00013763
NOVARTIS EXHIBIT 1017
Novartis v. Regents, IPR2023-01346
Page 2509 of 4460

N^1-(3-pyridyl)sulfanilamide and ascribed to some contribution of the imide form which sulfapyridine is known to exhibit (8). Unfortunately, a comparison between SMZ structure in the complexed and in the free state can not be effected at present. The double bond character in the C(7)-N(2) bond may have a limiting effect on the conformational flexibility about this bond. The conformational state of the SMZ molecule can be specified by three torsion angles τ_1, τ_2 and τ_3 (Table III: see refs. 11 and 12). The torsion angles showing the orientation of the benzene ring respect to O(1) and O(2) oxygen atoms are also reported.

TABLE III

Torsion angles (*) describing the conformations adopted by the SMZ and TMP molecules in TSC.

Sulfamethoxazole		
N(2)-S-C(4)-C(3)	τ_1 =	64.3°
C(4)-S-N(2)-C(7)	τ_2 =	—90.3°
S-N(2)-C(7)-N(3)	τ_3 =	—170.6°
C(3)-C(4)-S-O(1)		—56.7°
C(3)-C(4)-S-O(2)		179.0°
C(5)-C(4)-S-O(1)		120.9°
C(5)-C(4)-S-O(2)		—3.4°
Trimethoprim		
C(12)-C(13)-C(15)-C(16)	τ_1 =	173.4°
C(13)-C(15)-C(16)-C(21)	τ_2 =	87.7°
C(22)-O(4)-C(18)-C(17)		—13.9°
C(23)-O(5)-C(19)-C(18)		—74.7°
C(24)-O(6)-C(20)-C(21)		—7.1°

(*) Mean σ for all angles 0.4°.

As far as the TMP molecule is concerned, the values of intramolecular bond distances and angles are in good agreement with the corresponding values observed for TMP alone (14) and its salts (15, 16).

Both benzene and pyrimidine rings are planar within the limits of experimental error and are connected by a methylene carbon atom in a non-coplanar fashion, making an angle of 84.5° with each other.

UM00013764
NOVARTIS EXHIBIT 1017
Novartis v. Regents, IPR2023-01346
Page 2510 of 4460

It must be pointed out that: a) the Ph-O(5) and CH_3-O(5) distances are both larger than those concerning O(4) and O(6); b) the angle C(19)-O(5)-C(23) is smaller than angles with vertex in O(4) and O(6); c) the angles C(21)-C(20)-O(6) and C(17)-C(18)-O(4) are larger than 120°, while the angles C(19)-C(20)-O(6) and C(19)-C(18)-O(4) are correspondingly lower than 120° (owing to the close interaction between *meta* methoxy groups and *orto* hydrogen atoms); d) the C(12)-C(13) bond is significantly longer than C(13)-C(14) (17); e) the angles in the pyrimidine ring are significantly distorted from a regular hexagon. In particular, the value of the angle C(11)-N(4)-C(14) [117.9(5)°] is significantly lower than the corresponding value in the free molecule [119.9(7)°] while it is of the same magnitude order as in TMP acetate salt (118°) (16). This can be attributed to the hydrogen bonding involving the ring nitrogen N(4).

The displacements of the ring-attached atoms C(15) and O(5) from the benzene plane and C(15) and N(7) from the pyrimidine plane are of greater significance. The substituent N(6), while markedly out of the pyrimidine ring plane in TMP free molecule (14), in TSC is equiplanar as in TMP acetate salt (16), being involved in the hydrogen bond in the linkage with the SMZ molecule [N(6)-H1(N6).....N(3)].

The TMP molecule has only two important degrees of conformational freedom, described by the torsion angles τ_1 and τ_2 around the bonds C(13)-C(15) and C(15)-C(16) (Table III: see ref. 14). The values of other torsion angles describing the orientation of methoxy groups respect to the ring plane are similar to those found in TMP acetate salt and show that the carbon atom on O(5) twists out of the ring plane about the O(5)-C(19) bond owing to intramolecular steric crowding (16) (C(23) out-of-plane displacement 1.113 Å).

In TSC the association between SMZ and TMP molecules is achieved through two hydrogen bonds between the aminoisoxazolic fragment [H(N2)N(2) (donor)-C(7)-N(3) (acceptor)] and the aminopyrimidine portion [N(4) (acceptor)-C(11)-N(6)H1(N6) (donor)]. The same aminopyrimidine moiety is involved in the bonding between TMP and acetic acid in TMP acetate salt where however the nitrogen ring atom is protonated (16).

Referring to the best plane formed by atoms N(2), C(7), N(3), N(4), C(11) and N(6) (plane 5 in Table IV), the isoxazole and pyrimidine ring systems are twisted about C(7)-N(3) and C(11)-N(4) bonds by 10 and 9°, respectively. The atoms of plane 5 opposite to each other N(2) $\longleftrightarrow$ N(4), C(7) $\longleftrightarrow$ C(11), N(3) $\longleftrightarrow$ N(6) show out-of-plane displacements almost equal as absolute value but of different sign. This is true also for H(N2) and H1(N6), although the H1(N6) displacement is very considerable when compared with H(N2).

UM00013765
NOVARTIS EXHIBIT 1017
Novartis v. Regents, IPR2023-01346
Page 2511 of 4460

TABLE IV

Least-squares planes.

Equations of planes (a)				
Plane (b)	A	B	C	D
1	2.4274	15.5167	13.0097	—13.5117
2	7.8444	—6.9030	12.2832	—8.3220
3	5.6325	13.5152	12.0306	—15.5439
4	—7.8875	—10.1045	11.0395	—1.0941
5	4.2575	16.0815	11.6040	—14.7579

Displacements from the plane (Å)				
Plane (c)	Displacement			
1	O(3)*	0.000	N(2)	0.056
	N(3)*	—0.004	C(10)	0.037
	C(7)*	0.007	H(8)	—0.014
	C(8)*	—0.006		
	C(9)*	0.004		
2	C(1)*	—0.010	S	—0.063
	C(2)*	0.010	N(1)	0.022
	C(3)*	—0.005	H1(N1)	—0.750
	C(4)*	—0.001	H2(N1)	0.001
	C(5)*	0.001	H(2)	0.052
	C(6)*	0.004	H(3)	—0.036
			H(5)	—0.015
			H(6)	0.036
3	N(4)*	—0.002	N(6)	0.006
	N(5)*	—0.015	N(7)	0.069
	C(11)*	0.014	H(14)	—0.002
	C(12)*	0.006	C(15)	—0.050
	C(13)*	0.005		
	C(14)*	—0.007		

UM00013766
NOVARTIS EXHIBIT 1017
Novartis v. Regents, IPR2023-01346
Page 2512 of 4460

(follows Table IV)

Plane (c)	Displacement			
4	C(16)*	0.006	O(4)	—0.041
	C(17)*	—0.005	O(5)	—0.094
	C(18)*	0.001	O(6)	0.010
	C(19)*	0.001	C(15)	—0.044
	C(20)*	—0.000	H(17)	—0.046
	C(21)*	—0.004	H(21)	0.043
			C(22)	0.203
			C(23)	1.113
			C(24)	—0.134
5	N(2)*	—0.170	H(N2)	—0.084
	N(3)*	0.134	H1(N6)	0.719
	N(4)*	0.172		
	N(6)*	—0.128		
	C(7)*	0.014		
	C(11)*	—0.022		

(a) The equations are in the form AX + BY + CZ + D = 0 referred to the crystallographic axes, with X, Y and Z in Å units.

(b) Plane number: 1, isoxazolic ring of SMZ; 2, benzene ring of SMZ; 3, pyrimidine ring of TMP; 4, benzene ring of TMP; 5, intermolecular ring N(2), C(7), N(3), N(6), C(11) and N(4).

(c) The asterisks denote the atoms used to define the planes.

The value for the most dominant hydrogen bond between the two molecular entities N(2).....N(4) (2.74 Å) is significantly smaller than the analogous values found in dimeric aminopyrimidine structures [3.09-3.37 Å (14, 17-20)] and the average value (3.10 ± 0.13 Å) tabulated by Pimentel and McClellan (21) for N-H.....N bridges. In the same range falls the other bridge (2.99 Å) between the two molecules.

The principal intermolecular binding forces joining the TSC molecules throughout the crystal lattice involve two N-H.....O hydrogen bridges between the two oxygen atoms of an —SO_2— grouping of one molecule of TSC and the —N(6)H2(N6) and —N(7)H2(N7) groups of other two molecules, respectively. Both N(6).....O(2) (2.84 Å) and H2(N6).....O(2) (1.97 Å) distances are significantly shorter than the average value of 3.04 Å ± 0.13 Å tabulated for N-H.....O hydrogen bonds (21) and the

UM00013767

NOVARTIS EXHIBIT 1017
Novartis v. Regents, IPR2023-01346
Page 2513 of 4460

TABLE V

Intermolecular hydrogen bonds (a, b) *and angles and intermolecular distances* (c) *less than* 3.40 Å.

Bond (Å)			Angle (°) and equivalent positions (d)
N(2).....N(4) (a)	N(2)-H(N2)	H(N2).....N(4)	$N(2)^{i}$-H(N2)^{i}.....N(4)^{i}
2.74	1.00	1.76	168
N(6).....O(2) (b)	N(6)-H2(N6)	H2(N6).....O(2)	$N(6)^{ii}$-H2(N6)^{ii}.....O(2)^{i}
2.84	0.96	2.00	145
N(7).....O(1) (b)	N(7)-H2(N7)	H2(N7).....O(1)	$N(7)^{iii}$-H2(N7)^{iii}.....O(1)^{i}
2.92	1.01	2.31	117
N(6).....N(3) (a)	N(6)-H1(N6)	H1(N6).....N(3)	$N(6)^{i}$-H1(N6)^{i}.....N(3)^{i}
2.99	0.98	2.59	105
N(1).....O(1) (b)	N(1)-H1(N1)	H1(N1).....O(1)	$N(1)^{iv}$-H1(N1)^{iv}.....O(1)^{i}
3.15	0.96	2.21	164
N(1).....N(5) (c)	N(1)-H2(N1)	H2(N1).....N(5)	$N(1)^{v}$-H2(N1)^{v}.....N(5)^{i}
3.23	0.99	2.53	128
C(10).....O(4) (c)	C(10)-H3(10)	H3(10).....O(4)	$C(10)^{vi}$-H3(10)^{vi}.....O(4)^{i}
3.31	1.00	2.60	128
N(7).....N(1) (c)	N(7)-H1(N7)	H1(N7).....N(1)	$N(7)^{vii}$-H1(N7)^{vii}.....N(1)^{i}
3.36	0.93	2.65	134

(a) Hydrogen bonds involved in the association between SMZ and TMP molecules.
(b) Hydrogen bonds holding together in the lattice the complex molecules.
(c) Intermolecular contacts.
(d) i = x,y,z; ii = x-1/2,1/2-y,1-z; iii = x,1/2-y,z-1/2; iv = 1-x,1-y,1-z; v = 3/2-x,y-1/2,z; vi = 3/2-x,1-y,1/2+z; vii = 3/2-x,1/2+y,z.

value of 2.4 Å, below which a hydrogen bond may be said to exist (22), respectively. Therefore this interaction is strong and more significant than N(7).....O(1) interaction. The arrangement of TSC molecules involving hydrogen bondings shorter than 3 Å is shown in Fig. 3.

As far as the N(1).....O(1) hydrogen bond between different SMZ molecules in crystal lattice is concerned, it can be pointed out that, although the length of 3.15 Å is somewhat greater than the accepted

UM00013768
NOVARTIS EXHIBIT 1017
Novartis v. Regents, IPR2023-01346
Page 2514 of 4460

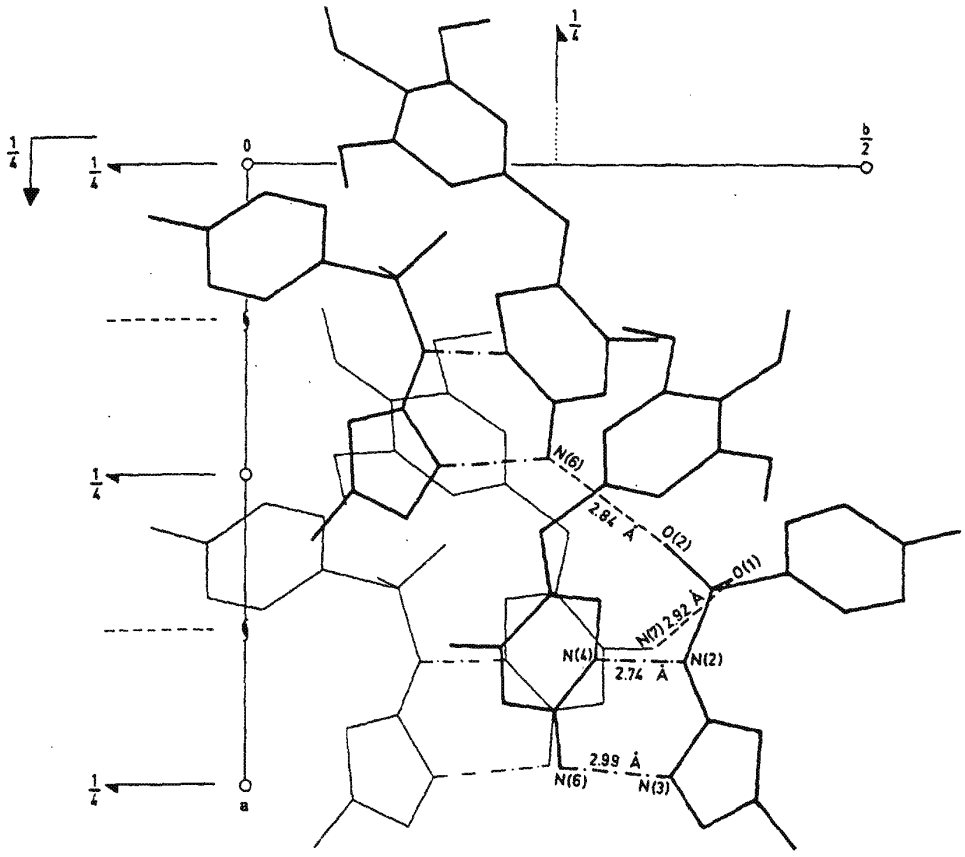


Fig. 3

Molecular arrangement of TSC molecules viewed along the c-axis involving hydrogen bondings shorter than 3 Å (— · — · —, N.....N bridges; — — —, N.....O bridges).

maximum for hydrogen bond (3.10 Å), the H1(N1).....O(1) length of 2.21 Å is well below the upper limit proposed for the H to O distance when hydrogen bonding takes place.

The SMZ aminogroup of TSC is involved in other two interactions with aminopyrimidine nitrogen atoms. These N.....N lengths fall in the upper range of such interaction (21); thus they can be considered extremely weak (intermolecular contacts).

Lastly, the C(10).....O(4) distance suggests weak association or polarization bonding (23) between the O(4) TMP methoxy group oxygen atom of one molecule of TSC and the SMZ methyl group of another TSC molecule.

UM00013769

NOVARTIS EXHIBIT 1017
Novartis v. Regents, IPR2023-01346
Page 2515 of 4460

In conclusion, hydrogen bonds appear to be the predominant stabilizing forces for TSC in the solid state, as already hypotized on the basis of I.R. spectra (1).

REFERENCES

1) GIORDANO F., BETTINETTI G.P., LA MANNA A., FERLONI P., *Il Farmaco, Ed. Sc.*, **32**, 889; 1977.
2) GERMAIN G., MAIN P., WOOLFSON M.M., *Acta Cryst.*, A27, 368; 1971.
3) BUSING W.R., MARTIN K.O., LEVY H.A., 1962, ORFLS, A Fortran Crystallographic Least Squares Program, ORNL-TM-305.
4) HANSON H., HERMAN F., LEA J.D., SKILLMAN S., *Acta Cryst.*, **17**, 1040; 1964.
5) ALLEAUME M., DECAP J., *Acta Cryst.*, B24, 214; 1968.
6) KRUGER G.J., GAFNER G., *Acta Cryst.*, B28, 326; 1971.
7) COOK D.S., TURNER M.F., *J. Chem. Soc. Perk. Trans. II*, **11**, 1021; 1975.
8) COOK D.S., TURNER M.F., *J. Chem. Soc. Perk. Trans. II*, **12**, 1379; 1976.
9) BREHM L., *Acta Cryst.*, B33, 146; 1977.
10) O'CONNEL A.M., MASLEN E.N., *Acta Cryst.*, **22**, 134; 1967.
11) SHEFTER E., CHMIELEWICZ Z.F., BLOUNT J.F., BRENNAN T.F., SACKMAN B.F., SACKMAN P., *J. Pharm. Sci.*, **61**, 872; 1972.
12) GIUSEPPETTI G., TADINI C., BETTINETTI G.P., GIORDANO F., *Cryst. Struct. Comm.*, **6**, 263; 1977.
13) SHEFTER E., SACKMAN P., *J .Pharm. Sci.*, **60**, 282; 1971.
14) KOETZLE T.F., WILLIAMS G.J.B., *J. Am. Chem. Soc.*, **98**, 2074; 1976.
15) PHILLIPS T., BRYAN R.F., *Acta Cryst.*, A25, S200; 1969.
16) HALTIWANGER R.C., M. Sc. Thesis, University of Virginia, Charlottesville, Va., 1971.
17) CLEWS C.J.B., COCHRAN W., *Acta Cryst.*, **2**, 46; 1949.
18) CLEWS C.J.B., COCHRAN W., *Acta Cryst.*, **1**, 4; 1948.
19) WHITE N.E., CLEWS C.J.B., *Acta Cryst.*, **9**, 586; 1956.
20) KVICK A., THOMAS R., KOETZLE T.F., *Acta Cryst.*, B32, 224; 1976.
21) PIMENTEL G.C., MCCLELLAN A.L., "The Hydrogen Bond", W.H., Freeman, San Francisco, Calif., 1960, chap. 9.
22) HAMILTON W.C., "Structural Chemistry and Molecular Biology", A. Rich and N. Davidson, Eds., W.H. Freeman, San Francisco, Calif., 1968, p. 468.
23) SUTOR D.J., *J. Chem. Soc.*, **1963**, 1105.

Pervenuto in Redazione il 10 *Aprile* 1979.

UM00013770
NOVARTIS EXHIBIT 1017
Novartis v. Regents, IPR2023-01346
Page 2516 of 4460

This Page is Inserted by IFW Indexing and Scanning Operations and is not part of the Official Record

BEST AVAILABLE IMAGES

Defective images within this document are accurate representations of the original documents submitted by the applicant.

Defects in the images include but are not limited to the items checked:

- ☐ BLACK BORDERS
- ☐ IMAGE CUT OFF AT TOP, BOTTOM OR SIDES
- ☐ FADED TEXT OR DRAWING
- ☐ BLURRED OR ILLEGIBLE TEXT OR DRAWING
- ☐ SKEWED/SLANTED IMAGES
- ☐ COLOR OR BLACK AND WHITE PHOTOGRAPHS
- ☐ GRAY SCALE DOCUMENTS
- ☐ LINES OR MARKS ON ORIGINAL DOCUMENT
- ☐ REFERENCE(S) OR EXHIBIT(S) SUBMITTED ARE POOR QUALITY
- ☐ OTHER: _____

IMAGES ARE BEST AVAILABLE COPY.
As rescanning these documents will not correct the image problems checked, please do not report these problems to the IFW Image Problem Mailbox.

Acta Cryst. (1999). C55, 583–585

2-Aminopyrimidine–fumaric acid cocrystal

SHYAMAPROSAD GOSWAMI,[a] AJIT KUMAR MAHAPATRA,[b] GUR DAYAL NIGAM,[c] KANDASAMY CHINNAKALI,[d]† HOONG-KUN FUN[d] AND IBRAHIM ABDUL RAZAK[d]

[a]*Department of Chemistry, Bengal Engineering College (Deemed University), Howrah 711 103, India,* [b]*Department of Chemistry, Indian Institute of Technology, Kharagpur 721 302, India,* [c]*Department of Physics and Meteorology, Indian Institute of Technology, Kharagpur 721 302, India, and* [d]*X-ray Crystallography Unit, School of Physics, Universiti Sains Malaysia, 11800 USM, Penang, Malaysia. E-mail: hkfun@usm.my*

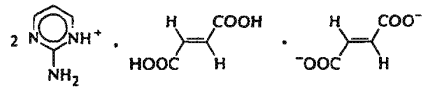
(*Received 18 August 1998; accepted 28 October 1998*)

Abstract

In crystals of the title compound, 2-aminopyrimidin-1-ium hemifumarate hemifumaric acid, $C_4H_6N_3^+ \cdot 0.5C_4H_2O_4^{2-} \cdot 0.5C_4H_4O_4$, the asymmetric unit contains one 2-aminopyrimidine cation, $C_4H_6N_3^+$, protonated at a pyrimidine ring-N atom, one half-molecule of fumaric acid, $C_4H_4O_4$, and one half of a fumarate ion, $C_4H_2O_4^{2-}$. These are linked by N—H···O, O—H···O and relatively strong C—H···O bonds, resulting in eight- and nine-membered hydrogen-bonded rings and an extended supramolecular structure.

Comment

Supramolecular assembly is a central theme in the design of new solid state structures with unusual conductance, electronic, non-linear optical or magnetic properties (Disalvo, 1990). Such an assembly has been observed in the cocrystal of 2-aminopyrimidine with terephthalic acid (1:1) (Goswami *et al.*, 1999). The crystal structure of 2-aminopyrimidine itself has been reported (Scheinbeim & Schempp, 1976), in which two equivalent proton donors and two equivalent acceptors make an eight-membered hydrogen-bonded self-assembly. This communication reports the crystal structure of 2-aminopyrimidine with fumaric acid, (I), in which 2-aminopyrimidine makes typically eight- and nine-membered hydrogen-bonded rings with fumaric acid. The structure of the complex shows that a strong interaction alone need not always dictate the crystal structure if other weaker interactions are of special significance. This indicates that caution must be taken to keep track of weak interactions while designing novel structures of new materials.



(I)

The asymmetric unit of (I) contains one 2-aminopyrimidine cation, one half-molecule of fumaric acid and one half of a fumarate dianion. The fumarate dianion is formed through the protonation of 2-aminopyrimidine by fumaric acid: this type of protonation is observed in other carboxylic acid and 2-aminopyrimidine cocrystals (Byriel *et al.*, 1992; Lynch *et al.*, 1994).

The bond lengths and angles in the 2-aminopyrimidine agree with the values observed for the protonated molecule (Byriel *et al.*, 1992; Lynch *et al.*, 1994). The geometries of the fumaric acid and fumarate dianion are comparable with those reported by Brown (1966) and Li & Mak (1997). The fumaric acid and its dianion form a dihedral angle of 12.51 (8)°, and they make dihedral angles of 27.66 (9) and 16.74 (9)°, respectively, with the 2-aminopyrimidine.

Within the asymmetric unit, the 2-aminopyrimidine is linked to the fumaric acid and fumarate dianion by N1—H···O3, N2—H···O4, O2—H···O4 and C2—H···O1 hydrogen bonds, through the formation of eight- and nine-membered hydrogen-bonded rings (Table 2 and Fig. 1). These hydrogen bonds, together with N1—H···O1($x, \frac{3}{2}-y, \frac{1}{2}+z$) and the crystallographic symmetry elements (the fumarate molecule and anion lie

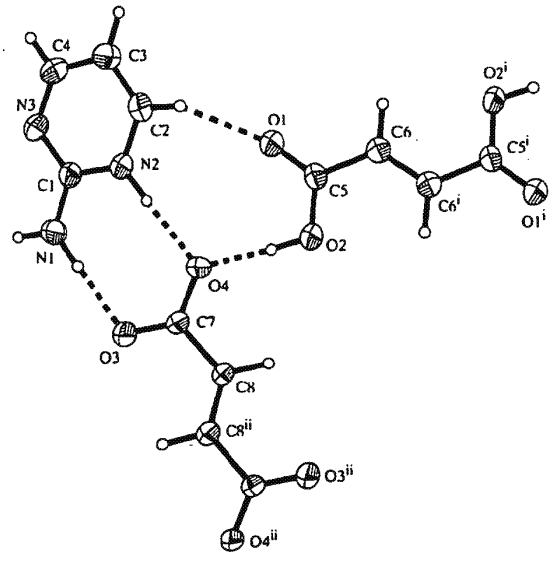


Fig. 1. The structure of title compound, showing 50% probability displacement ellipsoids and the atom-numbering scheme. Symmetry codes are as in Table 1.

† On leave from: Department of Physics, Anna University, Chennai 600 025, India.

© 1999 International Union of Crystallography
Printed in Great Britain – all rights reserved

UM00013772
NOVARTIS EXHIBIT 1017
Novartis v. Regents, IPR2023-01346
Page 2518 of 4460

on inversion centres), result in extended 'wavy' sheets parallel to the (100) plane. Adjacent sheets are linked by three weaker C—H···O hydrogen bonds to form a supramolecular assembly, which is further stabilized by the interactions between the pyrimidines within their stacks (Fig. 2).

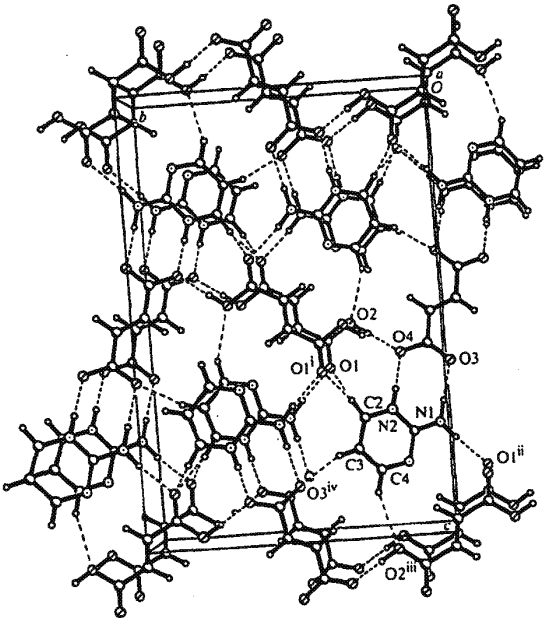


Fig. 2. Packing of the molecules of (I), viewed normal to the (100) plane. Symmetry codes are as in Table 2.

Experimental

Single crystals were grown by slow evaporation of a solution of 2-aminopyrimidine and fumaric acid (1:1 molar ratio) in a 6:1 mixture of dry acetone and methanol.

Crystal data

$C_4H_6N_3^+ \cdot 0.5C_4H_2O_4^{2-} \cdot \cdot 0.5C_4H_4O_4$
$M_r = 211.18$
Monoclinic
$P2_1/c$
$a = 3.7946\ (2)$ Å
$b = 19.1766\ (7)$ Å
$c = 13.0641\ (6)$ Å
$\beta = 96.893\ (1)°$
$V = 943.77\ (7)$ Å^3
$Z = 4$
$D_x = 1.486$ Mg m^{-3}
D_m not measured
Mo $K\alpha$ radiation
$\lambda = 0.71073$ Å
Cell parameters from 3463 reflections
$\theta = 3.14–33.12°$
$\mu = 0.121$ mm^{-1}
$T = 293\ (2)$ K
Slab
0.48 × 0.24 × 0.18 mm
Colourless

Data collection

Siemens SMART CCD area-detector diffractometer
ω-scans
Absorption correction: none
7257 measured reflections
2752 independent reflections
1830 reflections with $I > 2\sigma(I)$
$R_{int} = 0.042$
$\theta_{max} = 30°$
$h = -5 \rightarrow 5$
$k = 0 \rightarrow 26$
$l = 0 \rightarrow 18$

Refinement

Refinement on F^2
$R[F^2 > 2\sigma(F^2)] = 0.067$
$wR(F^2) = 0.184$
$S = 1.055$
2752 reflections
172 parameters
All H atoms refined
$w = 1/[\sigma^2(F_o^2) + (0.0917P)^2 + 0.1819P]$ where $P = (F_o^2 + 2F_c^2)/3$
$(\Delta/\sigma)_{max} < 0.001$
$\Delta\rho_{max} = 0.387$ e Å^{-3}
$\Delta\rho_{min} = -0.227$ e Å^{-3}
Extinction correction: none
Scattering factors from *International Tables for Crystallography* (Vol. C)

Table 1. *Selected bond lengths (Å)*

O1—C5	1.209 (3)	N3—C1	1.349 (3)
O2—C5	1.306 (3)	C2—C3	1.364 (3)
O3—C7	1.233 (2)	C3—C4	1.394 (3)
O4—C7	1.284 (2)	C5—C6	1.491 (3)
N1—C1	1.322 (3)	C6—C6'	1.310 (4)
N2—C2	1.352 (3)	C7—C8	1.494 (3)
N2—C1	1.355 (3)	C8—C8''	1.311 (4)
N3—C4	1.324 (3)		

Symmetry codes: (i) $-x, 1-y, 1-z$; (ii) $-x, 1-y, 2-z$.

Table 2. *Hydrogen-bonding geometry (Å, °)*

D—H···*A*	*D*—H	H···*A*	*D*···*A*	*D*—H···*A*
N1—H1N1···O3	0.96 (3)	1.84 (3)	2.796 (3)	176 (3)
N2—H1N2···O4	0.91 (3)	1.80 (3)	2.708 (2)	170 (3)
O2—H1O2···O4	0.93 (3)	1.63 (3)	2.551 (2)	172 (3)
C2—H2···O1	0.96 (3)	2.48 (3)	3.068 (3)	119 (2)
C2—H2···O1^i	0.96 (3)	2.56 (3)	3.378 (3)	143 (2)
N1—H2N1···O1^{ii}	0.95 (3)	1.93 (3)	2.875 (3)	174 (2)
C4—H4···O2^{iii}	0.97 (3)	2.58 (3)	3.440 (3)	149 (2)
C3—H3···O3^{iv}	0.97 (3)	2.43 (3)	3.367 (3)	162 (2)

Symmetry codes: (i) $1+x, y, z$; (ii) $x, \frac{3}{2}-y, \frac{1}{2}+z$; (iii) $1-x, \frac{1}{2}+y, \frac{3}{2}-z$; (iv) $1+x, \frac{3}{2}-y, z-\frac{1}{2}$.

The data collection covered a hemisphere of reciprocal space by a combination of three sets of exposures; each set had a different φ angle (0, 88 and 180°) for the crystal and each exposure of 30 s covered 0.3° in ω. The crystal-to-detector distance was 4 cm ($2\theta_{max} = 66.24°$) and the detector swing angle was −35°. Coverage of the unique set is over 99% complete. Crystal decay was monitored by repeating 30 initial frames at the end of data collection and analysing the duplicate reflections, and was found to be negligible. Only reflections having 2θ less than 60° were used for structure solution and refinement, as only a few reflections were found to be observed at higher angles. All H atoms were located from a difference Fourier map and refined isotropically.

Data collection: *SMART* (Siemens, 1996). Cell refinement: *SAINT* (Siemens, 1996). Data reduction: *SAINT*. Program(s) used to solve structure: *SHELXTL* (Sheldrick, 1997). Program(s) used to refine structure: *SHELXTL*. Molecular graphics: *SHELXTL*. Software used to prepare material for publication: *SHELXTL* and *PARST* (Nardelli, 1995).

UM00013773
NOVARTIS EXHIBIT 1017
Novartis v. Regents, IPR2023-01346
Page 2519 of 4460

SG and AKM are thankful to the CSIR, New Delhi, India, for financial support. The authors would also like to thank the Malaysian Government for research grant R&D No. 190-9609-2801. KC thanks the Universiti Sains Malaysia for a Visiting Post-Doctoral Fellowship.

Supplementary data for this paper are available from the IUCr electronic archives (Reference: HA1239). Services for accessing these data are described at the back of the journal.

References

Brown, C. J. (1966). *Acta Cryst.* **21**, 1–5.
Byriel, K. A., Kennard, C. H. L., Lynch, D. E., Smith, G. & Thompson, J. G. (1992). *Aust. J. Chem.* **45**, 969–981.
Disalvo, F. J. (1990). *Science*, **247**, 649–655.
Goswami, S., Mahapatra, A. K., Ghosh, K., Nigam, G. D., Chinnakali, K. & Fun, H.-K. (1999). *Acta Cryst.* C**55**, 87–89.
Li, Q. & Mak, T. C. W. (1997). *Acta Cryst.* B**53**, 252–261.
Lynch, D. E., Smith, G., Freney, D., Byriel, K. A. & Kennard, C. H. L. (1994). *Aust. J. Chem.* **47**, 1097–1115.
Nardelli, M. (1995). *J. Appl. Cryst.* **28**, 659.
Scheinbeim, J. B. & Schempp, E. (1976). *Acta Cryst.* B**32**, 566–571.
Sheldrick, G. M. (1997). *SHELXTL. Structure Determination Programs.* Version 5.10. Bruker Analytical X-ray Systems Inc., Madison, Wisconsin, USA.
Siemens (1996). *SMART* and *SAINT. Area Detector Control and Integration Software.* Siemens Analytical X-ray Instruments Inc., Madison, Wisconsin, USA.

Acta Cryst. (1999). C**55**, 585–586

5,10-Dimethoxy-1,4-methano-1,4,4a,11a-tetrahydrobenzo[*b*]fluoren-11-one oxime

KANDASAMY CHINNAKALI,[a]† HOONG-KUN FUN,[a] DIPAKRANJAN MAL,[b] NIRMAL KUMAR HAZRA,[b] SUJIT KUMAR GHORAI[b] AND GUR DAYAL NIGAM[c]

[a]*X-ray Crystallography Unit, School of Physics, Universiti Sains Malaysia, 11800 USM, Penang, Malaysia,* [b]*Department of Chemistry, Indian Institute of Technology, Kharagpur 721 302, West Bengal, India, and* [c]*Department of Physics and Meteorology, Indian Institute of Technology, Kharagpur 721 302, West Bengal, India. E-mail: hkfun@usm.my*

(Received 27 July 1998; accepted 16 November 1998)

Abstract

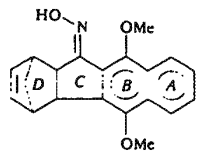
In the title compound, $C_{20}H_{19}NO_3$, the oxime moiety C=N—O—H adopts a *trans* conformation. Furthermore, the molecule as a whole exists in a dimeric form through hydrogen bonding between the oxime groups.

† On leave from: Department of Physics, Anna University, Chennai 600 025, India.

© 1999 International Union of Crystallography
Printed in Great Britain – all rights reserved

Comment

The title compound was prepared in connection with our work on the synthesis of phenanthroviridin, an anticancer drug (Gore *et al.*, 1992). The X-ray structure determination of the title compound, (I), was undertaken in order to determine the stereochemistry of the oxime moiety, which is very important for the planned Beckmann rearrangement.



(I)

The bond lengths and angles observed in this structure have normal values (Allen *et al.*, 1987; Beddoes *et al.*, 1993); the C9—C10 and N1—C6 bonds show double-bond character. The oxime moiety C=N—O—H adopts a *trans* conformation. The six-membered ring, *D*, of the norbornene ring system is a fairly symmetrical boat with asymmetry parameters ΔC_s(C7—C12) = 0.019 (1) and ΔC_s(C8) = 0.024 (1) (Nardelli, 1983). The two five-membered rings in the norbornene moiety formed by the bridging atom C14 adopt envelope conformations. The angles between the three-atom bridge plane C8—C14—C11 and four-atom planes of the six-membered rings (C8, C9, C10, C11 and C7, C8, C11, C12) are 52.0 (2) and 60.2 (2)°, respectively. The C9—C10—C7—C12 plane is nearly perpendicular [dihedral angle 87.59 (8)°] to the five-membered ring *C*. In the solid state, inversion-related molecules exist in dimeric form through O—H···N hydrogen bonding (Table 2).

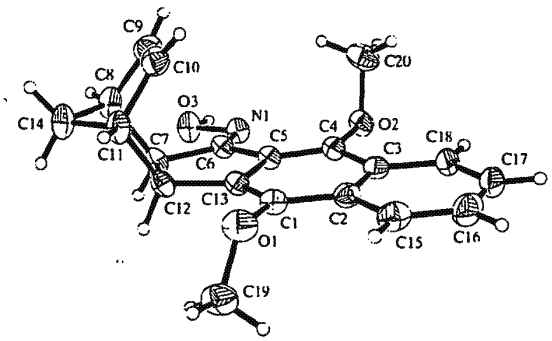


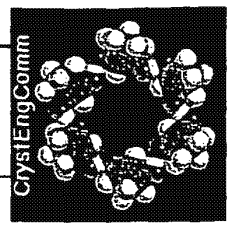
Fig. 1. The structure of the title compound showing 50% probability displacement ellipsoids and the atom-numbering scheme.

Experimental

To synthesize the title compound, 3-phenylsulphonylphthalide (1.100 mg, 4.0 mmol) was allowed to react with tricyclo-

UM00013774
NOVARTIS EXHIBIT 1017
Novartis v. Regents, IPR2023-01346
Page 2520 of 4460

Supramolecular synthon competition in organic sulfonates: A CSD survey



Paper

Delia A. Haynes,[a] James A. Chisholm,[a,b] William Jones[a] and W. D. Samuel Motherwell*[a,b]

[a]*Pfizer Institute for Pharmaceutical Materials Science, Department of Chemistry, Lensfield Road, Cambridge CB2 1EW, UK. E-mail: motherwell@ccdc.cam.ac.uk*
[b]*Cambridge Crystallographic Data Centre, 12 Union Road, Cambridge CB2 1EZ, UK*

Received 9th September 2004, Accepted 28th September 2004
First published as an Advance Article on the web 2nd November 2004

The hydrogen bonding motifs seen in sulfonate salts have been examined using the CSD. In a total sample of 1069 sulfonate salts, 594 structures contain NH-donors, and this subset of structures has been investigated in detail. Several robust hydrogen-bonding motifs have been identified. A particularly robust R(2,2)8 motif, here called the *bidentate* motif, has been investigated in more detail. This motif occurs with a probability of 75.4% in the CSD, and 78.6% in the sulfonate salts. A set of rules for the prediction of the occurrence of the *bidentate* motif in sulfonate salts has been developed.

1. Introduction

In the development of new pharmaceutical materials, it is often necessary to form the salt of a drug molecule in order to improve such physical properties as solubility and stability.[1,2] A typical example of a group of counterions used for this purpose are the $R–SO_3^-$ derivatives.[3] In the hope of discovering preferred patterns of hydrogen bonding with specific functional groups on drug-like cationic molecules, the hydrogen-bonding motifs exhibited by the sulfonate anion have been investigated.

A previous study investigating hydrogen bonding in structures containing sulfate ions[4] made several interesting observations regarding the characteristics of hydrogen bonding involving this anion. It was found that the sulfate anion exhibited no preference for either nitrogen or oxygen donors, but that hydrogen bonds from O-donors were shorter and stronger than those to N-donors. It was also found that N-donors often form two- or three-centred H-bonds, and also that in most cases a sulfate O accepted two or three (seldom one) H-bonds. The formation of hydrates, which occurred in around 60% of the structures studied, allowed the completion of the coordination sphere around the sulfate ion. It was concluded that the sulfate ion "will behave as a steric 'tightener', placing the attracted partners in close contact."[4] It was hoped that the present study would reveal whether the sulfonate anion exhibits similar characteristics.

Previous work on the geometrical features of hydrogen bonding of N-donors to the sulfonate group[5] gave a mean value for the N···O distance of 2.946 Å. This value is slightly larger than those obtained for hydrogen bonds by N-donors to carboxylates and monohydrogen phosphates (2.836 and 2.810 Å, respectively), indicating that sulfonates form longer, and weaker, hydrogen bonds to N-donors than carboxylates and monohydrogen phosphates. This was attributed to the differences in electron densities on the O atoms of the various groups. This study[5] also showed that the hydrogen bonds formed to sulfonates by N-donors were generally linear.

The Cambridge Structural Database (CSD) (version 5.24, November 2002),[6] which contains structural data for 272 066 organic and organometallic compounds, was used in this study. As many in-depth studies have shown, the CSD can provide a useful tool for examining structural motifs and discovering new supramolecular synthons.[7,8] The identification of frequently occurring specific interactions in the CSD could indicate that these interactions are fairly robust, and may be useful in crystal design and structure prediction: if an interaction occurs with a high enough probability, it can be predicted to occur in unknown compounds containing the same groups. In this study, the CSD has been used to collect information on the hydrogen bond motifs formed in a sample of sulfonate salts.

2. Methodology

Searches to determine the number of CSD hits for each ion were performed using ConQuest,[6] and hits were restricted to organic-only structures with 3D coordinates present. Variable bond types were allowed for in the sketches of SO_3^- groups. Unless otherwise stated, contact searches were performed using a van der Waals sum of 3.2 Å for N···O and O···O contacts (NH···O and OH···O hydrogen bonds were identified using these contact distances). This cutoff point of 3.2 Å is in agreement with values used previously in the literature.[4,5] In all cases, water was defined as H_2O or H_3O^+.

3. Results and discussion

3.1. Hydrogen bonding in sulfonates

There are 21146 S-containing compounds in the CSD. 7445 contain S bonded to an O atom, of which 1069 structures contain a sulfonate moiety. An investigation of the interactions of the SO_3^--group with several different hydrogen bond donors is summarised in Table 1. These results agree well with previous studies.[4] This sample of 1069 structures contains a wide range of chemical environments for SO_3^-. There are a small number of special cases such as $S–SO_3$(13) and $N–SO_3$(27), which perhaps should be treated separately. (Also, the SO_4^{2-} ion is a special case and has been excluded). Our main focus of interest is on $C–SO_3$, 1019 structures.

The 1069 sulfonate-containing structures can be sub-divided. We are interested in strong hydrogen bonding only, so we have eliminated the 268 structures that contain no N- or O-hydrogen bond donors, leaving 801 structures that can be

 DOI: 10.1039/b413797c

This journal is © The Royal Society of Chemistry 2004

UM00013775
NOVARTIS EXHIBIT 1017
Novartis v. Regents, IPR2023-01346
Page 2521 of 4460

Table 1 Hydrogen bonds formed by SO_3^- to a selection of donors

			RSO_3^- R ≠ O	SO_3OH	SO_3OX	SO_4
Total hits			1069	63	58	162
Hydrogen bond donors	NH	N_{pos}[a]	594	39	25	146
		N_{occ}[b]	522	35	23	140
		%	87.9	89.7	92.0	95.9
	OH	N_{pos}	488	29[c]	35	125
		N_{occ}	433	26	34	115
		%	88.7	89.7	97.1	92.0
	HNXNH	N_{pos}	192	7	6	59
		N_{occ}	182	7	6	54
		%	94.8	100	100	91.5
	COOH	N_{pos}	78	6	0	43
		N_{occ}	39	4		36
		%	50.0	66.7		83.7
	SH	N_{pos}	4	0	0	0
		N_{occ}	0			
		%	0			

[a] N_{pos} is the number of refcodes where an H-bond between two particular groups could possibly occur, *i.e.* the number of hits where both components (*e.g.*, SO_3^- and NH) occur in the same structure. [b] N_{occ} is the number of refcodes with an H-bond between the two components. [c] This number refers to OH groups other than SO_3OH.

subdivided according to donor types present in the structure as follows:

R–SO_3, R ≠ O	1069
R–SO_3 + NH or OH	801
R–SO_3 + NH only	313
R–SO_3 + NH + water only	100
R–SO_3 + OH only (no water)	47
R–SO_3 + OH + water only	64
R–SO_3 + NH + OH only (no water)	100
R–SO_3 + NH + OH + water	81
R–SO_3 + H_2O only	96

The overall picture of how the SO_3^- group interacts with other chemical groups in these 801 structures may be summarised by a simple count of the number of cases where we have at least one strong H-bond to each of the oxygens of the SO_3^- (Fig. 1). These data show that in more than half of the structures, all three sulfonate oxygen atoms are involved in hydrogen bonding to a strong donor. This indicates that the sulfonate moiety behaves as a 'steric tightener', *i.e.* brings several hydrogen bond donors into close contact, in the same way as the sulfate anion.[4] There are 50 structures which show no sulfonate oxygen atoms are involved in H-bonding to a N- or O-donor. Of these structures, 18 are alkali metal salts, and often the cation forms short contacts to the anion. Also, there are a number of cases where there are no available N- or O-donors due to intramolecular H-bonding or complexation. There are also some cases where an existing H-bond is not detected in the search process, due to atoms not being present in the structure, or due to the H-bond being longer than 3.2 Å.

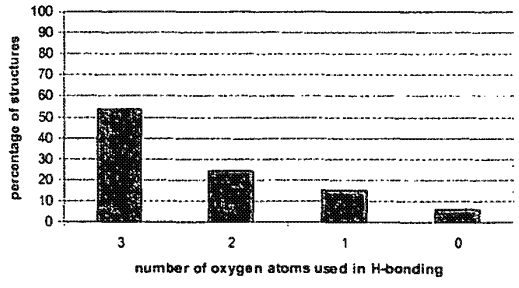


Fig. 1 Percentage of structures using 0, 1, 2 or 3 oxygen atoms of SO_3^- in hydrogen bonding in a sample of 801 structures.

However, when a strong H-bond donor is available there is a 94% probability of a contact to the sulfonate moiety.

It must again be noted here that there is a large variety of chemical compounds in this sample, and this distribution is influenced by the 'random' acquisition of structures into the CSD. For example, there are cases of metal salts with no H-bonds but metal coordination, as in calcium methylsulfonate, CAMSUL; other cases have only one available H-donor (BAZRAV, DICKIJ). It is quite common to find when there are two donors available that they form H-bonds to two different oxygens of SO_3^-, *e.g.* CEBTIZIO, DETRID, FIDYIA. When we have 3 or more donors available we normally find H-bonds to all 3 oxygens of SO_3^-. Some structures have as many as 18 available donors, *e.g.* HEJRAP. This effect of increasing H-bond acceptance by a group with increasing donor/acceptor ratio for the compound has been studied in detail by Infantes and Motherwell.[9] Further detailed analysis of the number of H-bonds accepted per SO_3^- group has not been reported in this paper, which is more concerned with identification of common H-bonding motifs.

As shown in Table 1, the sulfonate group forms H-bonds to N-donors in 87.9% of possible cases, and to O-donors in 88.7% of possible cases. Table 2 shows the number of structures containing $SO_3\cdots HN$ hydrogen bonds, $SO_3\cdots HO$ hydrogen bonds, or both, in the 181 structures containing both NH and OH donors. These results seem to imply that when both N- and O-donors are present in a structure which does not contain water, the SO_3^- group has a greater tendency to form an H-bond to the N-donor. However, when water is also present, there is a high tendency to form H-bonds to the water. In fact, 341 (31.8%) of the 1069 sulfonate structures contain water (which is considerably lower than the occurrence of hydrates of around 60% reported for sulfates[4]), and in 317 of these structures (93.0%), an H-bond forms between SO_3^- and water.

The 341 hydrates have been investigated further. 39 structures contain H_3O^+, and in all cases this is the only cation. Removing these oxonium salts from the sample leaves 302 structures, of which 48% (145 structures) contain metal ions. In fact, of those organic structures in the CSD containing a metal and an SO_3^- group, 76% are hydrates (compared to 42% of structures containing any charge and any metal which are hydrates in the whole CSD). The high frequency of hydrates in metal salts has already been noted,[10] but the 76% occurrence of hydrates in sulfonate metal salts is particularly high. Aside from this correlation however, no obvious reason for hydrate formation in the sulfonates could be identified.

3.2. Hydrogen bonding in NH-containing structures

There are a total of 594 sulfonate structures containing nitrogen donors, and these have been examined in detail. A variety of cyclic hydrogen bonding motifs have been identified in these structures. Some of these are represented diagrammatically in Fig. 2. We are conscious of the great variety of competing groups among these 594 structures, and the varying amounts of competing donors present, *e.g.* C–NH–C,

Table 2 Number of structures showing particular hydrogen bonds in sulfonates containing both NH and OH donors

	Donors present in structure	
H-bonds formed	NH and OH, no water 100 structures	NH, OH and water 81 structures
$SO_3\cdots N$	92 (92%)	67 (82.7%)
$SO_3\cdots O$	73 (73%)	79 (97.5%)
$SO_3\cdots N$ and $SO_3\cdots O$	66 (66%)	65 (80.2%)
$SO_3\cdots N$ not $SO_3\cdots O$	26 (26%)	2 (2.5%)
$SO_3\cdots O$ not $SO_3\cdots N$	7 (7%)	14[a] (17.3%)
$SO_3\cdots H_2O$	—	76 (93.8%)

[a] 13 of these are to water.

UM00013776
NOVARTIS EXHIBIT 1017
Novartis v. Regents, IPR2023-01346
Page 2522 of 4460

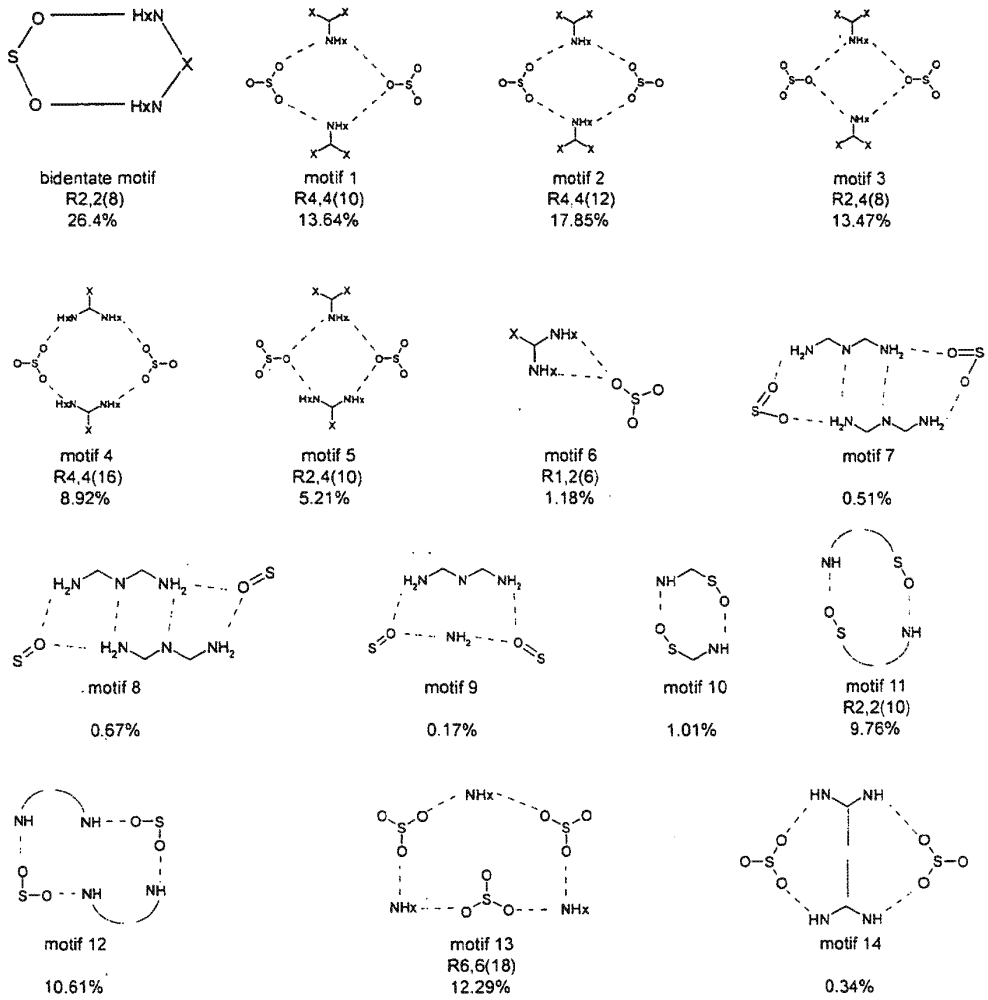


Fig. 2 A diagrammatic representation of some of the hydrogen-bonded motifs formed in sulfonates, along with the graph set and a percentage occurrence in the sample of 594 sulfonate salts containing NH donors. The percentage occurrence was determined using 3DSEARCH.[12]

$C{=}NH_2^+$, $C{-}NH_3^+$, and also OH, COOH and water. Because of these competing groups it is not very meaningful to examine the total sample for detailed motifs in an exhaustive manner, without careful subdivision into classes with defined ratios of donor/acceptor groups (which will be the subject of a further study). Rather, we have chosen a number of ring motifs which seem reasonably persistent in different environments and have the chemical significance of binding molecules together in energetically stable configurations, and often extended networks. Fig. 2 shows these motifs, as well as percentage occurrence of each motif within the sample of 594 structures. The motifs were chosen on the basis of either relatively frequent occurrence (*e.g.* motifs 1–5), or frequent occurrence within a particular subset of structures (*e.g.* motifs 7–9).

The bidentate motif. One of the simplest and most commonly occurring motifs formed between the SO_3^- oxygen atoms and NH donors is a *bidentate* motif resulting in an 8-membered H-bonded ring with graph set R2,2(8) (Fig. 2). This motif has been recognised as occurring with a 55% probability in the database in a previous study.[11] In this study, a total of 264 structures in the whole CSD were found to contain the required groups for forming this motif (*i.e.* HNXNH and SO_3), and of these 194 do in fact show the motif. In other words, in 75.4% of cases where it is feasible for this interaction to form, it does. A more in-depth analysis of the structures where the expected interaction did not form showed that there were often steric reasons: the two hydrogen donors were in a 5- or 6-membered ring, and therefore not correctly positioned to H-bond to the SO_3 group, or the central X-atom had an R-group which prevented the interaction from taking place. When these steric impossibilities are removed from the count, the percentage of structures showing the interaction increases to approximately 85%.

Searching for the components to form the *bidentate* motif in the subset of 594 sulfonates gives 192 structures. The motif is formed in 151 of these structures, or 78.6% of cases. Again, adjustment of samples to take steric factors leads to an even higher percentage of occurrence of the bidentate motif (*ca.* 90%). It seems that this is a very robust motif.

3.2.1. Guanidinium salts. 122 of the 594 NH-containing sulfonate salts are guanidinium salts, with the sulfonate group often attached to an aromatic ring. These structures are remarkably consistent: 121(*ca.* 99%) contain the *bidentate* motif (see Fig. 2), and in 119 of these there are ribbons of *bidentate* motifs. These ribbons are held together either in hexagons *via* the *bidentate* motif (83 structures), or in a slightly

UM00013777
NOVARTIS EXHIBIT 1017
Novartis v. Regents, IPR2023-01346
Page 2523 of 4460

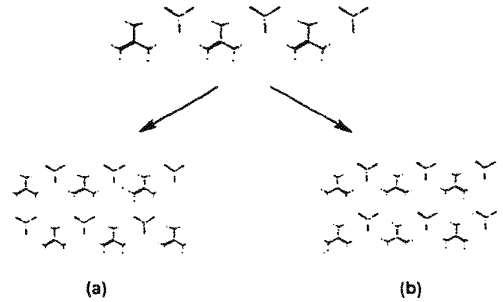


Fig. 3 Extended motifs formed in guanidinium sulfonate salts (a) From WETNEO and (b) From HEGQAL.

slipped manner *via* motif 1 (Fig. 3). We note that the structures that do not form the *bidentate* motif or ribbons of this motif all contain 2 or 3 NO_2 groups on the same aromatic ring as the sulfonate group. Only 1 of these 122 structures is a hydrate, and it is one of the structures with 2 NO_2 groups. The structures of these salts have been described in detail by Ward *et al*,[13] and exploited to predictively synthesize new crystals.

A preliminary analysis of the electrostatic potential of these compounds mapped onto their electron density reveals that it appears to be the electron-withdrawing effect of the nitro-groups on the rest of the molecule that influences the formation (or not) of the *bidentate* motif. A more positive potential on the sulfur atom combined with a less negative potential on the oxygen atoms could be the cause of the perturbation in the ribbon motif seen in all the other structures of this nature. Calculations indicate that the di- or tri-CN or $-CF_3$ derivatives would also exhibit perturbation of the *bidentate* motif.

3.2.2. Structures containing H_xNXNH_x. Aside from the guanidinium salts described above, 70 of the 594 NH-containing sulfonate salts contain an H_xNXNH_x moiety, of which 26 (*ca.* 37%) are hydrates. These 70 structures can be subdivided into those containing H_2NXNH_2 groups, those containing $HNXNH_2$ and those with HNXNH groups.

Fifteen structures contain H_2NXNH_2, and only 3 of these do not show the *bidentate* motif at all, but contain motif 3, (3 of those that do show the *bidentate* motif have N···O > 3.2 Å). The *bidentate* motifs are joined into more extended patterns in several ways: by a single O···H–N connection, or *via* motif 2 or 3 (Fig. 4), or the *bidentate* motifs are joined into ribbons as in the guanidinium salts. Two of these H_2NXNH_2-containing structures are uronium salts. One (UBESAV) forms flat sheets of connected *bidentate* motifs in a manner analogous to the sheets formed in the guanidinium salts. In the other uronium salt (BIKYUP), the H_2NCOH functionality successfully competes for the SO_3 functionality, and the *bidentate* motif is not seen.

28 structures contain an $HNXNH_2$ moiety, 7 of which contain water (*ca.* 25%). 24 of these structures have the *bidentate* motif (only 1 has N···O > 3.2 Å). In two cases, the *bidentate* motif is unable to form for steric reasons, and motif 2

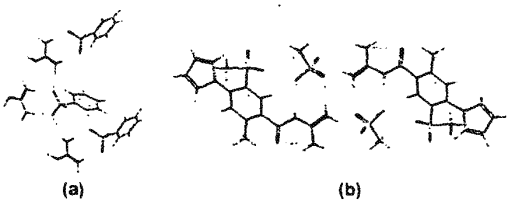


Fig. 4 Extended motifs seen in some sulfonate salts. (a) Two *bidentate* motifs joined by a single hydrogen bond (UBESAV) and (b) two *bidentate* motifs joined by motif 3, *i.e. bidentate-motif 3-bidentate* (NEGTIC).

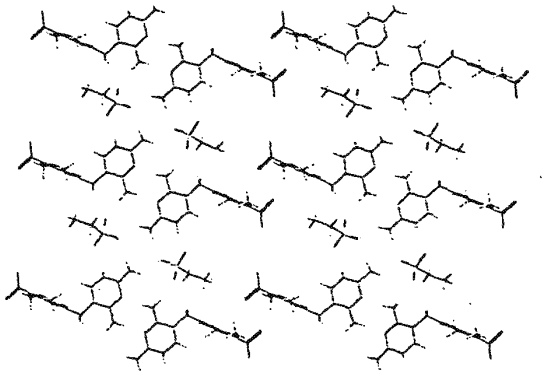


Fig. 5 'Hydrophobic' and 'hydrophilic' regions in CIDWOB, showing extended patterns of motifs, including the *bidentate-motif 3-bidentate* pattern.

or simple single NH···OS links form instead. Taking this into account, *ca.* 92% of these structures show the *bidentate* motif, which is almost as high an occurrence as in the guanidinium sulfonate salts (*ca.* 99%). In both structures where the *bidentate* motif could form but is not seen, there is a water molecule hydrogen-bonded to one of the N-donors, obstructing the formation of the expected motif.

A subgroup of these structures contain 2,4-diaminopyrimidine derivatives (or very similar functional groups such as triaminotriazine). This combination of functional groups always results in motifs 7, 8 or 9 (see Fig. 2) which, when combined with the *bidentate-motif 3-bidentate* pattern mentioned above, leads to layers of 'hydrophobic' and 'hydrophilic' regions in the crystal structure (Fig. 5). 9 structures contain this particular combination of functional groups, of which two are hydrates.

27 structures contain an HNXNH group, of which 14 (*ca.* 52%) are hydrates. In 17 of these structures the NH groups are cyclic, and several motifs are seen to occur. In three cases there are no NH···OS hydrogen bonds formed, and in all three of these structures X is C=O, and an alternative *bidentate*-type motif occurs (Fig. 6). In many of the remaining cases, two of the SO_3 oxygen atoms form hydrogen bonds to nitrogen donors, linking the molecules into chains (4), or other cyclic motifs such as motif 2 (2), motif 3 (1), motif 10 (1) and motif 14 (2).

Of the remaining 10 structures, 5 are sterically unable to form the *bidentate* motif. In these structures the molecules are linked by single NH···OS hydrogen bonds in four cases, and motif 2 in one case. Of the other 5 cases, 3 show the *bidentate* motif, and 2 structures contain a urea functionality, which forms the well-known urea hydrogen-bonding motif.

3.2.3. NH_4^+- and NH_3^+-containing structures. Once the structures containing H_xNXNH_x have been eliminated from the sample of 594 NH-containing sulfonates, 402 structures remain. We now discuss the 165 which contain only N-donors, and no O-donors.

8 structures contain NH_4^+. 6 of these structures contain no other N-donors, and the structures form layers of NH_4^+ and SO_3^- ions in an analogous manner to the guanidinium salts (see above). These layers are formed from ladders of various cyclic motifs (Fig. 7).

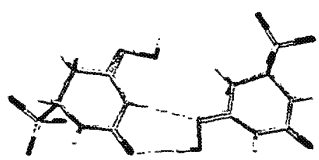


Fig. 6 Hydrogen bonding motif seen in BIFBOH.

NOVARTIS EXHIBIT 1017
Novartis v. Regents, IPR2023-01346
Page 2524 of 4460

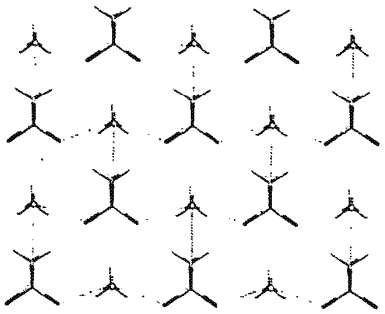


Fig. 7 Layers of ions in FASJUE.

30 structures contain NH_3^+. Of these, 15 have no other N-donors, and once again layers of NH_3^+ and SO_3^- are formed. 10 structures contain other N-donors, and of these 9 structures show motif 2. In 6 of the 10 structures, there is some type of extended motif such as ladders or chains of motifs. However, as the complexity of the molecule increases, the degree of extended pattern formation decreases. The 5 remaining NH_3^+-containing structures have O atoms (for example, in crown ethers) that accept hydrogen bonds from NH.

44 structures contain only NH_2 groups as hydrogen bond donors, and 83 have only NH groups. Very few of these structures show any motifs more complex than simple chains of hydrogen bonds, $NH_2\cdots SO_3^-\cdots NH_2\cdots SO_3^-$.

3.3. Structures containing only water as a donor

96 of the 1069 SO_3-containing structures have water as the only hydrogen-bond donor present in the structure. Approximately 47% of these structures are alkali or alkaline earth metal salts (see above), and in *ca.* 24% of the structures the cation is the oxonium ion (H_3O^+). Many of the hydrogen bonding motifs and patterns (ladders of motif 2, *etc.*) seen in the oxonium salts are similar to those seen in the ammonium salts. The oxonium salts are also similar to the ammonium salts in that often nets of ions form, separated by interstitial hydrophobic regions (Fig. 8). In fact, this separation of hydrophilic and hydrophobic regions into layers is characteristic of CSD structures where water is the only strong hydrogen-bond donor.

3.4. Prediction of the *bidentate* motif

Using the information described above, a set of rules have been developed for predicting the occurrence of the *bidentate* motif in sulfonate salts. These have then been tested against new structures added to the database since the collection of the 1069 sample. The rules, which apply in cases where the groups are sterically able to form the *bidentate* motif (*i.e.* not *trans* to one another) are as follows:

(i) All guanidinium sulfonate salts will show the *bidentate* motif, with the exception of those containing two or more strongly electron-withdrawing groups (NO_2, CF_3, CN) on the same molecule as the sulfonate group.

(ii) Sulfonate salts with no guanidinium cation, but containing an H_xNXNH_x group, will show the *bidentate* motif, with the exception of structures where X is C=O or C=OH, in which case there will be strong competition for the formation of the *bidentate* motif. However, the O···N distance in the motif may be greater than 3.2 Å.

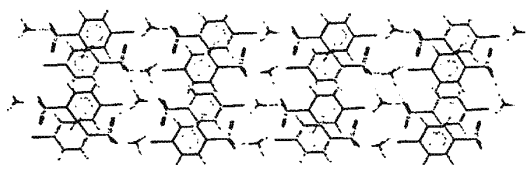


Fig. 8 'Hydrophilic' and 'hydrophobic' layers seen in JEHPAN.

Searching version 5.25 of the CSD, plus 1 update (January 2004) gave 20 new structures that contained $R\text{–}SO_3^-$ and an H_xNXNH_x group. 13 of these are guanidinium salts, and it was predicted that all of these salts would exhibit the *bidentate* motif. In fact, 1 salt (OFOXAI) does not exhibit the *bidentate* motif. This could perhaps be rationalised by examining the electrostatic potential of this sulfonate ion. Of the remaining 7 structures, 2 were sterically unable to form the *bidentate* motif (MOTCON and WUYRUD), and so were removed from this analysis, leaving 5 structures. According to rule 2 above, all of these structures should contain the bidentate motif. In fact, only 1 structure (LUHWOA) does not show this motif.

4. Conclusions

This work describes the analysis of hydrogen bonding motifs formed in sulfonate salts, particularly with nitrogen donors. The robust nature of a particular R2,2(8) motif,[11] here called the *bidentate* motif, has been confirmed. It has been shown that certain functional groups will compete with HNXNH for the formation of this motif, particularly groups containing C=O or C–OH, and that certain motifs may form in favour of this motif, for example the urea hydrogen bonding motif. However, the *bidentate* motif can be predicted to occur with a fair degree of confidence.

Other cyclic motifs formed between the $R\text{–}SO_3^-$ functionality and nitrogen donors have been described, and their occurrence noted. The nature of the functional groups involved obviously affects the motif that is seen in the structure. Extended networks of motifs have also been described. Guanidinium sulfonate salts are extremely likely to form extended motifs made up of ribbons of the *bidentate* motif, whereas NH_4^+ and NH_3^+-containing sulfonate salts are more likely to form nets made up of ladders of motifs 1–5.

Acknowledgements

Discussions with Dr Neil Feeder and Dr Pete Marshall are appreciated. We also thank the Pfizer Institute for Pharmaceutical Materials Science for funding.

References

1 L. D. Bighley, S. M. Berge and D. C. Monkhouse, *Encyclopaedia of Pharmaceutical Technology Volume 13*, ed. J. Swarbrick and J. C. Boylan, Marcel Dekker Inc., New York, 1996, 453.
2 P. J. Gould, *Int. J. Pharm.*, 1986, 33, 201.
3 See for example, *Handbook of Pharmaceutical Salts*, ed. P. H. Stahl and C. G. Wermuth, Wiley-VCH, Weinheim, 2002.
4 L. Chertanova and C. Pascard, *Acta Crystallogr., Sect. B*, 1996, 52, 677.
5 B. Pirard, G. Baudoux and F. Durant, *Acta Crystallogr., Sect. B*, 1995, 51, 103.
6 F. H. Allen, *Acta Crystallogr., Sect. B*, 2002, 58, 380; I. J. Bruno, J. C. Cole, P. R. Edgington, M. Kessler, C. F. Macrae, P. McCabe, J. Pearson and R. Taylor, *Acta Crystallogr., Sect. B*, 2002, 58, 389.
7 F. H. Allen and W. D. S. Motherwell, *Acta Crystallogr., Sect. B*, 2002, 58, 407.
8 A. Nangia, *CrystEngComm*, 2002, 4, 93.
9 L. Infantes and W. D. S. Motherwell, *Chem. Commun.*, 2004, 1166.
10 L. Infantes, J. Chisholm and S. Motherwell, *CrystEngComm*, 2003, 5, 480.
11 F. H. Allen, P. R. Raithby, G. P. Shields and R. Taylor, *Chem. Commun.*, 1998, 1043.
12 J. A. Chisholm and S. Motherwell, *J. Appl. Crystallogr.*, 2004, 37, 331.
13 See for example, V. A. Russell and M. D. Ward, *J. Mater. Chem.*, 1997, 7, 1123 K; T. Holman, A. M. Pivovar and M. D. Ward, *Science (Washington, D. C.)*, 2001, 294, 1907.

UM00013779
NOVARTIS EXHIBIT 1017
Novartis v. Regents, IPR2023-01346
Page 2525 of 4460

This Page is Inserted by IFW Indexing and Scanning Operations and is not part of the Official Record

BEST AVAILABLE IMAGES

Defective images within this document are accurate representations of the original documents submitted by the applicant.

Defects in the images include but are not limited to the items checked:

- ❑ BLACK BORDERS
- ❑ IMAGE CUT OFF AT TOP, BOTTOM OR SIDES
- ❑ FADED TEXT OR DRAWING
- ❑ BLURRED OR ILLEGIBLE TEXT OR DRAWING
- ❑ SKEWED/SLANTED IMAGES
- ❑ COLOR OR BLACK AND WHITE PHOTOGRAPHS
- ❑ GRAY SCALE DOCUMENTS
- ❑ LINES OR MARKS ON ORIGINAL DOCUMENT
- ❑ REFERENCE(S) OR EXHIBIT(S) SUBMITTED ARE POOR QUALITY
- ❑ OTHER: _____

IMAGES ARE BEST AVAILABLE COPY.
As rescanning these documents will not correct the image problems checked, please do not report these problems to the IFW Image Problem Mailbox.

Acta Crystallographica Section C
Crystal Structure Communications
ISSN 0108-2701

1:1 Hetero-assembly of 2-amino-pyrimidine and (+)-camphoric acid

Shyamaprosad Goswami,[a] Reshmi Mukherjee,[a] Kumaresh Ghosh,[a] Ibrahim Abdul Razak,[b] S. Shanmuga Sundara Raj[b] and Hoong-Kun Fun[b]*

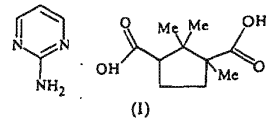
[a]Department of Chemistry, Bengal Engineering College, Botanic Garden, Howrah 711103, India, and [b]X-ray Crystallography Unit, School of Physics, Universiti Sains Malaysia, 11800 USM, Penang, Malaysia
Correspondence e-mail: hkfun@usm.my

Received 26 October 1999
Accepted 17 January 2000

In the title cocrystal, 2-aminopyrimidine–(+)-camphoric acid (1/1), $C_4H_5N_3{\cdot}C_{10}H_{16}O_4$, the 2-aminopyrimidine forms two eight-membered hydrogen-bonded rings with two different camphoric acid molecules. This results in infinite wave-like chains of molecules in which neighbouring chains are connected by weak C—H···O contacts. The five-membered ring in the acid molecule adopts a half-chair conformation.

Comment

Because of their strength as well as directional nature compared with other intermolecular non-covalent interactions (Lehn, 1995), hydrogen bonds are normally used as a tool in designing the structure of molecular crystals. Weak C—H···O contacts play a significant role in determining the molecular packing of organic solids (Taylor & Kennard, 1982). The crystal structure of 2-aminopyrimidine itself has been reported previously (Scheinbeim & Schempp, 1976; Furberg *et al.*, 1979) and both of the pyrimidine-ring N atoms and the amine group form eight-membered rings which leads to hydrogen-bonded self-assembly. The pattern can be changed to a hetero-assembled structure where the donors (acid OH) are paired with the acceptors (ring N) (Etter *et al.*, 1990). This communication reports the structure of the hydrogen-bonded heterodimer of 2-aminopyrimidine with camphoric acid, (I), where the 2-aminopyrimidine is hydrogen-bonded with the camphoric acid moiety to form typical eight-membered rings.



(I)

The bond lengths and bond angles of the 2-amino-pyrimidine and the camphoric acid molecules are comparable with the reported values (Etter *et al.*, 1990; Furberg *et al.*, 1979; Barnes *et al.*, 1991). The five-membered ring of the acid molecule adopts a half-chair conformation, as observed in *trans*-π-camphanic acid (Hudson & Mills, 1972), with δC_2(C3) = 0.007 (2) Å (Nardelli, 1983). The twofold axis passes through C3 and intersects the C1—C5 bond. Atoms C1 and C5 deviate from the mean plane defined by the atoms C2, C3 and C4 by 0.316 (5) and −0.376 (5) Å, respectively.

In the crystal (Fig. 1), each acid molecule is linked to two 2-aminopyrimidine molecules and *vice versa* by N—H···O and O—H···N intermolecular hydrogen bonds to form two symmetry-independent eight-membered rings each of which has the graph-set motif of $R_2^2(8)$ (Bernstein *et al.*, 1995). The eight-membered ring formed between the two moieties belonging to the same asymmetric unit (*i.e.* that ring involving N2 and O2) is almost planar with a maximum deviation from the plane of 0.111 (4) Å for O1. The second eight-membered ring, which contains O4 and N1^{i} [symmetry code: (i) $\frac{3}{2}-x, 1-y, z-\frac{1}{2}$], is more twisted with the angle between the two four-atom planes defined by the acid and amine moieties being

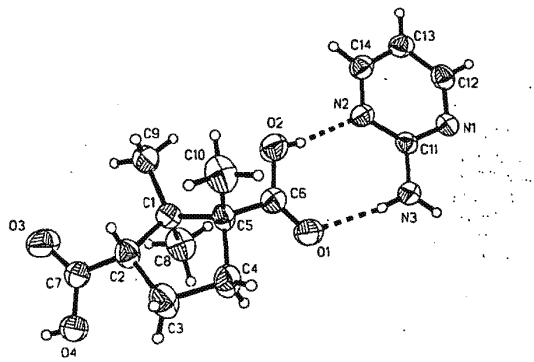


Figure 1
The structure of the title compound showing 30% probability displacement ellipsoids and the atom-numbering scheme.

23.8 (4)°. The maximum deviation from the mean ring plane is 0.321 (5) Å for O3. The mean plane through the five-membered ring in the acid molecule makes dihedral angles of 33.9 (2) and 38.3 (2)°, respectively, with the two adjacent pyrimidine rings described above. These hydrogen bonds thereby link the acid and amine moieties into infinite wave-like chains which extend parallel to the *c* axis (Fig. 2). The crystal structure is also characterized by alternate layers of camphoric acid and 2-aminopyrimidine molecules which lie parallel to the *ab* plane. This pattern has also been reported by De Santis *et al.* (1997). The neighbouring chains are interconnected by weak C—H···O interactions (Table 1) and are stacked along the *b* axis with C—H···π interactions involving the 2-aminopyrimidine molecules of 3.602 Å [C13—H13*A* = 0.93, H13*A*—*Cg*($-\frac{1}{2}+x, \frac{3}{2}-y, 1-z$) = 2.893 Å and C13—H13*A*···*Cg*($-\frac{1}{2}+x, \frac{3}{2}-y, 1-z$) = 134° (*Cg* = centroid of pyrimidine ring)].

 © 2000 International Union of Crystallography · Printed in Great Britain – all rights reserved

UM00013781
NOVARTIS EXHIBIT 1017
Novartis v. Regents, IPR2023-01346
Page 2527 of 4460

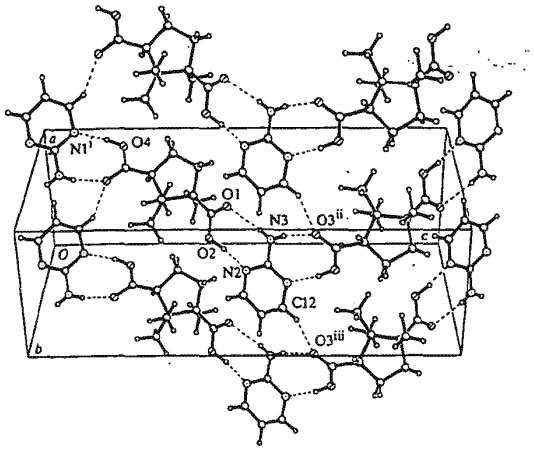


Figure 2
The C—H···O interactions connecting neighbouring chains. The symmetry operators are given in Table 1.

Experimental

Single crystals of (I) were grown by evaporation of a 1:1 mixture of 2-aminopyrimidine and (1*R*,3*S*)-(+)-camphoric acid in ethanol.

Crystal data

$C_4H_5N_3{\cdot}C_{10}H_{16}O_4$
M_r = 295.34
Orthorhombic, $P2_12_12_1$
a = 7.146 (1) Å
b = 10.561 (1) Å
c = 21.306 (1) Å
V = 1607.9 (3) Å^3
Z = 4
D_x = 1.220 Mg m^{-3}
Mo $K\alpha$ radiation
Cell parameters from 2297 reflections
θ = 1.91–28.33°
μ = 0.090 mm^{-1}
T = 293 (2) K
Needle, colourless
0.36 × 0.16 × 0.12 mm

Data collection

Siemens SMART CCD area-detector diffractometer
ω scans
8732 measured reflections
2837 independent reflections
1522 reflections with $I > 2\sigma(I)$
R_{int} = 0.066
θ_{max} = 25.01°
$h = -7 \rightarrow 8$
$k = -12 \rightarrow 12$
$l = -23 \rightarrow 25$

Refinement

Refinement on F^2
$R[F^2 > 2\sigma(F^2)]$ = 0.065
$wR(F^2)$ = 0.159
S = 1.05
2837 reflections
190 parameters
H atoms constrained
$w = 1/[\sigma^2(F_o^2) + (0.0551P)^2 + 0.2628P]$ where $P = (F_o^2 + 2F_c^2)/3$
$(\Delta/\sigma)_{max} < 0.001$
$\Delta\rho_{max}$ = 0.15 e Å^{-3}
$\Delta\rho_{min}$ = −0.15 e Å^{-3}

Table 1
Hydrogen-bonding geometry (Å, °).

D—H···A	D—H	H···A	D···A	D—H···A
O2—H2*B*···N2	0.82	1.87	2.665 (5)	163
O4—H4*C*···N1^{i}	0.82	1.90	2.713 (4)	170
N3—H3*D*···O1	0.86	2.06	2.910 (5)	170
N3—H3*C*···O3^{ii}	0.86	2.13	2.951 (5)	161
C12—H12*A*···O3^{iii}	0.93	2.59	3.221 (6)	125

Symmetry codes: (i) $\frac{1}{2}-x, 1-y, z-\frac{1}{2}$; (ii) $\frac{1}{2}-x, 1-y, \frac{1}{2}+z$; (iii) $\frac{1}{2}-x, 1-y, \frac{1}{2}+z$.

After checking their presence in the difference map, the positions of all H atoms were geometrically idealized and allowed to ride on their parent atoms.

Data collection: *SMART* (Siemens, 1996); cell refinement: *SAINT* (Siemens, 1996); data reduction: *SAINT*; program(s) used to solve structure: *SHELXTL* (Sheldrick, 1997); program(s) used to refine structure: *SHELXTL*; molecular graphics: *SHELXTL*; software used to prepare material for publication: *SHELXTL* and *PARST* (Nardelli, 1995).

The authors would like to thank the Malaysian Government and Universiti Sains Malaysia for research grant R & D No. 305/PFIZIK/622004. SSSR thanks the Universiti Sains Malaysia for a Visiting Postdoctoral Fellowship.

Supplementary data for this paper are available from the IUCr electronic archives (Reference: LN1090). Services for accessing these data are described at the back of the journal.

References

Barnes, J. C., Paton, J. D., Blyth, C. S. & Howie, R. A. (1991). *Acta Cryst.* C47, 1888–1892.
Bernstein, J., Davis, R. E., Shimoni, L. & Chang, N.-L. (1995). *Angew. Chem. Int. Ed. Engl.* 34, 1555–1573.
De Santis, P., Camalli, M., Spagna, R., Gallo, G., Giorgi, F. & Tinti, M. O. (1997). *Acta Cryst.* C53, 1679–1682.
Etter, M. C., Adsmond, D. A. & Britton, D. (1990). *Acta Cryst.* C46, 933–934.
Furberg, S., Grøgaard, J. & Smedsrud, B. (1979). *Acta Chem. Scand. Ser. B*, 33, 715–724.
Hudson, D. W. & Mills, O. S. (1972). *Chem. Commun.* pp. 647–648.
Lehn, J. M. (1995). *Supramolecular Chemistry*, edited by U. Anton, pp. 1–171. New York: VCH.
Nardelli, M. (1983). *Acta Cryst.* C39, 1141–1142.
Nardelli, M. (1995). *J. Appl. Cryst.* 28, 659.
Scheinbeim, J. & Schempp, E. (1976). *Acta Cryst.* B32, 607–609.
Sheldrick, G. M. (1997). *SHELXTL*. Version 5.10. Bruker AXS Inc., Madison, Wisconsin, USA.
Siemens (1996). *SMART* and *SAINT*. Siemens Analytical X-ray Instruments Inc., Madison, Wisconsin, USA.
Taylor, R. & Kennard, O. (1982). *J. Am. Chem. Soc.* 104, 5063–5070.

UM00013782
NOVARTIS EXHIBIT 1017
Novartis v. Regents, IPR2023-01346
Page 2528 of 4460

This Page is Inserted by IFW Indexing and Scanning Operations and is not part of the Official Record

BEST AVAILABLE IMAGES

Defective images within this document are accurate representations of the original documents submitted by the applicant.

Defects in the images include but are not limited to the items checked:

- ☐ BLACK BORDERS
- ☐ IMAGE CUT OFF AT TOP, BOTTOM OR SIDES
- ☐ FADED TEXT OR DRAWING
- ☐ BLURRED OR ILLEGIBLE TEXT OR DRAWING
- ☐ SKEWED/SLANTED IMAGES
- ☐ COLOR OR BLACK AND WHITE PHOTOGRAPHS
- ☐ GRAY SCALE DOCUMENTS
- ☐ LINES OR MARKS ON ORIGINAL DOCUMENT
- ☐ REFERENCE(S) OR EXHIBIT(S) SUBMITTED ARE POOR QUALITY
- ☐ OTHER: _____

IMAGES ARE BEST AVAILABLE COPY.
As rescanning these documents will not correct the image problems checked, please do not report these problems to the IFW Image Problem Mailbox.

SUPRAMOLECULAR CHEMISTRY, Vol. 11, pp. 25 - 33
Reprints available directly from the publisher
Photocopying permitted by license only

© 1999 OPA (Overseas Publishers Association) N.V.
Published by license under
the Gordon and Breach Science
Publishers imprint.
Printed in Malaysia.

Molecular Recognition Induced Supramolecular Array of 2-Aminopyrimidine with Terephthalic Acid, 1,4-Phenylenediacetic Acid and Fumaric Acid in Solid State *via* H-bonding and π-stacking Interactions*

SHYAMAPROSAD GOSWAMI† and AJIT KUMAR MAHAPATRA

Department of Chemistry, Bengal Engineering College (Deemed University), Howrah-711 103, India

(Received 8 October 1998; In final form 11 January 1999)

The crystal structures of molecular complexes of 2-aminopyrimidine (2AP) with terephthalic acid (1) (1:1; Complex A), 1,4-phenylenediacetic acid (2) (1:1; Complex B) and fumaric acid (3) (1:2; Complex C) were determined. Complex A is orthorhombic, space group Pnma, with $a = 13.0323(3)$, $b = 23.9443(1)$, $c = 3.7927(1)$ Å; $\alpha = \beta = \gamma = 90^\circ$; $Z = 4$; $D_{calc} = 1.466$ Mg/m^3; final $R = 0.0384$, $wR^2 = 0.0939$ for 1381 independent reflections. Complex B is orthorhombic, space group Pbcn with $a = 4.5686(1)$, $b = 15.7687(2)$, $c = 20.1621(4)$ Å; $\alpha = \beta = \gamma = 90^\circ$; $Z = 4$; $D_{calc} = 1.323$ Mg/m^3; final $R = 0.0461$, $wR^2 = 0.1158$ for 1662 independent reflections. Complex C is monoclinic, space group $P2_1/c$ with $a = 3.7946(2)$, $b = 19.1766(7)$, $c = 13.0641(6)$ Å; $\alpha = 90^\circ$, $\beta = 96.893(1)^\circ$, $\gamma = 90^\circ$; $Z = 4$; $D_{calc} = 1.486$ Mg/m^3; final $R = 0.0665$, $wR^2 = 0.1626$ for 2752 independent reflections. 2AP generates supramolecular assembly with 2 and 3 *via* non-conventional weak C-H—O hydrogen bonding. Interestingly only in the case of Complex C, proton transfer occurs to the ring nitrogen of 2AP from 3. A novel hydrogen-bonding motif for the control of solid-state structures has been developed. The motif is based on the hydrogen bonding complementarity of dicarboxylic acids with 2AP.

Keywords: Molecular recognition, hydrogen bonding, π-stacking and molecular hetero-assembly

INTRODUCTION

Molecular self-assembly is the spontaneous association of molecules under equilibrium conditions into stable aggregates, joined by noncovalent bonds, with well defined composition and structure [1]. Careful choice of complementary binding groups will lead not only to strong but also discriminating interaction in the solid state. Most of the supramolecular crystals are originated from conventional, strong N-H—X and O-H—X (X = O, N) hydrogen bonds. The weak hydrogen bonds such as C-H—O [2] and C-H—N [3] are known to play a significant role in the determining the molecular packing of organic solids. In continuation

* Dedicated to J.-M. Lehn, D. J. Cram and C. J. Pedersen for their contribution in the opening up of Molecular Chemistry into the Intermolecular Science of life and materials.

†Corresponding author.

UM00013784
NOVARTIS EXHIBIT 1017
Novartis v. Regents, IPR2023-01346
Page 2530 of 4460

of our research interest in molecular recognition studies on dicarboxylic acids [4], we report here the crystal structures of some interesting molecular complexes of 2AP with terephthalic acid, 1,4-phenylenediacetic acid and fumaric acid respectively.

2AP has two equivalent proton donors and two equivalent proton acceptors [5] available for hydrogen bonding with neighbouring molecules. Hetero-assembly with 2AP could be prepared by the addition of a dicarboxylic acid guest that forms preferentially hydrogen bonds with 2AP rather than forming self-assembled [6, 7] hydrogen bonds and they form cyclic hydrogen bonded dimers like 2AP [6]. The crystal structures of 2AP with succinic acid [8] and terephthalic acid [9] have been reported, but in both cases C-H—O hydrogen bondings were not observed to form a supramolecular hydrogen bonding array though succinic acid contains α-hydrogens. The goal of this co-crystal structural study was to investigate the ability of 2AP in the formation of different hydrogen bonding pattern with different dicarboxylic acids although the basic hydrogen bonding units are same.

RESULTS AND DISCUSSION

Complex A

Terephthalic acid typically associates with 2-aminopyrimidine by N-H—O and O-H—N hydrogen bonds through the formation of eight-membered hydrogen bonded rings (Fig. 1). The acid molecule (within $\pm 0.028(1)$ Å) makes a dihedral angle of 22.34(6)° with the planar pyrimidine ring. These heterodimers form hydrogen-bonded zig-zag chains extended along [010] axis (Fig. 2).

The pyrimidine and benzene rings are stacked independently along [001] axis (Fig. 3) with N1-C2 $(x, y, z+1)$ 3.364 (2) Å being the shortest contacts for the pyrimidine rings and C5—C6 $(x, y, z+1)$ 3.513 (2) Å for the benzene rings respectively.

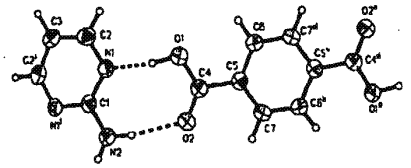


FIGURE 1 ORTEP diagram of complex A showing displacement ellipsoids at the 50% probability level.

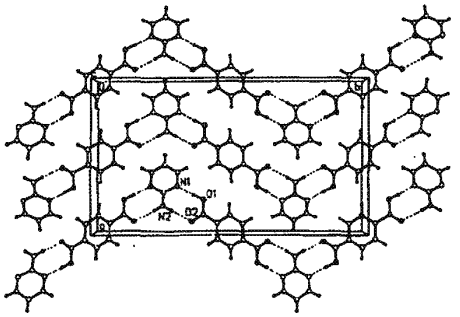


FIGURE 2 Hydrogen bonding network in crystal lattice of complex A.

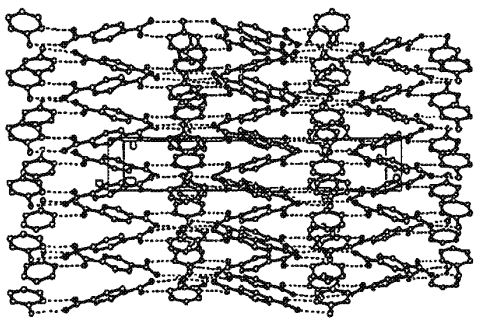


FIGURE 3 Supramolecular array of complex A showing stacking mode along (001) axis.

The bond lengths and bond angles observed in the molecules of the co-crystal agree with those observed in the independent crystal structures [10].

UM00013785
NOVARTIS EXHIBIT 1017
Novartis v. Regents, IPR2023-01346
Page 2531 of 4460

Complex B

The asymmetric unit contains one-half molecule for each 2-aminopyrimidine and 1,4-phenylenediacetic acid with other-half being symmetry related (Fig. 4). 2-Aminopyrimidine is related by a crystallographic two-fold axis passing through the atoms N2, C6 and C8 whereas 1,4-phenylenediacetic acid is inversion related. The carboxylic acid group (O1, O2, C4 and C5) makes a dihedral angle of 77.54(8)° with the phenyl ring.

The planar 2-aminopyrimidine molecule is linked to the 1,4-phenylenediacetic acid by N-H—O and O-H—N intermolecular hydrogen bonds (N2-H1N2 0.91(2), H1N2—O1 2.02(2), N2-O1 2.921(2)Å, N2-H1N2—O1 174(2)Å; O2-H1O2 1.04(3), H1O2—N1 1.65(3), O2—N1 2.676(2)Å, O2-H1O2—N1 172(2)Å. The donor and acceptor atoms in these hydrogen bonds along with C5 and C6 form a eight-membered ring which is coplanar with the pyrimidine moiety. Since these molecules lie across the crystallographic symmetry elements they form an infinite wave like chain in the solid state.

The chains translated one unit along [100] axis are linked by weak C-H—O contacts involving C4 and O1(C4-H4A 1.00(3), H4A—O1 2.56(3), C4A—O1 3.541(3)A, C4-H4A—O1 167(2)°. The pyrimidine and phenyl rings translated one unit along [100] axis are stacked (Fig. 5) with perpendicular distances of 3.605 and 3.614Å, respectively. The line joining the centroids of adjacent rings form angles of 37.91° and 37.72° respectively with the normal to the planes. Thus benzylic hydrogens of the acid molecule of one layer are linked to carboxylic carbonyl oxygen

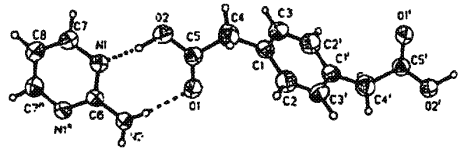


FIGURE 4 ORTEP diagram of complex B showing displacement ellipsoids at the 50% probability level.

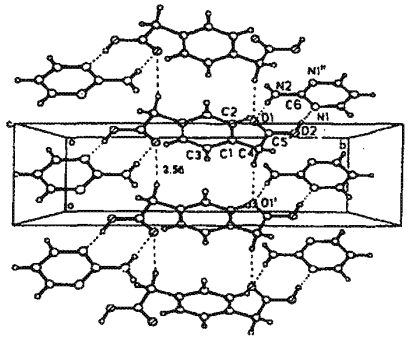


FIGURE 5 Interlayer Hydrogen bondings through C-H—O of complex B.

atoms of another layer through hydrogen bonds in the crystal sheet and thus results a three point fixation [11] of carboxylic acid motif in the complex.

Complex C

The asymmetric unit contains a molecule of 2-aminopyrimidine and half molecule each of two fumaric acids (Fig. 6). The 2-amino pyrimidine is protonated at the N2 position which is transferred from one of the fumaric acid (all the hydrogen atoms were located from a difference Fourier map and no sign of any peak was seen near the O4 atom). Proton transfer is also corroborated from the ^{1}H NMR spectrum [12] (a broad signal appeared at δ 8.19 for ring N-H) of the complex crystal.

In complex C (Fig. 6), O4 makes two hydrogen bonds with N2-H (due to proton transfer from carboxylic group to ring N of 2AP) and O2-H of another formic acid molecule. Thus the charge density on O4 atom of carboxylate group is partially shared by these two hydrogen bonds showing the unequal bond distances in carboxylate group. The fumaric acid molecules form a dihedral angle of 12.51(8)° between them and they make dihedral angles of 27.66(9) and 16.74(9)° with the 2-aminopyrimidine.

UM00013786
NOVARTIS EXHIBIT 1017
Novartis v. Regents, IPR2023-01346
Page 2532 of 4460

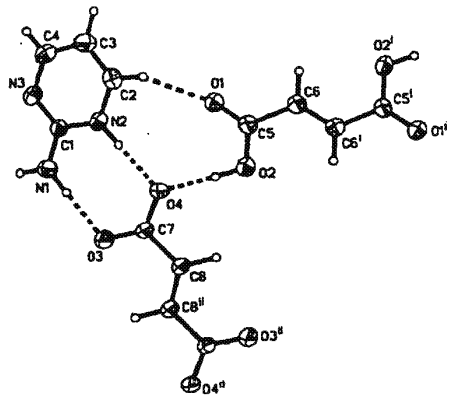


FIGURE 6 ORTEP diagram of complex C showing displacement ellipsoids at the 50% probability level.

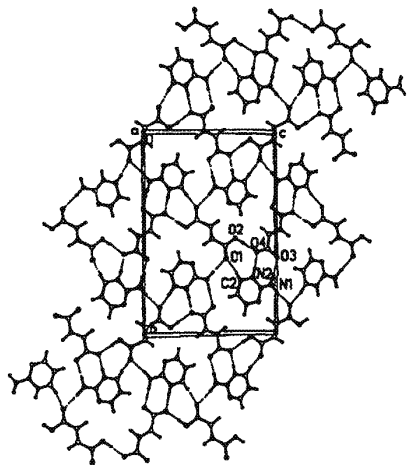


FIGURE 7 Hydrogen bonding network of Complex C.

The contents of the asymmetric unit are linked by two N-H—O, one O-H—O and one very weak C-H—O hydrogen bonds. In the solid state they extend along (010) axis to form an infinite plane wave like structure. The adjacent wave-like structures are linked by a network of N-H—O and weak C-H—O intermolecular hydrogen bonds to form a supramolecular structure (Fig. 7). The 2-amino pyridimine and both acid molecules translated along [100] axis are stacked (Fig. 8) as individual columns.

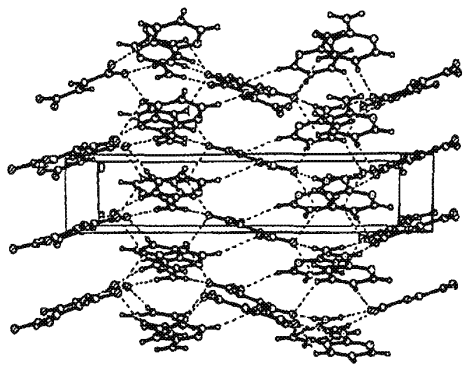


FIGURE 8 Column like stacked H-bonding network of Complex C.

EXPERIMENTAL

General: Melting points were recorded (uncorrected) in open capillaries with a hot-stage apparatus (Toshniwal). IR spectra were recorded on a PERKIN-ELMER, MODEL No. 883, spectral bands are reported in cm^{-1}. Proton NMR (200 MHz) spectra were measured with a BRUKER AM-200 spectrometer; chemical shifts are expressed in ppm down field from internal Me_4Si. Elemental analysis was carried out in the Microanalytical Laboratory of Indian Association for the Cultivation of Science, Calcutta. Solvents were purified and dried in the usual manner before use.

Synthesis

Complex A

Single crystal was grown by slow evaporation of 5:1 mixture of a dry acetone and methanol solution of the 2-aminopyrimidine and terephthalic acid (1:1 mol. ratio). MP : 192°C. IR(KBr) cm^{-1}: 3369, 3322, 3199, 2436, 1672, 1289; ^1H NMR (200 MHz $CDCl_3$): δ8.27 (d, 2H, J = 6 Hz), 8.09 (bs, 4H), 6.59 (t, 1H, J =

UM00013787
NOVARTIS EXHIBIT 1017
Novartis v. Regents, IPR2023-01346
Page 2533 of 4460

6 Hz), 4.73 (bs, 2H, $-NH_2$); Anal. Calcd. for C12H11N3O4; C, 55.17; H, 4.24; N, 16.09%. Found: C, 55.18; H, 4.28; N, 16.14%.

Complex B

The complex B was prepared by mixing 2-aminopyrimidine with 1,4-phenylenediacetic acid (1 : 1) in dry acetone. The resulting solution was allowed to evaporate at rt to give the desired crystals, MP 154°C.

IR (KBr) cm^{-1}: 3384, 3332, 2455, 1904, 1695, 1566, 1341, 1243; ^1H NMR (200 MHz, $CDCl_3$): δ 8.19 (d, 2H, J = 6 Hz), 7.19 (s, 4H), 6.53 (t, 1H, J = 6 Hz), 5.49 (bs, 2H, $-NH_2$), 3.52 (s, 4H); Anal. Calcd. for C14H15N3O4: C, 58.13; H, 5.23; N, 14.53%. Found: C, 58.21; H, 5.32; N, 14.49%.

Complex C

The Complex C was grown by slow evaporation of 3:1 mixture of dry acetone and methanol solution of the 2-aminopyrimidine and fumaric acid (1:1 mol ratio). Colourless slab crystals of the complex appeared which was suitable for X-ray study. MP: 180–182°C.

IR (KBr) cm^{-1}: 3248, 2930, 1664, 1430, 1362, 1294, 1234; ^1H NMR (200 MHz $CDCl_3$): δ 8.19 [bs, 1H, (ring −NH)], 8.04 (d, 2H, J = 6 Hz), 6.56 (t, 2H, J = 6 Hz), 6.36 (d, 2H, J = 9.6 Hz), 4.71 (bs, 2H, $-NH_2$). Anal. Calcd. for C8H9N3O4: C, 45.50; H, 4.29; N, 19.89%. Found: C, 45.59; H, 4.27; N, 19.91%.

Experimental conditions are summarized in Table I. Positional and thermal parameters for non-hydrogen atoms are listed in Table II. Bond distances and bond angles are contained in Table III and the hydrogen bond data are listed in Table IV.

X-ray Structure Analysis

Data were collected on a SMART CCD area detector diffractometer using graphite monochromated MoK_α radiation ($\lambda = 0.71073$ Å) with

TABLE I Crystal data and structure refinement for complex A, complex B and complex C

Complex	A	B	C
Empirical formula	C12H11N3O4	C14H15N3O4	C8H9N3O4
Formula weight	261.24	289.29	211.18
Wavelength, Å	0.71073	0.71073	0.71073
Crystal system	Orthorhombic	Orthorhombic	Monoclinic
Space group	Pnma	Pbcn	$P2_1/c$
Unit cell dimensions (Å):			
a	13.0323 (3)	4.5686 (1)	3.7946 (2)
b	23.9443 (1)	15.7687 (2)	19.1766 (7)
c	3.7927 (1)	20.1621 (4)	13.0641 (6)
α	90°	90°	90°
β	90°	90°	96.893°
γ	90°	90°	90°
Volume (Å^3)	1183.51 (4)	1452.50 (5)	943.77 (7)
Z	4	4	4
Density (calculated)	1.466 Mg/m^3	1.323 Mg/m^3	1.486 Mg/m^3
Absorption coefficient (mm^{-1})	0.113	0.099	0.121
F(000)	544	608	440
Reflections collected	6833	8468	7257
Independent reflections	1381 [*R*(int) = 0.0280]	1662 [*R* (int) = 0.0287]	2752 [*R*(int) = 0.0417]
Refinement method	Full-matrix least-squares	Full-matrix least-squares	Full-matrix least-squares
Goodness-of-fit on F^2	1.073	1.078	1.055
Final *R* indices [$I > 2$ sigma(I)]	$R1 = 0.0384$, $wR^2 = 0.0939$	$R1 = 0.0461$, $wR^2 = 0.1158$	$R1 = 0.0665$, $wR^2 = 0.1626$
R indices (all data)	$R1 = 0.0532$, $wR^2 =$	$R1 = 0.0716$, $wR^2 = 0.1355$	$R1 = 0.1031$, $wR^2 = 0.1836$
Largest diff. peak and hole	0.175 and −0.140 e.A^{-3}	0.118 and −0.094 e.A^{-3}	0.387 and −0.227 e.A^{-3}

UM00013788

NOVARTIS EXHIBIT 1017
Novartis v. Regents, IPR2023-01346
Page 2534 of 4460

TABLE II Atomic coordinates ($\times 10^4$) and equivalent isotropic parameters ($A^2 \times 10^3$). U_{eq} is defined as one third of the trace of the orthogonalised U_{ij} tensor

Atoms	x	y	z	U(eq)
		Complex A		
O (1)	7904 (1)	3995 (1)	107 (4)	53 (1)
O (2)	9270 (1)	3576 (1)	2425 (4)	60 (1)
N (1)	6965 (1)	3000 (1)	88 (3)	37 (1)
N (2)	8256 (1)	2500	2775 (5)	41 (1)
C (1)	7382 (1)	2500	938 (5)	33 (1)
C (2)	6066 (1)	2988 (1)	-1596 (4)	41 (1)
C (3)	5570 (2)	2500	-2456 (6)	44 (1)
C (4)	8868 (1)	3983 (1)	1118 (4)	40 (1)
C (5)	9940 (1)	4514 (1)	523 (4)	36 (1)
C (6)	8965 (1)	4986 (1)	-863 (4)	40 (1)
C (7)	10478 (1)	4531 (1)	1378 (4)	40 (1)
		Complex B		
O (1)	-1401 (3)	6495 (1)	3543 (1)	96 (1)
O (2)	-10 (3)	7763 (1)	3885 (1)	96 (1)
N (1)	-3388 (3)	8492 (1)	2963 (1)	76 (1)
N (2)	-5000	7247 (2)	2500	90 (1)
C (1)	970 (4)	5770 (1)	4733 (1)	69 (1)
C (2)	1813 (5)	5006 (1)	4470 (1)	89 (1)
C (3)	-850 (5)	5751 (1)	5268 (1)	87 (1)
C (4)	1966 (5)	6603 (2)	4448 (1)	93 (1)
C (5)	16 (4)	6939 (1)	3912 (1)	72 (1)
C (6)	-5000	8091 (2)	2500	68 (1)
C (7)	-3460 (5)	9338 (1)	2954 (1)	87 (1)
C (8)	-5000	9794 (2)	2500	93 (1)
		Complex C		
O (1)	1905 (6)	6291 (1)	6139 (1)	54 (1)
O (2)	801 (6)	5292 (1)	6887 (1)	55 (1)
O (3)	1719 (6)	6273 (1)	10140 (1)	53 (1)
O (4)	2351 (5)	6016 (1)	8517 (1)	47 (1)
N (1)	3200 (6)	7655 (1)	9664 (2)	42 (1)
N (2)	5257 (5)	7271 (1)	8169 (1)	33 (1)
N (3)	5203 (6)	8471 (1)	8576 (1)	40 (1)
C (1)	4566 (6)	7800 (1)	8804 (2)	31 (1)
C (2)	6686 (6)	7399 (1)	7289 (2)	37 (1)
C (3)	7389 (7)	8069 (1)	7026 (2)	42 (1)
C (4)	6561 (7)	8588 (1)	7704 (2)	43 (1)
C (5)	1165 (6)	5678 (1)	6083 (2)	36 (1)
C (6)	602 (7)	5319 (1)	5063 (2)	38 (1)
C (7)	1541 (6)	5858 (1)	9415 (2)	34 (1)
C (8)	346 (6)	5125 (1)	9556 (2)	37 (1)

a detector distance of 4 cm and swing angle of $-35°$. A hemisphere of the reciprocal space was covered by combination of three sets of exposures; each set had a different angle (0, 88, 180°) and each exposure of 10 s covered 0.3° in ω. The collected data were reduced by using the program SAINT [G.M. Sheldrick SAINT v4 Software Reference Manual, Siemens Analytical X-ray systems, Inc., Madison, Wisconsin, USA (1996)] and for reflections with $2\theta \leq 55°$ were used for further processing. The structure was solved by direct methods and refined by least-squares on F^2_{obs} by using the SHELXTL [G.M. Sheldrick, SHELXTL v5 Reference Manual, Siemens Analytical X-ray System, Inc., Madison, Wisconsin, USA (1996)] software package. All non-H atoms were anisotropically refined. The hydrogen atoms were located by difference

UM00013789
NOVARTIS EXHIBIT 1017
Novartis v. Regents, IPR2023-01346
Page 2535 of 4460

TABLE III Selected bond lengths (Å) and angles (deg)

Complex A	
O(1)-C(4)	1.314 (2)
O(2)-C(4)	1.211 (2)
N(1)-C(2)	1.334 (2)
N(1)-C(1)	1.354 (14)
N(2)-C(1)	1.335 (3)
C(1)-N(1) #1	1.354 (14)
C(2)-C(3)	1.375 (2)
C(3)-C(2) #1	1.375 (2)
C(4)-C(5)	1.491 (2)
C(5)-C(7)	1.392 (2)
C(5)-C(6)	1.393 (2)
C(6)-C(7) #2	1.378 (2)
C(7)-C(6) #2	1.378 (2)
C(2)-N(1)-C(1)	116.65 (13)
N(2)-C(1)-N(1) #1	117.85 (9)
N(2)-C(1)-N(1)	117.85 (9)
N(1) #1-C(1)-N(1)	124.3 (2)
N(1)-C(2)-C(3)	122.9 (2)
C(2)-C(3)-C(2) #1	116.5 (2)
O(2)-C(4)-O(1)	123.50 (14)
O(2)-C(4)-C(5)	122.00 (13)
O(1)-C(4)-C(5)	114.50 (13)
C(7)-C(5)-C(6)	119.65 (13)
C(7)-C(5)-C(4)	118.48 (13)
C(6)-C(5)-C(4)	121.87 (13)
C(7) #2-C(6)-C(5)	120.07 (14)
C(6) #2-C(7)-C(5)	120.28 (13)
Complex B	
O(1)-C(5)	1.208 (2)
O(2)-C(5)	1.300 (2)
N(1)-C(7)	1.335 (2)
N(1)-C(6)	1.347 (2)
N(2)-C(6)	1.332 (3)
C(1)-C(3)	1.362 (3)
C(1)-C(2)	1.373 (3)
C(1)-C(4)	1.503 (3)
C(2)-C(3) #3	1.378 (3)
C(3)-C(2) #3	1.378 (3)
C(4)-C(5)	1.498 (3)
C(6)-N(1) #4	1.347 (2)
C(7)-N(1)-C(6)	116.5 (2)
C(3)-C(1)-C(2)	117.3 (2)
C(3)-C(1)-C(4)	120.5 (2)
C(2)-C(1)-C(4)	122.3 (2)
C(1)-C(2)-C(3) #3	121.5 (2)
C(1)-C(3)-C(2) #3	121.3 (2)
C(5)-C(4)-C(1)	113.9 (2)
O(1)-C(5)-O(2)	123.2 (2)
O(1)-C(5)-C(4)	123.8 (2)
O(2)-C(5)-C(4)	112.9 (2)
N(2)-C(6)-N(1)	117.99 (11)
N(2)-C(6)-N(1) #4	117.99 (11)
N(1)-C(6)-N(1) #4	124.0 (2)
N(1)-C(7)-C(8)	123.4 (2)
C(7) #4-C(8)-C(7)	116.2 (3)
Complex C	
O(1)-C(5)	1.209 (3)
O(2)-C(5)	1.306 (3)
O(2)-H1O2	0.92 (3)
O(3)-C(7)	1.233 (2)
O(4)-C(7)	1.284 (2)
N(1)-C(1)	1.322 (3)
N(1)-H1N1	0.96 (3)
N(1)-H2N1	0.95 (3)
N(2)-C(2)	1.352 (3)
N(2)-C(1)	1.355 (3)
N(2)-H1N2	0.91 (3)
N(3)-C(4)	1.324 (3)
N(3)-C(1)	1.349 (3)
C(2)-C(3)	1.364 (3)
C(2)-H(2)	0.96 (3)
C(3)-C(4)	1.394 (3)
C(3)-H(3)	0.96 (3)
C(4)-H(4)	0.97 (3)
C(5)-C(6)	1.491 (3)
C(6)-C(6) #3	1.310 (4)
C(6)-H(6)	1.02 (3)
C(7)-C(8)	1.494 (3)
C(8)-C(8) #5	1.311 (4)
C(8)-H(8)	1.03 (3)
C(5)-O(2)-H1O2	111.0 (18)
C(1)-N(1)-H1N1	118.6 (18)
C(1)-N(1)-H2N1	118.4 (16)
H1N1-N(1)-H2N1	123 (2)
C(2)-N(2)-C(1)	120.79 (18)
C(2)-N(2)-H1N2	119.9 (18)
C(1)-N(2)-H1N2	119.0 (18)
C(4)-N(3)-C(1)	116.82 (19)
N(1)-C(1)-N(3)	119.15 (19)
N(1)-C(1)-N(2)	119.20 (18)
N(3)-C(1)-N(2)	121.65 (18)
N(2)-C(2)-C(3)	119.8 (2)
N(2)-C(2)-H(2)	114.1 (15)
C(3)-C(2)-H(2)	126.1 (15)
C(2)-C(3)-C(4)	116.5 (2)
C(2)-C(3)-H(3)	121.9 (18)
C(4)-C(3)-H(3)	121.6 (18)
N(3)-C(4)-C(3)	124.5 (2)
N(3)-C(4)-H(4)	114.8 (16)
C(3)-C(4)-H(4)	120.7 (16)
O(1)-C(5)-O(2)	123.2 (2)
O(1)-C(5)-C(6)	120.69 (19)
O(2)-C(5)-C(6)	116.07 (19)
C(6) #3-C(6)-C(5)	123.6 (3)
C(6) #3-C(6)-H(6)	119.2 (15)
C(5)-C(6)-H(6)	117.1 (15)
O(3)-C(7)-O(4)	123.51 (19)
O(3)-C(7)-C(8)	120.06 (17)
O(4)-C(7)-C(8)	116.43 (17)
C(8) #5-C(8)-C(7)	123.4 (2)
C(8) #5-C(8)-H(8)	118.1 (18)
C(7)-C(8)-H(8)	118.5 (18)

Symmetry transformations: #1 $x, -y+1/2, z$ #2, $-x+2, -y+1, -z$ #3 $-x, -y+1, -z+1$ #4 $x-1, -y, z+1/2$ #5 $-x, -y+1, -z+2$.

synthesis and refined isotropically. Final conventional $R(F)$ and $wR(F^2)$ for observed reflections $[I > 2\sigma(I)]$ with weighting scheme, $w = 1/[\sigma^2(F_0^2) + (0.0534P)^2 + 0.2173P]$, where

UM00013790

NOVARTIS EXHIBIT 1017
Novartis v. Regents, IPR2023-01346
Page 2536 of 4460

TABLE IV Hydrogen bond parameters (Å,°)

	Complex A		
D-H—A	H—A	D—A	D-H—A
N2-H1N2—O2	2.02 (2)	2.89 (1)	166 (2)
O1-H1O1—N1	1.69 (3)	2.68 (2)	169 (2)
	Complex B		
D-H—A	H—A	D—A	D-H—A
O2-H1O2—N1	1.65 (2)	2.68 (2)	171.5 (2)
N2-H1N2—O1	2.02 (2)	2.92 (2)	173.8 (2)
C3-H3—O2	2.59 (2)	3.46 (3)	153.9 (2)
C4-H4A—O1	2.56 (2)	3.54 (3)	166. 7 (2)
	Complex C		
D-H—A	H—A	D—A	D-H—A
N1-H1N1—O3	1.84 (3)	2.79 (3)	176 (3)
N2-H1N2—O4	1.80 (3)	2.71 (2)	170 (3)
O2-H1O2—O4	1.63 (3)	2.55 (2)	172 (3)
C2-H2—O1	2.48 (3)	3.06 (3)	119 (2)
C2-H2—O1 #1	2.56 (3)	3.31 (3)	143 (2)
N1-H2N1—O1 #2	1.93 (3)	2.88 (3)	174 (2)
C4-H4—O2 #3	2.58 (3)	3.44 (3)	149 (2)
C3-H3—O3 #4	2.43 (3)	3.37 (3)	162 (2)

Symmetry transformations: #1 $x+1, y, z$; #2 $x, -y+3/2, z+1/2$; #3 $-x+1, y+1/2, -z+3/2$; #4 $x+1, -y+3/2, z-1/2$.

$P = (F_0^2 + 2F_c^2)/3$. The molecular graphics were done using SHELXTL.

CONCLUSIONS

This article thus demonstrates the role of 2AP in the formation of supramolecular structure with various dicarboxylic acids by utilising weak forces like hydrogen bonding, π-stacking *etc.*, and also shows how 2AP can be used to probe the hydrogen-bond preferences of carboxylic acid. All the crystal structures reported here involve a wave like or zig-zag pattern except the case of fumaric acid. In case of complex B and complex C, 1,4-phenylenediacetic acid and fumaric acid take part in unconventional C-H—O hydrogen bonding [C(sp^3)-H—O and C(sp)^2-H—O for complex B and C respectively] along with pyrimidine-pyrimidine (3.605 Å) and phenyl-phenyl (3.614 Å) stacking. This results an infinite wave like chain structures in the solid state. Most interestingly in complex C fumaric acid is complexed with 2AP *via* the formation of fused eight-nine membered hydrogen-bonded rings after the transfer of one proton to the pyrimidine ring nitrogen and ultimately forms a plane wave like structure. This is in contrast to succinic acid although it has the same geometrical orientation with succinic acid. All these supramolecular structures therefore demonstrate that acidity of the carboxylic acid as well as acidity of C-H proton of methylene or aromatic ring, govern the pattern of supramolecular structure in the solid state. Also in the solid state design, besides the arrays of conventional hydrogen bonds, C-H—O contacts play a significant role in futher modification of the structure of supramolecular assemblies.

Acknowledgments

We thank DST and CSIR, New Delhi for financial support. We thank Professor G.D. Nigam (IIT Kharagpur), Professor H. K. Fun and Dr. K. Chinnakali of Universiti Sains Malaysia for X-ray analysis and R. Mukherjee for her constant help. We also thank Professor U.R. Ghatak and Professor A. Chakraborty of IACS, Calcutta for research encouragement at this new place.

References

[1] Whitesides, G. M., Mathias, J. P. and Seto, C. T. (1991). *Science*, **254**, 1312; Desiraju, G. (1989). *Crystal Engineering: The Design of Organic Solids*, Elsevier, New York.
[2] Taylor, R. and Kennard, O. (1982). *J. Am. Chem. Soc.*, **104**, 5063; Desiraju, G. R. (1991). *Acc. Chem. Res.*, **24**, 290.
[3] Reddy, D. S., Goud, S. B., Panneerselvam, K. and Desiraju, G. R. (1993). *J. Chem. Soc. Chem. Commun.*, p. 663.
[4] Goswami, S. P. and Ghosh, K. (1997). *Tetrahedron Letters*, **38**, 4503; Goswami, S. P., Ghosh, K. and Halder, M., *Tetrahedron Letters*, (in press); Tellado, F. G., Goswami, S. P., Chang, S. K., Geib, S. J. and Hamilton, A. D. (1990). *J. Am. Chem. Soc.*, **112**, 7393; Hosseini, M. W. and Lehn, J. M. (1982). *J. Am. Chem. Soc.*, **104**, 3525; Rebek, J. Jr. Nemeth, D., Ballester, P., Breslow, R., Rajagopalan, R. and Schwatz, J. (1981). *J. Am. Chem. Soc.*, **103**, 2905; Liao, R. F. and Lin, F. T. (1987). *J. Am. Chem. Soc.*, **109**, 3474; Lauher, J. W. and Fowler, F. W. (1996). *Tetrahedron.*, **52**, 3153.
[5] Etter, M. C. (1990). *Acc. Chem. Res.*, **23**, 120; Aakeroy, C. B., Nieuwenhuyzen, M. and Price, S. L. (1998). *J. Am. Chem. Soc.*, **120**, 8986.

UM00013791
NOVARTIS EXHIBIT 1017
Novartis v. Regents, IPR2023-01346
Page 2537 of 4460

[6] Scheinbein, S. and Schempp, E. (1976). *Acta Cryst. Sec B*, p. 32.
[7] Leiserowitz, L. (1976). *Acta Cryst.*, Sec B, **32**, 775; Tamura, C., Sakurai, N. and Sato, S. (1971). *Bull. Chem. Soc. Jpn.*, **44**, 1473.
[8] Etter, M. C., Adsmond, D. A. and Briton, D. (1990). *Acta Cryst.*, C-32, 933.
[9] Goswami, S. P., Mahapatra, A. K., Ghosh, K., Nigam, G. D., Chinnakali, K. and Fun, H. K. (1998). *Acta Cryst.*, C-54, (in press).
[10] Bailey, M. and Brown, C. J. (1966). *Acta Cryst.*, **21**, 566; Brown, C. J. (1966). *Acta Cryst.*, **21**, 1.
[11] Goswami, S. P., Ghosh, K. and Dasgupta, S. (1996). *Tetrahedron*, **52**, 12223; Raposo, C., Martin, M., Mussons, M. L., Crego, M., Anaya, J., Caballero, M. C. and Maran, J. R. (1994). *J. Chem. Soc. Perkin Trans.*, **1**, 2113.
[12] All ^{1}H NMR, IR, Analysis and M.P. were noted by taking co-crystal of the corresponding complex.

UM00013792
NOVARTIS EXHIBIT 1017
Novartis v. Regents, IPR2023-01346
Page 2538 of 4460

This Page is Inserted by IFW Indexing and Scanning Operations and is not part of the Official Record

BEST AVAILABLE IMAGES

Defective images within this document are accurate representations of the original documents submitted by the applicant.

Defects in the images include but are not limited to the items checked:

- ☐ BLACK BORDERS
- ☐ IMAGE CUT OFF AT TOP, BOTTOM OR SIDES
- ☐ FADED TEXT OR DRAWING
- ☐ BLURRED OR ILLEGIBLE TEXT OR DRAWING
- ☐ SKEWED/SLANTED IMAGES
- ☐ COLOR OR BLACK AND WHITE PHOTOGRAPHS
- ☐ GRAY SCALE DOCUMENTS
- ☐ LINES OR MARKS ON ORIGINAL DOCUMENT
- ☐ REFERENCE(S) OR EXHIBIT(S) SUBMITTED ARE POOR QUALITY
- ☐ OTHER: _____

IMAGES ARE BEST AVAILABLE COPY.
As rescanning these documents will not correct the image problems checked, please do not report these problems to the IFW Image Problem Mailbox.

19 November 1999

ELSEVIER

Chemical Physics Letters 313 (1999) 725–732

CHEMICAL PHYSICS LETTERS

www.elsevier.nl/locate/cplett

Interplay of acceptor molecule shape, crystal structure and physical properties of a new molecular complex $C_{70} \cdot 2[(Ph_3P)AuCl]$

A. Graja [a,b,*], R. Lipiec [a], S. Waplak [a], S. Król [a], I. Turowska-Tyrk [c], N.V. Drichko [a,d]

[a] *Institute of Molecular Physics, Polish Academy of Sciences, ul. Smoluchowskiego 17, 60-179 Poznań, Poland*
[b] *L.P.M.C., University of Nice, Sophia Antipolis, 06108 Nice, France*
[c] *Institute of Physical and Theoretical Chemistry, Technical University of Wrocław, 50-370 Wrocław, Poland*
[d] *Ioffe Physical-Technical Institute, Russian Academy of Sciences, St. Petersburg, Russian Federation*

Received 1 March 1999; in final form 6 September 1999

Abstract

Investigations of crystal structure, electronic and vibrational absorption spectra and electron spin resonance of the complex of the fullerene C_{70} with chloro(triphenylphosphine)gold have been performed. Optical anisotropy, in particular the anisotropy of normal vibrations of the donor, has been observed and discussed. It was stated that the $C_{70} \cdot 2[(Ph_3P)AuCl]$ complex undergoes a first-order phase transition at ~ 160 K and shows an anomaly between 225 and 250 K. The role of the shape of C_{70} molecule in the structural organization and physical properties of the electron donor–acceptor complex is emphasized. © 1999 Elsevier Science B.V. All rights reserved.

1. Introduction

The fullerenes are the subject of wide interdisciplinary interest in materials science. Amongst their various kinds, C_{60} and C_{70} are the most abundant and the most investigated. Although the chemistry and physics of C_{70} have developed more slowly than that of C_{60}, its properties are being studied currently. In contrast to the C_{60} molecule with I_h symmetry, the C_{70} molecule has the lower symmetry D_{5h} and lacks inversion symmetry; it is no longer spherical, but has a slightly elongated rugby-ball shape. Owing to its form and reduced symmetry, the electronic, vibrational and dynamical properties of C_{70} differ from those of C_{60}. Although there is more strain in the C_{70} molecule than in C_{60} and fewer pyracylene bonds in the former molecule, it exhibits the same first reduction wave potentials in various solvents [1].

However, despite a similar chemical nature, materials made out of C_{70} differ much in their properties from their C_{60} analogues [2]. Similarly, the number of reports on the physical properties of both groups of derivatives is quite different. It seems that only a few C_{70} complexes with organic donors are characterized by X-ray diffraction [3–7]. Knowledge of the physical properties of C_{70} complexes is still poor

* Corresponding author. Fax: +48-61-8684524; e-mail: graja@ifmpan.poznan.pl

0009-2614/99/$ - see front matter © 1999 Elsevier Science B.V. All rights reserved.
PII: S0009-2614(99)01038-6

UM00013794
NOVARTIS EXHIBIT 1017
Novartis v. Regents, IPR2023-01346
Page 2540 of 4460

[2,6,8]. Recently, electronic and vibrational spectroscopies were used to investigate the electron processes in C_{70} complexes with crown-shaped sulfur and 9,9′-bis-*trans*-(telluraxanthenyl) donors as well as in C_{70} salt $(Ph_4P)_2C_{70}Br$ [8].

In this Letter we describe the crystal structure and spectral characterization of a new complex of C_{70} with an electron donor chloro(triphenylphosphine) gold – $(Ph_3P)AuCl$. The aim of these investigations is the selection of the spectral (UV–VIS–NIR–IR and ESR) effects typical for the complex, in particular studies of its optical anisotropy and an evolution of these spectra versus temperature. A comparison of its physical properties with the properties of the C_{60} complex with the same donor is also given.

2. Experimental

The complex of C_{70} with $(Ph_3P)AuCl$ was grown from solutions of stoichiometric amounts of C_{70} and the donor in toluene or benzene according to the procedure which have been applied for preparation of a similar complex with C_{60}. Details of the synthesis of the latter complex have been reported elsewhere [9,10]. The compound formula $C_{70} \cdot 2[(Ph_3P)AuCl]$ was suggested on the ground of the elemental analysis and X-ray diffraction studies. However, it is necessary to mention that the elemental analysis as well as infrared (IR) spectral studies show some contamination of solvent molecules.

Methods used for data collection and structure solution will be given in Section 3.

Electronic absorption spectra of the $C_{70} \cdot 2[(Ph_3P)AuCl]$ complex, in KBr pellets containing dispersed samples with concentration 1:10000, were recorded with a Perkin Elmer Lambda 19 spectrometer at room temperature. The transmission IR spectra of a single crystal of the complex as well as its C_{60} analogue were recorded for polarized light, for various crystal orientations, in the spectral range 650–4000 cm^{-1} with a FT IR Perkin Elmer 1725 X spectrometer equipped with an IR microscope. The IR spectra of $C_{70} \cdot 2[(Ph_3P)AuCl]$ were taken in the temperature range from 4 to 300 K using an Oxford Instruments cryostat.

The ESR spectra of powered sample of $C_{70} \cdot 2[(Ph_3P)AuCl]$ were recorded within the temperature range from 80 to 300 K on a SE/X 2544 spectrometer with TE_{102} cavity and 100 kHz magnetic modulation. Temperature was measured by a thermocouple mounted inside the sample.

A standard four-probe technique for the determination of dc conductivity along the long crystal axis has been applied. Electrical contacts were made by sticking the silver wires with silver past paint. At room temperature the samples' resistance exceeded 2 GΩ.

3. Crystal structure

A crystal of the title compound was examined on a Kuma KM4CCD diffractometer equipped with a CCD camera. The method used for data collection with KM4CCD, as for other area detectors [11], was rotational: for each small rotation of the crystal, a two-dimensional image of data was taken. An image increment and integration time used in the case of the $C_{70} \cdot 2[(Ph_3P)AuCl]$ crystal were 0.3° and 20 s, respectively. The data were collected for two tilt angles of the area detector, 27° and 40°, in four sweeps for each tilt: two 100° rotations of ω at $\kappa = 0°$ (separated by 90° in ϕ) and two 70° rotations of ω at $\kappa = 90°$ (separated by 90° in ϕ). The cell constants were determined precisely by the least-squares method on the ground of four sweeps for the detector tilt angle 27°. The data collection was performed at 190 K. The reflections were corrected for Lorentz-polarization and absorption effects [12].

The structure was solved by Patterson techniques from the SHELXS86 program [13]. Only 1/6 of C_{70} and 1/3 of $(Ph_3P)AuCl$ is crystallographically asymmetric. Positions of almost all atoms of the $(Ph_3P)AuCl$ species were revealed. The remaining atoms of this fragment were found by the difference synthesis. The phenyl rings appeared to be disordered on two equally occupied positions. In the fullerene molecule only one atom (situated on a three-fold axis) was clearly seen by SHELXS86 and by the difference syntheses in SHELXL93 [14]. For this molecule the model was constructed on the ground of coordinates taken from [15]. The model molecule was disordered on six orientations around the three-fold axis and the inversion center. In the refinement process, the geometry of the C_{70} model

UM00013795
NOVARTIS EXHIBIT 1017
Novartis v. Regents, IPR2023-01346
Page 2541 of 4460

was fixed and only translational and rotational movements of the molecule were regarded. The structure was refined by SHELXL93. During the structure determination, many constraints and restraints were applied. Most of them were also kept in final stages of the refinement. The non-hydrogen atoms of the $(Ph_3P)AuCl$ were treated anisotropically and the hydrogen atoms of only one disordered phenyl group were included. The C_{70} molecule was refined isotropically. The ratio between a number of observed reflections and a number of such refined parameters was 6.7. The partly occupied solvent molecule was not identified in a crystal lattice. The crystal data and refinement details were given in Table 1.

The long axis of the C_{70} molecule is situated perpendicularly to a crystallographic three-fold axis and simultaneously on an inversion center. The Cl, Au and P atoms of the $(Ph_3P)AuCl$ fragment are placed on a three-fold axis. There are three C_{70} and six $(Ph_3P)AuCl$ species in a unit cell. Fig. 1 presents a stereoscopic view of the $(Ph_3P)AuCl$ content in the unit cell. As it was mentioned both species are disordered in the crystal lattice. The disorder of C_{70} is a requirement of the symmetry. The disorder in $(Ph_3P)AuCl$ can be a result of two possible, energetically equally preferred, orientations of the phenyl ring in a free $(Ph_3P)AuCl$ molecule. In the crystal lattice an angle between the (110) and phenyl ring planes is 54° for both occupations. The exactly equal occupancy of the Ph rings is demanded by a connectivity pattern in the crystal. The *meta* atoms of the phenyl rings of one orientation form bonds to the phenyl *meta* atoms of adjacent species of the second occupation creating in this way a two-dimensional network. The C_{70} molecules are arranged in layers situated between such networks.

Table 1
Crystal data structure refinement for $C_{70} \cdot 2[(Ph_3P)AuCl]$

Formula	$C_{106}H_{30}Au_2Cl_2P_2$
M_r	1830.07
Crystal system	trigonal
Space group	$R\bar{3}$
a (Å)	12.371(5)
c (Å)	35.752(5)
V (Å^3)	4739(3)
Z	3
$F(000)$	2664
D_x (Mg/m^3)	1.92
λ (Å)	0.71073
μ (mm^{-1})	4.84
Crystal size (mm)	$0.12 \times 0.12 \times 0.35$
Temperature (K)	190(2)
θ_{max} (deg)	24
Number of all reflections	4521
Number of independent reflections	1629
Number of observed reflections	1232
R_{int}	0.041
R indices [$I > 2\sigma(I)$]	$R_1 = 0.093$, $wR_2 = 0.254$
R indices (all data)	$R_1 = 0.123$, $wR_2 = 0.254$
Goodness-of-fit on F^2	1.07
$\Delta\rho_{max}$ and $\Delta\rho_{min}$ (Å^{-3})	1.17 and −0.94 (close to Au and C_{70})

4. Spectral properties

Spectra of $C_{70} \cdot 2[(Ph_2P)AuCl]$ in the range from near IR to ultraviolet (UV) (3000–200 nm) show only some features at visible and UV regions. Broad and weak absorption is observed between 500 and 600 nm, farther a local minimum covers the blue-violet region and maxima of intermediate strength appear in the near UV region at ~340, ~365 and ~385 nm. Following a weaker maximum at ~325 nm, very strong absorption appears below 290 nm. These bands are typical for a neutral C_{70} molecule [16,17], but they are broadened in comparison with the bands of C_{70} crystals. On the other hand no absorption was found between 750 and 3000 nm; it means also that there is no the absorption band at ~1370 nm, typical for C_{70}^- anion [17]. From this investigation one can conclude that the electronic structure of C_{70} is not disturbed by the complex. Thus, $C_{70} \cdot 2[(Ph_2P)AuCl]$ is a weak, molecular complex with negligible charge transfer from the electron donor to C_{70}.

A vibrational spectrum of the single crystal of the investigated complex is strongly anisotropic (Fig. 2). It consists of tens of bands for both polarizations of light. The bands at about 1462, 1433, 1417, 1135, 795, 674 and 642 cm^{-1} can be attributed to normal vibrations of C_{70} molecule. Their wavenumbers are the same or are shifted by 1–3 cm^{-1} but their width

UM00013796
NOVARTIS EXHIBIT 1017
Novartis v. Regents, IPR2023-01346
Page 2542 of 4460

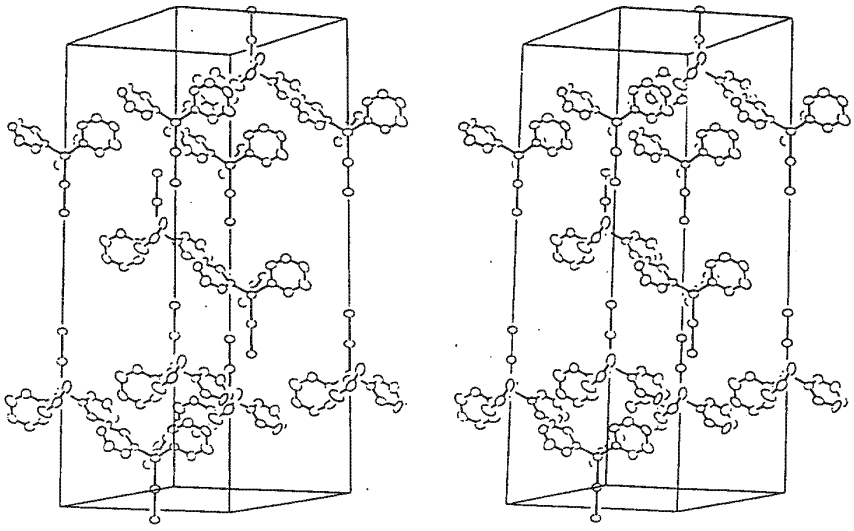


Fig. 1. A stereoscopic view presenting the $(Ph_3P)AuCl$ content in the unit cell.

is bigger with respect to the dominant bands of C_{70} [18]. There are also many weak lines similar to those observed in the transmission spectra of C_{70} complexes [8]. This structure of IR spectrum is due to silent and combination modes typical of the broken D_{5h} symmetry of the free C_{70} molecule. The spectrum of $C_{70} \cdot 2[(Ph_2P)AuCl]$ is dominated however by the absorption lines of the donor molecule $(Ph_2P)AuCl$. The bands at 1584, 1481, 1433, 1312, 1182, 1100, 1028, 1000, 749, 712, 693 and 668 cm^{-1} are typical for the donor. They are shifted by 1–2 cm^{-1} with respect to the normal vibrations of $(Ph_3P)AuCl$, observed in its transmission spectra in KBr pellets. Some very weak bands can be assigned to solvent contaminations – if this attribution is correct, the solvent content is only residual. It seems, that an assignment of these bands to the silent or combination modes of C_{70} is equally probable.

There are several absorption bands whose origin is not clear. The band at 1182 cm^{-1} shows too strong intensity for the band of the donor. On the other hand, it coincides with the strongest band of C_{60} – thus one could suspect the band to be a result of contamination of C_{70} with C_{60}. However, this suspicion is not confirmed by the IR spectrum of the pure C_{70} used for the complex synthesis neither by the UV-VIS spectra of the complex that is typical for C_{70}. An attribution of the bands at 987, 922 and 848 cm^{-1} is also not clear. These bands are observed neither in the spectra of C_{70} or in the spectra of the donor or solvent. We can find the same bands in the IR spectra of a similar complex with C_{60}. Thus, we suggest that in both $C_{60} \cdot 2[(Ph_2P)AuCl]$ and $C_{70} \cdot 2[(Ph_2P)AuCl]$ complexes one or more phenyl rings are strongly deformed and have normal mode frequencies different from that of their undeformed configuration. It is highly probable because short $C \cdots C$ contacts between the phenyl rings of

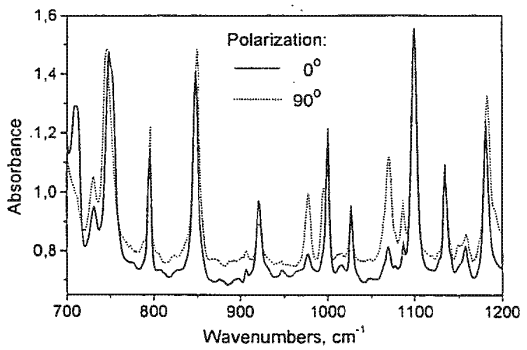


Fig. 2. The FT IR polarized spectrum of $C_{70} \cdot 2[(Ph_3P)AuCl]$ at room temperature for two perpendicular light polarizations.

UM00013797
NOVARTIS EXHIBIT 1017
Novartis v. Regents, IPR2023-01346
Page 2543 of 4460

$(Ph_3P)AuCl$ and some kind of polymerization have been suggested for $C_{60} \cdot 2[(Ph_2P)AuCl] \cdot 0.1C_6H_5CH_3$ [19]. The short contacts between the phenyl rings of $(Ph_3P)AuCl$ in its complex with C_{60} have been also emphasized [10]. As mentioned before, each phenyl ring is not only disordered on two positions but the rings creat a two-dimensional, oriented network in the structure of $C_{70} \cdot 2[(Ph_2P)AuCl]$. Thus, some shifts of the frequencies of the normal vibrations of phenyl rings are expected for both complexes of $(Ph_3P)AuCl$ with C_{60} or C_{70}.

The above discussion of the vibrational spectrum of the complex confirms our conclusion from an analysis of the visible and ultraviolet spectra that interactions between donor and acceptor molecules are weak in $C_{70} \cdot 2[(Ph_2P)AuCl]$ and that it is a complex of Van der Waals type. On the other hand the broadening of some IR and UV-VIS bands suggests a disorder in the positions of C_{70} molecules and phenyl rings of the donor.

A good quality of the single crystals of C_{70} and C_{60} complexes with $(Ph_3P)AuCl$ enables us to study an anisotropy of their IR spectra. The spectra have been recorded for two light polarizations: parallel (0°) and perpendicular (90°) to the long single crystal axis.

The spectrum of $C_{70} \cdot 2[(Ph_2P)AuCl]$ (Fig. 2) is strongly anisotropic. The band at 712 cm^{-1} disappears, at 749 cm^{-1} is shifted by ~ 5 cm^{-1} and shows a complex structure, at 1000 cm^{-1} loses its weaker component at ~ 997 cm^{-1}, the bands at 1070 and 1091 cm^{-1} lose distinctly their intensities, a doublet at 1158 and 1163 cm^{-1} changes its form and the band at 1182 cm^{-1} is weaker and narrowed for 90° polarization. All these bands are attributed to the donor normal vibrations. Much smaller changes occur for normal vibrations of C_{70}. The intensity of the band at 795 cm^{-1} decreases without a change of its frequency for 90° polarization. The band at 1135 cm^{-1} is more or less independent of the crystal orientation.

A similar spectrum of $C_{60} \cdot 2[(Ph_2P)AuCl]$ is isotropic, in principle. One can see only some changes in the form of the bands at ~ 720 and ~ 750 cm^{-1}; the intensity of the band at 1182 cm^{-1} shows also a small decrease for 90° polarization.

The anisotropy of F_{1u} mode (1182 cm^{-1}) of the fullerene is very small in $C_{60} \cdot 2[(Ph_2P)AuCl]$ but the bands typical for C_{70} molecule (795 and 1135 cm^{-1}) in the $C_{70} \cdot 2[(Ph_2P)AuCl]$ complex show small anisotropy adequate to a natural orientation of the elongated C_{70} molecules in the crystals. The ordering effect is better seen if one analyses the bands of the donor. The spectral isotropy of the $C_{60} \cdot 2[(Ph_2P)AuCl]$ testifies the isotropic distribution of the donor molecules, in particular their phenyl rings. It is seen first of all in the X-ray crystal structure [10]. On the other hand, the distribution of the phenyl ring orientations is strongly anisotropic in the C_{70} complex – the phenyl rings form a two-dimensional network in $C_{70} \cdot 2[(Ph_2P)AuCl]$. It seems that this crystal structure anisotropy is caused by the

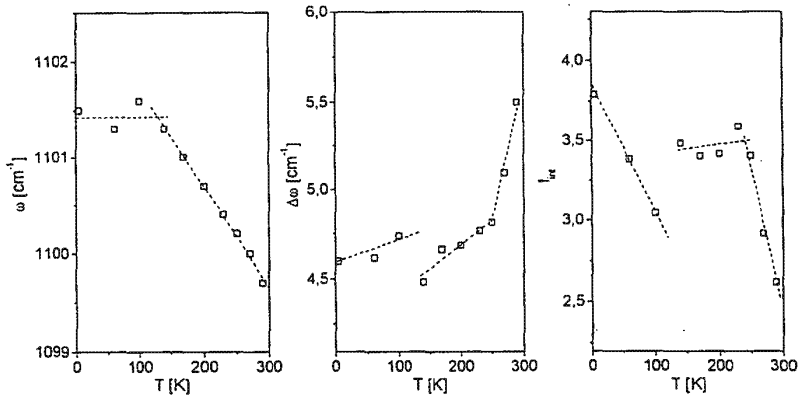


Fig. 3. The temperature dependence of the spectral parameters of the band at 1001 cm^{-1} for $C_{70} \cdot 2[(Ph_3P)AuCl]$.

UM00013798
NOVARTIS EXHIBIT 1017
Novartis v. Regents, IPR2023-01346
Page 2544 of 4460

orientation of the C_{70} molecules; as it was mentioned before, the long axis of C_{70} is situated perpendicularly to the crystallographic three-fold axis. The structural anisotropy of $C_{70} \cdot 2[(Ph_2P)AuCl]$ is perfectly reflected by its IR spectra. From this investigation it is clear that the spectral study for polarized light are useful tool for investigation of the structural anisotropy of the crystals of the fullerene complexes. Recently, this method has been used successfully for the study of C_{60} complexes with TMTSF [20].

A detailed temperature study of anywhere from ten to twenty separable bands of $C_{70} \cdot 2[(Ph_2P)AuCl]$ has been carried out. Temperature variations of the IR line wavenumbers (ω) linewidths ($\Delta\omega$), amplitudes (I) and integral intensities (I_{int}) have been analysed for the range 5–300 K. It was stated that investigated bands show a distinct anomaly of their parameters at ~ 150 K – it is exemplified in Fig. 3 where temperature dependencies of the investigated spectral parameters of the band at 1100 cm^{-1} are presented. Another anomaly is seen at ~ 225–250 K. Usually, the frequency of the bands of $C_{70} \cdot 2[(Ph_2P)AuCl]$ increases monotonically with decreasing the temperature down to 150 K and stabilizes below this temperature. The linewidth decreases down to 250 K and further stabilizes showing however an anomaly below 150 K. The amplitude and integral intensity increase with lowering the temperature down to 250 K, are rather stable between 250 and 150 K and further increase. The anomaly at 150 K is also perfectly seen as an appearance of a new band at ~ 1020 cm^{-1}, but that at 250 K is marked as an appearance of the bands at 1040 cm^{-1} and 1055 cm^{-1} above adequate temperatures. It is characteristic that mainly the modes attributed to normal vibrations of the donor are significantly perturbed at the critical temperatures.

For elucidation of these anomalies, the temperature studies of the crystal unit cell have been performed. The crystal structure and the cell parameters can be stated only for temperatures above 160 K – below this temperature diffraction spots are so smeared that one cannot find good unit cell. However assuming the trigonal crystal system in the whole temperature range, one can evaluate the crystal cell parameters versus temperature. The temperature dependence of the a parameter of the unit cell

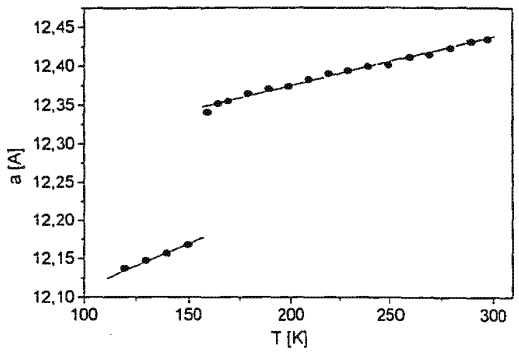


Fig. 4. The temperature variation of the unit cell parameter a of $C_{70} \cdot 2[(Ph_3P)AuCl]$.

obtained this way is shown in Fig. 4. A similar anomaly is seen for parameter c between 160 and 150 K. If even the crystal system in low temperature is changed and values of the unit cell parameters are not correct below 160 K, it is unquestionable that $C_{70} \cdot 2[(Ph_2P)AuCl]$ undergoes the first order phase transition at ~ 160 K. The anomalies in the spectral parameters of the selected absorption bands, which have been presented above are of course a consequence of this phase transition. The second anomaly, detected by IR spectral studies at ~ 250 K, is not seen in the X-ray investigation. Thus, this anomaly is not caused by a structural phase transition but can reflect changes of the oscillator forces provoked or by a redistribution of the charges on the donor molecule or by changes in the molecular dynamics of the phenyl rings.

The EPR spectrum of $C_{70} \cdot 2[(Ph_2P)AuCl]$ consists of one line with ΔB_{pp} linewidth equal 0.15 mT in the (80–300) K temperature region. In contrast, the g-value is temperature-dependent. The distinct anomaly of $g(T)$ at ~ 159 K show the I-order phase transition like as anomaly of a-lattice constant (Fig. 4). The $g(T)$ anomalies for $C_{70} \cdot 2[(Ph_2P)AuCl]$ and $C_{60} \cdot 2[(Ph_2P)AuCl]$ are shown in Fig. 5 for comparison. For $C_{60} \cdot 2[(Ph_2P)AuCl]$ the temperature dependence of $g(T)$ is well described by the equation [10]:

$$g(T) = g_0 + AT, \tag{1}$$

where

$$A = \frac{\partial^2 g}{\partial Q^2} \frac{k}{m\omega^2},$$

UM00013799
NOVARTIS EXHIBIT 1017
Novartis v. Regents, IPR2023-01346
Page 2545 of 4460

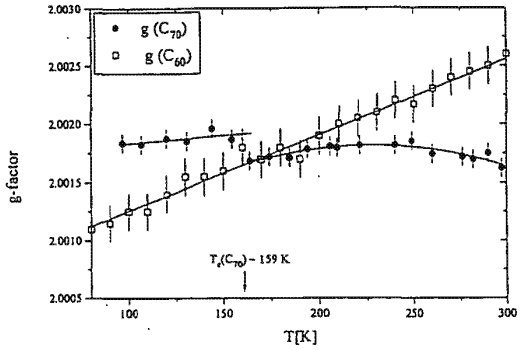


Fig. 5. The temperature dependence of the g-factor of the ESR line of $C_{70} \cdot 2[(Ph_3P)AuCl]$ (●); for comparison the g-factor of a narrow line of $C_{60} \cdot 2[(Ph_3P)AuCl]$ is shown (□).

and Q is the normal coordinate, and ω the frequency of normal mode vibration.

For $C_{70} \cdot 2[(Ph_2P)AuCl]$ with IR spectra show strong anisotropy due to ellipsoidally shaped C_{70} molecule, the transitional and rotational motion of C_{70} cannot be described by Eq. (1) applied for only harmonic vibration regarded for $C_{60} \cdot 2[(Ph_2P)AuCl]$. In our opinion the tendency to lowering the $g(T)$ value about 250 K is due to enhancement of rotational motion of C_{70}. At this temperature also the linewidth of normal mode of donor vibration grows up (Fig. 3).

5. Conclusions

We have performed complex investigations of the properties of the new compound $C_{70} \cdot 2[(Ph_3P)AuCl]$. It was stated that its crystal structure is different from the structure of $C_{60} \cdot 2[(Ph_3P)AuCl]$ – the differences are mainly caused by the elongated form of the fullerene C_{70}. Both donor and acceptor species are disordered in the crystal lattice. The disorder has been confirmed by UV-VIS-NIR-IR spectral studies. It was stated also that $C_{70} \cdot 2[(Ph_3P)AuCl]$ is a weak molecular complex with negligible charge transfer from the electron donor to C_{70}. IR spectra of the complex are strongly anisotropic – they reflect the crystal structure organization. The anomaly in the temperature dependence of the IR spectral parameters is confirmed by the temperature variation of the unit cell parameter and ESR studies. It was shown that $C_{70} \cdot 2[(Ph_3P)AuCl]$ undergoes a first-order phase transition at ~ 160 K.

Acknowledgements

This work was supported by the Polish State Committee for Scientific Research (grant No. 7T08A 004 11) and Russian Scientific Program 'Fullerenes and Atomic Clusters'. The support of the Foundation for Polish Science for the purchase of the CCD camera (grant MOLTEK'96) is gratefully acknowledged. We thank Professor B. Kuchta for providing coordinates suitable for the construction of the C_{70} molecular model. One of us (A.G.) acknowledges the University of Nice-Sophia Antipolis (France) for hospitality.

References

[1] P.-M. Allemand, A. Koch, F. Wudl, Y. Rubin, F. Diederich, M.M. Alvarez, S.J. Anz, R.L. Whetten, J. Am. Chem. Soc. 113 (1991) 1050.
[2] A. Graja, J.-P. Farges, Adv. Mater. Opt. Electr. 8 (1998) 215.
[3] G. Roth, P. Adelmann, J. Phys. (Paris) I 2 (1992) 1541.
[4] H.A. Romberg, M. Knupfer, J.F. Armbruster, G. Roth, Synth. Met. 69-71 (1995) 1379.
[5] B.Z. Narimbetov, L.V. Zorina, S.S. Hasanov, L.P. Rosenberg, R.P. Shibaeva, D.V. Konarev, R.N. Lyubovskaya, Kristallografiya 42 (1997) 851, (in Russian).
[6] A. Pénicaud, A. Pérez-Benitez, R. Escudero, C. Coulon, Solid State Commun. 96 (1995) 147.
[7] O. Ermer, C. Robke, J. Am. Chem. Soc. 115 (1993) 10077.
[8] V.N. Semkin, N.V. Drichko, A.V. Talysin, A. Graja, S. Król, D.N. Konarev, R.N. Lyubovskaya, Synth. Met. 93 (1998) 207.
[9] A. Graja, A. Łapiński, S. Król, J. Mol. Struct. 404 (1997) 147.
[10] A. Graja, S. Waplak, V.V. Gritsenko, N.G. Spitsina, N.V. Drichko, Synth. Met. 106 (1999) 29.
[11] W. R Sheidt, I. Turowska-Tyrk, Inorg. Chem. 33 (1994) 1314.
[12] Kuma KM4CCD Sooftware, version 146, Kuma Diffraction, Wrocław, 1998.
[13] G.M. Sheldrick, Acta Crystallogr. A 46 (1990) 467.
[14] G.M. Sheldrick, SHELXL93. Program for the Refinement of Crystal Structures, University of Göttingen, Göttingen, 1993.
[15] G.B.M. Vaughan, Ph.D. Thesis, University of Pennsylvania, Philadelphia, PA, 1993.
[16] H. Ajie, M.M. Alvarez, S.J. Anz, R.D. Beck, F. Diederich,

UM00013800
NOVARTIS EXHIBIT 1017
Novartis v. Regents, IPR2023-01346
Page 2546 of 4460

K. Fostiropoulos, D.R. Huffman, W. Krätschmer, Y. Rubin, K.E. Schriver, D. Sensharma, R.L. Whetten, J. Phys. Chem. 94 (1990) 8630.
[17] D.V. Konarev, N.V. Drichko, A. Graja, J. Chim. Phys. 95 (1998) 2143.
[18] D.S. Bethune, G. Meijer, W.C. Tang, H.J. Rosen, W.G. Golden, H. Seki, C.A. Brown, M.S. de Vries, Chem. Phys. Lett. 179 (1991) 181.
[19] A. Mucha, Thesis, Wrocław Technical University, Wrocław, 1997.
[20] I. Olejniczak, V.N. Semkin, N.G. Spitsina, A. Graja, Fullerenes Sci. Technol. (submitted).

UM00013801
NOVARTIS EXHIBIT 1017
Novartis v. Regents, IPR2023-01346
Page 2547 of 4460

This Page is Inserted by IFW Indexing and Scanning Operations and is not part of the Official Record

BEST AVAILABLE IMAGES

Defective images within this document are accurate representations of the original documents submitted by the applicant.

Defects in the images include but are not limited to the items checked:

- ☐ BLACK BORDERS
- ☐ IMAGE CUT OFF AT TOP, BOTTOM OR SIDES
- ☐ FADED TEXT OR DRAWING
- ☐ BLURRED OR ILLEGIBLE TEXT OR DRAWING
- ☐ SKEWED/SLANTED IMAGES
- ☐ COLOR OR BLACK AND WHITE PHOTOGRAPHS
- ☐ GRAY SCALE DOCUMENTS
- ☐ LINES OR MARKS ON ORIGINAL DOCUMENT
- ☐ REFERENCE(S) OR EXHIBIT(S) SUBMITTED ARE POOR QUALITY
- ☐ OTHER: _____

IMAGES ARE BEST AVAILABLE COPY.

As rescanning these documents will not correct the image problems checked, please do not report these problems to the IFW Image Problem Mailbox.

Table 1. *Fractional atomic coordinates and equivalent isotropic temperature factors* (Å²) *with e.s.d.'s in parentheses*

$U_{eq} = \frac{1}{3}\sum_i\sum_j U_{ij}a_i^*a_j^*\mathbf{a}_i.\mathbf{a}_j$.

	x	y	z	U_{eq}
O(1)	0.1762 (2)	0.2957 (2)	0.6906 (1)	0.0251
O(2)	0.2936 (2)	0.1747 (2)	0.5382 (1)	0.0282
N(1)	−0.0399 (2)	0.4862 (2)	0.8453 (1)	0.0257
C(1)	0.1673 (2)	0.2368 (2)	0.5901 (1)	0.0181
C(2)	0.0000	0.2500	0.5254 (2)	0.0162
C(3)	0.0159 (3)	0.3401 (2)	0.4109 (2)	0.0260
H(1*a*)	−0.098 (3)	0.424 (3)	0.899 (2)	0.051 (3)†
H(1*b*)	−0.136 (3)	0.558 (3)	0.811 (2)	0.051 (3)†
H(1*c*)	0.045 (3)	0.549 (3)	0.879 (2)	0.051 (3)†
H(1*d*)	0.010 (3)	0.421 (3)	0.782 (2)	0.051 (3)†
H(3*a*)	0.138 (3)	0.381 (3)	0.391 (2)	0.051 (3)†
H(3*b*)	−0.080 (3)	0.420 (3)	0.390 (2)	0.051 (3)†

† Isotropic *U*.

Table 2. *Interatomic distances* (Å) *and angles* (°) *with e.s.d.'s in parentheses*

O(1)—C(1)	1.259 (2)	C(2)—C(3)	1.517 (3)
O(2)—C(1)	1.256 (2)	C(3)—C(3^{i})	1.474 (4)
C(1)—C(2)	1.505 (2)		
O(2)—C(1)—O(1)	123.3 (2)	C(3)—C(2)—C(1^{i})	118.1 (1)
C(2)—C(1)—O(1)	118.7 (2)	C(3)—C(2)—C(1)	113.4 (1)
C(2)—C(1)—O(2)	117.9 (1)	C(3)—C(2)—C(3^{i})	58.1 (2)
C(1)—C(2)—C(1^{i})	120.4 (2)	C(3)—C(3^{i})—C(2)	60.93 (8)
Hydrogen bonds			
O(1)···N(1)	2.897 (2)	O(2)···N(1^{iii})	2.890 (2)
O(1)···H(1*d*)	1.95 (3)	O(2)···H(1*a*^{iii})	1.99 (3)
O(1)···H(1*d*)—N(1)	161 (1)	O(2)···H(1*a*^{iii})—N(1^{iii})	168 (2)
O(1)···N(1^{ii})	2.855 (2)	O(2)···N(1^{iv})	2.794 (2)
O(1)···H(1*b*^{ii})	1.88 (3)	O(2)···H(1*c*^{iv})	1.87 (3)
O(1)···H(1*b*^{ii})—N(1^{ii})	158 (2)	O(2)···H(1*c*^{iv})—N(1^{iv})	175 (2)

Symmetry codes: (i) $-x, \frac{1}{2}-y, z$; (ii) $\frac{1}{2}+x, 1-y, \frac{1}{2}-z$; (iii) $\frac{1}{2}+x, \frac{1}{2}-y, z-\frac{1}{2}$; (iv) $\frac{1}{2}-y, y-\frac{1}{2}, \frac{1}{2}-z$.

Colourless needles of the compound were crystallized from water/ethanol at 277 K. The structure was solved by direct methods (*SHELXS*86; Sheldrick, 1986) and refined by full-matrix least squares.

We thank Professor J. C. Chottard for helpful discussions.

Lists of structure factors and anisotropic thermal parameters have been deposited with the British Library Document Supply Centre as Supplementary Publication No. SUP 55269 (5 pp.). Copies may be obtained through The Technical Editor, International Union of Crystallography, 5 Abbey Square, Chester CH1 2HU, England. [CIF reference: PA1005]

References

Bitha, P., Child, R. G., Hlavka, J. J., Lang, S. A. Jr & Lin, Y. (1988). *Inorg. Chim. Acta*, **151**, 89–93.

Bondi, A. (1964). *J. Chem. Phys.* **68**, 441–451.

Carruthers, J. R. & Watkin, D. W. (1985). *CRYSTALS*. Advanced crystallographic computer program. Chemical Crystallography Laboratory, Univ. of Oxford, England.

Jaulmes, S., Laruelle, P. & Fabrègue, E. (1987). *Acta Cryst.* C**43**, 238–241.

McQuillin, F. J. (1972). *Alicyclic Chemistry*, p. 13. Cambridge Univ. Press.

Meester, M. A. M., Schenk, H. & MacGillavry, C. H. (1971). *Acta Cryst.* B**27**, 630–634.

Neidle, S., Ismail, M. I. & Sadler, P. J. (1980). *J. Inorg. Biochem.* **13**, 205–212.

Pajunen, A. & Pajunen, S. (1979). *Acta Cryst.* B**35**, 2401–2403.

Sheldrick, G. M. (1986). *SHELXS*86. Program for the solution of crystal structures. Univ. of Göttingen, Germany.

Soltzberg, L. & Margulis, T. N. (1971). *J. Chem. Phys.* **55**, 4907–4913.

Acta Cryst. (1992). C**48**, 2096–2098

Structure of the 1:1 Complex of 6,6′-Diquinolyl Ether with 5,5-Diethylbarbituric Acid

LIU HAIXIN AND WANG XIN*

Analysis and Research Centre, Lanzhou University, Lanzhou 730000, People's Republic of China

ZHANG XINMIN

Department of Pharmacy, Lanzhou Medical College, Lanzhou 730000, People's Republic of China

(*Received* 19 *November* 1991; *accepted* 30 *July* 1992)

Abstract

The crystal structure shows that barbital (5,5-diethylbarbituric acid) is bonded to 6,6′-diquinolyl ether by two short NH···N hydrogen bonds with N···N 2.88 Å. This arrangement is similar to those reported for hydrogen bonds in the molecular complexes of barbiturates.

Comment

Barbiturates are widely used medicinally and are among the most frequently encountered drugs for the treatment of epilepsy. This class of antiepileptic drug is of special interest since many of them and their active metabolites form metal complexes. Various metal complexes of barbiturates have been synthesized and studied (Caira, Fazakerley, Linder & Nassimbeni, 1973; Pezeshk, Greenaway & Sorenson, 1983). A series of crystal structure determinations of molecular complexes of barbiturates with other molecules, such as 9-ethyladenine (Voet & Rich, 1972; Voet, 1972), caffeine (Craven & Gartland, 1970), aminopyrine (Kiryu, 1971), urea (Gartland & Craven, 1974), acetamide (Hsu & Craven, 1974*a*), salicylamide (Hsu & Craven, 1974*b*) and imidazole (Hsu & Craven, 1974*c*), have been reported. In crystal complexes of barbiturates with these ligands there are stronger NH···O—C and NH···N hydrogen bonds between the two components than are found in the crystal structures of the individual components.

0108-2701/92/112096-03$06.00

© 1992 International Union of Crystallography

UM00013803
NOVARTIS EXHIBIT 1017
Novartis v. Regents, IPR2023-01346
Page 2549 of 4460

Quinoline is one of the ligands often used in coordination chemistry. Zhang and co-workers synthesized 6,6′-diquinolyl ether and described its structure (Zhang, Tan & Li, 1986; Wang, Zhang & Kong, 1988). It was found that 6,6′-diquinolyl ether is an important ligand in the syntheses of some complexes with biomedical activity. The present paper reports an X-ray diffraction study of the crystal structure of the molecular addition compound of 6,6′-diquinolyl ether with barbital (Fig. 1).

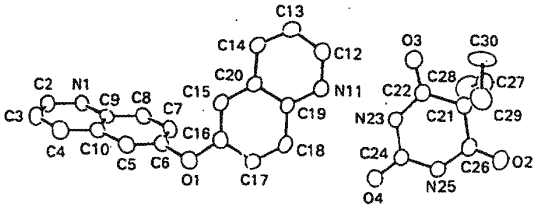


Fig. 1. An *ORTEP* (Johnson, 1965) drawing of the molecular structure.

In the quinolyl ring, the C—C bond lengths are between 1.352 and 1.419 Å, average 1.392 Å. The C—N bond lengths are between 1.314 and 1.367 Å, average 1.340 Å. The C—H bond lengths are in the expected range 0.93–1.01 Å. The average value of the C—O bond length is 1.394 Å; the C6—O—C16 bond angle is 117.5°. The above results are similar to those for the 6,6′-diquinolyl ether hydrate (Wang, Zhang & Kong, 1988). All atoms for each quinolyl ring are coplanar.

The 6,6′-diquinolyl ether molecule adopts a conformation with a dihedral angle of 108.8° between the two quinolyl rings.

The C30 atom in the ethyl group of the barbital molecule has abnormally high thermal parameters suggesting that it is disordered.

Strong intermolecular N1···H—N25 (N···N 2.88, N···H 1.90, H—N 0.99 Å, N···H—N 178°) and N11···H—N23 (N···N 2.88, N···H 1.95, H—N 0.94 Å, N···H—N 173°) hydrogen bonds occur. N11 is hydrogen bonded to N23 of the barbital of the same asymmetric unit while N1 is hydrogen bonded to N25 of the barbital of the asymmetric unit at $\frac{1}{2}+x, \frac{1}{2}-y, -\frac{1}{2}+z$. Thus barbital is linked with 6,6′-diquinolyl ether to form chains by the NH···N hydrogen bonds in which the barbital NH groups are donors and 6,6′-diquinolyl ether N atoms are acceptors (Hsu & Craven, 1974*a*). The dihedral angles between the planes of the two quinolyl rings and the barbital molecule of the same asymmetric unit are 105.12 and 5.23°, respectively.

Experimental

Crystal data

$C_{26}H_{24}N_4O_4$	$Z = 8$
$M_r = 456.51$	$D_x = 1.315$ Mg m^{-3}
Monoclinic	Mo $K\alpha$ radiation
$C2/c$	$\lambda = 0.7107$ Å
$a = 24.565$ (2) Å	Cell parameters from 25 reflections
$b = 17.750$ (2) Å	$\theta = 10$–$20°$
$c = 10.959$ (3) Å	$\mu = 0.0846$ mm^{-1}
$\beta = 105.24$ (3)°	$T = 294$ K
$V = 4610.4$ Å^3	0.40 × 0.25 × 0.25 mm

Data collection

CAD-4 four-circle diffractometer	2657 observed reflections $[I>2\sigma(I)]$
$\omega/2\theta$ scans	$R_{int} = 0.017$
Absorption correction: empirical	$\theta_{max} = 27°$
$T_{min} = 0.925$, $T_{max} = 1.000$	$h = 0 \rightarrow 32$
5384 measured reflections	$k = 0 \rightarrow 23$
4548 independent reflections	$l = -14 \rightarrow 14$
	3 standard reflections
	frequency: 90 min
	intensity variation: 1.5%

Refinement

Refinement on F	$\Delta\rho_{max} = 0.32$ e Å^{-3}
Final $R = 0.052$	$\Delta\rho_{min} = -0.40$ e Å^{-3}
$wR = 0.047$	Extinction correction: none
$S = 3.75$	Atomic scattering factors from *International Tables for X-ray Crystallography* (1974, Vol. IV)
2657 reflections	
379 parameters	
$(\Delta/\sigma)_{max} = 0.60$	

Table 1. *Fractional atomic coordinates and equivalent isotropic thermal parameters* (Å^2)

$$B_{eq} = (4/3)[a^2B(1,1)+b^2B(2,2)+c^2B(3,3)+ab(\cos\gamma)B(1,2)+ac(\cos\beta)B(1,3)+bc(\cos\alpha)B(2,3)].$$

	x	y	z	B_{eq}
O1	0.54456 (9)	0.1666 (2)	0.0807 (2)	5.66 (6)
O2	0.0831 (1)	0.1581 (2)	0.0483 (3)	7.56 (7)
O3	0.1826 (1)	0.0204 (2)	−0.1932 (3)	7.96 (8)
O4	0.2717 (1)	0.1735 (2)	0.1222 (3)	7.99 (8)
N1	0.6912 (1)	0.2277 (2)	−0.2129 (2)	4.27 (6)
N11	0.3260 (1)	0.0670 (2)	−0.1173 (2)	3.99 (6)
N23	0.2259 (1)	0.0959 (2)	−0.0341 (3)	5.05 (7)
N25	0.1769 (1)	0.1643 (2)	0.0853 (3)	5.05 (7)
C2	0.7431 (1)	0.2018 (2)	−0.1774 (3)	4.77 (8)
C3	0.7635 (1)	0.1567 (2)	−0.0702 (4)	5.17 (9)
C4	0.7293 (1)	0.1392 (2)	0.0050 (3)	4.87 (9)
C5	0.6341 (1)	0.1508 (2)	0.0427 (3)	4.48 (8)
C6	0.5810 (1)	0.1783 (2)	0.0037 (3)	4.17 (7)
C7	0.5631 (1)	0.2225 (2)	−0.1061 (3)	4.53 (8)
C8	0.5998 (1)	0.2376 (2)	−0.1768 (3)	4.43 (8)
C9	0.6555 (1)	0.2100 (2)	−0.1403 (3)	3.73 (7)
C10	0.6730 (1)	0.1661 (2)	−0.0294 (3)	3.92 (7)
C12	0.3134 (1)	0.0238 (2)	−0.2182 (3)	4.39 (8)
C13	0.3530 (2)	−0.0017 (2)	−0.2801 (3)	4.84 (8)
C14	0.4078 (1)	0.0181 (2)	−0.2337 (3)	4.62 (8)
C15	0.4796 (1)	0.0910 (2)	−0.0764 (3)	4.24 (7)
C16	0.4910 (1)	0.1390 (2)	0.0236 (3)	4.03 (7)
C17	0.4488 (1)	0.1634 (2)	0.0799 (3)	4.52 (8)
C18	0.3949 (1)	0.1394 (2)	0.0324 (3)	4.52 (8)
C19	0.3808 (1)	0.0896 (2)	−0.0724 (3)	3.58 (7)
C20	0.4240 (1)	0.0659 (2)	−0.1274 (3)	3.65 (7)
C21	0.1228 (1)	0.0762 (2)	−0.0782 (3)	4.65 (8)
C22	0.1789 (1)	0.0619 (2)	−0.1072 (3)	5.09 (9)
C24	0.2276 (1)	0.1464 (2)	0.0618 (3)	5.16 (9)
C26	0.1254 (1)	0.1363 (2)	0.0223 (3)	4.95 (9)
C27	0.0800 (2)	0.1000 (3)	−0.1991 (4)	5.7 (1)
C28	0.0968 (2)	0.1685 (3)	−0.2608 (5)	8.1 (1)
C29	0.1054 (2)	0.0019 (3)	−0.0205 (4)	6.9 (1)
C30	0.0957 (6)	−0.0606 (6)	−0.104 (1)	34.6 (6)

UM00013804
NOVARTIS EXHIBIT 1017
Novartis v. Regents, IPR2023-01346
Page 2550 of 4460

Table 2. *Geometric parameters* (Å, °)

O1—C6	1.399 (4)	C7—C8	1.362 (5)
O1—C16	1.388 (4)	C8—C9	1.409 (4)
O2—C26	1.211 (5)	C9—C10	1.413 (4)
O3—C22	1.219 (5)	C12—C13	1.400 (5)
O4—C24	1.212 (5)	C13—C14	1.355 (5)
N1—C2	1.315 (4)	C14—C20	1.411 (4)
N1—C9	1.367 (5)	C15—C16	1.358 (5)
N11—C12	1.314 (4)	C15—C20	1.407 (4)
N11—C19	1.365 (4)	C16—C17	1.407 (5)
N23—C22	1.360 (4)	C17—C18	1.358 (4)
N23—C24	1.375 (5)	C18—C19	1.419 (4)
N25—C24	1.373 (5)	C19—C20	1.414 (5)
N25—C26	1.366 (4)	C21—C22	1.516 (5)
C2—C3	1.399 (5)	C21—C26	1.522 (5)
C3—C4	1.359 (6)	C21—C27	1.519 (5)
C4—C10	1.419 (5)	C21—C29	1.569 (6)
C5—C6	1.352 (5)	C27—C28	1.501 (7)
C5—C10	1.416 (5)	C29—C30	1.41 (1)
C6—C7	1.406 (5)		
C6—O1—C16	117.5 (2)	C15—C16—C17	121.8 (3)
C2—N1—C9	118.0 (3)	C16—C17—C18	119.5 (3)
C12—N11—C19	117.9 (3)	C17—C18—C19	120.9 (3)
C22—N23—C24	126.2 (4)	N11—C19—C18	118.9 (3)
C24—N25—C26	125.9 (3)	N11—C19—C20	122.5 (3)
N1—C2—C3	123.6 (4)	C18—C19—C20	118.6 (3)
C2—C3—C4	119.8 (3)	C14—C20—C15	123.4 (3)
C3—C4—C10	118.6 (3)	C14—C20—C19	116.8 (3)
C6—C5—C10	119.3 (4)	C15—C20—C19	119.8 (3)
O1—C6—C5	118.2 (3)	C22—C21—C26	113.8 (3)
O1—C6—C7	119.5 (3)	C22—C21—C27	108.9 (4)
C5—C6—C7	122.1 (3)	C22—C21—C29	107.5 (3)
C6—C7—C8	119.4 (4)	C26—C21—C27	109.0 (4)
C7—C8—C9	120.7 (4)	C26—C21—C29	105.2 (3)
N1—C9—C8	118.6 (3)	C27—C21—C29	112.7 (3)
N1—C9—C10	122.1 (3)	O3—C22—N23	119.9 (3)
C8—C9—C10	119.3 (3)	O3—C22—C21	121.4 (4)
C4—C10—C5	122.8 (4)	N23—C22—C21	118.7 (3)
C4—C10—C9	118.0 (3)	O4—C24—N23	121.3 (3)
C5—C10—C9	119.3 (3)	O4—C24—N25	122.1 (4)
N11—C12—C13	123.7 (3)	N23—C24—N25	116.6 (3)
C12—C13—C14	118.9 (3)	O2—C26—N25	120.2 (3)
C13—C14—C20	120.1 (3)	O2—C26—C21	121.3 (3)
C16—C15—C20	119.5 (3)	N25—C26—C21	118.6 (3)
O1—C16—C15	123.7 (4)	C21—C27—C28	114.2 (3)
O1—C16—C17	114.4 (3)	C21—C29—C30	114.7 (7)

A solution of sodium barbital (1 mmol) in 10 ml H_2O was added dropwise to a solution of 6,6′-diquinolyl ether (1 mmol) in 15 ml absolute alcohol at room temperature (294 K), with constant stirring for 2 h. Brown stick-like or plate-like crystals were grown from the mixed solution after 10 d. The crystals were filtered, washed with H_2O and absolute alcohol. Analysis: calculated for $C_{26}H_{24}N_4O_4$: C 68.40, H 5.30, N 12.28%; found: C 68.18, H 5.12, N 12.40%.

Structure analysis was performed with the *SDP* program on a PDP11/44 computer. The crystal structure was solved by direct methods. The positions of 34 non-H atoms in the asymmetric unit were determined with *MULTAN*82 (Main *et al.*, 1982). The positions of all H atoms were determined by difference Fourier syntheses. The refinements were carried out with unit weights by full-matrix least squares for the coordinates of all atoms and anisotropic thermal parameters for the non-H atoms (isotropic thermal parameters for H atoms were fixed at 5 Å^2).

Lists of structure factors, anisotropic thermal parameters, and H-atom coordinates have been deposited with the British Library Document Supply Centre as Supplementary Publication No. SUP 55380 (19 pp.). Copies may be obtained through The Technical Editor, International Union of Crystallography, 5 Abbey Square, Chester CH1 2HU, England. [CIF reference: CR0411]

0108-2701/92/112098-03$06.00

References

Caira, M. R., Fazakerley, G. V., Linder, P. W. & Nassimbeni, L. R. (1973). *Inorg. Nucl. Chem. Lett.* **9**, 1101–1104.

Craven, B. M. & Gartland, G. L. (1970). *J. Pharm. Sci.* **59**, 1666–1670.

Gartland, G. L. & Craven, B. M. (1974). *Acta Cryst.* B**30**, 980–987.

Hsu, I.-N. & Craven, B. M. (1974*a*). *Acta Cryst.* B**30**, 974–979.

Hsu, I.-N. & Craven, B. M. (1974*b*). *Acta Cryst.* B**30**, 843–846.

Hsu, I.-N. & Craven, B. M. (1974*c*). *Acta Cryst.* B**30**, 988–993.

Johnson, C. K. (1965). *ORTEP*. Report ORNL-3794. Oak Ridge National Laboratory, Tennessee, USA.

Kiryu, S. (1971). *J. Pharm. Sci.* **60**, 699–703.

Main, P., Fiske, S. J., Hull, S. E., Lessinger, L., Germain, G., Declercq, J.-P. & Woolfson, M. M. (1982). *MULTAN*82. *A System of Computer Programs for the Automatic Solution of Crystal Structures from X-ray Diffraction Data*. Univs. of York, England, and Louvain, Belgium.

Pezeshk, A., Greenaway, F. T. & Sorenson, J. R. J. (1983). *Inorg. Chim. Acta*, **80**, 191–195.

Voet, D. (1972). *J. Am. Chem. Soc.* **94**, 8213–8222.

Voet, D. & Rich, A. (1972). *J. Am. Chem. Soc.* **94**, 5888–5891.

Wang, X., Zhang, G. & Kong, Q. (1988). *Ningxiadaxue Xuebao* (*Zirankexueban*), 3, 70–76. [In Chinese.]

Zhang, G., Tan, Z. & Li, Y. (1986). *Yingyong Huaxue*, 3(4), 48–50.

Acta Cryst. (1992). C**48**, 2098–2100

(*E*)-Methyl 2-Phenyl-2-(3-pyridyl)vinyl Sulfide

JACQUES METIN* AND DANIELLE ROCHE

Groupe de Recherche en Pharmacochimie, UFR de Pharmacie, BP 38, 63001 *Clermont-Ferrand CEDEX, France*

HENRI VESCHAMBRE

Laboratoire de Chimie Organique Biologique, URA 485 *CNRS, Université Blaise-Pascal,* 63117 *Aubière CEDEX, France*

MICHEL MADESCLAIRE*

Groupe de Recherche en Pharmacochimie, UFR de Pharmacie, BP 38, 63001 *Clermont-Ferrand CEDEX, France*

(*Received* 2 *April* 1992; *accepted* 6 *July* 1992)

Abstract

The unambiguous identification by X-ray diffraction of the (*E*) configuration of the title compound confirms a previous tentative assignment by NMR. The two planar rings (phenyl and pyridyl) are at an angle of about 70°. Crystal cohesion is ensured by a dense network of van der Waals contacts.

© 1992 International Union of Crystallography

UM00013805
NOVARTIS EXHIBIT 1017
Novartis v. Regents, IPR2023-01346
Page 2551 of 4460

Disappearing and Reappearing Polymorphs. The Benzocaine:Picric Acid System

Jan-Olav Henck,*,†,‖ Joel Bernstein,*,‡ Arkady Ellern,‡ and Roland Boese§

Contribution from the Institut für Pharmakognosie der Universität Innsbruck Innrain 52, Josef-Moeller-Haus, 6020 Innsbruck, Austria, Department of Chemistry, Ben-Gurion University of the Negev, Beer Sheva, Israel 84105, and FB8/Anorganische Chemie, Universität-GH Essen, Universitätstrasse 5, 45117 Essen, Germany

Received June 12, 2000

Abstract: The low-melting polymorphic modification of the 1:1 complex of benzocaine (**BC**) and picric acid (**PA**) had earlier been reported to be an example of a "disappearing polymorph". The **BC**:**PA** system has been reinvestigated by thermomicroscopy, calorimetry, solid-state NMR, and X-ray crystallography. The phase diagram has been derived, and robust procedures for the crystallization of the two 1:1 complexes, a hydrate of the 1:1 complex, and a 2:1 complex have been devised. The structures of all four phases have been determined and compared using graph set analysis to characterize the hydrogen-bonding patterns. It is shown that the thorough microscopic investigation of the thermal behavior, combined with calorimetric methods, can lead to the development of strategies to crystallize metastable polymorphic forms which may be difficult to obtain once their stable congeners have been obtained.

Introduction

Polymorphism, the ability of a substance to exist in several different crystal forms or modifications, is a frequently observed phenomenon in molecular compounds.[1] If a solid substance includes a solvent during crystallization, this structure is known as a pseudopolymorph, and in case of, e.g., water such crystal forms are generally called hydrates.[2] The polymorphic modifications of a compound are chemically identical but usually differ in their physical and chemical properties, such as density, vibrational spectra, and diffraction patterns.

Since a particular polymorph may have desirable properties, it may be useful to develop a robust method to obtain that polymorphic modification consistently and reproducibly. There are many documented cases of difficulties in obtaining crystals of a particular known modification.[3,4] Such difficulties may have serious practical consequences: a material designed to give a particular structure may exhibit an undesired polymorphic one;[5] a plant manufacturing a particular modification may have to close because it has been "poisoned" by an undesired polymorph;[6] a commercial drug formulation may no longer be available on the market due to the appearance of an undesired polymorphic modification.[7] We recently documented a number of representative cases in which it was difficult to obtain a given polymorphic form even though previously it had often been obtained routinely over long periods of time—so-called "disappearing polymorphs".[3] In the conclusion to that review, we stated our belief "that once a particular polymorph has been obtained, it is always possible to obtain it again; it is only a matter of finding the right experimental conditions". One of the challenges to those dealing with the preparation of solids is to be able to rationally develop those conditions and to control the polymorphic form obtained—in many instances to recover the disappeared polymorph. In this paper we present a case study of how such a challenge might be met.

One of the examples cited in the above-mentioned review was the case of benzocaine picrate (**BC**:**PA**). This binary system has been studied previously at least three separate times.[8−10] In 1972, Nielsen and Borka[8] reported the first preparation of the complex (now known as Mod. II) with a melting point of 130−132 °C. At the time, this modification was used as a pharmacopoeial standard for the identification of benzocaine (a topical anesthetic). Subsequently, the same authors prepared a high-melting modification (now known as Mod. I), mp 162−163 °C, whereupon they encountered severe difficulties in preparing and maintaining Mod. II for more than several hours before it transformed into Mod. I.[11] The low-melting modification is thermodynamically unstable at 20 °C.[8]

In 1974, Borka and Kuhnert-Brandstätter[9] reinvestigated the system using thermomicroscopy and found four modifica-

* To whom correspondence should be addressed.
† Universität Innsbruck.
‡ Ben-Gurion University of the Negev.
§ Universität-GH Essen.
‖ Current address: Bayer AG, PH-PD PQCD1, Building E39, 51368 Leverkusen, Germany.

(1) The April 1, 1998, release of the Cambridge Structural Database contains 181 309 entries, of which 5641 contain the qualifier "form", 163 the qualifier "polymorph", 172 the qualifier "modification", and 146 the qualifier "mod". Not all of these are entries for the structures of all polymorphs for a particular substance, but these numbers indicate that roughly 3% of the entries in the database are for polymorphic materials.

(2) Byrn, S. R. *Solid State Chemistry of Drugs*, 2nd ed.; SSCI, Inc.: West Lafayette, IN, 1999; pp 513−514.

(3) Dunitz, J. D.; Bernstein, J. *Acc. Chem. Res.* **1995**, *28*, 193−200.

(4) Webb, J.; Anderson, B. *J. Chem. Educ.* **1978**, *55*, 644.

(5) Aakeröy, C. B.; Nieuwenhuyzen, M.; Price, S. L. *J. Am. Chem. Soc.* **1998**, *120*, 8986−8993.

(6) Anonymous. *Ind. Eng. Chem.* **1953**, 11a.

(7) Chemburkar, S. R.; Bauer, J.; Deming, K.; Spiwek, H.; Patel, K.; Morris, J.; Henry, R.; Spanton, S.; Dziki, W.; Porter, W.; Quick, J.; Bauer, P.; Donaubauer, J.; Narayanan, B. A.; Soldani, M.; Riley, D.; McFarland, K. *Org. Process Res. Dev.* **2000**, *4*, 413−417.

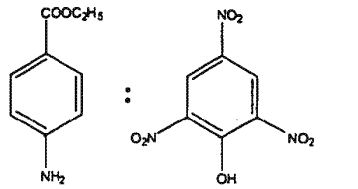
(8) Nielsen, T. K.; Borka, L. *Acta Pharm. Suecica* **1972**, *9*, 503−505.

(9) Borka, L.; Kuhnert-Brandstätter, M. *Arch. Pharmaz.* **1974**, *307*, 377−384.

(10) Togashi, A.; Matsunaga, Y. *Bull. Chem. Soc. Jpn.* **1987**, *60*, 1171−1173.

10.1021/ja002113o CCC: $20.00 © 2001 American Chemical Society
Published on Web 02/10/2001

UM00013806
NOVARTIS EXHIBIT 1017
Novartis v. Regents, IPR2023-01346
Page 2552 of 4460



Benzocaine (BA) Picric acid (PA)

tions of **BC**:**PA**. They further identified two modifications of a (**BC**)$_2$:**PA** complex as well as a monohydrate. Apparently unaware of both of these earlier works, Togashi and Matsunaga also reported a (**BC**)$_2$:**PA** complex and an additional charge-transfer complex between the two compounds, observed by using differential scanning calorimetry (DSC).[10] No structural studies on any of the complexes were reported.

The aims of the work we report here were (1) to develop a general strategy and specific methods for controllably and reproducibly obtaining the "disappearing" modification II of **BC**:**PA**; (2) to develop methods for obtaining single crystals suitable for X-ray structure determination of as many as possible of the **BC**:**PA** species reported by earlier authors; and (3) to fully characterize the **BC**:**PA** phases by spectroscopic and structural techniques.

Experimental Strategy

Since the discovery of polymorphism in 1822,[12] one of the principal techniques for investigating the phenomenon has been optical microscopy and, in the latter part of the 20th century, thermomicroscopy.[13−16] These methods are particularly useful in detecting the existence of polymorphs and polymorphic transitions quickly and easily. In the last few decades, more sophisticated analytical techniques have supplanted the two classic ones,[17] but the net result of years of effort by a number of groups is that many polymorphic materials have been identified and characterized.[16,18−20] Despite the success of these methods, very few of these findings have been utilized as the starting point for structural studies.[21] The general problem apparently lies in the difficulty of translating the microscopic observations to the growth of single crystals that can be used for structure determination. In this work, we adopted a strategy for crystal growth experiments aimed at obtaining crystals for X-ray determination of the various phases of **BC**:**PA** based on the observations made using optical and thermomicroscopy and on the appearance and disappearance of those phases. We believe that this approach can be widely utilized and thus can provide the means for greatly expanding our understanding of the structural basis for polymorphic behavior.

Results

The Phase Diagram. The phase diagram can provide very useful information and guidelines for the preparation of a particular polymorphic modification. Much of the data for the preparation of the phase diagram may be readily obtained from thermomicroscopic studies. In fact, for a two-component system, such as **BC**:**PA**, Kuhnert-Brandstätter pointed out that "Kofler's contact method of thermal analysis offers the possibility of investigating organic two component systems qualitatively in the shortest possible time in the simplest possible manner."[16,22] More quantitative details may be added from DSC measurements.

Details on the preparation of the **BC**:**PA** contact sample and analysis are given in the Experimental Procedures section. Figure 1a shows the photomicrograph of the recrystallized contact preparation of **BC** and **PA** at 25 °C. The interference colors are due to the use of crossed polarizers. The pure compounds are at the extremities of the preparation, while in the region where the original compounds have merged, a number of different areas may be observed, due to the formation of different crystalline species combining the two components. Heating this preparation on the hot-stage microscope to a temperature of about 88 °C shows (Figure 1b) the eutectic melt of **BC** and the broad dark yellow crystals of a new compound. Due to the crossed polarizers, the isotropic melt appears black. As can be seen in Figure 1c, at about 120 °C on the left side of the preparation **BC** is melted, and on the right side the eutectic between **PA** and the remaining crystals of the **BC**:**PA** 1:1 complex melts. Figure 1d shows the situation which is observed at 122 °C. **PA** is almost melted, and in the middle of the preparation a eutectic melt appears. Thus, two chemically different kinds of complexes between **BC** and **PA** have been formed. The one on the right side is the 1:1 complex, while the small strip on the left side (the **BC** side) is a complex with composition (**BC**)$_2$:**PA**.[9] The former melts at 129 °C, while the latter shows a melting point at 124 °C.

The results obtained by means of thermomicroscopy and DSC experiments on different mixtures of benzocaine and picric acid led to the phase diagram (Figure 2). These investigations indicate the existence of two modifications of the 1:1 complex as well as of one modification of the 2:1 complex. The eutectic points of Mod. II of the 1:1 complex with benzocaine and picric acid are located at mole fractions of 0.07 (88 °C) and 0.85 (109 °C), respectively. The peritectic of Mod. II with the 2:1 complex appears at a mole fraction 0.33 and about 120 °C, and the eutectic between the 2:1 complex and benzocaine is located at 0.3 and at 110 °C.

Preparation of Single Crystals. The thermodynamic phase relationship between the two forms of **BC**:**PA** may be

(11) The authors reported the disappearing phenomenon and their attempts to overcome it as follows:[8] "As a matter of curiosity, it ought to be mentioned that once the stable modification was obtained, the metastable modification could no longer be isolated. It was first observed by one of us (TKN). This observation was later confirmed in a separate laboratory (LB). Further, it was found that after discarding all samples, washing the equipment and laboratory benches and waiting for 8−12 days, the low melting modification could be isolated again. This has now been repeated several times in our laboratories. Obviously the seeding effect during the formation of the primary crystals (or during the very procedure of determination of the melting point) is exceptionally strong."

(12) Mitscherlich, E. *Ann. Chim. Phys.* **1822**, *19*, 350−419.

(13) Chamot, E. M.; Mason, C. W. *Handbook of Chemical Microscopy, Volume I, Principles and Use of Microscopes and Accessories: Physical Methods for the Study of Chemical Problems*, 3rd ed.; John Wiley and Sons: New York, 1958.

(14) Kofler, L.; Kofler, A. *Thermo-MikroMethoden zur Kennzeichnung organischer Stoffe und Stoffgemische*; Wagner: Innsbruck, 1954.

(15) McCrone, W. C. *Fusion Methods in Chemical Microscopy*; Interscience: New York, 1956.

(16) (a) Kuhnert-Brandstätter, M. *Thermomicroscopy in the Analysis of Pharmaceuticals*; Pergamon Press: Oxford, 1971 Kuhnert-Brandstätter, M. In *Thermomicroscopy of Organic Compounds*; Svehla, G., Ed.; Comprehensive Analytical Chemistry, Vol. XVI; Elsevier: Amsterdam, 1982; pp 329−513.

(17) Threlfall, T. *Analyst* **1995**, *120*, 2435−2460.

(18) Burger, A.; Ramberger, R. *Mikrochim. Acta* **1979**, *II*, 259−271.

(19) Haleblian, J. K.; Borka, L. *Acta Pharm. Jugosl.* **1990**, *40*, 71−94.

(20) Borka, L. *Pharm. Acta, Helv.* **1991**, *66*, 16−22.

(21) For a more detailed account of the use and decline of the use of the microscope in polymorphism research, see: Bernstein, J.; Henck, J.-O. *Cryst. Eng.* **1998**, *1*, 119−128.

(22) For a summary of the contact method, see also: Emons, H.-H.; Keune, H.; Seyfarth, H.-H. In *Chemical Microscopy*; Svehla, G., Ed.; Comprehensive Analytical Chemistry, Vol. XVI; Elsevier: Amsterdam, 1982; pp 180−184.

UM00013807
NOVARTIS EXHIBIT 1017
Novartis v. Regents, IPR2023-01346
Page 2553 of 4460

BEST AVAILABLE COPY

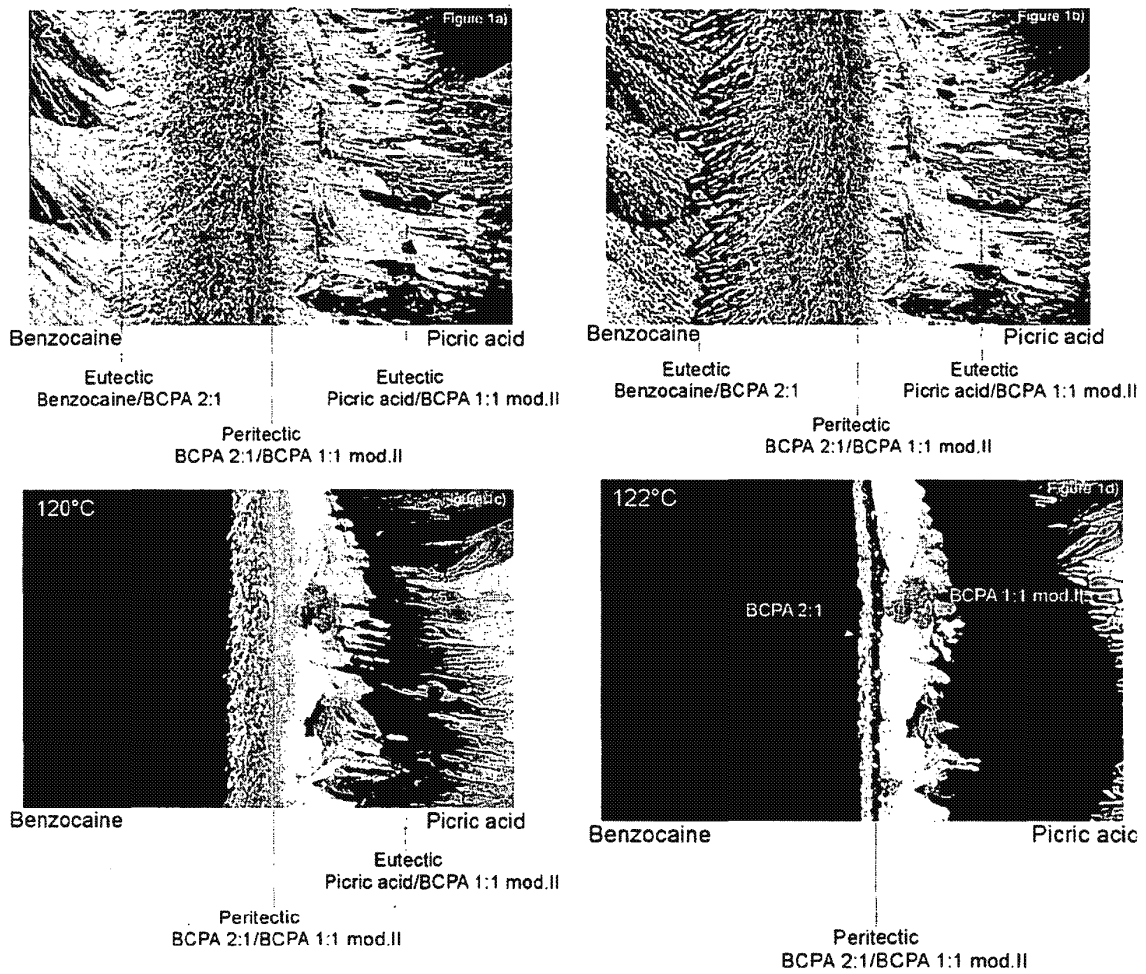


Figure 1. Photographs of the microscope slide Kofler preparations showing the various phases of the **BC**:**PA** binary system: (a) 25 °C, (b) 87 °C, (c) 120 °C, and (d) 123 °C (see text for explanation and discussion of details of the phenomena observed here).

enantiotropic or monotropic.[16] In the former case, the choice of crystallization conditions for one of the two polymorphs would be more facile, because thermodynamically controlled crystallization conditions could be chosen at temperatures below the thermodynamic transition point. To determine the monotropism/enantiotropism, we crystallized microcrystalline **BC**:**PA** Mod. II by means of thermomicroscopy and carried out DSC measurements on the resulting solid. The DSC trace shows an exothermic transition of Mod. II into Mod. I. We could then apply the empirical heat-of-transition rule[23] to conclude that these two crystal forms are monotropically related (Table 1). This means that Mod. I is the thermodynamically stable crystal form from absolute zero up to its melting point.

Since the lower melting Mod. II is thermodynamically less stable at all temperatures below the melting point, "kinetic" conditions must be created to attempt to crystallize this form. Therefore, a high-temperature (80 °C) crystallization was attempted, with water as the solvent, yielding single crystals up to 1 mm in maximum dimension. Since the prior work of Nielson and Borka[8] indicated that seeds of the stable form must be excluded, we obtained the less stable form prior to carrying out crystallization experiments aimed at obtaining the more stable one.

As Mod. I is the thermodynamically preferred form, an "equilibrium" crystallization is preferred over a "kinetic" one. Nielsen and Borka[8] obtained Mod. I by "excessive drying of [Mod. II] at 105 °C", conditions which are not particularly conducive to an "equilibrium" situation, nor to the growth of single crystals. Also, the existence of the hydrate (determined in the thermomicroscopic studies) suggests that the presence of water might be problematic in attempting to obtain nonhydrated phases. Hence, we resorted to a nonaqueous gel-diffusion crystallization,[24] using Sephadex as the gel medium, and obtained large single crystals (1−2 mm maximum dimension) after 3 days at 20 °C.

The rather drastic drying procedure described by Nielsen and Borka[8] to obtain Mod. I, Borka and Kuhnert-Brandstätter's report,[9] and our own observations on the hot-stage microscope indicated the existence of a hydrate of **BC**:**PA**. To obtain single crystals of this material, we attempted a crystallization from a

(23) According to the "heat-of-transition rule",[18] if the phase transition is exothermic, then there is no transition point below the experimentally observed transition temperature. This is generally observed if two transitions are monotropically related. As can be seen in Table 1, the phase transition has been determined by DSC measurements to be exothermic.

(24) Desiraju, G. R.; Curtin, D. Y.; Paul, I. C. *J. Am. Chem. Soc.* **1977**, *99*, 6148−6149.

UM00013808
NOVARTIS EXHIBIT 1017
Novartis v. Regents, IPR2023-01346
Page 2554 of 4460

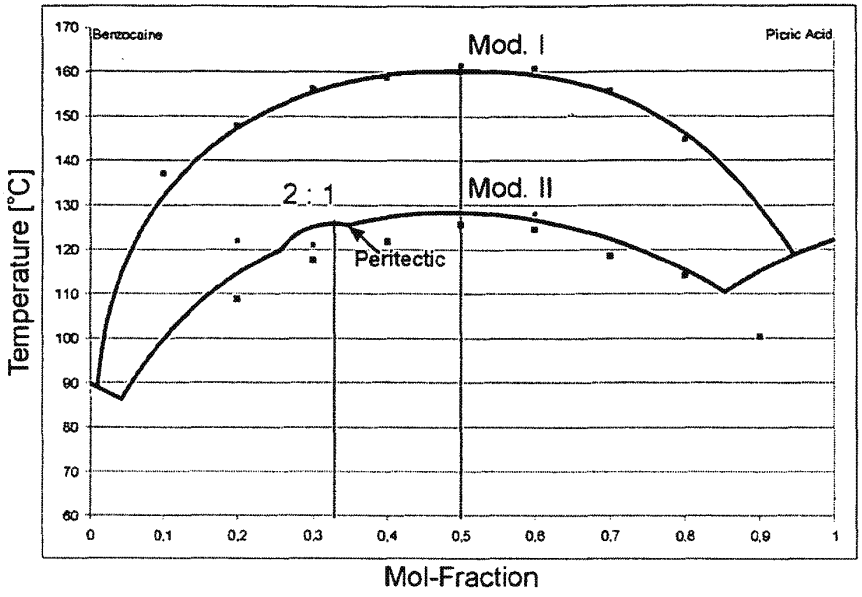


Figure 2. Phase diagram of the **BC**:**PA** system.

Table 1. Physicochemical Data of **BC**:**PA** Mod. I, **BC**:**PA** Mod. II, and $(BC)_2$:**PA**

	BC:**PA** Mod. I	**BC**:**PA** Mod. II	$(BC)_2$:**PA**
mp (°C), DSConset	161	129	119
thermomicroscopy	161	128	120
enthalpy of fusion (kJ mol^{-1})	63	56	
enthalpy of transition (kJ mol^{-1})		−9 → Mod. I	
entropy of fusion[a] (J mol^{-1} K^{-1})	145	118	

[a] Calculated by $\Delta S_f = \Delta H_f\ mp^{-1}$.

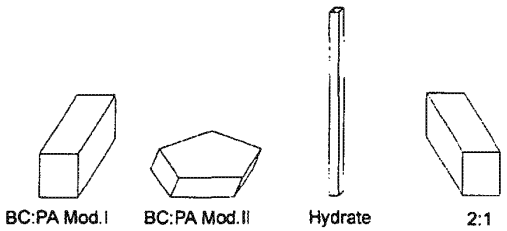


Figure 3. Line drawing representation of the morphologies of the four different crystalline materials obtained, as labeled.

saturated water solution in a sealed virgin flask (to prevent the unintentional incursion of seeds of any of the other forms) at 20 °C; needle-shaped crystals (up to 4 mm long) appeared after 48 h.

Crystals of the 2:1 complex were obtained by slow evaporation (ca. 4 weeks) of a 1:1 mixture of the components in 2-propanol at 4 °C. Admittedly, this was not an experiment designed to obtain the 2:1 complex, but the ample evidence to indicate its existence increased our interest in examining all the crystals obtained and motivated our attempts to obtain the crystals, using conditions different from those used for the other three species.

The crystals of all four complexes were yellow but were easily distinguished by their morphology (Figure 3) and, very clearly, by their melting points.

Crystal data for the four structures are given in Table 2; details of the structure determination are given in the Experimental Procedures section.

Crystal Structures. (a) General Features. All four structures are ionic picrates, the acidic hydrogen of the hydroxyl group on picric acid having been transferred to an amino group on benzocaine. The atomic numbering, given in a the ORTEP diagram (for $(BC)_2$:**PA**), is identical for all four structures

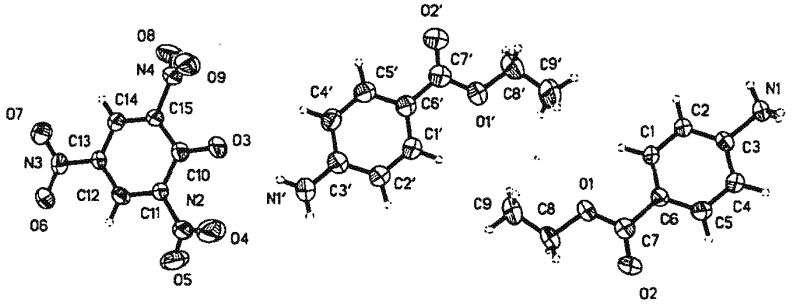


Figure 4. ORTEP diagram of the molecules in the $(BC)_2$:**PA** structure, showing the atomic numbering. Hydrogens are numbered according to the atoms to which they are attached. Numbering is identical for the other structures; the oxygen of the water molecule in **BC**:**PA**·H_2O is O01.

UM00013809
NOVARTIS EXHIBIT 1017
Novartis v. Regents, IPR2023-01346
Page 2555 of 4460

Table 2. Summary of Crystallographic Data for the Four Compounds Studied

	BC:PA Mod. I	BC:PA Mod. II	$(BC)_2$:PA	BC:PA·H_2O
formula	$C_{15}H_{14}N_4O_9$	$C_{15}H_{14}N_4O_9$	$C_{24}H_{25}N_5O_{11}$	$C_{15}H_{16}N_4O_{10}$
formula weight	394.3	394.3	559.5	412.3
crystal system	monoclinic	triclinic	triclinic	monoclinic
space group	$P2_1/n$	$P\bar{1}$	$P\bar{1}$	$P2_1$
color of crystal	yellow	yellow	yellow	yellow
Z	4	2	2	2
a (Å)	7.149(3)	7.304(3)	8.190(2)	4.1478(8)
b (Å)	12.240(7)	8.231(2)	8.857(3)	12.732(3)
c (Å)	19.594(9)	15.361(5)	19.747(5)	17.518(4)
α (°)	90	99.91(2)	78.59(2)	90
β (°)	96.77(3)	99.53(2)	85.13(2)	93.84(3)
γ (°)	90	106.73(3)	67.93(2)	90
R-factor (%)	5.1	3.3	4.0	3.8
GOF (on F^2)	0.988	0.969	0.908	0.980

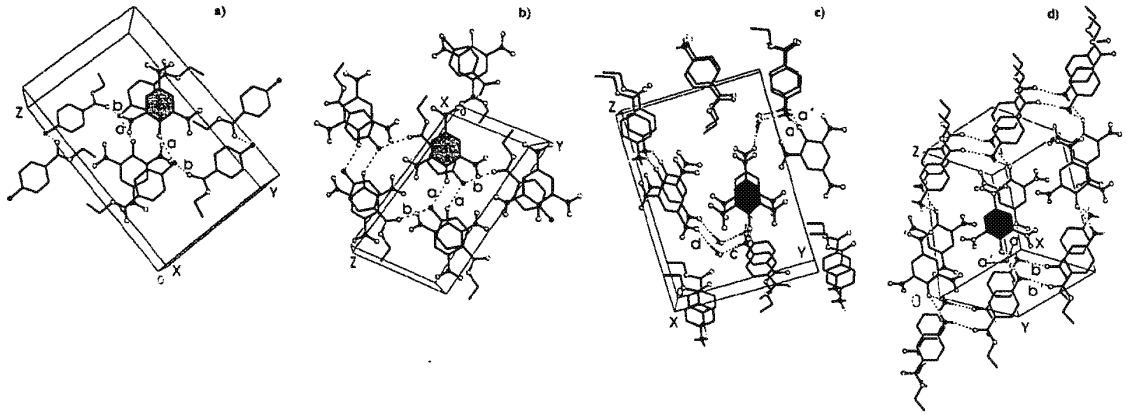


Figure 5. Packing diagrams the four crystal structures. For ease of comparison, in all cases the view is chosen on the best plane of the shaded picrate anion as a reference, with the C−O vector pointing down. Some slight rotational adjustments of the views have been made to facilitate better viewing of the packing and the hydrogen bonds. Carbon atoms are not explicitly drawn. Oxygens are represented by empty circles, and nitrogens are represented by filled circles. Hydrogens have been eliminated for clarity except where noted. The unit cell axes are marked as *X,Y,Z*, while hydrogen bonds are identified by lowercase letters (see text). (a) **BC**:**PA** Mod. I, (b) **BC**:**PA** Mod. II, (c) **BC**:**PA**·H_2O (hydrogens are included on the water molecule and on N1 of **BC**), and (d) $(BC)_2$:**PA** (hydrogens on N1 and N1′ are included).

Table 3. Rotation Angles (deg) of Nitro Groups in **PA** in the Four Crystal Structures

angle about C−N bond	BC:PA Mod. I	BC:PA Mod. II	BC:PA·H_2O	$(BC)_2$:PA
C11−N2	−176.0	−144.4	−168.5	−152.8
C13−N3	4.7	11.3	8.2	0
C15−N4	−37.9	147.4	19.2	−49.4

(Figure 4). There are no unusual bond lengths or angles. Only two of the torsion angle values for the ethyl ester chain of the **BC** moiety suggest some conformational variation, namely that for C5−C6−C7−O1 of **BC**:**PA** Mod. I (157.6°) and that for C7−O1−C8−C9 of **BC**:**PA** Mod. II (161.0°) compared to the others, which are all in the range 170−180°. These conformational differences were not investigated further.

The rotations of the nitro groups in **PA** are summarized in Table 3. That para to the phenolate oxygen is essentially coplanar with the benzene ring in all cases. The ortho nitro groups are rotated out of the phenyl plane, those about C11−N2 all in the same sense but to varying degrees, while those about C15−N4 are also rotated to approximately the same degree, but the rotation in the hydrate is opposite in sense from the other three instances.

BC:**PA** Mod. I in (Figure 5a) may be described as mixed stacks of ···BC^+··· PA^-··· with apparently $\pi-\pi$ plane-to-plane interactions along the [100] direction. The best planes of the BC^+ and PA^- within a stack make an angle of 2.3° with each other, the distance between centers of rings being 4.04 Å. **BC**:**PA** Mod. II (Figure 5b) also crystallizes in mixed $\pi-\pi$ stacks of ···$\mathbf{BC}^+$···$\mathbf{PA}^-$···, again essentially along [100]. The mode of overlap along the stack is such that the four atom chain of the ester group is nearly parallel to the long (O--C···*p*-NO_2) axis of the molecule, while in Mod. I the chain of the ester group is nearly perpendicular to that axis. The angle between the phenyl rings (7.6°) is slightly larger, but the distance between centers is smaller (3.70 Å), indicating a greater degree of overlap between neighboring molecules in Mod. II.

In contrast to the two anhydrous complexes, in **BC**:**PA**·H_2O (Figure 5c) the cations and anions are arranged in segregated stacks ···$\mathbf{BC}^+$···$\mathbf{BC}^+$··· and ···$\mathbf{PA}^-$···$\mathbf{PA}^-$···. The perpendicular distance between planes in the BC^+ stack is 3.73 Å, while that in the PA^- stack is 3.45 Å. Sheets of cations or anions are generated by the screw operation along the *b* axis, and in these sheets cations and anions alternate along the *c* axis. The angle between the phenyl rings of BC^+ and PA^- is 35°. There are sheets of cations and sheets of anions, both parallel to the stacking direction, so that the structure is built up of parallel sheets of cations and anions, in a manner similar to zinc blende. Since the structure is polar, this means that, as drawn in Figure 5c, the (001) and (00$\bar{1}$) faces of the crystal should be oppositely

UM00013810
NOVARTIS EXHIBIT 1017
Novartis v. Regents, IPR2023-01346
Page 2556 of 4460

Table 4. Geometric Features of the Hydrogen Bonds Discussed in the Text (The Designations a, a'...d Correspond to the Hydrogen Bonds in Figure 4, and Are Defined for Each Section)

(a) N^+—H···$^-$O—C

	$N^+\cdots{}^-O$ (Å)	H···$^-$O (Å)
BC:PA Mod. I	2.681(4)	1.772(3)
BC:PA Mod. II	2.667(3)	1.716(3)
(BC)$_2$:PA	2.762(4)	1.792(4)
a'[a]	3.024(4)	2.182(4)
BC:PA·H_2O	2.678(7)	1.709(8)
a'	2.791(7))	2.083(7)

(b) N^+—H···O=C

	$N^+\cdots$O (Å)	H···O (Å)
BC:PA Mod. I	2.834(4)	1.956(3)
BC:PA Mod. II	2.883(3)	2.279(3)
(BC)$_2$:PA	2.860(4)	1.945(4)
b'[b]	2.994(4)	2.163(4)
BC:PA·H_2O	–	–

(c) N^+—H···O(w), (d) O(w)—H···O=N(nitro)

BC:PA·H_2O[c]	D···A (Å)	H···A (Å)
c[c]	2.803(8)	1.983(7)
d	2.948(7)	1.787(7)

[a] For this entry, a' is the hydrogen bond from the *neutral* **BC** to the PA^- in the 2:1 complex. [b] For this entry, b' is the hydrogen bond from the *neutral* **BC** to the PA^- in the 2:1 complex. [c] The generic notation (D—H···A) for the hydrogen bond is used here, since c and d are different hydrogen bonds.

charged as in zinc blende.[25] The **(BC)$_2$:PA** complex (Figure 5d) is composed of BC^+ cations, PA^- anions, and an additional neutral **BC** molecule, confirming the conclusion of Togashi and Matsunaga from IR data.[10] The PA^- anions are arranged across successive inversion centers at $^1/_2$, $^1/_2$, $^1/_2$, forming a stack in the *b* axis direction, with a perpendicular distance between atoms of one picrate ring and the plane of its centrosymmetric neighbor of 3.48−3.51 Å and a distance between ring centers of 5.90 Å. Translation of these stacks along the *a* crystallographic axis generates a sheet of picrate anions. The **BC** molecules are also stacked along the *b* crystallographic axis, with alternating neutral **BC** and BC^+ cations. The angle between the phenyl rings for the two species is 13.6°, with a center-to-center distance of 3.82 Å. Sheets of these **BC** moieties are then generated by the *a* axis translation.

(b) Hydrogen Bonding. There are clearly a number of possibilities for hydrogen bonding in these four structures, and a comparison of the hydrogen-bonding patterns facilitates recognizing the similarities and differences among them.

The hydrogen bonds are defined and their metrics are compared in Table 4. Hydrogen bond **a** appears in all structures and is remarkably constant, save for the bond to the neutral **BC** in **(BC)$_2$:PA** and for the second hydrogen bond of the type (noted as **a'**) in the hydrate. Hydrogen bond **b** appears in all but the hydrate, but the H···O distance is longer in **BC:PA** Mod. II and to the neutral **BC** in **(BC)$_2$:PA** than in the two other cases.

The two hydrogen bonds involving water (once as donor and once as acceptor) in the hydrate are denoted as **c** and **d** in Table 4. It is not clear if the long O—H and concomitantly short H···O distances for the latter are of significance or merely a result of the unconstrained refinement of the hydrogen atom position in the crystal structure analysis.

The most direct way of summarizing the hydrogen-bonding patterns and comparing them is through the use of graph sets.[26,27] The graph set assignments are conveniently summarized in (symmetric) matrix-type tables,[27] in which the diagonal elements are the first level graph set assignments and the off-diagonal elements are the second level assignments. Consistent ordering of the columns and rows with chemically identical hydrogen bonds through the four molecules (to the extent that it is possible) greatly facilitates comparison of hydrogen-bonding patterns among the structures. These graph set assignments are summarized in Figure 6.

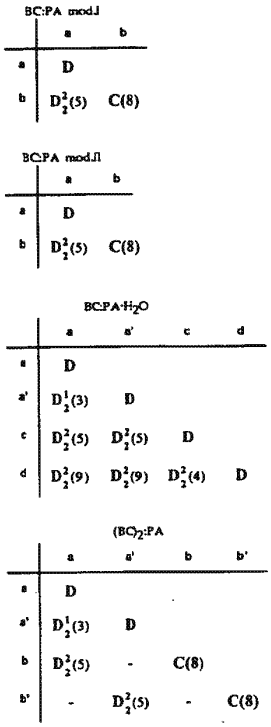


Figure 6. Graph set assignments for the hydrogen bond patterns in the four structures studied. The hydrogen bonds are denoted by lowercase letters that correspond to the tabulation in Table 5 and the notation in Figure 6. As in ref 27, diagonal elements represent first level graph assignments, while off-diagonal ones represent second level graph sets composed of the two hydrogen bonds forming that element. A hyphen indicates that there is no connectivity between the hydrogen bonds at the second level.

The same two *individual* hydrogen bonds are present in **BC:PA** Mod. I and **BC:PA** Mod. II. The monotropic transformation from mod. II to mod. I is not accompanied by any overall pattern change. Also, the fact that the ~7 Å axis is maintained suggests that the transformation takes place within the sheets nearly perpendicular to this axis. The transformation, observed by microscope, is seen to be a solid−solid transformation but involves extensive shattering of the crystalline material, indicating that quite drastic structural changes are, indeed, taking place. However, a careful visual examination and comparison of the two structures with all of these considerations did not reveal a simple geometric mechanism for the phase change.

Thermal Studies and Thermodynamic Relationships among the Structures Studied. The structural properties of Mod. I

(25) Mak, T. C. W.; Zhou. G.-D. *Crystallography in Modern Chemistry*; Wiley-Interscience: New York, 1992; pp 77−80.

(26) Etter, M. C. *Acc. Chem. Res.* **1990**, *23*, 120−127.

(27) Bernstein, J.; Davis, R. E.; Chang. N.-L.; Shimoni, L. *Angew. Chem., Int. Ed. Engl.* **1995**, *35*, 1555−1567.

UM00013811
NOVARTIS EXHIBIT 1017
Novartis v. Regents, IPR2023-01346
Page 2557 of 4460

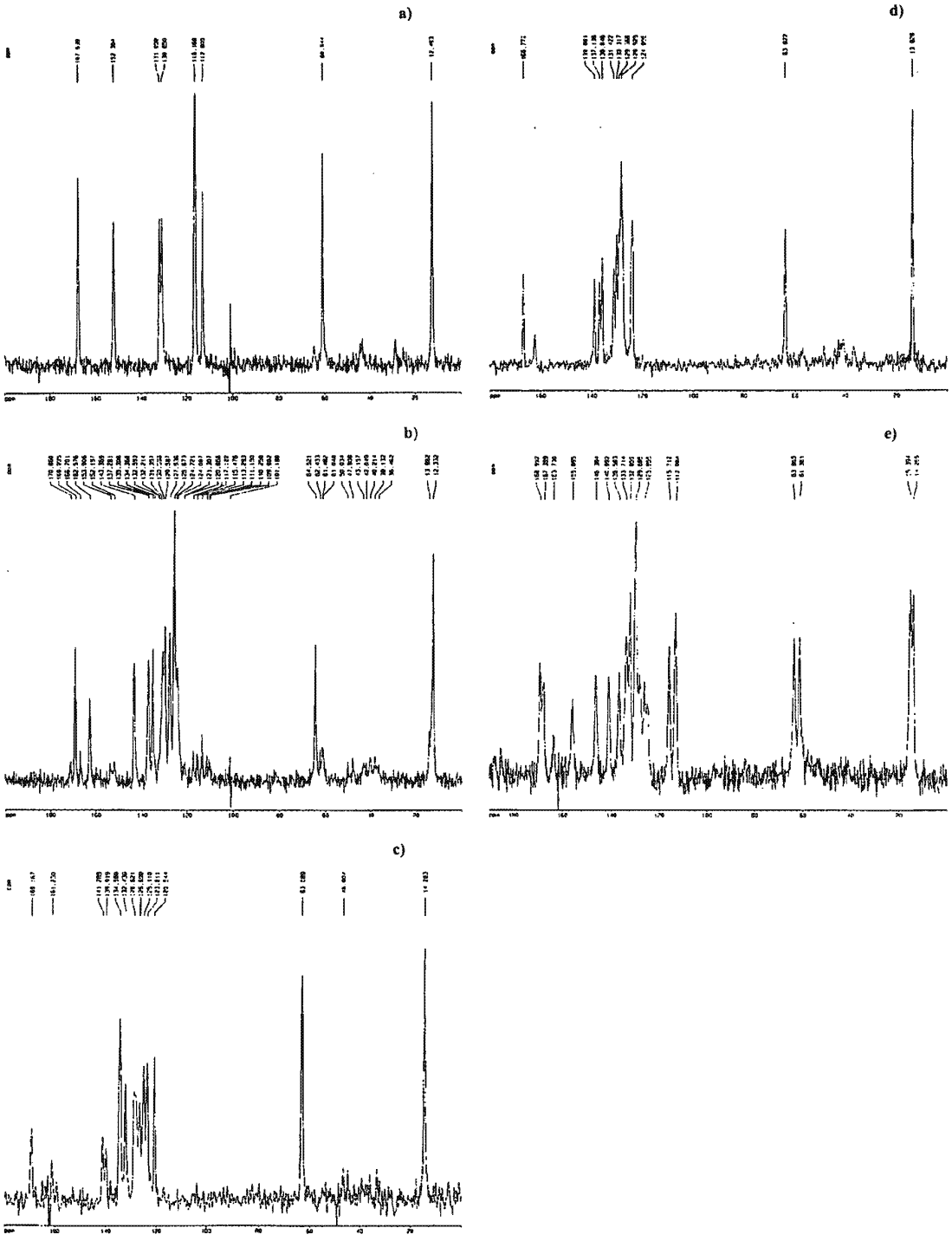


Figure 7. CP-MAS solid-state NMR spectra: (a) benzocaine, (b) **BC**:**PA** Mod. I, (c) **BC**:**PA** Mod. II, (d) **BC**:**PA**·H_2O, and (e) $(\mathbf{BC})_2$:**PA**.

and Mod. II are quite similar. Lacking the structural data, one might be tempted to suggest the 30 K difference in melting point as being due to extraordinary differences in the packing properties of the two modifications. The system studied here shows that it is questionable whether differences in melting can be used to try to relate thermodynamic properties of crystalline systems to structural features. It is the difference in entropy of fusion between the two forms which is the thermodynamic quantity for comparison here. The thermoanalytical results on **BC**:**PA** (Table 1) indicate that the entropy of fusion of the two crystal forms is also close. Since melting point, enthalpy of fusion, transition temperature, or enthalpy of transition can be

UM00013812
NOVARTIS EXHIBIT 1017
Novartis v. Regents, IPR2023-01346
Page 2558 of 4460

measured by "power compensation" DSC, the entropy of fusion is usually more readily available than the enthalpy of sublimation, which is a direct measure of the lattice energy.

Solid-State NMR Studies. The four crystalline complexes studied here (Figure 7) show different ^{13}C solid-state NMR spectra, which can be used as fingerprint identifiers. One of the most distinguishing signals is that for the methylene carbon atom of the ethyl group of benzocaine. For Mod. I, Mod. II, and the hydrate, this chemical shift appears at approximately 64 ppm, whereas the 2:1 complex shows two signals at 64 and 61 ppm, respectively, clearly reflecting two different kinds of benzocaine species. The chemical shift for this carbon atom in pure solid benzocaine is 61 ppm. Another observation reflecting the ionic and neutral nature of the two benzocaine molecules in the 2:1 complex is the fact that the chemical shift for the carbon atom which is connected to the amino group is at 152 ppm for pure solid benzocaine and 156 ppm in the 2:1 complex. This peak is not observed in the other crystal forms, in which all benzocaines are cationic.

Experimental Procedures

Kofler's Contact Method for Determination of the Binary Phase Diagram.[14,16] A few crystals of the lower melting substance picric acid (mp 122 °C) were placed on a microscope slide at the edge of a cover glass. The amount of substance is chosen in such a way that the melt, which is pulled by capillary forces between the microscope slide and cover glass, occupies about half of the space between them. The preparation is solidified by cooling, and benzocaine (mp 90 °C) is treated in the same manner. In the zone where the melts come into contact, the two compounds merge. The thermal behavior observed on the Kofler hot-stage microscope during heating of the resulting preparation was used to construct and confirm the phase diagram. DSC experiments were also performed to construct the isobar phase diagram (Figure 2) using the melting points and enthalpies of fusion of mixtures of benzocaine and picric acid, determined from DSC studies.

Production of Single Crystals of the Crystal Forms. Crystal growth experiments were carried out using commercially available benzocaine and picric acid (Sigma), and the solvents were of analytical grade. *Note*: *Picric acid is potentially explosive*!

The crystallization of Mod. II as described by Nielsen and Borka[8] leads to a microcrystalline precipitate, which is not suitable for single-crystal X-ray structure determination. However, a mixture of 50 mL of a room temperature saturated water solution of benzocaine and picric acid in a virgin one-neck 250-mL flask covered with Parafilm leads after 48 h at 20 °C to needlelike single crystals of benzocaine−picrate monohydrate. Another preparation of a solution maintained at 80 °C yields, by slow evaporation, platelike single crystals of Mod. II within 24 h. Mod. II resulted only if particular care was taken to exclude seeds of Mod. I. Therefore, it is preferable to perform the crystallization of Mod. II directly from of the synthesis of the compound.

Single crystals of Mod. I suitable for crystallographic analysis were obtained by means of nonaqeous gel diffusion.[24] In this procedure, 0.5 g of Sephadex LH-60-120 (Sigma) was placed in a sealable flask, and 0.5 g of benzocaine dissolved in 6 mL of a 3:1 mixture of chloroform: methanol was added. The gel sets immediately. A solution of 0.2 g of picric acid in 6 mL of the same solvent mixture was placed above the gel. Diffusion of the two solutions and a crystallization period of 3 days at 20 °C yielded yellow crystals of columnar habit with dimensions about 2.5 × 1 × 1 mm^3.

Single crystals of **(BC)$_2$:PA** were obtained by slow evaporation (4 weeks) of a solution of a 1:1 mixture of **BA** and **PA** in 2-propanol at 4 °C. The procedure for obtaining the hydrate was described above.

Thermoanalytical Methods. Polarized microscopy was performed using a Kofler hot-stage microscope (Thermovar, Reichert, Vienna, Austria). DSC was carried out with a Perkin-Elmer DSC-7. The binary phase diagram was constructed from DSC data (heating rate of 5 K min^{-1}) on several ground mixtures of known composition.

(a) Single-Crystal X-ray Diffraction. Crystallographic Data. The X-ray data for **BC:PA** Mod. 1, **BC:PA** Mod. 2, and **(BC)$_2$:PA** were collected on a conventional Syntex $P\bar{1}$ diffractometer [λ(Mo Kα) = 0.711069 Å, graphite monochromator, $\omega/2\theta$ scan, T = 293 K]. The data for **BC:PA·H$_2$O** were collected on a Siemens SMART 1000 CCD diffractometer. All structures were solved by direct methods and refined by full-matrix least-squares for non-hydrogen atoms. All the hydrogen atoms were located from a difference Fourier map and were refined isotropically. The only exceptions were the H atoms of the $-NH_3^+$ group in the **(BC)$_2$:PA** structure, which were found as above, but refined as a "riding group". SHELXTL[29] was used for all calculations. All the metric parameters are collected in Table 2. Atomic coordinates, bond lengths, angles, and anisotropic parameters have been deposited at the Cambridge Crystallographic Data Center.

(b) Solid-State NMR. The solid-state ^{13}C CP-MAS NMR spectra were measured on a Bruker DMX-500 spectrometer, at a measurement frequency of 125.8 MHz and a rotation frequency of 11 000 Hz.

Conclusion

Careful consideration of the thermodynamics and phase diagram along with observation of crystallization phenomena can provide information about the relationship among phases and suggest conditions for growing different polymorphic forms and solvates. Although Mod. II of **BC:PA** has been reported to be a "disappearing polymorph", we have demonstrated a strategy for determining the conditions to consistently produce it. We believe that this strategy can be useful for the exploratory search for polymorphs, the development of robust procedures for selectively obtaining a particular polymorph, and the preparation of single crystals of polymorphs for single-crystal X-ray structure determination. The success of this strategy reinforces our earlier contention[3] that once a particular polymorph has been prepared, in principle it should always be possible to find the conditions to obtain it again.

Acknowledgment. This work is dedicated to Professor Maria Kuhnert-Brandstätter on the occasion of her 80th birthday. J.-O.H. is grateful to the Alexander von Humboldt Foundation for a Feodor Lynen Postdoctoral Fellowship in Beer Sheva. This work was supported in part by the U.S.-Israel Binational Science Foundation (Jerusalem) under Grant 94-00394-2, and by an Austria-Israel Scientific and Cultural Exchange Program. We thank Prof. J. D. Dunitz for constant encouragement. The warm hospitality of the Cambridge Crystallographic Data Centre during the sabbatical leave of J.B. is greatly appreciated. CP-MAS spectra were obtained by Prof. Robert Glaser at The University Laboratory for Magnetic Resonance (Ben-Gurion University of the Negev). The Bruker DMX-500 spectrometer was purchased with a matching funds grant from the Israel Ministry of Science and Industry, and the Bruker solid-state CP-MAS accessory was purchased with a matching funds grant from the Equipment Program of the Israel Council for Higher Education.

JA002113O

(28) McNaughton, J. L.; Mortimer, C. T. *IRS*; Physical Chemistry Series 2, Vol. 10, Butterworths, London, 1975; pp 1−44.

(29) Sheldrick, G. M. *SHELXTL*, Version 5.0; Bruker Analytical X-ray Instruments, Inc.: Madison, WI, 1994.

UM00013813
NOVARTIS EXHIBIT 1017
Novartis v. Regents, IPR2023-01346
Page 2559 of 4460

J. Pharm. Sci. Vol. 50 p905-9 (1961)

Complexation of Organic Substances in Aqueous Solution by Hydroxyaromatic Acids and Their Salts

Relative Contributions of Several Factors to the Overall Effect

By TAKERU HIGUCHI and ARGE DRUBULIS

Apparent stability constants in water of approximately 100 molecular complexes formed between aromatic acids hydroxylated to varying degrees and their salts, on one hand, and four organic compounds, theophylline, hydrocortisone, prednisolone, and phenacetin, on the other, are reported. The data show that introduction of —OH into the first group, particularly *ortho* to a carboxylate grouping, produced marked enhancement in binding. The relative magnitude of the constants suggest that neither the squeezing out force nor hydrogen bonding is significantly responsible in most instances for the observed effects.

THE PRESENT communication is concerned with the results of experimental studies designed to obtain further information on the nature of physical interaction responsible for formation of organic molecular complexes in dilute aqueous solutions. The relative roles of such factors as hydrophobic binding, hydrogen bonding, donor-acceptor forces, etc., have been considered. Data have been obtained specifically on the complexing behavior, as reflected in their solubilizing action, of various hydroxybenzoic acids, corresponding benzoates, several hydroxynaphthoates, and related compounds for theophylline, hydrocortisone, prednisolone, and phenacetin. The latter group was selected to provide a spectrum of compounds. Experimental techniques and interpretive approaches employed follow our earlier reports in this area

Information of this nature is of biological and pharmaceutical interest from two standpoints, (*a*) actions of drugs, hormones, enzymes, etc., are believed to be mediated by formation of complexes in aqueous environment, and (*b*) thermodynamic activities and solubilities of physiologically potent chemicals can be modified by complex formation.

EXPERIMENTAL

Reagents

All organic compounds used in these studies were purified prior to use by recrystallization from water or water-ethanol mixtures.

Procedure

Solubility Studies.—An amount of material to be tested equivalent to at least three times its normal solubility was weighed into 15-ml. vials containing varying amounts of complexing agent (acid or salt) and 10 ml. of distilled water. When the complexing agent was an acid, the water was replaced by an equivalent amount of 0.005 *M* sulfuric acid solution to decrease the ionization of the complexing agent. When the salt of an acid was used as the complexing agent, aliquots from a stock solution were added from a buret into the vials and the necessary volume of distilled water was added.

Each system was equilibrated by rotation for twenty-four hours for systems involving theophylline or phenacetin, and for forty-eight hours for those containing the steroids. This equilibration was effected in a thermostated water bath at a temperature of 30.0 ± 0.1°. The respective equilibration times were evaluated previously as sufficient time for each of the substrates.

Following equilibration, appropriate aliquots of clear solution were removed and analyzed for the material solubilized.

Analysis.—The aliquots were extracted with chloroform from a 0.5 *M* aqueous sodium bicarbonate solution. For theophylline, the extracting solvent was composed of three parts chloroform to one part isopropyl alcohol.

Analysis for theophylline or phenacetin was made directly in the chloroformic solutions. Analysis for the steroids was carried out in ethanolic solution. In these instances, the chloroform was evaporated with the use of mild heat and the substrate residue dissolved in 95% ethanol.

In all cases the spectral characteristics of the analyzed component, as determined previously in the proper solvents, were used as standards. The wavelengths chosen for spectral analyses were: theophylline, 275 mμ; hydrocortisone, 242 mμ; prednisolone, 245 mμ; and phenacetin, 249 mμ.

RESULTS

The complexing tendencies of the several free acids and the sodium salts of these aromatic and hydroxyaromatic acids, as reflected in their respective solubilizing power for theophylline, hydrocortisone, prednisolone, and phenacetin, are presented in Tables I and II. For the majority of the cases, the results are listed as first-order interaction constants (K_1), since the phase diagrams describing those systems indicated that the amount of material solubilized increased generally linearly with the

Received January 26, 1961, from the University of Wisconsin, School of Pharmacy, Madison 6.
Accepted for publication February 13, 1961.
Presented to the Scientific Section, A.PH.A., Chicago meeting, April 1961.
This study was supported in part by a grant from Chas. Pfizer and Co., Brooklyn, N. Y., and in part by a grant from the National Institutes of Health (RG 5830).

UM00013814
NOVARTIS EXHIBIT 1017
Novartis v. Regents, IPR2023-01346
Page 2560 of 4460

TABLE I.—APPARENT STABILITY CONSTANTS[a] (L/M) FOR INTERACTIONS OF SOME MONO- AND DIHYDROXYBENZOIC ACIDS AND SALTS

Compound		Theophylline	Hydrocortisone	Prednisolone	Phenacetin
Benzoic	Acid	[c]	12	11	2.6
	Salt	5.3	2.9	3.7	1.0
o-Hydroxybenzoic	Acid	[c]	12	10	5.4
	Salt	20	7.2	7.3	1.9
m-Hydroxybenzoic	Acid	[c]	13	12	3.9
	Salt	11	4.9	6.1	1.1
p-Hydroxybenzoic	Acid	[c]	10[b]	11[b]	4.0
	Salt	12	4.1	5	1.2
2,4-Dihydroxybenzoic	Acid	[c]	12[b]	15	4.5
	Salt	58	13	12	2.4
2,5-Dihydroxybenzoic	Acid		16	15[b]	4.6
	Salt	43[b]	10[b]	12	2.4
2,6-Dihydroxybenzoic	Acid	[c]	12[b]	13	4.5
	Salt	300	13[b]	10[b]	3.3
3,4-Dihydroxybenzoic	Acid	[c]	12	14[b]	4.3
	Salt	14	6.8	6.5	1.5
3,5-Dihydroxybenzoic	Acid	[c]	18[b]	17[b]	4.9
	Salt	20	6.0[b]	8.5	2.0
3,4,5-Trihydroxybenzoic	Acid	[c]	19[b]	17[b]	5.3
	Salt	22[b]	7.3	6.2[b]	2.1

[a] Calculated by use of Eq. 1. [b] Best fit single linear constant describing interactions exhibiting curvature. [c] The interactions of these acids with theophylline were not studied since these compounds gave insoluble complexes.

TABLE II.—APPARENT STABILITY CONSTANTS[a] (L/M) FOR INTERACTIONS OF SOME NAPHTHOATE AND HYDROXYNAPHTHOATE IONS

Compound	Theophylline	Hydrocortisone	Prednisolone	Phenacetin
1-Naphthoate	38	8.2[c]	8.0[c]	2.5
2-Naphthoate	1:1.2[b]	19[c]	20[c]	5.8[c]
2-Hydroxy-1-naphthoate	1:1.4[b]	21[c]	23[c]	6.6[c]
1-Hydroxy-2-naphthoate	1:1.7[b]	35[c]	35[c]	7.0[c]
3-Hydroxy-2-naphthoate	1:1.6[b]	32	39	6.3

[a] Calculated by use of Eq. 1. [b] Stoichiometric ratios (salt : theophylline). [c] Best fit single linear constant describing interactions exhibiting some curvature.

amount of aromatic compound present, in accordance with the relationship

$$A + B \rightleftharpoons AB$$
$$\uparrow\downarrow$$
$$[B]_{solid}$$

$$K_1 = \frac{[AB]}{[A][B]} \qquad \text{(Eq. 1)}$$

where A is the acid or its salt, B is the substance solubilized, and AB is the complex formed.

A typical phase diagram exhibiting this linearity is that for the interaction of theophylline with sodium 1-naphthoate shown in Fig. 1. The stability constant can be calculated from such a diagram if any observed increase in solubility is assumed to be due to complex formation (1). Because of the nature of the experimental method employed this technique cannot, unfortunately, give any information as to the dependency of the complexing reaction on the concentration of B.

In a number of instances the dependency did not appear to be completely linear, the plots having an upward curvature. The solubilization of prednisolone by sodium 2-hydroxy-1-naphthoate, as shown in Fig. 2, for example, seems to be best described by a combination of more than one equilibrium occurring in solution at the same time. Although a better fit for such cases can be obtained by a combination of linear and quadratic terms, the data do not warrant such a refined treatment. For this reason the values for the best fit linear constant (K_1) (best fit linear constant, describing interactions exhibiting curvature) are given in these instances.

The values describing the binding behavior of some of the naphthoates with theophylline require additional explanation. Since, for these systems, one molecule of the naphthoate ion added usually brought more than one molecule of the xanthine into solution, as shown in Fig. 3, it is evident that the constant K_1, as defined above, is meaningless. The observations strongly support the suggestion that two or more theophylline molecules may interact with individual naphthoate or hydroxy-naphthoate ions. Since the experimental determinations were carried out at constant theophylline activity, the dependency of the complex formation on theophylline could not, of course, be established. Since these systems appear to be more or less linearly dependent on the concentration of naphthoate ion added, the results for these interactions are given as the molar ratio

$$\frac{\text{naphthoate added}}{\text{theophylline solubilized}}$$

It is possible that complexes of similar higher order dependency, relative to the solubilized species, may exist in systems other than those specifically cited in the preceding paragraph. The results are listed, nevertheless, in terms of interactions of first-order dependency since this probably is the most significant interaction occurring in these dilute systems.

DISCUSSION

As indicated in the data given in Tables I and II, aromatic acids and their salts appear to have definite affinity for the four organic compounds.

UM00013815
NOVARTIS EXHIBIT 1017
Novartis v. Regents, IPR2023-01346
Page 2561 of 4460

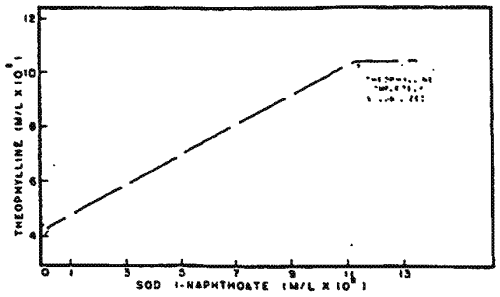


Fig. 1.—Plot showing the solubilization of theophylline by sodium 1-naphthoate exhibiting first-order dependency of complex formation on the salt concentration.

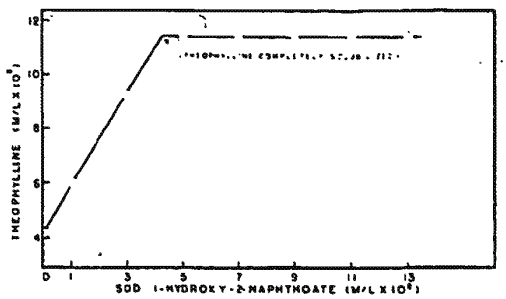


Fig. 3.—Plot showing the solubilization of theophylline by sodium 1-hydroxy-2-naphthoate exhibiting stoichiometric ratio greater than 1:1.

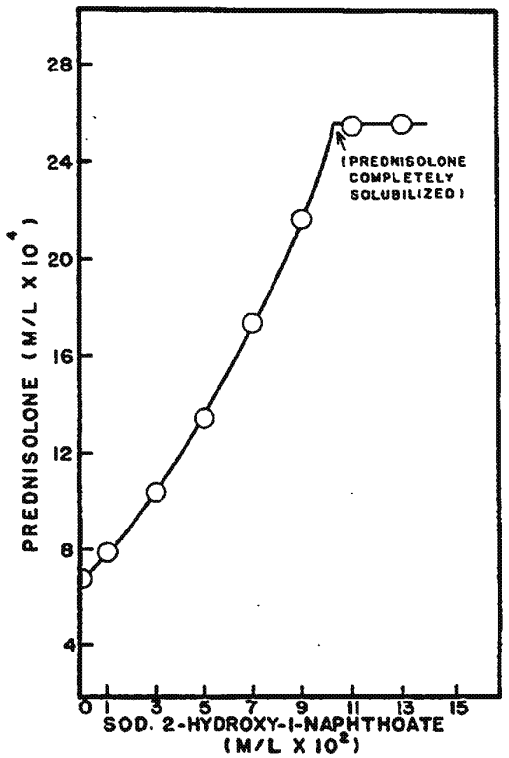


Fig. 2.—Plot showing the solubilization of prednisolone by sodium 2-hydroxy-1-naphthoate exhibiting mixed order dependencies of complex formation on the salt concentration.

The calculated apparent stability constants range from 1.0 L./mole for phenacetin and benzoate to 39 L./mole for prednisolone-3-hydroxy-2-naphthoate systems. For low concentrations of the complexed material this would mean that 0.1 molar concentration of the complexing agent would render roughly 10% of the first and 80% of the second system into their respective complexed species.

If we were to look only at the phenacetin systems, the weakness of the solubilization effects produced by the carboxylate salts hardly seems to justify attributing them to complex formation. Yet it is of interest to note that these largely parallel the behavior of the theophylline systems: a weak binder for phenacetin is a relatively weak binder for theophylline, and a strong binder for one is also a strong binder for the other. The binding constants for the xanthine are, on the other hand, generally so large that there is very little doubt that formal formation of new molecular species is involved in the solubilization process.

The same relative order of solubilizing action produced by the salt solutions appears to hold not only for theophylline and phenacetin but also for the two steroids, with only a few minor exceptions. This was somewhat surprising in view of the wide structural differences among the three classes of substrate compounds used. The relationship holds best with the two steroids since these structures are very similar, but the tendency is definitely evident even for the other systems. These results tend to suggest that much of the binding behavior exhibited in these instances, by these aromatic and hydroxy-aromatic compounds, was largely of a nonspecific nature as opposed to a behavior where more definite "lock and key" can exist between the components of a complex (2).

This lack of specificity does not, however, appear to extend to the acids. Salicylic acid, for example, appears to complex twice as much with phenacetin as does benzoic (5.4 L./mole *vs.* 2.6 L./mole), whereas with respect to the steroids, the activities of the two acids are essentially the same.

Interactions of Acid *vs.* Salt Forms.—In instances where both the free acid and its sodium salts were studied, the acid proved to be the stronger binder in every case. It is possible that this effect is a consequence of the lower hydrophilicity or the greater electrophilicity of the acid. With salt, the ions in solution are probably associated with several molecules of water situated near the carboxylate group. The directing effect of the formal charge on this group can influence the movement and the freedom of the water molecules, possibly resulting in the formation of ice-like structures. It is possible that the presence of such structures may hinder the association involving the aromatic ring materially. The negative charge on the ionized species may, on the other hand, be responsible for sufficient reduction of the electrophilicity of these compounds to reduce their affinity for electron donating agents.

No data are reported for interactions of free acids with theophylline as these systems led, in nearly all cases, to formation of insoluble complex species.

UM00013816
NOVARTIS EXHIBIT 1017
Novartis v. Regents, IPR2023-01346
Page 2562 of 4460

The solubility of the molecular compounds found were usually so low that no reliable stability constants could be determined (3).

Hydroxy- and Methoxybenzoates.—The relative complexing abilities of salicylic acid, *m*-hydroxybenzoic acid, and *p*-hydroxybenzoic acids, together with those of their salts, are shown in Table I. The introduction of an hydroxyl group into the ring markedly enhanced the binding tendencies of the carboxylate forms. With the *ortho* substituent, the effect is essentially doubling of the observed stability constants over those found for the simple benzoate. The enhancement for the *meta* and *para* isomers is somewhat less but still significant, being roughly one-half of that of the *ortho*. The binding tendencies of the free acids do not appear to be markedly influenced by the addition of an hydroxyl group except with phenacetin. With the latter, the *ortho* substitution again produced doubling of the constant over that with benzoic acid.

The reason for the apparent greater complexing efficacy of hydroxybenzoates, particularly salicylate, over that of benzoate is not altogether clear at the moment. Certainly if the driving force behind these interactions were largely due to the squeezing out effect (1) or hydrophobic bonding, the introduction of an —OH grouping would not be expected *a priori* to increase the associative tendencies. A possible explanation for the observed nonspecific increase in binding may be in the changes produced in the relative electrophilicity of these compounds. The four compounds against which these aromatic compounds were tested are largely electron donors in nature. If the major effect in going, for example, from benzoate to salicylate is in the relative affinity for the π-electrons of the donor molecules, the observed results may be rationalized.

Possible participation in a molecularly dispersed state by dipolar or, specifically, hydrogen bonds in promoting molecular association between these hydroxy compounds and xanthine, steroids, and phenacetin appeared to be small. For one thing, such interactions would be in direct competition with the water molecules, the net gain in energy being small. Also, more significantly, although the position and presence of the hydroxyl groups markedly enhanced the intensity of interaction, the effect was largely nonspecific with respect to the solubilized component. There could not be direct fits, since the relative order of interaction did not appear to differ markedly for each of the substances.

To shed additional light on the nature of the hydroxyl contribution, the binding tendencies of *ortho*- and *meta*-methoxybenzoates with respect to theophylline were determined. The first-order constant found for *o*-methoxybenzoate was 5.3 L./mole and that for *m*-methoxybenzoate was 17 L./mole. The marked *ortho* effect noted for the phenolic benzoate thus appears to be absent for the methoxy system. For the *meta* isomer, the replacement of the proton seems to enhance the binding tendency. These results, again, seem to preclude hydrogen bonding as a major factor in these interactions.

Interactions of Di- and Trihydroxybenzoates.—Comparison of the results obtained for the interactions of the dihydroxybenzoates with those of the monohydroxybenzoates indicates that the effect of the additional hydroxyl group further intensified these interactions. Again, to substantiate the thought that this was not due to hydrogen bonding, the binding tendency of 3,4,5-trimethoxybenzoate with respect to theophylline was determined. The first-order constant for this interaction was 23 L./mole; this compares well to that obtained for the trihydroxy compound (22 L./mole). Thus, it is further evident that the presence of the phenolic protons was not of major importance in these interactions.

In general, the total effect that additional groups may have on the binding ability of a bifunctional or trifunctional compound may conceivably be of two types. It is possible that the added groups may enhance the strength of the initial complex maintaining essentially the same structure, or the new groups may lead to the formation of another complex species independent of the initial complex. In the former case, the energies of interaction are, in a sense, additive, while in the latter case, the extents of the interactions are statistically additive.

If the effect of the two hydroxy groups is such that the interaction energies are additive, then it can be easily seen that the interaction constant (K) for the dihydroxy isomer may be approximately related to the interaction constants for the monohydroxy compounds in the following manner

$$K_D = \frac{K_A}{K_C} \times K_B \qquad \text{(Eq. 2)}$$

K_D is the interaction constant for the dihydroxybenzoate, where K_A and K_B are the interaction constants for the respective monohydroxybenzoates, and K_C is the interaction consant for benzoate alone. The assumption made here, of course, is that the two hydroxyl groups do not interact appreciably with each other.

If, on the other hand, the hydroxyl groups do not make use of the same structure in exerting their binding action, then it is apparent that

$$K_D = K_A + K_B - K_C \qquad \text{(Eq. 3)}$$

The data obtained in this study with the dihydroxybenzoates suggest that in these associations the hydroxyl groups generally appear to reinforce the initial binding of the benzoate nucleus and the interaction constants for these compounds follow the relationship expressed by Eq. 2. A comparison between the experimentally observed values and the calculated values is presented in Table III. It is evident that these values agree for each of the substrates in a very approximate sense. In view of the obvious assumptions implicit in such treatment, these data should be considered only as qualitative indications.

Interaction of Naphthoates.—Expansion of the ring system from a benzenoid to the naphthalene structure may be expected to lead to increased complexing tendencies on at least two counts. The greater hydrophobic surface of the flat naphthalene ring surely must contribute more substantially to the "squeezing out" tendency. Also, the relative electron affinity of the two systems must be sufficiently different to produce some changes. Data show, in any case, very strong binding tendencies by these compounds.

As is evident from Table II, β-naphthoate was a markedly stronger binder than its isomer, α-naphthoate. Since this relative difference in bind-

UM00013817
NOVARTIS EXHIBIT 1017
Novartis v. Regents, IPR2023-01346
Page 2563 of 4460

TABLE III.—COMPARISON OF EXPERIMENTAL (*E*) AND CALCULATED[a] (*C*) INTERACTIONS CONSTANTS FOR DIHYDROXYBENZOATES

	Theophylline		Hydrocortisone		Prednisolone		Phenacetin	
	E	C	E	C	E	C	E	C
2,4-Dihydroxybenzoate	56	45	13	10	12	10	2.4	2.3
2,5-Dihydroxybenzoate	43	42	10	12	12	12	2.4	2.1
2,6-Dihydroxybenzoate	300	75	13	18	11	14	3.3	3.6
3,4-Dihydroxybenzoate	14	25	6.8	6.9	6.4	8.4	1.5	1.3
3,5-Dihydroxybenzoate	20	23	5.6	8.3	6.5	10	2.0	1.2

[a] Obtained by use of Eq. 2.

ing was true for all four systems, it is somewhat unlikely that the effect could be attributed to specific steric interactions. There is a possibility, however, that steric interference between the carboxylate group and the second ring may confer flatter configuration to the β-isomer; this may be generally more conducive to binding. The observed greater interactions, on the other hand, may again be attributed to the possibly greater electron affinity of the β-isomer, although it would be difficult to explain why this would be the case.

The results for the few hydroxynaphthoates studied indicate that the added effect due to the presence of a hydroxyl group on the naphthalene ring was approximately the same as it was for the presence of this group on the benzene ring. This observation tends to suggest that the factors responsible for the increased complexation of the monohydroxybenzoates over benzoate apparently hold for these naphthoate systems as well. Again, it is difficult to make any conclusions which would be more than speculative, particularly in view of the limited systems studied.

Considerations from the Standpoint of the Material Solubilized.—The degree of solubilization achieved is, as expected, strongly dependent on the nature of the compound. The data of Tables I and II reveal that the most nucleophilic compound, theophylline, was the strongest binder in all instances. Previous studies (1, 2) have shown that the xanthines generally are strong binders of electron acceptors. It is probable that the contribution from this type of binding, reinforced by other factors, is also important in the interactions with these aromatic and hydroxyaromatic compounds.

One might expect from the type of structures involved that hydrophobic associations would be responsible, on the other hand, for the binding tendencies of the steroids. Contributions from such binding alone could not, however, explain the enhancing ability of phenolic groupings. Consequently, it is felt that π-electrons in the keto group and in the double bond(s) of the A ring must participate to some extent in these interactions.

The relatively low associative tendency of phenacetin was somewhat unexpected.

CONCLUSIONS

It is evident from the above sections that we are presently of the opinion that the major contributions of the interactions between these aromatic or hydroxyaromatic compounds and the four substrates studied have been of the "donor-acceptor" type and that the contributions from hydrophobic bonding and hydrogen bonding were possibly of lesser magnitude. The general considerations discussed herein can, however, only be considered as speculative. Further work along these lines may bring to light additional factors which have not been evident in this limited study.

REFERENCES

(1) Higuchi, T., and Lach, J., THIS JOURNAL, 43, 465, 524(1954).
(2) Higuchi, T., Sciarrone, B., and Haddad, A., *J. Med. and Pharm. Ch.*, 3, 195(1961).
(3) Higuchi, T., and Lach, J., THIS JOURNAL, 43, 527 (1954).

UM00013818
NOVARTIS EXHIBIT 1017
Novartis v. Regents, IPR2023-01346
Page 2564 of 4460

This Page is Inserted by IFW Indexing and Scanning Operations and is not part of the Official Record

BEST AVAILABLE IMAGES

Defective images within this document are accurate representations of the original documents submitted by the applicant.

Defects in the images include but are not limited to the items checked:

- ☐ BLACK BORDERS
- ☐ IMAGE CUT OFF AT TOP, BOTTOM OR SIDES
- ☐ FADED TEXT OR DRAWING
- ☐ BLURRED OR ILLEGIBLE TEXT OR DRAWING
- ☐ SKEWED/SLANTED IMAGES
- ☐ COLOR OR BLACK AND WHITE PHOTOGRAPHS
- ☐ GRAY SCALE DOCUMENTS
- ☐ LINES OR MARKS ON ORIGINAL DOCUMENT
- ☐ REFERENCE(S) OR EXHIBIT(S) SUBMITTED ARE POOR QUALITY
- ☐ OTHER: _____

IMAGES ARE BEST AVAILABLE COPY.
As rescanning these documents will not correct the image problems checked, please do not report these problems to the IFW Image Problem Mailbox.

ELSEVIER

Thermochimica Acta 374 (2001) 85–92

thermochimica acta

www.elsevier.com/locate/tca

Assessment of nicotinamide polymorphs by differential scanning calorimetry

Tomoaki Hino[1], James L. Ford*, Mark W. Powell

School of Pharmacy and Chemistry, James Parsons Building, Liverpool John Moores University, Byrom Street, Liverpool L3 3AF, UK

Received 23 October 2000; received in revised form 27 February 2001; accepted 28 February 2001

Abstract

The thermal behaviour of nicotinamide was investigated by differential scanning calorimetry (DSC). Nicotinamide was heated to 140°C, cooled and subsequently re-heated using DSC. Nicotinamide displayed four polymorphs. The melting points of Forms I, II, III and IV were 126–128, 112–117, 107–111 and 101–103°C, respectively. Untreated nicotinamide composed only of Form I. When molten and subsequently cooled, a mixture of polymorphs recrystallised. When the molten liquid was cooled to temperatures <80°C, the main product was Form I. In these scans, conversion from the metastable forms to the stable one without accompanying melting was observed at low re-heating rates. At higher rates, the melting of the metastable form became more obvious and it occurred concomitantly with recrystallisation of the stable form. When molten samples were cooled to 80 or 85°C and held isothermally, Form II was predominantly formed and the formation of Form I could not be detected. Form II was converted to Form I by cooling to 30°C. Form I was the stable form; others were metastable.
© 2001 Elsevier Science B.V. All rights reserved.

Keywords: Nicotinamide; Polymorphs; DSC; Scanning rate dependence; Isothermal hold

1. Introduction

Solid dispersions are extensively investigated for improving the dissolution properties of poorly water-soluble drugs [1–3]. These are prepared with drugs and carriers by intermediate action of heat [4–6], solvent or a combination of heat and solvent [7,8]. The heating method should result in no inherent toxicity from residual solvent. However, the heating method may require careful control of heating and cooling conditions because of the potential problems of polymorphic modifications.

Nicotinamide, viz. pyridine-3-carboxyamide, is one of the components of vitamin B. It was reported that the solubilities of nifedipine [9,10], indomethacin [11] or halofantrine [12] are increased by forming solid dispersions with nicotinamide. In spite of these potential utilities of nicotinamide, the thermal properties of this compound have not been fully investigated. Fused nicotinamide shows a different differential scanning calorimetry (DSC) scan to the scan of the untreated material [13]. The polymorphic modifications of nicotinamide and their interconversion have not been explained in detail. In the present paper, the relationships between nicotinamide polymorphs and the heating and cooling conditions are reported.

* Corresponding author. Tel.: +44-151-231-2096; fax: +44-151-231-2170.
E-mail address: j.l.ford@livjm.ac.uk (J.L. Ford).
[1] Present address: Faculty of Pharmaceutical Sciences, The University of Tokushima, Sho-machi 1-78-1, Tokushima 770-8505, Japan.

0040-6031/01/$ – see front matter © 2001 Elsevier Science B.V. All rights reserved.
PII: S0040-6031(01)00491-9

UM00013820
NOVARTIS EXHIBIT 1017
Novartis v. Regents, IPR2023-01346
Page 2566 of 4460

2. Materials and methods

2.1. Materials

Reagent grade nicotinamide was purchased from BDH Laboratories (Poole, England) and used without further purification.

2.2. DSC analysis

The DSC scans were carried out using a Perkin-Elmer DSC7 calorimeter. The calorimeter was calibrated for temperature against the melting points of indium and zinc (156.60 and 419.47°C, respectively) and for enthalpies against the heat of fusion of indium ($\Delta H_f = 28.45\ J\ g^{-1}$).

Samples (normally 2–5 mg) were placed in aluminum pans and aluminum lids were crimped in position. Each sample was initially held at 50°C for 1 min prior to analysis. These samples were heated to 140°C, maintained at this temperature for 0.5 min, cooled to 30, 50, 70, 80, 85 or 90°C, held isothermally at these temperatures for periods varying from 0 to 20 min and subsequently re-heated to 140°C. The heating, cooling and re-heating scans were carried out under the rates specified in the discussion.

2.3. Thermogravimetic analysis

Thermogravimetic (TG) analysis of nicotinamide was determined using a Perkin-Elmer TGA7 thermogravimetric analyser equipped with a Perkin-Elmer TAC7 controller. The apparatus was calibrated against the magnetic transition temperatures of nickel and iron (354 and 780°C, respectively) and weight against a 100-mg Class M calibration standard (Part No. 0990-8397, Perkin-Elmer).

The initial weights of samples analysed were 4.5–7.7 mg. Samples were heated from 30 to 140°C at a rate of 1.0 or 10.0°C min^{-1}.

2.4. Hot stage microscopic observation

Untreated nicotinamide was placed on a glass microscope slide and covered by a glass cover slip. The thermal behaviour of the sample was observed using hot stage microscopy. The hot stage, the microscope and the central processor of the system used were a Mettler FP82, an Olympus BH-2 and a Mettler FP80, respectively. Samples were heated from 50 to 140°C, cooled to ambient temperature by removing the slide out of the stage and subsequently heating to 140°C again. The heating and re-heating rates were in the range 1–20°C min^{-1}. Accuracy of the hot stage was routinely checked against the melting of indomethacin B.P. and ibuprofen B.P.

2.5. Stability of nicotinamide during heating

The stability of nicotinamide during heating was checked by high performance liquid chromatography (HPLC). Nicotinamide samples were placed in uncovered aluminum pans and heated in the DSC7 calorimeter. Samples were held at 50°C for 1 min, heated to and maintained at 140°C for 0.5 min, and subsequently cooled to 30°C. Heating and cooling rates were 20°C min^{-1}. Following heat treatment, samples were also maintained at 80°C for 20 min during the cooling procedure. Samples were dissolved in methanol and the quantity of nicotinamide remaining determined by HPLC using a Model 2690 Separation Module (Waters Limited, Watford, UK) with a Waters 996 photodiode array detector. The data system used was a Millenium 32. The injection volume was 3 μl and the column used was a Symmetry Shield™ RP_8 (3.9 × 150 mm, 5 μm d.p., Waters Limited, Watford, UK) at a temperature of 30°C. A gradient elution profile was used, comprising initially 1 v/v% aqueous acetonitrile, containing 0.1 v/v% trifluoroacetic acid. This composition was maintained for 2 min, and then the proportion of acetonitrile increased linearly over 8 min to 70 v/v%. This ratio was maintained for 2.90 min and subsequently decreased linearly over 0.1 min to the starting composition. The column was allowed to equibrate for 5 min prior to the next injection. Nicotinamide was determined by UV detection at 260 nm.

3. Results and discussion

3.1. Thermal behaviour of the untreated nicotinamide

Untreated nicotinamide was heated to 140°C at 1–30°C min^{-1} using DSC. Each scan (represented

UM00013821
NOVARTIS EXHIBIT 1017
Novartis v. Regents, IPR2023-01346
Page 2567 of 4460

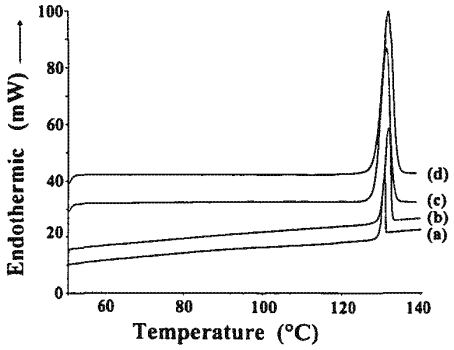


Fig. 1. DSC heating scans of untreated nicotinamide. Heating rate: (a) 1°C min^{-1}, (b) 5°C min^{-1}, (c) 10°C min^{-1}, (d) 20°C min^{-1}.

by Fig. 1) exhibited one sharp peak with onset temperature of 126–128°C and melting enthalpies of ~209 J g^{-1} (Table 1). The fact that no other events were apparent indicated that the untreated nicotinamide contained one crystal form. Slight baseline displacements were observed between the baselines prior to the onset and following the offset temperatures of the melting peaks. This suggests that slight decomposition of nicotinamide might have occurred on melting. However, the weight loss after heating to 140°C at rates of 1 and 10°C min^{-1}, determined by TG, were in the ranges 0.31–0.34 w/w% and <0.02 w/w% ($n = 2$), respectively. Neither significant reduction in peak areas nor new peaks originating from decomposition of nicotinamide with heating were detected by HPLC. Therefore, nicotinamide was considered to be stable under the DSC conditions employed.

The thermal behaviour of nicotinamide during heating to 140°C was observed using hot stage microscopy. Crystals melted in the range 124–130°C. No changes were observed at lower temperatures. These observations confirm that nicotinamide was originally composed of one crystal form.

3.2. Characterisation of nicotinamide polymorphs

Heating, cooling and re-heating of nicotinamide were carried out at various rates. Several patterns of endothermic peaks due to melting of the samples were

Table 1
Characterisation of nicotinamide crystal forms

Heating rate (°C min^{-1})	1	5	10	20	30	Mean	S.D.[a]	n
Form I (untreated)								
Onset temperature (°C)	125.9–128.3	127.8–128.2	126.5–128.4	128.0–128.3	127.9–128.4	128.1	0.9	20
Peak temperature (°C)	130.7–132.5	130.8–133.1	131.2–133.5	130.2–134.6	131.0–133.8	131.5	1.5	20
ΔH (J g^{-1})	207.5–218.8	208.8–219.2	204.3–205.2	182.8–228.3	197.7–221.9	208.9	9.6	20
Form I (from recrystallised material)								
Onset temperature (°C)	127.7–128.4	128.1–129.6	124.8–128.8	127.9–130.1	127.5–128.5	128.0	0.9	32
Peak temperature (°C)	128.8–129.3	129.5–133.6	130.1–130.7	131.1–135.6	131.5–134.5	131.3	1.7	33
ΔH (J g^{-1})	182.7–242.7	208.8–261.7	189.3–210.2	208.6–228.3	191.7–191.9	208.6	22.0	13
Form II								
Onset temperature (°C)	113.3–116.9	112.2–115.4	112.6–115.4	113.5–116.2	111.6–116.1	114.5	1.4	26
Peak temperature (°C)	113.7–117.2	113.1–117.5	113.3–117.7	114.7–120.2	114.9–120.9	115.9	1.9	48
ΔH (J g^{-1})	156.1–160.2	153.8–171.3	146.7–164.6	150.3–180.5	167.6–180.5	161.6	9.7	12
Form III								
Onset temperature (°C)	107.6	108.2		109.1–110.6	106.9–110.7	108.9	1.1	12
Peak temperature (°C)	108.9	109.1		110.0–113.6	109.1–113.5	111.5	1.5	15
ΔH (J g^{-1})	148.6				167.3	158.0	13.2	2
Form IV[b]								
Onset temperature (°C)	103.1	101.1–102.0		102.0		102.1	0.7	4
Peak temperature (°C)	104.2	103.9		102.2–105.2		103.9	0.9	6

[a] Standard deviation.
[b] ΔH of Form IV was not determined.

UM00013822
NOVARTIS EXHIBIT 1017
Novartis v. Regents, IPR2023-01346
Page 2568 of 4460

observed in the re-heating scans, depending on the operating conditions of DSC. These peaks were classified into four types, i.e. Forms I, II, III and IV, defined by the temperatures when the onset of melting and the peak temperature occurred. The DSC characteristics of the four polymorphic forms of nicotinamide are shown in Table 1. The peak maxima of the endotherms of Forms I, II, III and IV were 131.5 ± 1.5, 115.9 ± 1.9, 111.5 ± 1.5 and 103.9 ± 0.9°C, respectively.

Onset temperatures are defined as the temperatures where the baselines intersected the extrapolated tangents at the midpoints of the peaks [14]. Although this analysis slightly overestimates the onset temperature, it diminishes the personal bias of judgement of the onset. Because sample weight, filling state and the heating rate affect the onset and peak temperatures [15], these conditions were carefully controlled. The peak temperature has somewhat larger variance compared with the onset temperature (Table 1). This is due to the fact that onset temperature reflects the temperature when the threshold of the energy for melting was supplied to the sample, while peak temperature is influenced by the dynamical equilibrium between supplied heat and the content of the solid portion which is gradually converted to the molten liquid in the sample [16]. On the contrary, the reproducibility of the onset temperature was such that the standard deviation was <1.4°C. Consequently in this study, the peaks were characterised by onset temperatures unless multiple peaks overlapped each other.

ΔH denotes the enthalpy change caused by melting of the sample per unit weight. The value of the Form I was significantly larger than that of the Form II ($P < 0.001$) or Form III ($P < 0.05$; t-test). It suggests that Form I is the stable form, the other forms are metastable and that these polymorphs are monotropic according to Burger's rule [17]. The ΔH values of the Form IV could not be calculated, because the peaks originating from the melting of Form IV could not be solely obtained and other peaks always appeared during re-heating.

3.3. Effect of cooling rates on the nicotinamide polymorphs

The DSC cooling and re-heating scans of nicotinamide are shown in Fig. 2. The initial heating rate and

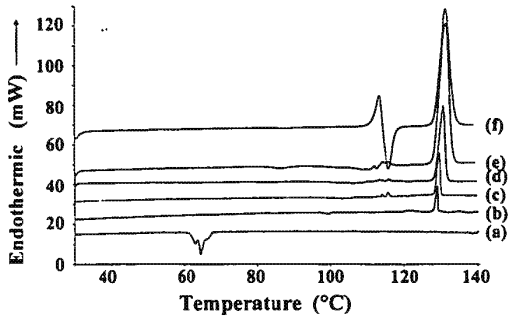


Fig. 2. DSC cooling and re-heating scans of nicotinamide. Initial heating rate: 20°C min^{-1}, cooling rate: (a) 5°C min^{-1}. Re-heating curves: (b) 1°C min^{-1}, (c) 5°C min^{-1}, (d) 10°C min^{-1}, (e) 20°C min^{-1}, (f) 30°C min^{-1}.

cooling rate were 20 and 5°C min^{-1}, respectively. The samples were heated to 140°C, held at 140°C for 0.5 min, cooled to 30°C and held for 0.5 min prior to subsequent re-heating. Fig. 2a shows a typical cooling scan under these heating and cooling conditions. A large split exothermic peak, due to the recrystallisation of nicotinamide, is observed at 68–60°C (Fig. 2a). Also several small exothermic peaks existed at lower temperatures. These complex aspects of the cooling scans were not reproducible. However, a large split exothermic peak in the range 85–60°C and several subsequent smaller peaks were observed in each scan. The enthalpy of the main recrystallisation peak was -129.8 ± 16.1 J g^{-1} ($n = 8$).

Fig. 2b–f are typical re-heating scans. The main peak is due to the melting of the Form I in each scan. Form I was thus considered as the main product of these heating and cooling operations. However, other endothermic peaks were obtained. It suggests that other forms, possibly Forms II, III and IV, were also produced under these conditions. Although the relative size between the endotherm of Form I and those of the other forms varied in each experimental run, the melting endotherm of Form I was always apparent. The variations in their relative size were probably due to the unpredictable nucleation process mentioned by Bottom [18], and He and Craig [19]. Exothermic peaks were observed in these scans (Fig. 2b, c, e and f). It suggests that recrystallisation occurred on re-heating as well as during cooling. Conversion from one solid form to another without accompanying melting was observed at the slow scanning rates of

UM00013823
NOVARTIS EXHIBIT 1017
Novartis v. Regents, IPR2023-01346
Page 2569 of 4460

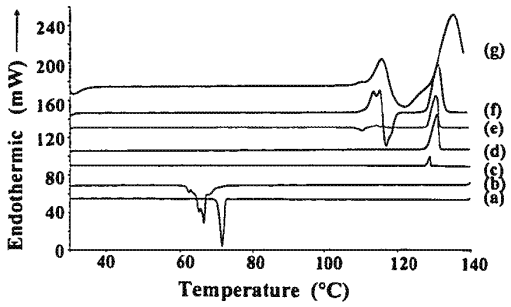


Fig. 3. DSC cooling and re-heating scans of nicotinamide. Initial heating rate: 20°C min^{-1}, cooling rate: (a) and (b) 10°C min^{-1}. Re-heating curves: (c) 1°C min^{-1}, (d) 5°C min^{-1}, (e) 10°C min^{-1}, (f) 20°C min^{-1}, (g) 50°C min^{-1}.

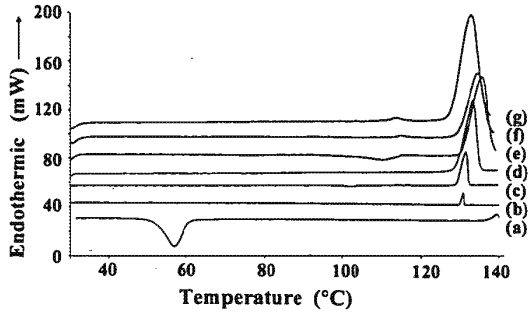


Fig. 4. DSC cooling and re-heating scans of nicotinamide. Initial heating rate: 20°C min^{-1}, cooling rate: (a) 30°C min^{-1}. Re-heating curves (b) 1°C min^{-1}, (c) 5°C min^{-1}, (d) 10°C min^{-1}, (e) 20°C min^{-1}, (f) 30°C min^{-1}, (g) 50°C min^{-1}.

1, 5 and 20°C min^{-1}. At the rate of 30°C min^{-1} (Fig. 2e), conversion from Form III to Form I occurred via melting of Form III and subsequent recrystallisation of Form I. This phenomenon is caused by insufficient heat supply due to the rapid heating. Melting of Form III occurred before the solid–solid conversion.

Fig. 3 shows typical DSC scans at a cooling rate of 10°C min^{-1} and subsequent re-heating. The cooling scans were not reproducible and showed either sharp peaks such as Fig. 3a or large split peaks as Fig. 3b. No relationship between sample weight and the peak aspects could be recognised. The enthalpy change was -132.3 ± 20.2 J g^{-1} ($n = 14$). Large endotherms due to the melting of Form I were observed in the re-heating scans (Fig. 3c–g). Other endothermic peaks also existed. A solid → liquid → solid conversion from Form III to Form I became more obvious with increase in the re-heating rate. This could be due to the fact that gradual recrystallisation at the lower temperature was suppressed because of the rapid supply of heat during the faster re-heating procedures. Consequently, recrystallisation of Form I occurred concomitantly with melting of Forms III and IV.

Fig. 4 shows typical DSC cooling and re-heating scans from samples examined following cooling rate at 30°C min^{-1}. The cooling scan exhibited only one sharp exotherm (Fig. 4a). The re-heating scans exhibited sharp endothermic peaks caused by melting of Form I and small endotherms originating from Form III. Similar results were obtained at an approximate cooling rate of 250°C min^{-1} (data not shown). Although a precise cooling rate of 250°C min^{-1} was not controllable, this rate was the fastest attainable with the DSC instrument used.

Nicotinamide, following fusion at 140°C and subsequent cooling, was re-heated and examined using a hot stage microscope. Recrystallisation was observed in the range 64–105°C although the temperature was not reproducible. This result suggests that the conversion of Form III to Form I occurred during re-heating and supported the DSC data that some conversion of the solid state occurred before melting took place.

From Figs. 2–4, Form I appeared to be the main product of cooling to 30°C and subsequent re-heating. Form III frequently existed. Forms II and IV might be formed under these conditions. The endotherm that originates from Form III became smaller and that from Form I became more predominant with increase in the cooling rate. The data suggest that Form I, which was preferentially formed by rapid cooling, is the stable form and other forms are metastable.

3.4. Recrystallisation of nicotinamide under isothermal conditions

Nicotinamide samples were heated to 140°C at 20°C min^{-1}, cooled to 80°C at 10°C min^{-1}, held at 80°C for 10 min and subsequently re-heated. The DSC isothermal scan at 80°C exhibited either only one sharp peak (Fig. 5a) or a complex one (Fig. 5b). Although recrystallisation occurred and ended mostly during the isothermal step (Fig. 5a and b), it occasionally started during the cooling step (Fig. 5c) or ended during re-heating (Fig. 5d).

UM00013824
NOVARTIS EXHIBIT 1017
Novartis v. Regents, IPR2023-01346
Page 2570 of 4460

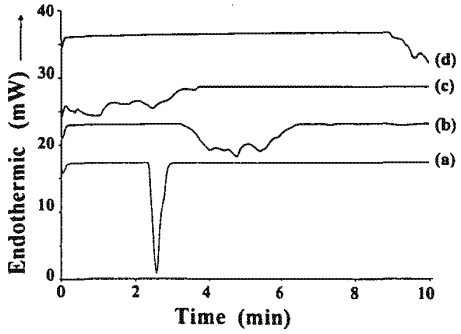


Fig. 5. Typical DSC isothermal scans of nicotinamide at 80°C. Initial heating rate: 20°C min^{-1}, cooling rate: 10°C min^{-1}, holding temperature: 80°C. (a) and (b) Recrystallisation occurred and ended during the holding time. (c) Recrystallisation was initiated during the cooling step and ended during the isothermal one. (d) Recrystallisation was initiated during the isothermal stage and ended during the re-heating one.

Fig. 6a–f shows the re-heating scans of samples, when recrystallisation started and ended during the isothermal step at 80°C. No scan exhibited the peak originating from Form I. At the low re-heating rate of 1°C min^{-1}, a sharp peak due to the melting of either Form III (Fig. 6a) or Form II (Fig. 6b) appeared. At faster rates, two peaks originating from Forms II and III are observed. The former endotherm was larger than the latter. A small exothermic peak was observed at 86°C in Fig. 6a. Such peaks were not observed in Fig. 6b–f. It is considered that Form II was the main product of these scanning conditions. The small

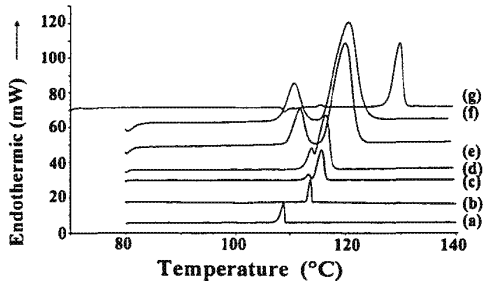


Fig. 6. DSC re-heating scans of nicotinamide after holding at 80 or 70°C. Initial heating rate: 20°C min^{-1}, cooling rate: 10°C min^{-1}. Holding temperature: (a)–(f) 80°C, (g) 70°C. Re-heating curves: (a) and (b) 1°C min^{-1}, (c) 5°C min^{-1}, (d) 10°C min^{-1}, (e) 20°C min^{-1}, (f) 30°C min^{-1}, (g) 10°C min^{-1}.

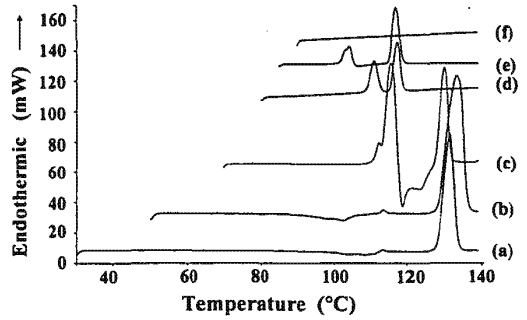


Fig. 7. Effect of holding temperature on the DSC re-heating scans of nicotinamide. Initial heating rate: 100°C min^{-1}, cooling rate: 100°C min^{-1}, re-heating rate: 20°C min^{-1}. Holding temperature: (a) 30°C, (b) 50°C, (c) 70°C, (d) 80°C, (e) 85°C, (f) 90°C.

exothermic peak in Fig. 6a was presumably due to the conversion of Form II to Form III. On the contrary, Form I was the main product when nicotinamide was cooled to 70°C and subsequently held at this temperature (Fig. 6g).

The effect of the holding temperature on the recrystallisation of nicotinamide is shown in Fig. 7. The re-heating rate was 20°C min^{-1}. In order to initiate and terminate the recrystallisation during the isothermal procedure, the cooling rate and holding time were 100°C min^{-1} and 20 min, respectively, rather than the conditions of Fig. 6. Consequently, the recrystallisation commenced and ended during the holding step, except at the holding temperature of 90°C. When nicotinamide was cooled to lower than 80°C, Form I was predominantly formed, while Form II was the main product under the holding temperature of 80 or 85°C. When the cooling was stopped at 90°C, neither melting nor recrystallisation occurred in the isothermal and re-heating scans.

3.5. Recrystallisation of nicotinamide during re-heating

Nicotinamide was cooled to 80°C and immediately heated without isothermal holding it at 80°C. When the re-heating rate was low (1 or 5°C min^{-1}), recrystallisation occurred at a lower temperature in the re-heating scan (Fig. 8a and b). The main product of these scans was Form II. Neither recrystallisation nor melting occurred in the re-heating scan at the faster rates

UM00013825
NOVARTIS EXHIBIT 1017
Novartis v. Regents, IPR2023-01346
Page 2571 of 4460

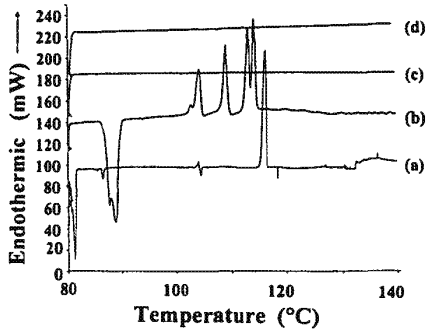


Fig. 8. Recrystallisataion of nicotinamide during re-heating procedure. Initial heating rate: 20°C min^{-1}, cooling rate: 10°C min^{-1}. Re-heating curves: (a) 1°C min^{-1}, (b) 5°C min^{-1}, (c) 10°C min^{-1}, (d) 20°C min^{-1}.

(10 or 20°C min^{-1}, Fig. 8c and d). This is due to the fact that nicotinamide was insufficiently cooled and subsequently re-heated before the solidification occurred at the larger re-heating rate.

3.6. Solid to solid conversion of nicotinamide

Nicotinamide was heated to 140°C, cooled to 80°C, held at 80°C for 20 min, cooled to 30°C and subsequently re-heated. The DSC cooling and re-heating scans are shown in Fig. 9. The product after cooling to 80°C and subsequent holding at the temperature is considered to be Form II, as described above. However, when it was cooled to 30°C, Form II was converted to

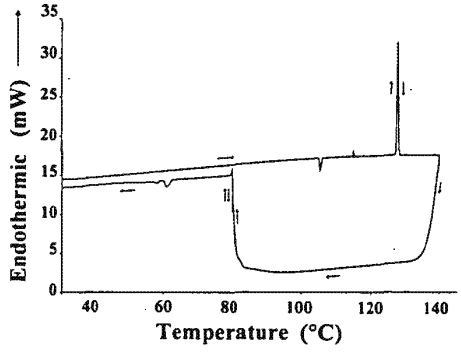


Fig. 9. DSC cooling and re-heating scans of nicotinamide obtained by heating to 140°C at 100°C min^{-1}, followed by cooling to 80°C at 100°C min^{-1}, holding at 80°C for 20 min, cooling to 30°C at 10°C min^{-1} and heating to 140°C at 1°C min^{-1}.

Form I. The exothermic peaks were observed at ca. 61 and 105°C in the further cooling and re-heating scans, respectively. These peaks are considered to be caused by the conversion from Form II to Form I without accompanying melting. The peak due to the melting of Form II is also detectable in the re-heating scan.

The original nicotinamide powder was heated to 80°C, held for 20 min and subsequently heated to 140°C. The heating curve exhibited only one small peak originating from Form I (data not shown). The conversion from Form I to Form II did not occur in these procedures. These results denote that Form I is a stable form and Form II is a metastable one. It was confirmed by these results as well as the ΔH data in Table 1 that the solid–solid polymorphic change from Form II to Form I is monotropic.

The X-ray diffraction patterns of nicotinamide investigated at ambient temperature have been reported earlier [20]. No significant change in the X-ray diffraction pattern of nicotinamide was obtained by heating to 140°C nor by subsequent cooling and holding at 80°C. This was due to a lack of significant decomposition and that Form II crystals were converted to Form I by cooling to ambient temperature.

This clarified the facts that nicotinamide displays polymorphic changes and that cooling conditions affects its polymorphs significantly. Fused nicotinamide shows a different DSC scan to the scan of the untreated material due to the co-existence of the polymorphs [13]. Consequently, precise control of cooling is necessary for the preparation of solid dispersions with nicotinamide.

4. Conclusion

Nicotinamide has at least four polymorphs. Form I is the stable form. When nicotinamide is melted and subsequently cooled to temperatures <80°C, Form I preferentially recrystallises. When cooling is stopped at the higher temperature (80 or 85°C), Form II predominantly forms.

References

[1] W.L. Chou, S. Riegelman, J. Pharm. Sci. 60 (1971) 1281.
[2] M. Moneghini, A. Carcano, G. Zingone, B. Perissutti, Int. J. Pharm. 175 (1998) 177.

UM00013826
NOVARTIS EXHIBIT 1017
Novartis v. Regents, IPR2023-01346
Page 2572 of 4460

[3] C. Rouchotas, O.E. Cassidy, G. Rowley, Int. J. Pharm. 195 (2000) 1.
[4] F. Damian, N. Blaton, L. Naesens, J. Balzarini, R. Kinget, P. Augustijins, G. Van den Mooter, Eur. J. Pharm. Sci. 10 (2000) 311.
[5] S. Hülsmann, T. Backensfeld, S. Keitel, R. Bodmeier, Eur. J. Pharm. Biopharm. 49 (2000) 237.
[6] C. Leuner, J. Dressman, Eur. J. Pharm. Biopharm. 50 (2000) 47.
[7] J.L. Ford, Pharm. Acta Helv. 61 (1986) 69.
[8] M.C. Martínez-Ohárriz, C. Martín, M.M. Goñi, C. Rodríguez-Espinosa, M.C. Tros-Ilarduya, A. Zornoza, Eur. J. Pharm. Sci. 8 (1999) 127.
[9] H. Suzuki, H. Sunada, Chem. Pharm. Bull. 45 (1997) 1688.
[10] H. Suzuki, H. Sunada, Chem. Pharm. Bull. 46 (1998) 1015.
[11] S. Bogdanova, D. Sidzhakova, V. Karaivanova, S. Georgieva, Int. J. Pharm. 163 (1998) 1.
[12] L.-Y. Lim, M.-L. Go, Eur. J. Pharm. Sci. 10 (2000) 17.
[13] H. Suzuki, H. Sunada, Chem. Pharm. Bull. 46 (1998) 482.
[14] T. Hatakeyama, F.X. Quinn, Thermal Analysis — Fundamentals and Applications to Polymer Science, Second Edition, Wiley, Chichester, 1999, p. 72.
[15] S.K. Dordunoo, J.L. Ford, M.H. Rubinstein, J. Pharm. Pharmacol. 48 (1996) 782.
[16] J.L. Ford, P. Timmins, Pharmaceutical Thermal Analysis. — Techniques and Applications, Ellis Horwood, Chichester, 1989, p. 25.
[17] B. Burger, Acta Pharm. Tochnol. 28 (1982) 1.
[18] R. Bottom, Int. J. Pharm. 192 (1999) 47.
[19] R. He, D.Q.M. Craig, J. Pharm. Pharmacol. 53 (2001) 41.
[20] T. Hino, J.L. Ford, Int. J. Pharm., in press.

UM00013827
NOVARTIS EXHIBIT 1017
Novartis v. Regents, IPR2023-01346
Page 2573 of 4460

J. Pharm. Pharmacol. 1987, 39: 787–796
Received February 10, 1987

© 1987 J. Pharm. Pharmacol.

Crystallographic, theoretical and molecular modelling studies on the conformations of the salicylamide, raclopride, a selective dopamine-D_2 antagonist*

THOMAS HÖGBERG†, ULF NORINDER, STEN RÄMSBY AND BIRGITTA STENSLAND‡

Research and Development Laboratories, Astra Alab AB, S-151 85 Södertälje, and ‡Department of Structural Chemistry, Arrhenius Laboratory, University of Stockholm, S-106 91 Stockholm, Sweden

The structure of the potent dopamine-D_2 antagonist, raclopride, (*S*)-3,5-dichloro-*N*-[(1-ethyl-2-pyrrolidinyl)methyl]-6-methoxysalicylamide (+)-tartrate, has been determined by X-ray crystallography. The benzamide moiety of raclopride is planar in accordance with other salicylamides (FLA 797 and eticlopride). The planar conformation is stabilized by two intramolecular hydrogen bonds, i.e. one between the amide hydrogen and the methoxy group and one between the phenol hydrogen and the carbonyl group. The side-chain of raclopride has an extended conformation in contrast to the solid state conformations of FLA 797 and eticlopride. The side-chain conformations were studied by rigid rotations followed by MM2PI relaxations of the eight local minima found. Small energy differences (<4·0 kcal mol^{-1}) exist between the various extended and folded conformations. Based on modelling studies with piquindone as template, it is suggested that the salicylamides with *N*-ethyl-2-pyrrolidinylmethyl side-chains interact with the dopamine-D_2 receptor in a folded or a half-folded conformation.

Two categories of central dopamine receptors, dopamine-D_1 and dopamine-D_2, have been identified (Stoof & Kebabian 1984). Dopamine-D_1 receptors are positively coupled to adenylate cyclase, whilst dopamine-D_2 receptors are either unconnected or negatively coupled to adenylate cyclase (Stoof & Kebabian 1981, 1984; Meunier & Labrie 1982). The substituted benzamides are a recently developed class of compounds, which preferentially block the dopamine-D_2 receptors (Jenner & Marsden 1981; Ögren et al 1984, 1986; de Paulis 1985; Hall et al 1986). The mode of action of antipsychotic agents has been suggested to be related to the ability to block dopamine-D_2 receptors (e.g. Seeman 1980).

There exist several main types of benzamide derivatives with different side chains and/or aromatic substituents. The common denominator is the 2-methoxybenzamide part often referred to as orthopramide. The side-chains are of four principal types, i.e. aminoethyl (metoclopramide), 2-pyrrolidinylmethyl (sulpiride), 3-pyrrolidinyl (YM 09151-2) and 4-piperidyl (clebopride) as shown in Fig. 1. Most of the first reported derivatives (e.g. sulpiride) are substituted in the 5-position and unsubstituted in the 6-position. Recently, a series of compounds containing 6-methoxy (remoxipride) or 6-hydroxy (eticlopride, raclopride, FLA 797) substituents have been reported from these laboratories (Fig. 2) (Florvall & Ögren 1982; Ögren et al 1984, 1986; de Paulis et al 1985a, b, 1986; Hall et al 1986). Remoxipride was shown to improve schizophrenic symptomatology in an open study (Lindström et al 1985). The salicylamides, [^{3}H]eticlopride and [^{3}H]raclopride, have proved to be potent and selective dopamine-D_2 receptor ligands under in-vitro as well as in-vivo conditions (Köhler et al 1985, 1986; Hall et al 1985; Hall & Wedel 1986; Köhler & Radesäter 1986). By virtue of these properties, [^{11}C]raclopride has been

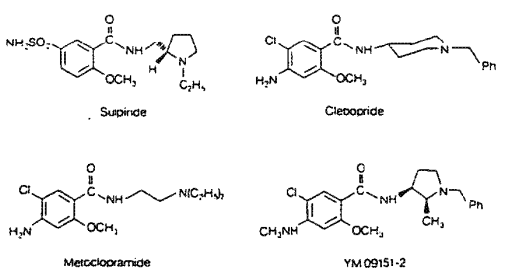


FIG. 1. Representative examples of antidopaminergic 2-methoxybenzamides containing the four main types of side-chains.

* Presented in part at the IXth International Symposium on Medicinal Chemistry, Berlin, 1986, P 2.2.2.

† Correspondence.

UM00013828

NOVARTIS EXHIBIT 1017
Novartis v. Regents, IPR2023-01346
Page 2574 of 4460

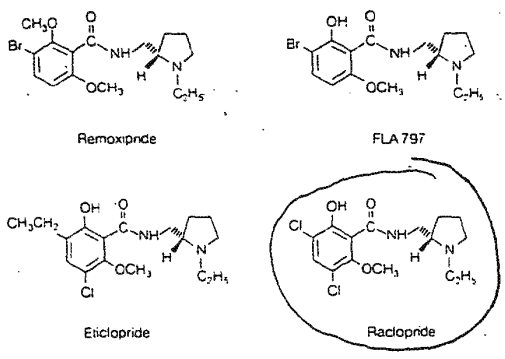


FIG. 2. Recently developed 2-methoxybenzamides with 6-methoxy or 6-hydroxy substituents.

used in positron emission tomography (PET) to visualize the dopamine-D_2 receptors in the living human brain (Farde et al 1985, 1986). Moreover, it has been suggested that raclopride is able to discriminate between various subclasses of functionally coupled dopamine-D_2 receptors (Ögren et al 1986).

Many experimental and theoretical studies have been done to elucidate how the substituted benzamides may interact with the dopamine receptor at the molecular level (e.g. Testa et al 1986). The 4-piperidyl derivatives (e.g. clebopride) exist exclusively in the extended form, whereas the 2-pyrrolidinylmethyl benzamides have considerable conformational flexibility (van de Waterbeemd & Testa 1983). By utilizing various topographical dopamine receptor models, both extended (Testa et al 1986) and folded (Högberg et al 1986) conformers of 2-pyrrolidinylmethyl derivatives have been proposed to be the conformation recognized by the receptor. Such receptor models have been derived from conformationally restricted compounds. Humber et al used butaclamol and isobutaclamol (Fig. 3) to define coordinates of a widely used 3-D receptor map including a naphthalene binding site (α and β regions), a nitrogen binding site and a lipophilic

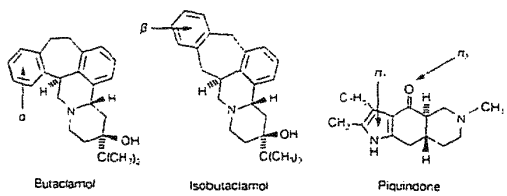


FIG. 3. Conformationally restricted neuroleptics used in dopamine receptor mapping. Pertinent pharmacophores are indicated according to original designations.

accessory binding site 4·5 Å away from the nitrogen site (Humber et al 1979b; Philipp et al 1979). Olson et al (1981) have used piquindone (Fig. 3) and other antipsychotics as model compounds. The pyrroloisoquinoline structure contains three recognition sites, i.e. a π-excessive pyrrole ring (π_1-site), a keto function (π_2-site) and an aliphatic nitrogen, which chemically relate to the 2-hydroxy-6-methoxyphenyl group, the amide carbonyl and the pyrrolidine nitrogen in the salicylamides. Contrary to the (iso)-butaclamol model, the piquindone model has no strict requirement for an accessory lipophilic binding.

Theoretical and crystallographic investigations provide essential information about possible low-energy conformations likely to be involved in the receptor interaction. As a part of the structure-activity studies of the 6-oxygenated 2-methoxybenzamides (Fig. 2), the solid state conformations of remoxipride, FLA 797 (Högberg et al 1986) and eticlopride (Wägner et al 1985; de Paulis et al 1985b) have been determined.

In the present paper we report on the X-ray structure of raclopride tartrate. Furthermore, the conformational behaviour of raclopride, a representative model for the group of substituted salicylamides (including eticlopride and FLA 797), has been investigated using molecular mechanics (force field) calculations (cf. Burkert & Allinger 1982). Finally, the different solid state conformations and the theoretically derived conformations have been related to the preferred rigid template, i.e. piquindone, by means of distance parameters and molecular modelling.

MATERIALS AND METHODS

Crystallography

Single crystals of raclopride (+)-tartrate, FLA 870, $C_{15}H_{20}O_3N_2Cl_2 \times C_4H_6O_6$ were obtained from recrystallization in absolute ethanol. The crystal chosen for the data collection was 0·08 × 0·62 × 0·64 mm in size and oriented with the crystallographic b-axis parallel to the ϕ-axis of the goniostat. A Philips PW 1100 automated diffractometer, equipped with monochromatized CuK(α)-radiation was used to measure 2011 unique reflections, utilizing the ω-2θ scan technique. The θ-range was: 1–67°; scan width 1·4° and scan speed 0·035° s^{-1}. All observed reflections were corrected for Lorenz and polarization factors as well as for absorption. Least squared refined unit cell parameters were calculated from an X-ray powder diffraction photograph taken in a Guinier-Hägg focusing camera with monochro-

NOVARTIS EXHIBIT 1017
Novartis v. Regents, IPR2023-01346
Page 2575 of 4460

matized CuK(α_1)-radiation (λ = 1·54056 Å) and Si (a = 5·4309 Å) as internal standard (Malmros & Werner 1973). The crystal structure was elucidated by a combination of Patterson- and direct methods. From the Patterson synthesis the positions of the pseudo-related Cl-atoms were determined and the knowledge was exploited in the MULTAN 80 program (Main et al 1980). Many successive Fourier maps had to be calculated before a reasonable structural model was found.

The structure was completed and refined in the program system SHELX 76 (Sheldrick 1976). All non-H atoms were refined anisotropically except for C(12), which was suffering from abnormal thermal vibration or disorder. Most H-atom positions were calculated from known geometrical considerations (C–H = 1·08 Å) and supplied with four different isotropic thermal factors. Exceptions were the hydrogen-bonded H-atoms H(3), H(8) and H(14) of the raclopride molecule and the hydroxyl H-atom H(3″) of the tartrate, which were refined individually with isotopic thermal parameters. The two carboxyl H-atoms of the tartrate group could, however, never be located. In the last cycle of refinement the largest parameter shift was 0·022 of the non-H atoms. Five reflections (11 5 5, –3 0 1, 1 0 0, –15 4 6, –16 0 5) were omitted due to their abnormally high δ/σ ratio.

A summary of some selected crystal and experimental data is given in Table 1. Lists of atomic coordinates and anisotropic thermal parameters have been deposited with the Director of the Cambridge Crystallographic Data Centre, University Chemical Laboratory, Lensfield Road, Cambridge CB2 1EW, UK. Any request should be accompanied by the complete literature citation of this paper. Structure factors and Bijvoet differences are available from the authors.

Table 1. Some selected crystal data for raclopride tartrate.

Formula	$C_{15}H_{20}O_9N_2Cl_2 \cdot C_2H_6O_6$
Space group	$P2_1$
Number of molecules in the unit cell	Z = 2
Cell dimensions	a = 16·214(7) Å b = 9·567(3) Å c = 7·581(2) Å β = 108·20 (3)°
Calculated density	d_c = 1·422 g cm^{-3}
Linear absorption coefficient (CuKα)	μ = 30·2 cm^{-1}
Number of unique collected reflections	2011
Number of reflections for which F ≥ 6σ (F)	1922
Number of parameters refined	309
Final linear R-value	R = 5·80%
Weighted R-value {w = 22·76 [σ^2(F) + 0·009(F)^2]$^{-1}$}	R_w = 5·91%

Calculations

We have used a molecular mechanics program MM2PI, which is similar to the MMPI-MM2 hybrid force field developed by Lipkowitz et al (1984). The MM2PI program uses the π-system routines of MMPI together with the MM2 equations and parameters. MM2PI provides geometries and energies that are comparable with those obtained by MMP2 (Norinder unpublished). The parent rigid trial structures of raclopride were obtained by using the MACCS program (Molecular Design Ltd, Hayward, California, USA) followed by MM2PI relaxation. The rigid rotations were carried out with a subroutine in the MIMIC program (Liljefors 1983). The molecular modelling was performed by comparison of the molecules with proper alignment according to the least-squares fitting routine in CHEM-X (developed and distributed by Chemical Design Ltd, Oxford, UK).

RESULTS

Crystallography

The molecular structure and atom numbering, shown in Fig. 4, refer to the correct absolute

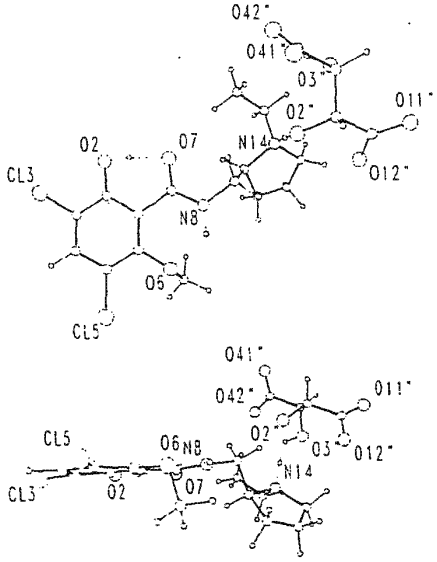


FIG. 4. Molecular structure and atom numbering of raclopride (+)-tartrate displayed from two different angles. Atoms with a prime refer to the tartrate anion.

UM00013830
NOVARTIS EXHIBIT 1017
Novartis v. Regents, IPR2023-01346
Page 2576 of 4460

configuration of raclopride (+)-(*R,R*)-tartrate. The pertinent possible intra- and intermolecular hydrogen bonds are shown in Table 2. The molecular packing arrangement is drawn in a mixed ball-and-stick/van der Waals style for clarity (Fig. 5). The absolute configuration, measured from Bijvoet differences of 14 reflections, entirely confirmed the (*S*)-enantiomeric form (Bijvoet et al 1951). The (+)-tartrate anion, being an asymmetric marker in itself, was determined to possess the (*R,R*)-configuration.

Table 2. Possible intra- and intermolecular hydrogen bonds in raclopride tartrate with estimated standard deviations in parentheses. Primed atoms refer to the tartrate molecule.

	Distances (Å)			Angle (°)
Donor-H · · · Acceptor	D · · · A	D–H	H · · · A	<D-H · · · A
O(2)-H(2) · · · O(7)	2·467(6)	0·88(5)	1·60(5)	169(6)
N(8)-H(8) · · · O(6)	2.704(6)	1·05(8)	1·94(7)	127(5)
N(14)–H(14) · · · O(2″)	2·880(7)[a]	0·63(9)	2·28(10)	163(11)
Intramolecular distances (Å)				
Tartrate				
O(12″) · · · O(2″)	2·630(5)			
O(3″) · · · O(2″)	2·816(6)			
O(3″) · · · O(42″)	2·626(6)			
Intermolecular distances (Å)				
Raclopride–Tartrate		Tartrate–Tartrate		
N(8) · · · O(11″)	3·009(6)[b]	O(2″) · · · O(42″)	2·637(6)[c]	
O(6) · · · O(11″)	3·130(5)[b]	O(12″) · · · O(41″)	2·492(5)[d]	

Symmetry operations: [a] x, y, z; [b] 2 − x, ½ + y, 2 − z; [c] 2 − x, ½ + y, 1 − z; [d] x, y, z + 1.

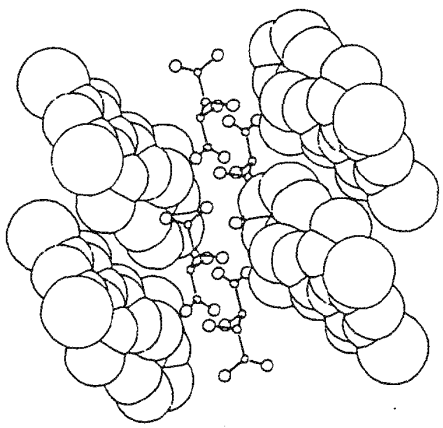


FIG. 5. Molecular packing arrangement of the raclopride (+)-tartrate, viewed along the crystallographic b-axis and drawn in a mixed ball-and-stick/van der Waals style. The four most closely packed molecules involved in short intermolecular contacts are shown. No H-atoms are included.

The benzamide part of the raclopride molecule adopts a rigid planar conformation stabilized by two intramolecular hydrogen bonds. Except for the common interaction from the amide nitrogen to the methoxy oxygen, N(8)–H(8) · · · O(6) = 2·704(6) Å, found in most *ortho*-methoxy benzamides, another hydrogen bond between the phenol and carbonyl oxygen atoms, O(2)–H(2) · · · O(7) = 2·467(6) Å, is also found. This observation is in agreement with other *ortho*-hydroxy substituted benzamides (salicylamides) (Wägner et al 1985; Högberg et al 1986). It is notable that the only component diverging from the plane is the methyl group of the methoxy moiety.

The side-chain in raclopride has an extended conformation in contrast to the other investigated salicylamides. The interchain torsion angles τ_3: C(7)N(8)–C(9)C(10) and τ_4: N(8)C(9)–C(10)-N(14), possessing the greatest conformational freedom, are −78° and 176°, respectively. The conformation of the pyrrolidine ring takes a half-chair form, with the two-fold axis through the C(12) atom and with a phase angle P = 88(5)° (Cremer & Pople 1975). The dihedral angle between the pyrrolidine and benzene ring least-squares planes is 41·8(3)°.

The distances between the centre of the benzene ring and the tertiary nitrogen N(14) is 7·32 Å and the out-of-plane distance is 0·84 Å. The distances to N(14) from the centres of the two pseudo-rings including N–H · · · O and O–H · · · O are 5·25 Å and 5·47 Å, respectively.

Bonds involving the tartrate carboxyl group C(1″)O(11″)O(12″) are normal with a separation of 0·1 Å of the C–O and C=O distances. The corresponding values of the deprotonated carboxyl group C(4″)O(41″)O(42″) are equal. Remarkably, the hydroxy oxygen O(2″), instead of the carboxylate oxygen in the tartrate, is involved in the hydrogen bonding to the protonated tertiary nitrogen N(14) of the raclopride molecule. Thus, the hydroxyl O(2″)H acts as a hydrogen bonding bridge between the two ionic centres. The short intermolecular interaction between the carboxyl oxygen O(11″) and the amine nitrogen N(8) of the raclopride molecule is also notable.

Calculations

To ascertain relevant basic structural parameters in the calculations, we have utilized salient features from the crystal structures (cf. Table 3). The benzamide moiety in the solid state conformations of all salicylamides examined so far (vide infra) has a planar arrangement, i.e. a torsion angle

UM00013831
NOVARTIS EXHIBIT 1017
Novartis v. Regents, IPR2023-01346
Page 2577 of 4460

Table 3. Selected topographical X-ray features of various antidopaminergic compounds.

Compound	Distances (Å)[a] Ar-N	N-plane	Torsion angles (°)[b] τ_1	τ_2	τ_3	τ_4	τ_5	Theor. min[c]	Ref.
Raclopride tartrate	7·3	−0·8	− 7	−173	− 78	176	−115	4	
Eticlopride HCl	6·2	2·6	− 5	−179	93	60	− 98	1	Wägner et al (1985)
FLA 797 (base)	6·0	0·5	− 4	177	−161	− 51	− 75	3	Högberg et al (1986)
(±)-Sulpiride (base)	7·4[d]	0·8[d]	−13	179	−124	171	− 69	5	Houttemane et al (1981)
(±)-Sulpiride HCl[e]	6·1[d]	2·3[d]	− 5	178	84	59	−103	1	Blaton et al (1981)
Piquindone HCl[e]	5·9	0·1							Olson et al (1981)
(±)-Butaclamol HBr	5·1[d]	0·5[d]							Bird et al (1976)
(+)-Isobutaclamol HBr	6·0[d]	1·1[d]							Humber et al (1979a, b)

[a] Distances from the nitrogen to the centre of the aromatic ring (Ar-N) and above the aromatic ring plane (N-plane).
[b] Positive sign for clockwise rotation. τ_1 to τ_5 corresponds to the string (from left to right): C(6)C(1)–C(7)–N(8)–C(9)–C(10)–N(14)C(15). Cf. Table 4.
[c] Corresponding conformation calculated in Fig. 6 (rigid rotation) and Table 4 (MM2PI).
[d] Distances calculated from the X-ray coordinates obtained from Cambridge Crystallographic Data File.
[e] Torsion angles refer to the (*s*)-enantiomer.

τ_1: C(6)C(1)–C(7)N(8) of about −5°. This torsion angle was held constant at −5° in the following calculations in order to mimic the intramolecular hydrogen bond. Likewise, the amide bond has a perfect *trans* orientation [τ_2: C(1)C(7)–N(8)C(9) being about 180°] in a variety of 2-methoxybenzamides (cf. references in Högberg et al 1986). Crystallographic data on various benzamides including sulpiride, remoxipride, eticlopride and raclopride have shown that the 1-ethyl group in the pyrrolidine ring is oriented *trans* to the 2-methylamino chain. For comparative purposes, both the *cis* and the *trans* configurations of raclopride were initially subjected to conformational analysis. The torsion angles τ_3 and τ_4, which consequently mainly determine the side-chain conformations, were changed by rigid rotation (10° increments) in the two trial structures obtained from MACCS–MM2PI. The final energy surface was calculated from the grid obtained by rigid rotation using spline-interpolation. The calculations showed consistently lower (>1·8 kcal mol^{-1}) energies for the local minima of the *trans* forms in comparison with the corresponding *cis* forms. The conformation τ_3 vs τ_4 energy surface of the *trans* configuration was found to contain eight local minima (Fig. 6), which subsequently were subjected to full MM2PI relaxation except for the torsion angle τ_1. Final energies and selected geometry data are presented in Table 4.

Our calculations indicate that a half-folded conformation (#8) is the global minimum and a folded conformation (#3) is less than 0·5 kcal mol^{-1} higher in energy. However, all local minima found in this conformational search are within 4 kcal mol^{-1} of each other and include various folded and extended forms. According to this calculation the distance between the centre of the aromatic ring and the nitrogen atom can easily range from 6 to about 7·5 Å (Table 4).

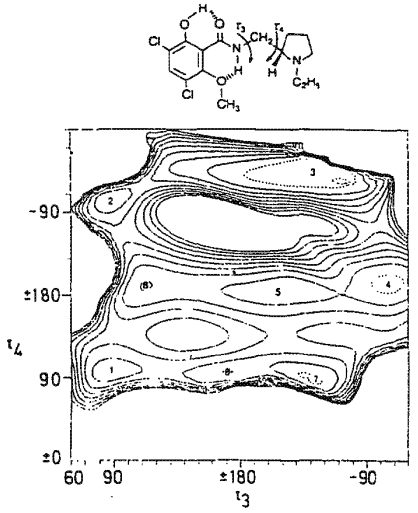


FIG. 6. Energy surface of raclopride generated by rigid rotations of τ_3 and τ_4 in 10° increments. The final energy surface was calculated from the grid using spline-interpolation.

Molecular modelling

As mentioned earlier, the most widely used conformationally restricted compounds for modelling of the dopamine receptor are (iso)butaclamol and piquindone shown in Fig. 3 (Humber et al 1979a, b; Philipp et al 1979; Olson et al 1981). The essential

UM00013832
NOVARTIS EXHIBIT 1017
Novartis v. Regents, IPR2023-01346
Page 2578 of 4460

distance parameters are the distance between the nitrogen atom and the centre of the aromatic ring and the height of the nitrogen atom above the aromatic ring plane. These parameters for the calculated conformations of raclopride and crystal conformations of different dopamine receptor blockers are shown in Tables 3 and 4.

Table 4. Prominent features of low-energy conformations of raclopride calculated by MM2PI.[a]

Minimum[b]	Energy[c] kcal/mol	Torsion angles (°)[d]		Distances (Å)[f]	
		τ_3[e]	τ_4[e]	Ar–N	N-plane
1	3·68	86	83	6·8	2·3
2	3·26	94	− 70	6·2	1·4
3	0·42	−118	− 49	6·0	−0·4
4	2·46	− 58	−168	7·1	−1·7
5	2·66	−164	−174	7·6	0·6
6	4·04	112	−173	6·5	1·3
7	2·16	−132	81	6·3	−2·2
8	0·00	−167	79	6·7	0·0

[a] The 1-ethyl group is oriented *trans* to the 2-methylamino chain of the pyrrolidine ring. Torsion angle τ_1C(6)C(1)–C(7)N(8) fixed at −5°.
[b] Calculated from the corresponding minimum in Fig. 6.
[c] Relative to minimum #8.
[d] Positive sign for clockwise rotation.
[e] τ_3 = C(7)N(8)–C(9)C(10). τ_4 = N(8)C(9)–C(10)N(14).
[f] Distances from the nitrogen to the centre of the aromatic ring (Ar–N) and above the aromatic ring plane (N-plane, positive sign when carbonyl is oriented upwards and nitrogen above plane of paper).

First, we compare the different solid-state conformations of the benzamides with the preferred template piquindone with respect to the distance parameters shown in Table 3. The salicylamide FLA 797 exhibits a remarkable fit both in terms of nitrogen distance from (6·0 Å) and height above (0·5 Å) the aromatic ring. The folded conformation found in eticlopride will place the nitrogen too high above the ring plane, but it might be argued that a π–π stacking or other type of interaction at the receptor can tolerate a smaller angular deviation which could bring the nitrogen within contact. However, the extended X-ray conformation of raclopride is inappropriate for an acceptable overlap. When the calculated conformations of raclopride in Table 4 are compared with piquindone, the closest match is obtained with #3, which is one of the energetically most favoured conformations.

Molecular modelling of the eight minimized raclopride conformations and the above mentioned X-ray structures, with piquindone as template, results in a more appropriate comparison than that by the simple distance parameters. The superimposition of the benzamide with piquindone was based on the three assumed recognition sites (π_1, π_2 and N) by minimization with respect to the aromatic ring atoms, carbonyl moieties and aliphatic nitrogens with attached lone-pairs. Four representative graphic overlays are shown from two different angles in Fig. 7 (a–d). The excess salicylamide volumes are contoured at the van der Waals radii.

The raclopride conformation #3, having ideal distance parameters, exhibits an excess volume primarily from the 3-, 4- and 5-pyrrolidine carbons and the 5-chloro substituent (Fig. 7a). The latter substituent, (5-Cl) in the *ortho* position with regard to the methoxy group, is not as crucial for activity as the substituent *para* to the methoxy group as mentioned earlier. Most antidopaminergic benzamides, e.g. sulpiride, clebopride and FLA 797, in fact lack a substituent in the position *ortho* to the essential methoxy group (de Paulis 1985; de Paulis et al 1985a). This is clearly seen in Fig. 7d having the solid state conformation of FLA 797 superimposed on piquindone. The overlays of these two structures (Fig. 7a, b) are similar with the exception of the excess volume generated by the less important chloro substituent in raclopride. This latter type of substituent *ortho* to the methoxy group can be tolerated by the receptor not only in the salicylamide class of compounds (de Paulis et al 1986) but also in other derivatives such as tropapride and veralipride (de Paulis 1985). It should be noted that the halogens in the 3-position of the salicylamides raclopride (Fig. 7a) and FLA 797 (Fig. 7d) are completely included in the van der Waals volume generated by piquindone. Thus, this particular type of superimposition with piquindone and *para*-substituted orthopramides is consistent with the observation that 2- and 3-alkyl substituents of limited size in the pyrrole part of piquindone related compounds are mandatory for high activity (Olson et al 1983).

The global minimum #8 of raclopride also shows a favourable overlap with piquindone (Fig. 7b), indicating that the slightly longer distance between the aromatic ring and the nitrogen in the half-folded conformation is more reasonable than originally anticipated. It should be noted that the *N*-ethyl group in conformation #8 occupies the same excess space as the pyrrolidine ring (i.e. carbons 3, 4 and 5) in conformation #3. However, conformation #2 is clearly less likely than might be expected on the basis of the distance parameters (Fig. 7c). The other structures showed less efficient overlays and are thus not depicted.

DISCUSSION

The crystal conformation of raclopride shows notable similarities with FLA 797 and eticlopride hydrochloride. The salicylamide part in all three

LIM00013833
NOVARTIS EXHIBIT 1017
Novartis v. Regents, IPR2023-01346
Page 2579 of 4460

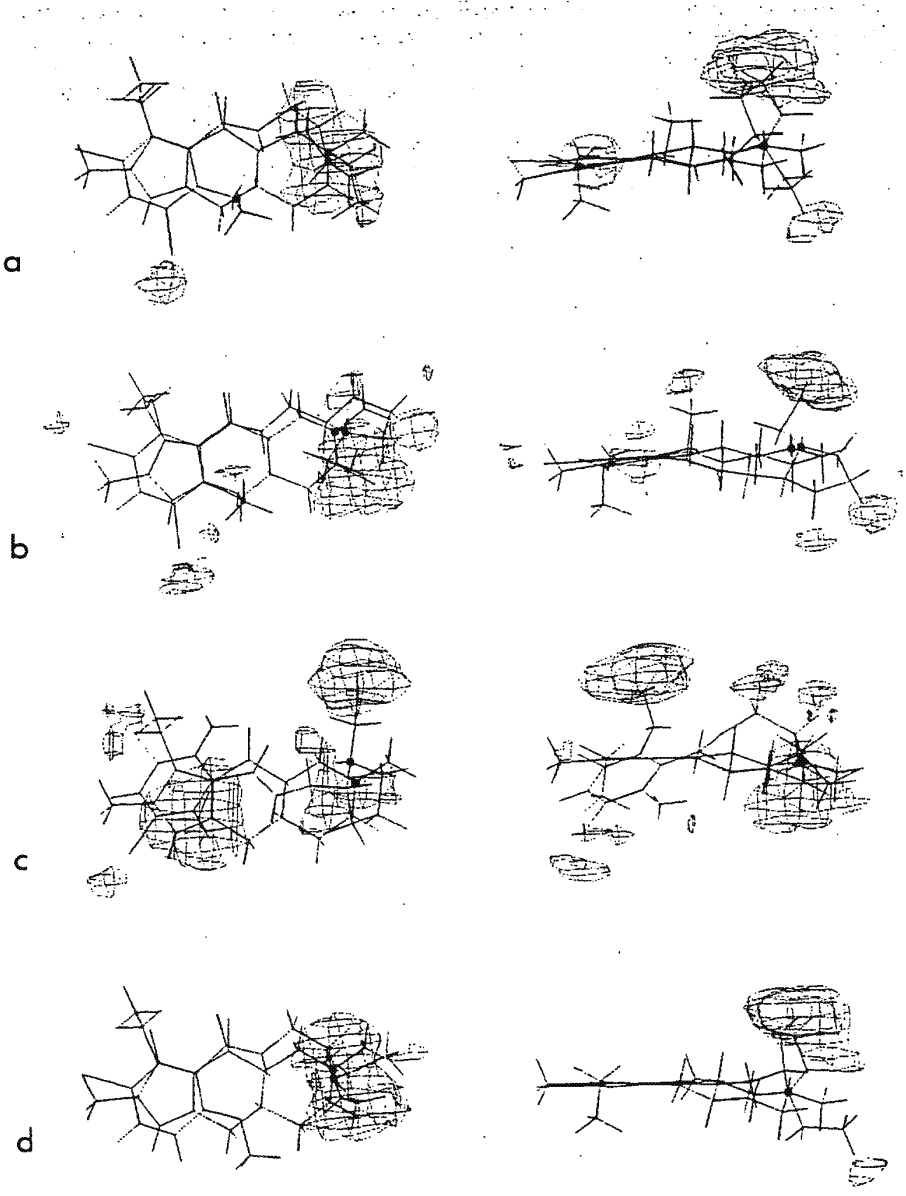


FIG. 7. Displays of two different views of the superimpositions of three pertinent calculated conformations of raclopride (a: #3, b: #8, c: #2) and the X-ray conformation of FLA 797 (d) with piquindone. The excess volume of the salicylamides is contoured at the van der Waals radii. The aliphatic nitrogens are marked.

UM00013834
NOVARTIS EXHIBIT 1017
Novartis v. Regents, IPR2023-01346
Page 2580 of 4460

compounds has a planar conformation which is stabilized by the two intramolecular hydrogen bonds from the amide hydrogen to the methoxy oxygen atom and from the phenol hydrogen to the carbonyl oxygen atom. This common feature, clearly shown in Table 3 by the practically identical values of τ_1 and τ_2, is thus not influenced by the differences in salt forms or aromatic substituents. It should be noted that this planar benzamide arrangement is present also in the solid state of other 2-methoxybenzamides lacking the 6-hydroxy substituent, e.g. sulpiride (Houttemane et al 1981; Blaton et al 1981), metoclopramide (Cesario et al 1981), YM-09151-2 (Furuya et al 1982) and its diastereomer YM-09151-1 (Furuya et al 1986).

The appearance of the side-chain in the crystal conformations of the salicylamides raclopride, eticlopride and FLA 797 differ considerably (τ_3, τ_4 and τ_5 shown in Table 3). The side-chain conformation is apparently independent of whether the pyrrolidine is in base or protonated form, which is underlined by comparison of the two sulpiride structures in Table 3. Thus, the extended conformation of raclopride is not necessarily due to the tartrate, which is involved in extensive hydrogen bonding in the crystal, since a similar conformation is found for sulpiride base. The X-ray studies indicate that the salicylamide moiety is also likely to be in a planar hydrogen bonded form when the compounds elicit the biological response. However, no conclusive information about which of the different side-chain conformations is preferred can be deduced on the basis of the crystal conformations alone.

The theoretical conformational analysis of the model salicylamide raclopride shows that there are a variety of folded and extended conformations possible within a small energetic span of 4 kcal mol^{-1}. In Table 3 it can be seen that the crystal conformations of raclopride, eticlopride, FLA 797 and sulpiride in fact correspond to four of the eight local minima found by the MM2PI calculations. An exact match of the torsion angles should not be expected due to the methodological differences. Yet, this fact underlines the relevance of the calculations since the X-ray analysis provides the three-dimensional arrangement of at least one of the minimum energy conformations, even if it is affected by crystal packing forces such as π–π stacking and hydrogen bonding (Kitaigorodsky 1973; Duax 1978; Högberg et al 1986).

A half-folded (#8) and a folded (#3) conformation are energetically most favoured, which partly is in line with the results obtained by van de Waterbeemd & Testa (1981). They investigated a model molecule [*N*-(1-methyl-2-pyrrolidinylmethyl)-2-methoxybenzamide] in the protonated form by the quantum mechanical PCILO method. The global minimum thus obtained was a folded conformer having a hydrogen bond between the carbonyl and the protonated nitrogen. This particular conformation stems from a *cis* orientation of the 1-methyl group and the 2-methylamino side-chain in the pyrrolidine ring. Consequently, this folded conformation has no corresponding minimum in our calculations, since we only refined the energetically more favoured *trans* forms of the free base by the MM2PI relaxation. Besides, the PCILO method is known to overestimate attractive interactions between non-bonded atoms, especially hydrogen bonds (Bendl & Pretsch 1982). However, the additional three local minima found by van de Waterbeemd & Testa (1981) are close to the minima #7, #4 and #6 obtained by the MM2PI calculation. It is important to note that low-energy folded conformations are found by force-field (MM2PI) calculations without any need for an internal hydrogen bond between the carbonyl and the pyrrolidinium group (cf. van de Waterbeemd & Testa 1983). Still, there are no conclusive arguments either for or against any of the possible side-chain conformations as being more relevant than the others in the receptor interaction. For this purpose one needs to study rigid analogues or to make comparisons with other geometrically defined antidopaminergic compounds as described in the preceding section (Fig. 7).

The 2-methoxybenzamides with *N*-ethyl-2-pyrrolidinylmethyl side-chains have several features that make piquindone the rigid template of choice, i.e. a reasonable chemical relationship, a flat aromatic/pseudo-ring arrangement and a small *N*-alkyl substituent without the requirement of accessory binding. The latter requirement is for example not met by 4-piperidyl derivatives such as clebopride which have the *N*-benzyl substituent as a prerequisite for activity (Prieto 1977). Besides, there are certain characteristics of the binding of piquindone that make it an attractive template for mapping of the benzamide conformations (Nakajima & Iwata 1984). Firstly, sulpiride, metoclopramide, molindone and domperidone exerted a more potent inhibition of [^{3}H]piquindone binding than of [^{3}H]spiperone binding, whereas other classical antipsychotics were almost equipotent at the two binding sites. Secondly, the binding of piquindone, sulpiride, metoclopramide and molindone to [^{3}H]spiperone binding sites was markedly sodium dependent in contrast to spiperone, chlor-

UM00013835
NOVARTIS EXHIBIT 1017
Novartis v. Regents, IPR2023-01346
Page 2581 of 4460

promazine and domperidone. Finally, pyrroloisoquinoline compounds having a nonlipophilic *N*-substituent (methyl, propyl, cyclopropylmethyl, allyl) were more potent at [^{3}H]piquindone binding sites whereas compounds with lipophilic *N*-substituents were equipotent at [^{3}H]piquindone and [^{3}H]spiperone binding sites. It has been argued that the *N*-substituents may influence the selectivity between dopamine-D_1 and -D_2 receptors (Olson et al 1983).

Based on the modelling studies of the salicylamides with piquindone shown in Fig. 7, it can be concluded that the benzamides with an *N*-ethyl-2-pyrrolidinylmethyl side-chain are likely to have a planar hydrogen-bonded pseudo-ring system and a folded or a half-folded side-chain conformation when interacting with the dopamine receptor. If this hypothesis is correct the distance between the centre of the aromatic ring and the nitrogen atom (ca 6 Å) is significantly longer than the corresponding distance in dopamine, having a fully extended *trans* side-chain (5 Å). An extended phenethylamine moiety has been proposed as an essential part of the pharmacophore in several dopamine agonists (Ernst 1967; Horn & Rodgers 1980; Cannon et al 1981; Cannon 1985; Seeman et al 1985) and antagonists (Horn & Snyder 1971; Humber et al 1975; Harbert et al 1980; van de Waterbeemd & Testa 1983) (cf. reviews by Seeman 1980; Andrews & Lloyd 1982; Kaiser & Jain 1985). For an agonist it is highly relevant to expect such a resemblance with the endogenous transmitter. However, for an antagonist this might be the case (Johansson et al 1986) but there are several other possible ways to block the receptor than merely by overlapping in a complementary fashion with the endogenous pharmacophore. Such explanations include binding to an allosteric site or binding to only one of the sites essential for the transmitter (e.g. aromatic or amine binding site) combined with one or several other accessory sites. This view lends support from the different structure–activity relationships found for agonists (e.g. Cannon 1983, 1985; Kaiser & Jain 1985) and antagonists (e.g. Kaiser et al 1980). Besides, dopamine agonists and antagonists exhibit certain different binding properties (e.g. Seeman 1980; Creese et al 1983; Seeman et al 1986; Creese & Leff 1986), which can make comparisons of their structures erroneous. This risk of using dopamine antagonists to probe the agonist binding site has been pointed out previously (e.g. Carnmalm et al 1979; Cannon et al 1981; McDermed 1983).

The phenethylamine moiety has been invoked in the pharmacophore of 2-methoxybenzamide antidopaminergics by regarding the hydrogen-bonded pseudo-ring as the aromatic counterpart (van de Waterbeemd & Testa 1983). By recent molecular electrostatic potential (MEP) studies, van de Waterbeemd et al (1986a, b) slightly revised this model due to an inadequate correspondence between regions of positive and negative potential generated by dopamine and orthopramides. The receptor topography thus proposed by van de Waterbeemd and Testa is based on an extended side-chain, contrasting with our own view. Further studies are needed to gain a deeper insight into which is the bioactive conformation. Different requirements might be involved for benzamides with a small alkyl nitrogen substituent (sulpiride, raclopride, eticlopride, etc) and for semi-rigidly extended benzamides which require lipophilic nitrogen substituents (clebopride, YM-09151-2, BRL 25594, etc).

REFERENCES

Andrews, P. R., Lloyd, E. J. (1982) Med. Res. Rev. 2: 355–393

Bendl, J., Pretsch, E. (1982) J. Comp. Chem. 3: 580–587

Bijvoet, J. M., Peerdeman, A. F., van Bommel, A. J. (1951) Nature 168: 271–272

Bird, P. H., Bruderlein, F. T., Humber, L. G. (1976) Can. J. Chem. 54: 2715–2722

Blaton, N. M., Peeters, O. M., De Ranter, C. J., Denisoff, O., Molle, L. (1981) Cryst. Struct. Comm. 10: 833–838

Burkert, U., Allinger, N. L. (eds) (1982) Molecular Mechanics, ACS Monograph 177, American Chemical Society, Washington, D.C.

Cannon, J. G. (1983) Ann. Rev. Pharmacol. Toxicol. 23: 103–130

Cannon, J. G. (1985) Progr. Drug. Res. 29: 303–414

Cannon, J. G., Long, J. P., Bhatnagar, R. (1981) J. Med. Chem. 24: 1113–1118

Carnmalm, B., Johansson, L., Rämsby, S., Stjernström, N. E., Wägner, A. (1979) Acta Pharm. Suec. 16: 239–246

Cesario, M., Pascard, C., El Moukhtari, M., Jung, L. (1981) Eur. J. Med. Chem. 16: 13–17

Creese, I., Leff, S. E. (1986) in: Woodruff, G. N., Poat, J. A., Roberts, P. J. (eds) Dopaminergic Systems and their Regulations, MacMillan, London, pp 79–95

Creese, I., Sibley, D. R., Hamblin, M. W., Leff, S. E. (1983) Ann. Rev. Neurosci. 6: 43–71

Cremer, D., Pople, J. A. (1975) J. Am. Chem. Soc. 97: 1354–1367

de Paulis, T. (1985) in: Dahlbom, R., Nilsson, J. L. G. (eds) VIIIth International Symposium on Medicinal Chemistry, Proceedings, Vol. 1, Swedish Pharmaceutical Press, Stockholm, pp 405–425

de Paulis, T., Kumar, Y., Johansson, L., Rämsby, S., Florvall, L., Hall, H., Angeby-Möller, K., Ögren, S.-O. (1985a) J. Med. Chem. 28: 1263–1269

de Paulis, T., Hall, H., Ögren, S.-O., Wägner, A., Stensland, B., Csöregh, I. (1985b) Eur. J. Med. Chem. 20: 273–276

de Paulis, T., Kumar, Y., Johansson, L., Rämsby, S., Hall, H., Sällemark, M., Angeby-Möller, K., Ögren, S.-O. (1986) J. Med. Chem. 29: 61–69

UM00013836
NOVARTIS EXHIBIT 1017
Novartis v. Regents, IPR2023-01346
Page 2582 of 4460

Duax, W. L. (1978) in: Sutton, L. E., Truter, M. R. (eds) Molecular Structure by Diffraction Methods. The Chemical Society, London, Vol. 6, pp 261–328

Ernst, A. M. (1967) Psychopharmacologia 10: 316–323

Farde, L., Ehrin, E., Eriksson, L., Greitz, T., Hall, H., Hedström, C.-G., Litton, J.-E., Sedvall, G. (1985) Proc. Natl. Acad. Sci. USA 82: 3863–3867

Farde, L., Hall, H., Ehrin, E., Sedvall, G. (1986) Science 231: 258–261

Florvall, L., Ögren, S.-O. (1982) J. Med. Chem. 25: 1280–1286

Furuya, T., Iwanami, S., Takenaka, A., Sasada, Y. (1982) Bull. Chem. Soc. Japan, 55: 2321–2326

Furuya, T., Iwanami, S., Takenaka, A., Sasada, Y. (1986) Acta Cryst. C42: 117–121

Hall, H., Wedel, I. (1986) Acta Pharmacol. Toxicol. 58: 368–373

Hall, H., Köhler, C., Gawell, L. (1985) Eur. J. Pharmacol. 111: 191–199

Hall, H., Sällemark, M., Jerning, E. (1986) Acta Pharmacol. Toxicol. 58: 61–70

Harbert, C. A., Plattner, J. J., Welch, W. M., Weissman, A., Koe, B. K. (1980) Mol. Pharmacol. 17: 38–42

Högberg, T., Rämsby, S., de Paulis, T., Stensland, B., Csöregh, I., Wägner, A. (1986) Ibid. 30: 345–351

Horn, A. S., Rodgers, J. R. (1980) J. Pharm. Pharmacol. 35: 521–524

Horn, A. S., Snyder, S. H. (1971) Proc. Natl. Acad. Sci. USA 2325–2328

Houttemane, C., Boivin, J. C., Nowogrocki, G., Thomas, D. J., Boute, J. P. (1981) Acta Cryst. B37: 981–984

Humber, L. G., Bruderlein, F. T., Voith, K. (1975) Mol. Pharmacol. 11: 833–840

Humber, L. G., Philipp, A. H., Voith, K., Pugsley, T. (1979a) J. Med. Chem. 22: 899–901

Humber, L. G., Bruderlein, F. T., Philipp, A. H., Götz, M., Voith, K. (1979b) Ibid. 22: 761–767

Jenner, P., Marsden, C. D. (1981) Neuropharmacology 20: 1285–1293

Johansson, A. M., Karlén, A., Grol, C. J., Sundell, S., Kenne, L., Hacksell, U. (1986) Mol. Pharmacol. 30: 258–269

Kaiser, C., Jain, T. (1985) Med. Res. Rev. 5: 145–229

Kaiser, C., Ali, F. E., Bondinell, W. E. et al (1980) J. Med. Chem. 23: 975–976

Kitaigorodsky, A. I. (1973) Molecular Crystals and Molecules. Academic Press, New York and London

Köhler, C., Radesäter, A.-C. (1986) Neurosci. Lett. 66: 85–90

Köhler, C., Hall, H., Ögren, S.-O., Gawell, L. (1985) Biochem. Pharmacol. 34: 2251–2259

Köhler, C., Hall, H., Gawell, L. (1986) Eur. J. Pharmacol. 120: 217–226

Liljefors, T. (1983) Mol. Graphics 1: 111–117

Lindström, L., Besev, G., Stening, G., Widerlöv, E. (1985) Psychopharmacology 86: 241–243

Lipkowitz, K. B., Naylor, A. M., Melchior, W. B. (1984) Tetr. Lett. 25: 2297–2300

Main, P., Fiske, S. J., Hull, S. E., Lessinger, L., Germain, G., Declercq, J.-P., Woolfson, M. M. (1980). MULTAN 80. A System of Computer Programs for the Automatic Solution of Crystal Structures from X-ray Diffraction Data. Univ. of York, England and Louvain, Belgium

Malmros, G., Werner, P.-E. (1973) Acta Chem. Scand. 27: 493–502

McDermed, J. (1983) in: Kaiser, C., Kebabian, J. W. (eds) Dopamine Receptors. ACS Symposium Series No. 224, American Chemical Society, Washington D.C., pp 247–250

Meunier, H., Labrie, F. (1982) Life Sci. 30: 963–968

Nakajima, T., Iwata, K. (1984) Mol. Pharmacol. 26: 430–438

Ögren, S. O., Hall, H., Köhler, C., Magnusson, O., Lindbom, L.-O., Angeby, K., Florvall, L. (1984) Eur. J. Pharmacol. 102: 459–474

Ögren, S. O., Hall, H., Köhler, C., Magnusson, O., Sjöstrand, S. E. (1986) Psychopharmacology 90: 287–294

Olson, G. L., Cheung, H.-C., Morgan, K. D., Blount, J. F., Todaro, L., Berger, L., Davidson, A. B., Boff, E. (1981) J. Med. Chem. 24: 1026–1035

Olson, G. L., Cheung, H.-C., Chiang, E., Berger, L. (1983) in: Kaiser, C., Kebabian, J. W. (eds) Dopamine Receptors, ACS Symposium Series No. 224, American Chemical Society, Washington D.C. pp 251–274

Philipp, A. H., Humber, L. G., Voith, K. (1979) J. Med. Chem. 22: 768–773

Prieto, J., Moragues, J., Spickett, R. G., Vega, A., Colombo, M., Salazar, W., Roberts, D. J. (1977) J. Pharm. Pharmacol. 29: 147–152

Seeman, P. (1980) Pharmacol. Rev. 2: 229–313

Seeman, P., Watanabe, M., Grigoriadis, D., Tedesco, J. L., George, S. R., Svensson, U., Nilsson, J. L. G., Neumeyer, J. L. (1985) Mol. Pharmacol. 28: 391–399

Seeman, P., Grigoriadis, D., George, S. R., Watanabe, M., Ulpian, C. (1986) in: Woodruff, G. N., Poat, J. A., Roberts, P. J. (eds) Dopaminergic Systems and their Regulation, MacMillan, London, pp 97–109

Sheldrick, G. M. (1976). SHELX 76. A Program for Crystal Structure Determination. Univ. of Cambridge, UK

Stoof, J. C., Kebabian, J. W. (1981) Nature 294: 366–368

Stoof, J. C., Kebabian, J. W. (1984) Life Sci. 35: 2281–2296

Testa, B., van de Waterbeemd, H., Carrupt, P.-A. (1986) J. Mol. Struct. (Theochem) 134: 351–366

van de Waterbeemd, H., Testa, B. (1981) Helv. Chim. Acta 64: 2183–2188

van de Waterbeemd, H., Testa, B. (1983) J. Med. Chem. 26: 203–207

van de Waterbeemd, H., Carrupt, P.-A., Testa, B. (1986a) Ibid. 29: 600–606

van de Waterbeemd, H., Carrupt, P.-A., Testa, B. (1986b) J. Mol. Graphics 4: 51–55

Wägner, A., Stensland, B., Csöregh, I., de Paulis, T. (1985) Acta Pharm. Suec. 22: 101–110

NOVARTIS EXHIBIT 1017
Novartis v. Regents, IPR2023-01346
Page 2583 of 4460

This Page is Inserted by IFW Indexing and Scanning Operations and is not part of the Official Record

BEST AVAILABLE IMAGES

Defective images within this document are accurate representations of the original documents submitted by the applicant.

Defects in the images include but are not limited to the items checked:

- ☐ BLACK BORDERS
- ☐ IMAGE CUT OFF AT TOP, BOTTOM OR SIDES
- ☐ FADED TEXT OR DRAWING
- ☐ BLURRED OR ILLEGIBLE TEXT OR DRAWING
- ☐ SKEWED/SLANTED IMAGES
- ☐ COLOR OR BLACK AND WHITE PHOTOGRAPHS
- ☐ GRAY SCALE DOCUMENTS
- ☐ LINES OR MARKS ON ORIGINAL DOCUMENT
- ☐ REFERENCE(S) OR EXHIBIT(S) SUBMITTED ARE POOR QUALITY
- ☐ OTHER: _____

IMAGES ARE BEST AVAILABLE COPY.
As rescanning these documents will not correct the image problems checked, please do not report these problems to the IFW Image Problem Mailbox.

Acta Cryst. (1974). B30, 994

The 2:1 Crystal Complex of 2-Aminopyridine and 5,5-Diethylbarbituric Acid (Barbital)

BY I-NAN HSU AND B.M. CRAVEN

Department of Crystallography, University of Pittsburgh, Pittsburgh, Pennsylvania 15260 *U.S.A.*

(*Received* 2 *November* 1973; *accepted* 10 *December* 1973)

The 2:1 complex of 2-aminopyridine ($C_5H_6N_2$) and 5,5-diethylbarbituric acid (barbital, $C_8H_{12}N_2O_3$), m.p. 82°C, is triclinic, space group $P\bar{1}$ with $a=9{\cdot}914$ (2), $b=10{\cdot}004$ (2), $c=10{\cdot}861$ (2) Å, $\alpha=108{\cdot}76$ (2), $\beta=92{\cdot}28$ (2), $\gamma=104{\cdot}24$ (2)°, (reduced cell) and with observed density (1·265 g cm^{-3}) in agreement with a calculated value (1·262 g cm^{-3}) for $4(C_5H_6N_2).2(C_8H_{12}N_2O_3)$ in the unit cell. The structure determination by direct methods was based on 4032 integrated intensities measured on a computer-controlled four-circle diffractometer with graphite monochromated Cu $K\alpha$ radiation. Least-squares refinement of two large blocks of atomic parameters gave a final R value of 0·065 for all data. The structure contains two strong NH···N hydrogen bonds with N···N distances 2·81, 2·85 Å, in which the two barbital NH groups are donors and pyridine nitrogen atoms are acceptors. These distances are similar to those reported for hydrogen bonds in which barbiturate or uracil is donor and adenine atom (N1) is acceptor. There are four weak NH···O=C hydrogen bonds with N···O distances 3·02, 3·03, 3·13 and 3·14 Å.

Introduction

The strong association of barbiturates with adenine derivatives in solution may be significant for an understanding of barbiturate drug action (Kyogoku, Lord & Rich, 1968). Structure determinations of crystal complexes of barbiturates with adenine derivatives (Kim & Rich, 1968; Voet & Rich, 1972; Voet, 1972) have shown examples of hydrogen bonding both in the Watson–Crick and Hoogsteen modes. The Watson–Crick mode of hydrogen bonding which involves one NH···N hydrogen bond with barbital as donor and adenine N(1) as acceptor, and a second NH···O=C hydrogen bond with the adenine amino group as donor and a barbital oxygen atom as acceptor, is very similar to the mode of hydrogen bonding which is observed in the complex of barbital with 2-aminopyridine.

Experimental

Prismatic crystals of the 2:1 complex 2-aminopyridine–barbital previously reported in the patent literature* were grown from a supersaturated solution of both components in a solvent mixture of 3 ml ethanol and 3 ml hexane. The crystals were observed to become opaque after about a week's exposure to air. A transparent crystal of dimensions 0·4 × 0·3 × 0·2 mm was coated with epoxy resin to prevent deterioration. The unit-cell dimensions and X-ray intensities were measured on a four-circle automatic diffractometer using graphite monochromated Cu $K\alpha$ radiation ($\lambda=1{\cdot}5418$ Å), and with the coated crystal oriented with [011] approximately along the goniostat φ axis. Reflections were scanned in the θ–2θ mode, with a θ scan width of $(0{\cdot}8+0{\cdot}5\tan\theta)°$. Among a total of 4032 independent reflections in the range $\theta\leq 75°$, there were 726 reflections for which the integrated intensity (I) was less than $2\sigma(I)$ as calculated from the counting statistics. These reflections were assigned intensities of $\sigma(I)/2$. X-ray absorption and extinction corrections were not applied.

The crystal structure was determined by direct methods (Germain, Main & Woolfson, 1971). Because of computing limitations, atomic parameters (Table 1) were refined alternately in two blocks by a least-squares procedure. The first block consisted of parameters for all heavier atoms and the second block consisted of parameters for all hydrogen atoms together with those of the atoms to which the hydrogens are bonded. The function minimized was $\sum_H w_H \Delta_H^2$, where $\Delta_H=|F_H^o|-|F_H^c|$. The weights were $w_H^{-1}=0{\cdot}13+0{\cdot}0034|F_H|^2$. The atomic scattering factors were those of Cromer & Waber (1965) for carbon, nitrogen and oxygen, and of Stewart, Davidson & Simpson (1965) for hydrogen. All hydrogen atom positions were obtained from a difference Fourier synthesis which was calculated after some refinement of heavier atom anisotropic thermal parameters. Hydrogen-atom thermal parameters were refined isotropically. In the final cycles of refinement, reflections with $I<2\sigma(I)$ and 14 strong reflections for which $|F_H^c|>|F_H^o|$ were given zero weight. The final R index* was 0·065 for all reflections and 0·044 for reflections with non-zero weights.†

* Chemische Fabrik von Heyden A-G, F. 769586 (1934).

* $R=\sum_H|\Delta_H|/\sum_H|F_H^o|$.

† The list of structure factors has been deposited with the British Library Lending Division as Supplementary Publication No. SUP 30319 (25 pp., 1 microfiche). Copies may be obtained through the Executive Secretary, International Union of Crystallography, 13 White Friars, Chester CH1 1NZ, England.

UM00013839
NOVARTIS EXHIBIT 1017
Novartis v. Regents, IPR2023-01346
Page 2585 of 4460

Discussion

(i) *Barbital*

The barbital bond lengths and angles (Fig. 1) are similar to those in barbital II (Craven, Vizzini & Rodrigues, 1969), the most significant differences being in the internal ring angles at the nitrogen atoms (125·5° *vs.* 126·8°) and at C(2) (116·8° *vs.* 115·1°). The e.s.d.'s in these differences are 0·3°. Corresponding bond lengths and angles are very similar on each side of the C(2)···C(5) ring diagonal, in contrast to the slight differences which have consistently been reported in other barbiturate crystal structures, in which atom O(4) is hydrogen bonded, but O(6) is not (Craven, Cusatis, Gartland & Vizzini, 1973). In the complex with 2-aminopyridine, both atoms O(4) and O(6) are hydrogen bonded and no such differences in bond lengths and angles are expected. The pyrimidine ring atoms are nearly coplanar except for C(5), which is displaced 0·06 Å from the best least-squares plane of the other five. The hydrocarbon chain C(10)–C(9)–C(5)–C(7)–C(8) is fully extended except for a twist of 3·1° (σ = 0·1°) about the C(5)–C(7) bond.

(ii) *2-Aminopyridine*

There is excellent agreement between corresponding

Table 1. *Atomic parameters with e.s.d.'s*

Positional parameters are given as fractions of the lattice translations. Anisotropic thermal parameters are given according to the expression: $T=\exp[-(\beta_{11}h^2+\beta_{22}k^2+\beta_{33}l^2+2\beta_{12}hk+2\beta_{13}hl+2\beta_{23}kl)]$ and isotropic thermal parameters according to the expression: $T=\exp[-B\sin^2\theta/\lambda^2]$. Estimated standard deviations given in parentheses refer to the least significant figures in the parameter values.

(*a*) Non-hydrogen atom parameters (× 10⁴)

(i) Barbital molecule

	x	*y*	*z*	β_{11}	β_{22}	β_{33}	β_{12}	β_{13}	β_{23}
N(1)	3588 (1)	3452 (1)	1232 (1)	95 (1)	76 (1)	118 (1)	8 (1)	25 (1)	7 (1)
O(2)	5857 (1)	4420 (1)	1049 (1)	108 (1)	109 (1)	176 (1)	15 (1)	60 (1)	10 (1)
N(3)	4829 (1)	5862 (1)	2543 (1)	84 (1)	80 (1)	110 (1)	2 (1)	19 (1)	9 (1)
C(4)	3717 (1)	6143 (1)	3165 (1)	95 (1)	83 (1)	95 (1)	10 (1)	18 (1)	14 (1)
O(4)	3844 (1)	7328 (1)	4030 (1)	126 (1)	102 (1)	135 (1)	7 (1)	36 (1)	−17 (1)
C(6)	2374 (1)	3548 (1)	1738 (1)	87 (1)	87 (1)	109 (1)	4 (1)	16 (1)	16 (1)
O(6)	1331 (1)	2497 (1)	1369 (1)	103 (1)	107 (1)	174 (1)	−16 (1)	31 (1)	−6 (1)
C(7)	1245 (1)	5586 (1)	2193 (1)	97 (1)	121 (2)	118 (1)	31 (1)	22 (1)	24 (1)
C(8)	1657 (2)	6027 (2)	1022 (2)	143 (2)	194 (2)	147 (2)	48 (2)	23 (2)	76 (2)
C(9)	1818 (2)	4654 (2)	3997 (1)	130 (2)	140 (2)	112 (1)	6 (1)	32 (1)	41 (1)
C(10)	2783 (2)	4065 (2)	4661 (2)	198 (3)	224 (3)	163 (2)	5 (2)	−4 (2)	109 (2)

(ii) 2-Aminopyridine (molecule *A*, above; molecule *B*, below)

	x	*y*	*z*	β_{11}	β_{22}	β_{33}	β_{12}	β_{13}	β_{23}
N(1)	3694 (1)	788 (1)	−623 (1)	105 (1)	94 (1)	96 (1)	16 (1)	13 (1)	25 (1)
	7432 (1)	8079 (1)	3181 (1)	100 (1)	91 (1)	101 (1)	14 (1)	18 (1)	24 (1)
C(2)	2752 (1)	−520 (1)	−960 (1)	110 (1)	97 (1)	96 (1)	16 (1)	−10 (1)	24 (1)
	7684 (1)	9440 (1)	4024 (1)	103 (1)	94 (1)	88 (1)	19 (1)	4 (1)	27 (1)
C(3)	2958 (2)	−1749 (2)	−1927 (2)	164 (2)	111 (2)	125 (2)	27 (2)	−20 (2)	0 (1)
	8893 (2)	10544 (1)	4051 (1)	128 (2)	99 (2)	130 (2)	0 (1)	1 (1)	30 (1)
C(4)	4146 (2)	−1593 (2)	−2522 (2)	208 (3)	183 (3)	103 (2)	93 (2)	4 (2)	−1 (2)
	9831 (2)	10199 (2)	3204 (2)	120 (2)	144 (2)	163 (2)	2 (1)	21 (1)	74 (2)
C(5)	5123 (2)	−241 (2)	−2171 (2)	162 (2)	216 (3)	109 (2)	76 (2)	42 (1)	54 (2)
	9584 (2)	8787 (2)	2336 (2)	128 (2)	166 (2)	153 (2)	43 (2)	58 (1)	70 (2)
C(6)	4854 (2)	903 (2)	−1222 (1)	129 (2)	145 (2)	113 (1)	33 (1)	34 (1)	50 (1)
	8378 (2)	7776 (2)	2358 (1)	129 (2)	116 (2)	123 (2)	33 (1)	36 (1)	30 (1)
N(7)	1625 (1)	−605 (1)	−286 (1)	108 (1)	121 (1)	157 (2)	−4 (1)	15 (1)	33 (1)
	6748 (1)	9710 (1)	4893 (1)	134 (2)	120 (1)	121 (1)	25 (1)	34 (1)	6 (1)

(*b*) Hydrogen atom parameters (× 10³)

(i) Barbital molecule

	x	*y*	*z*	*B* (Å²)
H(1)	359 (2)	258 (2)	64 (2)	5·6 (4)
H(3)	564 (2)	654 (2)	279 (2)	4·6 (3)
H(71)	30 (2)	482 (2)	193 (2)	5·7 (4)
H(72)	109 (2)	645 (2)	290 (2)	6·2 (4)
H(81)	93 (2)	637 (2)	64 (2)	6·6 (4)
H(82)	195 (3)	523 (3)	34 (2)	9·4 (6)
H(83)	246 (3)	681 (3)	129 (2)	9·3 (6)
H(91)	88 (2)	400 (2)	375 (2)	5·4 (4)
H(92)	169 (2)	555 (2)	464 (2)	5·3 (4)
H(101)	243 (3)	389 (3)	536 (3)	9·6 (7)
H(102)	300 (2)	312 (3)	403 (2)	7·5 (6)
H(103)	379 (3)	477 (3)	494 (2)	7·8 (6)

(ii) 2-Aminopyridine (molecule *A*, above; molecule *B*, below)

	x	*y*	*z*	*B* (Å²)
H(3)	229 (2)	−270 (2)	−210 (2)	7·5 (5)
	898 (2)	1156 (2)	466 (2)	6·8 (5)
H(4)	425 (2)	−250 (2)	−321 (2)	7·2 (5)
	1074 (2)	1096 (2)	323 (2)	7·3 (5)
H(5)	599 (2)	−7 (2)	−256 (2)	7·7 (5)
	1021 (2)	854 (2)	173 (2)	7·0 (5)
H(6)	552 (2)	191 (2)	−90 (2)	6·2 (4)
	814 (2)	673 (2)	179 (2)	6·1 (4)
H(71)	97 (2)	−128 (2)	−64 (2)	6·6 (5)
	595 (2)	908 (2)	471 (2)	6·0 (4)
H(72)	143 (2)	27 (2)	19 (2)	5·6 (4)
	672 (2)	1060 (2)	522 (2)	5·8 (4)

UM00013840
NOVARTIS EXHIBIT 1017
Novartis v. Regents, IPR2023-01346
Page 2586 of 4460

bond lengths and angles in molecules *A* and *B* (Fig. 1). In each molecule, the pyridine ring atoms are coplanar, with root-mean-square atomic displacements from the best least-squares planes of 0·003 and 0·004 Å respectively. However, in molecules *A* and *B* the amino nitrogen atoms are distant (0·06 and 0·07 Å) from the pyridine ring planes on one side, and the amino hydrogen atoms are distant (0·18, 0·15 Å and 0·12, 0·22 Å) from these planes on the opposite side. The sums of the bond angles at the amino nitrogen atoms are 349·3° and 347·6°. The differences from 360° (10·7° and 12·4°) are possibly significant in terms of their e.s.d.'s (2·9° and 3·0°). Thus, the bonds at the amino nitrogen atom in both molecules appear to be pyramidal rather than coplanar. The hydrogen atoms all form more nearly collinear N–H···O hydrogen bonds (NHO angles 157, 171, 175 and 168°) than would be the case if the covalent bonds at the nitrogen atoms were coplanar.

(iii) *The molecular association*

Barbital molecules hydrogen bond exclusively with 2-aminopyridine and *vice versa*, forming ribbons as shown in Fig. 2. All hydrogen atoms capable of hydrogen bonding are, in fact, hydrogen bonded. Hydrogen atoms at C(6) of each 2-aminopyridine molecule are at H···O van der Waals distances (2·65, 2·68 Å) from the same barbital O(2) atom. These interactions are not hydrogen bonds. In addition to the crystallographic centers of symmetry in Fig. 2, there are pseudomirror planes which pass through atoms C(2), C(5) and the ethyl groups of each barbital molecule. The pyridine ring planes of molecules *A* and *B* are nearly parallel (dihedral angle, 2·5°). Both rings are tilted (13·2°, 14·2°) with respect to the plane of the barbital pyrimidine ring. The hydrogen bonded ribbons are stacked so that 2-aminopyridine molecules overlap each other (Fig. 3). Stacking also results in an association of antiparallel barbital C(2)=O(2) carbonyl groups, with C(2)···O(2) distances of 3·40 Å.

The barbital NH groups are both donors in hydrogen bonds with pyridine nitrogen acceptor atoms. The N···N distances are 2·81 and 2·85 Å, the H···N distances are 1·91 and 1·97 Å and the NH···N angles are 176° and 174°. These are strong hydrogen bonds with short N···N distances like those in Watson–Crick hydrogen bonded adenine/uracil or adenine/barbiturate pairing. Hsu & Craven (1974) list N···N distances for eight such hydrogen bonds, ranging from 2·78 Å to 2·85 Å with a mean value of 2·81 Å.

The four NH···O=C hydrogen bonds in which 2-aminopyridine is donor and a barbital oxygen atom is acceptor are weak, with N···O distances, 3·14, 3·02, 3·13 and 3·03 Å. These distances are longer than the longest (2·98 Å) of the 48 distances listed by Gartland & Craven (1974) for NH···O=C hydrogen bonds in which barbiturate is both donor and acceptor. The N···O distances in the 2-aminopyridine–barbital complex are more like those found in barbiturate–

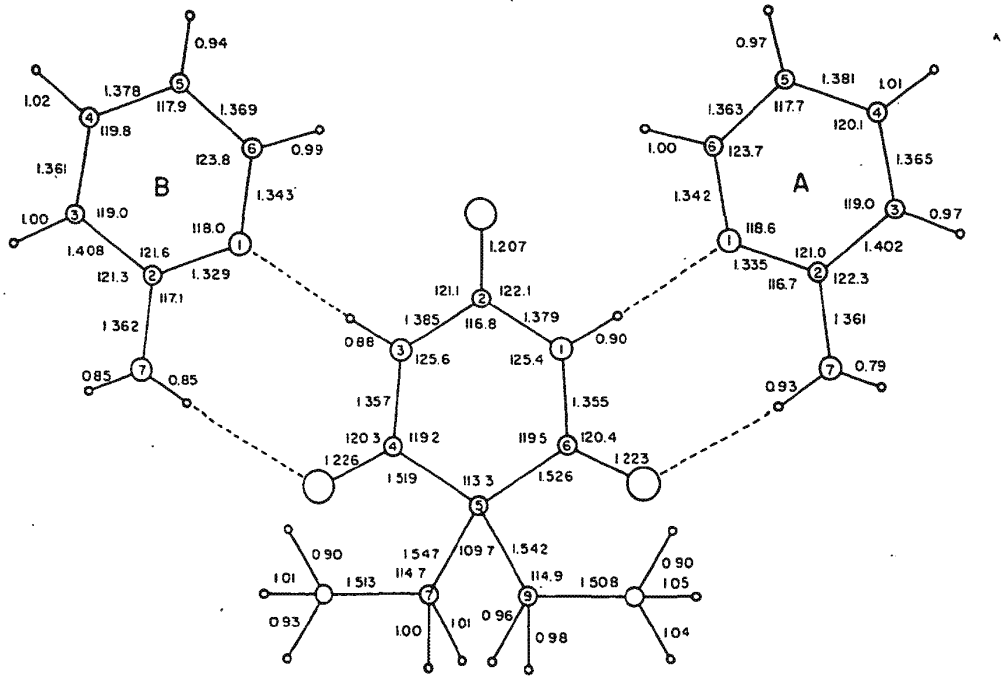


Fig. 1. Bond lengths and angles. The e.s.d.'s are 0·002 Å and 0·1° in bond lengths and angles which do not involve hydrogen atoms. The C–H and N–H bond lengths have e.s.d.'s of 0·02 Å.

UM00013841
NOVARTIS EXHIBIT 1017
Novartis v. Regents, IPR2023-01346
Page 2587 of 4460

adenine complexes. In these complexes, there are six NH···O=C hydrogen bonds in which adenine is donor and a barbiturate is acceptor. The N···O distances range from 2·97 to 3·39 Å, with a mean value of 3·21 Å. In the 1:1 complex of barbital with 9-ethyladenine, Voet (1972) attributes the long N···O distances (3·22 and 3·39 Å) to the constraint of crystal-packing forces which require molecules related by lattice translations to have the same orientation. However, this constraint does not apply to the 2-aminopyridine molecules *A* and *B* in the 2:1 complex with barbital. In this crystal structure, the vectors C(2) → NH_2 in non-symmetry-related 2-aminopyridine molecules (Fig. 2) make an angle of 14·8°. Thus, the long NH···O=C hydrogen bonds between 2-aminopyridine or adenine and barbital appear to be due, at least in part, to the rather low affinity for hydrogen bonding of the donor and acceptor groups which are involved.

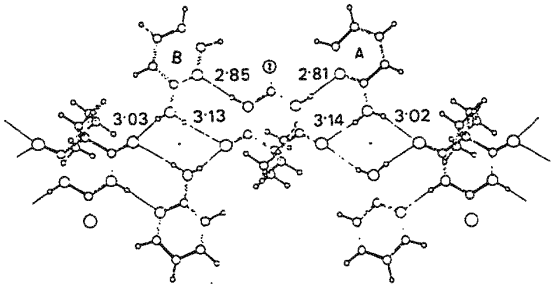


Fig. 2. The hydrogen bonding. Distances N···O and N···N are shown in Å.

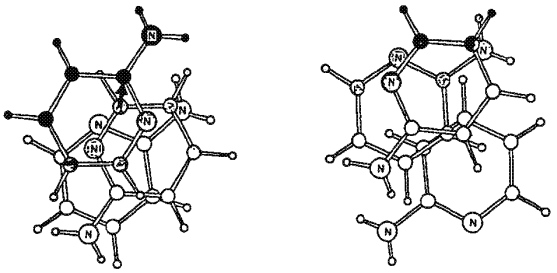


Fig. 3. The overlap of 2-aminopyridine molecules viewed normal to the plane of the central molecules *A* on the left and *B* on the right. The shortest interatomic distance between overlapping molecules (indicated by the arrow) is 3·46 Å.

In the crystal structures of the complexes of barbital with adenine, with 2-aminopyridine and with imidazole (Hsu & Craven, 1974), there is a recurrent pattern of short NH···N and long NH···O=C hydrogen bonds, both in the Watson–Crick and Hoogsteen configurations. A single NH···N hydrogen bond does not confer specificity upon the overall molecular interaction. However, this hydrogen bond appears to be important for the strong association of adenine or its analogs with barbiturate derivatives.

This work was supported by Grant No. NS-02763 of the U. S. Public Health Service, National Institutes of Health. We thank Prof. R. Shiono for the use of computer programs.

References

CRAVEN, B. M., CUSATIS, C., GARTLAND, G. L. & VIZZINI, E. A. (1973). *J. Mol. Struct.* **16**, 331–342.

CRAVEN, B. M., VIZZINI, E. A. & RODRIGUES, M. M. (1969). *Acta Cryst.* B**25**, 1978–1993.

CROMER, D. T. & WABER, J. T. (1965). *Acta Cryst.* **18**, 104–109.

GARTLAND, G. L. & CRAVEN, B. M. (1974). *Acta Cryst.* B**30**, 980–987.

GERMAIN, G., MAIN, P. & WOOLFSON, M. M. (1971). *Acta Cryst.* A**27**, 368–376.

HSU, I-N. & CRAVEN, B. M. (1974). *Acta Cryst.* B**30**, 988–993.

KIM, S. H. & RICH, A. (1968). *Proc. Natl. Acad. Sci. U.S.* **60**, 402–408.

KYOGOKU, Y., LORD, R. D. & RICH, A. (1968). *Nature, Lond.* **218**, 69–72.

STEWART, R. F., DAVIDSON, E. R. & SIMPSON, W. T. (1965). *J. Chem. Phys.* **42**, 3175–3187.

VOET, D. (1972). *J. Amer. Chem. Soc.* **94**, 8213–8222.

VOET, D. & RICH, A. (1972). *J. Amer. Chem. Soc.* **94**, 5888–5891.

UM00013842
NOVARTIS EXHIBIT 1017
Novartis v. Regents, IPR2023-01346
Page 2588 of 4460

Acta Cryst. (1974). B30, 998

The 1:1 Crystal Complex of *N*-Methyl-2-pyridone and 5,5-Diethylbarbituric Acid (Barbital)

BY I-NAN HSU AND B. M. CRAVEN

Department of Crystallography, University of Pittsburgh, Pittsburgh, Pennsylvania 15260, *U.S.A.*

(*Received* 19 *November* 1973; *accepted* 18 *December* 1973)

The 1:1 crystal complex of *N*-methyl-2-pyridone (C_6H_7NO) and 5,5-diethylbarbituric acid (barbital, $C_8H_{12}N_2O_3$), m.p. 90°C, is monoclinic, with space group $P2_1/c$ and $a=7{\cdot}257$ (2), $b=19{\cdot}339$ (2), $c=11{\cdot}127$ (2) Å, $\beta=105{\cdot}20$ (1)°. The structure determination, by direct methods, was based on 3094 integrated intensities measured on an automatic diffractometer with graphite monochromated Cu $K\alpha$ radiation. Refinement by a full-matrix least-squares procedure gave a final R value of 0·053. Both NH···O=C hydrogen bonds, with N···O distances 2·86 and 2·89 Å, involve the pyridone oxygen atom as acceptor so that the barbital oxygen atoms are not hydrogen bonded.

Experimental

Crystals of the 1:1 complex of *N*-methyl-2-pyridone and 5,5-diethylbarbituric acid (barbital) were obtained by slow cooling of an ethanolic solution which was slightly supersaturated with respect to both components. The crystal density (1·292 g cm^{-3}), which was determined by flotation in a mixture of carbon tetrachloride and cyclohexane, agrees with the calculated value (1·293 g cm^{-3}) assuming four molecules of each component in the unit cell. The lattice constants and X-ray intensity data were measured on a four-circle computer-controlled diffractometer using graphite-monochromated Cu $K\alpha$ radiation ($\lambda=1{\cdot}5418$ Å). The crystal, which had dimensions of $0{\cdot}37\times0{\cdot}36\times0{\cdot}15$ mm, was coated with lacquer and mounted with the longest dimension (the c axis) along the φ axis of the goniostat. Integrated intensities were measured for 3094 independent reflections in the range $\theta\leq75°$. Reflections were scanned in the $\theta/2\theta$ mode with a θ scan width of $(0{\cdot}6+0{\cdot}2\tan\theta)°$. There were 385 reflections for which the integrated intensity (I), was less than 2·0 $\sigma(I)$ as calculated from counting statistics. These reflections were assigned intensities of $\sigma(I)/2$. No corrections were applied for X-ray absorption or extinction.

The crystal structure was determined by direct methods (Germain, Main & Woolfson, 1971). Atomic parameters (Table 1) were refined by a full-matrix least-squares procedure. The function minimized was $\sum_H w_H\Delta_H^2$, where $\Delta_H=|F_H^o|-|F_H^c|$, and $w_H^{-1}=0{\cdot}1+0{\cdot}045|F_H|^2$. The atomic scattering factors were those of Cromer & Waber (1965) for carbon, nitrogen and oxygen, and Stewart, Davidson & Simpson (1965) for hydrogen. All hydrogen-atom positions were obtained from difference Fourier syntheses which were calculated after one cycle of refinement of anisotropic thermal parameters of the non-hydrogen atoms. Hydrogen-atom positional parameters were subsequently refined, but owing to computer limitations, hydrogen-atom temperature factors were fixed with values the same as those of the atoms to which they are covalently bonded. During the last cycles of refinement, six strong reflections for which $|F^c|>|F^o|$ and reflections with $I<2\sigma(I)$ were given zero weight.* The final R index† was 0·053 for all reflections and 0·045 for those with non-zero weight.

Discussion

(*a*) *Barbital*

The ring atoms are almost coplanar (Fig. 1) as found in a number of other crystal structures involving barbital (Craven, Cusatis, Gartland & Vizzini, 1973).

* The list of calculated and observed structure amplitudes has been deposited with the British Library Lending Division as Supplementary Publication No. SUP 30321 (20 pp., 1 microfiche). Copies may be obtained from the Executive Secretary, International Union of Crystallography, 13 White Friars, Chester CH1 1NZ, England.

† $R=\sum_H|\Delta_H|/\sum_H|F_H^o|$.

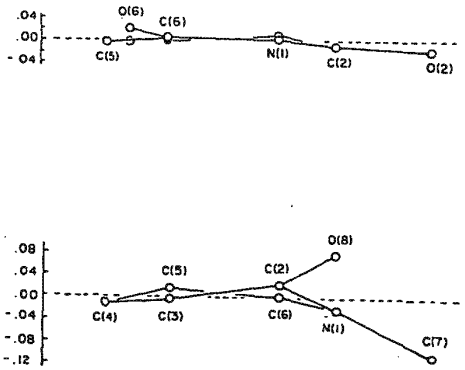


Fig. 1. The ring conformations of barbital (above) and *N*-methyl-2-pyridone (below). In each case, the dashed line is the trace of the best least-squares plane through the six ring atoms. The vertical scale (Å) is ten times the horizontal scale.

UM00013843
NOVARTIS EXHIBIT 1017
Novartis v. Regents, IPR2023-01346
Page 2589 of 4460

However, there is a slight displacement (0·02 Å) of atom C(2) from the plane of the other five ring atoms. The barbital ethyl groups and C(5) form a chain which is almost fully extended, with torsion angles C(7)–C(5)–C(9)–C(10) and C(8)–C(7)–C(5)–C(9) of −179·7° and 177·6° respectively, and e.s.d.'s of 0·14 Å. In other barbiturate crystal structures, slight differences in oxopyrimidine bond lengths and angles in the halves of the molecule on either side of C(2)···C(5) have been attributed to atom O(4) being hydrogen bonded while O(6) is not (Craven *et al.*, 1973). In the present complex, none of the barbital oxygen atoms are hydrogen bonded. Thus no significant bond length and angle differences of this kind are expected, and indeed none is observed (Fig. 2).

(*b*) *N-methyl-2-pyridone*

The molecule is almost planar (Fig. 1) but with a slight fold along C(2)···C(5), which increases the intramolecular distance (2·69 Å) of the carbonyl oxygen and *N*-methyl carbon atoms. There are significant differences among the C–C bond lengths. The alternating long and short bonds in the sequence C(2)–C(3)=C(4)–C(5)=C(6) are consistent with the formal single- and double-bond character of the expected principle valence-bond structure for the mole-

Table 1. *Atomic parameters and their e.s.d.'s*

Positional parameters are given as fractions of the unit cell translations ($\times 10^4$) for non-hydrogen atoms and ($\times 10^3$) for hydrogen atoms. Anisotropic thermal factors ($\times 10^5$) are given by the expression: $T=\exp[-\sum_i \sum_j (\beta_{ij}h_ih_j)]$. The e.s.d.'s are in brackets and refer to the least significant digit of the corresponding parameter.

(i) Barbital

(*a*) Non-hydrogen atom parameters

	x	*y*	*z*	β_{11}	β_{22}	β_{33}	β_{12}	β_{13}	β_{23}
N(1)	5990 (2)	2590 (1)	1160 (1)	1821 (25)	187 (3)	685 (10)	−115 (6)	230 (13)	32 (4)
N(3)	6179 (2)	1715 (1)	2637 (1)	1710 (23)	227 (3)	480 (9)	23 (6)	161 (11)	33 (4)
C(2)	6781 (2)	2356 (1)	2353 (1)	1544 (26)	218 (4)	638 (11)	−21 (7)	212 (13)	−40 (5)
C(4)	4838 (2)	1306 (1)	1872 (1)	1509 (24)	189 (3)	594 (10)	25 (7)	318 (13)	23 (4)
C(5)	3922 (2)	1559 (1)	556 (1)	1568 (25)	191 (3)	524 (10)	−74 (7)	199 (13)	6 (4)
C(6)	4641 (2)	2259 (1)	250 (1)	1482 (25)	188 (3)	574 (10)	20 (7)	242 (13)	31 (4)
C(7)	1750 (2)	1610 (1)	385 (2)	1465 (28)	362 (5)	835 (14)	−113 (9)	74 (16)	83 (7)
C(8)	1167 (3)	2096 (1)	1286 (2)	1921 (37)	487 (7)	1197 (20)	276 (13)	618 (22)	133 (10)
C(9)	4343 (3)	1026 (1)	−375 (2)	3265 (45)	219 (4)	726 (13)	−173 (10)	591 (19)	−83 (6)
C(10)	6442 (3)	926 (1)	−295 (2)	4043 (61)	243 (5)	1456 (24)	112 (13)	1601 (33)	−18 (8)
O(2)	7961 (2)	2687 (1)	3097 (1)	2392 (27)	325 (3)	819 (10)	−236 (7)	−14 (13)	−91 (5)
O(4)	4398 (2)	752 (1)	2235 (1)	2667 (28)	232 (3)	898 (11)	−113 (7)	322 (13)	134 (4)
O(6)	4051 (2)	2518 (1)	−771 (1)	2442 (25)	269 (3)	666 (9)	−30 (7)	107 (12)	130 (4)

(*b*) Hydrogen atom parameters

	x	*y*	*z*		*x*	*y*	*z*
H(1)	648 (2)	298 (1)	98 (1)	H(83)	185 (3)	257 (1)	138 (2)
H(3)	669 (2)	158 (1)	338 (2)	H(91)	371 (3)	120 (1)	−123 (2)
H(71)	126 (2)	111 (1)	51 (2)	H(92)	378 (3)	56 (1)	−22 (2)
H(72)	120 (2)	181 (1)	−43 (2)	H(101)	698 (3)	133 (1)	−50 (2)
H(81)	−21 (3)	219 (1)	101 (2)	H(102)	664 (3)	59 (1)	−83 (2)
H(82)	161 (3)	191 (1)	210 (2)	H(103)	717 (3)	77 (1)	64 (2)

(ii) *N*-Methyl-2-pyridone

(*a*) Non-hydrogen atom parameters

	x	*y*	*z*	β_{11}	β_{22}	β_{33}	β_{12}	β_{13}	β_{23}
N(1)	10145 (2)	4369 (1)	1378 (1)	1676 (24)	217 (3)	595 (9)	−50 (6)	185 (11)	4 (4)
C(2)	9448 (2)	3927 (1)	390 (1)	1711 (27)	178 (3)	591 (10)	−82 (7)	209 (13)	21 (4)
C(3)	10736 (2)	3767 (1)	−344 (2)	2364 (36)	241 (4)	880 (14)	−57 (9)	581 (18)	−72 (6)
C(4)	1250 (2)	4057 (1)	−107 (2)	2026 (34)	306 (5)	1143 (17)	79 (10)	695 (20)	60 (7)
C(5)	13097 (2)	4530 (1)	871 (2)	1603 (30)	294 (5)	1154 (17)	−107 (9)	250 (18)	74 (7)
C(6)	11911 (2)	4669 (1)	1593 (1)	1838 (30)	245 (4)	800 (13)	−142 (9)	6 (15)	3 (6)
C(7)	8945 (3)	4507 (1)	2224 (2)	2486 (41)	377 (6)	761 (14)	−79 (12)	518 (20)	−101 (7)
O(8)	7778 (2)	3699 (1)	192 (1)	1943 (23)	281 (3)	734 (9)	−245 (6)	274 (11)	1 (4)

(*b*) Hydrogen atom parameters

	x	*y*	*z*		*x*	*y*	*z*
H(3)	1030 (3)	342 (1)	−103 (2)	H(71)	793 (3)	473 (1)	178 (2)
H(4)	1335 (3)	394 (1)	−62 (2)	H(72)	852 (3)	405 (1)	255 (2)
H(5)	1428 (3)	477 (1)	106 (2)	H(73)	960 (3)	481 (1)	287 (2)
H(6)	1220 (2)	500 (1)	230 (2)				

UM00013844
NOVARTIS EXHIBIT 1017
Novartis v. Regents, IPR2023-01346
Page 2590 of 4460

cule. Similar C–C bond-length variations were also observed in the crystal structure of 2-pyridone (Penfold, 1953). The most notable differences in the two molecules are in the C(2)–N(1) and C(6)–N(1) bond lengths, which are nearly the same in *N*-methyl-2-pyridone (1·379, 1·370 Å; e.s.d., 0·002 Å), but are significantly different in 2-pyridone (1·401, 1·335 Å; e.s.d., 0·01 Å).

(c) The molecular association

The crystal structure contains hydrogen-bonded ribbons which run parallel to **c** (Fig. 3). The ribbons are packed together with no unusual features, such as short intermolecular distances. The hydrogen bonds N(1)H···O(8) and N(3)H···O(8) have N···O distances 2·86 and 2·89 Å, H···O distances 2·01 and 2·04 Å and NH···O angles 164 and 176°, respectively. There is also a short (3·03 Å) intraribbon N(3)···O(6) distance between barbital molecules. However, this is not a hydrogen bond because the corresponding H(3)···O(6) distance (2·92 Å) is long, even for a van der Waals interaction, and the N(3)H(3)···O(6) angle is 89°.

This structure determination is one of a series of crystal complexes of drug-active barbiturates with other amides such as urea (Gartland & Craven, 1974), acetamide (Hsu & Craven, 1974*a*) and salicylamide (Hsu & Craven, 1974*b*). The aim is to see whether the modes of NH···O=C hydrogen bonding and the hydrogen bonding N···O distances are suggestive of differences in the inherent hydrogen-bonding affinities of the various NH and O=C groups involved. Gartland & Craven (1974) have pointed out that the N···O distances in NH···O=C hydrogen bonds involving barbiturates tend to be short (2·75 to 2·82 Å) when barbiturate is donor and a non-barbiturate oxygen atom is acceptor. The N···O distances are of intermediate length (2·82 to 2·98 Å) when barbiturate is both donor and acceptor, and longer (2·95 to 3·39 Å) when barbiturate is acceptor and a non-barbiturate is donor. This pattern of N···O distances suggests that barbiturates are more effective as hydrogen-bonding donors than as acceptors.

The hydrogen bonds in the complex of barbital with *N*-methyl-2-pyridone have longer N···O distances than the others in which barbiturate is involved as donor. The range of such distances must thus be extended (2·75 to 2·89 Å) so as to overlap the range for hydrogen bonds in which barbiturates hydrogen bond with each other (2·82 to 2·98 Å).

It must be noted that both hydrogen bonds involve the 2-pyridone oxygen atom as acceptor, so that none of the three barbital oxygen atoms is hydrogen bonded. Similarly, in the complex of barbital with urea (Gartland & Craven, 1974) and acetamide (Hsu & Craven, 1974*a*), the barbital NH groups hydrogen bond only

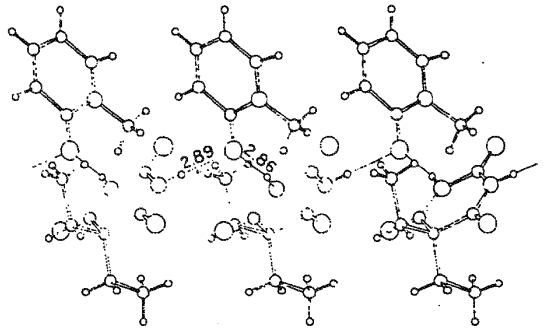


Fig. 3. A hydrogen-bonded ribbon in the projection down b. The hydrogen bond distances N···O are in Å.

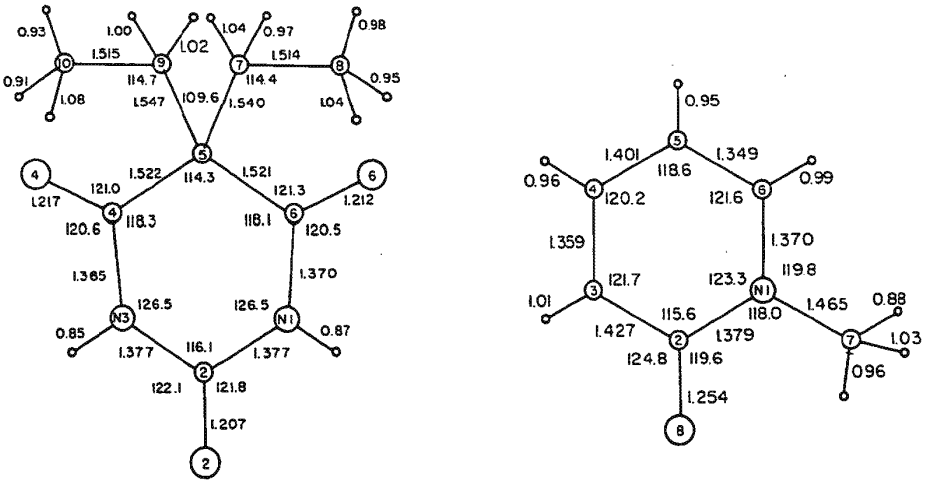


Fig. 2. Bond lengths and angles in barbital (left) and *N*-methyl-2-pyridone (right). The C–H and N–H bond lengths have e.s.d.'s of 0·02 Å. The e.s.d.'s are 0·002 Å in other bond lengths and 0·1° in bond angles.

UM00013845
NOVARTIS EXHIBIT 1017
Novartis v. Regents, IPR2023-01346
Page 2591 of 4460

with the urea or acetamide oxygen atoms. There are also weak hydrogen bonds involving the amide amino group as donor and barbital oxygen atoms as acceptor, but these have no counterpart in the *N*-methyl-2-pyridone complex because of *N*-methylation. Thus, the mode of hydrogen bonding in each of these complexes is consistent with the barbital oxygen atoms being relatively poor hydrogen-bonding acceptors.

This work was supported by Grant No. NS-02763 from the U. S. Publich Health Service, National Institutes of Health. We thank Dr R. Shiono for the use of computer programs.

References

CRAVEN, B. M., CUSATIS, C., GARTLAND, G. L. & VIZZINI, E. A. (1973). *J. Mol. Struct.* **16**, 331–342.

CROMER, D. T. & WABER, J. T. (1965). *Acta Cryst.* **18**, 104–109.

GARTLAND, G. L. & CRAVEN, B. M. (1974). *Acta Cryst.* B**30**, 980–987.

GERMAIN, G., MAIN, P. & WOOLFSON, M. M. (1971). *Acta Cryst.* A**27**, 368–376.

HSU, I. & CRAVEN, B. M. (1974*a*). *Acta Cryst.* B**30**, 974–979.

HSU, I. & CRAVEN, B. M. (1974*b*). *Acta Cryst.* B**30**, 843–846.

PENFOLD, B. R. (1953). *Acta Cryst.* **6**, 591–600.

STEWART, R. F., DAVIDSON, E. R. & SIMPSON, W. T. (1965). *J. Chem. Phys.* **43**, 3175–3187.

Acta Cryst. (1974). B**30**, 1001

The Crystal and Molecular Structure of Methyl 3,3,4-Trichloro-5-methoxyindolenine-2-carboxylate

BY E. HOUGH* AND D. ROGERS

Chemical Crystallography Laboratory, Imperial College, London SW7 2AY, England

(*Received* 8 *December* 1973; *accepted* 10 *December* 1973)

The structure of a trichlorinated intermediate in the synthesis of isatin compounds by a new pathway has been determined by X-ray crystallography. The compound crystallizes in the orthorhombic system with $a=22{\cdot}450$, $b=13{\cdot}292$, $c=8{\cdot}558$ Å, space group $Pna2_1$, and two molecules of $C_{11}H_8NO_3Cl_3$ in the asymmetric unit. The structure was solved by the symbolic addition method, the phases of the 150 strongest $|E|$'s being found close to 0 or π. This is probably due to the near centrosymmetric distribution of the chlorine atoms. The structure, based on 1297 diffractometer intensities, has been refined to $R=0{\cdot}036$.

Introduction

Recent investigations of the products and mechanism of attack by the positive chlorine ion (Cl^+) on indole-2-carboxylic acid (Hinman & Bauman, 1964; Foglio & Swern, 1968; Muchowski, 1970) have provided a novel route for the synthesis of substituted isatins. R. J. Bass of Pfizer (U.K.) Ltd., who aroused our interest in this matter, proposed a reaction sequence (Fig. 1) involving an unstable 'intermediate compound' [Fig. 1 (I)]. Later, Muchowski (1970) suggested that this intermediate consists rather of a sequence of reactions (Fig. 2) leading to the formation of a trichloro species [Fig. 2 (7)] which subsequently loses the elements of hydrogen chloride and carbon dioxide before tautomerizing to an oxindole [Fig. 2 (8)]. Attack by a further Cl^+ ion then yields the 3,3,4-trichloro-oxindole shown in Fig. 2 (2).

Bass found that treatment of the intermediate with diazomethane yielded a more stable and isolable com-

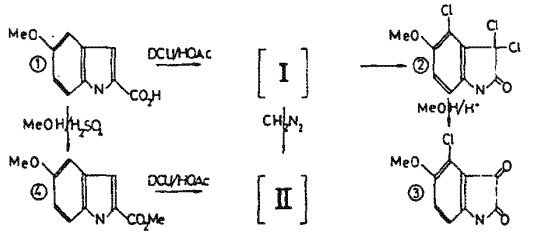


Fig. 1. Reaction sequence for synthesis of substituted isatins.

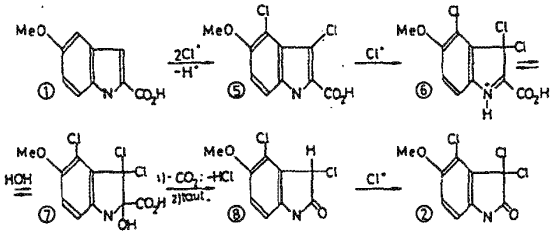


Fig. 2. Sequence of reactions comprising intermediate in Fig. 1 (I).

* Present address: Kjemisk institutt, Universitetet i Oslo, Postboks 1033, Blindern, Oslo 3, Norway.

UM00013846
NOVARTIS EXHIBIT 1017
Novartis v. Regents, IPR2023-01346
Page 2592 of 4460

Acta Cryst. (1974). B30, 843

The Crystalline Complex (1:1) of Salicylamide and 5-Ethyl-5-isoamylbarbituric Acid (Amobarbital)

BY I-NAN HSU AND B. M. CRAVEN

Department of Crystallography, University of Pittsburgh, Pittsburgh, Pennsylvania 15260, *U.S.A.*

(*Received* 12 *October* 1973; *accepted* 21 *November* 1973)

$[C_7H_7NO_2].[C_{11}H_{18}N_2O_3]$, m.p. 124°, is monoclinic, space group $P2_1/c$, with $a=13{\cdot}028$ (5), $b=12{\cdot}558$ (5), $c=12{\cdot}719$ (5) Å, $\beta=107{\cdot}60$ (1)°; $D_{meas}=1{\cdot}216$ g cm^{-3} and $D_{calc}=1{\cdot}217$ g cm^{-3} for $Z=4$. The crystal structure was determined by direct methods from 4089 integrated intensities measured with a computer-controlled four-circle diffractometer and graphite-monochromated Cu $K\alpha$ radiation. Refinement gave a final R index of 0·072. The crystal structure of the complex resembles the crystal structures of the components in many respects, including some apparent disorder in the isoamyl group of amobarbital, a strong O–H···O intramolecular hydrogen bond (2·49 Å) in salicylamide, and the nature of the intermolecular NH···O hydrogen bonding.

Introduction

The drug-active barbiturates form crystal complexes with a number of amides (Gartland & Craven, 1973). A comparison of the mode of hydrogen bonding in these complexes and in the crystal structures of the component molecules is of interest since it may suggest differences in the hydrogen-bonding affinity of the donor and acceptor groups involved.

Experimental

The 1:1 complex of salicylamide and amobarbital (Fig. 1) was first prepared by Kuroyanagi (1956). Our crystals were grown by cooling a solution consisting of ethanol and cyclohexane (5:1, v/v) supersaturated with respect to both salicylamide and amobarbital. Crystal data were measured on a computer-controlled four-circle diffractometer, using graphite-monochromated Cu $K\alpha$ radiation ($\lambda=1{\cdot}5418$ Å). The crystal, which measured approximately $0{\cdot}32\times0{\cdot}16\times0{\cdot}16$ mm was mounted with its long dimension (a) along the diffractometer φ axis. Integrated intensities for 4089 non-symmetry-related reflections were collected with the $\theta/2\theta$ scan method. There were 868 reflections with integrated intensity (I) less than $2\sigma(I)$. These were assigned intensities $I=\sigma(I)/2$.

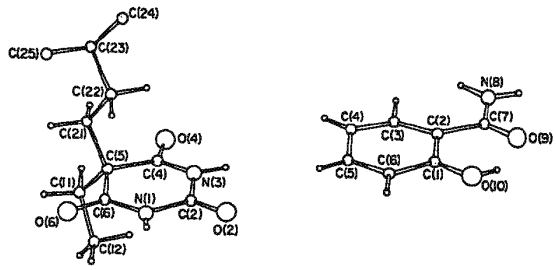


Fig. 1. Molecular structures and atomic nomenclature for 5-ethyl-5-isoamylbarbituric acid or amobarbital (left) and salicylamide (right).

The crystal structure was determined by direct methods with the computer-programmed procedure of Germain, Main & Woolfson (1971), applied to the 389 reflections with normalized structure factors $|E|\geq 1{\cdot}5$. A set of phases was obtained which correctly revealed all but three atoms when used to calculate an E synthesis.

Refinement of the atomic parameters (Table 1) was by least-squares methods, minimizing the function $\sum_h w\Delta^2$ where $\Delta=|F_{meas}|-|F_{calc}|$, and $w^{-1}=0{\cdot}54+0{\cdot}0017|F_{meas}|^2$. The atomic form factors which were used were those of Cromer & Waber (1965) for carbon, nitrogen and oxygen, and of Stewart, Davidson & Simpson (1965) for hydrogen. Because of computer limitations, parameters were refined alternately in two blocks. The first block consisted of all 235 non-hydrogen atom parameters. The second block consisted of 208 parameters for the hydrogen atoms together with parameters of heavier atoms to which they are bonded. The latter parameters were included so as to have overlapping of the two blocks. The refinement was terminated when the largest change in a non-hydrogen atom positional parameter was $0{\cdot}5\sigma$. In the final cycles, reflections with $I<2\sigma(I)$ and 15 low-angle reflections for which $|F_{calc}|$ was significantly less than $|F_{meas}|$, were assigned zero weight. The final R values* were 0·072 for all reflections and 0·055 for reflections with non-zero weight.†

* $R=(\sum_h|\Delta|/\sum_h|F_{meas}|)$.

† The table of observed and calculated structure amplitudes has been deposited with the British Library Lending Division as Supplementary Publication No. SUP 30291 (25 pp., 1 microfiche). Copies may be obtained through the Executive Secretary, International Union of Crystallography, 13 White Friars, Chester CH1 1NZ, England.

UM00013847
NOVARTIS EXHIBIT 1017
Novartis v. Regents, IPR2023-01346
Page 2593 of 4460

As was observed in the crystal structure determinations of amobarbital I and amobarbital II [see Fig. 2 in Craven & Vizzini (1969)] the calculated electron density peaks are diffuse for the terminal atoms C(23), C(24), and C(25) of the isoamyl group. The largest principal values for the r.m.s. amplitudes of thermal vibration of these atoms is 0·59 Å for C(25). In amobarbital I the corresponding value is 0·60 Å. In all three of these crystal structures, the hydrogen atoms bonded to C(23), C(24) and C(25) could not be found in electron density difference maps. However, in the final stages of the present refinement, a diffuse hydrogen-atom-like peak (0·5 e Å^{-3}) was observed at the expected tetrahedral bond angle, and at a distance of 1·4 Å from atom C(23). This peak may be the result of a partial conformational disordering with respect to rotation about the C(22)–C(23) bond. No attempt was made to incorporate such disordering into the assumed model of the crystal structure.

Discussion

The amobarbital bond lengths and angles (Fig. 2) and conformation agree well with those reported for the two crystalline forms of amobarbital itself (Craven & Vizzini, 1969). The geometry of the salicylamide molecule (Fig. 3) has been determined with greater accuracy

Table 1. *Atomic parameters*

Positional parameters are given as fractions of the lattice translations. Anisotropic temperature factors correspond to the expression $T=\exp[-(\beta_{11}h^2+\beta_{22}k^2+\beta_{33}k^2+2\beta_{12}hk+2\beta_{13}hl+2\beta_{23}kl)]$, and isotropic temperature factors to the expression $\exp(-B\sin^2\theta/\lambda^2)$. E.s.d.'s given in parentheses refer to the least significant figures in parameter values. Atom labels are consistent with those of Craven & Vizzini (1969) and Sasada *et al.* (1964).

(*a*) Carbon, nitrogen and oxygen atom parameters (× 10^4)

(i) Amobarbital

	x	*y*	*z*	β_{11}	β_{22}	β_{33}	β_{12}	β_{13}	β_{23}
N(1)	−314 (1)	1597 (1)	2058 (1)	53 (1)	92 (1)	87 (1)	−18 (1)	38 (1)	−31 (1)
C(2)	−211 (1)	1038 (2)	1175 (2)	48 (1)	72 (1)	67 (1)	−5 (1)	22 (1)	−13 (1)
O(2)	−917 (1)	454 (1)	634 (1)	55 (1)	95 (1)	89 (1)	−17 (1)	24 (1)	35 (1)
N(3)	740 (1)	1179 (1)	934 (1)	53 (1)	84 (1)	66 (1)	−9 (1)	27 (1)	−22 (1)
C(4)	1583 (1)	1813 (2)	1493 (1)	49 (1)	69 (1)	65 (1)	−5 (1)	22 (1)	−8 (1)
O(4)	2378 (1)	1880 (1)	1189 (1)	54 (1)	101 (1)	87 (1)	−8 (1)	35 (1)	−16 (1)
C(5)	1508 (1)	2385 (2)	2515 (2)	52 (1)	80 (1)	73 (1)	−15 (1)	25 (1)	−23 (1)
C(6)	444 (2)	2229 (2)	2763 (2)	60 (1)	96 (2)	80 (2)	−16 (1)	34 (1)	−33 (1)
O(6)	262 (1)	2645 (2)	3541 (1)	89 (1)	166 (2)	118 (2)	−40 (1)	61 (1)	−80 (1)
C(11)	1647 (2)	3589 (2)	2369 (2)	86 (2)	78 (2)	113 (2)	−18 (1)	41 (2)	−25 (1)
C(12)	775 (3)	4069 (2)	1412 (3)	128 (3)	86 (2)	169 (3)	10 (2)	41 (2)	−2 (2)
C(21)	2415 (2)	1947 (2)	3510 (2)	65 (1)	112 (2)	70 (1)	−15 (1)	18 (1)	−17 (1)
C(22)	2361 (3)	730 (2)	3655 (2)	131 (3)	114 (2)	88 (2)	−12 (2)	12 (2)	−1 (2)
C(23)	3351 (3)	229 (3)	4478 (2)	161 (3)	135 (3)	101 (2)	42 (3)	34 (2)	8 (2)
C(24)	3215 (5)	−993 (4)	4429 (4)	401 (10)	112 (3)	167 (5)	37 (4)	21 (5)	9 (3)
C(25)	3501 (5)	581 (4)	5630 (3)	260 (6)	212 (5)	122 (3)	89 (5)	−15 (4)	−42 (3)

(ii) Salicylamide

C(1)	6972 (1)	1954 (2)	2681 (2)	50 (1)	70 (1)	78 (1)	−1 (1)	27 (1)	−9 (1)
C(2)	5852 (1)	1862 (1)	2208 (1)	48 (1)	59 (1)	69 (1)	−1 (1)	24 (1)	−5 (1)
C(3)	5195 (1)	2535 (2)	2593 (2)	56 (1)	80 (1)	91 (2)	8 (1)	25 (1)	−18 (1)
C(4)	5624 (2)	3280 (2)	3399 (2)	74 (2)	101 (2)	111 (2)	9 (1)	32 (1)	−43 (2)
C(5)	6730 (2)	3378 (2)	3830 (2)	80 (2)	101 (2)	105 (2)	−5 (1)	23 (2)	−45 (2)
C(6)	7402 (2)	2723 (2)	3478 (2)	58 (1)	98 (2)	93 (2)	−7 (1)	20 (1)	−30 (1)
C(7)	5428 (1)	1078 (1)	1314 (1)	49 (1)	57 (1)	69 (1)	−2 (1)	23 (1)	−3 (1)
N(8)	4381 (1)	1030 (1)	797 (1)	49 (1)	75 (1)	89 (1)	−1 (1)	20 (1)	−21 (1)
O(9)	6062 (1)	465 (1)	1040 (1)	54 (1)	75 (1)	95 (1)	2 (1)	25 (1)	−27 (1)
O(10)	7660 (1)	1303 (1)	2376 (1)	47 (1)	96 (1)	111 (1)	−4 (1)	29 (1)	−37 (1)

(*b*) Hydrogen atom positional parameters (× 10^3)

(i) Amorbarbital

	x	*y*	*z*	*B*(Å^2)
H(1)	−92 (1)	150 (2)	218 (2)	5·0 (5)
H(3)	89 (2)	80 (2)	39 (2)	5·7 (5)
H(111)	238 (2)	371 (2)	228 (2)	5·5 (5)
H(112)	173 (2)	397 (2)	307 (2)	6·5 (6)
H(121)	73 (3)	371 (3)	73 (3)	8·6 (9)
H(122)	14 (3)	393 (3)	153 (3)	9·4 (10)
H(123)	88 (3)	480 (3)	137 (3)	10·2 (10)
H(211)	309 (2)	212 (2)	339 (2)	5·2 (5)
H(212)	240 (2)	235 (2)	421 (2)	6·9 (6)
H(221)	224 (3)	33 (3)	295 (4)	10·7 (10)
H(222)	174 (3)	60 (3)	389 (3)	9·6 (10)

(ii) Salicylamide

	x	*y*	*z*	*B*(Å^2)
H(3)	440 (2)	247 (2)	229 (2)	4·0 (4)
H(4)	510 (2)	373 (2)	365 (2)	7·4 (7)
H(5)	701 (2)	391 (2)	446 (2)	5·8 (5)
H(6)	819 (2)	273 (2)	373 (2)	5·4 (5)
H(81)	417 (2)	52 (2)	30 (2)	5·3 (5)
H(82)	390 (2)	142 (2)	99 (2)	5·6 (6)
H(10)	725 (2)	91 (2)	186 (2)	7·0 (7)

UM00013848
NOVARTIS EXHIBIT 1017
Novartis v. Regents, IPR2023-01346
Page 2594 of 4460

than in the crystal structure of salicylamide itself (Sasada, Takano & Kakudo, 1964). The atoms of the benzene ring are coplanar within ±0·01 Å, with the amide carbon atom C(7) and the phenolic oxygen atom O(10) displaced 0·07 Å and 0·05 Å from the ring plane in opposite senses. There is a dihedral angle of 5·4° between the planes of the benzene ring and the amide group C(7), O(9), N(8). The internal hydrogen bond involving the phenolic group and the amide oxygen atom has an O···O distance (2·49 Å) shorter than the corresponding hydrogen bond in salicylic acid (2·62 Å, Sundaralingam & Jensen, 1965). The shorter O···O distance occurs together with a longer carbonyl bond length (1·253 *vs.* 1·234 Å) suggesting that the internal hydrogen bond in salicylamide is stronger because the carbonyl oxygen is more electronegative than in salicylic acid.

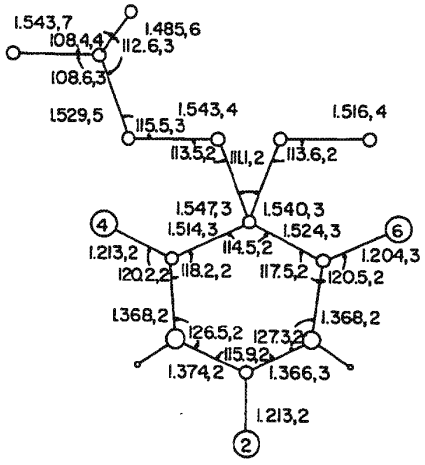


Fig. 2. Bond lengths (Å) and angles (°) with e.s.d.'s for amobarbital. Each parameter is separated from its e.s.d. by a comma. The e.s.d. refers to the least significant digit in the parameter.

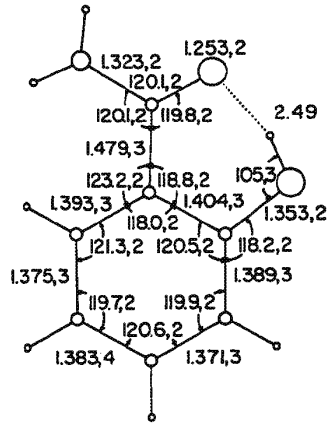


Fig. 3. Bond distances (Å) and angles (°) for salicylamide. Each parameter is separated from its e.s.d. by a comma. The e.s.d. refers to the least significant digit in the parameter.

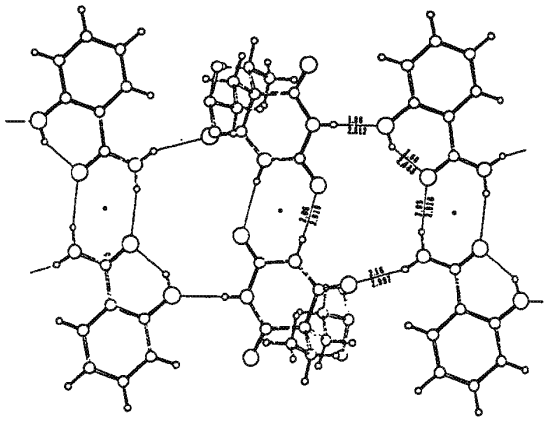


Fig. 4. Hydrogen bonding in the crystal structure. A single hydrogen-bonded chain is viewed normal to (110).

The crystal structure consists of hydrogen-bonded chains made up of alternating hydrogen-bonded dimers of amobarbital and salicylamide (Fig. 4). The planes of adjacent dimers are at an angle of 29°. The chains run parallel to a, which is the direction of fastest crystal growth, and are oriented parallel to (1 1 0) and (1$\bar{1}$0). The chains are packed so that in the view down a there are tunnels with minimum cross-sectional dimensions of about 6 × 7 Å, into which project the ethyl and isoamyl groups. The terminal isoamyl atoms are enclosed by four benzene rings. However, there are no short intermolecular distances, so that the arrangement is consistent with the observed large apparent amplitudes of thermal vibration, and possible conformational disorder of atoms C(24) and C(25).

Our principal aim in determining this crystal structure was to compare the hydrogen-bonding arrangements in the molecular complex with those in the crystal structures of the individual components. In the crystal structure of salicylamide (Sasada *et al.*, 1964), there are hydrogen-bonded chains similar to those of the complex (Fig. 4). The N···O hydrogen-bond distance between molecules of salicylamide within a dimer is 2·94 Å, which is very similar to the corresponding distance in the complex with amobarbital (2·92 Å). Both amobarbital I and II (Craven & Vizzini, 1969) contain hydrogen-bonded chains in which there can be recognized the same kind of amobarbital dimers as in the complex with salicylamide. The N···O distances (2·92, 2·92, 2·88 Å) in these dimers are also very similar to the corresponding distance in the complex (2·92 Å).

It is of interest to compare the inter-dimer NH···O hydrogen bonds, which occur between unlike molecules in the complex, and between like molecules in the crystal structures of the separate components. The N···O distance in $NH_{barb}\cdots O(10)_{sal}$ is shorter

UM00013849
NOVARTIS EXHIBIT 1017
Novartis v. Regents, IPR2023-01346
Page 2595 of 4460

(2·81 Å) than in the corresponding $NH_{sal}\cdots O(10)_{sal}$ (3·05 Å) hydrogen bond and the distance in $NH_{sal}\cdots O(4)_{barb}$ is longer (3·00 Å) than in the corresponding $NH_{barb}\cdots O(4)_{barb}$ hydrogen bonds (2·89, 2·91, 2·86 Å), in amobarbital I and II, and other hydrogen bonds of this type involving barbiturate as both donor and acceptor (Gartland & Craven, 1974). These distances are thus compatible with the conclusion that the barbiturates are more effective hydrogen-bonding donors than acceptors.

This work was supported by the U. S. Public Health Service, National Institutes of Health, Grant No. NS-02763. We thank Dr R. Shiono for the use of computer programs.

References

CRAVEN, B. M. & VIZZINI, E. A. (1969). *Acta Cryst.* B25, 1993–2009.
CROMER, D. T. & WABER, J. T. (1965). *Acta Cryst.* 18, 104–109.
GARTLAND, G. L. & CRAVEN, B. M. (1974). *Acta Cryst.* B 30. in the press.
GERMAIN, G., MAIN, P. & WOOLFSON, M. M. (1971). *Acta Cryst.* A27, 368–376.
KUROYANAGI, S. (1956). Japanese Patent, 897.
SASADA, Y., TAKANO, T. & KAKUDO, M. (1964). *Bull. Chem. Soc. Japan*, 37, 940–946.
STEWART, R. F., DAVIDSON, E. R. & SIMPSON, W. T. (1965). *J. Chem. Phys.* 42, 3175–3187.
SUNDARALINGAM, M. & JENSEN, L. H. (1965). *Acta Cryst.* 18, 1053–1058.

Acta Cryst. (1974). B30, 846

Lithium Nuclear-Magnetic-Resonance in Lithium Acetate Dihydrate, $Li(CH_3COO).2H_2O$

BY S. V. BHAT, A. C. PADMANABHAN AND R. SRINIVASAN
Department of Physics, Indian Institute of Science, Bangalore-12, India

(*Received* 19 *November* 1973; *accepted* 22 *November* 1973)

^{7}Li n.m.r. in single crystals of lithium acetate dihydrate is used to determine the quadrupole coupling parameters: (e^2qQ/h) and η. The orientations of the principal z, y and x components of the electric field gradient tensor are determined to be along the crystallographic b, a and c axes respectively. The parameters experimentally determined are $(e^2qQ/h) = 154{\cdot}6$ kHz; and $\eta = 0{\cdot}9$. This study indicates a tetrahedral configuration around the Li ion, confirming the recent X-ray and p.m.r. results.

Introduction

The interaction between the quadrupole moment of a nucleus and the gradient of the electric field at the nuclear site perturbs the nuclear magnetic transitions between the Zeeman levels. The electric field gradient (e.f.g.) at a site thus reflects the local structural symmetry. It is possible, therefore, to obtain information regarding structural details around the resonating nucleus from a study of the quadrupole splitting of the nuclear-magnetic-resonance lines. With this objective a study of ^{7}Li n.m.r. in $Li(CH_3COO).2H_2O$ is described.

Amirthalingam & Padmanabhan (1958) first studied the structure of $Li(CH_3COO).2H_2O$ and fixed the space group as *Cmm*2. Clark (1964) however, after a calculation of the various bond lengths, drew attention to certain inconsistencies, and Galigné, Mouvet & Falgueirettes (1970), after a redetermination of the structure, concluded that the space group is *Cmmm* rather than *Cmm*2 and further that the Li coordination is fourfold and not sixfold. The results of a proton-magnetic-resonance study in our laboratory by Padmanabhan & Srinivasan (1972) confirmed the results of Galigné *et al.* (1970) and indicated more probable locations for the water protons. It was therefore thought worth while to look at the structure of this crystal from the point of view of the quadrupolar interaction at the Li sites.

According to Galigné *et al.* (1970), $Li(CH_3COO).2H_2O$ crystals are orthorhombic with $Z=4$. Two mirror symmetry elements, one in the *ac* plane and a second in the *bc* plane, pass through the Li sites, thus fixing the directions of the principal components of the e.f.g. tensor along the three crystallographic axes. The four Li ions in the unit cell are identical from the point of view of e.f.g. because of the mirror in the *ab* plane and the screw axis along a. So the structure predicts a spectrum characteristic of a single nucleus in each of the crystallographic planes: a central signal and a pair of satellites. Our n.m.r. study confirms this prediction.

Experimental

Single crystals of sufficient size ($3 \times 2 \times 1{\cdot}5$ cm) were grown by slow evaporation of a saturated solution of AnalaR grade lithium acetate in distilled water, over calcium chloride in a desiccator. A Robinson oscillator working at 8·7 MHz was used with a 6 inch electromagnet. A magnetic field sweep calibrated by the ^{7}Li signal in

UM00013850
NOVARTIS EXHIBIT 1017
Novartis v. Regents, IPR2023-01346
Page 2596 of 4460

FINGER, L. (1972). Private communication.
GARRETT, B. S. (1954). Oak Ridge National Laboratory Report No. 1745, pp. 97–148.
GHOSE, S. (1962). *Acta Cryst.* **15**, 1105–1109.
GHOSE, S., LEO, S. R. & WAN, C. (1974). *Amer. Min.* In the press.
GRANGER, A. & DE SCHULTEN, A. (1904). *Bull. Soc. Minér. Fr.* **27**, 137–146.
IBERS, J. A. (1956). *Acta Cryst.* **9**, 225–231.
KEVE, E. T., ABRAHAMS, S. C. & BERNSTEIN, J. L. (1971). *J. Chem. Phys.* **54**, 2556–2563.
LARSON, A. C. & CROMER, D. T. (1961). *Acta Cryst.* **14**, 128–132.
MANOTTI LANFREDI, A. M., PELLINGHELLI, M. A., TIRIPICCHIO, A. & TIRIPICCHIO CAMELLINI, M. (1972). *Acta Cryst.* B**28**, 679–682.
MCGILLAVRY, C. H. & VAN ECK, C. L. P. (1943). *Rec. Trav. Chim. Pays-Bas*, **62**, 729.

Acta Cryst. (1974). B**30**, 974

The Crystal Structure of the 1:1 Complex of Acetamide with 5,5-Diethylbarbituric Acid (Barbital)

BY I-NAN HSU AND B. M. CRAVEN

Department of Crystallography, University of Pittsburgh, Pittsburgh, Pennsylvania 15260 *U.S.A.*

(*Received* 12 *October* 1973; *accepted* 10 *December* 1973)

The 1:1 complex of acetamide and barbital ($C_2H_5NO.C_8H_{12}N_2O_3$), m.p. 116°C, is orthorhombic with space group $P2_12_12_1$. Lattice translations are $a=10{\cdot}615$ (2), $b=10{\cdot}568$ (2), $c=11{\cdot}243$ (2) Å. The crystal density (1·283 g cm^{-3}) agrees with the calculated density (1·281 g cm^{-3}) for four molecules of each component in the unit cell. The crystal structure has been determined from 1500 integrated intensities measured on a computer-controlled diffractometer with nickel-filtered Cu $K\alpha$ radiation. The final R index is 0·044. The crystal structure is isomorphous with the urea/barbital complex. The acetamide complex has slight differences in barbital conformation as well as in the relative translations and orientations of the component molecules, but is similar in having two strong hydrogen bonds (N···O, 2·84 Å) in which barbital is donor and the oxygen of the second component (acetamide) is acceptor.

Introduction

This crystal structure determination is one of a series involving NH···O=C hydrogen bonded complexes of drug-active barbiturates with various other amides. The crystal structure of the 1:1 complex of 5,5-diethylbarbituric acid (barbital, Fig. 1) with acetamide is of interest because it is isomorphous with the corresponding urea complex (Gartland & Craven, 1974). Thus the acetamide methyl group which does not hydrogen bond, replaces a urea amino group which does hydrogen bond, with only minor perturbation of the crystal structure.

Experimental

Transparent, prismatic crystals of the complex were grown from a saturated solution of barbital and acetamide in a solvent mixture of propanol and cyclohexane (4:1). The crystal density was determined by flotation in a mixture of benzene and carbon tetrachloride. Intensity data and unit-cell dimensions were measured on a four-circle computer-controlled diffractometer (Enraf–Nonius CAD-4) using nickel-filtered Cu $K\alpha$ radiation ($\lambda=1{\cdot}5418$ Å). The crystal data for the isomorphous complexes of barbital with acetamide and urea are given in Table 1.

Table 1. *Crystal data for the isomorphous* (1:1) *complexes barbital/acetamide and barbital/urea*

	Barbital/acetamide (This work)	Barbital/urea (Gartland & Craven, 1974)
	$C_8H_{12}N_2O_3.C_2H_5NO$	$C_8H_{12}N_2O_3.CH_4N_2O$
	Orthorhombic, space group $P2_12_12_1$	
m.p.	116°C	146–150°C
a	10·615 (2) Å	10·302 (5) Å
b	10·568 (2)	10·181 (2)
c	11·243 (2)	11·627 (3)
V	1261·2 Å^3	1219·5 Å^3
D_{meas}	1·283 g cm^{-3}	1·320 g cm^{-3}
D_x	1·281	1·330

1500 independent reflections were measured in the range $\theta\leq 75°$. The crystal, which had dimensions 0·3 × 0·2 × 0·2 mm, was mounted so that there was an angle of 15° between the crystal axis a and the φ axis of the goniostat. Reflections were scanned in the ω–2θ mode at different rates to obtain a minimum net count of 5000 within a specified maximum scan time (90 s). The background counts were taken at each of the scan limits for ¼ of the scan time. The 2θ scan width in degrees was 1·2 + 0·4 tan θ. There were 86 reflections for which the integrated intensity (I) was less than $2\sigma(I)$ as calculated from the counting statistics. These

UM00013851
NOVARTIS EXHIBIT 1017
Novartis v. Regents, IPR2023-01346
Page 2597 of 4460

reflections were assigned intensities of $\sigma(I)/2$. No corrections were made for X-ray absorption or extinction.

In retrospect this crystal structure could have been determined most readily from its isomorphism with the barbital/urea complex (Gartland & Craven, 1974). However, at the time, this relationship was not appreciated, and the crystal structure was determined by direct methods with the *MULTAN* program of Germain, Main & Woolfson (1971).

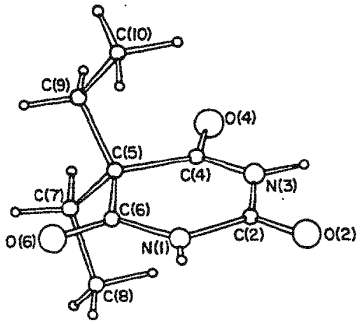


Fig. 1. Molecular structure of 5,5-diethylbarbituric acid (barbital).

Atomic parameters (Table 2) were refined by a full-matrix least-squares procedure. The function minimized was $\sum w_H \Delta_H^2$, where $\Delta_H = |F_H^{obs}| - |F_H^{calc}|$. The weights were assumed to be $w_H^{-1} = 0{\cdot}15 + 0{\cdot}002\,|F_H|^2$. The atomic scattering factors were those of Cromer & Waber (1965) for O, N, C, and of Stewart, Davidson & Simpson (1965) for H. All hydrogen atomic positions were obtained from a difference Fourier map which was calculated after refinement of anisotropic temperature factors had been applied for the non-hydrogen atoms. Hydrogen-atom positional and isotropic thermal parameters were subsequently refined. During the last three cycles of least-squares refinement, reflections with $I < 2\sigma(I)$ and 17 strong reflections for which $|F^{obs}| > |F^{calc}|$ were given zero weights. Refine-

Table 2. *Atomic parameters with e.s.d.'s*

Positional parameters are given as fractions of the lattice translations. Thermal parameters are given according to the expression: $T = \exp[-(\beta_{11}h^2 + \beta_{22}k^2 + \beta_{33}l^2 + 2\beta_{12}hk + 2\beta_{13}hl + 2\beta_{23}kl)]$, or $T = \exp[-B\sin^2\theta/\lambda^2]$, and U_k is the r.m.s. displacement (Å) along the kth principal axis of the thermal ellipsoid. The parameters are listed $\times 10^4$, except for hydrogen atoms positional parameters ($\times 10^3$) and U_k ($\times 10^2$).

(i) The barbital molecule

				B (Å^2) / β_{11}	β_{22}	β_{33}	β_{12}	β_{13}	β_{23}	U_1	U_2	U_3
	x	y	z									
N(1)	5757 (1)	4077 (1)	4916 (1)	88 (1)	59 (1)	55 (1)	−1 (1)	21 (1)	−2 (1)	17	18	24
H(1)	524 (2)	398 (3)	557 (2)	4·8 (5)								
C(2)	6551 (2)	3097 (2)	4653 (1)	106 (2)	54 (1)	55 (1)	6 (1)	11 (1)	1 (1)	17	18	25
O(2)	6584 (2)	2136 (1)	5245 (1)	200 (2)	73 (1)	88 (1)	26 (1)	43 (1)	30 (1)	17	23	36
N(3)	7313 (2)	3246 (1)	3677 (1)	94 (1)	57 (1)	57 (1)	18 (1)	17 (1)	2 (1)	16	18	25
H(3)	777 (2)	258 (2)	350 (3)	3·5 (4)								
C(4)	7318 (1)	4266 (2)	2920 (1)	61 (1)	64 (1)	46 (1)	−4 (1)	−2 (1)	−3 (1)	17	18	19
O(4)	7986 (1)	4259 (1)	2043 (1)	87 (1)	98 (1)	59 (1)	1 (1)	20 (1)	1 (1)	17	23	24
C(5)	6499 (1)	5390 (1)	3223 (1)	69 (1)	49 (1)	52 (1)	−3 (1)	−2 (1)	3 (1)	16	18	20
C(6)	5726 (2)	5230 (2)	4358 (1)	67 (1)	54 (1)	57 (1)	3 (1)	2 (1)	−7 (1)	17	20	20
O(6)	5071 (1)	6070 (1)	4744 (1)	103 (1)	78 (1)	96 (1)	28 (1)	19 (1)	−11 (1)	17	25	27
C(7)	5567 (2)	5634 (2)	2190 (2)	93 (2)	80 (2)	66 (1)	6 (1)	−17 (1)	4 (1)	19	22	24
H(71)	513 (2)	643 (2)	242 (2)	3·8 (4)								
H(72)	605 (2)	575 (2)	149 (2)	4·1 (5)								
C(8)	4677 (2)	4548 (2)	1930 (2)	89 (2)	127 (3)	88 (2)	−6 (2)	−22 (2)	−20 (2)	19	25	28
H(81)	417 (3)	432 (3)	263 (3)	5·5 (6)								
H(82)	511 (3)	378 (3)	168 (2)	5·6 (6)								
H(83)	414 (3)	473 (3)	127 (3)	6·5 (7)								
C(9)	7377 (2)	6550 (2)	3377 (2)	99 (2)	60 (1)	73 (1)	−21 (1)	−0 (1)	3 (1)	17	22	25
H(91)	690 (2)	736 (2)	349 (2)	4·2 (5)								
H(92)	777 (2)	672 (2)	256 (2)	4·0 (5)								
C(10)	8359 (2)	6385 (2)	4343 (2)	89 (2)	100 (2)	80 (2)	−28 (2)	−4 (1)	−19 (1)	18	23	27
H(101)	787 (3)	625 (3)	514 (3)	5·7 (6)								
H(102)	900 (3)	554 (3)	419 (3)	6·5 (7)								
H(103)	889 (3)	719 (4)	437 (3)	8·4 (9)								

(ii) The acetamide molecule

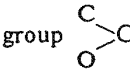
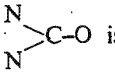
C(1)	3793 (1)	4477 (2)	7644 (1)	62 (1)	77 (2)	57 (1)	−10 (1)	3 (1)	−10 (1)	18	19	22
O(1)	4048 (1)	3721 (1)	6832 (1)	122 (1)	88 (1)	74 (1)	−42 (1)	35 (1)	−29 (1)	18	19	32
N(2)	4191 (2)	5659 (2)	7620 (2)	104 (2)	69 (1)	88 (1)	−11 (1)	22 (1)	−17 (1)	19	21	27
H(21)	477 (3)	591 (3)	707 (3)	6·1 (7)								
H(22)	414 (2)	616 (3)	821 (2)	4·7 (5)								
C(3)	3041 (2)	4058 (2)	8699 (2)	102 (2)	103 (2)	67 (1)	−17 (2)	22 (1)	−11 (2)	19	22	27
H(31)	283 (3)	478 (3)	921 (3)	5·7 (6)								
H(32)	227 (3)	365 (3)	843 (2)	5·6 (6)								
H(33)	339 (3)	337 (4)	911 (3)	7·3 (9)								

UM00013852
NOVARTIS EXHIBIT 1017
Novartis v. Regents, IPR2023-01346
Page 2598 of 4460

ment was concluded when all parameter changes were less than $\sigma/3$. The final overall R index* is 0·044.†

The molecular structures

(i) *Barbital*

The oxopyrimidine ring is almost planar with C(5) and the ethyl carbon atoms forming the spine of a hydrocarbon chain which extends perpendicular to the ring. The slight ring puckerings, which occur in the barbital rings in both the acetamide and the urea complexes are shown in Fig. 2. In the acetamide complex the ring is skewed with respect to a twist about the C(2)···C(5) axis. In the urea complex, this feature is coupled with a displacement of atom C(5) from the mean plane of the remaining ring atoms. In both molecules, each four-atom group  and  is nearly planar. These puckering modes have both been noted in other barbiturate crystal structures (Craven, Cusatis, Gartland & Vizzini, 1973). Their occurrence presumably depends on the nature of the barbiturate molecular environment in the crystal structure. It is interesting that this conformational difference is now found to occur in a pair of isomorphous crystal structures as a result of substituting acetamide for urea.

Torsion angles C(8)–C(7)–C(5)–C(9) and C(10)–C(9)–C(5)–C(7) are 178·5 and 182·1°, corresponding to small twists of the hydrocarbon chain from the fully extended conformation. In the urea complex, these angles are 184·6 and 180·9° respectively, the greater difference being a twist of 5·9° about the C(5)–C(7) bond.

The bond lengths and angles in the oxopyrimidine ring (Table 3) are in excellent agreement with those reported for the urea complex. There is a small but significant difference (1·5°) in the bond angle C(6)–C(5)–C(7) which may be associated with the conformational differences in the two barbital molecules.

(ii) *Acetamide*

The carbon, oxygen and nitrogen atoms are nearly coplanar, with the central carbon atom C(1) only 0·008 Å from the plane through the other atoms. There appears to be a rotation of the methyl group about the C–CH_3 bond of about 5° from the configuration in which hydrogen atom H(31) is *anti* with respect to the carbonyl oxygen atom. The amide hydrogen atoms are displaced (0·13, 0·16 Å; e.s.d. 0·03 Å) from the molecular plane on the opposite side from H(31), so that the bonds at the amide nitrogen atom are possibly significantly non-coplanar.

The bond lengths and angles (Table 3) agree with those reported in the two crystal forms of acetamide itself [rhombohedral, Senti & Harker (1940) and Denne & Small (1971); orthorhombic, Hamilton (1965)] although in the latter structure determinations, the e.s.d.'s are greater (0·05, 0·005 and 0·016 Å respectively in bond lengths).*

Table 3. *Bond lengths and angles for barbital and acetamide*

These values have not been corrected for the effects of anisotropic thermal motion. The e.s.d.'s are given in parentheses and refer to the least significant digit of the parameter. The C–H bond lengths in both barbital and acetamide range from 0·94 to 1·13 Å. The H–C–H and C–C–H bond angles range from 98 to 114°.

(*a*) Bond lengths (Å)

(*i*) Barbital		C(7)–C(8)	1·514 (3)
C(6)–N(1)	1·370 (2)	C(9)–C(10)	1·516 (3)
N(1)–C(2)	1·367 (2)	N(1)–H(1)	0·92 (3)
C(2)–N(3)	1·372 (2)	N(3)–H(3)	0·88 (2)
N(3)–C(4)	1·373 (2)		
C(6)–O(6)	1·208 (2)	(*ii*) Acetamide	
C(2)–O(2)	1·214 (2)	C(1)–O(1)	1·242 (2)
C(4)–O(4)	1·213 (2)	C(1)–N(2)	1·318 (2)
C(5)–C(4)	1·511 (2)	C(1)–C(3)	1·497 (3)
C(5)–C(6)	1·525 (2)	N(2)–H(21)	0·91 (3)
C(5)–C(7)	1·547 (3)	N(2)–H(22)	0·85 (3)
C(5)–C(9)	1·549 (2)		

(*b*) Bond angles (°)

(*i*) Barbital		C(6)—C(5)–C(7)	107·6 (1)
N(1)–C(2)–O(2)	122·2 (2)	C(7)—C(5)–C(9)	109·6 (1)
N(1)–C(2)–N(3)	116·7 (2)	C(5)—C(7)–C(8)	114·6 (2)
N(3)–C(2)–O(2)	121·1 (2)	C(5)—C(9)–C(10)	113·7 (2)
C(2)–N(3)–C(4)	126·0 (1)	C(6)—N(1)–H(1)	117 (2)
N(3)–C(4)–O(4)	120·1 (1)	C(2)—N(1)–H(1)	117 (2)
N(3)–C(4)–C(5)	118·3 (1)	C(4)—N(3)–H(3)	119 (1)
C(5)–C(4)–O(4)	121·6 (1)	C(2)—N(3)–H(3)	114 (1)
C(4)–C(5)–C(6)	114·3 (1)		
C(5)–C(6)–O(6)	121·9 (1)	(*ii*) Acetamide	
C(5)–C(6)–N(1)	117·9 (1)	N(2)—C(1)–O(1)	121·6 (2)
N(1)–C(6)–O(6)	120·1 (2)	O(1)—C(1)–C(3)	120·5 (2)
C(6)–N(1)–C(2)	126·1 (1)	C(3)—C(1)–N(2)	117·9 (2)
C(4)–C(5)–C(7)	109·3 (1)	C(1)—N(2)–H(21)	120 (2)
C(4)–C(5)–C(9)	107·5 (1)	C(1)—N(2)–H(22)	124 (2)
C(6)–C(5)–C(9)	108·5 (1)	H(21)–N(2)–H(22)	113 (3)

Differences between the isomorphous complexes

There are both intra- and intermolecular differences between the isomorphous complexes of acetamide and urea with barbital. The intramolecular differences consist of the obvious difference between acetamide and urea, and the small conformational differences in the barbital molecule which have already been described. The intermolecular differences will be de-

* $R=\sum_H|\Delta_H|/\sum_H|F_H^{obs}|$.

† A list of structure amplitudes has been deposited with the British Library Lending Division as Supplementary Publication No. SUP 30318 (10 pp., 1 microfiche). Copies may be obtained through the Executive Secretary, International Union of Crystallography, 13 White Friars, Chester CH1 1NZ, England.

* The present results should be compared with those of Denne & Small (1971) before correction for molecular librations.

UM00013853
NOVARTIS EXHIBIT 1017
Novartis v. Regents, IPR2023-01346
Page 2599 of 4460

scribed in terms of the relative translations and orientations of the two components in each complex.

The atoms which are close to the center of mass of each component are C(5) in barbital and the carbonyl carbon of acetamide and urea. The C(5)···C distance between these atoms (Table 1) is almost the same in both complexes (5·82 and 5·84 Å). However, the components of the C → C(5) intermolecular vector differ by 0·25 Å, 0·31 Å and 0·21 Å along the crystal axes x, y and z respectively, corresponding to a relative translation of 0·45 Å between these atoms in the two complexes.

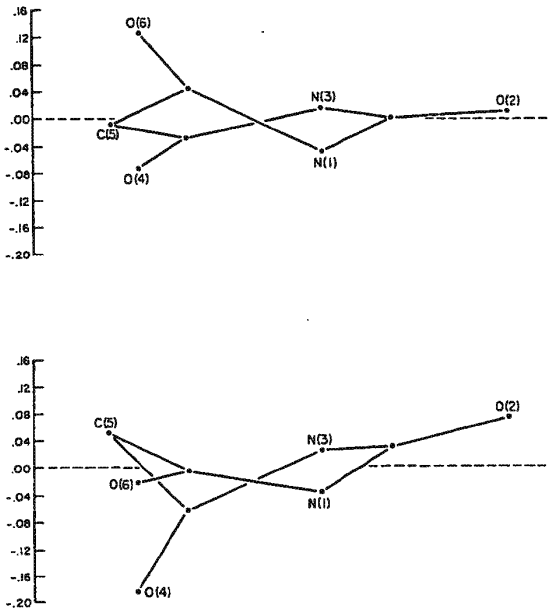


Fig. 2. Conformations of the barbiturate trioxopyrimidine ring in the complex with acetamide (above) and urea (below). The dashed lines are the traces of the best least-squares plane through the six ring atoms. The vertical scale (Å) is seven times that of the horizontal.

Molecular orientations are given in Table 4 in terms of the direction cosines of the normals to the molecular planes with respect to crystal axes, and the direction cosines of a selected C=O bond which lies in each of these molecular planes. In each case, the molecules chosen are those for which atomic parameters are given [see Table 1 in this paper, and in Gartland & Craven (1974)]. These molecules are shown as the central acetamide (or urea) and the barbital at the bottom right in Fig. 3. The angle between the plane normals of the barbiturate ring and acetamide in one complex is different by only 1·4° from the angle between the plane normals of the barbiturate ring and urea in the other. Similarly the angle between the directions of the C(2)=O(2) barbital bond and the carbonyl bond in acetamide differ by only 2·3° from the corresponding angle in the urea complex. The greatest differences in molecular orientation in the two complexes are in the normals to the barbiturate rings (5·9°) and the direction of the barbital C(2)=O(2) carbonyl group (7·1°). It is noteworthy that these differences in intramolecular and intermolecular configuration have little effect on the N···O distances in corresponding NH···O=C hydrogen bonds in the two complexes.

The hydrogen bonding

The important molecular interactions in this crystal structure are the NH···O=C hydrogen bonds (Table 5). Both NH groups from barbital are hydrogen

Table 4. *Molecular orientations in the isomorphous complexes of barbital with acetamide and urea*

Molecular orientations are expressed as best least-squares planes, $Lx+My+Nz=D$, or as directions (L,M,N) where L,M,N are direction cosines with respect to the crystal axes, and D is in Å. The appropriate angle is listed underneath each direction cosine.

	Barbital/acetamide				Barbital/urea			
	L	*M*	*N*	*D*	*L*	*M*	*N*	*D*
(1)	0·7295	0·3858	0·5648	9·2874	0·7524	0·4464	0·4843	9·0873
	43·2°	67·3°	55·6°		41·2°	63·5°	61·0°	
(2)	0·8398	−0·2670	0·4726	6·1860	0·8244	−0·2407	0·5123	6·6990
	32·9°	105·5°	61·8°		34·5°	103·9°	59·2°	
(3)	0·0292	−0·8364	0·5481	-	0·0984	−0·7692	0·6316	-
	88·3°	146·8°	56·8°		84·4°	140·3°	50·8°	
(4)	0·2175	−0·6428	−0·7351	-	0·2345	−0·6755	−0·6997	-
	77·4°	130·0°	137·3°		76·4°	132·5°	134·4°	

(1) Plane of pyrimidine ring
(2) Plane of acetamide or urea
(3) Direction cosines for barbital C(2)=O(2) bond
(4) Direction cosines for acetamide or urea C=O bond

Angles between plane normals, or between bond directions. Subscripts a and u refer to the acetamide and urea complexes respectively.

$(1)_a \wedge (2)_a$	39·1°	$(1)_a \wedge (1)_u$	5·9°
$(1)_u \wedge (2)_u$	40·5	$(2)_a \wedge (2)_u$	2·9
$(3)_a \wedge (4)_a$	81·9	$(3)_a \wedge (3)_u$	7·1
$(3)_u \wedge (4)_u$	84·2	$(4)_a \wedge (4)_u$	1·8

UM00013854
NOVARTIS EXHIBIT 1017
Novartis v. Regents, IPR2023-01346
Page 2600 of 4460

bonded to the acetamide oxygen atom, with N···O distances (2·84 Å) slightly longer than the corresponding distances (2·80 and 2·78 Å) in the barbital/urea complex. Only one of the acetamide amide hydrogen atoms H(22), forms a normal hydrogen bond, and this is with the barbital O(2) atom. The N···O distance is rather long (2·98 Å). The remaining amide hydrogen atom appears (Fig. 3) as if it might be hydrogen bonded to a barbital O(4) atom, with N···O distance 3·07 Å. However, the N(2)–H(21)···O(4) angle is 131° and the H···O distance is 2·39 Å, indicating that this is at most a very weak interaction.* The acetamide methyl hydrogen atom H(31), which corresponds to the amine hydrogen atom in the urea complex, is at a normal van der Waals distance (2·64 Å) from the barbital O(2) atom. This hydrogen atom is not considered to be involved in C–H···O hydrogen bonding.

* In barbital/urea, the corresponding interaction is even weaker, with N···O distance 3·10 Å, H···O distance 2·60 Å and N–H···O angle of 123°.

Table 5. *Hydrogen-bonding distances and angles*

Parameters for atoms not in the crystal chemical unit (Table 1) may be derived by operations which are specified by subscripts *i*, *j*, where *i* is $(\frac{1}{2}+x, \frac{1}{2}-y, 1-z)$ and *j* is $(1-x, \frac{1}{2}+y, \frac{1}{2}-z)$. The e.s.d.'s given in parentheses refer to the least significant figures in the distances and angles.

N(1)···O(1)	2·841 (2) Å
H(1)···O(1)	1·92 (3)
N(3)···O(1)$_i$	2·836 (2)
H(3)···O(1)$_i$	1·96 (3)
N(2)···O(2)$_j$	2·980 (3)
H(22)···O(2)$_j$	2·16 (3)
N(1)···O(1)——C(1)	127·7 (1)°
N(1)——H(1)···O(1)	175 (2)
N(3)···O(1)$_i$——C(1)$_i$	118·6 (1)
N(3)——H(3)···O(1)$_i$	170 (2)
N(2)···O(2)$_j$——C(2)$_j$	150·6 (1)
N(2)——H(22)···O(2)$_j$	161 (3)

In the crystal structures of simple aliphatic amides both amide hydrogen atoms are usually involved in NH···O=C hydrogen bonds. Often, the amide molecules form cyclic dimers linked by pairs of hydrogen bonds which involve the hydrogen atom *cis* to the carbonyl oxygen atom. The hydrogen atom which is *trans* to the oxygen atom forms hydrogen bonds which further link dimers to give ribbons. Table 6 lists the

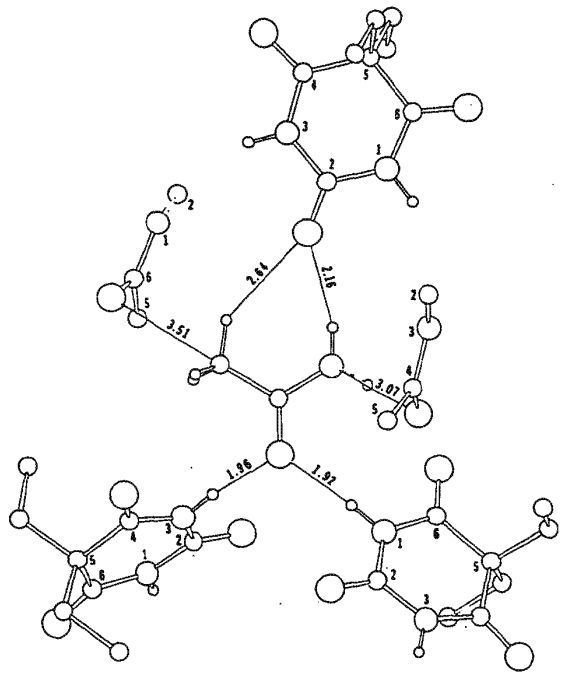


Fig. 3. The environment of the acetamide molecule, viewed normal to the plane of the amide group.

Table 6. *Distances* N···O *in* NH···O=C *hydrogen bonds in the crystal structures of aliphatic amides*

Amide*	N···O distances: N–H *trans* to C=O	N···O distances: N–H *cis* to C=O
Formamide (Ladell & Post, 1954)	2·88 Å	2·94 Å
Acetamide, orthorhombic (Hamilton, 1965)	2·87, 2·94	2·97, 3·01
Acetamide, rhombohedral (Denne & Small, 1971)	2·91	2·95
Chloroacetamide, α-form (Penfold & Simpson, 1956)	2·95	2·99
Chloroacetamide, β-form (Katayama, 1956)	3·05	–
Fluoroacetamide (Hughes & Small, 1962)	2·88	2·96
Cyanoacetamide (Chieh & Trotter, 1970)	–	2·96, 2·94
Decanamide (Brathovde & Lingafelter, 1958)	2·90	2·88
Tetradecanamide (Turner & Lingafelter, 1955)	2·93	2·99
Oxamide (Ayerst & Duke, 1954)	2·94	2·95
Malonamide (Chieh, Subramanian & Trotter, 1970)	2·89, 2·92 2·95, 2·95	2·89, 2·94 3·04, 3·14
Dichloromalonamide (Leibscher, Krishna Rao & Trotter, 1971)	3·05	2·96
Succinamide (Davies & Pasternak, 1956)	2·94	2·94
Glutaramide (Hospital & Housty, 1966*a*)	2·94	2·97
Adipamide (Hospital & Housty, 1966*b*)	2·93	2·94
Suberamide (Hospital & Housty, 1966*c*)	2·97	2·91
Azelamide (Hospital, 1971)	2·97	2·99

* This tabulation was compiled from the bibliography of Kennard & Watson (1970, 1971).

UM00013855
NOVARTIS EXHIBIT 1017
Novartis v. Regents, IPR2023-01346
Page 2601 of 4460

N···O distances for the two kinds of hydrogen bonds in amide crystal structures. The distributions of these two kinds of hydrogen bonds are very similar, with the 20 *cis* N···O distances ranging from 2·88 to 3·14 Å with an average value of 2·97 Å and the 21 *trans* distances ranging from 2·87 to 3·05 Å with an average value of 2·94 Å. The combined average distance is 2·95 Å.

The N···O distances for the NH···O=C hydrogen bonds in which barbital provides the donor (NH) and acetamide the acceptor (O=C) group are shorter (2·84 and 2·84 Å) than any of the distances in Table 6. They are also shorter than all but four of the 49 N···O distances in which a barbiturate is both donor and acceptor [see Table 5 in Gartland & Craven (1974)].

The N···O distance (2·98 Å) for the hydrogen bond in which acetamide provides the donor and barbital the acceptor is near the average value (2·95 Å) of the distances in Table 6, but is longer than all but one of the 49 barbiturate–barbiturate N···O distances.

These results are consistent with the conclusion (Gartland & Craven, 1974) that in NH···O=C hydrogen bonds the drug-active barbiturates are more effective as donor than acceptor. Analogous conclusions regarding the hydrogen bonding properties of acetamide and other simple amides must await crystal structure determinations of other complexes in which they are involved.

This work was supported by the U. S. Public Health Service, National Institues of Health, Grant No. NS-02763. We thank Dr R. Shiono for the use of computer programs.

References

Ayerst, E. M. & Duke, J. R. C. (1954). *Acta Cryst.* **7**, 588–590.

Brathovde, J. R. & Lingafelter, E. C. (1958). *Acta Cryst.* **11**, 729–732.

Chieh, P. C., Subramanian, E. & Trotter, J. (1970). *J. Chem. Soc.* (*A*), pp. 179–184.

Chieh, P. C. & Trotter, J. (1970). *J. Chem. Soc.* (*A*), pp. 184–187.

Craven, B. M., Cusatis, C., Gartland, G. L. & Vizzini, E. A. (1973). *J. Mol. Struct.* **16**, 331–342.

Cromer, D. T. & Waber, J. T. (1965). *Acta Cryst.* **18**, 104–109.

Davies, D. R. & Pasternak, R. A. (1956). *Acta Cryst.* **9**, 334–340.

Denne, W. A. & Small, R. W. H. (1971). *Acta Cryst.* B**27**, 1094–1098.

Gartland, G. L. & Craven, B. M. (1974). *Acta Cryst.* B**30**, 980–987.

Germain, G., Main, P. & Woolfson, M. M. (1971). *Acta Cryst.* A**27**, 368–376.

Hamilton, W. C. (1965). *Acta Cryst.* **18**, 866–870.

Hospital, M. (1971). *Acta Cryst.* B**27**, 484–494.

Hospital, M. & Housty, J. (1966*a*). *Acta Cryst.* **21**, 413–417.

Hospital, M. & Housty, J. (1966*b*). *Acta Cryst.* **20**, 626–630.

Hospital, M. & Housty, J. (1966*c*). *Acta Cryst.* **20**, 368–373.

Hughes, D. O. & Small, R. W. H. (1962). *Acta Cryst.* **15**, 933–940.

Katayama, M. (1956). *Acta Cryst.* **9**, 986–991.

Kennard, O. & Watson, D. G. (1970). *Molecular Structures and Dimensions*, Vol. 1. Utrecht: Oosthoek.

Kennard, O. & Watson, D. G. (1971). *Molecular Structures and Dimensions*, Vol. 3. Utrecht: Oosthoek.

Ladell, L. & Post, B. (1954). *Acta Cryst.* **7**, 559–564.

Leibscher, J. A., Krishna Rao, K. V. & Trotter, J. (1971). *J. Chem. Soc.* (*A*), pp. 1505–1508.

Penfold, B. R. & Simpson, W. S. (1956). *Acta Cryst.* **9**, 831.

Senti, F. & Harker, D. (1940). *J. Amer. Chem. Soc.* **62**, 2008–2019.

Stewart, R. F., Davidson, E. R. & Simpson, W. T. (1965). *J. Chem. Phys.* **42**, 3175–3187.

Turner, J. D. & Lingafelter, E. C. (1955). *Acta Cryst.* **8**, 551–557.

UM00013856
NOVARTIS EXHIBIT 1017
Novartis v. Regents, IPR2023-01346
Page 2602 of 4460

This Page is Inserted by IFW Indexing and Scanning Operations and is not part of the Official Record

BEST AVAILABLE IMAGES

Defective images within this document are accurate representations of the original documents submitted by the applicant.

Defects in the images include but are not limited to the items checked:

- ☐ BLACK BORDERS
- ☐ IMAGE CUT OFF AT TOP, BOTTOM OR SIDES
- ☐ FADED TEXT OR DRAWING
- ☐ BLURRED OR ILLEGIBLE TEXT OR DRAWING
- ☐ SKEWED/SLANTED IMAGES
- ☐ COLOR OR BLACK AND WHITE PHOTOGRAPHS
- ☐ GRAY SCALE DOCUMENTS
- ☐ LINES OR MARKS ON ORIGINAL DOCUMENT
- ☐ REFERENCE(S) OR EXHIBIT(S) SUBMITTED ARE POOR QUALITY
- ☐ OTHER: _____

IMAGES ARE BEST AVAILABLE COPY.
As rescanning these documents will not correct the image problems checked, please do not report these problems to the IFW Image Problem Mailbox.

All the calculations were carried out on the FACOM 270-30 at this Institute with a local version of the Universal Crystallographic Computation Program System, UNICS (1967, Crystallographic Society of Japan). Part of the cost of this research was met by a Scientific Research Grant from the Ministry of Education, to which the authors' thanks are due.

References

ANDERSON, G. R. & FRITCHIE, C. J. (1963). Second National Meeting, Society for Applied Spectroscopy, San Diego, October 14–18, paper 111.
BOER, J. L. DE & VOS, A. (1972). *Acta Cryst.* B28, 839–848.
FRITCHIE, C. J. & ARTHUR, P. (1966). *Acta Cryst.* **21**, 139–145.
HOEKSTRA, A., SPOELDER, T. & VOS, A. (1972). *Acta Cryst.* B28, 14–25.
International Tables for X-ray Crystallography (1962). Vol. III. Birmingham: Kynoch Press.
ITO, T. (1950). *X-ray Studies on Polymorphism.* Tokyo: Maruzen.
KONNO, M. & SAITO, Y. (1973). *Acta Cryst.* B29, 2815–2824.
LONG, R. E., SPARKS, R. A. & TRUEBLOOD, K. N. (1965). *Acta Cryst.* **18**, 932–939.
SAKAI, N., SHIROTANI, I. & MINOMURA, S. (1972). *Bull. Chem. Soc. Japan*, 45, 3321–3328.
SAKURAI, K. (1958). *Acta Cryst.* **11**, 840–842.
SHIBAEVA, R. P., ATOVMYAN, L. O. & ROZENBERG, L. P. (1969). *Chem. Commun.* pp. 649–650.
SHIROTANI, I. & KOBAYASHI, H. (1974). *Bull. Chem. Soc. Japan.* In the press.
SUNDARESAN, T. & WALLWORK, S. C. (1972*a*). *Acta Cryst.* B28, 491–497.
SUNDARESAN, T. & WALLWORK, S. C. (1972*b*). *Acta Cryst.* B28, 1163–1169.
VEGTER, J. G., HIMBA, T. & KOMMANDEUR, J. (1969). *Chem. Phys. Lett.* **3**, 427–429.
VEGTER, J. G., KUINDERSMA, P. I. & KOMMANDEUR, J. (1971). *Conduction in Low-Mobility Materials*, edited by KLEIN, N., TANNHAUSER, D. S. & POLLAK, M., pp. 363–373. London: Taylor and Francis.

Acta Cryst. (1974). B30, 1299

The Crystal Structure of the Triclinic 1:2 Complex of Hexamethylphosphoramide with 5,5-Diethylbarbituric Acid (Barbital)

BY I-NAN HSU* AND B. M. CRAVEN

Department of Crystallography, University of Pittsburgh, Pittsburgh, Pennsylvania 15260, *U.S.A.*

(*Received* 26 *December* 1973; *accepted* 4 *February* 1974)

Hexamethylphosphoramide, $[(CH_3)_2N]_3PO$, (M.W. 179·2) and barbital, $C_8H_{12}N_2O_3$, (M.W. 184·2) form a 1:2 triclinic complex, m.p. 124°C, space group $P\bar{1}$, with $a=6{\cdot}889$ (1), $b=12{\cdot}568$ (1), and $c=17{\cdot}944$ (2) Å, $\alpha=75{\cdot}76$ (1), $\beta=87{\cdot}85$ (1), and $\gamma=76{\cdot}31$ (1)°, $d_{meas}=1{\cdot}246$ g cm^{-3}, $Z=2[(CH_3)_2N]_3+4C_8H_{12}N_2O_3$, and a monoclinic complex of undetermined composition, m.p. 67 °C, space group Cc or $C2/c$ with $a=45{\cdot}64$, $b=20{\cdot}29$, and $c=13{\cdot}91$ Å, $\beta=106{\cdot}4$°, $d_{meas}=1{\cdot}172$ g cm^{-3}, $Z=48$ molecules. The crystal structure of the triclinic complex has been determined by the heavy-atom method, from 6020 integrated X-ray intensities measured on a computer-controlled four-circle diffractometer, using graphite-monochromated Cu $K\alpha$ radiation. Refinement by a block-diagonal least-squares procedure gave a final R value of 0·062 for all reflections. The hydrogen bonding is of interest as a model for possible barbiturate–phospholipid interactions. There are two rather strong NH···O=P hydrogen bonds (N···O distances 2·81, 2·84 Å) formed at the phosphoryl oxygen atom. There are also two NH···O=C hydrogen bonds which both form at the same barbital oxygen atom (N···O distances 2·92, 2·93 Å).

Introduction

The drug-active barbiturates, such as 5,5-diethylbarbituric acid or barbital (Fig. 1), form crystal complexes with a variety of molecules which are of biological interest, such as adenine derivatives (Kyogoku, Lord & Rich, 1968; Kim & Rich, 1968; Voet, 1972), amides (Gartland & Craven, 1974; Hsu & Craven, 1974*a*), and imidazole (Hsu & Craven, 1974*b*). The most important molecular interactions in these crystal structures are the hydrogen bonds. Those hydrogen bonds in which the barbiturate NH groups are donors tend to be short, whereas those in which barbiturate oxygen atoms are acceptors tend to be long (Gartland & Craven, 1974; Hsu & Craven, 1974*b*). This suggests that barbiturates are better hydrogen-bonding donors than acceptors and that the preferred barbiturate binding sites in bio-

* Present address: Department of Chemistry, University of Toronto, Ontario, Canada M5S 1A1.

UM00013858
NOVARTIS EXHIBIT 1017
Novartis v. Regents, IPR2023-01346
Page 2604 of 4460

chemical systems are likely to involve a strong hydrogen-bonding acceptor group. The phosphoryl oxygen atoms of phospholipids might satisfy this requirement. Thus, n.m.r. studies in deuterochloroform solution (Novak & Swift, 1972) provide evidence of complexation between phenobarbital and phosphatidylcholine. We have been unable to crystallize this complex, but we have obtained crystal complexes of a barbiturate with hexamethylphosphoramide (Fig. 2). Thermodynamic properties of hexamethylphosphoramide in carbon tetrachloride solution (Arnett, Joris, Mitchell, Murty, Gorrie & Schleyer, 1970) show this molecule to be a particularly strong hydrogen-bonding acceptor. For the complex formed with *p*-fluorophenol as donor, the heat of formation of a hydrogen-bonded dimer is 8 kcal mole^{-1}. We now report the crystal structure determination of the 1:2 triclinic complex of hexamethylphosphoramide (Fig. 2) with barbital, and crystal data for a monoclinic complex.

Experimental

Crystal data for two complexes of hexamethylphosphoramide and barbital are given in Table 1. The monoclinic crystals were obtained as plates elongated along c by slow cooling to room temperature of a solution of barbital in liquid hexamethylphosphoramide. The triclinic crystals were obtained as needles elongated on **a**, from a solution of both components in absolute ethanol. In order to exclude atmospheric moisture, crystals of both complexes were grown in a sealed flask, and were coated in lacquer before X-ray data were measured. Otherwise, the crystals decomposed in a few hours. X-ray oscillation and Weissenberg photographs (Cu $K\alpha$ radiation) showed that the monoclinic complex has an unusually large unit cell. The crystal density (1·172 g cm^{-3}) corresponds to a total of 48 molecules per unit cell, or 12 molecules in the asymmetric unit if the space group has the lower symmetry *Cc*. The composition of this complex could not be established with confidence from the unit-cell volume and crystal density because the two components have similar molecular weights.

Table 1. *Crystal data for the complexes of hexamethylphosphoramide with barbital*

	Hexamethylphosphoramide $[(CH_3)_2N]_3PO$ M.W. 179·2 Triclinic,* m.p. 124°	Barbital $C_8H_{12}N_2O_3$ M.W. 184·2 Monoclinic m.p. 67°
Space group	$P\bar{1}$	*Cc* or *C2/c*
a	6·889 (1) Å	45·64 Å
b	12·568 (1)	20·29
c	17·944 (2)	13·91
α	75·76 (1)°	–
β	87·85 (1)	106·4°
γ	76·31 (1)	–
d_{meas}	1·246 g cm^{-3}	1·172 g cm^{-3}
d_{calc}	1·243 g cm^{-3}	1·172 g cm^{-3}
Z	$2[(CH_3)_2N]_3PO + 4(C_8H_{12}N_2O_3)$	48 molecules with M.W. of 182

* The crystal data refer to the Niggli reduced cell, which was used throughout the structure determination.

The crystal structure determination of the triclinic form was undertaken first because of its relative simplicity. A needle-shaped crystal was cut to give dimensions 0·29 × 0·29 × 0·15 mm and was mounted with the *a* axis approximately along the φ axis of a computer-controlled four-circle diffractometer. Unit-cell dimensions and the integrated intensities for 6020 reflections with $\theta \leq 75°$ were measured with graphite-monochromated Cu $K\alpha$ radiation ($\lambda = 1{\cdot}5418$ Å). Reflections were scanned in the $\theta/2\theta$ mode with θ scan width $(0{\cdot}6 + 0{\cdot}3 \tan\theta)°$. There were 1316 weak reflections for which the intensity I was less than $2{\cdot}0\sigma(I)$. These reflections were assigned intensities of $\sigma(I)/2$. No corrections were made for X-ray absorption and extinction.

The phase problem was solved by the heavy-atom method, based on the phosphorus atoms. Atomic parameters (Table 2) were refined by a block-diagonal

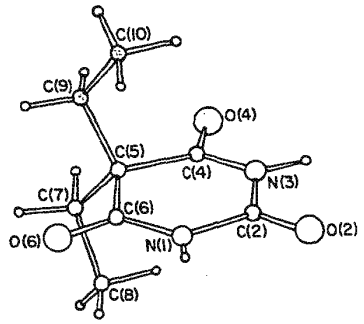


Fig. 1. Atomic nomenclature and conformation of barbital.

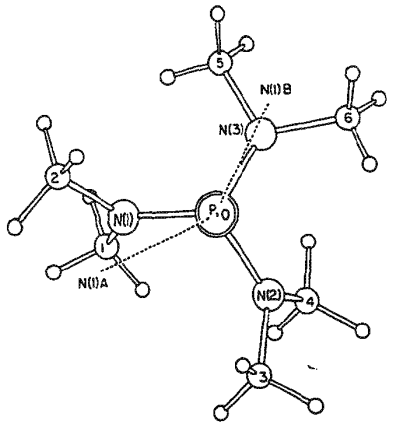


Fig. 2. The hexamethylphosphoramide molecule viewed down the phosphoryl bond. The dotted lines are the projections of the hydrogen bonds which are formed at the phosphoryl oxygen atom.

UM00013859
NOVARTIS EXHIBIT 1017
Novartis v. Regents, IPR2023-01346
Page 2605 of 4460

least-squares procedure in which the function minimized was $\sum_H w_H \Delta_H^2$, where $\Delta_H = |F_H^{obs}| - |F_H^{calc}|$. The weights were given by $w_H^{-1} = 0{\cdot}1 + 0{\cdot}002|F_H|^2$. The atomic scattering factors were those of Cromer & Waber (1965) for phosphorus (including $\Delta f' = 0{\cdot}2$), oxygen, nitrogen and carbon, and of Stewart, Davidson & Simpson (1965) for hydrogen. All hydrogen atomic positions were obtained from a difference Fourier map which was computed after refinement of anisotropic temperature factors had been made for the non-hydrogen atoms. Hydrogen atom positional parameters were then refined, but hydrogen atom thermal parameters were fixed with values the same as those of the atoms to which they are bonded. During the final cycles of least-squares calculation, reflections with $I < 2\sigma(I)$ and two strong reflections for which $|F_H^{calc}| > |F_H^{obs}|$ were given zero weight. The final R index* was 0·062 for all reflections and 0·046 for reflections with non-zero weight.†

Discussion

The crystal structure determination shows a hydrogen-bonded 1:2 complex with one hexamethylphosphoramide molecule and two barbital molecules (A and B) in the asymmetric unit of space group $P\bar{1}$.

In both barbital molecules, the oxopyrimidine ring

* $R = \sum_H |\Delta_H| / \sum_H |F_H^{obs}|$.

† The table of structure factors has been deposited with the British Library Lending Division as Supplementary Publication No. SUP 30367 (32pp., 1 microfiche). Copies may be obtained from the Executive Secretary, International Union of Crystallography, 13 White Friars, Chester CH1 1NZ, England,

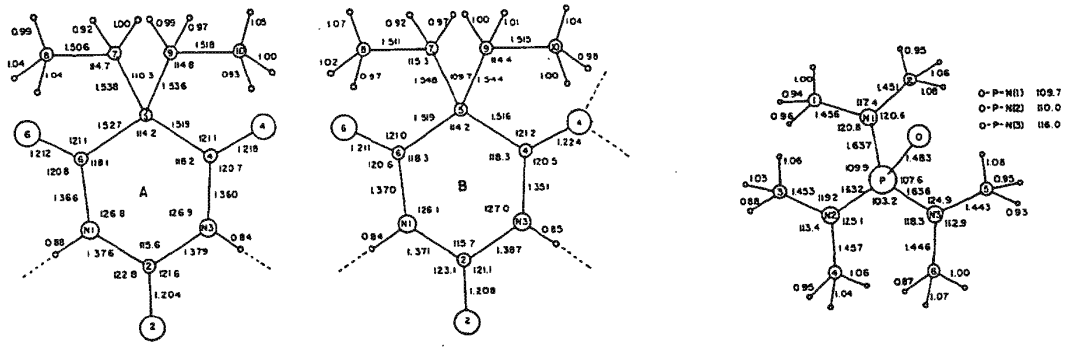


Fig. 3. Bond lengths and angles. The e.s.d.'s are 0·005 Å in C–N, C=O and C–C bond lengths, 0·3° in corresponding bond angles. 0·003 Å in P–N and P–O bond lengths, and 0·2° in corresponding angles, and 0·05 Å in bond lengths involving hydrogen atoms.

Table 2. *Atomic parameters and their e.s.d.'s*

Positional parameters are given as fractions of the unit-cell translations ($\times 10^4$) for non-hydrogen atoms and ($\times 10^3$) for hydrogen atoms. Anisotropic thermal factors ($\times 10^4$) are given by the expression $T = \exp[-\sum(\beta_{ij}h_ih_j)]$. The e.s.d.'s which are given in parentheses refer to the least significant digit in the corresponding parameters.

(*a*) Hexamethylphosphoramide

	x	y	z	β_{11}	β_{22}	β_{33}	β_{12}	β_{13}	β_{23}
P	1097 (1)	−21 (1)	3015 (1)	201 (2)	47 (1)	24 (1)	−21 (1)	−1 (1)	−6 (1)
O	1386 (4)	1138 (2)	2707 (1)	338 (8)	47 (2)	32 (1)	−27 (3)	21 (2)	−7 (1)
N(1)	−1274 (5)	31 (3)	3176 (2)	193 (7)	91 (3)	48 (1)	−29 (4)	1 (3)	−16 (2)
N(2)	2403 (5)	−622 (3)	3811 (2)	249 (8)	79 (3)	26 (1)	−19 (3)	−8 (2)	−7 (1)
N(3)	1869 (5)	−907 (3)	2474 (2)	256 (8)	66 (2)	36 (1)	−17 (3)	−8 (2)	−20 (1)
C(1)	−1903 (8)	−905 (6)	3700 (3)	291 (13)	185 (7)	50 (2)	−125 (8)	14 (4)	−12 (3)
C(2)	−2804 (8)	895 (5)	2693 (6)	276 (14)	97 (5)	145 (6)	−20 (6)	−79 (7)	−24 (4)
C(3)	2479 (7)	34 (5)	4368 (3)	301 (12)	160 (6)	39 (2)	−14 (7)	−13 (4)	−40 (3)
C(4)	3066 (8)	−1836 (4)	4127 (3)	369 (14)	95 (4)	41 (2)	−22 (6)	−21 (4)	21 (2)
C(5)	599 (8)	−1206 (4)	1977 (3)	399 (14)	100 (4)	42 (2)	−86 (6)	−3 (4)	−28 (2)
C(6)	3963 (7)	−1099 (4)	2244 (3)	291 (11)	86 (3)	43 (2)	−4 (5)	4 (3)	−28 (2)

	x	y	z		x	y	z
H(11)	−100 (7)	−134 (5)	415 (3)	H(41)	225 (7)	−212 (4)	453 (3)
H(12)	−250 (7)	−127 (5)	340 (3)	H(42)	451 (7)	−200 (4)	435 (3)
H(13)	−311 (7)	−60 (5)	393 (3)	H(43)	291 (7)	−227 (4)	370 (3)
H(21)	−225 (8)	144 (4)	235 (4)	H(51)	56 (7)	−69 (4)	140 (3)
H(22)	−372 (8)	121 (4)	311 (4)	H(52)	104 (7)	−198 (4)	197 (3)
H(23)	−338 (8)	42 (4)	237 (4)	H(53)	−68 (7)	−114 (4)	217 (3)
H(31)	150 (7)	−20 (4)	482 (3)	H(61)	412 (7)	−64 (4)	172 (3)
H(32)	391 (7)	−5 (4)	457 (3)	H(62)	452 (6)	−197 (4)	225 (3)
H(33)	221 (7)	75 (5)	412 (3)	H(63)	465 (6)	−97 (4)	260 (3)

UM00013860
NOVARTIS EXHIBIT 1017
Novartis v. Regents, IPR2023-01346
Page 2606 of 4460

Table 2 (*cont.*)

(*b*) Barbital (molecule *A*, above; molecule *B*, below)

	x	*y*	*z*	β_{11}	β_{22}	β_{33}	β_{12}	β_{13}	β_{23}
O(2)	−1581 (5)	3553 (3)	1570 (2)	398 (10)	97 (3)	32 (1)	3 (4)	5 (2)	−21 (1)
	3330 (5)	3528 (3)	1926 (2)	486 (11)	103 (3)	30 (1)	−113 (4)	27 (3)	−26 (1)
O(4)	−5269 (6)	6091 (3)	2749 (2)	437 (11)	70 (2)	46 (1)	58 (4)	−16 (3)	−11 (1)
	4764 (4)	4112 (2)	−587 (1)	275 (6)	55 (2)	25 (1)	−53 (3)	0 (2)	−4 (1)
O(6)	−499 (5)	2898 (2)	4124 (2)	332 (8)	82 (2)	32 (1)	19 (3)	−13 (2)	−4 (1)
	2045 (5)	1040 (2)	692 (2)	355 (8)	65 (2)	39 (1)	−89 (3)	9 (2)	−10 (1)
N(1)	−1039 (5)	3244 (2)	2852 (2)	259 (8)	55 (2)	31 (1)	4 (3)	1 (2)	−9 (1)
	2805 (4)	2241 (2)	1312 (2)	247 (7)	51 (2)	26 (1)	−41 (3)	14 (2)	−6 (1)
C(2)	−1932 (6)	3859 (3)	2157 (2)	268 (9)	59 (3)	29 (1)	−21 (4)	5 (3)	−9 (1)
	3366 (6)	3205 (3)	1344 (2)	258 (9)	60 (2)	26 (1)	−45 (4)	7 (2)	−11 (1)
N(3)	−3301 (5)	4851 (2)	2173 (2)	289 (8)	54 (2)	27 (1)	−9 (3)	−10 (2)	−3 (1)
	4004 (5)	3798 (2)	658 (2)	285 (8)	52 (2)	26 (1)	−58 (3)	5 (2)	−11 (1)
C(4)	−3952 (6)	5234 (2)	2806 (2)	284 (10)	50 (2)	32 (1)	−5 (4)	−4 (3)	−7 (1)
	4135 (5)	3524 (2)	−27 (2)	174 (7)	40 (2)	24 (1)	−18 (3)	−5 (2)	−5 (1)
C(5)	−2961 (6)	4580 (3)	3578 (2)	273 (10)	59 (3)	29 (1)	3 (4)	−10 (3)	−13 (1)
	3516 (5)	2463 (2)	−77 (2)	191 (7)	43 (2)	25 (1)	−26 (3)	−5 (2)	−8 (1)
C(6)	−1392 (5)	3508 (3)	3547 (2)	237 (9)	55 (2)	29 (1)	−14 (4)	1 (3)	−6 (1)
	2707 (5)	1859 (3)	665 (2)	189 (7)	44 (2)	29 (1)	−24 (3)	−2 (2)	−6 (1)
C(7)	−4595 (7)	4242 (4)	4130 (2)	309 (12)	100 (4)	29 (1)	28 (5)	9 (3)	−9 (2)
	5393 (6)	1640 (3)	−262 (2)	271 (9)	52 (2)	35 (1)	−22 (4)	18 (3)	−15 (1)
C(8)	−5556 (8)	3384 (5)	3933 (3)	316 (13)	144 (6)	49 (2)	−62 (7)	5 (4)	3 (3)
	7034 (7)	1196 (4)	329 (3)	222 (10)	83 (3)	63 (2)	13 (5)	−3 (4)	−18 (2)
C(9)	−1937 (9)	5356 (4)	3879 (3)	447 (17)	76 (3)	64 (2)	−5 (6)	−51 (5)	−31 (2)
	1904 (6)	2770 (3)	−719 (2)	294 (10)	74 (3)	32 (1)	−62 (5)	−32 (3)	−3 (2)
C(10)	−421 (11)	5827 (5)	3342 (5)	466 (21)	94 (5)	132 (5)	−73 (8)	−58 (8)	−29 (4)
	80 (7)	3671 (5)	−624 (3)	232 (11)	111 (4)	64 (2)	−34 (5)	−43 (4)	7 (3)

	x	*y*	*z*		*x*	*y*	*z*
H(1)	−27 (6)	258 (3)	285 (2)	H(83)	−448 (7)	263 (5)	396 (3)
	236 (6)	189 (3)	171 (2)		817 (6)	69 (4)	17 (3)
H(3)	−380 (6)	520 (3)	174 (2)	H(91)	−133 (8)	493 (4)	439 (3)
	437 (6)	440 (3)	66 (2)		252 (6)	304 (3)	−122 (2)
H(71)	−405 (7)	394 (4)	467 (2)	H(92)	−286 (8)	603 (4)	396 (3)
	498 (6)	100 (3)	−38 (2)		146 (6)	206 (3)	−72 (2)
H(72)	−552 (7)	490 (4)	415 (2)	H(101)	−131 (9)	637 (5)	287 (4)
	578 (6)	205 (3)	−74 (2)		43 (7)	443 (4)	−61 (3)
H(81)	−661 (7)	322 (5)	431 (3)	H(102)	1 (9)	631 (5)	364 (4)
	651 (6)	68 (4)	82 (3)		−82 (7)	384 (4)	−107 (3)
H(82)	−607 (7)	366 (4)	336 (3)	H(103)	48 (9)	530 (5)	314 (4)
	747 (6)	183 (4)	49 (3)		−40 (7)	338 (4)	−10 (3)

is almost planar and the ethyl carbon atoms and atom C(5) form an almost fully extended chain at right angles to the ring. The slight ring puckerings in molecules *A* and *B* closely resemble those found in molecules *C* and *D* in polymorph IV of barbital (Craven & Vizzini, 1971; Craven, Cusatis, Gartland & Vizzini, 1973). The greatest atomic displacements from the best least-squares planes through the six ring atoms are 0·07 Å for atom O(2) in molecule *A* and 0·11 Å for atom O(6) in molecule *B*. The torsion angles in the chain C(10)–C(9)–C(5)–C(7)–C(8) in molecules *A* and *B* respectively are −174·8 (5)° and −173·7 (4)° about the bond C(9)–C(5) and −174·0 (5)°, −175·4 (3)° about the bond C(5)–C(7).

There is good agreement between the bond lengths and angles of molecules *A* and *B* (Fig. 3). The differences between bond lengths such as C(4)–O(4) and C(6)–O(6) in molecule *B* are too small (0·013 Å) to be highly significant in terms of their e.s.d.'s (0·004 Å). However, this bond-length difference has the same sense and order of magnitude as have been consistently observed in other barbiturate molecules in which O(4) is hydrogen bonded, while O(6) is not (Craven, Cusatis, Gartland & Vizzini, 1973). In molecule *A*, where none of the barbiturate oxygen atoms is hydrogen bonded, bond-length differences across the C(2)···C(5) axis are even smaller than in molecule *B*.

The hexamethylphosphoramide molecule shows marked departures from threefold rotational symmetry about the P=O bond. This asymmetry involves the P–N torsion angles (Fig. 2) and valence bond angles (Fig. 3), but not bond lengths (Fig. 3). The torsion angles O–P–N(1)–C(2), O–P–N(2)–C(3) and O–P–N(3)–C(6) are all different (32·8°, 41·3°, 56·3°, e.s.d. 0·4°), in a way which appears to be uncorrelated with differences among the three O–P–N, the three N–P–N, and the six P–N–C bond angles. The bonds at the three nitrogen atoms are almost planar, but each is significantly displaced (0·09, 0·13, and 0·17 Å) from the plane through the phosphorus and methyl carbon atoms to which it is bonded. The nitrogen atoms N(1) and N(2) are on the same side of the plane as the phosphoryl oxygen atom, but nitrogen atom N(3) is on the opposite side.

UM00013861
NOVARTIS EXHIBIT 1017
Novartis v. Regents, IPR2023-01346
Page 2607 of 4460

The bond lengths in hexamethylphosphoramide (Fig. 3) are similar to those reported in crystal structure determinations of related molecules, such as *N,N*-dimethyldiphenylphosphinamide [P–O, 1·47 Å; P–N, 1·67 Å; N–CH_3, 1·52 and 1·47 Å; Haque & Caughlan (1966)], the trimeric diethylamide of metaphosphoric acid [mean P=O bond length 1·44 Å, mean P–N bond length 1·67 Å; Andrianov, Bokii, Cherepinskii-Malov, Tarnopolskii & Struchkov (1969)], 2,4,5-trimethoxy-1,3,5-trimethyl-2,4,6-trioxotriphosphazane [mean phosphoryl P=O bond length 1·46 Å, mean P–N bond length 1·66 Å; Ansell & Bullen (1968)] and triethylene thiophosphoramide [mean P–N bond length 1·64 Å; Subramanian & Trotter (1969)]. The phosphoryl bond length in hexamethylphosphoramide (1·483 Å) is nearly the same as the phosphodiester phosphoryl bond lengths found in glycerylphosphorylcholine [mean value 1·486 Å; Abrahamsson & Pascher (1966)] and glycerylphosphorylethanolamine monohydrate [mean value 1·488 Å; De Titta & Craven (1973)]. Since it appears that these phosphoryl bonds have similar double-bond character, the phosphoryl oxygen atom in hexamethylphosphoramide should have similar affinity as a hydrogen-bonding acceptor to the phosphoryl oxygen atoms of phospholipids.

In the 1:2 complex of hexamethylphosphoramide with barbital there are hydrogen-bonded chains which are parallel to **a** and have the thickness of one unit cell in the **b** and **c** directions (Fig. 4). Non-polar methyl or methylene groups from both kinds of molecules form the outer surface of each chain. Each barbital molecule *A* and *B* is the donor in one hydrogen bond to the O(4) oxygen atom of a barbital *B* molecule, and is also donor in a second hydrogen bond to the hexamethylphosphoramide oxygen atom. The hydrogen bonds N(3,*A*)H···O(4,*B*) and N(3,*B*)H···O(4,*B*) respectively have N···O distances 2·93 and 2·92 Å, H···O distances 2·10 and 2·07 Å, and N–H···O angles 171° and 177°. The N(3,*A*)···O(4,*B*)···N(3,*B*) angle is 86·0°. The hydrogen bonds N(1,*A*)H···O=P and N(1,*B*)H···O=P respectively have N···O distances 2·84 and 2·81 Å, H···O distances 1·97 and 1·98 Å and N–H···O angles 173° and 176°. The N(1,*A*)···O···N(1,*B*) angle is 89·5°. Thus, the arrangement of pairs of hydrogen bonds at the carbonyl O(4) and phosphoryl oxygen atoms is very similar except that the latter hydrogen bonds are shorter by about 0·1 Å.

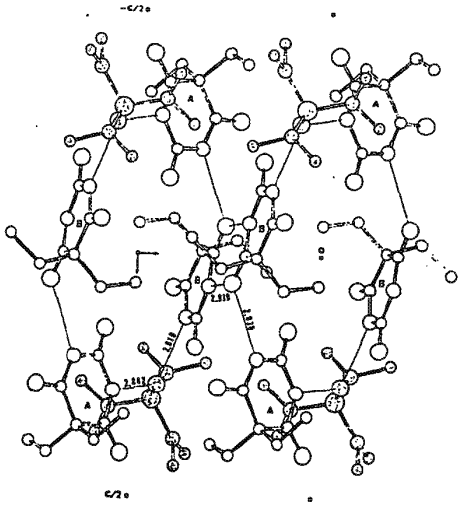


Fig. 4. The crystal structure viewed down **b**. Atoms of the hexamethylphosphoramide molecules are shaded.

The N···O distances for the hydrogen bonds involving only barbital are near the center of the range (2·81 to 2·98 Å) which has been observed for all such hydrogen bonds (Gartland & Craven, 1974). The N···O distances for the hydrogen bonds involving the phosphoryl oxygen are near the short limit of this range, but are longer than the NH···O=C hydrogen bond in which barbital is donor and aminopyridine is acceptor (2·75 Å; Kiryu, 1971). They are also longer than one of the NH···O=P hydrogen bonds (N···O distances 2·71, 2·85 Å) in glycerylphosphorylethanolamine monohydrate (DeTitta & Craven, 1973). Thus, in the 1:2 complex of hexamethylphosphoramide and barbital, the N···O distances are consistent with strong NH···O=P hydrogen bonds, but these do not appear to be markedly stronger than some hydrogen bonds in related crystal structures. We note that NH···O=C hydrogen bonds between barbiturate molecules have N···O distances which differ over a range of almost 0·2 Å, presumably as a result of crystal packing effects. The two NH···O=P hydrogen bonds in the triclinic complex of hexamethylphosphoramide with barbital do not provide an adequate estimate of the range of N···O distances which is to be expected for such hydrogen bonds. However, the crystal structure determination of the monoclinic complex (in progress) should give considerably more data concerning the nature of NH···O=P hydrogen bonds involving barbiturates.

This work was supported by Grant No. NS-02763 of the U. S. Public Health Service, National Institutes of Health. We thank Professor R. Shiono for the use of computer programs.

References

ABRAHAMSSON, S. & PASCHER, I. (1966). *Acta Cryst.* **21**, 79–87.

ANDRIANOV, V. I., BOKII, N. G., CHEREPINSKII-MALOV, V. C., TARNOPOLSKII, B. L. & STRUCHKOV, YU. T. (1969). *Zh. Strukt. Khim.* **10**, 865–871.

ANSELL, G. B. & BULLEN, G. J. (1968). *J. Chem. Soc.* (*A*), pp. 3026–3036.

ARNETT, E. M., JORIS, L., MITCHELL, E., MURTY, T. S. S. R., GORRIE, T. M. & SCHLEYER, P. v. R. (1970). *J. Amer. Chem. Soc.* **92**, 2365–2377.

UM00013862
NOVARTIS EXHIBIT 1017
Novartis v. Regents, IPR2023-01346
Page 2608 of 4460

CRAVEN, B. M., CUSATIS, C., GARTLAND, G. L. & VIZZINI, E. A. (1973). *J. Mol. Struct.* **16**, 331–342.
CRAVEN, B. M. & VIZZINI, E. A. (1971). *Acta Cryst.* B**27**, 1917–1924.
CROMER, D. T. & WABER, J. T. (1965). *Acta Cryst.* **18**, 104–109.
DETITTA, G. T. & CRAVEN, B. M. (1973). *Acta Cryst.* B**29**, 1354–1357.
GARTLAND, G. L. & CRAVEN, B. M. (1974). *Acta Cryst.* B**30**, 980–987.
HAQUE, M.-V. & CAUGHLAN, C. N. (1966). *Chem. Commun.* pp. 921–922.
HSU, I. & CRAVEN, B. M. (1974*a*). *Acta Cryst.* B**30**, 974–979.
HSU, I. & CRAVEN, B. M. (1974*b*). *Acta Cryst.* B**30**, 988–993.
KIM, S. H. & RICH, A. (1968). *Proc. Natl. Acad. Sci. U.S.* **60**, 402–408.
KIRYU, S. (1971). *J. Pharm. Sci.* **60**, 699–703.
KYOGOKU, Y., LORD, R. C. & RICH, A. (1968). *Nature, Lond.* **218**, 69–72.
NOVAK, R. F. & SWIFT, T. J. (1972). *Proc Natl. Acad. Sci. U.S.* **69**, 640–642.
STEWART, R. F., DAVIDSON, E. R. & SIMPSON, W. T. (1965). *J. Chem. Phys.* **42**, 3175–3187.
SUBRAMANIAN, E. & TROTTER, J. (1969). *J. Chem. Soc.* (*A*), pp. 2309–2312.
VOET, D. (1972). *J. Amer. Chem. Soc.* **94**, 8213–8222.

Acta Cryst. (1974). B**30**, 1304

The Crystal Structure of 1,4-Diiodobicyclo[2,2,2]octane

BY DOYLE BRITTON*

Laboratory for Organic Chemistry, Swiss Federal Institute of Technology, 8006 Zürich, Switzerland

(*Received* 26 *July* 1973; *accepted* 31 *January* 1974)

1,4-Diiodobicyclo[2,2,2]octane is tetragonal, probable space group $P4_12_12_1$, with $a=6{\cdot}653$ and $c=23{\cdot}311$ Å, $Z=4$. The structure, determined from Fourier maps and partial least-squares refinement, gave a final conventional R value of 0·045 for a disordered model with assumed tetrahedral bond angles and normal C–C bond lengths. The disorder arises from the molecules being rotated $\pm 20°$ about the three-fold molecular axis (*i.e.* the I···I axis) away from an orientation appropriate to the space-group symmetry. A less probable alternative structure requiring twinned crystals with space group $P4_1$ fits the data equally well.

Introduction

The packing of diiodoacetylene (Dunitz, Gehrer & Britton, 1972) shows unusual features, and it was thought that diiodobicyclooctane, which is another diiodide molecule with approximately cylindrical symmetry, would be worth examining. Accordingly, its structure is reported here.

Experimental

A sample of the compound, which had previously been provided for another purpose by Dr J. C. Kauer of the Central Research Department of E. I. du Pont de Nemours and Co., Inc. (*Chem. Eng. News*, 1970), was recrystallized from carbon tetrachloride. The crystals, mostly thin, square plates with no extinction perpendicular to the plate direction, were not well enough formed for any useful conclusions to be drawn about the crystallographic point group. Precession photographs showed the crystals to be tetragonal with Laue symmetry $4/mmm$. Systematic extinctions ($h00$, $h\neq 2n$; $00l$, $l\neq 4n$) indicate the space group to be $P4_12_12$ (No. 92) or its enantiomorph. The cell constants, determined from a least-squares fit of the diffractometer positions of 20 peaks (Mo $K\alpha$ radiation, $\lambda=0{\cdot}71069$ Å), are $a=6{\cdot}653$, $c=23{\cdot}311$ Å; the estimated error is less than 0·1%. For $Z=4$ the molecular volume is 258 Å^3 and the calculated density is 2·329 g cm^{-3}. The linear absorption coefficient is 61·0 cm^{-1} (Mo $K\alpha$).

A crystal $0{\cdot}10\times 0{\cdot}15\times 0{\cdot}20$ mm was used for intensity measurements. It was mounted on the end of a fine glass fibre, which was then sealed in a thin-walled glass capillary. Data were collected at room temperature using a 4-circle Hilger and Watts Y290 diffractometer with monochromatic Mo $K\alpha$ radiation. One complete octant of data (1295 reflexions) was collected for θ between 0 and 26°. Reflexions between 0 and 20° were scanned in 80 steps of 0·01° in θ and ω with 1 s counting times per step and 10 s background counts at each end of the scan; for 20–26° 100 such steps were used and the background counting time was increased to 25 s at each end. The 50 most intense reflexions were also scanned using reduced intensity to test for saturation of the counter and the seven most intense reflexions were corrected for this effect. The intensities of two check reflexions were measured every 25 reflexions; although the crystal turned dark yellow with use, there was no variation with time of the intensities of the check reflexions and the average deviation from the mean was 1·1%.

* Permanent address: Chemistry Department, University of Minnesota, Minneapolis, Minnesota 55455, U.S.A.

UM00013863
NOVARTIS EXHIBIT 1017
Novartis v. Regents, IPR2023-01346
Page 2609 of 4460

Acta Cryst. (1974). B30, 988

Hydrogen Bonding NH...N of Barbiturates: The 1:1 Crystal Complex of Imidazole and 5,5-Diethylbarbituric Acid (Barbital)

BY I-NAN HSU AND B. M. CRAVEN

Department of Crystallography, University of Pittsburgh, Pittsburgh, Pennsylvania 15260, *U.S.A.*

(*Received* 26 *October* 1973; *accepted* 12 *December* 1973)

The 1:1 crystal complex of imidazole and barbital (m.p. 122°C) is monoclinic, space group $P2_1/c$, with $a = 10{\cdot}133$ (4), $b = 11{\cdot}261$ (4), $c = 13{\cdot}715$ (5) Å, $\beta = 123{\cdot}12$ (1)° and four molecules of each component in the unit cell ($D_{meas} = 1{\cdot}276$, $D_x = 1{\cdot}278$ g cm^{-3}). The X-ray crystal structure has been determined from 2115 integrated intensities measured on a four-circle computer-controlled diffractometer using nickel-filtered Cu $K\alpha$ radiation. The phase problem was solved by a combination of direct and Patterson methods. The atomic parameters were refined by a full-matrix least-squares procedure to give a final R index of 0·065 for all reflections. The crystal structure consists of NH···O=C hydrogen-bonded dimers of barbital which are cross-linked by pairs of imidazole molecules to form hydrogen-bonded ribbons. Barbital provides the NH donor in a strong hydrogen bond to imidazole, with N···N distance 2·78 Å. Similar short hydrogen-bond distances occur in crystal complexes in which uracil, thymine or barbiturate provides the NH donor, and adenine provides the nitrogen atom acceptor.

Introduction

Kyogoku, Lord & Rich (1968) have reported that the association between barbiturates and 9-ethyladenine in carbon tetrachloride solution is strong, with equilibrium constants ($K_{HB} \sim 1000$ M^{-1}) which are an order of magnitude greater than those between uracil and adenine derivatives (100 M^{-1}). Highly specific interactions of this kind may be involved in the drug action of barbiturates. An important factor in the interaction is likely to be the barbiturate/adenine hydrogen bonding. Kyogoku, Lord & Rich (1968) point out that barbiturates may form stronger hydrogen bonds than uracil derivatives because of their greater acidity in aqueous solution (pK_a 7·8, 9·4 for barbital and uridine respectively). This would be in accord with Taft, Gurka, Joris, Schleyer & Rakshys (1969) who have found linear relationships between pK_a and pK_{HB} for the interactions of families of closely related hydrogen-bonding bases with a common hydrogen-bonding acid. In crystal complexes of barbiturates with adenine derivatives (Kim & Rich, 1968; Voet & Rich, 1972; Voet, 1972) there are indeed short NH···N hydrogen bonds between the two components, although not markedly shorter than those found in crystal complexes of uracil or thymine with adenine derivatives.

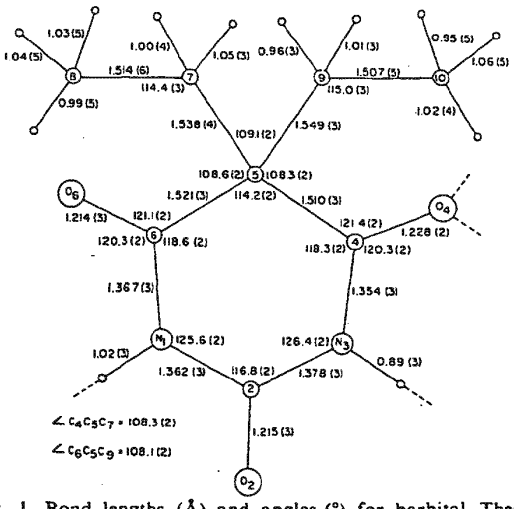
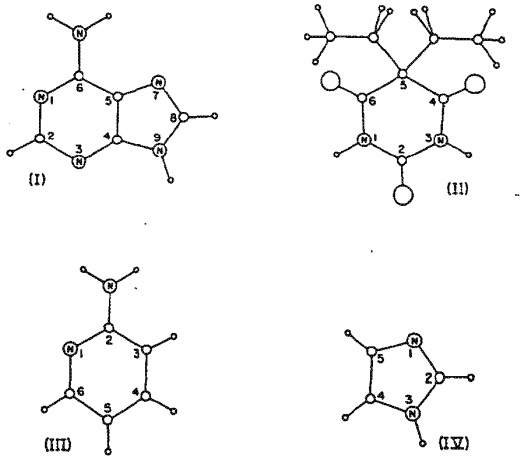


Fig. 1. Bond lengths (Å) and angles (°) for barbital. These values have not been corrected for the effects of anisotropic thermal motion. The e.s.d.'s are given in parentheses and refer to the least significant digit in the parameters.



It is interesting that in addition to the crystal complex with 9-ethyladenine [(I), Voet, 1972], 5,5-diethylbarbituric acid [barbital, (II)] also forms crystal complexes with 2-aminopyridine (III) and imidazole (IV). Molecules (III) and (IV), if fused together, comprise a molecule which closely resembles adenine. We report the crystal structure determinations of the latter complexes in this and the following paper (Hus & Craven,

UM00013864
NOVARTIS EXHIBIT 1017
Novartis v. Regents, IPR2023-01346
Page 2610 of 4460

1974). As in the barbiturate/adenine complexes, these structures involve short NH···N hydrogen bonds in which barbital NH groups are donors.

Experimental

The 1:1 crystal complex of imidazole with barbital, m.p. 122°C, was obtained by slow cooling to room temperature of an alcoholic solution which had been slightly supersaturated with respect to both components. We know of no previous report in the literature concerning this complex. The crystals are monoclinic with space group $P2_1/c$ and lattice translations $a=10{\cdot}133$ (4), $b=11{\cdot}261$ (4), $c=13{\cdot}715$ (5) Å, $\beta=123{\cdot}12$ (1)°. The crystal density (1·276 g cm^{-3}), which was determined by flotation in a mixture of CCl_4 and benzene, agrees with the calculated value (1·278 g cm^{-3}) assuming four molecules of each component in the unit cell. The lattice translations and X-ray intensity data were measured on a four-circle computer-controlled diffractometer using nickel-filtered Cu $K\alpha$ radiation ($\lambda=1{\cdot}5418$ Å). Integrated intensities were measured for 2115 symmetry-independent reflections in the range $\theta\leq 63°$, with the prism axis of the crystal (b) making an angle of 5° with the φ axis of the goniostat. The crystal dimensions were $0{\cdot}37\times 0{\cdot}29\times 0{\cdot}20$ mm. Reflections were scanned in the θ–2θ mode at a rate of 2° min^{-1} with 20 s background counts being taken at each of the scan limits. The 2θ scan width was based on 2·0° and was increased to allow for spectral dispersion. There were 385 reflections for which the integrated intensity, I, was less than $2{\cdot}0\sigma(I)$ as calculated from the counting statistics. These reflections were arbitrarily assigned intensity of $\sigma(I)/2$. No corrections were applied for X-ray absorption or extinction.

The crystal structure was determined by a combination of direct and Patterson methods. The most promising phase-set resulting from direct-method procedures as described by Germain, Main & Woolfson (1971) corresponded to an E map in which a barbital

Table 1. *Atomic parameters for the imidazole–barbital complex*

Positional parameters are given as fractions of the lattice translations. Anisotropic temperature factors correspond to the expression: $T=\exp[-(\beta_{11}h^2+\beta_{22}k^2+\beta_{33}l^2+2\beta_{12}hk+2\beta_{13}hl+2\beta_{23}kl)]$, and isotropic temperature factors to the expression: $\exp(-B\sin^2\theta/\lambda^2)$. E.s.d.'s given in parentheses refer to the least significant figures in parameter values.

(*a*) Carbon, nitrogen and oxygen atom parameters (× 10^4)

	x	y	z	β_{11}	β_{22}	β_{33}	β_{12}	β_{13}	β_{23}
(i) Imidazole									
N(1)	−172 (2)	1523 (2)	−2149 (2)	116 (3)	133 (2)	85 (2)	−18 (2)	25 (2)	−30 (2)
C(2)	661 (3)	1179 (2)	−1047 (2)	128 (3)	95 (2)	107 (2)	−13 (2)	55 (2)	1 (2)
N(3)	1839 (2)	1890 (2)	−410 (1)	129 (3)	128 (2)	61 (1)	−28 (2)	30 (2)	12 (1)
C(4)	1736 (3)	2736 (2)	−1154 (2)	157 (4)	122 (3)	79 (2)	−49 (3)	51 (2)	2 (2)
C(5)	519 (3)	2518 (3)	−2219 (2)	179 (4)	159 (3)	68 (1)	−16 (3)	36 (2)	19 (2)
(ii) Barbital									
N(1)	4033 (2)	1623 (2)	1966 (1)	128 (3)	87 (2)	54 (1)	−17 (2)	35 (2)	7 (1)
C(2)	3515 (2)	870 (2)	2465 (2)	114 (3)	64 (2)	62 (2)	−6 (2)	39 (2)	−3 (1)
O(2)	2195 (2)	453 (1)	1934 (1)	120 (2)	98 (1)	84 (1)	−29 (1)	37 (1)	−5 (1)
N(3)	4564 (2)	595 (1)	3622 (1)	117 (2)	70 (1)	60 (1)	−16 (1)	40 (1)	9 (1)
C(4)	6039 (2)	1036 (2)	4324 (2)	113 (3)	57 (1)	59 (1)	−2 (2)	44 (2)	4 (1)
O(4)	6844 (2)	754 (1)	5356 (1)	135 (2)	89 (1)	56 (1)	−7 (1)	35 (1)	17 (1)
C(5)	6658 (2)	1871 (2)	3802 (2)	114 (3)	76 (2)	54 (1)	−17 (2)	36 (2)	7 (1)
C(6)	5486 (2)	2145 (2)	2521 (2)	141 (3)	83 (2)	58 (2)	−21 (2)	46 (2)	3 (1)
O(6)	5822 (2)	2817 (2)	1996 (1)	226 (3)	146 (2)	72 (1)	−69 (2)	62 (2)	22 (1)
C(7)	8137 (3)	1313 (3)	3943 (2)	131 (3)	149 (3)	102 (2)	−1 (3)	69 (3)	16 (2)
C(8)	7844 (5)	151 (4)	3298 (4)	275 (7)	171 (4)	177 (5)	57 (5)	147 (5)	−6 (4)
C(9)	7114 (3)	3056 (2)	4485 (2)	214 (4)	81 (2)	65 (2)	−52 (2)	41 (2)	1 (2)
C(10)	5800 (5)	3656 (3)	4505 (4)	365 (8)	89 (3)	149 (4)	2 (4)	139 (5)	−14 (3)

(*b*) Hydrogen atoms (positional parameters × 10^3)

(i) Imidazole

	x	y	z	B (Å^2)
H(1)	−112 (4)	126 (3)	−276 (3)	7·4 (8)
H(2)	40 (3)	49 (3)	−74 (3)	7·4 (7)
H(4)	252 (3)	332 (3)	−88 (3)	7·1 (7)
H(5)	13 (4)	292 (3)	−288 (3)	8·4 (9)

(ii) Barbital

	x	y	z	B (Å^2)
H(1)	326 (3)	175 (3)	109 (3)	7·3 (7)
H(3)	419 (3)	8 (2)	391 (2)	6·2 (6)
H(71)	891 (3)	122 (2)	484 (2)	6·1 (6)
H(72)	861 (4)	191 (3)	368 (3)	8·3 (8)
H(81)	884 (5)	−17 (4)	337 (4)	12 (1)
H(82)	737 (5)	−48 (4)	358 (3)	11 (1)
H(83)	705 (5)	30 (4)	246 (4)	11 (1)
H(91)	802 (3)	288 (2)	531 (2)	6·0 (6)
H(92)	749 (3)	356 (3)	412 (2)	7·0 (7)
H(101)	546 (5)	317 (4)	489 (4)	11 (1)
H(102)	486 (5)	387 (3)	364 (4)	10 (1)
H(103)	621 (4)	447 (4)	490 (3)	10 (1)

UM00013865
NOVARTIS EXHIBIT 1017
Novartis v. Regents, IPR2023-01346
Page 2611 of 4460

molecule could be recognized. The molecular orientation was consistent with the origin region of the Patterson function, but the position of the molecule was inconsistent with hydrogen-bonding requirements. The correct position was determined using the Q-function of Tollin (1966). Atomic parameters (Table 1) were refined by a full-matrix least-squares procedure. The function minimized was $\sum_H w_H \Delta_H^2$, where $\Delta_H = |F_H^{obs}| - |F_H^{calc}|$. The weights were $w_H^{-1} = 0{\cdot}5 + 0{\cdot}002|F_H|^2$. The atomic scattering factors were those of Cromer & Waber (1965) for C, N, O, and of Stewart, Davidson & Simpson (1965) for H. All hydrogen atomic positions were obtained from difference Fourier syntheses which were calculated after refinement of anisotropic thermal parameters had been introduced for the non-hydrogen atoms. Hydrogen-atom positional and isotropic thermal parameters were subsequently refined. Before the last three cycles of least-squares refinement, 11 strong reflections for which $|F^{calc}| > |F^{obs}|$ were given zero weight. In the final cycle, all parameter changes were less than $0{\cdot}2\sigma$. The final overall R index was 0·065.*†

The molecular structures

The crystal structure consists of a hydrogen-bonded molecular complex and not of the imidazolium barbiturate salt. This conclusion is based upon the position of the hydrogen atom which was found to be at covalent bonding distance from barbital N(1), and also upon the barbiturate bond distances and angles, which closely resemble those of the acid rather than the barbiturate anion (Berking & Craven, 1971).

(i) *Barbital*

The bond lengths and angles are shown in Fig. 1. The oxopyrimidine bond lengths are very similar to those reported in the crystal structures of barbiturates in which oxygen atom O(4) is acceptor for two NH···O=C hydrogen bonds, and atom O(6) is acceptor for none (Craven, Cusatis, Gartland & Vizzini, 1973). There are slight differences of about 0·01 Å in corresponding bond lengths in the two halves of the oxopyrimidine ring which appear to be related to the mode of hydrogen bonding. Thus the bond C(4)=O(4) is longer (1·228 Å) than C(6)=O(6), (1·214 Å). Bond lengths and angles in the ethyl groups are similar to those found in the crystal structures of the three polymorphs of barbital (Craven, Vizzini & Rodrigues, 1969; Craven & Vizzini, 1971).

The atoms of the oxopyrimidine ring are nearly coplanar (Table 2), being more so than in all but one of the 14 molecules from barbiturate crystal structures which are shown in Fig. 3 of Craven *et al.* (1973). The largest atomic displacement from the best least-squares plane of the six pyrimidine ring atoms is 0·038 Å for atom O(2). The carbon atoms of the ethyl groups and C(5) form a chain which is nearly in the extended configuration, with torsion angles of 180·9° and 184·7° about the bonds C(5)–C(7) and C(5)–C(9) respectively.

Table 2. *Best least-squares planes through selected atoms*

The equations for the planes have the form $Lx + My + Nz = D$, where (L, M, N) are direction cosines of the plane normal with respect to the orthogonal axes a^*, b and c, and D is the distance of the plane from the crystallographic origin in Å.

(i) Plane equations

	L	M	N	D
(1)	−0·5812	0·7744	0·2500	0·462
(2)	−0·2787	−0·4932	0·8240	1·505
(3)	0·8117	−0·5552	−0·1814	0·662

(1): Plane through pyrimidine ring carbon and nitrogen atoms.
(2): Plane through atoms C(5) and the ethyl carbon atoms.
(3): Plane through imidazole ring carbon and nitrogen atoms.

(ii) Dihedral angles

(1)∠(2) = 90·8° (1)∠(3) = 18·7°

(iii) Atomic displacements from the planes (Å)

Plane (1)			
N(1)	−0·001	O(2)*	0·038
C(2)	0·008	O(4)*	0·036
N(3)	−0·013	O(6)*	0·008
C(4)	0·010	H(1)*	−0·07
C(5)	−0·003	H(3)*	−0·03
C(6)	−0·001		
Plane (2)			
C(5)	−0·032		
C(7)	0·023		
C(8)	0·006		
C(9)	−0·029		
C(10)	0·032		
Plane (3)			
N(1)	−0·001	H(1)*	−0·12
C(2)	−0·001	H(2)*	−0·04
N(3)	0·003	H(4)*	0·06
C(4)	−0·003	H(5)*	−0·03
C(5)	0·002		

* Atom not included in the best least-squares plane.

* At the request of the referee, a second refinement was carried out with zero weight assigned to reflections with $I < 2\sigma(I)$ as well as the 11 strong reflections. After two cycles, all parameter changes were less than $0{\cdot}2\sigma$. The final value of $R = \sum_H |\Delta_H| / \sum_H |F_H^{obs}|$ remained 0·065 for all reflections and 0·043 excluding reflections with zero weight. In the first refinement, the final weighted R index was 0·060 or 0·053, if reflections with $I < 2\sigma(I)$ were included or excluded respectively. In the second refinement, the weighted R index remained 0·053. A comparison of the two refinements showed that 25 out of 227 parameters were different by more than $1{\cdot}0\sigma$. The largest differences in thermal and positional parameters were $1{\cdot}6\sigma$ for β_{33} of C(5) for imidazole and $1{\cdot}3\sigma$ for x of C(4) in barbital. The most significant differences ($1{\cdot}0\sigma$) in bond lengths and angles observed in the second refinement are the bond lengths N(3)–C(4) of imidazole (1·360 Å) and the internal ring angles at N(3) and C(2) of imidazole (105·0°, 111·6° respectively). Parameter values in Table 1 are those of the first refinement. All interatomic distances and angles are based on these values.

† The table of structure amplitudes has been deposited with the British Library Lending Division as Supplementary Publication No. SUP 30314 (14 pp., 1 microfiche). Copies may be obtained through the Executive Secretary, International Union of Crystallography, 13 White Friars, Chester CH1 1NZ, England.

UM00013866
NOVARTIS EXHIBIT 1017
Novartis v. Regents, IPR2023-01346
Page 2612 of 4460

(ii) *Imidazole*

The atoms of the imidazole molecule are coplanar except possibly for the hydrogen atom at N(1), which is displaced by 0·12 Å (4σ) from the best least-squares plane of the carbon and nitrogen atoms (Table 2). The bond distances and angles (Fig. 2) show small but significant differences from those reported by Will (1969) and Martínez-Carrera (1966) for imidazole itself at room temperature and −150°C respectively. In the case of the bond length C(4)–C(5) which showed the poorest agreement in the previous determinations (1·31 *vs.* 1·35 Å) the value from the barbiturate complex agrees well (1·32 Å) with the room temperature value. In the case of the internal ring angles at N(1), C(2) and N(3), each of which differ by almost 3° in the previous determinations, the values from the barbiturate complex agree well with the low-temperature values. Other differences, which are possibly significant, are that the bond lengths N(1)–C(5) and N(3)–C(4) are somewhat shorter (1·353, 1·357 Å) than previously reported values (1·37, 1·38 Å). We can find no explanation for these differences.

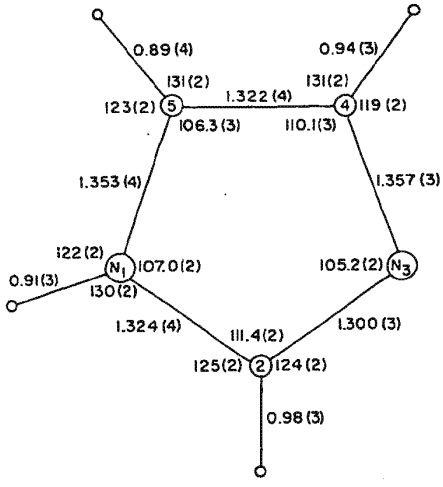


Fig. 2. Bond lengths (Å) and angles (°) for imidazole.

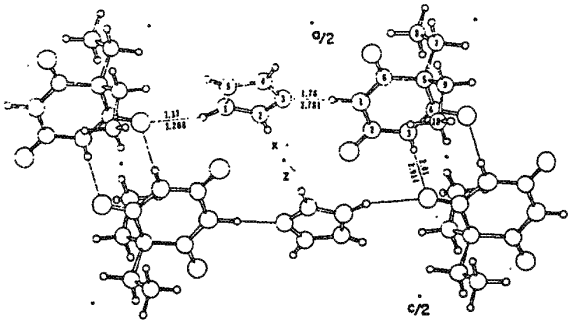


Fig. 3. The crystal structure viewed down b.

The molecular association

The crystal structure consists of hydrogen-bonded ribbons extending along [101] (Fig. 3). The intra-ribbon angle between the planes of the imidazole and barbiturate rings is 18·7° (Table 2). The ribbon plane is approximately parallel to (11$\bar{1}$), with the ribbons packed in a herringbone pattern, when viewed edge on. The barbiturate alkyl substituents from one ribbon fit against the region between two imidazole molecules of one adjacent ribbon and are close to the alkyl substituents of a second adjacent ribbon. The shortest intermolecular distances involving ethyl carbon atoms are $C(7)_{barb}\cdots C(2)_{imid}$ and C(7)···C(10) which are 3·78 and 3·97 Å respectively.

Barbital molecules hydrogen bond both with each other in cyclic dimers, and with imidazole molecules, whereas imidazole molecules hydrogen bond exclusively with barbital.* Within the barbital dimers, the NH···O=C hydrogen bonds have N···O distances (2·91 Å) which are within the range (2·9 ± 0·1 Å) of those observed in the crystal structures of the barbituric acids themselves (Gartland & Craven, 1974). The NH···O=C hydrogen bond in which imidazole is donor and barbital is acceptor is very weak. The N···O distance is long (3·21 Å) and the H···O distance (2·37 Å) is only 0·2 Å shorter than the corresponding van der Waals distance. Gartland & Craven (1974) have noted that NH···O=C hydrogen bonds in barbiturate crystal complexes are generally short when barbiturate participates only as donor, and long, as in the imidazole complex, when barbiturate participates only as acceptor. They have suggested that this is because the barbiturates are stronger hydrogen-bonding donors than acceptors.

If this were the case, similar variations should exist in N···N distances for NH···N hydrogen bonds involving barbiturates. With one exception,† distances are available only for NH···N hydrogen bonds in which barbiturate is donor. However, these do appear to be generally short, and thus consistent with the view that barbiturates are strong hydrogen-bonding donors.

In the barbital–imidazole complex, the NH···N hydrogen bond in which barbital is donor and imidazole is acceptor has N···N distance 2·78 Å and H···N distance 1·76 Å. This N···N distance is slightly shorter than in the hydrogen bonds in the crystal structure of imidazole itself at room temperature (2·81 Å) and at −150°C (2·86 Å) and the N(7)H···N(9) hydrogen bond involving the imidazole moiety of purine (2·85 Å; Watson, Sweet & Marsh, 1965).

* There is a short distance (3·06 Å) between atoms C(2) of imidazole and O(2) of barbital within the same ribbon. This would not appear to be a CH···O hydrogen bond since the H···O distance (2·46 Å) is rather long and the CHO angle is only 119°.

† In guanidinium barbiturate dihydrate (McClure & Craven, 1973) the guanidinium cation is donor and the barbital anion deprotonated nitrogen atom is acceptor for a hydrogen bond with N···N distance 3·00 Å.

UM00013867
NOVARTIS EXHIBIT 1017
Novartis v. Regents, IPR2023-01346
Page 2613 of 4460

A more extensive comparison of such distances is possible by considering those NH···N hydrogen bonds formed by adenine, both in self association and in complexes of adenine derivatives with uracil and uracil-like molecules, including the barbiturates. Table 3 lists the N···N distances for N(6)H···N(1) and N(6)H···N(7) hydrogen bonds in which adenine (I) is both donor and acceptor. There are six distances involving N(1) as acceptor and they range from 2·86 to 3·12 Å with a mean value of 3·00 Å. There are 11 distances involving N(7) as acceptor and they range from 2·93 to 3·13 Å with a mean value of 3·02 Å. These distances are combined and shown as a histogram in Fig. 4. The distribution is similar to that observed by Wallwork (1962) for 25 NH···N hydrogen bonds in crystal structures of various kinds, presumably including purines. He reported a mean N···N distance of 3·07 Å and a standard deviation of 0·11 Å.

The N···N hydrogen bond distance in the barbital/imidazole complex is significantly shorter than any of the distances in Table 3. However, it does fall within the range of distances for NH···N hydrogen bonds in which a uracil-like molecule provides the NH donor and an adenine N(1) or N(7) atom is acceptor. Hydrogen bonds involving N(1) and N(7) of adenine arise in pairings of the Watson–Crick and Hoogsteen type respectively. The N···N distances for these hydrogen

Table 3. *Hydrogen-bonding distance* N···N *between adenine derivatives*

The distances d_1 and d_7 are for hydrogen bonds NH···N in which the 6-amino group is donor and either atom N(1) or N(7) respectively is acceptor.

Crystal structure	d_1	d_7
9-Methyladenine (Stewart & Jensen, 1964)	2·96 Å	3·06 Å
Adenosine (Lai & Marsh, 1972)	–	3·13
Deoxyadenosine hydrate (Watson, Sutor & Tollin, 1965)	2·88	3·03
Adenine hydrochloride hemihydrate (Broomhead, 1948; Cochran, 1951)	–	2·99
N^6-(Δ^2-isopentenyl)-2-methylthioadenine (McMullan & Sundaralingam, 1971)	–	2·99
Uridyl-(3′,5′)-adenosine hemihydrate (Sussman, Seeman, Kim & Berman, 1972; Rubin, Brennan & Sundaralingam, 1972)	–	2·94, 2·98
1-Ethylthymine/8-methyl-9-ethyladenine (Tavale & Sobell; see Sobell, 1972)	3·04	–
1-Methyl-5-bromouracil/9-ethyladenine (Baklagina, Volkenshtein & Kondrashev, 1966)	3·00	–
1-Methyl-5-bromouracil/8-bromo-9-ethyladenine (Tavale, Sakore & Sobell, 1969)	–	3·03
1-Methyl-5-bromouracil/8-methyl-9-ethyladenine/9-ethyladenine (Ambady & Sobell; see Sobell, 1972)	3·12	2·93
5-Phenyl-5-ethylbarbituric acid/8-bromo-9-ethyladenine (Kim & Rich, 1968)	–	3·09, 3·02
8-Bromo-9-ethylhypoxanthine/8-bromo-9-ethyladenine (Sakore & Sobell, 1969)	3·01	–

Table 4. *Hydrogen bonding distances* N···N *between pyrimidine and adenine derivatives*

The distances d_1 and d_7 are for hydrogen bonds in which a pyrimidine NH is donor and either adenine N(1) or N(7) respectively is acceptor.

Crystal structure	d_1	d_7
Sodium adenosyl-(3′,5′)-uridinephosphate.$24H_2O$ (Rosenberg, Seeman, Park-Kim, Suddath, Nicholas & Rich, 1973)	2·82 Å, 2·83	–
5-Bromouridine/adenosine monohydrate (Haschemeyer & Sobell, 1965)	–	2·80 Å
1-Methylthymine/9-methyladenine (Hoogsteen, 1963)	–	2·92
1-Ethylthymine/8-methyl-9-ethyladenine (Tavale & Sobell; see Sobell, 1972)	–	2·89
1-Methyluracil/9-ethyladenine (Mathews & Rich, 1964)	–	2·83
1-Methyl-4-thiouracil/9-methyladenine (Saenger & Suck, 1970)	–	2·94
1-Methyl-5-fluorouracil/9-ethyladenine (Tomita, Katz & Rich, 1967)	–	2·78
1-Methyl-5-bromouracil/9-methyladenine (Baklagina, Volkenshtein & Kondrashev, 1966)	–	2·86
1-Methyl-5-bromouracil/9-ethyladenine (Katz, Tomita & Rich, 1965)	–	2·80
1-Methyl-5-bromouracil/8-methyl-9-ethyladenine/9-ethyladenine (Ambady & Sobell; see Sobell, 1972)	–	2·87
1-Methyl-5-bromouracil/8-bromo-9-ethyladenine (Tavale, Sakore & Sobell, 1969)	2·85	–
1-Methyl-5-iodouracil/9-ethyladenine (Sakore, Tavale & Sobell, 1969)	2·80	2·82
5-Phenyl-5-ethylbarbituric acid/8-bromo-9-ethyladenine (Kim & Rich, 1968)	2·78, 2·80	–
5,5-Diethylbarbituric acid/9-ethyladenine (Voet, 1972)	2·83	2·83
5-Isopropyl-5-bromoallylbarbituric acid/9-ethyladenine (Voet & Rich, 1972)	2·79	2·81
Riboflavin/5′-bromo-5′-deoxyadenosine trihydrate (Voet & Rich, 1971)	–	2·84

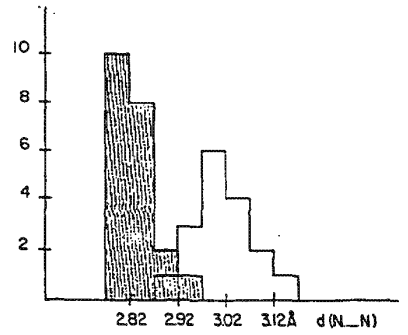


Fig. 4. Histogram of N···N distances in NH···N hydrogen bonds involving adenine. The shaded distribution is for distances from Table 4 (hydrogen bonds in which a uracil-like molecule provides the NH donor and adenine atom N(1) or N(7) is acceptor). The unshaded distribution is for distances from Table 3 (hydrogen bonds in which adenine provides both donor and acceptor). The two distributions overlap at the N···N distance of 2·9 Å.

UM00013868
NOVARTIS EXHIBIT 1017
Novartis v. Regents, IPR2023-01346
Page 2614 of 4460

bonds are listed in Table 4. There are eight distances involving adenine N(1) which range from 2·78 to 2·85 Å with a mean value of 2·81 Å and 13 distances involving N(7) which range from 2·78 to 2·94 Å with a mean value of 2·85 Å. These distances have been combined and their distribution shown as a histogram in Fig. 4. Katz, Tomita & Rich (1965) first noted that uracil-adenine hydrogen bonds at adenine N(7) were short. The distances in Table 3 and Fig. 4 show that their conclusion can be supported by data from more recent crystal structure determinations, and can also be extended to include hydrogen bonds at adenine N(1) and donor NH groups from uracil-like moieties, as found in the barbiturates and riboflavin.

The shortening of NH···N hydrogen bonds in crystal complexes of uracil and adenine derivatives is consistent with the hydrogen-bonding enthalpy change for their association in chloroform solution being greater by about 2 kcal mole^{-1} than for the self association of adenine (Kyogoku, Lord & Rich, 1966). However, the relationship between structural and thermodynamic properties is complex. In particular there may be a significant enthalpy change associated with the second hydrogen bond which accomplishes cyclic dimerization. This hydrogen bond changes from the type NH···N in the self association of adenine to NH···O=C in the adenine-uracil or adenine-barbiturate complexes.* In the case of the crystal complexes of barbiturates with adenine derivatives, with imidazole (IV) and 2-aminopyridine (III), the NH···O=C hydrogen bonds involving barbiturate as acceptor are weak (Hsu & Craven, 1974). This suggests that these complexes involve essentially the interaction of a hydrogen bonding acid (barbiturate) with a hydrogen bonding base [adenine or its analogs (III) and (IV)].

This work was supported by a grant NS-02763 from the U.S. Public Health Service, National Institutes of Health. We thank Dr R. Shiono for the use of computer programs.

* Enthalpy and entropy changes for barbiturate adenine interactions in solution have not been reported.

References

Baklagina, Yu. G., Volkenshtein, M. V. & Kondrashev, Yu. D. (1966). *Zh. Strukt. Khim.* **7**, 399–407.

Berking, B. & Craven, B. M. (1971). *Acta Cryst.* B**27**, 1107–1115.

Broomhead, J. M. (1948). *Acta Cryst.* **1**, 324–329.

Cochran, W. (1951). *Acta Cryst.* **4**, 81–92.

Craven, B. M., Cusatis, C., Gartland, G. L. & Vizzini, E. A. (1973). *J. Mol. Struct.* **16**, 331–342.

Craven, B. M. & Vizzini, E. A. (1971). *Acta Cryst.* B**27**, 1917–1924.

Craven, B. M., Vizzini, E. A. & Rodrigues, M. M. (1969). *Acta Cryst.* B**25**, 1978–1993.

Cromer, D. T. & Waber, J. T. (1965). *Acta Cryst.* **18**, 104–109.

Gartland, G. L. & Craven, B. M. (1974). *Acta Cryst.* B**30**, 980–987.

Germain, G., Main, P. & Woolfson, M. M. (1971). *Acta Cryst.* A**27**, 368–376.

Haschemeyer, A. E. V. & Sobell, H. M. (1965). *Acta Cryst.* **18**, 525–532.

Hsu, I-N. & Craven, B. M. (1974). *Acta Cryst.* B**30**, 994–997.

Hoogsteen, K. (1963). *Acta Cryst.* **16**, 907–916.

Katz, L., Tomita, K.-I. & Rich, A. (1965). *J. Mol. Biol.* **13**, 340–350.

Kim, S. H. & Rich, A. (1968). *Proc. Natl. Acad. Sci. U.S.* **60**, 402–408.

Kyogoku, Y., Lord, R. C. & Rich, A. (1966). *J. Amer. Chem. Soc.* **89**, 496–504.

Kyogoku, Y., Lord, R. C. & Rich, A. (1968). *Nature Lond.* **218**, 69–72.

Lai, T. F. & Marsh, R. E. (1972). *Acta Cryst.* B**28**, 1982–1989.

McClure, R. J. & Craven, B. M. (1973). *Acta Cryst.* B**29**, 1860–1864.

McMullan, R. K. & Sundaralingam, M. (1971). *J. Amer. Chem. Soc.* **93**, 7050–7054.

Martínez-Carrera, S. (1966). *Acta Cryst.* **20**, 783–798.

Mathews, F. S. & Rich, A. (1964). *J. Mol. Biol.* **8**, 89–95.

Rosenberg, J. M., Seeman, N. C., Park-Kim, J. J., Suddath, F. L., Nicholas, H. B. & Rich, A. (1973). *Nature, Lond.* **243**, 150–154.

Rubin, J., Brennan, T. & Sundaralingam, M. (1972). *Biochemistry*, **11**, 3112–3138.

Saenger, W. & Suck, D. (1970). *Nature, Lond.* **227**, 1046–1047.

Sakore, T. D. & Sobell, H. M. (1969). *J. Mol. Biol.* **43**, 77–87.

Sakore, T. D., Tavale, S. S. & Sobell, H. M. (1969). *J. Mol. Biol.* **43**, 361–374.

Sobell, H. M. (1972). *Jerusalem Symposia on Quantum Chemistry and Biochemistry*, Vol. 4, edited by E. D. Bergmann & B. Pullman, pp. 124–146. Jerusalem: Israel Academy of Sciences and Humanities.

Stewart, R. F., Davidson, E. R. & Simpson, W. T. (1965). *J. Chem. Phys.* **43**, 3175–3187.

Stewart, R. F. & Jensen, L. H. (1964). *J. Chem. Phys.* **40**, 2071–2075.

Sussman, J. L., Seeman, N. C., Kim, S. H. & Berman, H. M. (1972). *J. Mol. Biol.* **66**, 403–421.

Taft, R. W., Gurka, D., Joris, L., Schleyer, P. von R. & Rakshys, J. W. (1969). *J. Amer. Chem. Soc.* **91**, 4801–4808.

Tavale, S. S., Sakore, T. D. & Sobell, H. M. (1969). *J. Mol. Biol.* **43**, 375–384.

Tollin, P. (1966). *Acta Cryst.* **21**, 613–614.

Tomita, K.-I., Katz, L. & Rich, A. (1967). *J. Mol. Biol.* **30**, 545–549.

Voet, D. (1972). *J. Amer. Chem. Soc.* **94**, 8213–8222.

Voet, D. & Rich, A. (1971). *Proc. Natl. Acad. Sci. U.S.* **68**, 1151–1156.

Voet, D. & Rich, A. (1972). *J. Amer. Chem. Soc.* **94**, 5888–5891.

Wallwork, S. C. (1962). *Acta Cryst.* **15**, 758–759.

Watson, D. G., Sutor, D. J. & Tollin, P. (1965). *Acta Cryst.* **19**, 111–125.

Watson, D. G., Sweet, R. M. & Marsh, R. E. (1965). *Acta Cryst.* **19**, 573–580.

Will, G. (1969). *Z. Kristallogr.* **129**, 211–221.

UM00013869
NOVARTIS EXHIBIT 1017
Novartis v. Regents, IPR2023-01346
Page 2615 of 4460

This Page is Inserted by IFW Indexing and Scanning Operations and is not part of the Official Record

BEST AVAILABLE IMAGES

Defective images within this document are accurate representations of the original documents submitted by the applicant.

Defects in the images include but are not limited to the items checked:

- ☐ BLACK BORDERS
- ☐ IMAGE CUT OFF AT TOP, BOTTOM OR SIDES
- ☐ FADED TEXT OR DRAWING
- ☐ BLURRED OR ILLEGIBLE TEXT OR DRAWING
- ☐ SKEWED/SLANTED IMAGES
- ☐ COLOR OR BLACK AND WHITE PHOTOGRAPHS
- ☐ GRAY SCALE DOCUMENTS
- ☐ LINES OR MARKS ON ORIGINAL DOCUMENT
- ☐ REFERENCE(S) OR EXHIBIT(S) SUBMITTED ARE POOR QUALITY
- ☐ OTHER: _____

IMAGES ARE BEST AVAILABLE COPY.
As rescanning these documents will not correct the image problems checked, please do not report these problems to the IFW Image Problem Mailbox.

Journal of Inclusion Phenomena and Macrocyclic Chemistry 34: 345–353, 1999.
© 1999 *Kluwer Academic Publishers. Printed in the Netherlands.*

Research Communication

A Simple Correlation between the Structures of Different Crystal Modifications of a Given Host–Guest Complex and their Crystallization Temperatures

BAKHTIYAR IBRAGIMOV
Institute of Bioorganic Chemistry, H. Abdullaev Str., 83, Tashkent, 700143, Uzbekistan

(Received: 8 February 1999)

Abstract. The formation of different crystal modifications of a given host-guest complex depending on the crystallization temperature (pseudopolymorphism) is studied. It is shown that such pseudopolymorphism is a characteristic feature of versatile host compounds. A very important rule for host-guest chemistry is derived from the results of the X-ray structural investigations of pseudopolymorphs: the higher the crystallization temperature of the modification the more closed is the space occupied by guest molecules. On the basis of the formulated rule a recommendation for the topological control and solution of some central problems of supramolecular chemistry is proposed.

Key words: pseudopolymorphism, crystallization temperature, versatile hosts, gossypol, cyclotriveratrylene.

1. Introduction

Many chemical substances are represented as inclusion (host-guest, clathrate) compounds in which molecules of one component (the guest) are enclosed in an intramolecular (monomolecular inclusion) or intermolecular (lattice type inclusion) space of the other component (the host) with no covalent bonds between the two compounds [1]. A very common topological classification of the lattice type inclusion complexes depends on whether there are two-dimensional open inclusions (intercalates or layer type clathrates), one dimensional open channel inclusions (tubulates) or totally enclosed cage inclusions (cryptates) [2]. Inclusion compounds are widely used in practice. They may serve, for example, as containers for storage of toxic, hazardous, very volatile and unpleasant odor compounds [3] or they may be used as matrices for controlled (retarded) release of odorous compounds, pesticides or pheromones [4]. Obviously for purposes of the former applications the containers should be in the form of cryptates whereas host-guest compounds

UM00013871
NOVARTIS EXHIBIT 1017
Novartis v. Regents, IPR2023-01346
Page 2617 of 4460

used for controlled release have to be at least in the tubulate form, i.e., the *topology* of the space occupied by guest molecules is of crucial importance.

If a given inclusion complex is, say, in the tubulate form instead of the desired cryptate form, is it possible to prepare the desired modification and *vice versa*? In other words, can we control the *topology* of the space in the given inclusion compound? This would be possible if at least two crystal modifications of the same host-guest complex exist, i.e., if polymorphism (more exactly pseudopolymorphism) is a characteristic feature of the compounds formed by the given host-guest pair.

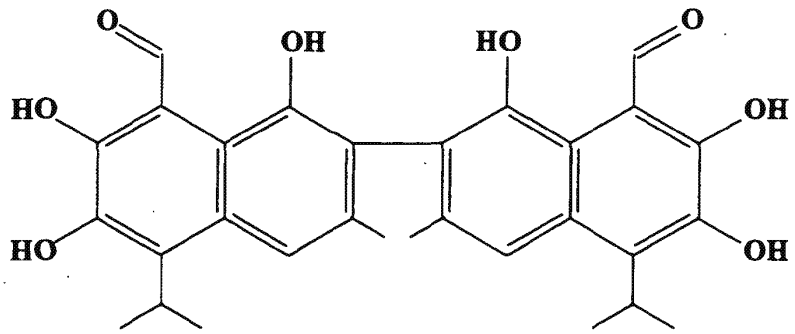
In order to obtain different polymorphs of polymorphic compounds, crystallization from solutions in various solvents, at different temperatures, pressures and concentrations is used. A similar approach should be suitable for searching for the pseudopolymorphs of host-guest compounds. However, to date, systematic investigations in this field have not been carried out apart from four studies in which pseudodimorphs were obtained at relatively high pressure and temperature [5], temperature [6], concentration [7] or by adding a third component to the crystallization solution [8]. Therefore in order to establish the presence of pseudopolymorphism for a given host-guest complex, at least in the case of versatile host compounds, and find out a correlation between the crystal structures of the modifications obtained and their formation conditions we started systematic investigations several years ago. Investigations were carried out on our traditional subject, the versatile host gossypol, its dianiline derivative and three other versatile host compounds. For simplicity a dependence on only crystallization temperature was studied keeping other parameters (pressure and concentration) constant. This communication presents a very important rule for supramolecular chemistry derived from these investigations.

2. Discussion

Gossypol (**I**), (2,2′-[1,1′,6,6′,7,7′-hexahydroxy-3,3′-dimethyl-5,5′ -diisopropyl-8,8′-diformyl]-naphthalene), is a yellow pigment of cotton seeds for which many types of bioactivity are known [9]. Its unique inclusion ability was discovered by our investigations [10]. Over 20 groups of different inclusion structures have been identified for this versatile host compound. Gossypol forms voids lined with apolar groups for inclusion of nonpolar guests and polar host cavities are prepared for the entrapment of polar guests able to form host-guest type H-bonds. Inclusion complexes of these two families never belong to the same isostructural group of crystals [10–12].

All three types of host-guest complexes with different topology are observed among gossypol inclusion complexes. For example, a very unstable 1 : 1 tubulate is formed from solutions of gossypol in dichloromethane. Its decomposition gives rise to the isostructural guest-free crystal with wide empty channels (organic zeolite) [13]. In the complex with trichloromethane the guest molecules are situated

UM00013872
NOVARTIS EXHIBIT 1017
Novartis v. Regents, IPR2023-01346
Page 2618 of 4460



I

in the space between host layers. This 1 : 1 intercalate slowly decomposes under ordinary conditions [14]. Tetrachloromethane forms a 1 : 1 complex with gossypol in which cages occupied by guest molecules are connected via channels [15]. However, the narrow channels restrict the movement of tetrachloromethane molecules because desolvation of this tubulato-cryptate takes place near the melting point of the crystals [16]. An authentic 1 : 0.5 cryptate formed from solutions of gossypol in benzene does not desolvate until melting [14].

An investigation of gossypol crystallization from solutions in dichloromethane at different temperatures shows that at least 3 modifications of the host-guest complex may be obtained (pseudotrimorphism) [17]. At 30 °C the 1 : 1 complex (β-phase), isostructural to that formed between gossypol and tetrachloromethane, is formed instead of the initial α-phase complex. The cryptate type 1 : 0.5 complex (γ-phase), isostructural to the complex between gossypol and benzene, is obtained at 36°C [17]. Thus instead of the wide channels of the α-phase, complex voids intermediate between channels and cages are formed in the β-phase which are replaced by well-defined cages in the γ-phase complex, i.e., the space for guest inclusion gradually becomes less open if the crystallization temperature increases. Crystallization from boiling solutions gives rise to the guest-free host identical with unsolvated gossypol obtained by desolvation of the α-phase complex.

Another low boiling solvent, diethyl ether, gives an unstable 1 : 1 tubulate with gossypol. As a result of its partial desolvation a stable 1 : 0.5 channel type complex is formed. This tubulate with half the amount of channels is also obtained by crystallization at 30 °C. In it guest molecules are situated in more closed channels and leave the crystals at 140 °C [18]. A new polymorph of unsolvated gossypol is crystallized from boiling solutions [19].

In the pyridine trisolvate of gossypol desolvating at 112 °C, the channels are wide and each of them accommodates 3 guest molecules H-bonded to host molecules [20]. At 40 °C a new 1 : 1 tubulate, isostructural to the complex of gossypol with acetone [21], is formed from solutions in pyridine. The total number of chan-

UM00013873
NOVARTIS EXHIBIT 1017
Novartis v. Regents, IPR2023-01346
Page 2619 of 4460

nels is halved and two pyridine molecules H-bonded to gossypol molecules are situated in relatively narrow channels. This complex does not decompose until its melting.

In all these 3 examples increasing the crystallization temperature leads to the formation of the inclusion complexes with "more closed" voids for guest entrapment and to a decrease of the guest component content. "More closed" entrapment has been reached here by alteration of the inclusion space topology (gossypol dichloromethane complex), reduction of the channel dimensions, reduction of the number of channels (gossypol diethyl ether complex) or simultaneous alteration of both of the last two characteristics (gossypol pyridine complex).

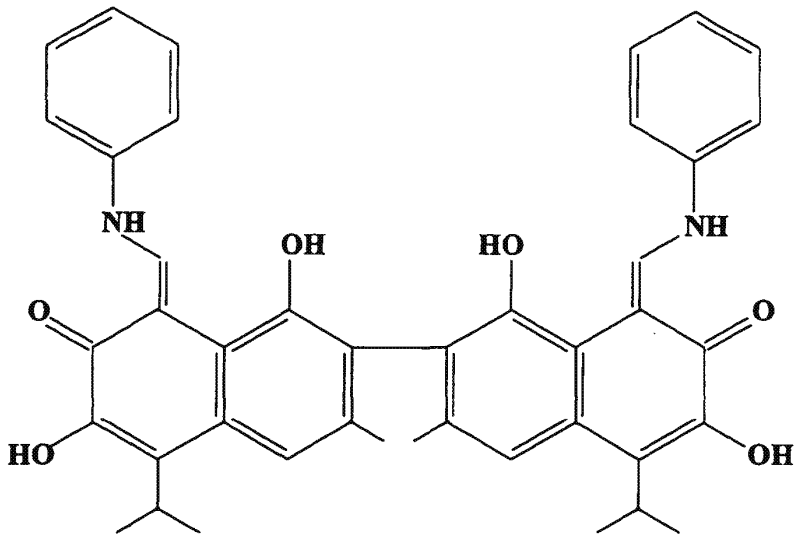
Gossypol is a host which easily includes any substances relating to any group of organic compounds, i.e., it is a highly versatile host compound. The observation of the pseudopolymorphism of a given host-guest complex may be connected with gossypol's unusual versatility. Therefore it is necessary to investigate less versatile hosts with respect to pseudopolymorphism. One such compound is dianilinegossypol (II) because it does not include, for example, alchohols, carboxylic acids and tetrachloromethane [11]. The host-guest complexes between dianilinegossypol and acetone, DMSO and ethylacetate are 1 : 2 cryptate [22], 1 : 2 intercalate [23] and 1 : 1 tubulate [24], respectively. Only cryptates are obtained from solutions of this host in acetone, DMSO and ethylacetate at 35 °C [22], 60 °C [23] and 35 °C [25], respectively, when the initial content of the guest component remains unchanged. These cryptates are absolutely new, i.e., in contrast to the case of gossypol they are not isostructural to any known complexes prepared at ordinary conditions. Two different polymorphs of the unsolvated host are crystallized from boiling solutions in acetone and ethylacetate.

Again crystallization at higher temperatures leads to formation of inclusion complexes with more closed voids. Obviously such behaviour is a universal feature of the host-guest systems. Therefore on the basis of these results the following rule may be formulated. *A pseudopolymorphic versatile host compound responds to an increase of the crystallization temperature by entrapping of the guest component into a "more closed" space in order to withstand the higher thermal mobility of the molecules being enclathrated (it is easy to observe the phenomenon if the solvent (guest) is low boiling). Near to the boiling temperature of the guest its thermal mobility increases to such a degree that an entrapment fails and the guest-free compound is crystallized instead of an inclusion complex.*

As a consequence of this rule it may be concluded that in high temperature complexes the guest content is generally not less than that in the low temperature modifications. Indeed, in order to construct an inclusion system with more closed voids a greater amount of the host molecules per one guest molecule (or a lesser amount of the guest molecules per one host molecule) are required and it is readily observed in practice.

Following this rule it is possible to make some important recommendations in order to obtain host-guest compounds with altered topology. *If a host-guest*

UM00013874
NOVARTIS EXHIBIT 1017
Novartis v. Regents, IPR2023-01346
Page 2620 of 4460



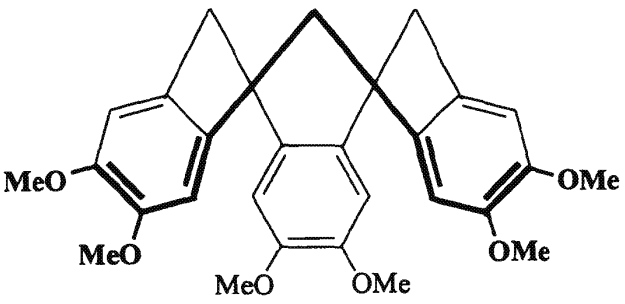
II

complex obtained at room temperature is tubulate, its cryptate (or another less open) modification can be prepared by increasing the crystallization temperature. If the host-guest complex is cryptate, its tubulate (or another more open) form can be prepared by decreasing the crystallization temperature.

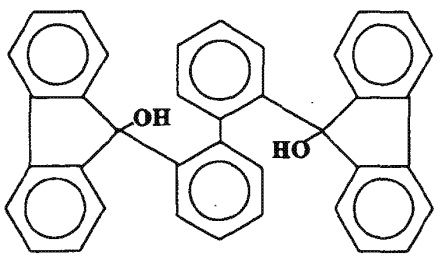
To check the validity of the postulated rule three versatile host compounds were chosen. Cyclotriveratrylene (**III**), a well known versatile host compound with a trigonal intramolecular cavity, forms tubulates with intermolecular inclusion of solvent molecules [26]. Intracavity (endocyclic) complexes of this compound with frequently used solvents have not been obtained to date. If this type of complex, especially a modification in which solvent molecules are entrapped between two facing host molecule cups exists, it will crystallize as a clathrate with more closed space for guest inclusion. According to the proposed recommendation in order to prepare such a modification, crystallization should be carried out at higher temperatures. Carrying out the crystallization of cyclotriveratrylene from its solution in acetone at 40 °C we found an absolutely new 1 : 0.25 sandwich type endocyclic cryptate [27, 28] instead of the usual 1 : 0.5 tubulate [26].

The host-guest complex of 2,2′-bis(9-hydroxy-9-fluorenyl) biphenyl (**IV**) with acetone is a 1 : 1 cryptate [29]. If another complex with more open voids for guest inclusion is possible it must be obtained by decreasing the preparation temperature. Indeed, the anticipated modification in the form of the very unstable 1 : 2 tubulate was obtained by crystallization at 10 °C [30].

UM00013875
NOVARTIS EXHIBIT 1017
Novartis v. Regents, IPR2023-01346
Page 2621 of 4460



III



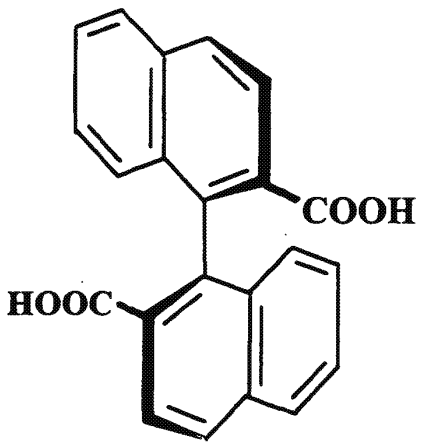
IV

Another example of the high temperature modification of the initial complex is provided by the versatile host, 1,1′-binaphthyl-2,2′-dicarboxylic acid (**V**), which forms a 1 : 2 tubulate with ethanol [31]. At 60 °C the 1 : 0.5 tubulate with half the number of channels is crystallized. The unsolvated host is obtained by crystallization at 100 °C [32]. Analysis of the crystal structures shows that the 1 : 0.5 tubulate is an intermediate phase between the initial modification and the unsolvated host.

These examples demonstrate the power and correctness of the formulated rule and the results following from its recommendations. Using this rule one may solve the following problems which are very important for practical supramolecular sciences:

- to obtain an inclusion complex with the required topology (topological control);
- to prepare pure (solvent free) substances or substances with a reduced content of solvent molecules if the compound of interest is represented by the stable inclusion complex of the versatile host compound;

UM00013876
NOVARTIS EXHIBIT 1017
Novartis v. Regents, IPR2023-01346
Page 2622 of 4460



V

- to introduce the new method for obtaining inclusion complexes with solid state guests (also with liquids in which the host is insoluble) according to which host and guest are dissolved in frequently used solvents and crystallization carried at temperatures slightly higher than the boiling point of the solvent;
- to prepare thermodynamically stable modifications of unstable host-guest complexes (as a rule, host-guest complexes with more closed voids for guest entrapment are more stable);
- to control the physico-chemical characteristics of the inclusion compounds and the biopharmaceutical properties (e.g., solubility, stability during storage *etc.*) of crystalline medicines (some solid state drugs are versatile host compounds);
- to explain the instability of physico-chemical (also biopharmaceutical for crystalline medicines) parameters of versatile host compounds caused by crystallization of different host-guest complex modifications under slightly different conditions (concentration, ambient temperature, pressure and humidity) for various samples;
- to explain the decomposition (desolvation) of inclusion complexes of the versatile hosts or sorption and desorption mechanisms between crystalline hosts (sensor materials) and organic vapours because these processes take place step by step passing through intermediate phases (pseudopolymorphic stages).

UM00013877
NOVARTIS EXHIBIT 1017
Novartis v. Regents, IPR2023-01346
Page 2623 of 4460

Acknowledgements

The author is grateful to his co-workers for their assistance in the investigations and to Professor E. Weber for samples of 1,1′-binaphthyl-2,2′-dicarboxylic acid and 2,2′-bis(9-hydroxy-9-fluorenyl) biphenyl and for his continuing interest in the research.

References

1. F. Cramer: *Angew.Chem*, **64**, 437 (1952).
2. E. Weber and H.-P. Josel: *J.Incl.Phenom.* **1**, 79 (1983)
3. D. Duchêne and D. Wouessidjewe: *J. Coord. Chem.* **27**, 223 (1992)
4. N. Rysanek, G. L. Bas, F. Villain and G. Tsoucaris: *Acta Crystallogr.* C**52**, 2932 (1996).
5. K. Hamada, M. Oh-hira, T. Fujiwara and F. Toda: *Acta Crystallogr.* C**48**, 1969 (1992).
6. A. T. Ung, R. Bishop, D. C. Craig, I. G. Dance and M. L. Scudder: *Tetrahedron* **49**, 639 (1993).
7. F. Toda, Y. Tagami and T. C. W. Mak: *Bull. Chem. Soc. Jpn.* **59**, 1189 (1986)
8. K. Nakano, K. Sada and M. Miyata: *J. Chem. Soc., Chem. Commun.* 989 (1996)
9. N. I. Baram and A. I. Ismailov: *Khimiya Prirodnyh Soedineniy* **3**, 334 (1993); *Chem. Abstr.* **123**, 245876b (1995).
10. B. T. Ibragimov, S. A. Talipov and P. M. Zorky: *Supramol.Chem.* **3**, 147 (1994).
11. M. Gdaniec, B. T. Ibragimov and S. A. Talipov: in Comprehensive Supramolecular Chemistry, Volume 6, (Solid-state Supramolecular Chemistry-Crystal Engineering). p. 117, eds. J.L. Atwood, J.E.D. Davies, D.D. MacNicol and F. Vögtle, Elsevier Science, Oxford, (1996).
12. B. T. Ibragimov and S. A. Talipov: *Mol. Cryst. Liq. Cryst.* **270**, 305 (1996).
13. B. T. Ibragimov, S. A. Talipov and T. F. Aripov: *J. Incl. Phenom.* **17**, 317 (1994).
14. M. Gdaniec, B. T. Ibragimov and S. A. Talipov: *J. Incl. Phenom.* **9**, 231 (1990).
15. B. T. Ibragimov, S. A. Talipov, G. B. Nazarov, B. N. Dadabaev, T. F. Aripov, A. I. Ismailov and A. S. Sadykov: *Khimiya Prirodnyh Soedineniy,* 113 (1986); *Chem. Abstr.* **105**, 227069j (1986).
16. B. T. Ibragimov, S. A. Talipov, T. F. Aripov and A. S. Sadykov: *J. Incl. Phenom.* **8**, 323 (1990).
17. B. T. Ibragimov, Z. G. Tiljakov, K. M. Beketov and S. A. Talipov: *J. Incl. Phenom.* **27**, 99 (1997).
18. S. A. Talipov, B. T. Ibragimov, N. G. Tishenko, T. F. Aripov, G. B. Nazarov, B. V. Strokopitov and K. M. Polyakov: *Krystallograhpiya* **33**, 384 (1988); *Chem. Abstr.* **109**, 170100j (1988).
19. B. T. Ibragimov and S. A. Talipov: *J. Incl. Phenom.* **17**, 325 (1994).
20. B. T. Ibragimov, B. N. Dadabaev, S. A. Talipov and A. A. Abduvakhabov: *Khimiya Prirodnyh Soedineniy*, 186 (1992).
21. B. T. Ibragimov, M. Gdaniec and B. N. Dadabaev: *J. Incl. Phenom.* **8**, 333 (1990).
22. K. M. Beketov, B. T. Ibragimov and S. A. Talipov: *J. Incl. Phenom.* **28**, 141 (1997).
23. B. T. Ibragimov, K. M. Beketov, S. A. Talipov and T. F. Aripov: *J. Incl. Phenom.* **29**, 23 (1997).
24. G. B. Nazarov, B. T. Ibragimov and T. F. Aripov: *Khimiya Prirodnyh Soedineniy,* 661 (1988); *Chem. Abstr.* **111**, 174420j (1989).
25. K. M. Beketov, B. T. Ibragimov, S. A. Talipov, K. K. Makhkamov and T. F. Aripov: *J. Incl. Phenom.* **27**, 105 (1997).
26. A. Collet: in Comprehensive Supramolecular Chemistry, Volume 6, (Solid-state Supramolecular Chemistry-Crystal Engineering). p. 281, eds. J.L. Atwood, J.E.D. Davies, D.D. MacNicol and F. Vögtle, Elsevier Science, Oxford, (1996).
27. B. T. Ibragimov, K. K. Makhkamov and K. M. Beketov: *Abstracts of 10th Inter. Symp. Org. Cryst. Chem. Poznan-Rydzyna*, Poland, 77 (1997).
28. B. T. Ibragimov, K. K. Makhkamov and K. M. Beketov: *J. Incl. Phenom.* in press, (1999).
29. N. Sardone: *Private Communication* (1996).

UM00013878
NOVARTIS EXHIBIT 1017
Novartis v. Regents, IPR2023-01346
Page 2624 of 4460

30. K. K. Makhkamov, K. M. Beketov, B. T. Ibragimov, E. Weber, and J. Seidel: *Abstracts of XII International Symposium on Molecular Inclusion and Recognition, Warsaw*, Poland, P-1-2 (1998).
31. E. Weber, I. Csoregh, B. Stensland and M. Czugler: *J. Am. Chem. Soc.* **106**, 3297 (1984).
32. B. T. Ibragimov, K. M. Beketov, K. K. Makhkamov and E. Weber: *J. Chem. Soc., Perkin Trans. 2*, 1349 (1997).

UM00013879
NOVARTIS EXHIBIT 1017
Novartis v. Regents, IPR2023-01346
Page 2625 of 4460

This Page is Inserted by IFW Indexing and Scanning Operations and is not part of the Official Record

BEST AVAILABLE IMAGES

Defective images within this document are accurate representations of the original documents submitted by the applicant.

Defects in the images include but are not limited to the items checked:

- ☐ BLACK BORDERS
- ☐ IMAGE CUT OFF AT TOP, BOTTOM OR SIDES
- ☐ FADED TEXT OR DRAWING
- ☐ BLURRED OR ILLEGIBLE TEXT OR DRAWING
- ☐ SKEWED/SLANTED IMAGES
- ☐ COLOR OR BLACK AND WHITE PHOTOGRAPHS
- ☐ GRAY SCALE DOCUMENTS
- ☐ LINES OR MARKS ON ORIGINAL DOCUMENT
- ☐ REFERENCE(S) OR EXHIBIT(S) SUBMITTED ARE POOR QUALITY
- ☐ OTHER: _____

IMAGES ARE BEST AVAILABLE COPY.
As rescanning these documents will not correct the image problems checked, please do not report these problems to the IFW Image Problem Mailbox.

which prevent the close approach of the appropriate γ-H atom to O.

In conclusion, the solid-state photolyses are topochemically controlled, with minimum motion resulting in formation of the *cis*-OH photoproduct (1) (Fig. 3) *via* interaction of *p*-orbital lobes *a* and *b* (Fig. 2), while the less-sterically hindered *trans*-OH compounds [(2) and (4)] are formed in solution reactions.

Asymmetric synthesis

The crystallographic study of 4-chloro-α-(3-methyladamantyl)acetophenone indicated that the material crystallized in the chiral space group $P2_12_12_1$ (Table 1). This suggested the possibility of producing an optically active product mixture from the achiral reactant material (Evans, Garcia-Garibay, Omkaram, Scheffer, Trotter & Wireko, 1986); the important factor is that the (chance) crystallization of the achiral reactant in a chiral space group provides a chiral environment for the reactant. Products formed by photolysis in solution or in a polycrystalline aggregate show no trace of optical activity. However, when a single crystal weighing 313 mg was photolysed, the major product was the *cis*-OH compound (1), with $[\alpha]_D = -21{\cdot}6°$, and an enantiomeric excess of 80% (as determined by the use of a chiral NMR shift reagent). The lack of total stereospecificity may be due to inversion twinning in the crystal, or to disruption of the crystal lattice as the reaction proceeds.

We thank Professor J. R. Scheffer and Dr N. Omkaram for collaborative photochemical studies, the Natural Sciences and Engineering Council of Canada for financial support, and the University of British Columbia Computing Centre for assistance.

References

EVANS, S. V., GARCIA-GARIBAY, M., OMKARAM, N., SCHEFFER, J. R., TROTTER, J. & WIREKO, F. (1986). *J. Am. Chem. Soc.* **108**, 5648–5650.

EVANS, S. V. & TROTTER, J. (1988). *Acta Cryst.* B**44**, 63–72.

EVANS, S. V. & TROTTER, J. (1989). *Acta Cryst.* B**45**, 159–162.

International Tables for X-ray Crystallography (1974). Vol. IV, pp. 99–102 and 149. Birmingham: Kynoch Press. (Present distributor Kluwer Academic Publishers, Dordrecht.)

OMKARAM, N. (1986). PhD Thesis, Univ. of British Columbia, Canada.

Acta Cryst. (1989). B**45**, 505–512

Structural Study of Histamine H_2-Receptor Antagonists. Five 3-[2-(Diaminomethyleneamino)-4-thiazolylmethylthio]propionamidine and -amide Derivatives

BY TOSHIMASA ISHIDA, YASUKO IN, MITSUNOBU DOI AND MASATOSHI INOUE

Osaka University of Pharmaceutical Sciences, 2-10-65 Kawai, Matsubara, Osaka 580, Japan

AND ISAO YANAGISAWA

Central Research Laboratories, Yamanouchi Pharmaceutical Co. Ltd, No. 1-8, Azusawa 1-chome, Itabashi-ku, Tokyo 174, Japan

(*Received 28 January 1989; accepted 1 June 1989*)

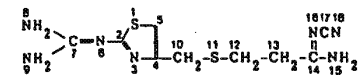
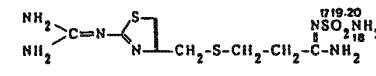
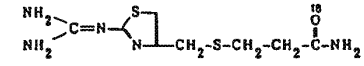
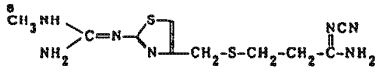
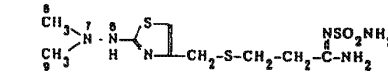
Abstract

(1) N^2-Cyano-3-[2-(diaminomethyleneamino)-4-thiazolylmethylthio]propionamidine monohydrate, $C_9H_{13}N_7S_2.H_2O$, $M_r = 301{\cdot}39$, $P\bar{1}$, $a = 11{\cdot}089$ (4), $b = 9{\cdot}130$ (6), $c = 7{\cdot}033$ (5) Å, $\alpha = 100{\cdot}99$ (6), $\beta = 83{\cdot}86$ (5), $\gamma = 86{\cdot}80$ (7)°, $V = 692{\cdot}9$ (6) Å^3, $Z = 2$, $D_m = 1{\cdot}443$ (2), $D_x = 1{\cdot}444$ g cm^{-3}, λ(Cu $K\alpha$) = 1·5418 Å, $\mu = 34{\cdot}86$ cm^{-1}, $F(000) = 316$, $T = 293$ K, $R = 0{\cdot}043$ for 2219 reflections. (2) 3-[2-(Diaminomethyleneamino)-4-thiazolylmethylthio]-N^2-sulfamoylpropionamidine (famotidine) hydrochloride, $C_8H_{15}N_7O_2S_3.HCl$, $M_r = 373{\cdot}90$, Cc, $a = 15{\cdot}205$ (3), $b = 14{\cdot}442$ (3), $c = 9{\cdot}262$ (1) Å, $\beta = 124{\cdot}00$ (5)°, $V = 1686{\cdot}1$ (7) Å^3, $Z = 4$, $D_m = 1{\cdot}470$ (2), $D_x = 1{\cdot}473$ g cm^{-3}, μ(Cu $K\alpha$) = 56·09 cm^{-1}, $F(000) = 776$, $T = 293$ K, $R = 0{\cdot}036$ for 1411 reflections. (3) 3-[2-(Diaminomethyleneamino)-4-thiazolylmethylthio]-propionamide, $C_8H_{13}N_5OS_2$, $M_r = 259{\cdot}35$, $P2_12_12_1$, $a = 5{\cdot}472$ (1), $b = 18{\cdot}260$ (5), $c = 11{\cdot}890$ (3) Å, $V = 1188{\cdot}0$ (5) Å^3, $Z = 4$, $D_m = 1{\cdot}448$ (1), $D_x = 1{\cdot}450$ g cm^{-3}, μ(Cu $K\alpha$) = 39·26 cm^{-1}, $F(000) = 544$, $T = 293$ K, $R = 0{\cdot}036$ for 1260 reflections. (4) 3-{2-[Amino(methylamino)methyleneamino]-4-thiazolylmethylthio}-N^2-cyanopropionamidine, $C_{10}H_{15}N_7S_2$, $M_r = 297{\cdot}40$, $P2_1/c$, $a = 14{\cdot}235$ (5), $b = 5{\cdot}453$ (2), $c = 17{\cdot}782$ (7) Å, $\beta = 90{\cdot}13$ (6)°, $V = 1380{\cdot}2$ (8) Å^3, $Z = 4$, $D_m = 1{\cdot}420$ (1), $D_x = 1{\cdot}431$ g cm^{-3}, μ(Cu $K\alpha$) =

0108-7681/89/050505-08$03.00 © 1989 International Union of Crystallography

UM00013881
NOVARTIS EXHIBIT 1017
Novartis v. Regents, IPR2023-01346
Page 2627 of 4460

Table 1. *Chemical structures with the atomic numberings and H_2-receptor antagonist activities of famotidine analogues*

	Chemical structure	$ED_{50}(M)$*
(1)		1.8×10^{-7}
(2)		2.7×10^{-7}
(3)		1.0×10^{-6}
(4)		1.2×10^{-6}
(5)		$> 10^{-4}$

*H_2-receptor antagonist activity in guinea pig atrium.

$34.39\ cm^{-1}$, $F(000) = 624$, $T = 293$ K, $R = 0.035$ for 2210 reflections. (5) 3-[2-(*N'*,*N'*-dimethylhydrazino)-4-thiazolylmethylthio]-*N*^{2}-sulfamoylpropionamidine–maleic acid (1/1), $C_9H_{18}N_6O_2S_3.C_4H_4O_4$, $M_r = 454.53$, $P\bar{1}$, $a = 14.802$ (4), $b = 13.275$ (3), $c = 5.236$ (2) Å, $\alpha = 93.42$ (2), $\beta = 93.68$ (2), $\gamma = 84.01$ (2)°, $V = 1019.8$ (5) Å^3, $Z = 2$, $D_m = 1.475$ (2), $D_x = 1.480\ g\ cm^{-3}$, $\mu(Cu\ K\alpha) = 36.57\ cm^{-1}$, $F(000) = 476$, $T = 293$ K, $R = 0.055$ for 3326 reflections. These molecules exhibit different activities as histamine H_2-receptor antagonists. The possible relationship between the molecular conformation and inhibitory activity is discussed.

Introduction

To design a biologically active compound, it is important to identify the key atoms and their spatial orientation responsible for the activity emergency. When information on the stereostructure of the receptor molecule is lacking, an alternative methodology is to compare the molecular conformations in a series of compounds of structural and physicochemical similarities but of different pharmaceutical activities. The conformational characteristics thus obtained would be useful for considering new potent compounds.

The therapeutic success of cimetidine as a histamine H_2-receptor antagonist (Brogden, Heel, Speight & Avery, 1978) led to the development of more potent and/or longer lasting drugs for human peptic ulcers. Consequently, 3-[2-(diaminomethyleneamino)-4-thiazolylmethylthio]-*N*^{2}-sulfamoylpropionamidine (famotidine) was designed as a more-potent ulcer drug (Takeda, Takagi & Maeno, 1981, 1983; Takeda, Takagi, Yashima & Maeno, 1982; Takagi, Takeda & Maeno, 1982; Harada, Terai & Maeno, 1983; Yanagisawa, Hirata & Ishii, 1987). The chemical structure of famotidine differs from cimetidine in the central aromatic ring and the end group of the side chain: a thiazole ring and an amidine group in the former, and an imidazole ring and a guanidine group in the latter.

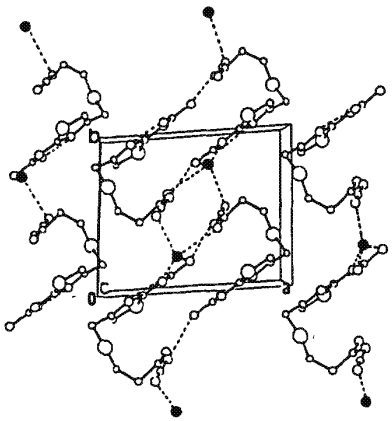
This paper deals with the X-ray crystal analyses of five famotidine analogues exhibiting different antagonist activities; their chemical formulae with the atomic numberings used are given in Table 1, along with their inhibitory activities (Yanagisawa, Hirata & Ishii, 1984, 1987). The conformational comparison of these compounds with cimetidine and ranitidine is useful for considering the structure–activity relationship of H_2-receptor antagonists (Ishida, In, Shibata, Doi, Inoue & Yanagisawa, 1987).

Experimental

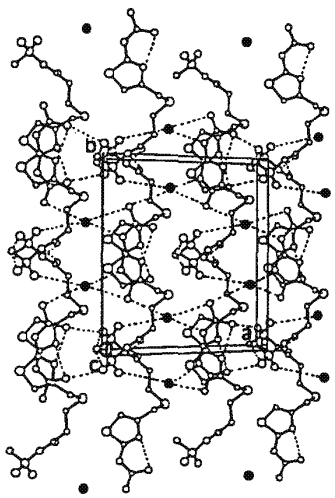
Synthesized by the method of Yanagisawa *et al.* (1984, 1987), recrystallized from methanol/acetone/water (1), methanol [(2) and (3)], ethanol (4) and methanol/water (5). Crystal size (mm): (1) 0·1 × 0·2 × 0·5; (2) 0·3 × 0·3 × 0·4; (3) 0·3 × 0·1 × 0·4; (4) 0·2 × 0·2 × 0·4; (5) 0·1 × 0·2 × 0·5. D_m by flotation method (benzene–carbon tetrachloride mixture). Rigaku four-circle diffractometer with graphite-monochromated Cu $K\alpha$ radiation. Cell parameters from 25 reflections with $15 < 2\theta < 30°$. Intensity data measured by ω–2θ continuous scan mode; scan speed 2–4° min^{-1} (θ); scan range ($A + 0.15\tan\theta$)° with A 0·8 to 1·2°; 5 s stationary background counts; 2θ range 2–130°; *hkl* range: (1) 0–±13, 0–±10, 0–8; (2) 0–±17, 0–16, 0–10; (3) 0–6, 0–21, 0–13; (4) 0–±16, 0–6, 0–20; (5) 0–±17, 0–±15, 0–6. Four standard reflections monitored every 100 reflections; no significant variation of intensities. Corrections for Lorentz and polarization effects; no absorption corrections. Number of measured reflections, number of observed [$I > \sigma(I)$] reflections in parentheses: (1) 2582 (2219); (2) 1439 (1411); (3) 1269 (1260); (4) 2443 (2210); (5) 3913 (3326). Structure solved by heavy-atom (2) or direct methods, *MULTAN*78 (Main, Hull, Lessinger, Germain, Declercq & Woolfson, 1978). All H atoms located on respective difference Fourier maps. Block-diagonal least-squares refinements with anisotropic temperature factors for non-H atoms and isotropic ones for H atoms. The function minimized was $\sum w(|F_o| - |F_c|)^2$, where the following w was used: $w = 1.0/[\sigma(F_o)^2 + m_1|F_o| + m_2|F_o|^2]$ for $|F_o| > \sigma(F_o)$; values

UM00013882
NOVARTIS EXHIBIT 1017
Novartis v. Regents, IPR2023-01346
Page 2628 of 4460

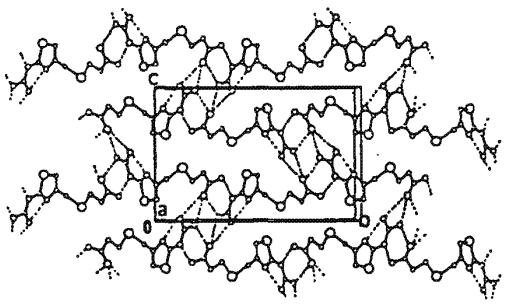
of m_1 and m_2: (1) 0·0302, −0·0004; (2) 0·0417, −0·0004; (3) 0·0454, −0·0006; (4) 0·0324, −0·0003; (5) 0·0627, −0·0009. Final wR and S: (1) 0·053, 1·198; (2) 0·030, 1·052; (3) 0·040, 1·109; (4) 0·034, 1·145; (5) 0·041, 1·326. $(\Delta/\sigma)_{max}$: (1) 0·40; (2) 0·33; (3) 0·38; (4) 0·32; (5) 0·35. $(\Delta\rho)_{max}$ and $(\Delta\rho)_{min}$ (e Å^{-3}): (1) 0·35, −0·28; (2) 0·22, −0·18; (3) 0·25, −0·19; (4) 0·25, −0·15; (5) 0·30, −0·22. Scattering factors from *International Tables for X-ray Crystallography* (1974). All numerical computations performed on an ACOS 900 computer at the Computation Center, Osaka University, using *The Universal Crystallographic Computing System – Osaka* (1979).*



(1)



(2)

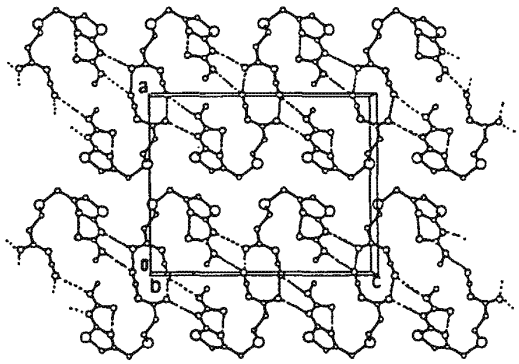


(3)

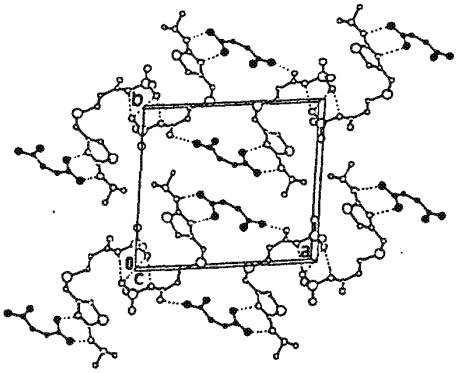
Discussion

Table 2 lists final coordinates and B_{eq} values for the non-H atoms. Fig. 1 shows the views of perspective molecular packings, in which dotted lines represent possible intra- or intermolecular hydrogen bonds. The hydrogen-bond distances and angles are summarized in Table 3.

* Lists of structure factors, anisotropic temperature factors and H-atom parameters have been deposited with the British Library Document Supply Centre as Supplementary Publication No. SUP 51975 (53 pp.). Copies may be obtained through The Executive Secretary, International Union of Crystallography, 5 Abbey Square, Chester CH1 2HU, England.



(4)



(5)

Fig. 1. Perspective views of crystal packings of (1)–(5). The dotted lines represent hydrogen bonds. The filled circles show waters of crystallization in (1), chloride ions in (2) and maleic acids in (5).

UM00013883
NOVARTIS EXHIBIT 1017
Novartis v. Regents, IPR2023-01346
Page 2629 of 4460

Table 2. *Fractional coordinates and equivalent isotropic temperature factors* (Å²) *of compounds* (1)–(5)

W represents the water molecule.

$$B_{eq} = \tfrac{4}{3}\sum_i\sum_j \mathbf{a}_i.\mathbf{a}_j B_{ij}.$$

	x	*y*	*z*	B_{eq}
(1)				
S(1)	0·79184 (6)	0·09405 (7)	0·64019 (9)	3·38 (3)
C(2)	0·7598 (2)	0·0187 (3)	0·4068 (3)	2·86 (9)
N(3)	0·8364 (2)	0·0484 (2)	0·2679 (3)	3·26 (9)
C(4)	0·9270 (2)	0·1354 (3)	0·3454 (4)	3·3 (1)
C(5)	0·9161 (2)	0·1696 (3)	0·5426 (4)	3·5 (1)
N(6)	0·6603 (2)	−0·0626 (2)	0·3913 (3)	3·34 (9)
C(7)	0·6196 (2)	−0·1026 (3)	0·2203 (4)	3·5 (1)
N(8)	0·5211 (2)	−0·1864 (3)	0·2193 (4)	4·8 (1)
N(9)	0·6650 (2)	−0·0704 (3)	0·0564 (3)	4·8 (1)
C(10)	1·0213 (2)	0·1841 (3)	0·2072 (4)	3·7 (1)
S(11)	0·95688 (6)	0·31350 (8)	0·0703 (1)	3·71 (3)
C(12)	0·8975 (2)	0·4669 (3)	0·2689 (4)	3·6 (1)
C(13)	0·7837 (3)	0·5472 (3)	0·2191 (4)	3·7 (1)
C(14)	0·6828 (2)	0·4425 (3)	0·1862 (4)	3·3 (1)
N(15)	0·6400 (2)	0·3825 (3)	0·3316 (3)	4·4 (1)
N(16)	0·6366 (2)	0·4072 (2)	0·0195 (3)	3·7 (1)
C(17)	0·6770 (3)	0·4682 (3)	−0·1285 (4)	4·0 (1)
N(18)	0·7044 (3)	0·5140 (3)	−0·2692 (4)	5·3 (1)
O(1)*W*	0·5755 (2)	0·7909 (2)	0·6884 (3)	4·36 (9)
(2)				
S(1)	0·46667 (9)	0·0758 (1)	0·4354 (2)	6·44 (5)
C(2)	0·3604 (3)	0·0053 (3)	0·3760 (6)	4·1 (2)
N(3)	0·2680 (3)	0·0413 (2)	0·2800 (5)	4·1 (1)
C(4)	0·2770 (4)	0·1345 (3)	0·2468 (5)	4·7 (2)
C(5)	0·3767 (4)	0·1629 (3)	0·3218 (7)	5·6 (2)
N(6)	0·3827 (2)	−0·0870 (2)	0·4323 (5)	4·5 (1)
C(7)	0·3060 (3)	−0·1534 (3)	0·3787 (5)	3·6 (1)
N(8)	0·3422 (3)	−0·2401 (2)	0·4385 (5)	4·5 (1)
N(9)	0·2069 (2)	−0·1364 (2)	0·2749 (5)	4·0 (1)
C(10)	0·1776 (4)	0·1899 (3)	0·1387 (5)	4·7 (2)
S(11)	0·1100 (1)	0·21254 (7)	0·2446 (2)	5·30 (4)
C(12)	0·2057 (4)	0·2813 (3)	0·4344 (6)	5·3 (2)
C(13)	0·1990 (3)	0·3831 (3)	0·3907 (5)	4·6 (2)
C(14)	0·2780 (3)	0·4420 (3)	0·5400 (5)	3·5 (1)
N(15)	0·2656 (3)	0·4502 (3)	0·6708 (4)	4·1 (1)
N(16)	0·3500 (2)	0·4801 (2)	0·5258 (4)	3·2 (1)
S(17)	0·43854 (8)	0·54953 (6)	0·6750 (1)	2·85 (3)
N(18)	0·5283 (2)	0·4913 (2)	0·8434 (4)	4·1 (1)
O(19)	0·4891 (2)	0·5894 (2)	0·5968 (4)	4·0 (1)
O(20)	0·3936 (2)	0·6128 (2)	0·7373 (4)	4·1 (1)
Cl(21)	0·10148 (8)	0·66179 (7)	0·2242 (2)	4·16 (3)
(3)				
S(1)	0·8771 (2)	0·54985 (5)	0·65159 (8)	2·87 (4)
C(2)	0·8993 (7)	0·5720 (2)	0·7946 (3)	2·3 (1)
N(3)	1·0785 (6)	0·5379 (2)	0·8464 (3)	2.5 (1)
C(4)	1·2065 (8)	0·4931 (2)	0·7744 (3)	2·5 (1)
C(5)	1·1265 (9)	0·4924 (2)	0·6660 (4)	3·3 (2)
N(6)	0·7329 (7)	0·6205 (2)	0·8340 (3)	2·8 (1)
C(7)	0·7382 (8)	0·6422 (2)	0·9411 (3)	2·6 (1)
N(8)	0·5666 (9)	0·6884 (2)	0·9758 (3)	4·2 (2)
N(9)	0·9027 (9)	0·6207 (2)	1·0154 (3)	4·1 (2)
C(10)	1·4100 (8)	0·4485 (2)	0·8192 (4)	2·9 (2)
S(11)	1·3074 (2)	0·37079 (5)	0·90363 (8)	2·81 (4)
C(12)	1·116 (1)	0·3243 (2)	0·8036 (4)	3·5 (2)
C(13)	0·9547 (9)	0·2691 (2)	0·8609 (4)	3·4 (2)
C(14)	0·7622 (8)	0·2383 (2)	0·7841 (3)	2·7 (1)
N(15)	0·6428 (7)	0·1796 (2)	0·8182 (2)	3·0 (1)
O(16)	0·7168 (7)	0·2675 (2)	0·6917 (3)	3·9 (1)
(4)				
S(1)	0·35214 (4)	0·9111 (1)	0·79372 (3)	3·43 (2)
C(2)	0·3046 (1)	0·6568 (4)	0·7477 (1)	2·71 (8)
N(3)	0·3435 (1)	0·6134 (3)	0·68222 (9)	2·94 (7)
C(4)	0·4120 (1)	0·7841 (4)	0·6663 (1)	2·99 (8)
C(5)	0·4261 (1)	0·9579 (4)	0·7181 (1)	3·56 (9)
N(6)	0·2339 (1)	0·5314 (3)	0·78251 (9)	2·80 (7)
C(7)	0·1896 (1)	0·3555 (4)	0·7441 (1)	2·70 (8)
N(8)	0·1247 (1)	0·2238 (4)	0·7815 (1)	3·31 (8)
C(8)	0·0719 (2)	0·0258 (5)	0·7479 (1)	4·0 (1)
N(9)	0·2025 (1)	0·3047 (4)	0·6720 (1)	3·63 (8)
C(10)	0·4637 (1)	0·7593 (4)	0·5936 (1)	3·56 (9)
S(11)	0·38785 (4)	0·7677 (1)	0·51151 (3)	3·20 (2)
C(12)	0·3323 (1)	1·0612 (4)	0·5279 (1)	3·10 (9)
C(13)	0·2504 (2)	1·1038 (4)	0·4739 (1)	3·42 (9)
C(14)	0·1708 (1)	0·9236 (4)	0·4848 (1)	3·06 (9)

Table 2 (*cont.*)

	x	*y*	*z*	B_{eq}
N(15)	0·1442 (1)	0·7961 (4)	0·4262 (1)	3·43 (8)
N(16)	0·1337 (1)	0·9118 (4)	0·5525 (1)	3·79 (8)
C(17)	0·0600 (2)	0·7655 (5)	0·5635 (1)	3·9 (1)
N(18)	−0·0043 (1)	0·6470 (5)	0·5794 (1)	4·9 (1)
(5)				
S(1)	0·33773 (6)	−0·31250 (7)	0·8029 (2)	3·99 (4)
C(2)	0·2684 (2)	−0·3385 (2)	0·5380 (6)	3·7 (1)
N(3)	0·1992 (2)	−0·2675 (2)	0·5066 (5)	3·7 (1)
C(4)	0·1971 (2)	−0·1899 (2)	0·6989 (6)	3·6 (1)
C(5)	0·2658 (2)	−0·2026 (3)	0·8722 (7)	3·9 (1)
N(6)	0·2835 (2)	−0·4186 (2)	0·3831 (6)	4·7 (1)
N(7)	0·3553 (2)	−0·4927 (2)	0·4597 (6)	4·5 (1)
C(8)	0·4166 (3)	−0·5154 (4)	0·2528 (9)	6·8 (3)
C(9)	0·3145 (3)	−0·5819 (3)	0·536 (1)	6·8 (3)
C(10)	0·1215 (2)	−0·1051 (3)	0·6892 (7)	3·9 (1)
S(11)	0·13001 (5)	−0·02229 (7)	0·4269 (2)	3·78 (3)
C(12)	0·2430 (2)	0·0174 (2)	0·4880 (6)	3·6 (1)
C(13)	0·2506 (2)	0·0907 (3)	0·7197 (7)	4·1 (2)
C(14)	0·3410 (2)	0·1338 (2)	0·7639 (6)	3·4 (1)
N(15)	0·3506 (2)	0·1876 (2)	0·9873 (6)	4·7 (1)
N(16)	0·4018 (2)	0·1114 (2)	0·5892 (5)	3·7 (1)
S(17)	0·50283 (5)	0·15041 (6)	0·6273 (1)	3·22 (3)
N(18)	0·5658 (2)	0·0746 (2)	0·8095 (5)	3·7 (1)
O(19)	0·5382 (2)	0·1343 (2)	0·3797 (4)	4·4 (1)
O(20)	0·5032 (2)	0·2482 (2)	0·7541 (5)	4·8 (1)
Maleic acid				
C(1)	0·9700 (3)	0·3896 (3)	1·2746 (8)	5·3 (2)
C(2)	0·9103 (2)	0·3820 (3)	1·0356 (7)	4·4 (2)
O(3)	0·9264 (2)	0·3096 (2)	0·8786 (5)	5·8 (1)
O(4)	0·8424 (2)	0·4443 (2)	1·0238 (6)	6·2 (2)
C(5)	1·0547 (2)	0·3433 (3)	1·3320 (8)	5·2 (2)
C(6)	1·1115 (2)	0·2683 (3)	1·1774 (7)	4·8 (2)
O(7)	1·0768 (2)	0·2241 (3)	0·9764 (7)	8·9 (2)
O(8)	1·1890 (2)	0·2432 (2)	1·2614 (6)	5·6 (1)

Table 3. *Hydrogen-bond distances* (Å) *and angles* (°)

W and *M* represent water and maleic acid, respectively.

Donor (*D*) at *x*, *y*, *z*	Acceptor (*A*) at	symmetry operation	*D*···*A*	H···*A*	*D*—H···*A*
(1)					
N(8)	N(16)	$-x+1, -y, -z$	3·110 (3)	2·31 (3)	140 (3)
N(9)	N(3)	x, y, z	2·686 (3)	1·99 (4)	127 (3)
N(9)	O(1)*W*	$x, y-1, z-1$	2·955 (3)	2·20 (3)	168 (3)
N(15)	N(18)	$x, y, z+1$	3·012 (4)	2·16 (3)	170 (3)
N(15)	O(1)*W*	$-x+1, -y+1, -z+1$	2·941 (3)	2·20 (4)	147 (4)
O(1)*W*	N(6)	$x, y+1, z$	2·797 (3)	1·75 (4)	167 (4)
O(1)*W*	N(18)	$x, y, z+1$	2·916 (4)	1·83 (4)	167 (3)
(2)					
N(6)	Cl(21)	$x+0·5, -y+0·5, z+0·5$	3·080 (4)	2·02 (5)	166 (4)
N(8)	O(19)	$x, y-1, z$	3·089 (5)	2·33 (5)	139 (4)
N(9)	N(3)	x, y, z	2·721 (5)	1·80 (5)	141 (4)
N(15)	N(16)	$x, -y+1, z+0·5$	2·959 (5)	1·86 (5)	179 (5)
N(18)	O(19)	$x, -y+1, z+0·5$	2·964 (5)	1·89 (5)	180 (4)
(3)					
N(8)	O(16)	$-x+1·5, -y+1, z+0·5$	2·941 (4)	2·20 (4)	153 (3)
N(8)	O(16)	$-x+1, y+0·5, -z+1·5$	2·903 (4)	2·00 (4)	169 (3)
N(9)	N(3)	x, y, z	2·691 (4)	2·21 (4)	118 (4)
N(9)	O(16)	$-x+1·5, -y+1, z+0·5$	3·003 (4)	2·11 (5)	161 (5)
N(15)	N(6)	$-x+1, y-0·5, -z+1·5$	2·942 (4)	2·00 (4)	151 (3)
(4)					
N(8)	N(18)	$-x, y-0·5, -z+1·5$	3·041 (3)	2·36 (2)	130 (2)
N(9)	N(3)	x, y, z	2·626 (2)	1·95 (3)	134 (2)
N(9)	N(16)	$x, y-1, z$	3·171 (3)	2·30 (2)	163 (2)
N(15)	N(6)	$x, -y+1·5, z-0·5$	3·010 (2)	2·08 (2)	168 (2)
N(15)	N(18)	$-x, -y+1, -z+1$	3·132 (3)	2·22 (3)	173 (2)
(5)					
N(6)	O(4)*M*	$-x+1, -y, -z+1$	2·769 (4)	1·83 (4)	178 (4)
N(15)	O(8)*M*	$x-1, y, z$	2·901 (4)	1·95 (4)	178 (4)
N(15)	O(20)	x, y, z	2·822 (4)	2·21 (4)	119 (3)
N(18)	O(19)	$x, y, z+1$	3·085 (4)	2·12 (4)	179 (3)
N(18)	N(16)	$-x+1, -y, -z+1$	3·155 (4)	2·20 (4)	176 (4)
O(3)*M*	N(3)	$-x+1, -y, -z+1$	2·727 (4)	1·72 (4)	179 (4)
O(7)*M*	O(3)*M*	x, y, z	2·429 (5)	1·54 (4)	155 (4)

UM00013884
NOVARTIS EXHIBIT 1017
Novartis v. Regents, IPR2023-01346
Page 2630 of 4460

Table 4. *Bond lengths* (Å) *of compounds* (1)–(5)

M represents maleic acid.

(1)			
S(1)—C(2)	1·737 (2)	C(7)—N(9)	1·300 (4)
S(1)—C(5)	1·712 (3)	C(10)—S(11)	1·822 (3)
C(2)—N(3)	1·303 (3)	S(11)—C(11)	1·817 (3)
C(2)—N(6)	1·366 (3)	C(12)—C(13)	1·530 (4)
N(3)—C(4)	1·406 (3)	C(13)—C(14)	1·520 (4)
C(4)—C(5)	1·353 (4)	C(14)—N(15)	1·307 (4)
C(4)—C(10)	1·495 (4)	C(14)—N(16)	1·320 (3)
N(6)—C(7)	1·323 (3)	N(16)—C(17)	1·320 (4)
C(7)—N(8)	1·368 (4)	C(17)—N(18)	1·163 (4)
(2)			
S(1)—C(2)	1·720 (5)	C(10)—S(11)	1·804 (5)
S(1)—C(5)	1·717 (6)	S(11)—C(12)	1·826 (5)
C(2)—N(3)	1·279 (6)	C(12)—C(13)	1·513 (7)
C(2)—N(6)	1·403 (6)	C(13)—C(14)	1·490 (6)
N(3)—C(4)	1·404 (6)	C(14)—N(15)	1·332 (6)
C(4)—C(5)	1·331 (7)	C(14)—N(16)	1·295 (5)
C(4)—C(10)	1·494 (7)	N(16)—S(17)	1·627 (4)
N(6)—C(7)	1·370 (6)	S(17)—N(18)	1·619 (4)
C(7)—N(8)	1·356 (6)	S(17)—O(19)	1·439 (3)
C(7)—N(9)	1·278 (6)	S(17)—O(20)	1·440 (3)
(3)			
S(1)—C(2)	1·752 (4)	C(7)—N(8)	1·328 (6)
S(1)—C(5)	1·730 (4)	C(7)—N(9)	1·321 (6)
C(2)—N(3)	1·316 (5)	C(10)—S(11)	1·826 (4)
C(2)—N(6)	1·353 (5)	S(11)—C(12)	1·799 (5)
N(3)—C(4)	1·376 (5)	C(12)—C(13)	1·503 (7)
C(4)—C(5)	1·361 (6)	C(13)—C(14)	1·503 (6)
C(4)—C(10)	1·479 (6)	C(14)—N(15)	1·320 (5)
N(6)—C(7)	1·335 (5)	C(14)—O(16)	1·246 (5)
(4)			
S(1)—C(2)	1·746 (2)	N(8)—C(8)	1·444 (3)
S(1)—C(5)	1·729 (2)	C(10)—S(11)	1·815 (2)
C(2)—N(3)	1·312 (3)	S(11)—C(12)	1·809 (2)
C(2)—N(6)	1·336 (3)	C(12)—C(13)	1·527 (3)
N(3)—C(4)	1·378 (3)	C(13)—C(14)	1·512 (3)
C(4)—C(5)	1·336 (3)	C(14)—N(15)	1·308 (3)
C(4)—C(10)	1·495 (3)	C(14)—N(16)	1·317 (3)
N(6)—C(7)	1·335 (2)	N(16)—C(17)	1·333 (3)
C(7)—N(8)	1·348 (3)	C(17)—N(18)	1·157 (3)
C(7)—N(9)	1·324 (3)		
(5)			
S(1)—C(2)	1·712 (3)	C(14)—N(15)	1·302 (4)
S(1)—C(5)	1·748 (4)	C(14)—N(16)	1·324 (4)
C(2)—N(3)	1·327 (4)	N(16)—S(17)	1·630 (3)
C(2)—N(6)	1·307 (4)	S(17)—N(18)	1·611 (3)
N(3)—C(4)	1·396 (4)	S(17)—O(19)	1·425 (3)
C(4)—C(5)	1·322 (5)	S(17)—O(20)	1·423 (3)
C(4)—C(10)	1·503 (5)	C(1)*M*—C(2)*M*	1·490 (5)
N(6)—N(7)	1·426 (4)	C(1)*M*—C(5)*M*	1·361 (6)
N(7)—C(8)	1·455 (6)	C(2)*M*—O(3)*M*	1·241 (5)
N(7)—C(9)	1·470 (6)	C(2)*M*—O(4)*M*	1·234 (5)
C(10)—S(11)	1·828 (4)	C(5)*M*—C(6)*M*	1·474 (6)
S(11)—C(12)	1·809 (3)	C(6)*M*—O(7)*M*	1·279 (5)
C(12)—C(13)	1·515 (5)	C(6)*M*—O(8)*M*	1·222 (5)
C(13)—C(14)	1·508 (5)		

Table 5. *Bond angles* (°) *of compounds* (1)–(5)

M represents maleic acid.

(1)			
C(2)—S(1)—C(5)	89·9 (1)	N(6)—C(7)—N(9)	126·0 (2)
S(1)—C(2)—N(3)	114·0 (1)	N(8)—C(7)—N(9)	118·2 (2)
S(1)—C(2)—N(6)	117·3 (1)	C(4)—C(10)—S(11)	112·2 (1)
N(3)—C(2)—N(6)	128·6 (1)	C(10)—S(11)—C(12)	100·2 (1)
C(2)—N(3)—C(4)	110·9 (2)	S(11)—C(12)—C(13)	110·6 (1)
N(3)—C(4)—C(5)	114·7 (2)	C(12)—C(13)—C(14)	111·6 (2)
N(3)—C(4)—C(10)	118·5 (1)	C(13)—C(14)—N(15)	117·9 (2)
C(5)—C(4)—C(10)	126·8 (2)	C(13)—C(14)—N(16)	124·1 (2)
S(1)—C(5)—C(4)	110·5 (1)	N(15)—C(14)—N(16)	118·1 (2)
C(2)—N(6)—C(7)	120·2 (2)	C(14)—N(16)—C(17)	119·1 (2)
N(6)—C(7)—N(8)	115·8 (2)	N(16)—C(17)—N(18)	173·2 (2)
(2)			
C(2)—S(1)—C(5)	87·3 (2)	C(10)—S(11)—C(12)	103·4 (2)
S(1)—C(2)—N(3)	116·9 (2)	S(11)—C(12)—C(13)	111·9 (2)
S(1)—C(2)—N(6)	117·1 (2)	C(12)—C(13)—C(14)	114·1 (3)
N(3)—C(2)—N(6)	126·0 (3)	C(13)—C(14)—N(15)	116·3 (3)
C(2)—N(3)—C(4)	109·8 (3)	C(13)—C(14)—N(16)	115·9 (3)
N(3)—C(4)—C(5)	113·8 (3)	N(15)—C(14)—N(16)	127·8 (3)
N(3)—C(4)—C(10)	118·3 (3)	C(14)—N(16)—S(17)	121·3 (2)
C(5)—C(4)—C(10)	127·9 (3)	N(16)—S(17)—N(18)	110·4 (2)
S(1)—C(5)—C(4)	112·2 (2)	N(16)—S(17)—O(19)	103·9 (2)
C(2)—N(6)—C(7)	123·4 (3)	N(16)—S(17)—O(20)	112·3 (2)
N(6)—C(7)—N(8)	115·4 (3)	N(18)—S(17)—O(19)	107·0 (2)
N(6)—C(7)—N(9)	123·0 (3)	N(18)—S(17)—O(20)	106·1 (2)
N(8)—C(7)—N(9)	121·5 (3)	O(19)—S(17)—O(20)	117·0 (2)
C(4)—C(10)—S(11)	113·8 (2)		
(3)			
C(2)—S(1)—C(5)	89·4 (2)	N(6)—C(7)—N(8)	118·0 (3)
S(1)—C(2)—N(3)	113·4 (1)	N(6)—C(7)—N(9)	124·3 (2)
S(1)—C(2)—N(6)	116·2 (1)	N(8)—C(7)—N(9)	117·6 (3)
N(3)—C(2)—N(6)	130·5 (2)	C(4)—C(10)—S(11)	113·2 (2)
C(2)—N(3)—C(4)	111·7 (2)	C(10)—S(11)—C(12)	100·5 (2)
N(3)—C(4)—C(5)	115·5 (2)	S(11)—C(12)—C(13)	111·0 (2)
N(3)—C(4)—C(10)	119·1 (2)	C(12)—C(13)—C(14)	112·7 (3)
C(5)—C(4)—C(10)	125·3 (3)	C(13)—C(14)—N(15)	117·6 (3)
S(1)—C(5)—C(4)	110·0 (2)	C(13)—C(14)—O(16)	121·1 (3)
C(2)—N(6)—C(7)	120·7 (2)	N(15)—C(14)—O(16)	121·3 (2)
(4)			
C(2)—S(1)—C(5)	89·4 (1)	N(8)—C(7)—N(9)	117·6 (1)
S(1)—C(2)—N(3)	113·3 (1)	C(7)—N(8)—C(8)	123·4 (1)
S(1)—C(2)—N(6)	118·1 (1)	C(4)—C(10)—S(11)	113·6 (1)
N(3)—C(2)—N(6)	128·7 (1)	C(10)—S(11)—C(12)	98·7 (1)
C(2)—N(3)—C(4)	111·1 (1)	S(11)—C(12)—C(13)	111·5 (1)
N(3)—C(4)—C(5)	116·3 (1)	C(12)—C(13)—C(14)	113·1 (1)
N(3)—C(4)—C(10)	117·8 (1)	C(13)—C(14)—N(15)	117·3 (1)
C(5)—C(4)—C(10)	125·8 (1)	C(13)—C(14)—N(16)	116·8 (1)
S(1)—C(5)—C(4)	109·9 (1)	N(15)—C(14)—N(16)	125·9 (1)
C(2)—N(6)—C(7)	118·3 (1)	C(14)—N(16)—C(17)	118·7 (1)
N(6)—C(7)—N(8)	117·0 (1)	N(16)—C(17)—N(18)	173·9 (1)
N(6)—C(7)—N(9)	125·4 (1)		
(5)			
C(2)—S(1)—C(5)	89·5 (2)	C(13)—C(14)—N(16)	117·9 (2)
S(1)—C(2)—N(3)	112·3 (1)	N(15)—C(14)—N(16)	127·4 (2)
S(1)—C(2)—N(6)	123·3 (1)	C(14)—N(16)—S(17)	121·2 (1)
N(3)—C(2)—N(6)	124·3 (2)	N(16)—S(17)—N(18)	108·6 (1)
C(2)—N(3)—C(4)	113·6 (2)	N(16)—S(17)—O(19)	104·2 (1)
N(3)—C(4)—C(5)	112·6 (2)	N(16)—S(17)—O(20)	113·3 (1)
N(3)—C(4)—C(10)	119·3 (2)	N(18)—S(17)—O(19)	105·9 (1)
C(5)—C(4)—C(10)	128·1 (2)	N(18)—S(17)—O(20)	105·6 (1)
S(1)—C(5)—C(4)	111·9 (1)	O(19)—S(17)—O(20)	118·8 (1)
C(2)—N(6)—N(7)	117·0 (2)	C(2)*M*—C(1)*M*—C(5)*M*	130·1 (2)
N(6)—N(7)—C(8)	109·5 (2)	C(1)*M*—C(2)*M*—O(3)*M*	119·0 (2)
N(6)—N(7)—C(9)	108·2 (2)	C(1)*M*—C(2)*M*—O(4)*M*	115·6 (2)
C(8)—N(7)—C(9)	113·4 (3)	O(3)*M*—C(2)*M*—O(4)*M*	125·0 (2)
C(4)—C(10)—S(11)	112·5 (1)	C(1)*M*—C(5)*M*—C(6)*M*	129·5 (2)
C(10)—S(11)—C(12)	102·5 (1)	C(5)*M*—C(6)*M*—O(7)*M*	120·1 (2)
S(11)—C(12)—C(13)	113·1 (1)	C(5)*M*—C(6)*M*—O(8)*M*	117·8 (2)
C(12)—C(13)—C(14)	115·2 (2)	O(7)*M*—C(6)*M*—O(8)*M*	121·8 (2)
C(13)—C(14)—N(15)	114·7 (2)		

The crystals are stabilized by intermolecular hydrogen bonds, in addition to van der Waals interactions. All of the H atoms bound to polar N or O atoms participate in hydrogen-bond formation; the bonding parameters are reasonable. It is characteristic that a hydrogen bond is formed between the cyanoamidine [N(15)···N(18)] or between the sulfamoylamidine [N(18)···O(19)] groups.

Water molecules in (1), chloride ions in (2) and maleic acid molecules in (5) exist in the cavities produced by the packing of the title molecules and contribute to the crystal lattice stabilization *via* hydrogen bonds. The water and maleic acid molecules do not appear to influence significantly the molecular conformations of (1) and (5), respectively; maleic acid in (5) exists as a neutral form of HOOCCH=CHCOOH, as evidenced from the difference Fourier map. In contrast, the molecular conformation of (2) appears to be largely affected by

UM00013885
NOVARTIS EXHIBIT 1017
Novartis v. Regents, IPR2023-01346
Page 2631 of 4460

the presence of hydrochloride (salt formation); the H atom of HCl is transferred to the N(6) atom of (2), so that the guanidine group is in a protonated state. There is a hydrogen bond [N(6)···Cl^- = 3·080 Å] and short contacts with the chloride ions [N(8)···Cl^- = 3·349, N(9)···Cl^- = 3·231 and N(15)···Cl^- = 3·235 Å].

The bond lengths and angles of (1)–(5) are listed in Tables 4 and 5. These values are all in the accepted region (Kennard, 1983) within their e.s.d.'s. It is interesting to note that each C—N bond in the guanidine group shows nearly equal double-bond character, and the conformation about C(2)—N(6)—C(7) is fixed to some limited regions because of the resonance between the thiazole ring and the guanidine group. On the other hand, the double-bond character of the amidine group is localized at the C(14)—N(15) and C(14)—N(16) bonds, and the C(4)—C(10)—S(11)—C(12)—C(13)—C(14) bond sequence is likely to rotate freely, judging from the bond lengths and angles.

The molecular conformations of (1)–(5) are shown in Fig. 2, where the dotted lines represent intramolecular hydrogen bonds. A characteristic common to (1)–(4) is the formation of a planar and highly polar six-membered-ring system by means of an intramolecular hydrogen bond [N(9)—H···N(3), see Table 3]. In (5), where such a hydrogen bond is not possible, a planar arrangement is also observed.

The torsion angles defining the side-chain conformation with respect to the thiazole ring are given in Table 6, together with the dihedral angles between the thiazole ring and amidine or amide group. This table also lists torsion angles of cimetidine (Hadicke, Fickel & Franke, 1978), cimetidine monohydrate (Kojić-Prodić, Ružić-Toroš, Bresciani-Pahor & Randaccio, 1980), ranitidine oxalate (Kojić-Prodić, Ružić-Toroš & Toso, 1982) and the free form of famotidine (Yanagisawa *et al.*, 1987). Interestingly, ω_1 and ω_2 torsion angles show the common *gauche* conformations. The same conformational characteristic has also been observed in cimetidine, cimetidine monohydrate, ranitidine oxalate and famotidine free form. This result implies that the conformation about C(4)—C(10)—S(11) is relatively fixed, and the conformational difference among the compounds is determined by ω_3–ω_5. Table 6 also shows that ω_3 and

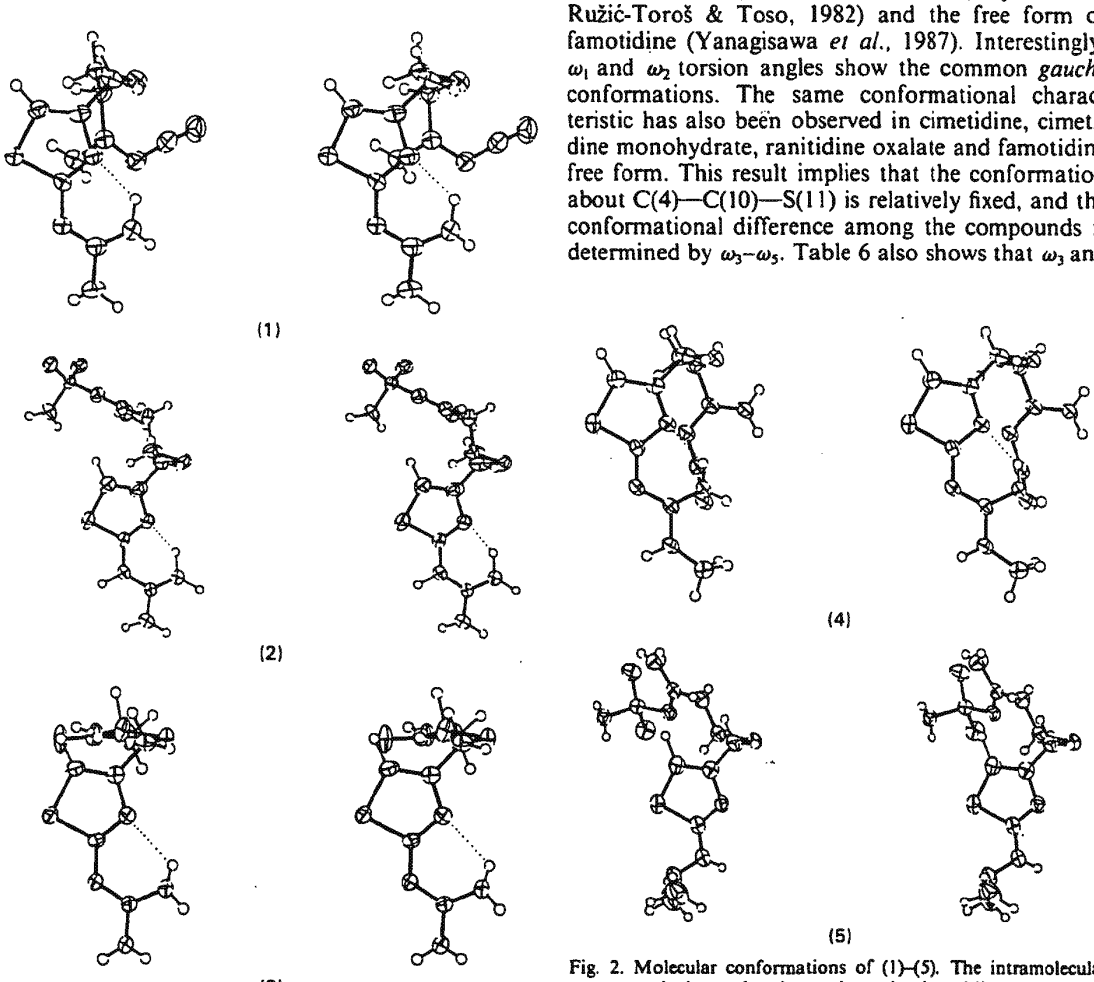


Fig. 2. Molecular conformations of (1)–(5). The intramolecular hydrogen bonds are shown by dotted lines.

UM00013886
NOVARTIS EXHIBIT 1017
Novartis v. Regents, IPR2023-01346
Page 2632 of 4460

Table 6. *Torsion angles (°) and dihedral angles (°) between the thiazole ring and the amidine or amide group*

The torsion angles of the famotidine (free form), cimetidine, cimetidine monohydrate and ranitidine oxalate are also given for comparison. Although the side chains of the cimetidine and ranitidine molecules are longer by an NH group than the present compounds, the listed torsion angles of the former molecules correspond to the latter ones.

Compound	ω_1 N(3)—C(4)—C(10)—S(11)	ω_2 C(4)—C(10)—S(11)—C(12)	ω_3 C(10)—S(11)—C(12)—C(13)	ω_4 S(11)—C(12)—C(13)—C(14)	ω_5 C(12)—C(13)—C(14)—N(15)	Dihedral angle
(1)	65·8 (2)	61·7 (2)	−148·5 (2)	60·9 (2)	61·4 (3)	19·6 (2)
(2)	68·8 (3)	62·5 (3)	84·8 (4)	−178·1 (4)	−67·4 (4)	86·7 (3)
(3)	73·5 (2)	57·0 (2)	−165·0 (3)	170·7 (3)	167·7 (3)	94·2 (2)
(4)	58·4 (1)	56·8 (1)	−170·3 (2)	64·4 (2)	−124·2 (2)	13·3 (1)
(5)	69·6 (2)	55·9 (2)	71·4 (2)	174·4 (3)	172·6 (3)	56·1 (2)
(2) (free form)	56·8	62·7	−170·6	68·1	−129·8	12·6
Cimetidine	69·8	−61·9	−62·6	175·7	−90·6	28·2
Cimetidine monohydrate	70·4	59·5	−137·2	67·6	75·8	10·7
Ranitidine oxalate	114·8	−59·0	−75·5	−176·0	−101·0	74·4

Table 7. *Conformational parameters and their correlation coefficients (r) with inhibitory activities*

The antagonist activity was classified as 0–3 according to the ED_{50} values: 0 for $ED_{50} > 10^{-4}$, 1 for $10^{-5} < ED_{50} < 10^{-4}$, 2 for $10^{-6} < ED_{50} < 10^{-5}$, and 3 for $10^{-7} < ED_{50}$.

Compound	ω_3	Dihedral angle (°)	D_{xy} of N(3)···N(15) (Å)	D_z of N(3)···N(15) (Å)	Activity
(1)	211·5	19·6	0·47	−0·08	3
(2)*	189·4	12·6	3·30	0·60	3
(3)	195·0	94·2	2·88	2·78	2
(4)	189·7	13·3	3·07	0·54	2
(5)	71·4	56·1	5·89	5·56	0
Cimetidine	297·4	28·2	3·90	−1·40	2
Cimetidine†	222·8	10·7	1·00	0·00	2
Ranitidine‡	284·5	74·4	2·80	−0·50	3
Linear correlation coefficient with activity					
r		0·8875	0·5334	0·8113	0·8333

* Famotidine free form.
† Cimetidine monohydrate.
‡ Ranitidine oxalate.

ω_4 torsion angles are restricted to either *gauche* or *trans*, while ω_5 has conformational freedom.

The geometry observed in the crystal structure may not represent the actual conformation bound to the H_2 receptor. Nevertheless, it is reasonable to consider the possible stereostructure–activity relationship using these X-ray data, particularly as structural data on the receptor binding site are lacking at present. Thus it is assumed that the combination of ω_3–ω_5 torsion angles could be closely related with the H_2-receptor antagonist activity. Before the discussion, it is important to say that the protonated structure of (2) (famotidine) shows a different conformation from the neutral one. The free form of (2) has a folded conformation (Yanagisawa *et al.*, 1987), while the present hydrochloride takes an extended conformation. This drastic conformational change from the neutral to the cationic state has also been observed in cimetidine (Shibata, Kagawa, Morisaka, Ishida & Inoue, 1983) and ranitidine (Ishida *et al.*, unpublished results). Thus it is questionable whether the conformation observed in the (2).HCl crystal reflects the intrinsic form of famotidine. Therefore, the data of (2).HCl were excluded from consideration. The relationships between the conformational parameters and H_2-receptor antagonist activities are given in Table 7.

As was expected, the compounds exhibiting high activities show the *trans* preference at the ω_3 torsion angle, while that without activity is in a *gauche* region ($r = 0{\cdot}8875$). On the other hand, the combination of ω_3, ω_4, ω_5 torsion angles determines the whole molecular conformation, as already stated. For example, when ω_3, ω_4, ω_5 takes the combination *trans, gauche, gauche* or *trans, gauche, anticlinal*, the side chain is folded back and the end group becomes close to parallel with the thiazole ring [(1), (2)(free form) and (4)], which is also observed for the potent cimetidine and ranitidine conformations. Therefore the dihedral angle may be related to the activity, although the correlation coefficient is not so high ($r = 0{\cdot}5334$).

Since the interatomic distances between the central aromatic ring and the side-chain end group are primarily determined by the combination of ω_3, ω_4, ω_5 torsion angles, on the other hand, these parameters were examined in relation to the activities. It is worthwhile to say that, among many possible interatomic pairs, the atomic distance between the thiazole N(3) atom and the end-group N(15) atom

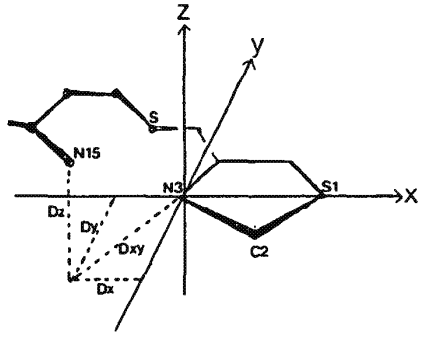


Fig. 3. Definition of D_x, D_y, D_z and D_{xy} distances between N(3) and N(15) atoms.

UM00013887
NOVARTIS EXHIBIT 1017
Novartis v. Regents, IPR2023-01346
Page 2633 of 4460

showed a high correlation. These two atoms could form the hydrogen bonds with the binding site of an H_2 receptor as the electron acceptor and donor atoms, respectively. In particular, the D_{xy} and D_y components of N(3)···N(15), which are defined in Fig. 3, were most strongly correlated with the activities ($r = 0.8113$ and 0·8333, respectively). Thus the linear combination of ω_3, D_{xy} and D_y led to the following correlation:

$$\begin{aligned} \text{activity} = {} & 1.9033 + 0.0058\omega_3 - 0.2678D_{xy} - 0.1613D_y \\ & (0.9160) \quad (0.0040) \quad (0.0987) \quad (0.1233) \\ r = {} & 0.9578 \\ & (0.3012). \end{aligned}$$

This equation clearly implies that the molecular conformation and spatial disposition of the N(15) atom with respect to the thiazole of imidazole ring are closely related to the emergence of antagonist activity.

References

BROGDEN, R. N., HEEL, R. C., SPEIGHT, T. M. & AVERY, G. S. (1978). *Drugs*, **15**, 93–131.

HADICKE, E., FICKEL, F. & FRANKE, A. (1978). *Chem. Ber.* **111**, 3222–3232.

HARADA, M., TERAI, M. & MAENO, H. (1983). *Eur. J. Pharmacol.* **91**, 371–376.

International Tables for X-ray Crystallography (1974). Vol. IV. Birmingham: Kynoch Press. (Present distributor Kluwer Academic Publishers, Dordrecht.)

ISHIDA, T., IN, Y., SHIBATA, M., DOI, M., INOUE, M. & YANAGISAWA, I. (1987). *Mol. Pharmacol.* **31**, 410–416.

KENNARD, O. (1983). *International Tables for X-ray Crystallography*, Vol. III, edited by C. H. MACGILLAVRY, G. D. RIECK & K. LONSDALE, pp. 275–276. Dordrecht: D. Reidel. (Present distributor Kluwer Academic Publishers, Dordrecht.)

KOJIĆ-PRODIĆ, B., RUŽIĆ-TOROŠ, Ž., BRESCIANI-PAHOR, N. & RANDACCIO, L. (1980). *Acta Cryst.* B**36**, 1223–1225.

KOJIĆ-PRODIĆ, B., RUŽIĆ-TOROŠ, Ž. & TOSO, R. (1982). *Acta Cryst.* B**38**, 1837–1840.

MAIN, P., HULL, S. E., LESSINGER, L., GERMAIN, G., DECLERCQ, J.-P. & WOOLFSON, M. M. (1978). *MULTAN78. A System of Computer Programs for the Automatic Solution of Crystal Structures from X-ray Diffraction Data*. Univs. of York, England, and Louvain, Belgium.

SHIBATA, M., KAGAWA, M., MORISAKA, K., ISHIDA, T. & INOUE, M. (1983). *Acta Cryst.* C**39**, 1255–1257.

TAKAGI, T., TAKEDA, M. & MAENO, H. (1982). *Arch. Int. Pharmacodyn.* **256**, 49–58.

TAKEDA, M., TAKAGI, T. & MAENO, H. (1981). *Jpn J. Pharmacol.* **31**, 222.

TAKEDA, M., TAKAGI, T. & MAENO, H. (1983). *Eur. J. Pharmacol.* **91**, 371–376.

TAKEDA, M., TAKAGI, T., YASHIMA, Y. & MAENO, H. (1982). *Arzneim. Forsch.* **32**, 734–737.

The Universal Crystallographic Computing System – Osaka (1979). The Computation Center, Osaka Univ., Japan.

YANAGISAWA, I., HIRATA, Y. & ISHII, Y. (1984). *J. Med. Chem.* **27**, 849–857.

YANAGISAWA, I., HIRATA, Y. & ISHII, Y. (1987). *J. Med. Chem.* **30**, 1787–1793.

Acta Cryst. (1989). B**45**, 512–518

Structures of Two 2-Oxyimino-α-D-pyranosides

BY ZBIGNIEW CIUNIK* AND HANS PAULSEN

Institut für Organische Chemie und Biochemie, Universität Hamburg, Martin-Luther-King-Platz 6, D-2000 Hamburg 13, Federal Republic of Germany

PETER LUGER

Institut für Kristallographie, Freie Universität Berlin, Takustrasse 6, D-1000 Berlin 33, Federal Republic of Germany

AND ZYGFRYD SMIATACZ AND HENRYK MYSZKA

Instytut Chemii, Uniwersytet Gdański, ul. Sobieskiego 18, 80-952 Gdańsk, Poland

(*Received* 2 *December* 1988; *accepted* 1 *June* 1989)

Abstract

1-(3-Acetamido-2-acetoxyimino-4-*O*-acetyl-2,3-dideoxy-α-D-*threo*-pentopyranosyl)pyrazole (I), $C_{14}H_{18}N_4O_6$, $M_r = 338.32$, orthorhombic, $P2_12_12_1$, $a = 9.257\ (2)$, $b = 9.306\ (2)$, $c = 19.582\ (5)$ Å, $V = 1687\ (1)$ Å^3, $Z = 4$, $D_x = 1.324\ (1)$ Mg m^{-3}, λ(Cu $K\alpha$) = 1·5418 Å, $\mu = 0.907$ mm^{-1}, $F(000) = 712$, room temperature, $R = 0.042$ for 1566 reflections with $I > 2\sigma(I)$. 1-(3,4,6-Tri-*O*-acetyl-2-hydroxyimino-2-deoxy-α-D-*arabino*-hexopyranosyl)-pyrazole (II), $C_{15}H_{19}N_3O_8$, $M_r = 369.33$, monoclinic,

* On leave from Instytut Chemii, Uniwersytet Wrocławski, ul. Fr. Joliot-Curie 14, 50-383 Wrocław, Poland.

0108-7681/89/050512-07$03.00

© 1989 International Union of Crystallography

UM00013888
NOVARTIS EXHIBIT 1017
Novartis v. Regents, IPR2023-01346
Page 2634 of 4460

TABLE II

COUPLING CONSTANTS FOR THE 1-X-2,4-DINITRONAPHTHALENES IN DIOXANE

J	X = Cl	X = Br	X = I
3,5	0	0	0
5,6	8.64 ± 0.04	8.49 ± 0.03	8.56 ± 0.04
5,7	1.17 ± 0.04	1.29 ± 0.03	1.05 ± 0.04
5,8	0.75 ± 0.03	0.57 ± 0.02	0.58 ± 0.03
6,7	7.16 ± 0.03	6.91 ± 0.02	6.93 ± 0.03
6,8	1.20 ± 0.04	1.12 ± 0.04	0.98 ± 0.04
7,8	8.59 ± 0.04	8.66 ± 0.04	8.56 ± 0.04

TABLE III

CHEMICAL SHIFTS AND COUPLING CONSTANTS FOR 1-X-2,4-DINITROBENZENES IN ACETONE

Substituent	Chemical shift			Coupling constant		
	ν_3	ν_5	ν_6	$J_{5,6}$	$J_{5,3}$	$J_{6,3}$
F[a]	530.2	515.7	466.1	3.0	0.2	9.3
Cl	530.8	512.6	483.4	2.49	0.10	8.85
Cl[b]	529.8	512.3	483.2	2.70	0.36	8.81
Br	527.9	506.6	494.0	2.63	0.26	8.76
I	523.5	495.4	510.7	2.54	0.02	8.80

[a] T. Schaefer, *Can. J. Chem.*, 40, 431 (1962). [b] S. L. Smith and A. M. Ihrig, *J. Mol. Spectrosc.*, 22, 241 (1967).

With the data of Spiesecki and Schneider,[8] a plot was made of the chemical shift of the halobenzene protons *vs.* the Pauling electronegativity of the halogen. The same type plot for the chemical shifts of the 2,4-dinitrohalobenzenes shows striking similarities. The H_3 and H_5 in the 2,4-dinitrohalobenzenes series are qualitatively similar to the meta protons of the halobenzene series; H_6 corresponds to the ortho protons in the halobenzenes. The two nitro groups affect the magnitude of the chemical shift, but the nature of the halogen still controls the relative chemical shift within the series.

The 2,4-dinitrohalonaphthalenes gave a much more complex spectra than the benzene series. H_3 appears as an intense singlet with a complex ABCD spectrum for the other protons, H_5, H_6, H_7, and H_8. Since the α protons of naphthalene have a greater chemical shift than β, the assignment of H_5 and H_8 to the downfield portion of the spectra is obvious. Since there is *no* coupling between the substituted and unsubstituted rings, the correct assignment of *one* of the protons (H_5 or H_8) is essential. From this one correct assignment, all other shifts and coupling constants are calculated *via* LAOCN3. The assignment of H_8 to the lower field is based on the data of Wells.[9] The effect of the nitro groups on H_5, H_6, H_7, and H_8 can be calculated.[9] These calculations indicate that $\nu_8 = 510$, $\nu_5 = 503$, $\nu_6 = 499$, and $\nu_7 = 437$ Hz. In other words, the order is $H_8 > H_5 > H_6 > H_7$. The data of Table I follow this pattern. If one draws resonance structures of the 1-halo-2,4-dinitronaphthalenes, both the 2- and the 4-nitro groups show resonance forms with + charges on the 6 and 8 positions. If electronegativity is the major factor in chemical shifts, these two protons should be downfield with respect to protons 5 and 7. The above argument has the implicit assumption that the halogens do not greatly affect the shift, and that their effect is a perturbation on the major effect of the nitro groups. Is this assumption correct or can we arrive at a satisfactory assignment on other bases? An alternative method is to apply the chemical shift changes of halogens in the ortho, meta, and para positions in benzene to the naphthalene series. If H_3 is regarded as meta to the halogen and H_5 as para, we arrive at the following qualitative result:

1-chloro	ν_8 = 510 (for NO_2 groups)	(−2)	(*m*-Cl) = 508 Hz
	ν_5 = 503 (for NO_2 groups)	(−8)	(*p*-Cl) = 495 Hz
1-bromo	ν_8 = 510	(−6)	(*m*-Br) = 504 Hz
	ν_5 = 503	(−2)	(*p*-Br) = 501 Hz
1-iodo	ν_8 = 510	(−15)	(*m*-I) = 495 Hz
	ν_5 = 503	(−3)	(*p*-I) = 500 Hz

These assumptions give the same qualitative order as the previous assumptions for the chloro and bromo compounds, but not for iodo. The iodine atom is large, and the peri positions of naphthalene are closer than the meta positions of the benzene. It is probable that the contributions of both the *m*-Br (−6) and the *m*-I (−15) are too negative; their real contribution would be more toward the ortho halogens, which are positive. This approach, though somewhat argumentative, supports the first. The peri effect has been discussed by Zweig, Lancaster, and Neglia.[10] The effect of a peri substituent is to shift that proton downfield; the low-field proton is always at the α position peri to the substituent. In our compounds, H_8 is the α and peri position and should be the low-field proton. Hence, the assignments $\nu_8 > \nu_5$ and $\nu_6 > \nu_7$ were accepted.

Comparison of the 2,4-dinitrohalonaphthalene series with the benzene series shows the meta pattern is followed. In each case, the chemical shift of the chloro compound is slightly greater than the bromo, which, in turn, is considerably greater than the iodo compounds.

Coupling constants do not vary much with respect to change in halogen. The ortho coupling constants, $J_{5,6}$ and $J_{7,8}$, are about equal (8.5 Hz) and greater than $J_{6,7}$ (7.0 Hz). The meta coupling constants, $J_{5,7}$ and $J_{6,7}$, show no pronounced trends and have the value of (1.0–1.3) Hz. The para coupling constants range from 0.75 to 0.6 Hz.

Registry No.—1-Cl-2,4-Dinitronaphthalene, 2401-85-6; 1-Br-2,4-dinitronaphthalene, 2401-86-7; 1-I-2,4-dinitronaphthalene, 4112-02-1; 1-Cl-2,4-dinitrobenzene, 97-00-7; 1-Br-2,4-dinitrobenzene, 584-48-5; 1-I-2,4-dinitrobenzene, 709-49-9.

(8) H. Spiesecki and W. G. Schneider, *J. Chem. Phys.*, 35, 731 (1961).
(9) R. P. Wells, *J. Chem. Soc.*, 1967 (1963).
(10) A. Zweig, J. E. Lancaster, and M. T. Neglia, *Tetrahedron*, 23, 2577 (1967).

Stepwise Synthesis of Oligopeptides with *N*-Carboxy-α-Amino Acid Anhydrides. IV. Glycine NCA

RYOICHI KATAKAI* AND MASANAO OYA

Department of Industrial Chemistry, College of Technology, University of Gunma, Kiryu-shi, Japan

KEIKICHI UNO AND YOSHIO IWAKURA

Department of Synthetic Chemistry, Faculty of Engineering, The University of Tokyo, Tokyo, Japan

Received July 6, 1971

A successful procedure for peptide synthesis using the controlled reaction of *N*-carboxy α-amino acid anhydrides (NCA's) in an aqueous system has been

UM00013889
NOVARTIS EXHIBIT 1017
Novartis v. Regents, IPR2023-01346
Page 2635 of 4460

TABLE I
RESULTS OF SYNTHESES OF N-GLYCYL PEPTIDES

Peptide	Yield, %	[α]D, deg	Calcd, % C	Calcd, % H	Calcd, % N	Found, % C	Found, % H	Found, % N
Gly-Gly	90		36.36	6.11	21.20	36.55	6.20	21.50
Gly-L-Ala	87	−59.0 (c 2.5, 0.5 N HCl)[a]	41.08	6.91	19.17	40.75	7.12	19.34
Gly-L-Val	91	−19.5 (c 2.0. water)[b]	48.25	8.12	16.08	48.33	8.25	16.26
Gly-L-Leu	92	−36.4 (c 2.5, water)[c]	51.04	8.58	14.88	51.12	8.61	14.80
Gly-L-Phe	89	41.0 (c 2.5, water)[d]	59.45	6.35	12.60	59.60	6.46	12.55
Gly-L-Leu-L-Ala	86	−59.2 (c 2.4, water)[e]	50.94	8.18	16.21	51.05	8.20	16.14

[a] −59.3° (c 2, 0.5 N HCl): B. F. Erlanger and E. Brand, *J. Amer. Chem. Soc.*, 73, 3508 (1951). [b] −19.9° (c 2, water): K. R. Rao, S. M. Birnbaum, R. B. Kingsley, and J. P. Greenstein, *J. Biol. Chem.*, 198, 507 (1952). [c] −36.3° (c 2, water): F. H. Carpenter and D. T. Gish, *J. Amer. Chem. Soc.*, 74, 3818 (1952). [d] 40.8° (c 2.5, water): ref 2. [e] −59.0° (c 2.5 water): E. Abderhalden and A. Fodor, *Z. Phys. Chem.*, 81, 1 (1912).

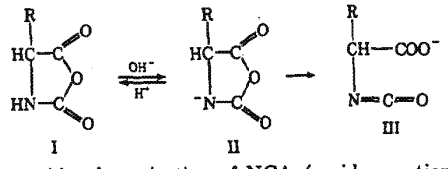
developed by the Merck group.[1,2] The procedure was satisfactorily used by Koppel and coworkers[3] to prepare some oligopeptides. The usefulness of this synthetic method was demonstrated by the total synthesis of the S protein of RNase A.[4-8] In the aqueous system, however, glycine NCA reacted with an amino acid as a nucleophile to give hydantoic acid as a side product to the extent of more than 20% even at the optimal pH of 10.2. 2,5-Thiazolidinedione (glycine NTA), therefore, was used to avoid the formation of the hydantoic acid.[9,10]

Another NCA method for peptide synthesis using the heterogeneous system acetonitrile–water has been reported by us.[11,12] With ordinary stirring and addition of sodium carbonate, the method permitted the synthesis of peptides without such side reactions as polymerization and hydrolysis of the NCA.

A distinct difference in the formation of the hydantoic acid was found between the NCA method in the aqueous system and that in the heterogeneous system. In the reaction of NCA with an amino acid or a peptide in our previous synthesis,[11] attention was not paid to the formation of the hydantoic acid because the desired peptide was obtained in high yield[12,13] and the by-product, if it had been formed, could not react with NCA. In the reaction of glycine NCA with glycine in heterogeneous system, glycylglycine was obtained in 90% yield. Such a yield could not be expected from the results in the aqueous system reported by the Merck group. Glycyl-L-leucine was also obtained in 92% yield by the reaction of L-leucine in the heterogeneous system acetonitrile–water containing sodium carbonate with glycine NCA in acetonitrile. A tripeptide with N-terminal glycine, glycyl-L-leucyl-L-alanine, was also synthesized by the NCA method in the heterogeneous system. The sodium salt of L-alanine was treated with L-leucine NCA and the dipeptide formed was treated with glycine NCA. The resulting tripeptide was recrystallized from aqueous ethanol to give pure tripeptide (86% overall yield). Some *N*-glycyl dipeptides were also prepared in high yields in the heterogeneous system and these results are summarized in Table I.

These results strongly suggest that few side reactions occurred in the heterogeneous system. This was demonstrated by the synthesis of glycyl-L-tryptophan. After the reaction of glycine NCA with L-tryptophan in the heterogeneous system, the aqueous layer of the system was analyzed by thin layer chromatography. All of the Ehrlich positive components detected on silica gel were ninhydrin positive. No component that was Ehrlich positive and ninhydrin negative could be detected by tlc. These components were quantitatively determined as unreacted L-tryptophan (1%), glycyl-L-tryptophan (96.5%), and glycylglycyl-L-tryptophan (2.5%).

The formation of N-terminal glycyl peptides in high yields without formation of hydantoic acid is consistent with our previous suggestion[11] that the NCA in the heterogeneous system may be protected from side reactions by the acetonitrile layer. The hydantoic acid formed in the homogeneous system may be derived from the isocyanate III formed from the NCA anion II.[3]



I II III

The rapid polymerization of NCA (a side reaction in the peptide synthesis by the NCA method) *via* the NCA anion[3,14] does not occur in acetonitrile[15] or in the heter-

(1) R. G. Denkewalter, H. Schwam, R. G. Strachan, T. E. Beesley, D. F. Veber, E. F. Schoenewaldt, H. Barkemeyer, W. J. Paleveda, Jr., T. A. Jacob, and R. Hirschmann, *J. Amer. Chem. Soc.*, 88, 3163 (1966).

(2) R. Hirschmann, R. G. Strachan, H. Schwam, E. F. Schoenewaldt, H. Joshua, B. Barkemeyer, D. F. Veber, W. J. Paleveda, Jr., T. A. Jacob, T. E. Beesley, and R. G. Denkewalter, *J. Org. Chem.*, 32, 3415 (1967).

(3) K. D. Kopple, T. Saito, and M. Ohnishi, *ibid.*, 34, 1631 (1969).

(4) R. G. Denkewalter, D. F. Veber, F. W. Holly, and R. Hirschmann, *J. Amer. Chem. Soc.*, 91, 502 (1969).

(5) R. G. Strachan, W. J. Paleveda, Jr., R. F. Nutt, R. A. Vitali, D. F. Veber, M. J. Dickinson, V. Garsky, J. E. Deak, E. Walton, S. R. Jenkins, F. W. Holly, and R. Hirschmann, *ibid.*, 91, 503 (1969).

(6) S. R. Jenkins, R. F. Nutt, R. S. Dewey, D. F. Veber, F. W. Holly, W. J. Paleveda, Jr., T. Lanza, Jr., R. G. Strachan, E. F. Schoenewaldt, H. Barkemeyer, M. J. Dickinson, J. Sondey, R. Hirschmann, and E. Walton, *ibid.*, 91, 505 (1969).

(7) D. F. Veber, S. L. Varga, J. D. Milkowski, H. Joshua, J. B. Conn, R. Hirschmann, and R. G. Denkewalter, *ibid.*, 91, 506 (1969).

(8) R. Hirschmann, R. F. Nutt, D. F. Veber, R. A. Vitali, S. L. Varga, T. A. Jacob, F. W. Holly, and R. G. Denkewalter, *ibid.*, 91, 507 (1969).

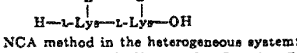
(9) R. S. Dewey, E. F. Schoenewaldt, H. Joshua, W. J. Paleveda, Jr., H. Schwam, H. Barkemeyer, B. H. Arison, D. F. Veber, R. G. Denkewalter, and R. Hirschmann, *ibid.*, 90, 3254 (1968).

(10) D. F. Veber, R. Hirschmann, and R. G. Denkewalter, *J. Org. Chem.*, 34, 753 (1969).

(11) Y. Iwakura, K. Uno, M. Oya, and R. Katakai, *Biopolymers*, 9, 1419 (1970).

(12) R. Katakai, M. Oya, K. Uno, and Y. Iwakura, *ibid.*, in press.

(13) Izumiya, *et al.*, synthesized



in 87% yield by the NCA method in the heterogeneous system: N. Mitsuyasu, S. Terada, K. Noda, M. Waki, T. Kato, and N. Izumiya, Proceedings of the 8th Symposium on Peptide Chemistry, Osaka, Japan, 1970, p 5.

(14) M. Goodman and J. Hutchison, *J. Amer. Chem. Soc.*, 88, 3527 (1966).

(15) Y. Iwakura, K. Uno, and M. Oya, *J. Polym. Sci., Part A-1*, 6, 2165 (1968).

UM00013890
NOVARTIS EXHIBIT 1017
Novartis v. Regents, IPR2023-01346
Page 2636 of 4460

ogeneous system of acetonitrile–water. Since glycine NCA cannot be transformed to the isocyanate through the NCA anion in the heterogeneous system, hydantoic acid is not formed in this system.

Experimental Section

Glycine NCA.[16]—Into a suspension of 10 g of finely powdered glycine in 400 ml of dry tetrahydrofuran, dry phosgene was bubbled at 45° with magnetical stirring. A clear solution was obtained after 2 hr. The solution was concentrated at reduced pressure at 30°, then glycine NCA crystallized out. To the residue was added 200 ml of *n*-hexane in order to crystallize out the NCA completely. The crystals of the product were filtered off and dried over P_2O_5 in a vacuum desiccator. The crude product was recrystallized twice from ethyl acetate to yield 9.8 g (73%) of the chlorine-free NCA,[17] mp 100° (lit.[18] 100°).

General Procedure for Synthesis of Glycyl Dipeptides.—To a solution of 0.01 mol of α-amino acid and 1 g of sodium carbonate in 10 ml of 1 *N* sodium hydroxide and 40 ml of water was added 40 ml of acetonitrile and the system was cooled to −10°. A solution of 1.2 g (0.012 mol) of glycine NCA in 24 ml of acetonitrile was added to the system and allowed to react for 3 hr at −10° with stirring. The aqueous layer of the system was washed with 50 ml of acetonitrile under cooling and neutralized with concentrated sulfuric acid. Sodium sulfate was removed by addition of 200 ml of ethanol followed by filtration and the alcoholic solution was concentrated *in vacuo* at 35°. Addition of 50 ml of ethanol and 100 ml of diethyl ether to the residue gave a crystalline product. The crude product was recrystallized from aqueous methanol to yield a crystalline dipeptide.

Glycyl-L-leucyl-L-alanine.—To a heterogeneous system of 50 ml of acetonitrile and 50 ml of 0.2 *N* sodium hydroxide containing 0.89 g (0.01 mol) of L-alanine and 1 g of sodium carbonate was added a solution of 1.73 g (0.011 mol) of L-leucine NCA in 17.3 ml of acetonitrile. The condensation reaction was allowed for 2 hr at −10° with stirring. After the reaction the acetonitrile layer of the system was separated off and the aqueous layer was washed with 100 ml of acetonitrile under cooling. The solution was warmed to 40° for 5 min. Then 50 ml of acetonitrile and 20 ml of 0.2 *N* sodium hydroxide were added to the solution and the system was cooled again to −10°. After the addition of 1.2 g (0.012 mol) of glycine NCA in 24 ml of acetonitrile, the system was kept at −10° for 3 hr with stirring. The aqueous layer of the system was treated by the same manner as above, washing, neutralization, and condensation. The crude product was recrystallized from aqueous ethanol.

Reaction of Glycine NCA with L-Tryptophan.—To a solution of 2.05 g (0.01 mol) of L-tryptophan and 1 g of sodium carbonate in 10 ml of 1 *N* sodium hydroxide and 40 ml of water, 40 ml of acetonitrile was added and the system was cooled to −10°. After the addition of 1.2 g of glycine NCA in 24 ml of acetonitrile the system was allowed to stand for 3 hr with stirring. The aqueous layer of the system was washed with 50 ml of acetonitrile and diluted with water to a volume of 50 ml. A 40-μl sample of the solution was analyzed by tlc on silica gel in pyridine–water (4:1). A strip showed three ninhydrin-positive spots, unreacted L-tryptophan (R_f 0.57), glycyl-L-tryptophan (R_f 0.39), and glycylglycyl-L-tryptophan (R_f 0.18). Three Ehrlich-positive spots were detected on another strip, L-tryptophan (R_f 0.57), glycyl-L-tryptophan (R_f 0.39), and glycylglycyl-L-tryptophan (R_f 0.18). Then the pertinent areas of the tlc developed anew were scraped off and extracted with 100 ml of water. The transmittancy of the extracts was measured at 280 mμ.[19] The residual sample was treated as above to isolate the dipeptide. The crude product was recrystallized from methanol to yield 2.33 g (89%) of a pure dipeptide: $[\alpha]_D$ 33.5° (*c* 2.5, 5 *N* HCl) [lit.[20] $[\alpha]_D$ 34.3° (*c* 2, 5 *N* HCl)]. *Anal.* Calcd for $C_{11}H_{11}N_3O_3$: C, 59.75; H, 5.80; N, 16.08. Found: C, 59.94; H, 6.06; N, 16.15.

Registry No.—Glycine NCA, 2185-00-4; Gly-Gly, 556-50-3; Gly-L-Ala, 3695-73-6; Gly-L-Val, 1963-21-9; Gly-L-Leu, 869-19-2; Gly-L-Phe, 3321-03-7; Gly-L-Leu-L-Ala, 32557-24-7; Gly-L-tryptophan, 2390-74-1.

(16) Y. Iwakura K. Uno, and S. Kang, *J. Org. Chem.*, **30**, 1158 (1965). We synthesized glycine NCA by the reaction of glycine with phosgene in tetrahydrofuran. The reaction time needed in phosgenation of the amino acid was shorter in this solvent than in any other solvents. High yield and high purity of the product were obtained in this solvent.

(17) M. Oya, K. Uno, and Y. Iwakura, *Kogyo Kagaku Zasshi*, **69**, 741 (1966).

(18) H. Leuchs, *Ber.*, **39**, 857 (1906).

(19) Uv spectra of peptides were measured with Shimazu MPS-50 L and Hitachi Perkin-Elmer 139 spectrophotometers.

(20) K. R. Rao, S. M. Birnbaum, R. B. Kingsley, and J. P. Greenstein, *J. Biol. Chem.*, **198**, 507 (1952).

A Convenient Synthesis of 5-Fluorouracil

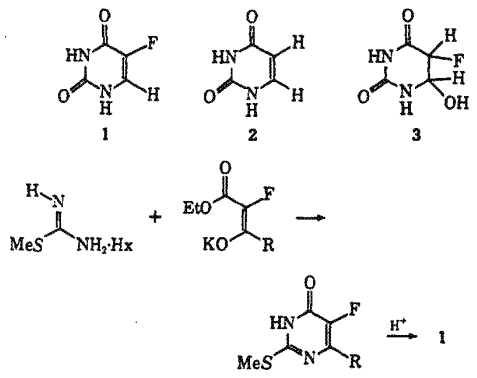
D. H. R. BARTON, R. H. HESSE,* H. T. TOH, AND M. M. PECHET

Communication No. 64[1] from the Research Institute for Medicine and Chemistry, Cambridge, Massachusetts 02142

Received August 18, 1971

5-Fluorouracil (1) is a cytotoxic analog of uracil of use in biochemical research and also of a certain value in medicine.[2] This derivative of uracil is typically prepared by a total synthesis as expressed in Chart I[3]

CHART I



which requires the use of a persistent and insidious toxin, fluoroacetic acid. The discovery that fluoroxytrifluoromethane (CF_3OF) is a useful reagent for the heretofore difficult direct electrophilic fluorination of aromatic compounds[4] led us to consider that the reaction of CF_3OF with uracil (2) (or an appropriate derivative thereof) might lead directly to 5-fluorouracil (or a derivative thereof) and thus constitute a convenient synthesis of such compounds. We now report that the direct conversion of uracil to 5-fluorouracil may be accomplished in high yield by electrophilic fluorination.

Electrophilic substitution at the 5 position of the pyrimidine ring is well known.[5] Uracil itself undergoes nitration at position 5 without complication,[6] and

(1) For no. 63, see D. H. R. Barton, T. J. Bentley, R. H. Hesse, F. Mutterer, and M. M. Pechet, *Chem. Commun.*, 912 (1971).

(2) G. Ramirez, *et al.*, *Amer. J. Surg.*, **120**, 400 (1970); J. Dule, *Bull. Soc. Fr. Dermatol. Syphiligr.*, **77**, 218 (1970); L. Y. Deemarsky, *et al.*, *Cancer*, **26**, 771 (1970); M. S. Mitchell, *et al.*, *ibid.*, **26**, 884 (1970); M. Hursthouse, *Brit. J. Dermatol.*, **82**, 218 (1970).

(3) R. Duschinsky, E. Pleven, and C. Heidelberger, *J. Amer. Chem. Soc.*, **79**, 4559 (1957).

(4) D. H. R. Barton, *et al.*, *Chem. Commun.*, 806 (1968).

(5) C. W. Kenner and A. Todd in "Heterocyclic Compounds," Vol. 6, R. C. Elderfield, Ed., Wiley, New York, N. Y., 1957, pp 235 ff.

(6) T. B. Johnson, *J. Amer. Chem. Soc.*, **30**, 19 (1908); *Chem. Abstr.*, **2**, 2792 (1909).

UM00013891
NOVARTIS EXHIBIT 1017
Novartis v. Regents, IPR2023-01346
Page 2637 of 4460

Pergamon

Bioorganic & Medicinal Chemistry, Vol. 4, No. 9, pp 1429–1446, 1996
Copyright © 1996 Elsevier Science Ltd
Printed in Great Britain. All rights reserved
PII: S0968-0896(96)00137-X
0968-0896/96 $15.00+0.00

The Rationale for E2020 as a Potent Acetylcholinesterase Inhibitor

Yoshiyuki Kawakami,[a,*] Atsushi Inoue,[a] Takatoshi Kawai,[a] Misako Wakita,[a] Hachiro Sugimoto[a] and Anton J. Hopfinger[b,*]

[a]*Tsukuba Research Laboratories, Eisai Co., Ltd., 1-3, Tokodai 5-chome, Tsukuba-shi, Ibaraki 300-26, Japan*
[b]*Department of Medicinal Chemistry and Pharmacognosy, MC 781, The University of Illinois at Chicago, 833 South Wood Street, Chicago, IL 60612-7231, U.S.A.*

Abstract—The phase III drug-candidate, E2020, developed for treatment of Alzheimer's disease, and possibly other dementias, and its analogues have been the focus of extensive molecular pharmacological and structural studies. The potency and selectivity of E2020 as an inhibitor of acetylcholinesterase, AChE, in the brain is established. A combination of molecular modeling and QSAR studies have been used throughout the evolution of the AChE inhibitor program leading to the benzylpiperidine series, and, ultimately, E2020. QSAR studies have identified requirements to optimize inhibition activity as a function of substituent choice on both the indanone and benzyl rings in the E2020 class of inhibitors. A combination of X-ray crystal structure studies of E2020 isomers and the molecular shape analysis, MSA, of E2020 and its analogues has led to a postulated active conformation, and molecular shape, for these AChE inhibitors. The active molecular shape corresponds to a high degree of shape similarity between the two E2020 isomers which, in turn, is consistent with the observed high inhibition potencies of both of these compounds. Intermolecular docking studies were carried out for E2020 and some analogues with the crystal structure of AChE when it became available. The docking simulations involving E2020 analogues suggest these inhibitors do not bind at the acetylcholine, ACh, active site, but rather at the most narrow location of the long channel leading to the active site. Intermolecular binding geometries are consistent with the postulated active conformations derived from structure–activity (receptor geometry independent) information. Copyright © 1996 Elsevier Science Ltd

Introduction

The reversible acetylcholinesterase (AChE) inhibitor, E2020 (1-benzyl-4-[5,6-dimethoxyl-(1-indanone)-2-yl]-methylpiperdine hydrochloride), see Figure 1, has been under clinical study as a candidate drug for the treatment of Alzheimer's disease (AD) where the cholinergic function is selectively, and irreversibly, affected in this senile demenita disease.[1] The mechanism proposed to explain the memory improvement through AChE inhibition is an increase in acetylcholine (ACh) levels in the central cholinergic synapses involved in the memory circuit.[2-5]

In principle, the synthesis of acetylcholine, its terminal release, interaction with synaptic receptors and ultimate degradation are straightforward mechanisms although the biochemical picture at each of these levels is becoming increasingly complex. Figure 2 shows a simplified metabolic pathway related to acetylcholine. The cholinergic hypothesis postulates that memory impairments in patients with AD result from a deficit of cholinergic functions in the brain. Several neurotransmitter systems undergo changes with advanced age. Significant cholinergic dysfunctions can occur in an aged and demented central nervous system. With respect to acetylcholine synthesis, it is generally accepted that the immediate precursors, acetyl coenzyme A and choline, are ultimately derived from circulating blood glucose and choline, respectively.[6] Activity of cholinergic markers, such as choline acetyltransferase and choline uptake, are markedly reduced (at least 40%) in the brains of patients with AD in comparison to age-matched controls. Biopsies indicate that cortical choline acetyltransferase loss can occur in AD, and certain areas, including the hippocampus, are most severely biochemically affected.

There exist relationships between the changes described above and loss of memory. Similar memory deficits can also be artifically induced by blocking cholinergic mechanisms in young subjects. Consequently, potentiation of central cholinergic action has been proposed as an approach for the palliative treatment of mild to moderate cases of AD.

The cholinergic hypothesis has provided the first rational approach to the treatment of AD by neurotransmitter replacement. ACh precursors, including various preparations of choline and lecithin, were the first compounds administered in the treatment of AD in an attempt to augment central cholinergic activity by enhancing ACh levels. However, the results of clinical studies have, so far, shown little or no evidence for the efficacy of this approach. AChE inhibitor type of drugs do show improvements in cognitive function in clinical study. Cholinergic agonists acting directly on muscarinic receptors may improve the cholinergic dysfunction. Five genetically defined muscarinic receptors subtypes (m1–m5) have been reported to date.[7]

UM00013892
NOVARTIS EXHIBIT 1017
Novartis v. Regents, IPR2023-01346
Page 2638 of 4460

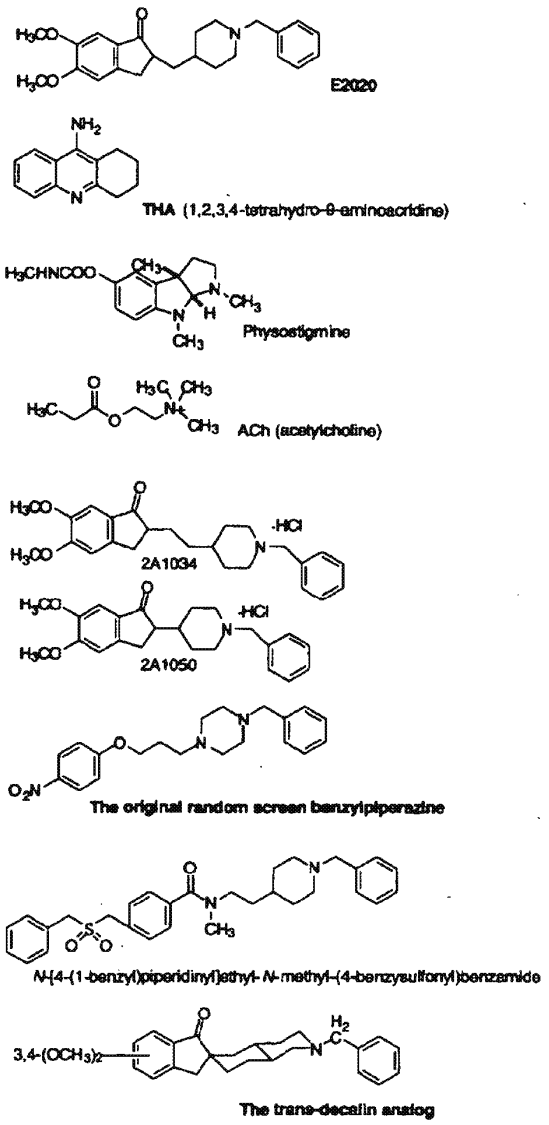


Figure 1. Structure of AChE inhibitors.

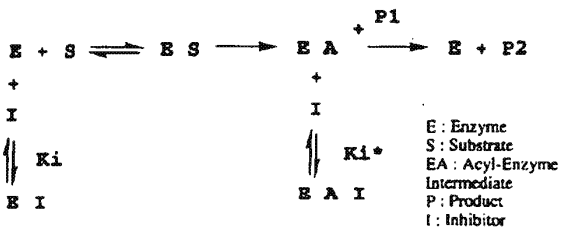


Figure 2. Reaction scheme in which the inhibitor combines with AChE and acylated AChE. E, free enzyme; S, substrates; ES, enzyme substrate complex; EA, acylated enzyme; P, product; I, inhibitor; ES, enzyme inhibitor complex; EAI, acylated enzyme inhibitor complex; K_i, dissociation constant for enzyme and inhibitor; K_i^*, dissociation constant for EA and inhibitor.

E2020 is the lead compound in a new class of AChE inhibitors having an *N*-benzylpiperidine and an indanone moiety which shows a greater selectivity for AChE than for butyrylcholinesterase, and is not expected to have any peripheral effects.[8] E2020 has been developed as a racemic mixture due to the same inhibitory profiles from each of the enantiomers.[9] Clinical studies of E2020 suggest that it is possibly effective in the treatment of patients with AD.[10] THA (tetrahydroaminoacridine, Fig. 1) recently became the first available agent for the treatment of AD in the U.S. However, the aminoacridines, in general, suffer from dose-limiting hepatotoxicity which is believed to be structure related.[11] Physostigmine, a carbamate-type inhibitor, has shown inconclusive results in the clinic, perhaps due to its short half-life and narrow therapeutic index. A controlled-released formulation of physostigmine is currently in phase-III trials. E2020 appears to be devoid of such an unfavorable side-effect profile probably because of its novel benzylpiperdine structure. Many groups have undertaken the design and synthesis of E2020-like compounds which incorporate bioisosteric replacements for the indanone ring.[12,13]

Methods and Results

Lead identification and optimization

A benzylpiperazine compound, see Figure 1, demonstrating weak (its IC_{50} is 14.5 μM), but definite inhibitory activity against AChE was identified in blind screening. Continued screening was performed around compounds of similar structures. Another type of 'seed' compound was found which has both benzylpiperidine and benzamide moieties in its structure. This compound has strong AChE activity, its IC_{50} being in excess of two orders of magnitude than that of the lead compound. Lead optimization synthesis, mainly involving modification of the benzamide moiety, led to *N*-[4-(1-benzyl)piperidinyl]ethyl-*N*-methyl-(4-benzylsulfonyl)benzamide, see Figure 1, which has an AChE IC_{50} five orders of magnitude smaller (higher inhibition potency) as compared to the original benzylpiperazine compound, as well as selective AChE inhibitory activity. However, compound **1** has a very short half-life due to hydrolyzation by proteases in the liver, which is believed to lead to an *N*-disubstituted amide metabolite.

Metabolic resistance was sought by incorporating bioisosteric replacements for the *N*-disubstituted amide moiety. A series of benzamide analogues possessing high AChE activity and which are readily transported into brain became the focus in the lead optimization process.

Over the course of the lead optimization it appeared that methyl substitution on the amide nitrogen enhanced activity. Thus, *trans* and *cis* forms of benzamide were considered as models since methyl substitution at the amide nitrogen may change the ratio of *cis* and *trans* isomers of the amide. Overall, conformation

UM00013893
NOVARTIS EXHIBIT 1017
Novartis v. Regents, IPR2023-01346
Page 2639 of 4460

$$\log 1/C = 0.019\,MR - 2.372\,\Delta E(C\text{-}T) + 22.94$$

$$n=19,\ s=0.256,\ r=0.833$$

log 1/C : negative logarithm of IC_{50} of AChE
MR : molar refractivity
$\Delta E(C\text{-}T)$: energy difference between cis and trans isomer (kcal/mol) by CNDO/2

Figure 3. QSAR of *para*-substituted benzamides.

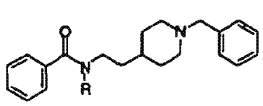
was considered an important component in a QSAR analysis used to guide the initial lead optimization process. A good correlation equation, QSAR, was found between activity, as measured by IC_{50}, and the difference in energy between the *cis* and *trans* isomers, $\Delta E(C\text{-}T)$ and the bulkiness of substituents (see Figure 3). The QSAR suggests that the intrinsic activity of *cis* isomers of benzamide are higher than the *trans* isomers, since there is a negative correlation between IC_{50} and $\Delta E(C\text{-}T)$.

Table 1 contains the structure–activity behavior of *N*-alkylated amides which have higher activity compared with non-*N*-alkylated analogues. Conformational analysis of the *N*-alkyl-substituted benzamides was performed using the MNDO quantum chemical method.[14] Figure 3 contains the estimated ratio of *trans* and *cis* isomers of some *N*-alkyl substituted benzamides. Nonsubstituted amides exist almost completely in the *trans* form, but *N*-substitution raises the *trans* conformational energy state so that, overall, the *cis* conformation becomes more stable. These results again indicate that AChE activity increases as the population of the *cis* isomer of the benzamide increases.

The QSAR analysis provided the structural requirements for lead evolution. The specific structural requirements identified in the QSAR analysis are as follows: (1) the *cis* conformation of the benzamide is the active conformation, (2) bulky groups at the *para* position of the benzamide increases activity, and (3) the carbonyl oxygen of the amide is a proton acceptor for an intermolecular hydrogen bond.

Flexible benzamide analogues having the *cis* conformation were made. One of these was E2020 which

Table 1. *N*-Alkyl analogues of *N*-[4-(1-benzyl)piperidinyl]ethylbenzamide



R	IC_{50} (mM)
H	560
Benzyl	180
Methyl	170
Ethyl	130
Phenyl	35

possesses benzylpiperidine and indanone moieties. E2020 was the first compound in which an indanone ring was part of the enzyme inhibitor.

E2020 as a selective AChE inhibitor

Pharmacology. E2020 was initially thought to be a mimic of ACh by structural similarity, and, therefore, a competitive inhibitor of AChE. The *N*-benzylpiperidines show outstanding in vitro selectivity for AChE. The IC_{50} of E2020 for AChE is 5.7 nM, while the IC_{50} for BuChE (butyrylcholinesterase) is ~7000 nM, a selectivity ratio in excess of three orders of magnitude. THA and physostigmine show poor selectivity having the same order of magnitude IC_{50}s for both AChE and BuChE. Inhibition of BuChE, which is abundant in plasma, may be associated with potentiating peripheral side effects.[15] Therefore, an AChE inhibitor which is essentially devoid of BuChE activity may display higher therapeutic indices than those which are also active BuChE inhibitors.

Dissociation constants. AChE catalysis involves an active serine residue, and the overall catalytic process proceeds in a three-step mechanism, as defined in Figure 2, like transfer within a catalytic triad. The activated serine residue enables a nucleophilic attack on ACh, resulting in hydrolysis and acetate products being released. Some reversible AChE inhibitors show a mixed type of inhibition by blocking the deacetylation process. The acetyl group is introduced into the esteratic site in this catalytic process. Therefore, acylated AChE can accept an external charged molecule at this vacant anionic site to form an EA–inhibitor complex (EAI). E2020 appears to bind to both the free enzyme and the acylated enzyme to block both Michaelis complex formation and deacetylation.

Molecular modeling and lead evolution

X-ray crystallography of E2020. A single crystal of E2020, crystallized from ethanol:acetone (1:2) mixed

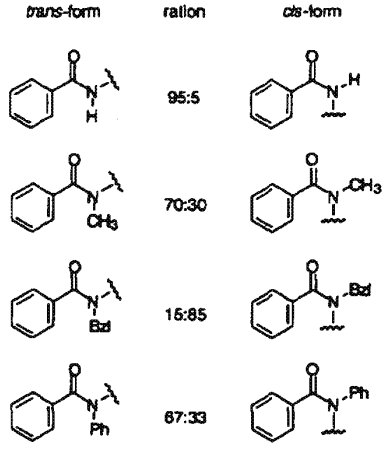


Figure 4. Estimated ratio of *trans* and *cis* isomer 5 in *N*-alkyl analogues of *N*-[4-(1-benzyl)piperidinyl]ethylbenzamide.

UM00013894
NOVARTIS EXHIBIT 1017
Novartis v. Regents, IPR2023-01346
Page 2640 of 4460

solution, was prepared and used. Data collection was performed with Cu K_α radiation ($\lambda = 1.54184$ Å) on an Enraf–Nonius CAD4 computer-controlled k axis diffractometer equipped with a graphite crystal, incident beam monochromator. The crystal was found to be triclinic with unit cell parameters $a = 9.977$ (2), $b = 13.347$ (4), $c = 8.541$ (6) Å, $\alpha = 92.72$ (4)°, $\beta = 100.59$ (3)°, $\gamma = 75.47$ (2)°, and $V = 1082.1$ Å^3. For $Z = 2$ and $M_r = 415.96$, the calculated density D_{calcd} is 1.28 g/cm^3. From least-squares refinement, the space group was determined to be $P\bar{1}$ (No. 2). The data were collected to a maximum 2θ–ω of 128.0° using the 2θ–ω scan technique. Lorentz and polarization corrections were applied to the data. No absorption correction was made and intensities of equivalent reflection were averaged. The structure was solved by direct methods. Full-matrix least-squares refinement of atomic positional and thermal parameters [anisotropic C, Cl, N, O; isotropic H (fixed at 4.0 Å^2)] converged at $R = 0.073$ over 2818 reflections with $I > 3\sigma(I)$.

The same procedures used to determine the crystal structure of E2020 at ambient temperature were also employed to solve the crystal structure of E2020 at low temperature (−20 °C). The unit-cell parameters were $a = 9.982$ (5), $b = 13.335$ (7), $c = 8.526$ (5) Å, $\alpha = 92.38$ (4)°, $\beta = 100.71$ (5)°, $\gamma = 75.38$ (4)°, and $V = 1079.0$ Å^3, $Z = 2$ and D_{calc} is 1.28 g/cm^3. The space group is $P\bar{1}$; $2\theta = 128.0°$. Thermal parameters were refined anisotropically for C, Cl, N, O and isotropically for H. The final R value is 0.075 over 3120 reflections with $I > 3\sigma(I)$.

Figure 5 shows the ORTEP[16] drawing of the racemic E2020 crystal structure. The ORTEP shows a pattern of irregular thermal ellipsoids. There is an asymmetric carbon atom at the 2-position of indanone ring and the irregular thermal motions phenomenon occurs around this chiral center. This thermal behavior is observed both at 23 and −20 °C and corresponds to two puckering structures of the indanone ring. Thus, the crystal structure of the indanone ring consists of two conformers. One conformer has a relative R configuration and the other has a relative S configuration. The most remarkable feature of R and S enantiomers is that they have the same molecular-shape except for small portions of the indanone and piperidine rings. The R and S configurations are so similar that they are not even recognized in the crystalline state. These two conformers also have almost equal heats of formation as computed by MNDO, and the crystal structure is one of the most stable intramolecular conformations of each E2020 enantiomer. This high intramolecular stability suggests that these two conformations may not only exist in the crystal state, but also in solution. However, solution structure studies of E2020 have not yet been performed.

Receptor independent molecular modeling and QSAR analyses. A comprehensive computer-assisted molecular design, CAMD, investigation of some of the E2020 analogues began at a point where crystals structures of E2020 had been determined, but a crystal structure of a AChE was not yet available. Approximately 80 analogues of E2020 had also been made and tested at the start of the on-going comprehensive CAMD study, and somewhere between 25 and 35 additional analogues have become available over the course of the CAMD investigation to date. This CAMD study is continuing with a focus on intermolecular ligand–receptor modeling.

The experimental design phase of the CAMD study identified that the maximum amount of structure–activity information would be derived from using only those analogues that could be placed into one of four structural feature sets. Each structural feature set corresponds to analogues differing from one another by a single, common location chemical change. This permits the differences in activity for analogues in a set to be considered only a function of the single chemical

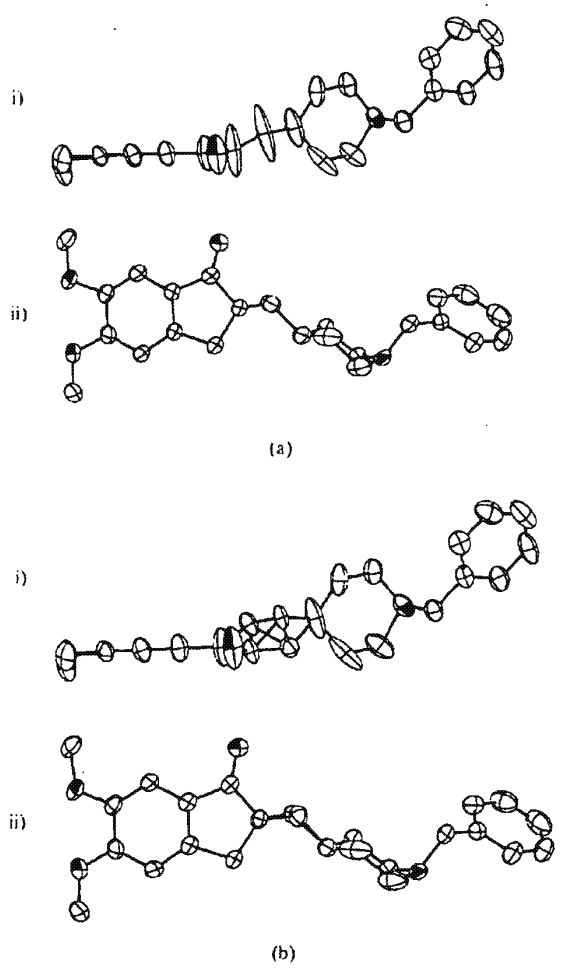


Figure 5. (a) X-ray crystal structure of racemic E2020 at −20 °C. (i, top) View along the plane of the indanone ring. (ii, bottom) View into the plane of the indanone ring. (b) X-ray crystal structure of racemic E2020 for discrete peaks. A racemic occupancy of 0.6(R) and 0.4(S) was found from the differential Fourier map. (i. top) View along the plane of the indanone ring. (ii, bottom) View into the plane of the indanone ring.

UM00013895
NOVARTIS EXHIBIT 1017
Novartis v. Regents, IPR2023-01346
Page 2641 of 4460

modification characteristic of the set. The composite experimental design led to the consideration of all E2020 analogues of the structural class shown in Figure 6. Within the framework of CAMD methods the construction of the four *feature* sets defined in Figure 6 corresponds to using the molecular decomposition–recomposition, MDR, technique[17] to construct databases for combined QSAR and molecular modeling studies on indanone benzyl piperidine inhibitors of AChE. The justification of using the particular MDR operation defined in Figure 6 is given in ref 18. The CAMD study for each feature is described below.

Feature 1. The set of 17 analogues reported in Table 2 were used to develop the feature 1 QSARs. These compounds were selected because all of them have the same general structure, I. The feature 1 structures differ from one another only by the substituents (R_1, R_2, R_3) on the aromatic ring of the indanone bicycle. Thus, the SAR for this set of compounds is due only to (R_1, R_2, R_3), and the MDR technique can be applied. In general, isomers at the *-carbon of the indanone ring are not resolved with respect to inhibition potency. The role of this chiral center on molecular conformation has been explored as part of the feature 2 analysis. The spacer link from C* to the piperidine ring is at least partially saturated, and in most cases totally saturated, so that resonance effects from substituent modifications on the rest of the molecule can be neglected.

The range on AChE inhibition potency for the 18 analogues is 1.3–380 nM IC_{50} units.

Conformational and electronic descriptors were determined using the model compound **I** to represent all analogues. The details of the molecular modeling procedures are given in ref 18.

Local minimum energy conformer states up to 6 kcal/mol above the apparent global minimum[19] were used to generate property measures of the descriptors used to generate feature 1 trial QSARs. The following set of descriptors was used in the QSAR analysis of feature 1: (1) Partial charge densities (from MNDO) on the C_1 to C_6 carbon atoms in 3. (2) The total dipole moment, U_T, and the angle the dipole makes with the C=O bond in the plane of the indanone ring. (3) Component of the dipole moment in the C=O direction, U_Z. (4) Lowest unoccupied molecular orbital energy, LUMO. (5) Highest occupied molecular orbital energy, HOMO. (6) Atomic orbital electron populations in C_3, C_4, and C_5. (7) Sum of the atomic orbital electron populations in C_1–C_6. (8) Sum of the atomic orbital electron populations in C_1–C_6 plus C_9 and O_{10}. HOMO π coefficient of each of the phenyl carbons C_1–C_6 as well as O_{10}. (10) Sum of the squares of the HOMO π coefficients of C_1–C_6 plus C_9 and O_{10}. (11) Partition coefficient, log P,[20] of X 3.

Trial QSARs were generated by considering all combinations of the descriptors for feature 1. Both linear and quadratic descriptor terms were used in the set of multidimensional linear regression, MLR, analyses. The SAS package[21] was used to carry out the statistical analyses.

GA discussion

The optimum 3-D QSAR that could be constructed using direct MLR for substitution onto the aromatic unit of the indanone ring, based upon all of the analogues in Table 2, is:

$$-\log(IC_{50}) = 2.73[C_4] + 1.86[U_T] - 0.14[U_T^2] - 156.7[\text{HOMO}] - 8.25[\text{HOMO}^2] - 740.93 \quad (1)$$

$N = 17$; $R = 0.804$; SD = 0.46; $F = 4.4$; $U_T(\max) = 6.6$ debye; HOMO(max) = −9.49 eV,

where C_4 is the HOMO out-of-plane π-orbital coefficient of ring carbon four, and the other terms in equation (1) have already been explicitly defined. An analysis of the residual of fit, $\Delta \log (IC_{50}) = (-\log (IC_{50}))_{obsd} - (-\log (IC_{50}))_{calcd}$, of equation (1) indicates that the marginal fit of this correlation equation is largely due to two outliers-compounds **4** and **17** of Table 2. Compound **4** is predicted to be less active that observed, while the opposite is true for **17**.

If compounds **4** and **17** are not considered in the direct MLR analysis, then the remaining 15 compounds can be described by the 3-D QSAR:

$$-\log (IC_{50}) = 2.21[C_4] - 6.65[U_T] + 1.18[U_T^2] - 162.9[\text{HOMO}] - 8.58[\text{HOMO}^2] - 757.52 \quad (2)$$

$N = 15$; $R = 0.939$; SD = 0.25; $F = 14.8$; $U_T(\max) = 2.8$ debye; HOMO(max) = −9.49 eV.

The most obvious difference between equations (1) and (2), besides the considerable increase in statistical

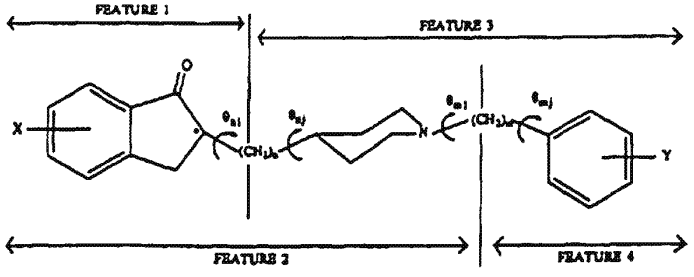
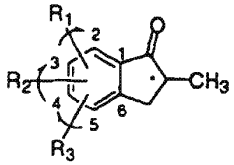


Figure 6. Definition of the four features of the E2020 analogue inhibitors of AChE.

UM00013896
NOVARTIS EXHIBIT 1017
Novartis v. Regents, IPR2023-01346
Page 2642 of 4460

Table 2. General SAR data for Feature I based upon model compound I



No.	R_1	R_2	R_3	C_4	U_T (debye)	HOMO energy (eV)	Obsd $-\log(IC_{50})$	Calcd [equation (2)] $-\log(IC_{50})$	Obsd−calcd [equation (1)] $-\log(IC_{50})$	Calcd [equation (2)] $-\log(IC_{50})$	Obsd−calcd [equation (2)] $-\log(IC_{50})$
1	3-OH	4-OMe	H	0.356	3.918	−9.305	8.88	8.46	0.42	8.81	0.07
2	3-OMe	4-OMe	H	0.454	2.301	−9.533	8.28	7.38	0.90	8.20	0.08
3	3-OEt	4-OEt	H	0.505	2.855	−9.631	8.20	8.00	0.20	7.86	0.34
4	H	H	5-Me	0.234	2.966	−9.593	8.15	7.46	0.69		
5	3-OMe	4-O-isop	H	0.449	3.332	−9.451	8.05	8.48	−0.43	8.19	−0.14
6	H	H	5-OMe	0.249	3.127	−9.545	7.92	7.72	0.20	7.55	0.37
7	2-OMe	3-OMe	4-OMe	0.468	2.765	−9.615	7.88	7.84	0.04	7.82	0.06
8	H	4-OMe	5-OMe	0.452	2.629	−9.461	7.70	7.77	−0.07	7.93	−0.23
9	3,4-Methylenedioxy		H	0.409	2.785	−9.314	7.64	7.58	0.06	7.51	0.13
10	2-OMe	4-OMe	H	0.364	2.845	−9.581	7.60	7.70	−0.10	7.64	−0.04
11	2-OMe	H	5-OMe	0.251	3.248	−9.443	7.44	7.86	−0.42	7.65	−0.21
12	3-Me	H	H	0.168	3.004	−9.615	7.16	7.27	−0.11	7.19	−0.03
13	3-OMe	H	H	0.247	2.980	−9.577	7.09	7.53	−0.44	7.42	−0.33
14	2-OMe	3-OMe	H	0.027	3.192	−9.376	7.06	7.10	−0.04	7.00	0.06
15	H	H	H	0.021	3.009	−9.716	6.83	6.58	0.25	6.58	0.25
16	3-F	H	H	0.226	3.467	−9.856	6.70	6.90	−0.20	6.80	−0.10
17	3-OMe	4-OH	H	0.463	1.946	−9.508	6.42	6.97	−0.55		

significance of equation (2), is the change in the dependence of $-\log(IC_{50})$ on U_T. According to equation (2), $-\log(IC_{50})$ increases with increasing U_T for $U_T > 2.8$ debye, while for equation (1), $-\log(IC_{50})$ decreases as U_T increase for U_T 6.6 debye. However, these two relationships between $-\log(IC_{50})$ and U_T are not inconsistent for most of the analogues in Table 2. Fifteen of the 17 compounds in Table 2 have U_T values in the 2.8–6.6 debye range. Both equations (1) and (2) predict $-\log(IC_{50})$ to increase with increasing U_T in this range of dipole values.

Neither equations (1) or (2) are particularly satisfying. Consequently, a subsequent QSAR analysis was undertaken using a genetic algorithm formalism called the genetic function approximation, GFA.[22] The GFA algorithm applied to the feature 1 dataset illustrates the automatic behavior of spline-based models in QSAR analysis.[23]

Feature 1 QSAR analysis using the GFA began with a population of 300 random models. The terms of the models were linear polynomials, linear splines, and quadratic splines. Only the three descriptors identified in the MLR study were used. However, spline basis functions were included to explore possible partitions of the data set. The population was evolved for 5000 crossover operations. By that point there was little continued improvement in the average score of the models in the population.

The splines used are *truncated power splines* and are denoted with angle brackets. For example, $<f(\mathbf{x})-a>$ is equal to zero if the value of $(f(\mathbf{x})-a)$ is negative, else it is equal to $(f(\mathbf{x})-a)$. The constant a is termed the *knot* of the spline. When a spline term is created, the knot is set using the value of the descriptor in a random data sample.

Splines are interpreted as performing either *range identification* or *outlier removal*. If there are many members in the nonzero partition, then the spline is identifying a range of effect. If there are only a few members of the nonzero set, the spline is identifying outliers. Regression can use the spline term to fit these members independent of the other terms of the model by, effectively, making them 'special cases' based on the extreme value of a descriptor.

The top 10 QSAR models discovered by the GFA algorithm are reported in Table 3. An example of outlier removal is the most frequent used spline, $<2.301-U_T>$. The only compound for which this item is nonzero is compound **17**, which was identified as one of the two outliers in the original study. All of the top 10 models isolate compound **17** in this manner. An example of range identification is the use of spline terms based on HOMO. For example, model 3 contains the term $<-9.545-\mathrm{HOMO}>^2$, which is nonzero for approximately half of the compounds: **3**, **4**, **7**, **10**, **12**, **13**, **15**, and **16**. The interpretation is the HOMO has an effect on activity only after it achieves a more negative value than −9.545. Four of the top 10 most frequently used basis functions are of this form.

An interesting effect in the selection of splines for the top 10 QSAR models was the isolation of the least

UM00013897
NOVARTIS EXHIBIT 1017
Novartis v. Regents, IPR2023-01346
Page 2643 of 4460

active compounds. If a histogram is constructed of the number of times each spline term is nonzero for each of the compounds in the data set, a strong skew toward the least active compounds is observed, as shown in Figure 7. The system is building general models of the most-active compounds and taking the least-active as special cases.

Feature 2. The set of model compounds encompassed in II was used to characterize the conformational behavior of the bicycle-piperidine portion of the AChE inhibitor analogues. In II, $W=(CH_2)_n$ [$n=0$, 1, 2, or 3], or a combination of single and double bond spacer units, A is usually CH_2, but can also be C=O, and X and Y are CH or N.

Table 4 contains the set of substructure II analogues used to investigate feature 2. Each structure in Table 4 corresponds to an analogue of E2020 for which the remainder of the molecule CH_2Ph is replaced by Me. Thus, the variations in IC_{50} reported in Table 4 are due solely to the structural changes represented by II. Note that a couple of key analogues in Table 4, with respect to modeling, correspond to changes on the piperidine ring of E2020: (1) compound **20** in which there is an additional nitrogen atom at position X and (2) compound **21** in which the piperidine nitrogen has been changed from Y to X. Table 4 is subdivided into (a) that contains active inhibitors which have one or two torsion angles (θ_1, θ_2) between the bicycle and the piperidine rings, (b) that contains substructure analogues for inactive inhibitors having zero, one, or two torsion angles between the rings, (c) that contains substructure analogues for active inhibitors having three or four torsion angles between the rings. It should be noted that some 6–6 bicycles were considered in exploring the SAR and one is given in Table 4. These analogues provide additional information to map the active molecular shape of feature 2 substructures.

Table 3. The top 10 3-D QSAR models derived for feature 1 based upon GFA analysis

(1) $-\log(IC_{50}) = 6.950$
$+2.046^{*}\ C_4$
$-6.523^{*} <2.301-U_1>$
$+1.037^{*}(U_1-2.845)^2$
$-22.090^{*} <-9.631-\mathrm{HOMO}>^2$
LOF: 0.209
r: 0.923
F: 17.16

(2) $-\log(IC_{50} = 7.101$
$+2.040^{*}\ C_4$
$-4.581^{*} <2.301-U_1>$
$+2.988^{*} <U_1-3.467>$
$-7.178^{*}\ (\mathrm{HOMO}+9.508)^2$
LOF: 0.216
r: 0.920
F: 16.55

(3) $-\log(IC_{50}) = 7.053$
$+1.983^{*} <C_4-0.027>$
$-6.468^{*} <2.301-U_1>$
$+0.987^{*}(U_1-2.845)^2$
$-11.185^{*} <-9.545-\mathrm{HOMO}>^2$
LOF: 0.221
r: 0.918
F: 16.10

(4) $-\log(IC_{50}) = 7.035$
$+1.771^{*}\ C_4$
$-7.683^{*} <2.301-U_1>$
$+1.241^{*}(U_1-2.966)^2$
$-18.192^{*} <-9.615-\mathrm{HOMO}>^2$
LOF: 0.224
r: 0.917
F: 15.84

(5) $-\log(IC_{50}) = 7.080$
$+1.778^{*} <C_4-0.027>$
$-7.686^{*} <2.301-U_1>$
$+1.242^{*}(U_1-2.966)^2$
$-18.196^{*} <-9.615-\mathrm{HOMO}>^2$
LOF: 0.224
r: 0.917
F: 15.82

(6) $-\log(IC_{50}) = 7.138$
$-1.615^{*} <C_4-0.027>$
$-7.619^{*} <2.301-U_1>$
$+1.231^{*}(U_1-2.966)^2$
$-4.616^{*} <-9.631-\mathrm{HOMO}>$
LOF: 0.225
r: 0.917
F: 15.80

(7) $-\log(IC_{50}) = 7.092$
$+1.756^{*} <C_4-0.027>$
$-7.667^{*} <2.301-U_1>$
$+1.234^{*}\ (U_1-2.966)^2$
$-15.250^{*} <9.593-\mathrm{HOMO}>^2$
LOF: 0.225
r: 0.917
F: 15.79

(8) $-\log(IC_{50}) = 7.098$
$+1.607^{*}\ C_4$
$-7.615^{*} <2.301-U_1>$
$+1.231^{*}(U_1-2.966)^2$
$-4.610^{*} <-9.631-\mathrm{HOMO}>$
LOF: 0.225
r: 0.917
F: 15.78

(9) $-\log(IC_{50}) = 8.076$
$-2.110^{*} <0.468-C_4>$
$+3.354^{*} <U_1-3.467>$
$-12.972^{*} <2.301-U_1>^2$
$-8.219^{*}(\mathrm{HOMO}+9.545)^2$
LOF: 0.225
r: 0.916
F: 15.74

(10) $-\log(IC_{50}) = 7.056$
$+1.739^{*}\ C_4$
$-21.539^{*} <2.301-U_1>^2$
$+1.223^{*}(U_1-2.966)^2$
$-13.468^{*} <-9.577-\mathrm{HOMO}>^2$
LOF: 0.226
r: 0.916
F: 15.65

UM00013898
NOVARTIS EXHIBIT 1017
Novartis v. Regents, IPR2023-01346
Page 2644 of 4460

Active conformations were sought by attempting to identify stable intramolecular conformer states for active analogues that are not stable for inactive analogues. This modeling strategy is called the LBA–LCS (loss in biological activity–loss in conformational stability) principle.[24] The details of the conformational analyses are given in ref 18.

Molecular-shape comparisons were performed by superimposing pairs of molecules under an initial three-atom constraint (spatial pharmacophore) and then performing an optimization with respect to the molecular-shape similarity measure. The measure of molecular-shape similarity has been based upon considering molecular geometry and corresponding conformational energetics. The geometric measures of molecular shape similarity include one, or more, pairs of interatomic distances and/or maximizing common overlap steric volume. Conformational energetics have been built into the estimation of molecular-shape similarity by using loss in conformational energy of an analogue (relative to the intramolecular global minimum energy conformation), to achieve an increase in the geometric measure of molecular-shape similarity, as a penalty function to the geometric measure.[25]

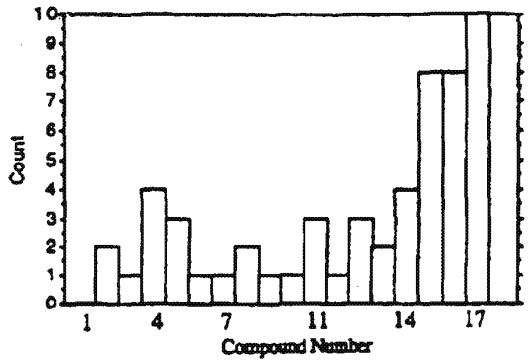
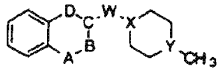


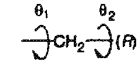
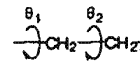
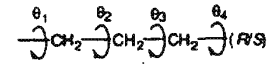
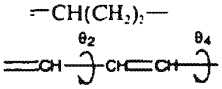
Figure 7. Histogram of the number of times a given compound was made a special case in the top 10 models. The histogram shows a skew toward the highest-numbered compounds, which are also the least active. In effect, the GFA algorithm is making special cases of the least-active compounds and modeling the patterns it found in the most active analogues.

The four compounds, two actives, **18A** and **20**, and two inactives, **21** and **22** (of Table 4), whose conformational energy maps are shown in Figures 8 and 9 have a common global minimum near ($q_1 = 300$, $q_2 = 300°$). These compounds also have various other local minimum energy regions as can be seen in Figures 8 and 9. At this point, any of the conformations near minima might be the active conformer. However, it is unlikely that any of the high-energy conformer minima of **18A** and **20** in the upper left-hand portion of their respective energy maps could be the active conformation. Hence, conformations ($\theta_1 = 300$, $\theta_2 = 300°$) and ($\theta_1 = 200$, $\theta_2 = 200°$) are considered the only possible candidates for the active (θ_1, θ_2) conformation.

Conformational analysis of the *trans* isomer of compound **19** the other active analogue of Table 4 (the *cis* isomer was found to be a high-energy isomer for all

Table 4. The analogues of, or similar to, E2020 used to map the active conformations, (q_1, q_2), with respect to feature 2



No.	A	B	C	D	X	Y	W	IC_{50}, nM
			(a) Active analogues with two torsion angles (θ_1, θ_2)*					
18A	CH_2	Bond	CH—	CH—O	CH	N		5.3
18B	CH_2	Bond	CH	C—O	CH	N	$-CH_2-(S)$	7.7
19	CH_2	Bond	C=	C=O	CH	N	=CH—	8.4
20	CH_2	Bond	CH—	C—O	N	N	$-CH_2-$	94.0
			(b) Inactive analogues with one, θ_1, or two torsion angles (θ_1, θ_2)					
21	CH_2	Bond	CH—	C=O	N	CH	$-CH_2-(R/S)$	480.0
22	CH_2	Bond	=C	HC—	CH	N	$-CH_2-$	4400.0
23	CH_2	Bond	CH—	C—O	CH	N	(R/S)	3300.0
24	CH_2	Bond	C—	C=O	=C	N	—	1200.0
			(c) Active analogues with three (θ_1, θ_2, θ_3) or four torsion angles (θ_1, θ_2, θ_3, θ_4)					
25	C=O	Bond	N—	C—O	CH	N		0.90
26	NH	C—O	CH	C—O	CH	N	$-(CH_2)_2-$	4.2
27	CH_2	Bond	CH	C—O	CH	N		1.5
28	CH_2	Bond	C=	C=O	CH	N	$=CH(CH_2)_2-$	0.82
29	CH_2	Bond	C—	C—O	CH	N		3.0

UM00013899
NOVARTIS EXHIBIT 1017
Novartis v. Regents, IPR2023-01346
Page 2645 of 4460

conformer states), indicates two minimum energy states with respect to θ_2.

Superposition of the conformational minima of compound **19**, with the two possible active conformations of **18A**, suggests that the conformer ($\theta_1 = 300$, $\theta_2 = 300°$) of **1A** is the only one which adopts a similar molecular shape to a minimum of **19**. Therefore, the ($\theta_1 = 300$, $\theta_2 = 300°$) intramolecular minimum energy state is postulated to be near the active conformation.

The postulated active conformation for **18A** is shown in Figure 10. The observed inhibition potencies of analogues **18B**, **20**, **23**, and **24** of Table 4 can be interpreted in terms of the molecular shape of **1A** in the postulated active conformation. Compound **18B** is active and, therefore, must adopt the postulated active conformation, or more correctly, active molecular shape, as a low energy stable state. Superposition of **18A** on **18B**, in their respective active molecular shapes, indicates that these two isomers have their indanone rings superimposed, and that their respective piperidine rings are perpendicular to the bicycle and exhibit significant overlapping.

The inactivity of both **23** and **24** is explained by their being too short, due to the lack of a bridging methylene group, to have their indanone and piperidine rings simultaneously superimpose on those of **18A** in the active conformation.

Analogue **20** is only 10–15 times less active than the most active analogue in Table 4(a). It is difficult to explain the lack of higher activity of this compound. One possible explanation for the observed activity profile of **20** is based on the active centers hypothesis of the E2020 derivatives. Compound **20** has two

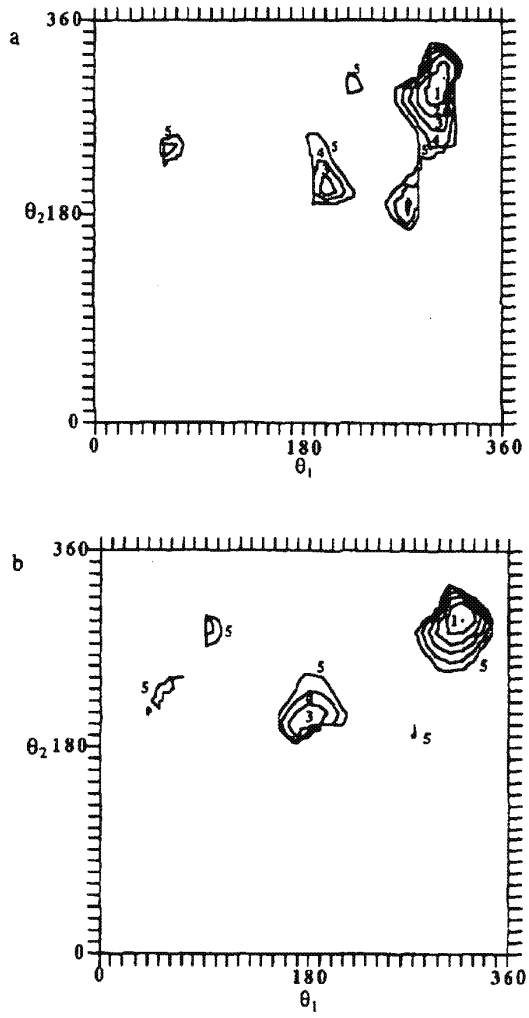


Figure 8. Conformational energy maps of key active analogues of II from Table 4 used to postulate the active conformation (shape) with respect to (θ_1, θ_2). The energy contours are in kcal per mole relative to the global minimum denoted by (●): (a. top) **18A**, (b. bottom) **20** of Table 4.

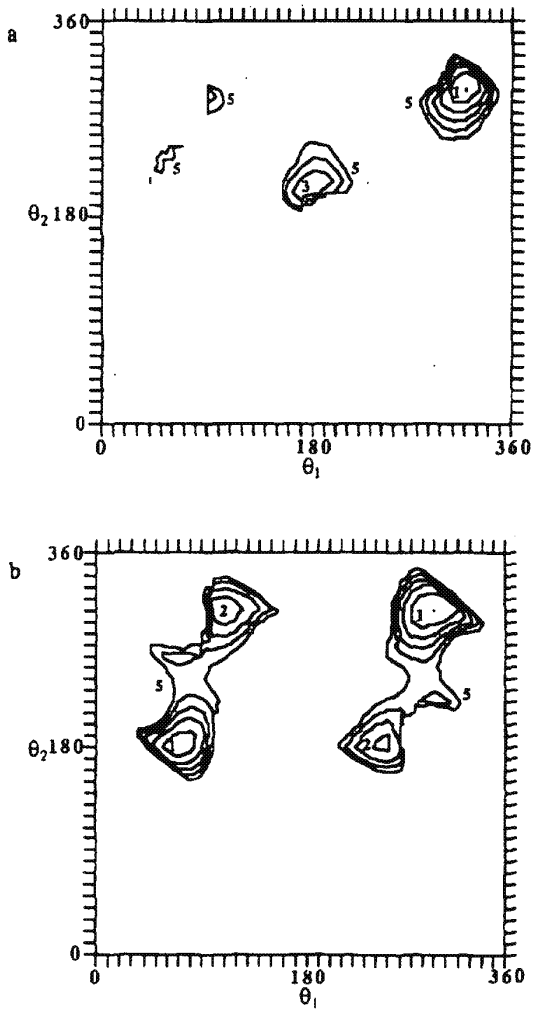


Figure 9. Same as Figure 8, but for key inactive analogues (a, top) **21**, (b, bottom) **22** of Table 4.

UM00013900
NOVARTIS EXHIBIT 1017
Novartis v. Regents, IPR2023-01346
Page 2646 of 4460

possible cationic nitrogen centers. The two nitrogens may compete for a single anionic site on the enzyme. These competitive interactions may lead **20** to a binding state for which both N atoms are at similar distances from the anionic receptor center. Such a virtual 'displacement' may then move the carbonyl group of the bicycle from its optimum binding position. A less favorable desolvation binding energy, as compared to **18A/B**, might also contribute to the loss in inhibitory potency.

The absence of a carbonyl oxygen and the relocation of the nitrogen in compounds **22** and **21**, respectively, each lead to major losses in activity. These structural changes also lead to losses in key AChE binding interaction which are discussed in the section on ligand docking.

Hypotheses for the 'active' conformations (shapes) of analogues of **II** having three or four torsion angles (W) between the indanone and piperidine rings are not definitive. There are two reasons for this ambiguity. First, the additional conformational flexibility in the three and four torsion angle analogues makes the exploration of conformational space more difficult. More significant, however, is that inactive three and four torsion angle analogues having structural changes which alter conformational behavior are not available. Hence, the LBA–LCS principle cannot be used.

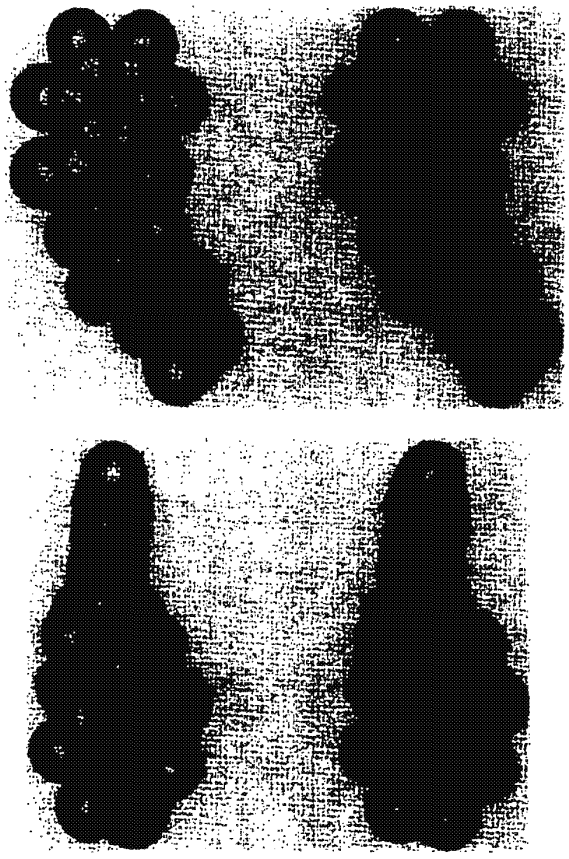


Figure 10. The postulated active conformation for analogues of **II** containing two torsion angles (θ_1, θ_2). The example here is the stereoview of **18A** of Table 4. (i, top) View into the plane of the indanone ring. (ii, bottom) View along the plane of the indanone ring.

An alternative approach to the LBA–LCS principle to probe for active conformation candidates for the analogues in Table 4(c) first focused on the conformational analysis of the most rigid analogue in this series, compound **29**. The double bonds induce conformational rigidity. All possible combinations of *cis* and *trans* isomers were considered in the conformational analyses of **29**. The all-*trans* conformational energy minima are generally lower than the minima of the other possible isomers by 3–5 kcal/mol. Thus, the assumption was made that the all *trans*-isomer was the relevant bioactive structure. No all-*trans* structure adopts a minimum energy conformation within 5 kcal/mol of its global intramolecular minimum that permits even marginal similarity superposition of its indanone and piperidine rings onto those of **18A**. It is not possible to determine any energetically reasonably superpositions of the highly flexible analogues **27** and **28** onto **18A**.

The molecular shape analysis becomes more confusing when stable conformations within 5 kcal/mol of the global minimum of each of the two active analogues having three torsions (compounds **25** and **26**) are compared to **18A**, in its active conformation, and to the stable conformations of **29**. In essence, no conformations near the relative minima of **25** or **26** meaningfully superimpose on either **18A** or **29**. One possible explanation of the differences in molecular shapes among the two, three, and four torsion angle classes of analogues of **II** is that each class has a distinct active molecular shape. This explanation is consistent with the docking simulations of E2020 and analogues to AChE that are discussed below.

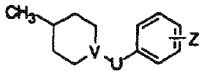
Feature 3. The set of feature 3 derivatives is given in Table 5, and the corresponding model compounds used in the conformational analyses can be represented by **III**.

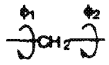
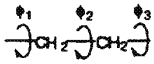
U is most often CH_2, but can also be C=O and $(CH_2)_2$. The substituted aromatic ring has also been replaced by cyclohexyl and naphthyl rings. Table 5 has been divided into parts: (a) contains active analogues which have two torsion angles (j_1, j_2); (b) contains inactive analogues which have two torsion angles (ψ_1, ψ_2); (c) contains a single inactive analogue which has three torsion angles (ψ_1, ψ_2, ψ_3).

The LBA–LCS principle was employed to map out the active conformation of the analogues of **III**, reported in Table 5, with respect to ϕ_1 and ϕ_2. An analysis of the (ϕ_1, ϕ_2) conformational energy maps of the active analogues **30** and **31**, and the inactive analogue **33**, suggests the minimum-energy conformation near ($\phi_1 = 200$, $\phi_2 = 240°$) as the active conformation, see Figure 11, the (ϕ_1, ϕ_2) map of 30.

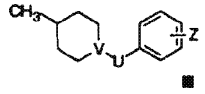
UM00013901
NOVARTIS EXHIBIT 1017
Novartis v. Regents, IPR2023-01346
Page 2647 of 4460

Table 5. The analogues of, or similar to, **III** used to map the active conformations, (f_1, f_2), with respect to feature 3



No.	U	V	Z	IC_{50} (nM)
(a) Active analogues with two torsion angles (ϕ_1, ϕ_2)				
30		N	H	5.3
31	CH_2	N	*o*-CH_3	10.0
32	$-CH_2-$	N	c-C_6H_{11}	8.9
(b) Inactive analogues with two torsion angles (ϕ_1, ϕ_2)				
33	$-CH_2-$	N	*o*-NO_2	160.0
34	$-C(O)-$	N	H	10000.0
35	$-CH_2-$	N	2-naphthyl	2900.0
36	$-CH_2-$	N	1-naphthyl	220.0
(c) An inactive analogue with three torsion angles (ϕ_1, ϕ_2, ϕ_3)				
37		N	H	180.0

[a] IC_{50} values correspond to analogues of structure 1.



The overall postulated active conformation for E2020, incorporating feature 3, is shown in Figure 12.

The crystal conformations of the isomers of E2020 (see Fig. 5) are the same as the postulated active conformation with respect to feature 1 (θ_1, θ_2). However, the postulated active conformation differs from the crystal structure with respect to feature 3, (ϕ_1, ϕ_2). The crystal structure adopts the ($\phi_1 = 300$, $\phi_2 = 300°$) conformation shown in Figure 11 in contrast to the postulated active conformation of ($\phi_1 = 200$, $\phi_2 = 240°$).

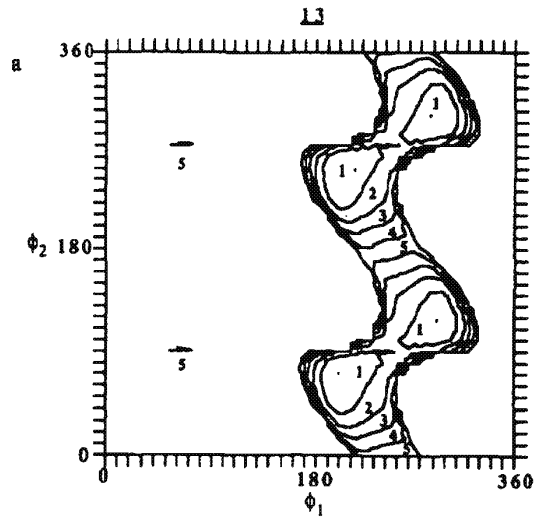


Figure 11. The conformational energy map of analogue **30** of Table 5. The energy contours are plotted the same as in Figures 8 and 9. The postulated active conformation is ($\phi_1 = 200$, $\phi_2 = 240°$).

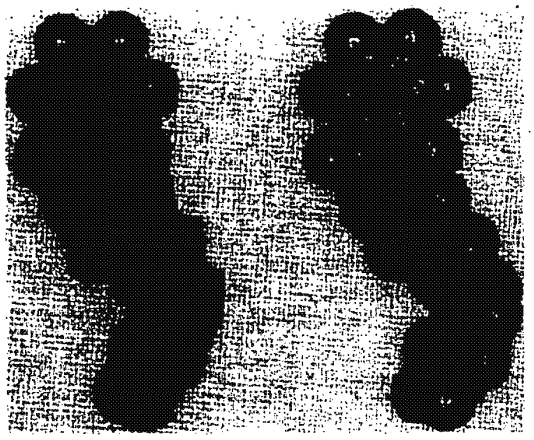


Figure 12. The postulated active conformation of the *R* isomer of E2020.

The inactive *o,m*-naphthyl analogue **36** has a conformational energy map nearly the same as **33**, thus accounting for its inactivity. However, the conformational energy map of **35**, the inactive *m,p*-naphthyl analogue, is almost identical to that of **30** (active). The inactivity of **35** can only be explained by hypothesizing an intermolecular, sterically forbidden, interaction between part of the *m,p*-naphthyl ring and the receptor wall. This explanation is consistent with the 3-D QSAR developed for substitution onto the phenyl ring in feature 4.

The active analogue **32** and the inactive analogue **34** would both be judged to be inactive based upon their (ϕ_1, ϕ_2) conformation energy profiles. However, these two profiles cannot be directly compared with any of the energy maps of analogues such as **26** and **27** because **32** and **34** possess changes in valence geometry. Nevertheless, the conformational energy minimum found for **32** at ($\phi_1 = 200$, $\phi_2 = 180°$), corresponds to the near perfect molecular superposition of **32** onto **30** in its active conformation, thus demonstrating **32** can adopt the postulated active molecular shape.

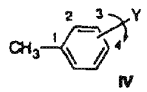
Compound **34** has a carbonyl group, in contrast to a methylene unit, as the spacer between the piperidine and phenyl rings. None of the conformational minima of **34** can be meaningfully superimposed on the proposed active conformation for **30** or for **31**. This lack of molecular-shape similarity is assumed to be a source for the inactivity of **34**. In addition, the nitrogen atom of the piperidine ring of **34** has a sp^2 hybridization as part of the amide group. Hence, it cannot protonate, and lacks a cationic head.

UM00013902
NOVARTIS EXHIBIT 1017
Novartis v. Regents, IPR2023-01346
Page 2648 of 4460

Finally, the inactivity of **37** of Table 5 can be accounted for by the fact that it does not possess any energetically reasonable intramolecular conformation which corresponds to a molecular shape that is close to the active molecular shape common to the active analogues **30**, **31**, or **32**. In essence, **37** is too 'long' due to the extra methylene spacer.

Feature 4. The set of 15 analogues given in Table 6 were used to develop feature 4 3-D QSARs. These E2020 analogues were selected because the only way in which these compounds differ from one another is in the substituent Y. Thus, model compound **IV** was used as the substructure in applying the MDR technique for the feature 4 QSAR analysis.

The range in IC_{50}s for the 16 analogues is 1–4900 nM. For Y substituents having conformational flexibility, the same molecular modeling and conformational analysis procedures used and referenced in 18 for feature 1 were used to determine the minimum-energy conformer states of Y. Once again, each intramolecular minimum-energy conformer state was used to compute measures of descriptors that are dependent upon substituent conformation. Each descriptor measure was considered in the QSAR analysis.



IV

The following set of descriptors were used as part of the feature 4 QSAR study: (1) The nonoverlap steric volume, S_n, using the aromatic ring as the molecular superposition criterium. (2) The principle moments of inertia. (3) The center of charge of each analogue. (4) The HOMO energy. (5) The partition coefficient, log *P*, of **IV**.

Trial QSARs were constructed in the same manner as those of feature 1. However, a GFA analysis was not performed.

For feature 4 the optimum 3-D QSAR that could be developed is:

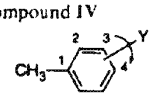
$$-\log(IC_{50}) = -0.107[S_n] + 0.046[IX] - 0.151[HOMO] + 6.683 \quad (3)$$

$N = 15$; $R = 0.905$; SD = 0.60; $F = 16.7$.

In equation (3) S_n is the nonoverlap steric volume between each analogue and the shape reference compound (Y = 3-OH) and IX is the largest principal moment of inertia of each analogue as represented by **IV**. The shape reference compound was determined by seeing which of the 15 analogues, each tested as the shape reference, gave the statistically most significant QSAR. The values of the QSAR descriptors, the predicted $-\log(IC_{50})$s and the corresponding residuals of fit are reported as part of Table 6.

AChE inhibition appears to be less sensitive, with respect to loss in potency, for substitutions onto the indanone ring (R_1, R_2, R_3), as compared to substitutions on the aromatic ring Y. This observation, coupled with the presence of a steric shape term in equation (3), suggests that substructure **IV** is in a more restricted steric environment than **III** when ligand–receptor binding occurs. Loss in inhibition potency seems particularly sensitive to the size of the Y substituent in the *para* position. This trend can be seen in Table 7 where the type and size (steric length) of *para* substituents are reported along with the corresponding $-\log(IC_{50})$. Using the unsubstitued ring as a reference, AChE inhibition potency decreases with increasing steric length of the *para* Y substituent. The only exception to this relationship is Y = 4-OH, which

Table 6. General SAR data for feature 4 based upon model compound IV



No.	Y	S_n (Å^3)	IX	HOMO energy (eV)	Obsd $-\log(IC_{50})$	Calcd $-\log(IC_{50})$	Obsd–calcd $-\log(IC_{50})$
38	3-F	0.86	17.47	−9.549	9.00	8.93	0.07
39	4-OH	6.80	15.24	−8.910	8.74	8.08	0.66
40	3-Me	11.47	23.46	−9.286	8.70	8.02	0.68
41	3-NO_2	14.06	31.96	−10.342	8.40	8.31	0.09
42	H	0.71	15.72	−9.339	8.28	8.83	−0.55
43	2-F	6.94	26.19	−9.527	8.02	8.67	−0.65
44	4-F	3.69	15.23	−9.478	8.02	8.51	−0.49
45	2-Me	21.40	26.57	−9.262	8.00	7.10	0.90
46	4-NH_2	9.72	15.47	−8.117	7.44	7.65	−0.21
47	4-Me	17.33	15.72	−9.225	7.40	7.03	0.37
48	4-NO_2	19.20	22.31	−10.391	7.00	7.32	−0.32
49	3-OMe	18.83	23.55	−8.954	6.66	7.19	−0.53
50	4-OMe	25.37	17.47	−8.895	5.44	6.20	−0.76
51	3,4-OMe	48.19	62.97	−9.198	5.40	5.90	−0.50
52	3,4,5-OMe	70.83	102.57	−9.367	5.31	5.32	−0.01

UM00013903
NOVARTIS EXHIBIT 1017
Novartis v. Regents, IPR2023-01346
Page 2649 of 4460

is also predicted to be less active by equation (3) than is observed (see Table 6).

Receptor dependent (docking) molecular modeling

Receptor model. Sussman and co-workers have reported the crystal structure of AChE from *Torpedo californica* electric organ.[26] The atomic coordinates of AChE were obtained from the Brookhaven Protein Data Bank (PDB entry: 1ACE). Hydrogen atoms were added after deleting the crystalline water molecules present in the X-ray structure, and aliphatic carbon–hydrogen groups were treated as united atoms. Docking studies for an acylated form of the enzyme, EA, were also carried out.[27] The 3-D structure of EA has not been determined so that the EA model used in this study was generated from the X-ray structure of AChE.

Table 7. *Para* substituents, Y, of feature 4, their steric length (sizes), and observed $-\log(IC_{50})$s

Y	Steric length (Å)	$-\log(IC_{50})$
H	2.23	8.28
F	2.60	8.02
OH	3.15	8.74
NH_2	3.20	7.44
CH_3	3.36	7.40
NO_2	3.92	7.00
OCH_3	4.84	5.44

AChE which contains 537 amino acids is schematically shown in Figure 13. AChE belongs to the class of α/β proteins and consists of 12 β-sheets surrounded by 14 α helices. A close-up view of the enzyme active site from the enzyme surface is shown in Figure 14. The active site serine residue can be seen from the surface of the enzyme. The active site consists of a catalytic triad composed of serine 200, histidine 440 and glutamic acid 327. The catalytic triad lies near the botton of a long and narrow gorge, which is lined with the side chain rings of fourteen aromatic amino acid residues. These aromatic residues are color-coded orange in Figure 14.



Figure 13. Global view of the AChE molecule looking down into the active site gorge.

UM00013904
NOVARTIS EXHIBIT 1017
Novartis v. Regents, IPR2023-01346
Page 2650 of 4460

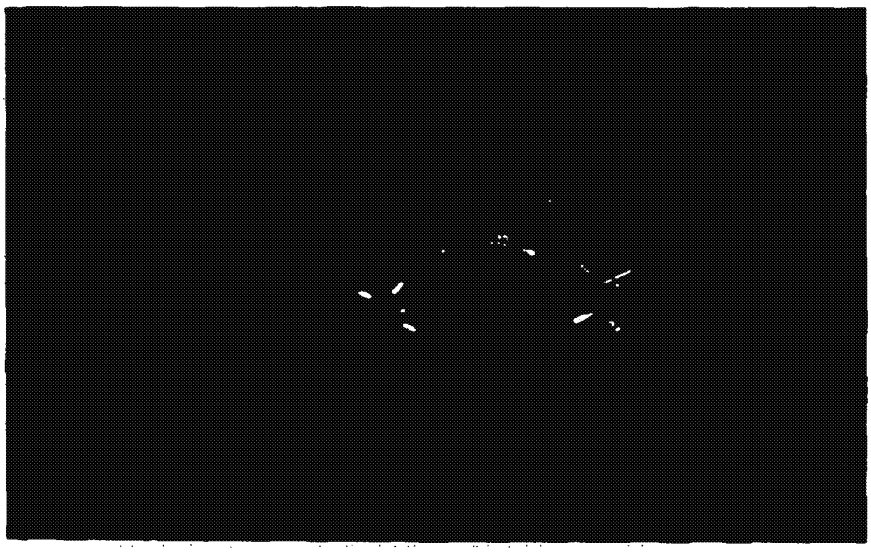


Figure 14. Close-up view of the AChE active site from the enzyme surface.

Figure 15 shows a schematic representation of the enzyme inhibition and the formation of intermediates. Catalysis by AChE involves the active serine residue, and the overall catalytic process proceeds in a three-step mechanism within the catalytic triad.[26] The activated serine residue enables a nucleophilic attack on ACh resulting in hydrolysis and acetate products being released. It is known that some reversible AChE inhibitors show a mixed type of inhibition by blocking the deacetylation process.[28-30] The acetyl group is introduced into the esteratic site in this catalytic process. Therefore, EA can accept an external charged molecule at this vacant anionic site to form an EA-inhibitor (EAI). Both the *R* and *S* forms of E2020 and THA appear to bind to both the free enzyme and the EA to block both Michaelis complex formation and the deacetylation process.[31]

Ligand models. The atomic coordinates of E2020 were taken from its crystal structure, and the other two analogues considered in the docking studies (2A1034, and 2A1050, see Figure 1) were built from E2020. The *S* form of each inhibitor considered in the docking simulation was optimized by the MNDO method. The atomic charges and dipole moments were calculated from these optimized structures. All three analogues

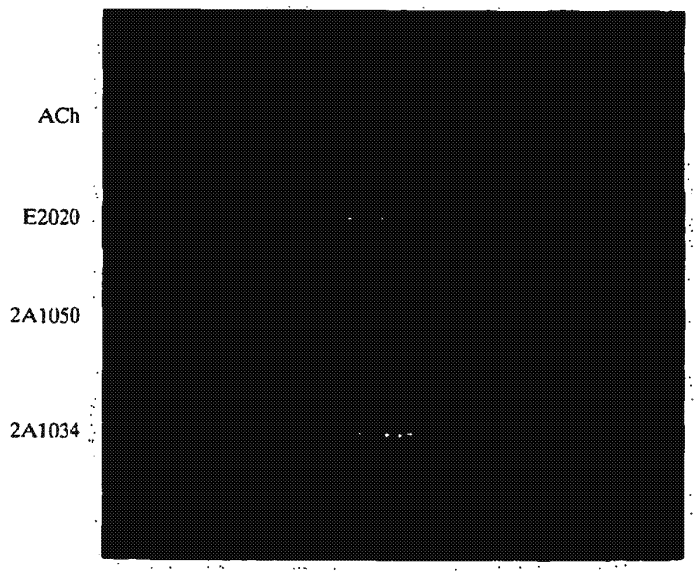


Figure 15. Dipole moments of ACh, E2020, 2A1034, and 2A1050 shown superimposed on the respective molecular structures.

UM00013905
NOVARTIS EXHIBIT 1017
Novartis v. Regents, IPR2023-01346
Page 2651 of 4460

possess large dipole moments, ca. 40–50 debye, and the direction of each dipole runs through the molecule from the benzylpiperidine moiety to the methoxy groups on the indanone ring, see Figure 16. ACh also has a large dipole moment of 23 Debye.

Docking procedures. The size of the active-site pocket of AChE is too small for E2020, and its related analogues, to mimic the binding geometry of ACh. Thus, it was necessary to search the long, narrow gorge leading to the active site in AChE for preferred binding locations. A sequential set of search operations were used to determine the enzyme–inhibitior structures and energies. The search operations consisted of: (1) identifying receptor 'hook' atoms using CAVHET;[32] (2) construction of initial inhibitor–receptor alignments based upon matching complementary ligand–receptor hook atoms, and the simultaneous alleviation of bad-contact atom-pair interactions by intermolecular ligand translations and rotations coupled with ligand torsion angle rotations; (3) Monte Carlo sampling, using the GREEN docking package,[33] to establish intermolecular low-energy locations and orientations, as well as conformations of the inhibitors, for each initial ligand–receptor model; and (4) molecular dynamics relaxation simulations,[25] using AMBER,[34] of the low-energy complexes generated in the Monte Carlo sampling analyses.

Docking models of AChE with ACh. Figure 17 shows a side view of the active site of AChE. The most remarkable feature of this structure is its deep and narrow channel, about 20 Å long and as narrow as 4.5 Å. This gorge penetrates halfway into the enzyme and widens out close to its interior terminus. It has been suggested that the quaternary group of the choline moiety of ACh makes a close contact with the indole ring of Trp 84.[24] However, our docking study indicates that the quaternary moiety of choline binds through interactions with the π electrons of the aromatic residues in the channel of AChE. Gly 118 and 119 might be part of the oxyanion hole since these glycines make close contacts to the carboxyl oxygen of ACh in the most stable AChE–ACh complex models.

Docking models of E2020 analogues to AChE and AE. The docking simulations show that stable conformations are adopted by the inhibitors upon binding to both AChE and acylated AChE. All three inhibitors considered dock to both AChE and the AE in a similar manner. The docking suggests two common features of binding for these compounds: (1) the *N*-benzyl substituent forms a *p*-stacking interaction with the indole side chain of Trp 84 and (2) the piperidine ring locates on the narrowest part of active-site cavity which is formed by four amino acid residues, Tyr 70, Asp72, Tyr 121, and Tyr 334.

E2020 exhibits five key binding interactions (KBI 1–5) involving the methoxy group, the phenyl ring, the carbonyl group in the indanone ring, the protonated nitrogen of piperidine, and the phenyl ring of the benzyl group attached to the nitrogen of piperidine. The carbonyl oxygen interacts with Tyr 121 (KBI 3a) and Tyr (KBI 3b). However, the *S* enantiomer of E2020 ($k_i = 17.5$ nM) only adopts the KBI 3b binding mode. 2A1034 ($k_i = 18.7$ nM) in the *R* form, which is the preferred binding isomer, interacts with the enzyme at only three of these five key sites. 2A1050 ($k_i = 122$ nM) binding involves only two of these interaction sites at the same time for the preferred binding *S* form.

The results of the docking study support the active conformation model discussed above which is characterized by the indanone and piperidine rings being 'perpendicular' to one another, where the larger of the two thickness dimensions of the piperidine ring contains its plane relative to the indanone ring.[18] The

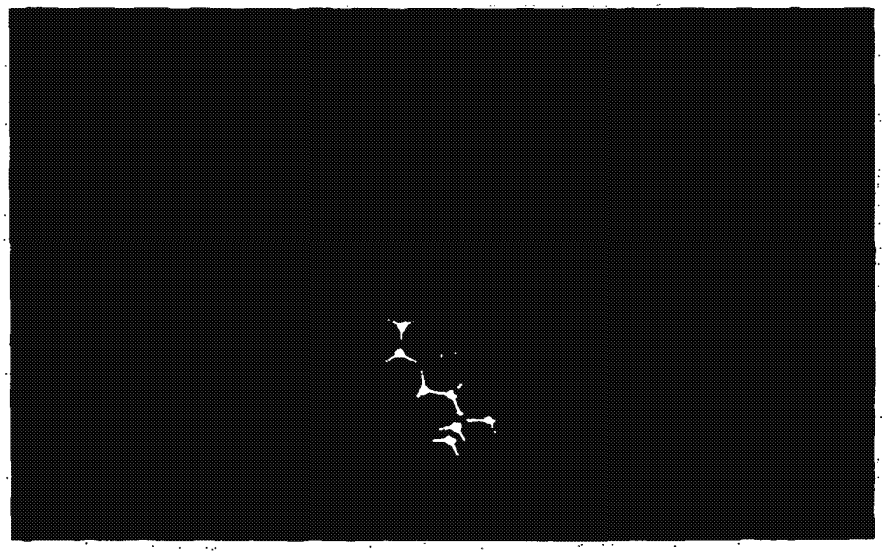


Figure 16. Side view of the AChE active site.

UM00013906
NOVARTIS EXHIBIT 1017
Novartis v. Regents, IPR2023-01346
Page 2652 of 4460

preferred mode of binding of E2020 to AChE is shown in Figure 18. Overall, these results suggest that E2020, and related analogues, are noncovalent AChE inhibitors which bind in the aromatic gorge, but do not interact with the catalytic residues. Consequently, the E2020 analogues can inhibit the Michaelis complex formation step/deacylation step of the hydrolytic reaction of AChE.

Discussion

QSAR, small molecule X-ray, and molecular modeling methods have been useful in the realization of the E2020 class of AChE inhibitors. These methods have been useful because they have been both functional and appropriate. The capacity to perform individual QSAR, X-ray, and molecular shape analyses quickly, relative to synthetic efforts, and at critical times in the evolution of the research program, are the reasons these methods have been functional. The insight to ask the 'right' questions when employing these methods has made their use appropriate. We note that not asking questions beyond the scope of a computer-assisted molecular design, CAMD, method qualifies as asking the 'right' question.

The intermolecular docking simulations have complemented the QSAR and molecular shape analyses in providing reasons for the high activity seen in E2020 analogues having differing numbers of spacers groups between the indanone and piperidine rings. E2020 analogues which can adopt long, narrow conformations as low-energy intramolecular states can fit in the long active-site gorge of AChE. The docking simulations indicate that the preferred binding site of E2020 (both isomers) to AChE is not at the ACh active site, but rather some distance away in the channel leading to the active site. This may be the reason E2020 is a potent inhibitor to both AChE and acylated AChE.

In addition, the docking simulations and 3-D QSARs support and reinforce one another. A detailed comparison of the AChE-E2020 docking modes to the

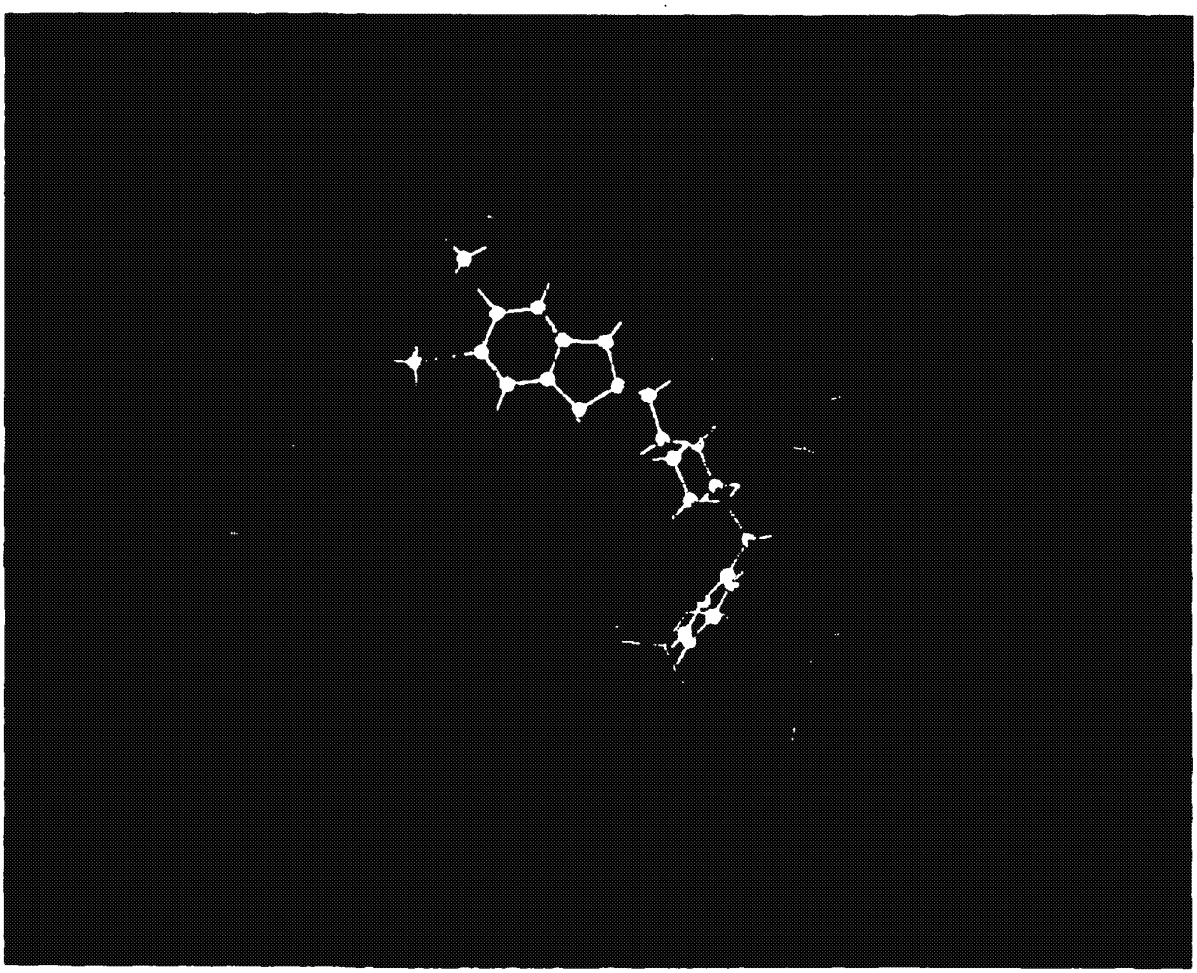


Figure 17. Superposition of the *R* and *S* enantiomers of E2020 binding models in the active site cavity with the five key binding interactions (KBIs) defined.

UM00013907
NOVARTIS EXHIBIT 1017
Novartis v. Regents, IPR2023-01346
Page 2653 of 4460

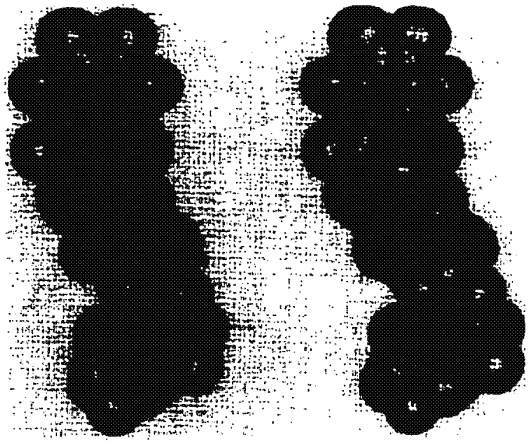


Figure 18. The *trans*-decalin analogue superimposed on the *R* enantiomer of E2020 in its postulated active conformation.

descriptor terms in the QSARs [equations (1)–(3)][25] reveals a self-consistency between sub-binding sites and descriptors. Binding simulations and the use of the QSARs jointly provide a robost tool to predict AChE inhibition activity in new analogues.

There are still pathways to take in the study and understanding of the family of E2020 AChE inhibitors. A better understanding of the geometric binding specificity in the active site channel would enhance inhibitor design capabilities. One measure of success in achieving an insight into inhibitor binding specificty would be to explain the inactivity of what we call the *trans* decalin analogue of E2020 whose structure is shown in Figures 1 and 18. This compound was predicted to be very active as an AChE inhibitor based upon its molecular shape similarity to E2020 (see Figure 18). However, the compound was made and tested and its IC_{50} was 2530 mM, a quite *inactive* inhibitor. The inactivity was assumed to be due to unfavorable intermolecular binding interactions not identified in the MSA study. At the time of the MSA study the AChE crystal structure was not available. Recent docking simulations of the *trans*-decalin analogue to AChE, carried out in the same manner as for E2020 and some of its other analogues and described above, also suggests it should be a potent inhibitor. Thus, future molecular modeling studies, and, in particular, docking simulations of the E2020 family of AChE inhibitors should keep the understanding of the low-activity of the *trans*-decalin analogue as both a goal and a corresponding measure of success.

Docking simulations may provide some guidelines for structural changes in the four features of E2020. A primary target for structural changes may be the indanone ring. There are other bicycles that lead to active analogues[18] suggesting a structure–activity mapping may be possible by docking simulation.

Implementation of docking simulations in a design mode is predicated upon reliable calculations. The ability to predict reliable and accurate ligand–receptor binding energies remains elusive in intermolecular modeling. Perhaps the best chances for success in the E2020 analogue—AChE docking simulations is to combine X-ray studies to elucidate AChE–inhibitor complex geometries with free-energy force-field refinement[35] docking simulations. The X-ray structures can provide realistic initial geometries to the docking simulations for a training set of inhibitors for which the inhibition potencies have been measured. The terms in the force field used to compute the binding energies of the inhibitors are then scaled, in a QSAR fashion, to establish a correlation between inhibition potency and binding free energy.

Overall, the E2020 project has had a successful past in terms of CAMD applications and there is every reason to believe in a bright future.

Acknowledgments

AJH is grateful for the financial support of Eisai for some parts of the work reported here. Mario Cardozo has been a major contributor to some of the QSAR studies (features 1 and 4) and the conformational and molecular shape analyses (features 2 and 3). We also appreciate the helpful discussions with S. Nochi of Eisai Co., Ltd.

References and Notes

1. Yamanishi, Y.; Ogura, H.; Kosasa, K.; Araki, S.; Sawa, Y.; Yamatsu, K. *Basic Clinical, and Therapeutic Aspects of Alzheimer's and Parkinson's Diseases*; Plenum: New York, 1990; Vol. 2, pp 409–413.

2. Bartus, R. T.; Dean, III, R. L.; Beer, B.; Lippa, A. S. *Science* **1982**, *217*, 408.

3. Sims, N. R.; Bowen, D. M.; Allen, S. J.; Tomalson, C. C. T.; Neary, D.; Thomas, D. J.; Davision, A. N. *J. Neurochem.* **1983**, *40*, 503.

4. Gottfries, C G. *Psychopharmacology* **1985**, *86*, 245.

5. Perry, E. K. *Br. Med. Bull.* **1986**, *42*, 63.

6. Hulme, E. C.; Birdsall, N. J. M.; Buckley, N. J. *Annu. Rev. Pharmacol. Toxicol.* **1990**, *30*, 633.

7. Yamanishi, Y.; Ogura, H.; Kosasa, K.; Araki, S.; Sawa, Y.; Yamatsu, K. *Basic Clinical, and Therapeutic Aspects of Alzheimer's and Parkinson's Diseases*; Plenum: New York, 1990; Vol. 2, p 409.

8. Sugimoto, H.; Tsuchiya, Y.; Sugumi, H.; Higurashi, K.; Karibe, N.; Iimura, Y.; Sasaki, A.; Kawakami, Y.; Nakamura, T.; Araki, S.; Yamanishi, Y. *J. Med. Chem.* **1990**, *33*, 1880.

9. Nochi, S. unpublished results.

10. Homma, A.; Hasegawa, K.; Nishimura, T.; Kameyama, M.; Hariguchi, S.; Imai, Y. In *proceedings of 6th Congress of the International Psychogeriatrica Association*, 1993.

11. Summers, W. K.; Koehler, A. L.; Marsh, A. M.; Tachiki, K.; Kling, A. *Lancet* **1989**, 729.

12. Ishihara, Y.; Hirai, K.; Miyamoto, M.; Goto, G. *J. Med. Chem.* **1994**, *37*, 2292.

UM00013908
NOVARTIS EXHIBIT 1017
Novartis v. Regents, IPR2023-01346
Page 2654 of 4460

13. Villalobos, A.; Blake, J.F.; Biggers, C.K.; Butler, T. W.; Chapin, D. S.; Chen, Y. L.; Ives, J. L.; Jones, S. B.; Liston, D. R.; Nage, A. A.; Nason, D. M.; Nielsen, J. A.; Shalaby, I. A.; White, W. F. *J. Med. Chem.* **1994**, *37*, 2721.

14. Dewar, M. J. S.; Thiel, W. *J. Am. Chem. Soc.* **1977**, *99*, 4899.

15. Hulme, E. C.; Birdsall, N. J. M.; Buckley, N. J. *Annu. Rev. Pharmacol. Toxicol.* **1990**, *30*, 633.

16. Johnson, C. K., *ORTEP* II. Report ORNL-5138. Oak Ridge National Laboratory, Tennesesce, U.S.A.

17. Hopfinger, A. J.; Malhotra, D.; Battershell, R. D.; Ho, A.; and Chen, J. A. *Pest. Sci.* **1984**, *9*, 631.

18 (a) Cardozo, M. G.; Iimura, Y.; Sugimoto, H.; Yamanishi, Y.; Hopfinger, A. J. *J. Med. Chem.* **1992**, *35*, 584. (b) Cardozo, M. G.; Kawai, T.; Iimura, Y.; Sugimoto, H.; Yamanishi, Y.; Hopfinger, A. J. *J. Med. Chem.* **1992**, *35*, 590.

19. Rhyu, K.-B.; Patel, H. C.; Hopfinger, A. J. *J. Chem. Inf. Comput. Sci.* **1995**, *35*, 771.

20. Medicinal Chemistry Software, *Medchem Software Manual, Release 3.51;* Pomona College: Claremont, California, April 1987.

21. *SAS User's Guide: Basics, SAS Release 5.18*; SAS Institute, Inc.: Cary, North Carolina, 1986.

22. Holland, J. *Adaptation in Artifical and Natural Systems*; University of Michigan: Ann Arbor, 1975.

23. Rogers, D.; Hopfinger, A. J. *J. Chem. Inf. Comput. Sci.* **1994**, *34*, 854.

24. Hopfinger, A. J.; Burke, B. J. In *3-D QSAR in Drug Design-Theory, Methods and Applications*, Kubinyi, H., Ed.; ESCOM Science: Leiden, 1993; pp 276–306.

25. Burke, B. J. Ph.D. Thesis, University of Illinois at Chicago, Illinois, 1992.

26. Sussman, J. L.; Harel, M.; Frolow, F.; Offner, C.; Goldman, A.; Toker, L.; Silman, I. *Science* **1991**, *253*, 872.

27. Inoue, A.; Kawai, T.; Wakita, M.; Iimura, Y.; Sugimoto, H.; Kawakami, Y., *J. Med. Chem.*, submitted.

28. Krupka, R. M.; Laidler, K. J. *J. Am. Chem. Soc.* **1961**, *83*, 1445.

29. Krupka, R. M.; Laidler K. J. *J. Am. Chem. Soc.* **1961**, *83*, 1454.

30. Krupka, R. M. *Biochemistry* **1965**, *4*, 429.

31. Nochi, S.; Asakawa, N.; Sato, T. *Biol. Pharm. Bull.* **1995**, *18*, 1145.

32. CAVHET is in the original program developed by A. Inoue.

33. Tomioka, N.; Itai, A. *J. Comput-Aided Mol. Design* **1994**, *8*, 347.

34. Weiner, S. J.; Kollman, P. A. *J. Comp. Chem.* **1986**, *7*, 230.

35. Hopfinger, A. J.; Tokarski, J. *J. Chem. Inf. Comput. Sci.*, submitted.

(*Received in U.S.A.* 5 *October* 1995)

UM00013909
NOVARTIS EXHIBIT 1017
Novartis v. Regents, IPR2023-01346
Page 2655 of 4460

This Page is Inserted by IFW Indexing and Scanning Operations and is not part of the Official Record

BEST AVAILABLE IMAGES

Defective images within this document are accurate representations of the original documents submitted by the applicant.

Defects in the images include but are not limited to the items checked:

- ☐ BLACK BORDERS
- ☐ IMAGE CUT OFF AT TOP, BOTTOM OR SIDES
- ☐ FADED TEXT OR DRAWING
- ☐ BLURRED OR ILLEGIBLE TEXT OR DRAWING
- ☐ SKEWED/SLANTED IMAGES
- ☐ COLOR OR BLACK AND WHITE PHOTOGRAPHS
- ☐ GRAY SCALE DOCUMENTS
- ☐ LINES OR MARKS ON ORIGINAL DOCUMENT
- ☐ REFERENCE(S) OR EXHIBIT(S) SUBMITTED ARE POOR QUALITY
- ☐ OTHER: _____

IMAGES ARE BEST AVAILABLE COPY.
As rescanning these documents will not correct the image problems checked, please do not report these problems to the IFW Image Problem Mailbox.

Protein Engineering vol.1 no.4 pp.301–303, 1987

SS

Automated protein crystallization and a new crystal form of a subtilisin:eglin complex

Henk A.Kelders, Kor H.Kalk, Piet Gros and Wim G.J.Hol

Laboratory of Chemical Physics, University of Groningen, Nijenborgh 16, 9747 AG Groningen, The Netherlands

A procedure is described for automating labour-intensive steps of the 'hanging drop' protein crystallization method. An automatic sample changer is employed to fill the wells in a multi-well plate so that concentration gradients in various components are obtained. The sample changer is also used for preparing droplets on a second multi-well plate. Subsequently, this second plate is manually turned around and placed on top of the first multi-well plate such that a large number of chambers with different conditions is obtained simultaneously. During initial trials a new crystal form of a subtilisin:eglin complex was obtained. The crystals have space group $P2_1$, contain two enzyme inhibitor complexes per asymmetric unit and diffract beyond 2.2 Å.

Key words: crystallization/automation/subtilisin:eglin complex

Introduction

With the advent of recombinant DNA techniques virtually every protein, either obtained from nature, modified by man or designed *de novo* can be obtained in large enough quantities to make X-ray crystallographic investigations feasible. The first step, however, in such investigations is the growth of high-quality crystals. This usually requires a trial-and-error process during which a wide variety of conditions have to be tested, (See e.g. Blundell and Johnson, 1976; McPherson, 1982). The possibility of expressing genes in high yield in fast growing bacteria, coupled with the great advances made in the field of protein purification in the last decade, means that large amounts of pure protein can be obtained. This implies that automatic methods for setting up crystallization trials in which robotics replace many of the manual steps, become feasible in order to test thousands or more different conditions.

Here we describe an almost completely automatic procedure for carrying out 'hanging drop' experiments which proved to be successful in obtaining a new crystal form of subtilisin Carlsberg complexed with its inhibitor eglin.

Materials and methods

The essential piece of equipment used in the automated 'hanging drop' crystallization procedure described here, is a computer-controlled sample changer. Two multi-well plates (purchased from Omnilabo Holland B.V., Breda, The Netherlands) were placed side-by-side within the working space of the sampler changer (model 221/401, kindly made available by the manufacturer, Gilson Medical Electronics, Villiers-le-Bel, France). One of the multi-well plates (plate I) eventually contained the mother liquor; the other plate (plate II) was used to accommodate the drops and was therefore siliconised with a silicon solution (Serva). Each well of the two plates has a volume of ~300 µl, and a flat and transparent bottom in order to be able to examine the drops with a microscope.

The Gilson sample changer model 221 is a so-called $x-y-z$ instrument. A vertical needle can be positioned at any $x-y$ coordinate within the working space with an accuracy of 0.1 mm, and at any height (up to 10 cm) above the working space with an accuracy of 1 mm. The needle is connected to a 'dilutor', model 401, equipped with a burette which can aspire a volume up to 1 ml in two different ways. Firstly, through the needle itself from any vial placed within the working space. In this manner, no dead-volume problems arise and manipulation of small volumes is possible. Secondly, from a reservoir placed outside the working space connected by a tube to the dilutor. Now a dead volume exists, i.e. the volume of the tubes leading to the needle plus that of the needle itself, but as the reservoir can contain large amounts of solution, repeated rinsing takes care of any mixing of solutions in the dead-volume. The accuracy with which the dilutor can dispense volumes from the needle is comparable to the accuracy of the well-known Eppendorf pipettes.

In the set-up used for our experiments the dilutor was connected to a PEG-containing reservoir. After completing the pipetting of the PEG solutions into the wells, the burette and tubes were rinsed with double-distilled water. Buffer and protein solutions were pipetted in a different manner by aspirating respectively thirty 5 µl amounts through the needle from a vial placed within the working space. In order to be able to manipulate such small amounts of protein solution, the tubing and needle were filled with distilled water. An air-gap prevented dilution of the 5 µl protein sample with the distilled water.

Hanging drop experiments which resulted in the subtilisin:eglin crystals, were carried out as follows. First, the following solutions were made by hand: (i) 60% PEG-6000 (Merck) in distilled water with 0.2% sodium azide added (PEG solution); (ii)

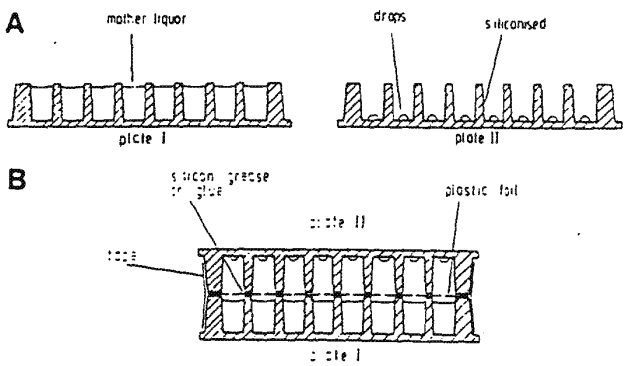


Fig. 1. (A) The two multi-well plates prior to the assembly are shown. Plate I contains the mother liquor, and plate II, which is siliconised, contains the drops. (B) The two plates after assembly. Plate I is covered airtight with plastic foil and silicon grease or glue, and plate II is placed upside down on top of plate I. Diffusion between the drop and the mother liquor is made possible by punching small holes in the plastic foil prior to the assembly.

© IRL Press Limited, Oxford, England

UM00013911

NOVARTIS EXHIBIT 1017
Novartis v. Regents, IPR2023-01346
Page 2657 of 4460

1.0 M potassium phosphate buffer, pH 6.0, containing 100 mM EDTA (buffer solution); and (iii) 20 mg/ml subtilisin:eglin, dialysed against 0.1 M potassium phosphate buffer, pH 6.0 (protein solution). The subtilisin used (Maxatase) was kindly provided by Gist Brocades, Delft; eglin was a gift from Dr H.P.Schnebli, Ciba-Geigy, Basle.

Second, the mother liquor was prepared in the wells of plate I by the sample changer. A concentration range of 6–48% PEG-6000 was made by pipetting 30–60–90 . . . 240 μl of the PEG solution into successive wells within a row. To each well, 30 μl of the buffer solution was added. Next, each well was filled up with double distilled water to make a final volume of 300 μl. Six identical rows were prepared in this way, making a total of 48 experiments [the other 48 wells could not be filled because of the small workspace of the sample changer used; another model (model 222) is available which allows preparation of 96 wells]. The mother liquor was mixed by aspiring 250 μl from each well and dispensing it back into the same well.

Third, the protein drops were made by the sampler changer. To this end, 5 μl of the 20 mg/ml subtilisin:eglin protein solution were pipetted into a well of plate II. Subsequently 8 μl of the mother liquor was taken from an appropriate well in plate I and carefully added to the protein drop in plate II, without mixing of the two solutions. This sequence was repeated for all 48 experiments.

Fourth, the multi-well plates were assembled. Plate II was covered with a piece of transparent adhesive foil (Alkor^R, obtained from Bijholt and Heuvelen B.V., The Netherlands). Silicon grease (Baysilone-paste, Bayer, Leverkusen) was applied to the non-adhesive side of the foil, and small holes were punched so that one hole was centered above each drop. Subsequently, plate II was carefully turned upside down and placed on top of plate I. In this way, each well of plate I was closed airtight except for the small hole in the plastic foil which allowed diffusion of vapour between the drop on plate II and the well with mother liquor on plate I. Finally, the two plates were taped tightly to each other and stored in a cupboard at 20°C.

Results

After ~2 months these cryallization experiments yielded crystals in drops equilibrated against 18 and 24% PEG-6000, which were subsequently investigated by precession photographs and diffractometer measurements. A few crystals were removed from a hanging drop after which plates I and II were taped together again. The space group appeared to be $P2_1$ with cell dimensions a = 38.3 Å, b = 46.5 Å, c = 89.5 and β = 93.4°. This yields a value of 2.5 Å^3/daltons, well within the usual range, if we assume that two subtilisin:eglin complexes of 35.6 daltons each are present in the asymmetric unit. The crystals diffract beyond 2.2 Å.

For the 48 experiments carried out the total time required was ~60 min. Pipetting had to be carried out slowly because the PEG solution was highly viscous. With further improvements, especially when less viscous solutions can be used, the final rate should be of the order of 200 experiments/h. It is clear that a significant reduction in the human time required to make the 96 different solutions in the wells and drops can be obtained by employing the 'robot'.

The reproducibility of the crystallization was excellent as judged by comparing the sets of six equivalent experiments. Large single crystals were observed in all six drops of the two successful conditions, i.e. 18 and 24% PEG. No useful crystals were observed in any other drop. This result shows that the reproducibility of the method employed is certainly acceptable, even when viscous solutions, such as quite high concentrations of PEG-6000, are used.

Discussion

The procedure employed has several advantages compared with conventional procedures. (i) Two time-consuming steps in the manual procedure, i.e. making the large number of different solutions in the wells and making the drops, are automated. (ii) The size of the drops can be 2 μl, or even somewhat smaller, which increases the number of experiments which can be done with a limited amount of protein. (iii) The setup is very compact. Many experiments can be stored in a small amount of space such as an oven. (iv) Because the vapour diffusion takes place through a small hole, equilibrium is reached quite slowly. Changing the size of the hole may be used as an extra parameter by which crystal growth can be controlled. (v) The compactness of the setup and the high transparency of the double-plate system allows rapid and easy screening with a microscope.

A major disadvantage of the current procedure is that all drops in a pair of plates have to be disturbed when mounting a crystal from one of the drops. We are trying various simple ways to overcome this shortcoming. It appeared, however, that hanging drops using the two-tray system can be stored for at least 3 months (even after separating the two plates, removing some crystals and sealing the plates together by tape) without affecting the quality of the crystals in the other drops.

The current method is already quite suitable for instance in cases where one intends to obtain a crude idea under what conditions precipitates form. In such cases quite large variations of conditions in neighbouring wells can be created and a beautiful overview of general solubility properties is obtained by one glance at the pair of multi-well plates. The procedure outlined in this paper also seems to be quite useful when small variations around a well-known crystallization condition have to be explored. This can be the case when the crystallization conditions are very sensitive to one or more parameters, e.g. protein concentration. A similar situation arises when one tries to crystallize a mutant, either obtained from nature or engineered by man, as it is not unreasonable to assume that suitable crystallization conditions will not differ too much from those of the wild-type protein. In other words, automated crystallization along such lines as described in this paper may be particularly suitable for protein engineering projects.

Crystals of subtilisin have, of course, been obtained by several groups. First in the native state (Wright *et al.*, 1969) or with a covalent inhibitor bound (Drenth *et al.*, 1972), later complexed with subtilisin *Streptomyces* inhibitor (Mitsui *et al.*, 1979) and with chymotrypsin inhibitor 2 (McPhalen *et al.*, 1985a). These studies concerned subtilisin BPN', or Novo, which are chemically identical but have different biological sources. Three-dimensional structures of engineered mutants of this subtilisin have also been reported (Katz and Kossiakoff, 1986). The structure of the Carlsberg type of subtilisins, to which the subtilisin in the present investigation belongs, has only been elucidated quite recently, but with high accuracy, and in both cases complexed with eglin in a triclinic cell (McPhalen *et al.*, 1985b, Bode *et al.*, 1985). Grütter *et al.* (1985) reported the same triclinic crystals of the eglin:subtilisin Carlsberg complex. The monoclinic crystal form described in the present communication may be of use to investigate, for instance, packing effects on structure and mobility of the subtilisin and inhibitor molecule. Furthermore, it is advantageous in protein engineering projects to know conditions

UM00013912
NOVARTIS EXHIBIT 1017
Novartis v. Regents, IPR2023-01346
Page 2658 of 4460

leading to different crystal modifications of the same protein. The reason being that mutations of a loop involved in crystal contacts of one crystal form prevent easy crystallization in that form, but such a loop may be freely exposed to solvent in another modification and, hence, mutants are likely to crystallize without difficulty in the second modification.

Acknowledgements

It is a pleasure to acknowledge stimulating as well as critical discussions with Drs Jan Metske van der Laan, Myra Swarte, Bauke Dijstra and Jan Drenth from the Groningen Protein Crystallography Group. This research was supported by Unilever, Vlaardingen, The Netherlands; Gist-Brocades, Delft, The Netherlands; the Groningen Protein Engineering Programme; and the Dutch Foundation of Chemical Research (SON) with financial aid from the Dutch Organisation for the Advancement of Pure Research (ZWO).

References

Blundell,T.L. and Johnson,L.N. (1976) In Horecker,B., Kaplan,N.O., Marmur,J. and Scheraga,H.A. (eds), *Protein Crystallography*. Academic Press, London, pp. 59–81.

Bode,W., Papamakos,E., Musil,D., Seemueller,U. and Fritz,H. (1985) *EMBO J.*, **5**, 813–818.

Drenth,J., Hol,W.G.J., Jansonius,J.N. and Koekoek,R. (1972) *Eur. J. Biochem.*, **26**, 177–181.

Grüner,M.G., Märki,W. and Walliser,H.-P. (1985) *J. Biol. Chem.*, **260**, 11436–11437.

Katz,B.A. and Kossiakoff,A. (1986) *J. Biol. Chem.*, **261**, 15480–15485.

McPhalen,C.A., Svendsen,I., Jonassen,I. and James,M.N.G. (1985a) *Proc. Natl. Acad. Sci. USA*, **82**, 7242–7246.

McPhalen,C.A., Schnebli,H.P. and James,M.N.G. (1985b) *FEBS Lett.*, **188**, 55–58.

McPherson,A. (1982) *Preparation and Analysis of Protein Crystals*. John Wiley and Sons, NY, pp. 82–127.

Mitsui,T., Satow,Y., Watanabe,Y., Hirono,S. and Iitaka,Y. (1979) *Nature*, **277**, 447–452.

Wright,C.S., Alden,R.A. and Kraut,J. (1969) *Nature*, **221**, 235–242.

Received on May 1, 1987; revised on June 17, 1987

UM00013913
NOVARTIS EXHIBIT 1017
Novartis v. Regents, IPR2023-01346
Page 2659 of 4460

This Page is Inserted by IFW Indexing and Scanning Operations and is not part of the Official Record

BEST AVAILABLE IMAGES

Defective images within this document are accurate representations of the original documents submitted by the applicant.

Defects in the images include but are not limited to the items checked:

- ☐ BLACK BORDERS
- ☐ IMAGE CUT OFF AT TOP, BOTTOM OR SIDES
- ☐ FADED TEXT OR DRAWING
- ☐ BLURRED OR ILLEGIBLE TEXT OR DRAWING
- ☐ SKEWED/SLANTED IMAGES
- ☐ COLOR OR BLACK AND WHITE PHOTOGRAPHS
- ☐ GRAY SCALE DOCUMENTS
- ☐ LINES OR MARKS ON ORIGINAL DOCUMENT
- ☐ REFERENCE(S) OR EXHIBIT(S) SUBMITTED ARE POOR QUALITY
- ☐ OTHER: _____

IMAGES ARE BEST AVAILABLE COPY.
As rescanning these documents will not correct the image problems checked, please do not report these problems to the IFW Image Problem Mailbox.

63

Egypt. J. Pharm. Sci., Vol. 33, No. 5-6, pp. 757 - 769 (1992).

Complexation of Paracetamol With Xanthine Derivatives.

R.M. Khalil

Department of Pharmaceutical Sciences, National Research Center, Dokki, Cairo, Egypt.

THE INTERACTION of paracetamol with certain xanthine derivatives, viz., caffeine, theophylline, acepifylline and dyphelline was investigated. Differential ultraviolet spectorphotometry revealed a marked effect of xanthines on the extinction coefficient of paracetamol. Applying the continuous variation method on spectrophotometric measurements revealed the formation of 1:1 complexes of paracetamol with caffeine and acepifylline. For the interaction between paracetamol and theophylline, two complexes of stoichiometric ratios of 1:1 and 2:1 are formed. On the other hand, two paracetamol dyphylline complexes of stoichiometric ratios 1:2 and 2:1 appear to be formed. Determination of the stability constant of the complexes by spectrophotometric method as well as the solubility methods revealed that acepifylline exhibits the highest tendency to complex with paracetamol. The dissolution rate of paracetamol as well as its xanthine complexes was determined and found to follow first order kinetics during the first 12 min of the run. The results revealed that there is a correlation between the stability constant of the xanthine complexes determined by the solubility method and the solubilizing power of the xanthine.

Many studies have shown that caffeine and related xanthines are capable of interacting in aqueous media with a variety of drugs through complexation [1-3]. Complex formation may be intended to increase the solubility and/or stability of drugs. The physical properties of the resulting drug complex most probably vary from that of the free drug. Complexation is one of the physicochemical factors that may profoundly affect drug bioavailability.

UM00013915
NOVARTIS EXHIBIT 1017
Novartis v. Regents, IPR2023-01346
Page 2661 of 4460

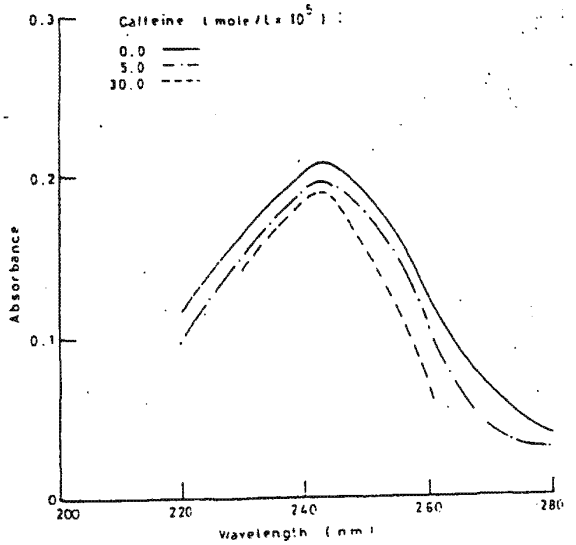


Fig. 1. Differential ultraviolet absorbance spectrum of aqueous solution of paracetamol (2 X 10^{-5} mole/L) in presence of caffeine.

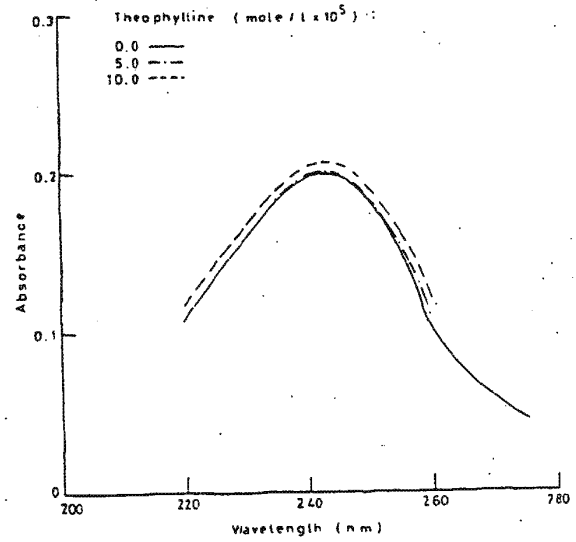


Fig. 2. Differential ultraviolet absorbance spectrum of aqueous solution of paracetamol (2 X 10^{-5} mole/L) in presence of theophylline.

UM00013916
NOVARTIS EXHIBIT 1017
Novartis v. Regents, IPR2023-01346
Page 2662 of 4460

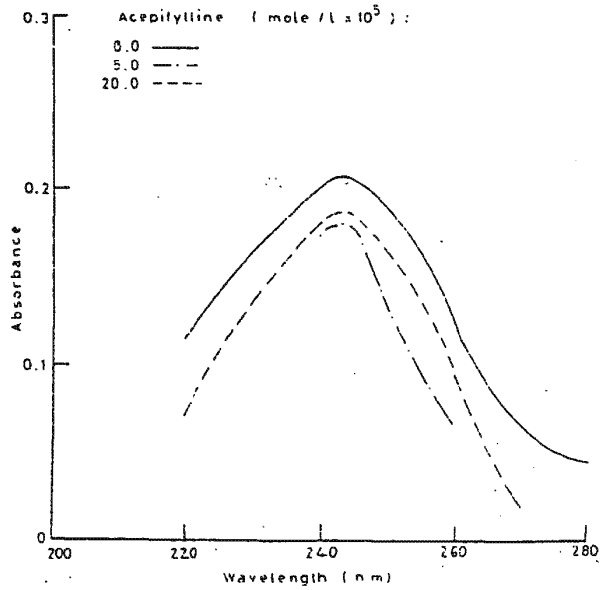


Fig. 3. Differential ultraviolet absorbance spectrum of aqueous solution of paracetamol (2 X 10^{-5} mole/L) in presence of acepifylline.

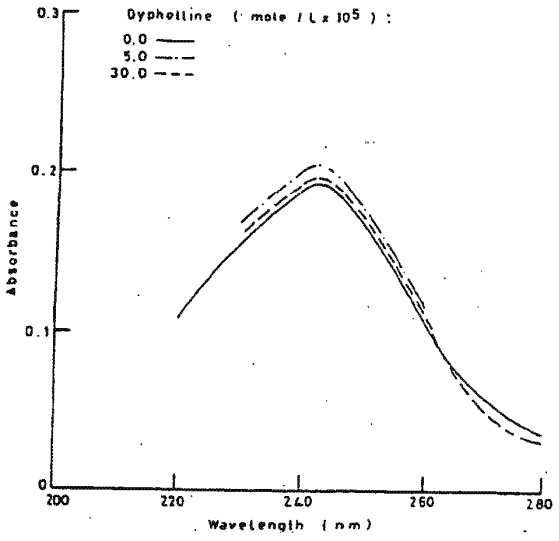


Fig. 4. Differential ultraviolet absorbance spectrum of aqueous solution of paracetamol (2 X 10^{-5} mole/L) in presence of dyphelline.

UM00013917
NOVARTIS EXHIBIT 1017
Novartis v. Regents, IPR2023-01346
Page 2663 of 4460

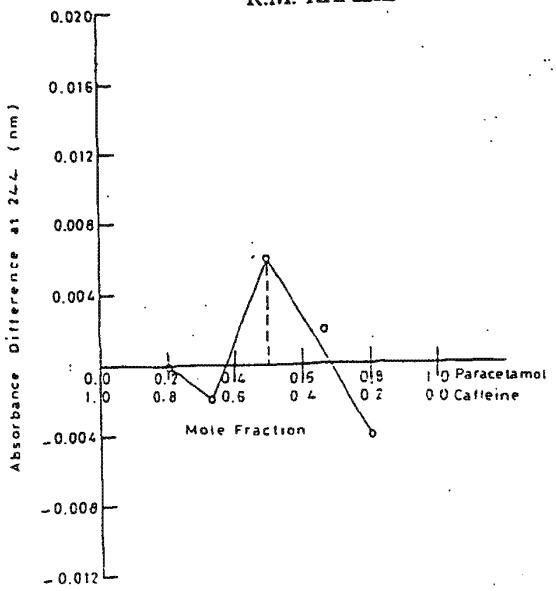


Fig. 5. Elucidation of the stoichiometric ratio of paracetamolcaffine complex by the spectrophotometric method.

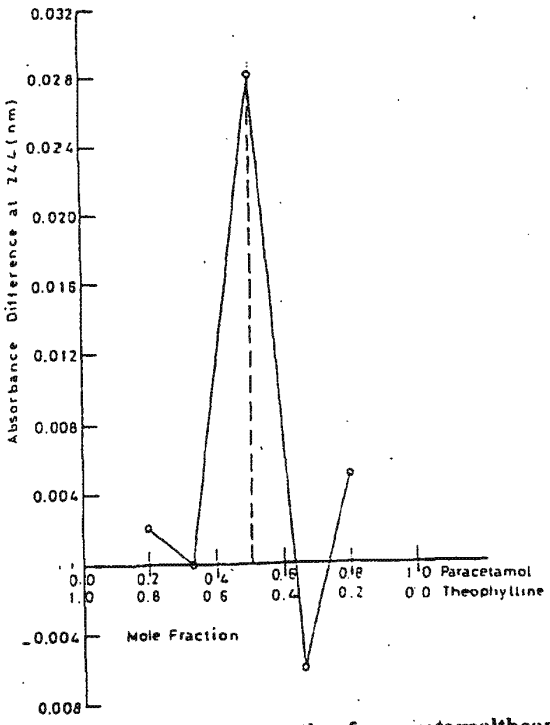


Fig. 6. Elucidation of the stoichiometric ratio of paracetamoltheophylline complex by the spectrophotometric method.

UM00013918
NOVARTIS EXHIBIT 1017
Novartis v. Regents, IPR2023-01346
Page 2664 of 4460

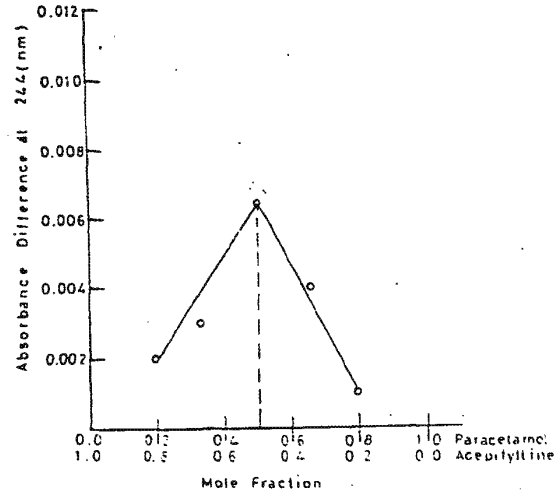


Fig. 7. Elucidation of the stoichiometric ratio of paracetamolacepifylline complex by the spectrophotometric method.

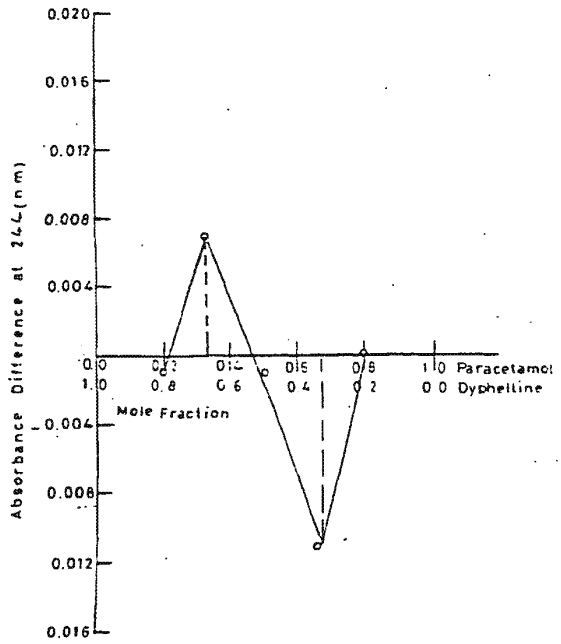


Fig. 8. Elucidation of the stoichiometric ratio of paracetamoldypheline complex by the spectrophotometric method.

UM00013919
NOVARTIS EXHIBIT 1017
Novartis v. Regents, IPR2023-01346
Page 2665 of 4460

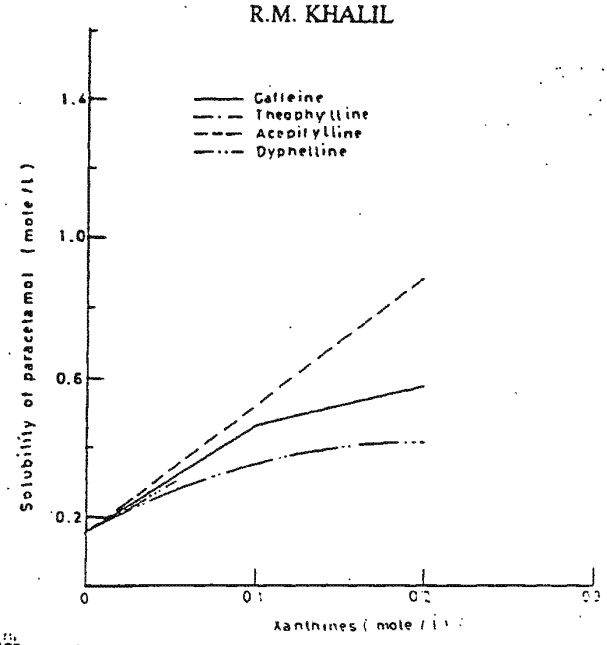


Fig. 9. Effect of xanthines on the solubility of paracetamol in water at 25°.

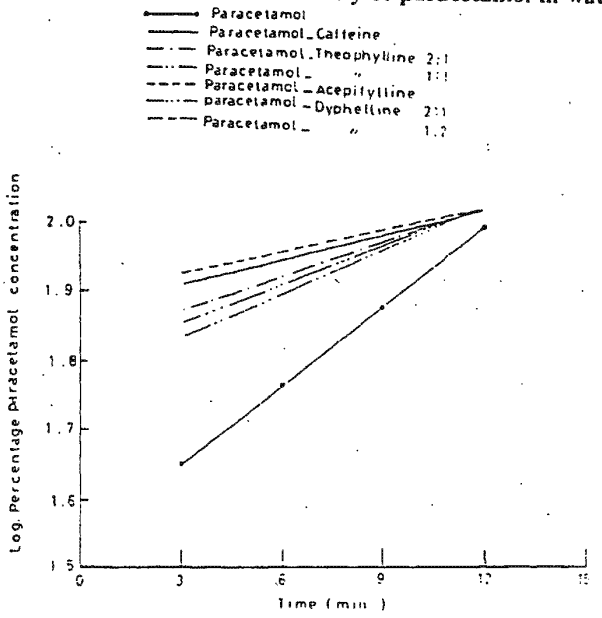


Fig. 10. Dissolution profile of paracetamol and paracetamolxanthine complexes in water at 37°.

UM00013920
NOVARTIS EXHIBIT 1017
Novartis v. Regents, IPR2023-01346
Page 2666 of 4460

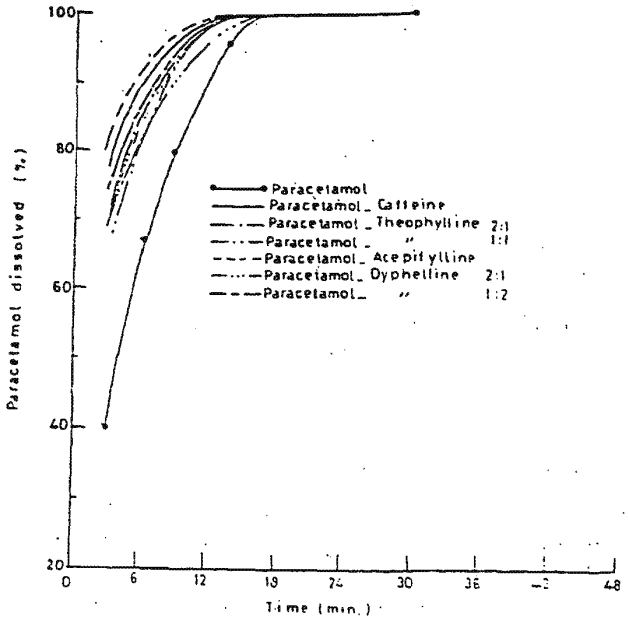


Fig. 11. Dissolution profile of paracetamol and paracetamolxanthine complexes in water at 37°.

The effect of the investigated xanthines on the solubility of paracetamol was studied (Fig. 9). It can be seen from the figure that there exists a linear relationship between the maximum additive concentration of the drug and xanthines concentration, except in the case of dyphelline. This can be considered as a further indication of the formation of 1:1 complexes between the drug and caffeine, theophylline as well as acepifylline.

The stability constant of the formed complexes was determined by the spectrophotometric method (8) as well as from the data of the solubility phase diagram of the drug in presence of xanthines. The results compiled in Table 1 reveal that theophylline and its derivatives form more or less more stable complexes with the drug compared to caffeine. Acepifylline seems to possess the highest complexing tendency towards the drug.

The dissolution rate of paracetamol as well as its xanthine complexes was determined by the beaker method.

The dissolution efficiency (D.E.) (11) which is a suitable comparative parameter for quantification of dissolution data was determined in each case and appear in Table 2.

UM00013921
NOVARTIS EXHIBIT 1017
Novartis v. Regents, IPR2023-01346
Page 2667 of 4460

TABLE 1. Stability Constant (k) of Paracetamol - Xanthine Complexes.

Complexes	Stability constant (k) determined by:	
	The spectrophotometric method	The solubility method
Paracetamol - Caffeine (1:1).	34.67	
Paracetamol - Theophylline.		20.0
(1:1)	4295.36	
(2:1)	8.02	18.5
Paracetamol - Acepifylline.		
(1:1)	10990.06	24.5
Paracetamol - Dyphelline:		
(1:2)	3572.73	
(2:1)	3.65	

TABLE 2. Dissolution Rate of Paracetamol and its Xanthine Complexes.

Time (min)	Paracetamole	% Paracetamol dissolved from:					
		Paracetamol complexes with:					
		Caffeine	Theophylline 2:1	Theophylline 1:1	Acepifylline	Dyphelline 2:1	Dyphelline 1:2
3	40	78.21	70.63	75.31	81.30	64.43	68.23
6	63.16	90.02	86.86	90.46	91.50	81.19	84.30
9	80.76	97.92	95.30	96.00	97.00	94.30	96.27
12	90.46	100	100	100	100	99.00	100
15	99.00	100	100	100	100	100	100
20	100	100	100	100	100	100	100
30	100	100	100	100	100	100	100
D.E. (%). 0-30 min.	81.68	91.62	90.28	91.18	92.00	88.89	89.96.
First-order dissolution rate constant min $^{-1}$).	0.09	0.03	0.04	0.03	0.02	0.05	0.04

It is evident from the data obtained that there are marked differences between the dissolution rate of paracetamol and its xanthine complexes.

UM00013922
NOVARTIS EXHIBIT 1017
Novartis v. Regents, IPR2023-01346
Page 2668 of 4460

The value of the dissolution efficiency of paracetamol - acepifylline complex is more or less higher than the other paracetamol complexes. In case of theophylline and dyphelline, the dissolution rate increases with increasing the mole fraction of the complexing agent in the complex.

The graphical illustration of the logarithm of paracetamol dissolved as a function of time (Fig. 10) revealed that the dissolution of paracetamol as well as the investigated paracetamol complexes follow first-order kinetics during the first tweleve minutes of the run. The values of the dissolution rate constant of paracetamol as well as its complexes during the first twelve minutes were calculated and compiled in Table 2. On the other hand, the solubilizing power of the investigated xathine derivatives expressed as mole of paracetamol solubilized per mole of xanthine was also calculated (Table 3).

TABLE 3. The Solubilizing Power of Xanthines, towards Paracetamol at 25°.

Xanthine	Mole drug solubilized per mole Xanthine			
(mole/L.)	Caffeine	Theophylline	Acepifylline	Dyphelline
0.00	–	–	–	–
0.01	–	3.5	–	–
0.02	4.15	2.8	3.60	0.8
0.03	–	2.67	–	–
0.04	3.35	2.8	3.15	1.45
0.05	–	2.9	–	–
0.06	3.17	–	3.79	2.27
0.08	3.25	–	3.89	1.89
0.10	3.06	–	3.57	2.39
0.20	2.14	–	3.68	1.34
Mean solubilizing Power.	3.19	2.93	3.61	1.69

Trying to correlate the stability of the formed complexes evidenced by the value of their formation constant with the dissolution rate constant of the complexes as well as with the solubilizing power of the complexing agent towards paracetamol, revealed that there is a correlation between the stability constant of the complex determined by the solubility method and the solubilizing power of the xanthine compound. However, it is evi-

UM00013923
NOVARTIS EXHIBIT 1017
Novartis v. Regents, IPR2023-01346
Page 2669 of 4460

dent from the results that there exists a correlation between the solubilizing power of the xanthines and the dissolution efficiency (D.E.) of their complexes with paracetamol.

From the results , we can see that the formed paracetamol - acepifylline complex possesses the highest value of stability constant and shows the most enhanced dissolution rate and in the same time acepifylline exhibits the greatest solubilizing power for paracetamol.

The above mentioned data throw a beam of light on the complexation of paracetamol with some xanthine derivatives which are commonly used. This complexation reflects itself on the solubility and dissolution properties of the drug and in the same time, this complexation appears to have an expected implication on the bioavailability of the drug which is worthy of thorough investigation.

References

1. Reilley, C.N., *"Advances in Analytical Chemistry and Instrumentation"*, Ed., Interscience, Vol. 4, p., 117, New York, N.Y. (1965).

2. Nishijo, J. and Takenaka, F., *Yokugaka Zasshi*, **103**, 819 (1983).

3. Nishijo, J., Ohno, K., *Nishimura, K., Hukuda, M. and Ishimaru, H.*; *Chem. Pharm. Bull*, **30**, 319 (1982).

4. Ameer, B. and Greenblatt, D.J. ; *Ann. Intern. Med.*, **87**, 202 (1977).

5. Griffenhagen, G.B. and Kawkins, L.L., *"Handbook of Non-Prescription Drugs"*, Eds., American Pharmaceutical Association, Washington, D.C., p. 44 (1971).

6. Chow, Y.P. and Repta, A.J., *J. Pharm. Sci.*, **61**, 1454 (1972).

7. Job, P., *Ann. Chim.* **9**, 113 (1928).

8. Morteil, A.E. and Calvin, M *Chemistry of the Metal Chelate Compounds*, Prentice-Hall, Inc., New York, p. 98 (1952).

9. Denbrow, M. and Jan, Z.A.; *J. Pharm. Pharmac.* **17**, 129S (1965).

10. Levy, G. and Hayes, B.; *New Eng. J. Med.*, **262**, 1053 (1960).

11. Khan, K.A. and Rhodes, G.T., *Pharm. Acta. Helv.*, **47**, 594, (1972).

(Recevid 10/91; accepted 12/91)

UM00013924
NOVARTIS EXHIBIT 1017
Novartis v. Regents, IPR2023-01346
Page 2670 of 4460

التراكيب بين الباراسيتامول ومشتقات الزانثين

راوية محمد خليل

قسم العلوم الصيدلية – المركز القومي للبحوث – الدقي – القاهرة – مصر

يتناول البحث دراسة التراكب بين الباراسيتامول وبعض مشتقات الزانثين المتمثلة في الكافيين ، الثيوفيللين ، الاسبيفيللين والداى فيللين.

وقد أوضحت نتائج الامتصاص الضوئي في المجال فوق البنفسجي ان مركبات الزانثين لها تأثير واضح علي الامتصاص الضوئي للباراسيتامول وهذا يشير إلي إحتمال وجود تراكب بين مركبات الزانثين والباراسيتامول . وقد تم دراسة نسبة مكونات المتراكبات بطريقة التغير المتواصل بأستخدام الامتصاص الضوئي وقد أكدت النتائج علي وجود النسب الاتية للمتراكبات ١ : ١ بين الباراسيتامول وكل من الكافيين والاسبيفيللين ١ :١, ٢ :١ للبارسيتامول مع الثيوفيللين ، ١ :٢, ٢ :١ للبارسيتامول مع الداي فيللين وبتعيين عامل الثبات لمتراكبات الباراسيتامول مع مشتقات الزانثين بطريقتين هما الامتصاص الضوئي والذائبية أثبتت النتائج أن الاسبيفيللين أكثر المركبات قابلية للتراكب مع الباراسيتامول.وأوضحت النتائج المستخلصة من دراسة تأثير الزانثين علي معدل الذائبية للباراسيتامول أن معدل الذائبية لكل من الباراسيتامول ومتراكبات الباراسيتامول يتبع معادلة الحركة من الدرجة الاولي خلال الاثني عشر دقيقة الاولي. وقد أوضحت النتائج أن هناك علاقة طردية ثابتة بين كل من عامل الثبات المعين بطريقة الذوبان وقوة الاذابة لمادة التراكب.

UM00013925
NOVARTIS EXHIBIT 1017
Novartis v. Regents, IPR2023-01346
Page 2671 of 4460

This Page is Inserted by IFW Indexing and Scanning Operations and is not part of the Official Record

BEST AVAILABLE IMAGES

Defective images within this document are accurate representations of the original documents submitted by the applicant.

Defects in the images include but are not limited to the items checked:

- ☐ BLACK BORDERS
- ☐ IMAGE CUT OFF AT TOP, BOTTOM OR SIDES
- ☐ FADED TEXT OR DRAWING
- ☐ BLURRED OR ILLEGIBLE TEXT OR DRAWING
- ☐ SKEWED/SLANTED IMAGES
- ☐ COLOR OR BLACK AND WHITE PHOTOGRAPHS
- ☐ GRAY SCALE DOCUMENTS
- ☐ LINES OR MARKS ON ORIGINAL DOCUMENT
- ☐ REFERENCE(S) OR EXHIBIT(S) SUBMITTED ARE POOR QUALITY
- ☐ OTHER: _____

IMAGES ARE BEST AVAILABLE COPY.

As rescanning these documents will not correct the image problems checked, please do not report these problems to the IFW Image Problem Mailbox.

Crystal Structure of the 1: 1 Complex of 5-Fluorouracil and 9-Ethylhypoxanthine

Sung-Hou Kim; Alexander Rich

Science, New Series, Volume 158, Issue 3804 (Nov. 24, 1967), 1046-1048.

Stable URL:
http://links.jstor.org/sici?sici=0036-8075%2819671124%293%3A158%3A3804%3C1046%3ACSOT11%3E2.0.CO%3B2-8

Your use of the JSTOR archive indicates your acceptance of JSTOR's Terms and Conditions of Use, available at http://www.jstor.org/about/terms.html. JSTOR's Terms and Conditions of Use provides, in part, that unless you have obtained prior permission, you may not download an entire issue of a journal or multiple copies of articles, and you may use content in the JSTOR archive only for your personal, non-commercial use.

Each copy of any part of a JSTOR transmission must contain the same copyright notice that appears on the screen or printed page of such transmission.

Science is published by American Association for the Advancement of Science. Please contact the publisher for further permissions regarding the use of this work. Publisher contact information may be obtained at http://www.jstor.org/journals/aaas.html.

Science
©1967 American Association for the Advancement of Science

JSTOR and the JSTOR logo are trademarks of JSTOR, and are Registered in the U.S. Patent and Trademark Office. For more information on JSTOR contact jstor-info@umich.edu.

©2003 JSTOR

http://www.jstor.org/
Mon Aug 11 12:45:27 2003

time" on Fig. 2. Clearly, no cloud about the spacecraft can be brighter than the difference (1.1×10^{-12} $B_\odot$) between the smaller day values and those of night. But the experiment is capable of determining a limit half this large.

To confirm the interpretation that the array of data points represents light scattered from a certain antenna with a known position, the situation was simulated in the laboratory with an identical photometer and light shield. The result is the solid curve (Fig. 2) which was normalized to pass thru the orbital data at 68°. The orbital data points appear to be approaching the brightness of the night sky at an antenna angle of 90° in the same manner as the laboratory data do. We may show an upper limit to cloud brightness by assuming that there is such a cloud and by showing that this causes disagreement between the orbital data and the laboratory simulation: If there had been around the spacecraft a cloud whose sunlit brightness in the antisolar direction was 5×10^{-13} $B_\odot$, then we should add this to the ground simulation before a comparison is made with the orbital data. The result (dashed curve, Fig. 2) is obtained by doing this and by normalizing the ground data again to fit the orbital data at an antenna angle of 68°. Since the functional forms are no longer within experimental error of each other, one concludes that there was no cloud as bright as 5×10^{-13} $B_\odot$. This upper limit determined experimentally is equivalent to 0.01 erg cm^{-2} sec^{-1} $sterad^{-1}$, or 12 fifth-visual-magnitude solar-type stars per square degree.

From the last form of the upper limit, there is evidently very little interference in measuring bright stars with instruments which, typically, have fields of view less than several minutes of arc. But the situation is different for observing extended sources of white light, in that the above limit is brighter than the Milky Way and much of the zodiacal light. In the antisolar direction, the true sky brightness is about 1×10^{-13} $B_\odot$, whereas the measured upper limit to the cloud brightness in this direction is five times larger. If the particle size distribution in the cloud were similar to that of the dust which causes the zodiacal light, then this brightness ratio of about 5 would be maintained over all portions of the zodiacal light to within 30° of the sun. Closer to the sun than 30°, scattering from free electrons enhances the zodiacal light and solar corona so that the ratio would fall, perhaps to 1. It is important to study the amount of solid debris in the vicinity of a spacecraft and to investigate the rates of formation and release of micron-size particles. Otherwise, observations of dim extended sources might be compromised whenever a large satellite is in sunlight.

CHARLES WOLFF

National Aeronautics and Space Administration, Goddard Space Flight Center, Greenbelt, Maryland 20771

References

1. F. E. Roach, L. Dunkelman, J. R. Gill, R. D. Mercer, in *Mid-Gemini Program Conference* (NASA SP-121, 1966), p. 315.
2. E. P. Ney and W. F. Huch, *Science* **153**, 297 (1966).
3. L. Dunkleman, paper presented at American Astronomical Society Meeting, June 1967.
4. I. Schmidt, *Science* **155**, 1136 (1967).
5. G. Newkirk, *Planetary Space Sci.*, **15**, 1267 (1967).
6. C. Wolff, *Appl. Opt.* **5**, 1838 (1966).

20 September 1967

Crystal Structure of the 1 : 1 Complex of 5-Fluorouracil and 9-Ethylhypoxanthine

Abstract. *9-Ethylhypoxanthine and 5-fluorouracil form a 1 : 1 crystalline complex. The structure of this complex has been solved by x-ray diffraction analysis. The molecules crystallize in a monoclinic lattice and form a sheet structure in which pairs of fluorouracil molecules are held together by two hydrogen bonds. The 9-ethylhypoxanthine residues fill up the rest of the molecular sheet by forming single hydrogen bonds with each uracil pair.*

The cocrystallization of two different molecules into the same lattice is usually a reflection of interactions which occur between these molecules in solution. A particularly important type of cocrystallization is that which has been observed with purine and pyrimidine derivatives of nucleic acids. It has been shown in a number of crystallographic studies that adenine derivatives cocrystallize with uracil (or thymine) derivatives (*1*, *2*), and guanine derivatives with those of cytosine (*3*). In these crystal structures, the purine-pyrimidine pairs are held together by two or three hydrogen bonds. The molecular packing and hydrogen bonding between these residues is of interest since many of them have a direct bearing on the molecular organization of the macromolecular nucleic acids. In these latter molecules, the specificity of hydrogen bonding plays a central role in the transmission of genetic information, in the production of messenger RNA as well as in the polymerization of amino acids to form proteins. Thus there is considerable interest in the way purines and pyrimidines associate with each other.

One of the characteristics of the crystallographic studies carried out in the past is the fact that only adenine derivatives have crystallized with uracil derivatives and likewise guanine derivatives with cytosine derivatives. No cases have been reported in which there has been cocrystallization of members of the adenine-uracil family with members of the guanine-cytosine family. Infrared and nuclear magnetic resonance studies (*4*) carried out on the association of these molecules in solution shows that there is a selective hydrogen bonding affinity between adenine and uracil derivatives and between guanine and cytosine derivatives. However, there is little or no hydrogen bonding association between members of these two families. Accordingly, it was of considerable interest when we found that it was possible to cocrystallize 5-fluorouracil with 9-ethylhypoxanthine. This appeared initially to be inconsistent with the specificity described above, since hypoxanthine is considered a derivative of guanine. Here we report the results of the crystal structure analysis of this 1 : 1 complex. Even though these molecules have crystallized together, they do not form pairs held together by two hydrogen bonds. Instead, there is a pairing of the uracil derivatives with each other, and the hypoxanthine derivatives are connected to these pairs with single hydrogen bonds.

5-Fluorouracil and 9-ethylhypoxanthine (Cyclo Chemical Co., Los Angeles) were dissolved in equimolar amounts in water and allowed to evaporate at room temperature. Well-developed prismatic crystals were formed, some of which had a diameter as great as 1 mm. Single crystals were isolated and redissolved and were

UM00013928
NOVARTIS EXHIBIT 1017
Novartis v. Regents, IPR2023-01346
Page 2674 of 4460

shown to have a 1 : 1 composition by spectrophotometric and chromatographic analyses. The crystals were found to be monoclinic, and the crystallographic data are presented in Table 1. The asymmetric unit contains one molecule each of 5-fluorouracil and 9-ethylhypoxanthine, and the unit cell contains four such pairs. The diffraction data were collected on a four-circle Picker automatic diffractometer out to a 2θ maximum value of 125°. This included a total of 1632 independent reflections, excluding systematic absences. Of these, 1464 reflections were above the background. The crystal measured 0.3 by 0.3 by 0.5 mm and no absorption correction was applied to the data.

The structure was solved by the reiterative application of the Sayre equations (*5*). The structure factors were reduced to normalized structure factors (E), and the method was applied with a program written by Long (*6*). This program produces various possible combinations of signs, and the correct one was among the first four which were examined. The first Fourier synthesis (E map) carried out with these phases revealed 20 out of the 21 atoms in the structure, excluding the hydrogen atoms. These 20 atoms were then refined isotropically by using a least squares program (*7*). After two cycles of refinement, the residual factor was reduced to 23.4 percent using all the data. A difference Fourier was calculated at that stage and the terminal carbon atom of the ethyl group was revealed. Anisotropic temperature factors were then introduced, and further refinement reduced the residual to 8.9 percent. Eight very strong reflections and the very weak reflections were then excluded and a difference Fourier was calculated from the remaining data. All of the hydrogen atoms were revealed at this stage except for two hydrogens found at the end of the ethyl group. These appeared in the difference Fourier after further refinement. Positional and thermal parameters for the hydrogen atoms were not refined. The final residual factor was 5.5 percent for the 1464 observed reflections.

The molecules form a layer structure in which they are organized into a hydrogen-bonded network, and these sheets are stacked, held together by van der Waal's interactions. The sheets are tilted off the *bc* plane at an angle of 46°42′, separated by a spacing of 3.24 Å. All of the atoms are in the plane of the sheet with the exception of the terminal carbon atom of the ethyl group, which lies halfway between the sheets. Figure 1 shows a section of the electron density map in the plane of the molecules. All of the atoms are seen in this plane except the terminal

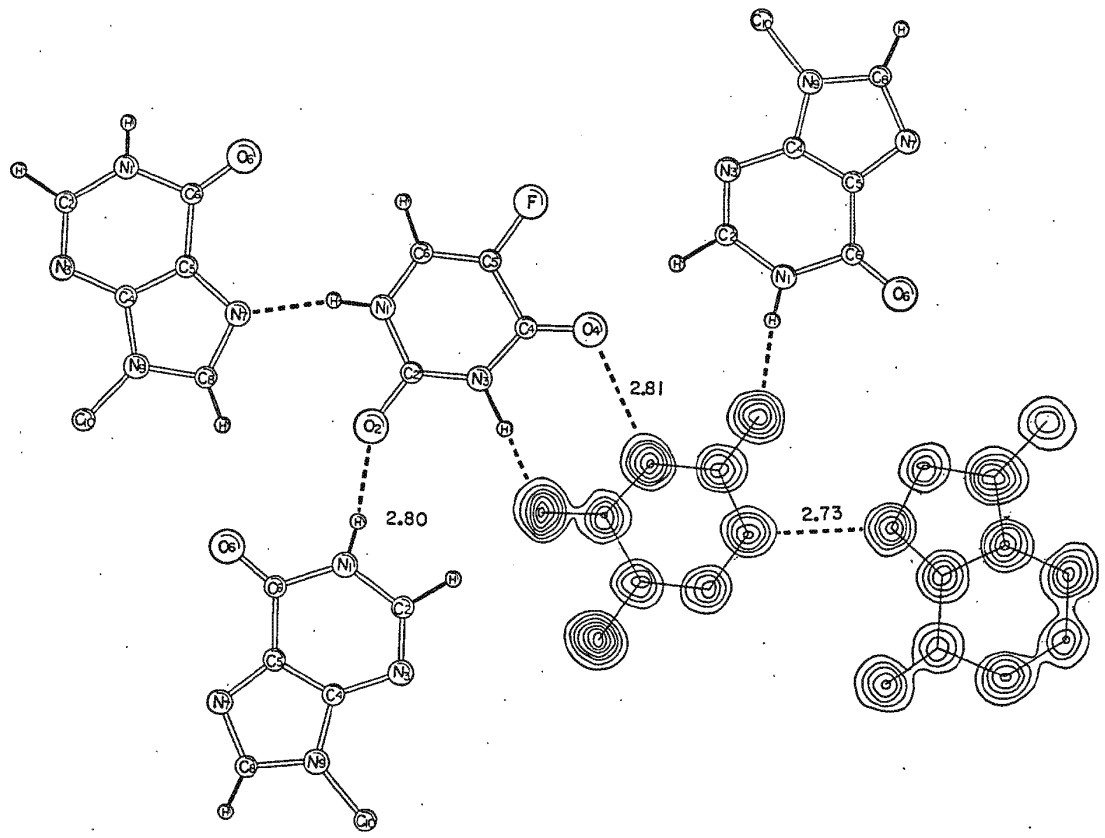


Fig. 1. The electron density map in the plane of the molecular sheet of the 5-fluorouracil : 9-ethylhypoxanthine structure. The contours occur at arbitrary levels of electron density in this section. The terminal carbon atom (C-11) on the ethyl group of 9-ethylhypoxanthine does not lie on the plane. The hydrogen bond lengths are indicated in angstrom units. The center of symmetry lies between the paired fluorouracil molecules.

UM00013929
NOVARTIS EXHIBIT 1017
Novartis v. Regents, IPR2023-01346
Page 2675 of 4460

Table 1. Crystallographic data for the 1 : 1 complex of 5-fluorouracil and 9-ethylhypoxanthine.

Space group	$P2_{1/c}$ $Z = 4$
Unit cell	$a = 4.656$ Å $b = 15.276$ Å $c = 17.807$ Å $\beta = 90°48'$
Calculated density	1.54 g/cm³
Observed density	1.55 g/cm³

carbon atom of the ethyl group. The 5-fluorouracil molecules are paired, held together by two hydrogen bonds of length 2.81 Å between N-3 and O-4. They are organized around a center of symmetry. This is the same pairing of uracil residues which is seen in the crystal structure of N-1-methyl uracil (*8*). The 9-ethylhypoxanthine molecules are connected to each fluorouracil pair by single hydrogen bonds. The hydrogen atom attached to the N-1 of hypoxanthine is bonded with O-2 of fluorouracil, while the hydrogen atom on N-1 of uracil is bonded to N-7 of a different hypoxanthine residue. The latter hydrogen bond is short (2.73 Å), as is frequently found in association with the purine imidazole group (*2*). The packing is quite compact and there are no open areas in the plane of the molecular sheet.

Although it is not shown in Fig. 1,

Table 2. Fractional atomic coordinates.

Position	*x/a*	*y/b*	*z/c*
	9-Ethylhypoxanthine		
N-1	0.8514	0.3024	0.3389
C-2	.0290	.2533	.3843
N-3	.0404	.1687	.3844
C-4	.8516	.1338	.3331
C-5	.6667	.1759	.2857
C-6	.6583	.2690	.2855
N-7	.5131	.1169	.2427
C-8	.6085	.0395	.2650
N-9	.8149	.0457	.3201
C-10	.0388	.4744	.1405
C-11	.2126	.4417	.0757
O-6	.5088	.3184	.2460
	5-Fluorouracil		
N-1	0.0812	0.1305	0.1380
C-2	.9950	.0508	.1143
N-3	.7709	.0493	.0622
C-4	.6333	.1216	.0333
C-5	.7440	.2034	.0616
C-6	.9565	.2060	.1124
O-2	.8930	.4831	.3635
O-4	.4323	.3855	.4874
F	.6178	.2762	.0353

the fluorine atom is in contact with the terminal carbon atoms of the ethyl side chain of hypoxanthine. However, it does not participate in any hydrogen bonding. The fluorine atoms are located in a column parallel to the *a*-axis, surrounded by ethyl groups from neighboring hypoxanthine molecules. There is very little overlap of the purine and pyrimidine rings of one layer with those of the layers on either side. A small amount of overlap occurs with the imidazole rings of hypoxanthine and N-1 and C-2 of the uracil rings immediately below. With this exception, the π-electrons of the unsaturated rings are not in contact with other π-electrons. Thus this crystal does not show a stacking of purine residues which is seen prominently in several layer structures involving cocrystals of adenine and uracil derivatives (*2*). Where overlapping of unsaturated rings does occur, the spacing between the adjacent layers is near 3.4 Å, as is found in the stacked bases of the nucleic acids. Partial overlap in the present structure is associated with a spacing of 3.24 Å. In the crystal of N-1-methyl uracil, the pyrimidine rings form a planar net with no overlap and there the spacing between the layers is 3.14 Å (*8*). The bond angles and distances of the purine and pyrimidine rings are similar to those which have been reported earlier in other crystallographic studies of similar compounds (*9*). Table 2 lists the atomic coordinates of all the atoms in this structure except hydrogens.

This crystal structure is of interest since it contains a guanine derivative and a uracil derivative. As such it might seem to violate the type of complementary pairing relationship which has been seen in the other crystal structures of base pairs. Both of these molecules have hydrogen donor and acceptor sites. However, an infrared study of hypoxanthine derivatives and uracil derivatives shows that there is no selective hydrogen bonding between these molecules in solution (*10*). The hydrogen-bonded pair involving two fluorouracil derivatives is similar to that found in N-1-methyl uracil (*8*) and this may also be related to the helical double-stranded hydrogen-bonded form of polyuridylic acid which is stable at lower temperatures (*11*). However, it is likely that the self-dimerization of fluorouracil is energetically less favorable than its association with adenine derivatives. The 1 : 1 crystalline complex of 9-ethyladenine and N-1-methyl-5-fluorouracil shows that these molecules form dimers held together with two hydrogen bonds (*12*).

In the present structure, the hypoxanthine molecules appear to fill space fully in the crystal lattice, and they are connected to individual uracil residues by single hydrogen bonds rather than a pair. In solution studies it has been shown that hydrogen bonding association between two molecules connected with a single hydrogen bond is much less stable than with a pair of bonds (*4*). In the present structure, the single hydrogen bond connecting the hypoxanthine with the fluorouracil pair undoubtedly stabilizes the crystal lattice, but it is unlikely that this could confer specificity to the interaction in a biological system. The existence of this 1 : 1 complex is probably determined more by the crystal lattice energy and the excellent packing and stacking than by a strong association of its component molecules. Thus the analysis of the present complex does not violate our understanding of the complementary nature of the hydrogen bonded pairs found between the purines and pyrimidines in the nucleic acids.

SUNG-HOU KIM
ALEXANDER RICH

Department of Biology,
Massachusetts Institute of Technology,
Cambridge 02139

References and Notes

1. K. Hoogsteen, *Acta Cryst.* **16**, 907 (1963); F. S. Mathews and A. Rich, *J. Mol. Biol.* **8**, 89 (1964); A. E. V. Haschemeyer and H. M. Sobell, *Proc. Nat. Acad. Sci. U.S.* **50**, 872 (1963).
2. L. Katz, K. Tomita, A. Rich, *J. Mol. Biol.* **13**, 340 (1965); *Acta Cryst.* **21**, 754 (1966).
3. H. M. Sobell, K. Tomita, A. Rich, *Proc. Nat. Acad. Sci. U.S.* **49**, 885 (1963); E. J. O'Brien, *Acta Cryst.* **23**, 92 (1967); A. E. V. Haschemeyer and H. M. Sobell, *Nature* **202**, 969 (1964).
4. R. M. Hamlin, R. C. Lord, A. Rich, *Science* **148**, 1734 (1965); Y. Kyogoku, R. C. Lord, A. Rich, *ibid.* **154**, 518 (1966); L. Katz and S. Penman, *J. Mol. Biol.* **15**, 220 (1966); Y. Kyogoku, R. C. Lord, A. Rich, *Proc. Nat. Acad. Sci. U.S.* **57**, 250 (1967).
5. D. Sayre, *Acta Cryst.*, **5**, 60 (1952).
6. R. E. Long, thesis, University of California, Los Angeles (1965).
7. W. R. Busing, K. O. Martin, H. A. Levy, *Oak Ridge Nat. Lab. Rep. TM-305* (1962).
8. D. W. Green, F. S. Mathews, A. Rich, *J. Biol. Chem.* **237**, P.C. 3573 (1962).
9. This information, together with more of the crystallographic details, is in preparation for presentation elsewhere.
10. Y. Kyogoku, R. C. Lord, A. Rich, *Biochim. Biophys. Acta*, in press.
11. M. Lipsett, *Proc. Nat. Acad. Sci. U.S.* **46**, 445 (1960).
12. K. Tomita, L. Katz and A. Rich, *J. Mol. Biol.*, in press.
13. We thank Professor G. A. Jeffrey, University of Pittsburgh, for the use of the diffractometer used in collecting the data. This research was supported by research grants from the NIH, NSF, and the American Cancer Society.

18 August 1967

UM00013930
NOVARTIS EXHIBIT 1017
Novartis v. Regents, IPR2023-01346
Page 2676 of 4460

ACKNOWLEDGMENTS AND ADDRESSES

Received May 11, 1970, from the *Bionucleonics Department, School of Pharmacy and Pharmacal Sciences, Purdue University, Lafayette, IN 47907*

Accepted for publication December 10, 1970.

This investigation was supported in part by the National Institute of Environmental Health Sciences, U. S. Public Health Service, and was conducted under the auspices of the Institute for Environmental Health.

* Present address: Department of Biology, South Campus of Allegheny County Community College, West Mifflin, PA 15122

Crystal Structure of a 1:1 Aminopyrine–Barbital Complex

SETSUO KIRYU

Abstract □ The crystal structure of a 1:1 complex of aminopyrine and barbital was determined from three-dimensional X-ray diffraction data. The unit cell dimensions are $a = 11.915$, $b = 26.922$, $c = 7.199$ Å, and $\beta = 97° 17'$. The space group is $P2_1/c$; $Z = 4$. The intensity data were collected photographically, and the structure was solved directly by the symbolic addition method. Molecules in the crystal are arranged in the series of aminopyrine–barbital–barbital–aminopyrine linked by hydrogen bondings. The ethyl groups and phenyl groups are in contact with the same groups of other molecules, with normal van der Waals' interactions.

Keyphrases □ Aminopyrine–barbital complex—crystal structure □ Crystal structure—1:1 aminopyrine–barbital complex □ Molecular structure—aminopyrine, barbital □ X-ray diffractometry—analysis

Since aminopyrine diethylbarbiturate appeared as a potent analgetic about half a century ago, numerous physicochemical as well as pharmacological investigations of this well-known system have been reported.

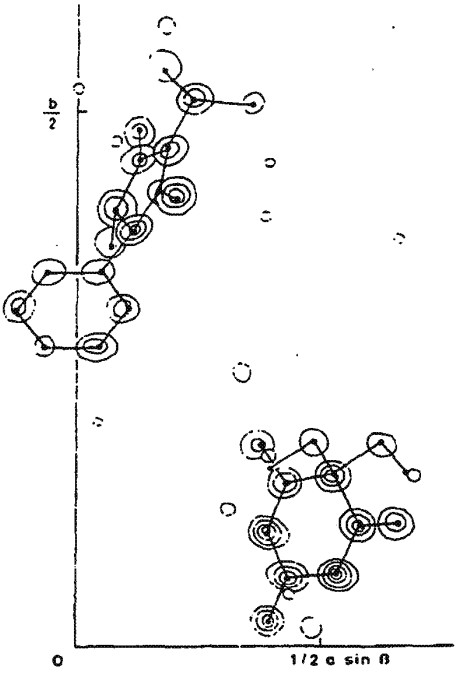


Figure 1—*Sections from a three-dimensional E-map projected along the c-axis. The contours are at equal intervals on an arbitrary scale.*

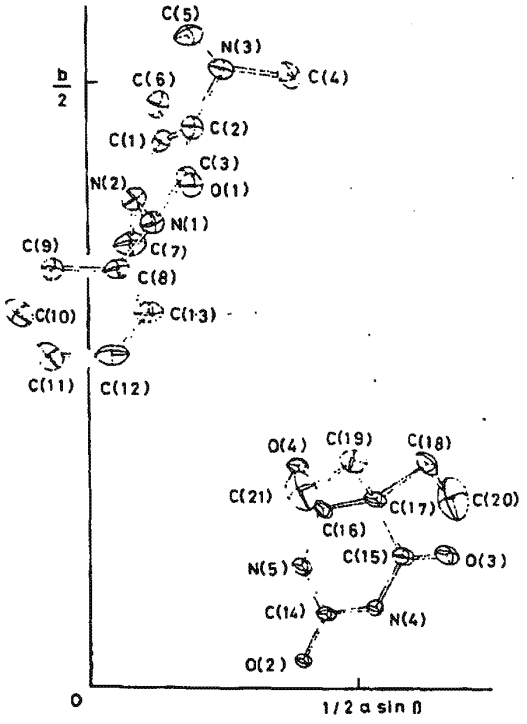


Figure 2—*Ellipsoidal representations of atomic thermal parameters and the atomic numbering scheme.*

Today a variety of information on this compound, such as its thermal or spectroscopic properties, is available; but the only study on its crystal structure was reported by Hertel in 1931 (1), and it does not offer sufficient information. Therefore, structure analysis by the X-ray diffraction method was undertaken to determine the exact crystal structure of this compound.

Table I—Initial Phase Assignments

h	*k*	*l*	*|Fo|*	*|E|*	Sign
5	10	5	35.2	4.34	+
−2	1	1	148.5	2.59	−
8	2	5	23.0	3.75	+
1	22	0	40.2	3.56	a
8	11	2	35.2	3.53	b
6	1	5	28.5	3.27	c

UM00013931
NOVARTIS EXHIBIT 1017
Novartis v. Regents, IPR2023-01346
Page 2677 of 4460

Table II—Positional Parameters and Their Estimated Standard Deviations (Fractional Coordinate × 10^4)

	x	y	z
Aminopyrine			
C (1)	1322 (4)	4522 (2)	0884 (7)
C (2)	1871 (4)	4638 (2)	2586 (7)
C (3)	1764 (4)	4227 (2)	3806 (7)
C (4)	3599 (6)	5055 (3)	3699 (11)
C (5)	1809 (7)	5374 (3)	4482 (11)
C (6)	1257 (5)	4818 (3)	−0893 (7)
C (7)	0726 (7)	3708 (3)	−0639 (8)
C (8)	0524 (5)	3495 (2)	3466 (7)
C (9)	−0653 (5)	3491 (2)	3058 (8)
C (10)	−1292 (7)	3136 (3)	3848 (9)
C (11)	−0727 (7)	2778 (3)	5079 (10)
C (12)	0434 (7)	2794 (3)	5478 (9)
C (13)	1092 (6)	3148 (2)	4668 (8)
N (1)	1169 (4)	3865 (2)	2721 (5)
N (2)	0819 (4)	4066 (2)	0934 (6)
N (3)	2385 (4)	5104 (2)	3077 (6)
O (1)	2070 (3)	4171 (1)	5520 (5)
Barbital			
C (14)	4360 (4)	0651 (2)	3912 (7)
C (15)	5788 (5)	1146 (2)	5774 (8)
C (16)	4294 (5)	1539 (2)	3415 (8)
C (17)	5280 (5)	1619 (2)	4925 (8)
C (18)	6226 (7)	1912 (3)	4122 (11)
C (19)	4864 (7)	1931 (3)	6501 (11)
C (20)	6713 (11)	1617 (6)	2561 (16)
C (21)	3922 (10)	1675 (6)	7405 (16)
N (4)	5293 (4)	0705 (2)	5236 (6)
N (5)	3915 (4)	1069 (1)	3052 (6)
O (2)	3956 (3)	0243 (1)	3522 (5)
O (3)	6613 (5)	1152 (2)	6968 (7)
O (4)	3851 (5)	1886 (2)	2537 (8)

Table IV—Least-Squares Planes

1. Equations of Planes[a]

Plane[b]	A	B	C	D
1	0.87750	−0.38927	−0.38909	−3.6277
2	−0.17236	0.61039	0.78873	7.6042
3	−0.70524	0.08008	0.78816	−1.3226

2. Displacements from the Plane (Å × 10^3)

Plane	Displacement
1	C(1) 25, C(2) 0, C(3) −24, N(1) 38, N(2) −39; atoms not forming the plane C(6) 145, C(7) 680, C(8) −457, N(3) −88, O(1) −125
2	C(8) −1, C(9) 4, C(10) 0, C(11) −6, C(12) 9, C(13) −5
3	C(14) 17, C(15) −19, C(16) −17, C(17) 28, N(4) −3, N(5) −6; atoms not forming the plane O(2) 48, O(3) −34, O(4) −69

[a] The equations are in the form $AX + BY + CZ = D$, referred to the crystallographic axes, with X, Y, and Z in Å units. [b] Plane number: 1, pyrazolone ring of aminopyrine; 2, benzene ring of aminopyrine; and 3, pyrimidine ring of barbital.

EXPERIMENTAL

Single crystals were prepared by slow evaporation of an ether solution, containing 0.7 g. of aminopyrine and 1.0 g. of barbital, in a refrigerator, whereupon colorless thin needles extending along the c-axis were obtained. The lattice constants of the monoclinic unit cell were determined from Weissenberg and precission photographs with Cu$K\alpha$ radiation (λ = 1.5418 Å); a = 11.915 ± 0.007, b = 26.922 ± 0.005, c = 7.199 ± 0.011 Å, and β = 97° 17′ ± 12′.

The cell contains four aminopyrine ($C_{13}H_{17}N_3O$) and four barbital ($C_8H_{12}N_2O_3$) molecules; the observed density is 1.26 g.·cm.$^{-3}$, calculated 1.20 g.·cm.$^{-3}$. Systematic absences of $0k0$ for k odd and $h0l$ for l odd indicate the space group to be $P2_1/c$. Linear absorption coefficient for Cu$K\alpha$ radiation is μ = 8.1 cm.$^{-1}$. The total number of electrons per unit cell is $F(000)$ = 888.

The dimensions of the specimen used for collecting the intensity data were 0.3 × 0.2 × 2.0 mm. Equi-inclination Weissenberg photographs, $hk0$-$hk6$ and $h0l$-$h2l$, were taken with Cu$K\alpha$ radiation, using the multiple-film technique. The intensities were estimated with a microphotometer and also visually by comparison with

Table III—Thermal Parameters and Their Estimated Standard Deviations (× 10^4)[a]

	B11	B22	B33	B12	B13	B23
Aminopyrine						
C (1)	73 (4)	16 (1)	122 (11)	14 (3)	32 (10)	7 (4)
C (2)	78 (4)	15 (1)	102 (10)	0 (3)	−1 (9)	0 (4)
C (3)	72 (4)	14 (1)	110 (10)	4 (3)	−17 (9)	−3 (4)
C (4)	92 (6)	28 (2)	350 (21)	−30 (5)	50 (17)	28 (9)
C (5)	136 (8)	22 (1)	340 (21)	−2 (5)	94 (19)	−69 (8)
C (6)	104 (6)	25 (1)	96 (12)	20 (4)	20 (11)	28 (5)
C (7)	161 (8)	20 (1)	114 (13)	3 (5)	0 (14)	−34 (6)
C (8)	95 (5)	14 (1)	105 (11)	5 (3)	23 (10)	−5 (4)
C (9)	92 (5)	20 (1)	179 (13)	1 (4)	18 (12)	−10 (6)
C (10)	133 (7)	25 (1)	186 (15)	−15 (5)	74 (16)	2 (7)
C (11)	126 (7)	26 (1)	229 (16)	−19 (5)	70 (16)	−10 (7)
C (12)	185 (9)	16 (1)	180 (15)	4 (5)	64 (17)	20 (6)
C (13)	126 (6)	13 (1)	149 (12)	3 (4)	−3 (13)	3 (5)
N (1)	95 (4)	16 (1)	84 (8)	5 (3)	−18 (8)	2 (3)
N (2)	95 (4)	18 (1)	85 (9)	6 (3)	−9 (8)	−6 (4)
N (3)	111 (5)	16 (1)	139 (10)	−7 (3)	15 (10)	1 (4)
O (1)	95 (3)	17 (1)	103 (7)	1 (2)	−53 (7)	6 (3)
Barbital						
C (14)	72 (4)	9 (1)	148 (11)	−1 (3)	−9 (9)	3 (4)
C (15)	98 (5)	11 (1)	224 (13)	−8 (3)	−47 (12)	6 (5)
C (16)	98 (5)	9 (1)	226 (14)	0 (3)	−26 (12)	10 (5)
C (17)	92 (5)	9 (1)	196 (13)	−13 (3)	−29 (11)	−2 (4)
C (18)	130 (8)	22 (1)	369 (21)	−45 (5)	0 (19)	57 (8)
C (19)	136 (8)	22 (1)	329 (20)	−2 (5)	10 (19)	−89 (8)
C (20)	195 (14)	65 (4)	445 (32)	−30 (12)	331 (35)	1 (19)
C (21)	179 (12)	57 (3)	432 (30)	−46 (10)	257 (30)	−145 (16)
N (4)	77 (4)	11 (1)	221 (11)	−4 (2)	−69 (9)	13 (4)
N (5)	89 (4)	10 (1)	161 (10)	1 (2)	−59 (9)	6 (3)
O (2)	78 (3)	9 (1)	235 (9)	−9 (2)	−69 (8)	2 (3)
O (3)	150 (5)	17 (1)	372 (14)	−23 (3)	−283 (14)	21 (5)
O (4)	160 (6)	10 (1)	426 (15)	−2 (3)	−237 (15)	42 (5)

[a] Thermal parameters are given according to the expression: $T = \exp[-(h^2B11 + k^2B22 + l^2B33 + hkB12 + hlB13 + klB23)]$.

UM00013932
NOVARTIS EXHIBIT 1017
Novartis v. Regents, IPR2023-01346
Page 2678 of 4460

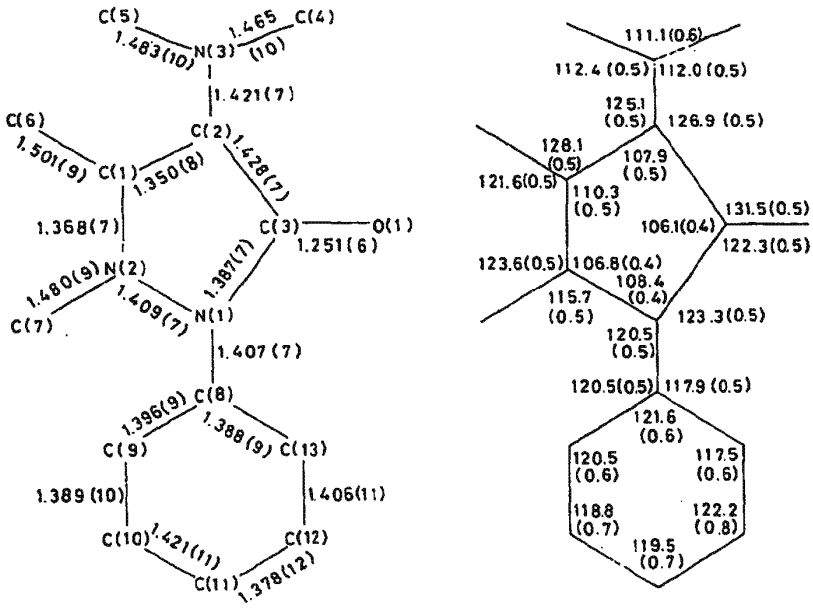


Figure 3—*Bond lengths (Å) and bond angles with their estimated standard deviations for aminopyrine.*

a calibrated scale. The number of unique reflections examined was 3669, among which were 1176 reflections of zero intensity. Corrections were applied for Lorentz and polarization factors but not for absorption.

STRUCTURE DETERMINATION

The structure was solved directly by the symbolic addition procedure for centrosymmetric crystals (2). Three reflections used to specify the origin and three additional reflections, each phase of which was designated by a symbol, are listed in Table I.

In the course of the phase determination, it became apparent that $a = b = +$ and $a = -c$. Phases were finally determined for 394 reflections of 477 with $|E| \geq 1.5$, and 382 of them were found to be correct after refinement. The positions of the atoms were readily found in the E-map computed with these 394 reflections (Fig. 1). Six cycles of block diagonal least-squares refinement applied to the positional parameters and the isotropic temperature and overall scale factors reduced the R-index from 0.50 to 0.27. Further refinement was carried out, introducing anisotropic temperature factors; after eight cycles of refinement the R-value was reduced to 0.177 (0.108 for observed reflections). The weighting scheme was $\sqrt{w} = 0.2$ for $Fo = 0$, $\sqrt{w} = 1.0$ for $0 < Fo < 11$, and $\sqrt{w} = 11/Fo$ for $Fo \geq 11$, and the function minimized was $\Sigma w(Fo - KFc)^2$.

The three-dimensional difference Fourier map, as well as the values of the positional and thermal parameters, showed no inconsistency with the structure obtained from the initial E-map, but few peaks of hydrogen atoms were clearly distinguishable in the difference Fourier map. Therefore, no further refinement, including the hydrogen atoms, was carried out. Maximum shifts of the positional and thermal parameters during the final cycle did not exceed a third of their standard deviations. The final positional and thermal parameters with their standard deviations are listed in Tables II and III, and the ellipsoidal representation of the thermal parameters is shown in Fig. 2.

The atomic scattering factors used for carbon, nitrogen, and oxygen were those of Berghuis *et al.* (3). Computations were carried out on the FACOM 230-60 of the Computer Center of Kyushu University with the programs UNICS (4), except for the computations of Fourier synthesis which were computed with a program written by the author.

DESCRIPTION OF THE STRUCTURE

The interatomic distances and the bond angles calculated on the basis of the parameters obtained are shown in Figs. 3 and 4.

Molecular Structure of Aminopyrine—In the five-membered pyrazolone ring, all the bond lengths lie between the corresponding

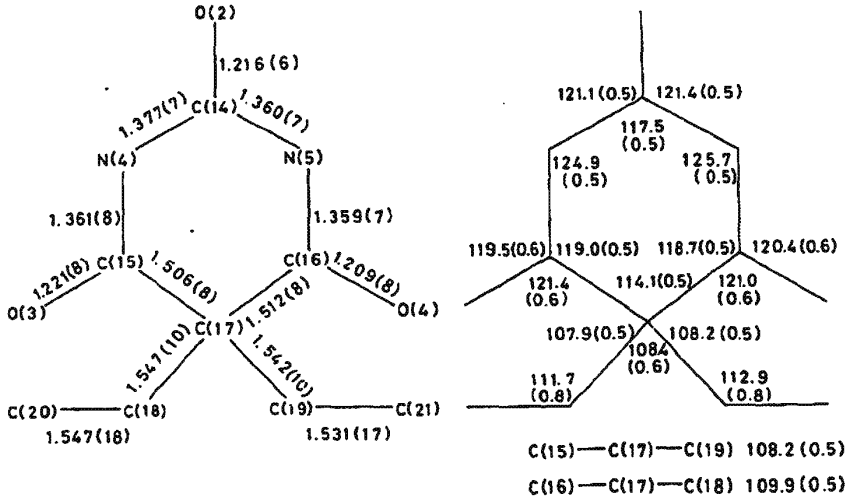


Figure 4—*Bond lengths (Å) and bond angles with their estimated standard deviations for barbital.*

UM00013933
NOVARTIS EXHIBIT 1017
Novartis v. Regents, IPR2023-01346
Page 2679 of 4460

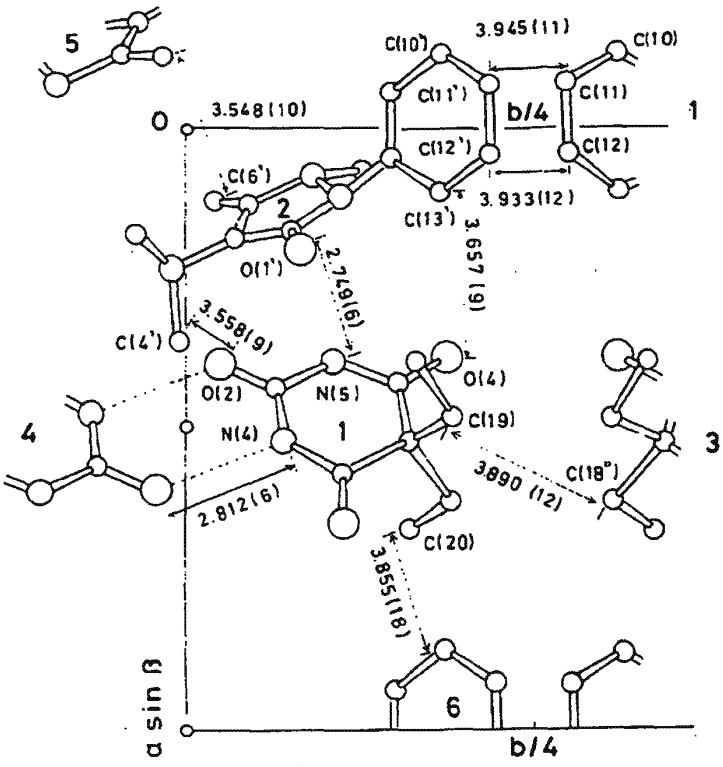


Figure 5—*Intermolecular atomic distances (Å) with their estimated standard deviations. The hydrogen bondings are shown by broken lines. The numbers on the molecules show following symmetry operations: (1)* x, y, z; *(2)* x, $^1/_2-y$, $-^1/_2+z$; *(3)* x, $^1/_2-y$, $^1/_2+z$; *(4)* $1-x$, $-y$, $1-z$; *(5)* $-x$, $-^1/_2+y$, $-^1/_2-z$; *and (6)* $1+x$, $^1/_2-y$, $-^1/_2+z$.

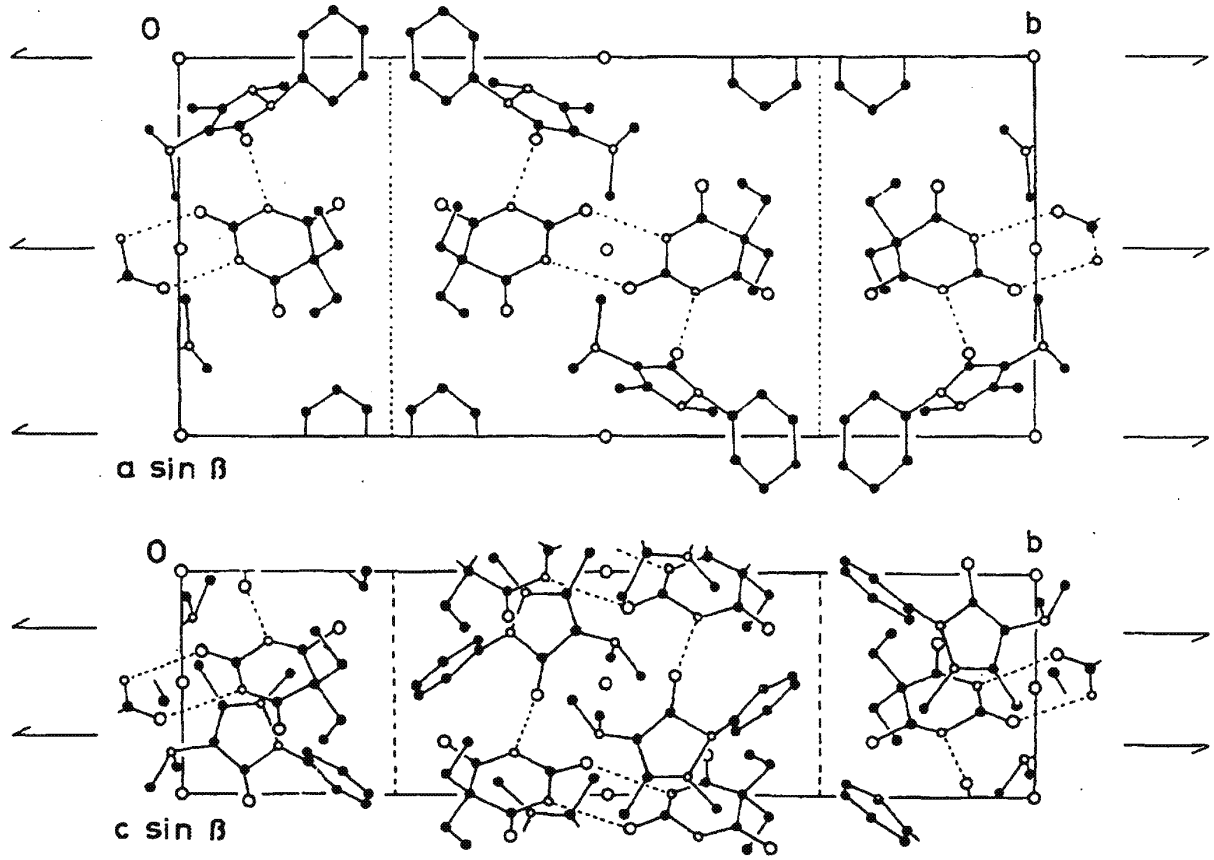


Figure 6—*The molecular arrangement viewed along the c- and a-axes. The hydrogen bondings are shown by broken lines.*

UM00013934
NOVARTIS EXHIBIT 1017
Novartis v. Regents, IPR2023-01346
Page 2680 of 4460

single- and double-bond values. The C(1)—N(2) bond length of 1.350 Å, however, shows an isolated double-bond character and the N(1)—N(2) distance 1.409 Å approximates a single-bond length.

Significant out-of-plane distortions occur in the ring (Table IV). The coordinations around the nitrogen atoms are not planar but pyramidal, and the substituents on N(1) and N(2), the phenyl and methyl groups, deviate from one another in a *trans*-configuration from the least-squares plane of the ring. The phenyl ring is completely planar (Table IV), and the C—C bond lengths (1.378–1.421 Å) and the bond angles (117.5–122.2°) are those of the typical benzenoid structure. The ring is inclined by 39° with respect to the plane of the pyrazolone ring. The dimethylamino group on C(2) is also of a pyramid configuration; the C(2)—N(3) bond length of 1.421 Å is a little shorter than that of a pure single bond at 1.47 Å (5) and is perhaps affected by the conjugated system of the pyrazolone ring.

Molecular Structure of Barbital—The values of bond lengths and angles are in reasonable agreement with the corresponding values for the same molecule in the barbital crystal (Form I) reported by Craven *et al.* (6). The C—N bond lengths of 1.359–1.377 Å in the pyrimidine ring show about 20–30% of double-bond characters, and there are no significant differences among the three C—O pure double-bond lengths. The C—C bond lengths of 1.506 and 1.512 Å in the pyrimidine ring approximate that of the single bond, while the steric requirement of the ring formation leads to a slight broadening of the angle at the tetrahedrally bonded atom C(17) from the tetrahedral angle of 109.4–114.1°. In the ethyl groups, the C—C—C angles and the C—C bond lengths agree quite well with those of normal paraffin. For an isolated barbital molecule, the ring atoms should be coplanar and the hydrocarbon chain of the ethyl groups should be normal to the ring plane. Some significant deviations of the ring atoms from the plane, however, were observed in this crystal (Table IV). The pyrimidine ring is slightly folded along the C(15)—C(16) line at an angle of about 4°. Similar distortions were also found in the pyrimidine rings in barbital I (6) and in other dialkylbarbiturate crystals (7, 8), in which the foldings of the planes were observed along the N(4)—C(16) diagonals.

Crystal Structure—The intermolecular atomic distances are shown in Fig. 5, and the arrangement of the molecules in the crystals is shown in Fig. 6. The short distances between the carbonyl and the imino groups, O(1)—N(5) 2.749 Å and O(2)—N(4) 2.812 Å, suggest hydrogen bondings. The interaction between two barbital molecules with hydrogen bonds is quite similar to that in barbital crystal I, in which the molecules are arranged in infinite planar ribbons with two kinds of hydrogen bonding (6). There are no infinite chains of molecules linked by hydrogen bonds in this compound: only two aminopyrine and two barbital molecules are linked in the series of aminopyrine–barbital–barbital–aminopyrine. The hydrocarbon groups, *i.e.*, the ethyl and phenyl groups, are in contact with one another in normal van der Waals' interactions. No other unusually close contacts or overlappings of molecules, which are found in some charge-transfer complexes, were observed.

REFERENCES

(1) E. Hertel, *Z. Phys. Chem.*, **1931**, 267.

(2) J. Karle and I. L. Karle, *Acta Crystallogr.*, **21**, 849(1966).

(3) J. Berghuis, I. J. M. Haanappel, M. Potters, B. O. Loopstra, C. H. MacGillavry, and A. L. Veenendaal, *ibid.*, **8**, 478(1955).

(4) "UNICS, The Universal Crystallographic Computation Program System," Crystallographic Society of Japan, 1967.

(5) W. J. Orville-Thomas, *Chem. Rev.*, **57**, 1179(1957).

(6) B. M. Craven, E. A. Vizzini, and M. M. Rodrigues, *Acta Crystallogr., Sect. B*, **25**, 1978(1969).

(7) B. M. Craven and E. A. Vizzini, *ibid.*, **25**, 1993(1969).

(8) B. M. Craven and C. Cusatis, *ibid.*, **25**, 2291(1969).

ACKNOWLEDGMENTS AND ADDRESSES

Received September 8, 1970, from the *Faculty of Pharmaceutical Science, Kyushu University, Katakasu, Fukuoka, Japan.*

Accepted for publication December 8, 1970.

The author expresses his thanks to Professor I. Ueda and Dr. A. Okazaki for facilities for X-ray diffraction measurement, and to Professor S. Iguchi for his continued guidance and encouragement.

Synthesis and Selected Pharmacology of Anthranilamides

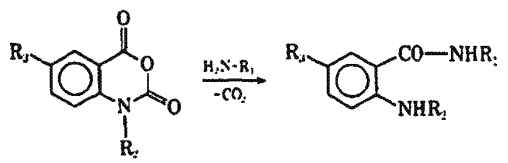
NED D. HEINDEL*, WILLIAM P. FIVES*, THOMAS F. LEMKE*, and RICHARD A. CARRANO†

Abstract □ A series of anthranilamides of diverse structure were prepared by the nucleophilic ring opening of isatoic anhydrides. Sixteen analogs, 10 of them previously unknown in the literature, were submitted to general pharmacologic screening. Several of the compounds displayed CNS depression, anti-inflammatory–analgesic, and antitremor activities.

Keyphrases □ Anthranilamides—synthesis from isatoic anhydrides □ CNS depressant activity—anthranilamides □ Anti-inflammatory, analgesic potential—anthranilamides □ Antitremor activity—anthranilamides

Literature reports regarding the general pharmacology of anthranilamides are sparse. In recent years, however, numerous studies appeared on the analgesic, antipyretic, and anti-inflammatory activities of anthranilamides (*o*-aminobenzamides) (1–5). One claim was made that their physiological activity rests, at least in part, on their metabolic conversion to salicylate analogs (6).

Synthetically, these compounds are obtained by nucleophilic ring opening of substituted isatoic anhydrides with amines (Scheme I). Although procedures



Scheme I

were suggested for these transformations (7, 8), an improved modification has been developed which simplifies the experimental method and enhances the yield by the use of *N,N*-dimethylformamide as a solvent when

UM00013935
NOVARTIS EXHIBIT 1017
Novartis v. Regents, IPR2023-01346
Page 2681 of 4460

This Page is Inserted by IFW Indexing and Scanning Operations and is not part of the Official Record

BEST AVAILABLE IMAGES

Defective images within this document are accurate representations of the original documents submitted by the applicant.

Defects in the images include but are not limited to the items checked:

- ☐ BLACK BORDERS
- ☐ IMAGE CUT OFF AT TOP, BOTTOM OR SIDES
- ☐ FADED TEXT OR DRAWING
- ☐ BLURRED OR ILLEGIBLE TEXT OR DRAWING
- ☐ SKEWED/SLANTED IMAGES
- ☐ COLOR OR BLACK AND WHITE PHOTOGRAPHS
- ☐ GRAY SCALE DOCUMENTS
- ☐ LINES OR MARKS ON ORIGINAL DOCUMENT
- ☐ REFERENCE(S) OR EXHIBIT(S) SUBMITTED ARE POOR QUALITY
- ☐ OTHER: _____

IMAGES ARE BEST AVAILABLE COPY.
As rescanning these documents will not correct the image problems checked, please do not report these problems to the IFW Image Problem Mailbox.

Chem. Pharm. Bull. 22(7)1588—1592(1974)

UDC 547.771.02 : 543.422.8

Crystal Structure of a 1:1 Aminopyrine-Cyclobarbital Complex

Setsuo Kiryu, Fumitoshi Hirayama, and Sadao Iguchi

Faculty of Pharmaceutical Sciences, Kyushu University[1]

(Received December 21, 1973)

The crystal structure of a 1:1 complex of aminopyrine and cyclobarbital was determined from X-ray diffraction data. The triclinic unit cell dimensions are $a=12.877$, $b=14.357$, $c=7.199$Å, $\alpha=91.49°$, $\beta=104.42°$, and $\gamma=100.05°$. The space group is $P\bar{1}$; $Z=2$. The intensity data were collected on a single crystal diffractometer and the structure was solved directly by the symbolic addition procedure. Molecules in the crystals were arranged in the series of aminopyrine-cyclobarbital-cyclobarbital-aminopyrine linked by hydrogen bonds. A partially disordered structure was observed of the cyclobarbital molecule.

As a part of a program for the pharmaceutical study on the molecular complex formation of drugs, the crystal structure of aminopyrine-barbital system was previously reported.[2] In this paper, the crystal structure determination of another molecular complex used as an analgetic, aminopyrine-cyclobarbital system, is reported.

Experimental and Structure Determination

Crystals were prepared by slow evaporation of ethanol solution including equimolar aminopyrine ($C_{13}H_{17}ON_3$) and cyclobarbital ($C_{11}H_{16}O_3N_2$) at room temperature. The lattice parameters and the reflection intensities were measured on Syntex $P\bar{1}$ automatic diffractometer using graphite monochromatized Cu$K\alpha$ radiation. The crystal data are: $C_{24}H_{33}O_4N_5$, triclinic system, $a=12.877\pm0.003$, $b=14.357\pm0.004$, $c=7.199\pm0.002$Å, $\alpha=91.49\pm0.02°$, $\beta=104.42\pm0.02°$, $\gamma=100.05\pm0.02°$, density observed 1.227, Calcd. 1.226 gcm^{-3}, $Z=2$, and space group $P\bar{1}$. Intensities for 3432 reflections were measured in the $\omega-2\theta$ scanning mode up to $2\theta=118°$, 797 reflections of which were considered to be unobserved ($I<3\sigma(I)$). Dimensions of specimen were about 0.3 mm and absorption corrections were not applied.

The structure was solved by the symbolic addition procedure and the atomic parameters were refined by block-matrix least-squares method. The function minimized was $\sum w(Fo-KFc)^2$, where $\sqrt{w}=0$ for unobserved reflections, $\sqrt{w}=1$ for $Fo<10$, $\sqrt{w}=10/Fo$ for $Fo\geqq10$, and K is a scale factor. An E-map computed from 316 signed E's with absolute values greater than 1.5 gave the positions of all the expected nonhydrogen atoms. There were found, however, two peaks for C(23) atom in the cyclohexene ring of cyclobarbital molecule, and either of them was not satisfactorily refined, giving an unusually large thermal parameter or chemically unacceptable bond lengths. Then two other possible structures were examined. One was a structure of noncentrosymmetric space group $P1$ and the other was a disordered one. The refinement of the $P1$ structure, however, did not improve the bond lengths in cyclohexene ring. The structure was finally assumed to be a disordered one and the two positions were given to the C(23) atom. The occupancy ratio was not refined but fixed at C(231): C(232)=0.6: 0.4 after several examinations (Fig. 1). The refinement of nonhydrogen atoms with the anisotropic temperature factors reduced R factor to 0.087. In the difference Fourier map at this stage, most hydrogen atom positions were readily found except those bonded to C(22), C(23), and C(24) located in the disordered region. Then 27 out of 33 hydrogen atoms were included in the final refinement with the isotropic temperature factors (R=0.056). The parameters determined are listed in Tables I and II.

Atomic scattering factors used for carbon, nitrogen, and oxygen were those of Berghuis, *et al.*[3] and that of McWeeny for hydrogen.[4] Computations were carried out in the Computer Center of Kyushu University with programs UNICS[5] and those written by one of authors (S.K).

1) Location: *1276, Katakasu Higashi-ku, Fukuoka.*
2) S. Kiryu, *J. Pharm. Sci.*, 60, 699 (1971).
3) J. Berghuis, I.J. Haanappel, M. Potters, B.O. Loopstra, C.H. McGillavry, and A.L. Veenendaal, *Acta Crystallogr.*, 8, 478 (1955).
4) R. McWeeny, *Acta Crystallogr.*, 4, 513 (1951).
5) "UNICS: The Universal Crystallographic Computation Program System," Crystallographic Society of Japan, Tokyo, 1967.

UM00013937
NOVARTIS EXHIBIT 1017
Novartis v. Regents, IPR2023-01346
Page 2683 of 4460

Description of the Structure

The interatomic distances and the bond angles calculated on the basis of the parameters obtained are shown in Fig. 2 and 3. C(22), C(23), and C(24) carbon atoms and all hydrogen atoms are excluded from the following discussion. The parameter values of the above three carbon atoms are less reliable due to the disorder, and some hydrogen atoms of the C(4) and C(5) methyl groups show unusually large thermal parameters and very diffused electron densities around the carbon atoms.

Molecular Structure of Aminopyrine

The values of bond lengths and angles are in good agreement with the corresponding values of the same molecule in the aminopyrine-barbital complex crystal.[2] In the five membered ring, the C(1)—C(2) bond length 1.352 Å shows an isolated double bond character and N(1)—N(2) distance 1.411 Å is approximately a single bond length. The coordinations around

Table I. Positional and Thermal Parameters with Their Standard Deviations ($\times 10^4$)

$T=\exp[-(h^2B_{11}+k^2B_{22}+l^2B_{33}+khB_{12}+hlB_{13}+klB_{23})]$

Atom	x	y	z	B_{11}	B_{22}	B_{33}	B_{12}	B_{13}	B_{23}
Aminopyrine									
C(1)	1465(2)	671(2)	5119(4)	71(2)	49(1)	181(6)	11(3)	56(5)	9(5)
C(2)	1985(2)	485(2)	6906(4)	76(2)	49(1)	193(6)	32(3)	60(5)	−1(5)
C(3)	1985(2)	1254(2)	8224(3)	57(2)	50(1)	169(5)	25(3)	42(5)	9(4)
C(4)	1853(3)	−925(2)	8625(6)	123(3)	58(2)	472(11)	56(4)	163(10)	101(7)
C(5)	3592(3)	−159(3)	8229(6)	88(3)	103(3)	469(12)	97(4)	130(9)	68(9)
C(6)	1286(3)	111(2)	3268(4)	105(3)	66(2)	194(6)	3(3)	85(7)	−31(5)
C(7)	1119(3)	2191(2)	3730(4)	102(3)	64(2)	193(6)	17(3)	29(6)	52(5)
C(8)	915(2)	2534(2)	7841(4)	69(2)	45(1)	205(6)	33(3)	68(5)	40(5)
C(9)	−196(2)	2479(2)	7124(5)	65(2)	62(2)	362(9)	33(3)	70(7)	51(6)
C(10)	−719(3)	3072(3)	7983(6)	83(3)	81(2)	545(13)	62(4)	203(9)	121(9)
C(11)	−120(3)	3717(2)	9506(5)	132(3)	72(2)	418(10)	83(4)	265(10)	68(8)
C(12)	978(3)	3780(2)	10160(4)	135(3)	61(2)	279(8)	60(4)	164(8)	23(6)
C(13)	1520(2)	3189(2)	9345(4)	95(2)	53(2)	197(6)	45(3)	74(6)	17(5)
N(1)	1469(2)	1894(1)	7107(3)	69(2)	50(1)	158(4)	34(2)	18(4)	1(4)
N(2)	1060(2)	1501(1)	5192(3)	80(2)	52(1)	149(4)	22(2)	17(4)	16(4)
N(3)	2413(2)	−357(2)	7391(3)	100(2)	60(1)	224(5)	66(3)	76(5)	12(4)
O(1)	2304(1)	1360(1)	10006(2)	77(1)	61(1)	157(4)	41(2)	3(4)	2(3)
Cyclobarbital									
C(14)	4465(2)	1190(2)	3935(4)	55(2)	51(1)	210(6)	25(3)	13(5)	25(5)
C(15)	5874(2)	2273(2)	6345(4)	57(2)	60(2)	219(6)	17(3)	17(5)	23(5)
C(16)	4470(2)	2892(2)	3754(4)	67(2)	54(2)	216(6)	29(3)	22(6)	7(5)
C(17)	5494(2)	3134(2)	5434(4)	62(2)	53(2)	200(6)	22(3)	21(5)	−14(5)
C(18)	5214(2)	3735(2)	7005(4)	80(2)	84(2)	225(7)	28(3)	64(6)	−41(6)
C(19)	6415(2)	3649(2)	4639(4)	70(2)	45(1)	192(6)	23(3)	31(5)	−2(5)
C(20)	4320(3)	3200(3)	7833(6)	89(3)	134(3)	349(10)	28(5)	138(9)	−7(9)
C(21)	6934(3)	4522(2)	5262(5)	109(3)	55(2)	323(8)	1(3)	147(8)	−38(6)
C(22)	7858(4)	5051(3)	4511(6)	160(4)	72(2)	447(12)	−37(5)	286(12)	−75(8)
C(231)[a]	8388(5)	4423(4)	3457(8)	116(5)	86(4)	332(15)	−22(7)	187(15)	−26(12)
C(232)	7729(9)	4565(6)	2445(14)	167(10)	74(6)	381(26)	11(12)	281(27)	68(19)
C(24)	7592(4)	3630(3)	2326(7)	184(5)	112(3)	569(15)	−101(6)	437(15)	−210(11)
C(25)	6710(3)	3103(2)	3111(5)	130(3)	68(2)	362(10)	−9(4)	208(9)	−77(7)
N(4)	5357(2)	1386(2)	5506(3)	62(2)	53(1)	237(5)	25(2)	−5(5)	40(4)
N(5)	4067(2)	1956(1)	3140(3)	61(2)	47(1)	218(5)	22(2)	−14(4)	14(4)
O(2)	4052(2)	386(1)	3305(3)	72(1)	48(1)	279(5)	18(2)	−32(4)	14(4)
O(3)	6626(2)	2340(1)	7787(3)	84(2)	76(1)	280(5)	6(2)	−101(5)	43(4)
O(4)	4018(2)	3502(1)	2967(3)	102(2)	55(1)	321(6)	60(2)	−70(5)	8(4)

a) C(231):C(232)=0.6:0.4

UM00013938
NOVARTIS EXHIBIT 1017
Novartis v. Regents, IPR2023-01346
Page 2684 of 4460

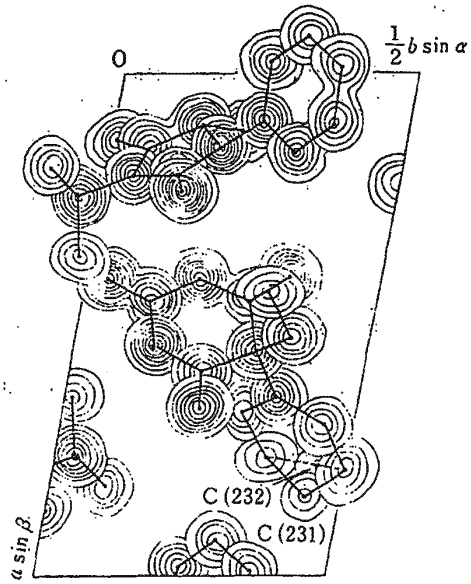


Fig. 1. Sections from the Final Electron Density Map projected along the *c*-Axis

Contours are at intervals of 1 eÅ^{-3} beginning with the 1 eÅ^{-3} contour.

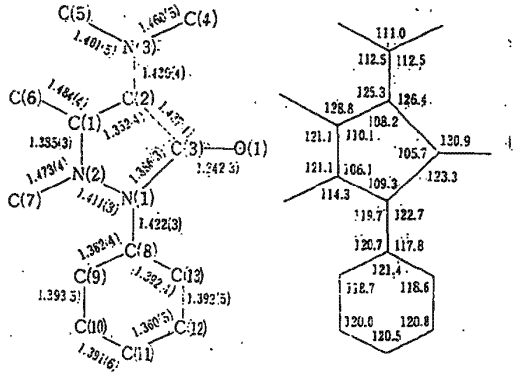


Fig. 2. Bond Lengths (Å) and Bond Angles with Their Estimated Standard Deviations for Aminopyrine

TABLE II. Hydrogen Atom Parameters with Their Standard Deviations

Atom	a)	$x \times 10^3$	$y \times 10^3$	$z \times 10^3$	B(Å^2)
H(1)	C(4)	197(3)	−55(3)	1004(6)	7.4(1.0)
H(2)		107(4)	−94(4)	809(8)	12.5(1.8)
H(3)		206(2)	−153(2)	869(4)	3.8(0.7)
H(4)	C(5)	393(4)	−80(3)	863(6)	8.0(1.1)
H(5)		374(5)	−5(5)	681(9)	14.3(2.0)
H(6)		374(4)	24(3)	952(7)	8.9(1.3)
H(7)	C(6)	169(3)	52(3)	242(5)	5.6(0.9)
H(8)		55(3)	−14(3)	279(5)	6.4(1.0)
H(9)		162(3)	−48(2)	355(5)	4.3(0.7)
H(10)	C(7)	188(3)	250(2)	399(5)	5.3(0.8)
H(11)		61(3)	265(2)	407(4)	4.1(0.7)
H(12)		81(3)	182(2)	245(5)	4.2(0.7)
H(13)	C(9)	−64(2)	200(2)	602(4)	3.5(0.7)
H(14)	C(10)	−162(3)	299(3)	725(5)	6.0(0.9)
H(15)	C(11)	−43(3)	414(3)	1026(6)	6.8(1.0)
H(16)	C(12)	141(3)	431(3)	1120(5)	5.9(0.9)
H(17)	C(13)	238(2)	324(2)	976(4)	3.0(0.6)
H(18)	N(4)	561(3)	84(3)	599(5)	5.6(0.9)
H(19)	N(5)	347(3)	183(3)	202(5)	5.5(0.9)
H(20)	C(18)	591(2)	397(2)	812(4)	3.8(0.7)
H(21)		501(3)	439(2)	641(5)	4.5(0.8)
H(22)	C(20)	414(4)	377(4)	876(7)	10.2(1.4)
H(23)		356(3)	302(3)	683(6)	6.7(1.0)
H(24)		454(3)	257(3)	852(6)	7.2(1.1)
H(25)	C(21)	670(3)	482(2)	635(5)	4.1(0.7)
H(26)	C(25)	704(3)	247(3)	388(6)	7.7(1.1)
H(27)		608(3)	273(3)	225(6)	7.2(1.1)

a) The atoms to which the hydrogen atoms are bonded.

UM00013939
NOVARTIS EXHIBIT 1017
Novartis v. Regents, IPR2023-01346
Page 2685 of 4460

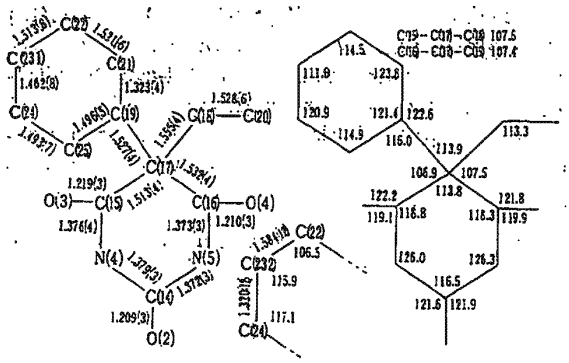


Fig. 3. Bond Lengths (Å) and Bond Angles with Their Estimated Standard Deviations for Cyclobarbital

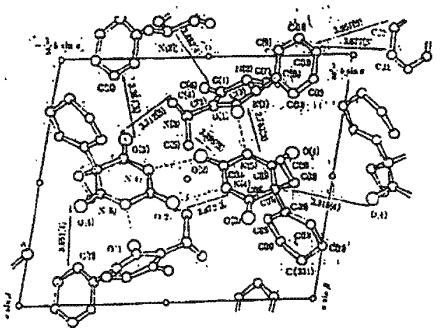


Fig. 4. The Molecular Arrangement viewed along the *c*-Axis and Intermolecular Atomic Distances (Å)

The hydrogen bonds are shown by broken lines.

TABLE III. Least-Squares Plane

1. Equation of plane[a]

Plane[b]	A	B	C	D
1	−0.85682	−0.33252	0.40413	−0.4176
2	−0.21028	−0.68297	0.73101	1.3821
3	−0.78680	0.05922	0.79272	−2.1640

2. Displacements from the plane (Å×10³)

Plane	
1	C(1) −29, C(2) 5, C(3) 22, N(1) −40, N(2) 42; atoms not forming the plane, C(6) −103, C(7) −778, N(3) 76, C(8) 479, O(1) 138
2	C(8) 12, C(9) −11, C(10) 2, C(11) 8, C(12) −7, C(13) −3
3	C(14) −13, N(4) −3, N(5) 1, C(15) 27, C(16) 23, C(17) −35; atoms not forming the plane, O(2) −22, O(3) 94, O(4) 84

a) The equations are in the form AX+BY+CZ=D, referred to the crystallographic axes, with X, Y, and Z in Å units.
b) plane number: 1, pyrazolone ring of aminopyrine; 2, benzene ring of aminopyrine; and 3, pyrimidine ring of cyclobarbital.

the nitrogen atoms are not planar but pyramidal, and the substituents on N(1) and N(2), the phenyl and methyl groups, deviate from one another in a *trans*-configuration from the least-squares plane of the pyrazolone ring (Table III). The structure is also very similar to that of antipyrine.[6]

Molecular Structure of Cyclobarbital

The structure of the cyclobarbital crystal at the stage of R=0.15 was reported as a note by Bideau, *et al.*[7] and has not been completely refined to be compared with the structure of this complex. The bond lengths and angles of the barbituric acid moiety of the complex, however, agree quite well with those of other barbiturates.[8] A slight folding of the pyrimidine ring plane[9] is also recognized along C(15)—C(16) line at an angle of about 5°.

The Crystal Structure

The intermolecular atomic distances and the arrangement of molecules in the crystals are shown in Fig. 4. The short distances between the carbonyl and imino groups, O(1)·····

6) T.P. Singh and M. Vijayan, *Acta Crystallogr., Sect. B*, 29, 714 (1973).
7) J.P. Bideau and M. Artaud, *C. R. Acad. Sc. Paris, Ser. C*, 271, 906 (1970).
8) B.M. Craven, E.A. Vizzini, and M.M. Rodorigues, *Acta Crystallogr., Sect. B*, 25, 1978 (1969); B.M. Craven and E.A. Vizzini, *ibid.*, 25, 1993 (1969).
9) B.M. Craven, C. Cusatis, G.L. Gartland, and E.A. Vizzini, *J. Mol. Struct.*, 16, 331 (1973).

UM00013940
NOVARTIS EXHIBIT 1017
Novartis v. Regents, IPR2023-01346
Page 2686 of 4460

H(19)—N(5) 2.765 Å (O(1)·····H(19) 1.82 Å) and O(2)·····H(18)—N(4) 2.872 A (O(2)·····H(18) 1.93 Å), suggest hydrogen bonds. Two aminopyrine and two cyclobarbital molecules are thus linked by hydrogen bonds in the series of aminopyrine-cyclobarbital-cyclobarbital-aminopyrine, while the hydrocarbon groups, phenyl and cyclohexenyl groups, are in contact with one another; these molecular interactions are quite similar to those of aminopyrine-barbital system in spite of its different crystal symmetry. No other close contacts or stackings of molecules are observed.

Acknowledgement The authors express their thanks to Drs. T. Komori and K. Miyahara for facilities for X-ray diffraction measurement.

UM00013941
NOVARTIS EXHIBIT 1017
Novartis v. Regents, IPR2023-01346
Page 2687 of 4460

This Page is Inserted by IFW Indexing and Scanning Operations and is not part of the Official Record

BEST AVAILABLE IMAGES

Defective images within this document are accurate representations of the original documents submitted by the applicant.

Defects in the images include but are not limited to the items checked:

- ☐ BLACK BORDERS
- ☐ IMAGE CUT OFF AT TOP, BOTTOM OR SIDES
- ☐ FADED TEXT OR DRAWING
- ☐ BLURRED OR ILLEGIBLE TEXT OR DRAWING
- ☐ SKEWED/SLANTED IMAGES
- ☐ COLOR OR BLACK AND WHITE PHOTOGRAPHS
- ☐ GRAY SCALE DOCUMENTS
- ☐ LINES OR MARKS ON ORIGINAL DOCUMENT
- ☐ REFERENCE(S) OR EXHIBIT(S) SUBMITTED ARE POOR QUALITY
- ☐ OTHER: _____

IMAGES ARE BEST AVAILABLE COPY.

As rescanning these documents will not correct the image problems checked, please do not report these problems to the IFW Image Problem Mailbox.

November 1985
Volume 74, Number 11

Journal of Pharmaceutical Sciences

A publication of the American Pharmaceutical Association

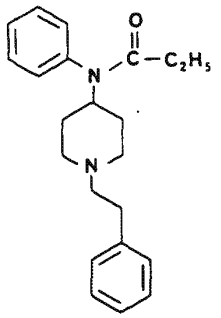
RESEARCH ARTICLES

Molecular Structure of Two Conformationally Restrained Fentanyl Analogues: cis- and trans-Isomers of *N*-{3-Methyl-1-[2-(1,2,3,4-tetrahydro)naphthyl]-4-piperidinyl}-*N*-phenylpropanamide

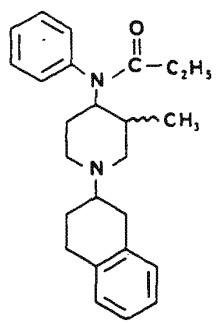
CHERYL L. KLEIN*x, EDWIN D. STEVENS*§, E. KIM FIFER‡, AND RONALD F. BORNE‡

Received December 5, 1984, from the *Department of Chemistry, Xavier University, New Orleans, LA 70125, §Department of Chemistry, University of New Orleans, New Orleans, LA 70148, and the ‡Department of Medicinal Chemistry, University of Mississippi, University, MS 38677. Accepted for publication July 11, 1985.

Abstract □ The X-ray crystallographic structures of two analogues of the potent analgetic fentanyl in which the *N*-phenethyl substituent is restrained through incorporation into a tetrahydronaphthyl ring system are reported. The tetrahydronaphthyl moiety exists in an equatorial conformation with respect to the piperidine ring which exists in the chair conformation. The propanilido group is also equatorial and antiperiplanar. The orientation of the *N*-phenyl group with respect to the *N*-acyl moiety is essentially invariant with an approximately 90° dihedral angle. The implications of these conformations in the interaction of fentanyl-type analgetics with opiate receptors are discussed. The following data were obtained: *cis*-$[C_{25}H_{33}N_2O^+]Cl^- \cdot 1/2\ C_2O_4H_2$, triclinic, $P\bar{1}$, a = 7.005(7), b = 13.189(2), c = 14.312(4)Å, α = 111.27(2), β = 99.15(5), γ = 93.52(4)°, V = 1205.9Å, Z = 2, T = 110K, R = 0.0596, R_w = 0.0760; *trans*-$[C_{25}H_{33}N_2O^+]\ C_2O_4H^- \cdot 1/2\ C_2O_4H_2 \cdot 2\ H_2O$, triclinic, $P\bar{1}$, a = 8.235(6), b = 10.546(8), c = 17.108(9)Å, α = 107.72(5), β = 95.73(5), γ = 90.63(6)°, V = 1406.8Å^3, Z = 2, T = 110K, R = 0.0737, R_w = 0.0934.



1



2 a = cis

b = trans

Fentanyl (1) is a potent narcotic analgetic agent which is representative of the 4-anilidopiperidine class of synthetic analgetics. This class of analgetics has been the subject of numerous structural and conformational studies. In an effort to clarify structure–activity relationships for analgetic activity there have been many reports regarding the synthesis of compounds related to fentanyl.[1-10] Several studies relating to the importance of conformational factors in the action of these analgetics have also been reported including efforts to restrict the *N*-propanilido group[11-13], the piperidine ring[14,15], and the *N*-phenethyl substituent.[16,17] Based on the reports that a 3-methyl substituent enhances activity[6,7] compounds 2a and b were prepared as analogues of 3-methylfentanyl in which the *N*-phenethyl substituent is restricted in an antiperiplanar conformation. The observation that 2a possesses approximately three times the analgetic activity of fentanyl and the proposal that the conformation of the *N*-phenyl rings plays an important role in the binding of fentanyl-type analgetics to the opiate receptor[13] prompted an investigation of its crystal structure.

Experimental Section

Compounds 2a and b were prepared as described previously.[16] Single crystals of both compounds were obtained separately from solutions of aqueous ethanol, and the structure was determined by X-ray crystallographic techniques as described below.

Crystal Data—*cis*-$[C_{25}H_{33}N_2O^+]Cl^- \cdot 1/2\ C_2O_4H_2$, triclinic space group, $P\bar{1}$, a = 7.005(7), b = 13.189(2), c = 14.312(4)Å, α = 111.27(2)°, β = 99.15(5)°, γ = 93.52(4)°, V = 1205.9Å^3, Z = 2, λ = 0.70930Å, D_x = 1.23 g/mL. *trans*-$[C_{25}H_{33}N_2O^+] \cdot 1/2\ C_2O_4H_2$, $C_2O_4H^- \cdot 2H_2O$, triclinic space group, $P\bar{1}$, a = 8.235(6), b = 10.546(8), c = 17.108(9)Å, α = 107.72(5)°, β = 95.73(5)°, γ = 90.63(6)°, V = 1406.8Å^3, Z = 2, λ = 0.70930Å, D_x = 1.25 g/mL.

***cis*-*N*-{3-Methyl-1-[2-(1,2,3,4-tetrahydro)naphthyl]-4-piperidinyl}-*N*-phenylpropanamide (2a)**—A single colorless plate-like

0022-3549/85/1100-1147$01.00/0
© 1985, American Pharmaceutical Association

UM00013943
NOVARTIS EXHIBIT 1017
Novartis v. Regents, IPR2023-01346
Page 2689 of 4460

Crystal (0.06 × 0.48 × 0.30 mm) was mounted on an Enraf-Nonius CAD-4 diffractometer with a molybdenum target X-ray tube and a graphite crystal monochromator. All three-dimensional intensity data were collected at 110 K in the $\omega:2\theta$ scan mode. Independent reflections (5138) were collected to a 2θ maximum of 52° Reflections with $I > 3\sigma(I)$ were considered observed (3059) and were included in the refinement. The data were corrected for Lorentz and polarization effects. Absorption as a function of psi was observed to be minimal and, therefore, not corrected. Three standard reflections measured every 2 h during data collection showed no significant change in intensity.

The structure was solved by direct methods using the MULTAN[18] series of programs which revealed the location of 31 non-hydrogen atoms, corresponding to the cis-isomer of the fentanyl analogue and one-half of an oxalic acid molecule which is located on an inversion center on the E map. These 31 atoms were refined isotropically using a full-matrix least-squares program to R = 0.131%. All hydrogen atoms, with the exception of the nitrogen proton and the oxalic acid hydrogens, were calculated on the basis of sp^2 or sp^3 geometry and a C — H bond distance of 0.95Å. The oxalic acid hydrogen and the hydrogen on the piperidine nitrogen atom were located on a difference Fourier map. Continued refinement of all-nonhydrogen atoms with anisotropic thermal parameters and hydrogen atoms with isotropic thermal parameters led to a final R = 0.0596 and R_w = 0.0760.[19]

trans-*N*-(3-Methyl-1-[2-(1,2,3,4-tetrahydro)naphthyl]-4-piperidinyl)-*N*-phenylpropanamide (2b)—A single, colorless, plate-like crystal (0.42 × 0.27 × 0.08 mm) was mounted on the instrument described above. Independent reflections (3727) were collected at 110 K to a 2θ maximum of 44°. Reflections with $I > 5\sigma(I)$ were considered observed (1243) and included in the refinement. The data were corrected for Lorentz and polarization effects. Absorption as a function of psi was observed to be minimal and therefore not corrected. Three standard reflections measured every 2 h showed a 15.8% loss in intensity over a 10-d data collection period which was corrected assuming a linear decay model.

The structure was solved using the MULTAN series of programs which revealed the location of all atoms in the trans-isomer, one hydrogen oxalate anion, one-half of an oxalic acid molecule, and two water oxygen atoms. Isotropic full-matrix least-squares refinement led to an R value of 0.136. All hydrogen atoms except those on the water molecules and those on the oxalates were calculated on the basis of sp^2 or sp^3 geometry and a C — H bond distance of 0.95Å. Two of the remaining hydrogen positions were located on a subsequent Fourier map. The remaining hydrogens could not be located. Continued refinement with all non-hydrogen atoms with anisotropic temperature factors and all hydrogen atom positions and thermal parameters fixed led to a final value of R = 0.0737 and R_w = 0.0934.

All computer programs used for data collection and refinement are part of the CAD-4 SDP package.[20] Scattering factors were taken from the International Tables for X-ray Crystallography[21] and included corrections for anomalous scattering contributions.

Results and Discussion

Final fractional coordinates for both isomers are given in Table I. The numbering system and bond lengths may be found in Fig. 1 for the cis-isomer and Fig. 2 for the trans-isomer. Bond lengths and bond angles may be found in Table II.[22] Crystals of the trans-isomer 2b were of lower quality than those of the cis-isomer 2a, leading to a lower ratio of observations with significant intensity. In addition, the crystals of the trans-isomer showed significant decay during the data collection. The overall precision of the structural results for the trans-isomer is therefore somewhat lower than for the cis-isomer, which is reflected in estimated SD of position thermal parameters, and bond distances and angles which are 3–4 times higher. Despite the lower precision, the basic information of chemical connectivity and molecular conformation of the trans-isomer are well defined.

The cis-isomer 2a crystallized as the hydrochloride salt with the piperidine nitrogen atom protonated and the methyl group bonded axially. An oxalic acid molecule, located on an inversion center in the unit cell, participated in an extensive

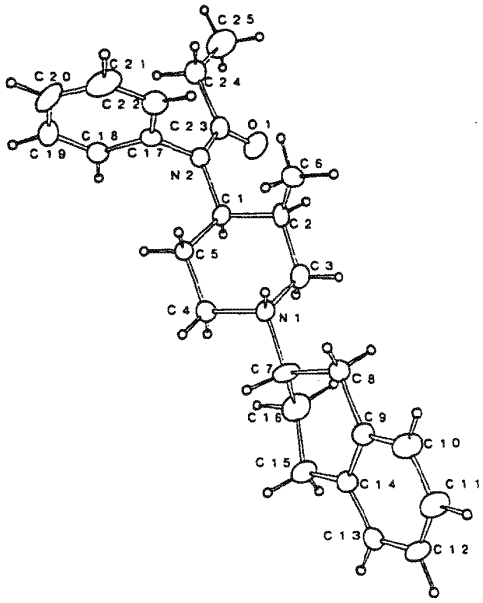


Figure 1—*Numbering system and bond lengths for* ***2a****, the cis-isomer.*

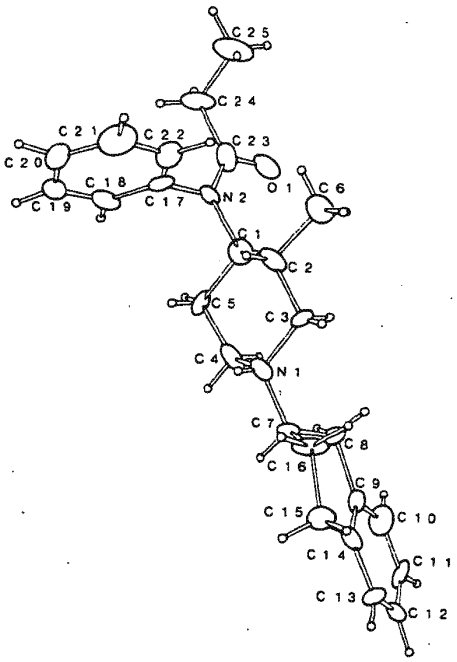


Figure 2—*Numbering system and bond lengths for* ***2b****, the trans-isomer.*

intermolecular hydrogen bonding network. The trans-isomer 2b crystallized as the oxalate salt, with the piperidine nitrogen atom also protonated and the methyl group bound equatorially. The unit cell contains two molecules of 2b, one oxalic acid molecule located on an inversion center, two monohydrogen oxalate anions, and four water molecules, all participating in an extensive intermolecular hydrogen bonding network.

Both the cis- and trans-isomers (2a and b) represent conformationally restrained analogues of fentanyl in which

UM00013944
NOVARTIS EXHIBIT 1017
Novartis v. Regents, IPR2023-01346
Page 2690 of 4460

Table I—Fractional Coordinates for 2a and 2b[a]

Atom	2a x	2a y	2a z	2a B_{equiv}(Å^2)	Atom	2b x	2b y	2b z	2b B_{equiv}(Å^2)
Cl(1)	0.3450(1)	0.85783(9)	0.15771(7)	2.47(2)	O(1)	0.846(1)	−0.1869(8)	0.5661(5)	3.3(2)
O(1)	−0.2122(4)	−0.2113(2)	0.7814(2)	2.99(7)	O(2)	0.270(1)	0.0749(7)	0.8034(5)	2.2(2)
O(3)	0.3673(4)	0.0884(2)	0.5803(2)	2.05(6)	O(3)	0.375(1)	0.2780(8)	0.8165(5)	3.6(2)
O(4)	0.6325(4)	0.0127(2)	0.6190(2)	2.23(6)	O(4)	0.106(2)	0.0811(9)	0.6653(7)	7.9(4)
N(1)	0.2572(4)	0.1626(2)	0.9051(2)	1.41(6)	O(5)	0.144(2)	0.2914(9)	0.6968(6)	5.4(3)
N(2)	0.0042(4)	−0.1632(2)	0.6990(2)	1.54(6)	O(6)	0.290(1)	0.0083(7)	0.9833(5)	2.2(2)
C(1)	0.1493(6)	0.0923(3)	0.9461(3)	1.99(8)	O(7)	0.481(1)	0.0520(7)	0.9120(5)	2.0(2)
C(2)	0.1279(6)	−0.0290(3)	0.8788(3)	2.17(8)	O(8)	−0.027(1)	0.274(1)	0.5623(6)	5.4(3)
C(3)	0.0213(5)	−0.0468(3)	0.7698(3)	1.53(7)	O(9)	−0.190(2)	0.036(1)	0.4947(7)	8.0(4)
C(4)	0.1261(5)	0.0282(3)	0.7295(3)	1.43(7)	N(1)	0.663(1)	−0.1994(8)	0.6529(5)	2.0(3)
C(5)	0.1471(5)	0.1479(3)	0.8008(3)	1.62(7)	N(2)	0.806(1)	0.0906(9)	0.8892(5)	2.0(2)
C(6)	0.3170(7)	−0.0774(3)	0.8831(3)	3.2(1)	C(1)	0.761(2)	0.139(1)	0.8154(6)	2.0(3)
C(7)	0.3094(6)	0.2823(3)	0.9741(3)	2.33(9)	C(2)	0.669(2)	0.035(1)	0.7452(7)	2.2(3)
C(8)	0.4727(5)	0.2944(3)	1.0629(3)	1.77(8)	C(3)	0.762(2)	−0.093(1)	0.7211(7)	2.2(3)
C(9)	0.5306(5)	0.4128(3)	1.1335(3)	1.83(8)	C(4)	0.802(2)	−0.139(1)	0.7979(7)	2.0(3)
C(10)	0.7058(6)	0.4427(3)	1.2035(3)	2.7(1)	C(5)	0.898(2)	−0.030(1)	0.8650(7)	2.7(3)
C(11)	0.7594(6)	0.5482(3)	1.2740(3)	2.8(1)	C(6)	0.640(2)	0.092(1)	0.6725(8)	3.4(4)
C(12)	0.6383(6)	0.6272(3)	1.2756(3)	2.34(9)	C(7)	0.891(2)	0.197(1)	0.9636(6)	1.8(3)
C(13)	0.4673(6)	0.5996(3)	1.2042(3)	2.04(8)	C(8)	1.050(2)	0.248(1)	0.9503(7)	1.7(3)
C(14)	0.4101(5)	0.4931(3)	1.1339(3)	1.73(8)	C(9)	1.132(2)	0.349(1)	1.0327(7)	1.6(3)
C(15)	0.2186(6)	0.4647(3)	1.0579(3)	2.59(9)	C(10)	1.297(2)	0.373(1)	1.0416(8)	2.7(3)
C(16)	0.1426(6)	0.3400(4)	1.0109(3)	2.9(1)	C(11)	1.377(2)	0.459(1)	1.1128(8)	2.3(3)
C(17)	0.0944(5)	−0.1921(3)	0.6112(3)	1.55(7)	C(12)	1.279(2)	0.522(1)	1.1745(7)	2.3(3)
C(18)	0.2765(6)	−0.2289(3)	0.6133(3)	2.24(9)	C(13)	1.117(2)	0.502(1)	1.1656(7)	2.4(3)
C(19)	0.3598(6)	−0.2552(4)	0.5291(4)	3.0(1)	C(14)	1.034(2)	0.413(1)	1.0945(7)	2.3(3)
C(20)	0.2652(6)	−0.2463(4)	0.4412(3)	2.9(1)	C(15)	0.852(2)	0.387(1)	1.0864(7)	2.3(3)
C(21)	0.0849(6)	−0.2083(3)	0.4390(3)	2.36(9)	C(16)	0.775(2)	0.310(1)	0.9976(7)	2.5(3)
C(22)	−0.0007(5)	−0.1821(3)	0.5229(3)	1.83(8)	C(17)	0.515(2)	−0.254(1)	0.6674(7)	1.7(3)
C(23)	−0.1240(6)	−0.2372(3)	0.7109(3)	2.08(8)	C(18)	0.516(2)	−0.362(1)	0.6965(7)	2.8(3)
C(24)	−0.1464(7)	−0.3541(3)	0.6331(3)	2.48(9)	C(19)	0.371(2)	−0.413(1)	0.7109(7)	3.1(4)
C(25)	−0.2812(9)	−0.4315(4)	0.6550(4)	4.6(1)	C(20)	0.222(2)	−0.362(1)	0.6906(8)	3.6(4)
C(26)	0.4917(5)	0.0307(3)	0.5557(3)	1.63(7)	C(21)	0.228(2)	−0.250(1)	0.6630(9)	3.9(4)
					C(22)	0.374(2)	−0.198(1)	0.6514(8)	2.9(3)
					C(23)	0.716(2)	−0.238(1)	0.5802(8)	2.6(3)
					C(24)	0.630(2)	−0.343(1)	0.5091(8)	4.3(4)
					C(25)	0.525(2)	−0.277(1)	0.4505(8)	5.3(5)
					C(26)	0.288(2)	0.185(1)	0.7836(8)	2.3(3)
					C(27)	0.164(2)	0.179(1)	0.7069(8)	3.8(4)
					C(28)	0.429(1)	0.015(1)	0.9708(6)	1.2(3)

[a] Estimated standard deviations are given in parentheses.

the *N*-phenethyl moiety is restricted to an antiperiplanar conformation by incorporation of this moiety as part of a tetrahydronaphthyl group. In the cis-isomer, the analgetic activity was slightly increased[16] and it was found to be approximately three times as potent as fentanyl. This is analogous to the effect observed in the increased potency of fentanyl upon addition of a *cis*-3-methyl group[6,7]. The trans-isomer, however, displays a slightly decreased activity relative to fentanyl. These data indicate that the conformation of the phenethyl group of fentanyl and related 4-anilidopiperidine analogues is most probably equatorial and antiperiplanar when interacting with the opiate receptor. This contradicts another model derived from molecular models which suggested a "folded" fentanyl conformation where the orientation of a phenyl ring of the phenethyl group is equivalent to the orientation of the comparable phenyl ring in other, more rigid, opiates.[23]

The piperidine ring in both the cis- and trans-isomers exists in a chair conformation with the 4-propanilido group extended and equatorially oriented. This is also the case in the crystal structure of fentanyl[24] itself and a 4-methoxymethyl derivative of fentanyl which shows analgetic activity 460 times that of fentanyl.[25] The *N*-acyl functions in all four of these compounds are essentially planar with nearly perpendicular dihedral angles between the *N*-acyl plane and the plane of the *N*-phenyl ring (fentanyl, 89°; 2a, 87.9°, 2b, 93.3°; and 4-CH_2OCH_3-fentanyl, 85°). In all cases, the orientation of the *N*-phenyl ring with respect to the *N*-acyl plane is essentially constant and the conformational differences result from the rotation of the *N*-phenyl/*N*-acyl groups about the C(3) — N(2) bond.

The torsion angles, C(17) — N(2) — C(3) — C(2), vary considerably (2b, −67.2°; fentanyl, −81.9°; and 2a, −118.1°). This must be a result of the orientation of the 3-methyl substituent with respect to the *N*-phenyl and propanilido substituents. This can be seen more clearly in Fig. 3. Figure 3a shows that rotation of the *N*-phenyl/propanilido groups around the C(3) — N(2) bond in 2a is hindered by the close proximity of an *N*-phenyl hydrogen atom and a methyl hydrogen atom [H(18) — H(6′), 2.32Å]. Rotation around the C(3) — N(2) bond in 2b is also hindered by the close proximity of an *N*-phenyl hydrogen atom and a methyl hydrogen atom [H(22) — H(6′), 2.32Å] (Fig. 3c). The comparable torsion angles in the 4-methoxymethyl fentanyl derivative [C(17) — N(2) — C(3) — C(2)] are −122.0° and −120.8° (for two unique molecules in the asymmetric unit).[25] These are similar to the torsion angles in the cis-isomer 2a.

In summary this structural investigation has resulted in the following information concerning the conformation of 2a and b. The apparently preferred conformation of the piperidine ring is a chair with the propanilido group equatorial and planar with respect to the C(3) — N(2) — C(23) —C(24)

UM00013945
NOVARTIS EXHIBIT 1017
Novartis v. Regents, IPR2023-01346
Page 2691 of 4460

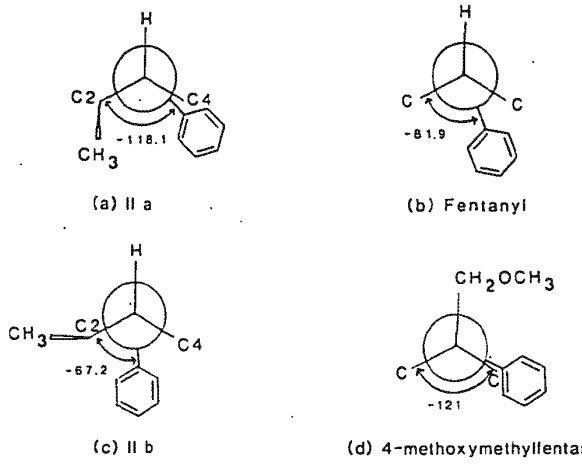


Figure 3—*Newman projections showing the degree of rotation of the N-phenyl/propanilido groups around the C3 — N2 bond (or comparable) in: a) 2a, b) fentanyl, c) 2b,and d) 4-methoxymethyl fentanyl.*

bond. The preferred conformation of the *N*-phenethyl moiety in fentanyl is, most probably, equatorial when interacting with the opiate receptor. This is confirmed by the observed effects on analgetic activity upon substitution of the *N*-phenethyl group with a tetrahydro naphthalene derivative which conformationally restrains the phenethyl group into an equatorial and antiperiplanar conformation. The orientation of the *N*-phenyl ring with respect to the *N*-acyl group is essentially invariant with an approximately 90° dihedral angle. Any variations that occur in the conformation of the *N*-phenyl and propanilido groups apparently result from rotation about the N(2) — C(3) bond. The increased activity of the *cis*-3-methyl derivative (**2a**) when compared with the corresponding trans-isomer (**2b**) and fentanyl (**1**) suggests that the axial *cis*-3-methyl substituent may allow the phenyl ring to assume a preferred conformation for interaction with the opiate receptor by avoiding unfavorable interactions between the phenyl ring and the methyl group. Likewise, the *N*-phenyl group in the trans-isomer is also forced into a conformation that avoids unfavorable interactions between the phenyl ring and the methyl groups. However, this orientation in the case of **2b** is apparently not one which is favorable to enhanced analgetic activity.

Table II—Bond Lengths (Å) and Bond Angles (°) for 2a and 2b

Atom 1	Atom 2	Distance	Atom 1	Atom 2	Atom 3	Angle
			2a			
O(1)	O(23)	1.222(4)	C(1)	N(1)	C(5)	109.2(2)
N(1)	C(1)	1.491(4)	C(1)	N(1)	C(7)	115.9(2)
N(1)	C(5)	1.507(3)	C(5)	N(1)	C(7)	111.9(2)
N(1)	C(7)	1.525(4)	C(3)	N(2)	C(17)	120.5(2)
N(2)	C(3)	1.487(4)	C(3)	N(2)	C(23)	117.5(2)
N(2)	C(17)	1.435(4)	C(17)	N(2)	C(23)	121.1(2)
N(2)	C(23)	1.360(4)	N(1)	C(1)	C(2)	112.3(3)
C(1)	C(2)	1.523(4)	C(1)	C(2)	C(3)	109.3(3)
C(2)	C(3)	1.547(4)	C(1)	C(2)	C(6)	113.3(3)
C(2)	C(6)	1.509(5)	C(3)	C(2)	C(6)	114.4(3)
C(3)	C(4)	1.519(4)	N(2)	C(3)	C(2)	111.9(2)
C(4)	C(5)	1.522(4)	N(2)	C(3)	C(4)	110.5(2)
C(7)	C(8)	1.524(4)	C(2)	C(3)	C(4)	110.0(2)
C(7)	C(16)	1.496(4)	C(3)	C(4)	C(5)	111.8(2)
C(8)	C(9)	1.509(4)	N(1)	C(5)	C(4)	109.9(2)
C(9)	C(10)	1.389(4)	N(1)	C(7)	C(8)	109.5(2)
C(9)	C(14)	1.395(4)	N(1)	C(7)	C(16)	115.5(3)
C(10)	C(11)	1.376(4)	C(8)	C(7)	C(16)	111.3(3)
C(11)	C(12)	1.382(5)	C(7)	C(8)	C(9)	111.4(2)
C(12)	C(13)	1.378(4)	C(8)	C(9)	C(10)	119.2(3)
C(13)	C(14)	1.387(4)	C(8)	C(9)	C(14)	122.2(3)
C(14)	C(15)	1.517(4)	C(10)	C(9)	C(14)	118.5(3)
C(15)	C(16)	1.554(5)	C(10)	C(9)	C(14)	118.5(3)
C(17)	C(18)	1.393(4)	C(9)	C(10)	C(11)	121.5(3)
C(17)	C(22)	1.387(4)	C(10)	C(11)	C(12)	119.9(3)
C(18)	C(19)	1.365(5)	C(11)	C(12)	C(13)	119.1(3)
C(19)	C(20)	1.374(5)	C(12)	C(13)	C(14)	121.5(3)
C(20)	C(21)	1.388(5)	C(7)	C(14)	C(13)	119.4(3)
C(21)	C(22)	1.370(5)	C(9)	C(14)	C(15)	120.4(3)
C(23)	C(24)	1.521(4)	C(13)	C(14)	C(15)	120.2(3)
C(24)	C(25)	1.495(5)	C(14)	C(15)	C(16)	113.4(3)
			C(7)	C(16)	C(15)	106.6(3)
			N(2)	C(17)	C(18)	121.3(3)
			N(2)	C(17)	C(22)	119.3(3)
			C(18)	C(17)	C(22)	119.4(3)
			C(17)	C(18)	C(19)	120.1(3)
			C(18)	C(19)	C(20)	120.7(3)
			C(19)	C(20)	C(21)	119.5(3)
			C(20)	C(21)	C(22)	120.5(3)
			C(17)	C(22)	C(21)	119.9(3)
			O(1)	C(23)	N(2)	121.6(3)
			O(1)	C(23)	C(24)	122.3(3)
			N(2)	C(23)	C(24)	116.1(3)
			C(23)	C(24)	C(25)	112.7(3)

continued

UM00013946
NOVARTIS EXHIBIT 1017
Novartis v. Regents, IPR2023-01346
Page 2692 of 4460

Table II—Continued

Atom 1	Atom 2	Distance	Atom 1	Atom 2	Atom 3	Angle
			2b			
O(1)	C(23)	1.27(1)	C(3)	N(2)	C(17)	121.0(8)
N(1)	C(1)	1.52(1)	C(3)	N(2)	C(23)	118.0(9)
N(1)	C(5)	1.46(1)	C(17)	N(2)	C(23)	121.0(9)
N(1)	C(7)	1.52(1)	C(1)	N(1)	C(5)	110.6(7)
N(2)	C(3)	1.50(1)	C(1)	N(1)	C(7)	113.5(6)
N(2)	C(17)	1.41(1)	C(5)	N(1)	C(7)	112.8(8)
N(2)	C(23)	1.30(1)	N(1)	C(1)	C(2)	112.6(7)
C(1)	C(2)	1.49(1)	C(1)	C(2)	C(3)	111.3(8)
C(2)	C(3)	1.53(1)	C(1)	C(2)	C(6)	107.9(8)
C(2)	C(6)	1.54(1)	C(3)	C(2)	C(6)	111.5(8)
C(3)	C(4)	1.54(1)	N(2)	C(3)	C(2)	110.3(8)
C(4)	C(5)	1.51(1)	N(2)	C(3)	C(4)	111.0(7)
C(7)	C(8)	1.47(1)	C(2)	C(3)	C(4)	109.6(7)
C(7)	C(16)	1.53(1)	C(3)	C(4)	C(5)	109.5(7)
C(8)	C(9)	1.57(1)	N(1)	C(5)	C(4)	111.4(9)
C(9)	C(10)	1.36(1)	N(1)	C(7)	C(8)	114.9(7)
C(9)	C(14)	1.39(1)	N(1)	C(7)	C(16)	110.7(8)
C(10)	C(11)	1.38(1)	C(8)	C(7)	C(16)	112.2(8)
C(11)	C(12)	1.39(1)	C(7)	C(8)	C(9)	110.4(8)
C(12)	C(13)	1.33(1)	C(8)	C(9)	C(10)	119.1(9)
C(13)	C(14)	1.40(1)	C(8)	C(9)	C(14)	119.3(9)
C(14)	C(15)	1.50(2)	C(10)	C(9)	C(14)	121.7(9)
C(15)	C(16)	1.56(1)	C(9)	C(10)	C(11)	122.(1)
C(17)	C(18)	1.38(1)	C(10)	C(11)	C(12)	116.(1)
C(17)	C(22)	1.34(1)	C(11)	C(12)	C(13)	122.(1)
C(18)	C(19)	1.38(1)	C(12)	C(13)	C(14)	123.(1)
C(19)	C(20)	1.39(1)	C(9)	C(14)	C(13)	115.(1)
C(20)	C(21)	1.41(1)	C(9)	C(14)	C(15)	122.6(9)
C(21)	C(22)	1.37(2)	C(13)	C(14)	C(15)	122.(1)
C(23)	C(24)	1.49(1)	C(14)	C(15)	C(16)	115.2(8)
C(24)	C(25)	1.58(2)	N(2)	C(17)	C(18)	121.(1)
			N(2)	C(17)	C(22)	118.2(9)
			C(18)	C(17)	C(22)	121.(1)
			C(17)	C(18)	C(19)	120.(1)
			C(18)	C(19)	C(20)	120.3(9)
			C(19)	C(20)	C(21)	117.(1)
			C(20)	C(21)	C(22)	122.(1)
			C(17)	C(22)	C(21)	119.5(9)
			O(1)	C(23)	N(2)	121.(1)
			O(1)	C(23)	C(24)	116.(1)
			N(2)	C(23)	C(24)	123.(1)
			C(23)	C(24)	C(25)	109.8(8)

References and Notes

1. Janssen, P. A. J.; Van der Eycken, C. A. M. in "Drugs Affecting the Central Nervous System," vol. 2; A. Burger, Ed.; Marcel Dekker: New York, 1968; chap. 2.
2. Maryanoff, B. E.; Simon, E. J.; Gioannini, T.; Gorissen, H. *J. Med. Chem.* 1982, *25*, 913.
3. Grossman, S.; Moser, U.; Mutschler, E. *Arch. Pharm. (Weinheim, Ger.)* 1978, *311*, 1010.
4. Lobbezoo, M. W.; Soudijn, W.; Van Wijngaarden, I. *Eur. J. Med. Chem.–Chim. Ther.* 1980, *15*, 357.
5. Lobbezzo, M. W.; Soudijn, W.; Van Wijngaarden, I. *J. Med. Chem.* 1981, *24*, 777.
6. Van Bever, W. F. M.; Niemegeers, C. J. E.; Janssen, P. A. J. *J. Med. Chem.* 1974, *17*, 1047.
7. Riley, T. N.; Hale, D. B.; Wilson, M. C. *J. Pharm. Sci.* 1973, *62*, 983.
8. Van Wijngaarden, I.; Soudijn, W. *Life Sci.* 1968, *7*, 1239.
9. Van Bever, W. F. M.; Neimegeers, C. J. E.; Schellekens, K. H. L.; Janssen, P. A. J. *Arzneim.–Forsch.* 1976, *26*, 1548.
10. Helsley, G. C.; Lunsford, D. C.; Welstead, W. J., Jr.; Boswell, R. F., Jr.; Funderburk, W. H.; Johnson, D. N. *J. Med. Chem.* 1969, *12*, 583.
11. Klein, W.; Back, W.; Mutschler, E. *Arch. Pharm. (Weinheim, Ger.)* 1975, *308*, 910.
12. Berger, J. G.; Davidson, F.; Langford, G. E. *J. Med. Chem.* 1977, *20*, 600.
13. Borne, R. F.; Fifer, E. K.; Waters, I. W. *J. Med. Chem.* 1984, *27*, 1271.
14. Borne, R. F.; Law, S.-J.; Kapeghian, J.; Masten, L. W. *J. Pharm. Sci.* 1980, *69*, 1104.
15. Riley, T. N.; Bagley, J. R. *J. Med. Chem.* 1979, *22*, 1167.
16. Fifer, E. K.; Davis, W. M.; Borne, R. F. *Eur. J. Med. Chem.–Chim. Ther.* in press.
17. Maryanoff, B. E.; McComsey, D. F.; Taylor, R. J., Jr.; Gardocki, J. F. *J. Med. Chem.* 1981, *24*, 79.
18. Main, P.; Woolfson, M. M.; Germain, G. *Acta Crystallogr.* 1971, *A27*, 368.
19. Conventional reliability indices $R = \Sigma||F_o| - |F_c||/\Sigma|F_o|$, $R_w = (\Sigma(|F_o| - |F_c|)^2/\Sigma w|F_o|^2)^{1/2}$, where F_o and F_c are observed and calculated structure factors, $w = 1/\sigma(F)^2$, and where $\sigma(F)$ is the estimated SD in F_o.
20. CAD-4 SDP package of computer programs written by B. Frenz (1982).
21. "International Tables for X-Ray Crystallography," vol. 4; Birmingham, England: Kynoch Press, 1974.
22. Observed and calculated structure factors, fractional coordinates for hydrogen atoms, and anistropic thermal parameters have been deposited with the British Lending Division. Copies may be obtained through The Executive Secretary, International Union of Crystallography, 13 White Friar, Chester Ch1 INZ, England.
23. Feinberg, A. P.; Creese, I.; Snyder, S. H. *Proc. Natl. Acad. Sci. U.S.A.* 1976, *73*, 4215.
24. D. Duchamp, the UpJohn Company, provided fractional coordinates of fentanyl citrate.
25. Koch, M. H. J.; DeRanter, C. J.; Rolies, M.; Dideberg, O. *Acta Crystallogr.* 1976, *B32*, 2529.

Acknowledgments

Partial support of this research by the National Institutes of Health (NS19789) is gratefully acknowledged. The authors would like to thank Dr. Dave Duchamp for providing fractional coordinates of fentanyl citrate prior to publication and Cathy Gatchell for recrystallizing the samples.

UM00013947
NOVARTIS EXHIBIT 1017
Novartis v. Regents, IPR2023-01346
Page 2693 of 4460

This Page is Inserted by IFW Indexing and Scanning Operations and is not part of the Official Record

BEST AVAILABLE IMAGES

Defective images within this document are accurate representations of the original documents submitted by the applicant.

Defects in the images include but are not limited to the items checked:

- ☐ BLACK BORDERS
- ☐ IMAGE CUT OFF AT TOP, BOTTOM OR SIDES
- ☐ FADED TEXT OR DRAWING
- ☐ BLURRED OR ILLEGIBLE TEXT OR DRAWING
- ☐ SKEWED/SLANTED IMAGES
- ☐ COLOR OR BLACK AND WHITE PHOTOGRAPHS
- ☐ GRAY SCALE DOCUMENTS
- ☐ LINES OR MARKS ON ORIGINAL DOCUMENT
- ☐ REFERENCE(S) OR EXHIBIT(S) SUBMITTED ARE POOR QUALITY
- ☐ OTHER: _____

IMAGES ARE BEST AVAILABLE COPY.
As rescanning these documents will not correct the image problems checked, please do not report these problems to the IFW Image Problem Mailbox.

Photoreactivities of two kinds of bimolecular crystals formed from acridine and phenothiazine

Hideko Koshima,*[a,b] Yang Wang,[a] Teruo Matsuura,[a] Ikuko Miyahara,[c] Hisashi Mizutani,[c] Ken Hirotsu,[c] Tsuyoshi Asahi[d] and Hiroshi Masuhara[d]

[a] *Department of Materials Chemistry, Faculty of Science and Technology, Ryukoku University, Seta, Otsu 520-21, Japan*
[b] *PRESTO, Japan Science and Technology Corporation, Ryukoku University, Seta, Otsu 520-21, Japan*
[c] *Department of Chemistry, Faculty of Science, Osaka City University, Sugimoto, Sumiyoshi, Osaka 558, Japan*
[d] *Department of Applied Physics, Osaka University, Suita, Osaka 565, Japan*

A yellow crystal 3 and a red crystal 4 simultaneously crystallize from a solution of acridine 1 and phenothiazine 2 in acetonitrile. Similar N···H–N hydrogen bonding pairs of 1 and 2 are formed in the two crystals. The 3:4 crystal 3 has a slightly uncommon molecular arrangement of which four acridine molecules out of twelve are disordered in the unit cell. The 1:1 crystal 4 has a more rigid packing of the hydrogen bonding pairs. Irradiation of 3 gives a photoadduct 5 as the sole product, whereas 4 shows almost no photoreactivity. The occurrence of photoinduced electron transfer has been confirmed by the measurement of transient absorption spectra of the crystals 3 and 4. However, the two-stage decay of the transient absorption of 3 with lifetimes of 2 and 50 ps is different from that of 4 with a single short lifetime of 2 ps. Upon irradiating 3, electron transfer, proton transfer and subsequent radical coupling occur over the shortest distance of 4.1 Å between the preradical carbon and nitrogen atoms in the crystal lattice followed by dehydrogenation to afford the product 5. In the case of the red crystal 4, the radical coupling is difficult because of the longer coupling distance of 5.6 Å and the more restricted movement in the rigid crystal lattice. The results indicate that the observed photochemical behaviour of 3 and 4 are controlled by the molecular arrangement in the crystal lattice.

Since the discovery of topochemical [2 + 2] photocycloadditions by Cohen and Schmidt,[1] a large number of solid state photoreactions of one-component molecular crystals have been reported. However, the reaction types were almost always limited to [2 + 2] cycloadditions and some intramolecular reactions, such as hydrogen abstraction, and so have not extended the scope of solid state organic photochemistry.[2,3] Recently, we have studied the photochemistry of two-component molecular crystals prepared by the self-assembly of different organic molecules[4] and developed several bimolecular reactions that occur in the crystal lattice.[5–9] An important advantage to utilizing a bimolecular crystal as a reaction medium is that induction of reactivity is possible *via* photoinduced electron transfer (PET) by combining an electron donor and acceptor species. Although a large number of PET reactions are already known in solution photochemistry, the product selectivities are low due to the high mobility of radical species in the solutions.[10] In contrast, solid state PET reaction can give high product selectivity due to the quite low mobility in the crystal lattice, as in photodecarboxylation of bimolecular crystals of indole-3-acetic acid and phenanthridine, for example.[6] The occurrence of a stereospecific reaction ultimately results in the success of absolute asymmetric synthesis.[9,11,12] Namely, solid state bimolecular photoreactivity depends not only on the nature of component molecules but also on the crystal structure.

Here, we report an interesting case of two kinds of bimolecular crystals 3 (yellow) and 4 (red) that are formed simultaneously from solutions of acridine 1 and phenothiazine 2. Irradiation of 3 causes photoaddition, while 4 has almost no photoreactivity. Further, we describe the first evidence for the occurrence of solid state PET by the successful measurement of transient absorption spectra in femtosecond diffuse reflectance spectroscopy.[13,14] The correlation between the molecular arrangement and photoreactivity of the two crystals is discussed.

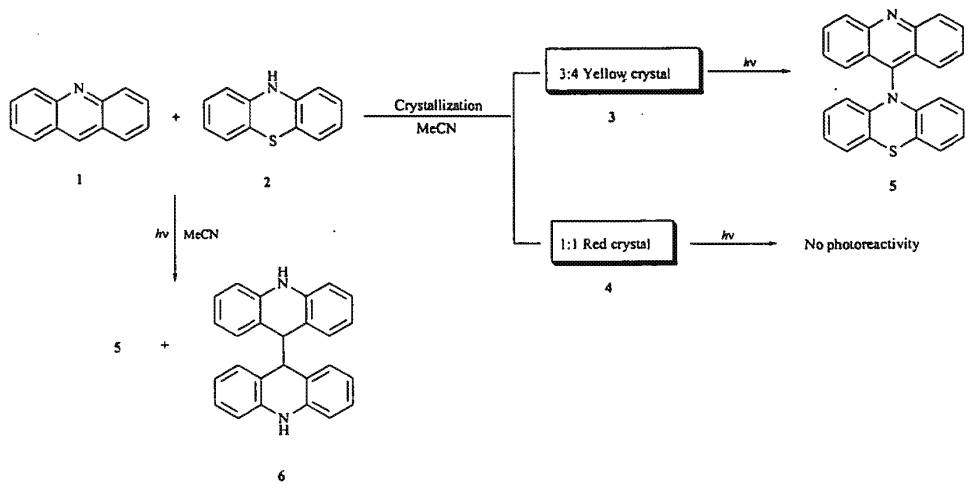
Results and discussion

Crystal structure

The 3:4 yellow crystal 3 and the 1:1 red crystal 4 are simultaneously crystallized from an equimolar solution of acridine 1 and phenothiazine 2 in acetonitrile. By seeding the desired crystals they can be prepared on a large scale. The ground-state absorption spectra of the microcrystals 3 and 4 were measured by a reflection method using $MgSO_4$ as a standard (Fig. 1). Although the yellow and red colours of the single crystals are visually very different, the two spectra seem to be quite similar at longer wavelengths. The melting point of 3 is 134 °C, falling between those of 1 (107 °C) and 2 (185 °C). The red colour of 4 changes to yellow at around 90 °C, which is a transition point, and the crystal melts at 134 °C, corresponding to the two endothermic peaks in DSC measurements. The powder X-ray diffraction (PXD) pattern of 3 is almost the same as that of 1:1 melting-resolidifying mixture of 1 and 2. When 4 was submitted to melting-resolidifying manipulation, the PXD pattern changed to be almost concordant with that of the 1:1 melting-resolidifying mixture of 1 and 2. It indicated that 4 can form only by crystallization from solution. The simultaneous crystallization of 3 and 4 from solution suggests that the difference in their formation energies is small; thermodynamics studies are under way.

Table 1 shows the X-ray crystal structure data for crystals 3 and 4 and product 5. It should be noted that crystals 3 and 4 have centrosymmetric space groups, $C2/c$ and $P2_1/c$, respectively, while phenothiazine crystal is known to have an enantiomorphous space group $P2_1$.[15] Crystalline 3 has a relatively

UM00013949
NOVARTIS EXHIBIT 1017
Novartis v. Regents, IPR2023-01346
Page 2695 of 4460



Scheme 1

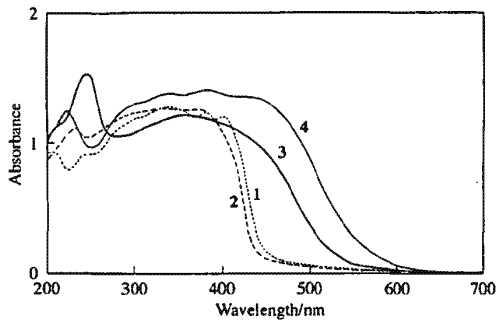


Fig. 1 Ground-state absorption spectra of **3** and **4** and components **1** and **2**

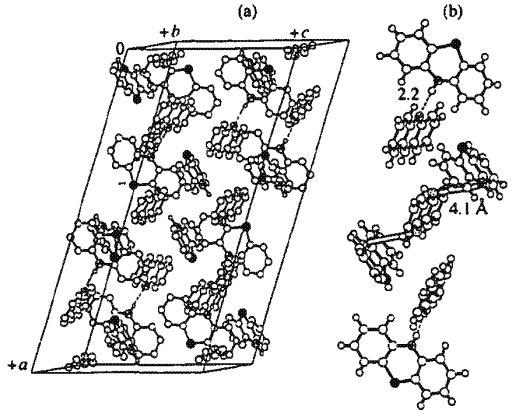


Fig. 2 (*a*) Molecular packing and (*b*) the radical coupling path in **3**. In (*a*), the hydrogens are omitted except for the NH hydrogens for clarity. Sulfur (●) and nitrogen ⊕. Dotted atoms in the disordered acridine molecules represent the coexistence of carbon and nitrogen atoms with occupancies of about 50%.

uncommon molecular arrangement in which twelve and sixteen molecules of **1** and **2**, respectively, are packed in the unit cell (Fig. 2). The molecular shape of **1** is almost flat, but that of **2** is butterfly-like due to the longer S–C bond (1.8 Å) than C–N and C–C bonds (1.4 Å). Molecular pairs of **1** and **2** are formed through N···H–N hydrogen bonding with H···N distance of 2.15 Å; the dihedral angle between the plane of **1** and the central C–C–C–C plane of **2** is 86.58°, *i.e.* almost perpendicular. The eight molecular pairs of **1** and **2** are packed head-to-tail with a distance of 6.4 Å between the two acridine planes in the crystal lattice. The eight molecules of each of **1** and **2** are arranged almost parallel to the *ab* face and the *ac* face, respectively. The residual four acridine molecules out of twelve are disordered, in which N and C atoms coexist at about 50% occupancy (Fig. 2). The four disordered acridine molecules and the residual eight phenothiazine molecules do not form hydrogen bonds in the unit cell. The disordered acridine is placed between the two phenothiazine molecules at a dihedral angle of 58.2°. Further, the acridine molecules with and without hydrogen bonds are arranged almost parallel to each other (dihedral angle 5.15°). On the other hand, the phenothiazine molecules with and without hydrogen bonds are almost perpendicular (dihedral angle 89.38°). The IR absorption band of **3** at 3342 cm^{-1} corresponds to the molecules of **2** with no hydrogen bonds in **3** in good accordance with the NH band of the crystal **2**. The bands at 3391, 3237 and 3164 cm^{-1} correspond to the N···H–N hydrogen bonds of **1** and **2**.

In crystalline **4**, similar hydrogen bonding pairs are formed with an H···N distance of 2.19 Å; the dihedral angle between the plane of **1** and the central C–C–C–C plane of **2** is 85.73° (Fig. 3). The IR absorption bands of **4** at 3395, 3240 and 3179 cm^{-1} correspond to the N···H–N hydrogen bonding, but are slightly shorter than those of **3**. Four molecular pairs exist in the unit cell. The molecular pairs are arranged head-to-tail to form two independent stacking columns (A) and (B) with plane distances of 3.9 and 8.9 Å between the two acridine molecules in the crystal lattice. The phenothiazine molecules in column (A) are arranged almost perpendicular to the acridine planes in the next stacking column (B) with the shortest distance of 2.9 Å between the aromatic H atom of **2** and the acridine plane. Such rigid molecular packing is a feature of crystal **4**.

Photoreactions

Crystals were pulverized and irradiated with a 400 W high-pressure mercury lamp through Pyrex glass (>290 nm transparent) under argon. Scheme 1 and Table 2 show the results together with the solution photoreaction. Irradiation of **3** caused an addition reaction to give photoadduct **5** in low yield as the sole product. The molecular structure of **5** was confirmed

UM00013950
NOVARTIS EXHIBIT 1017
Novartis v. Regents, IPR2023-01346
Page 2696 of 4460

Table 1 X-Ray crystallographic data for the bimolecular crystals and the product

	Yellow crystal 3	Red crystal 4	Product 5
Formula	$C_{37}H_{33}N_7S_4$	$C_{25}H_{18}N_2S$	$C_{25}H_{16}N_2S$
M_w	1334.74	378.49	376.47
Crystal system	Monoclinic	Monoclinic	Monoclinic
Space group	*C2/c*	$P2_1/c$	$P2_1/n$
Z	4	4	4
Cell constants			
a/Å	30.194(3)	13.121(2)	8.460(8)
b/Å	14.686(3)	9.126(3)	9.870(2)
c/Å	15.996(3)	17.318(2)	22.633(7)
β/°	107.930(9)	110.83(1)	99.39(6)
V/Å^3	6748(1)	1938.1(8)	1864(2)
D_c/g cm^{-3}	1.314	1.297	1.341
μ/cm^{-1}	17.16	1.79	1.86
Radiation	Cu-Kα	Mo-Kα	Mo-Kα
$2\theta_{max}$/°	120.3	50.0	50.0
Scan mode	$\omega - 2\theta$	$\omega - 2\theta$	$\omega - 2\theta$
No. of reflections measured	5367	3809	3745
No. of unique reflections	5252	3642	3493
No. with $I > 3.00\sigma(I)$	4540	2583	1006
No. of variables	566	257	254
R (%)	8.9	5.6	5.6
R_w (%)	8.0	8.0	7.5

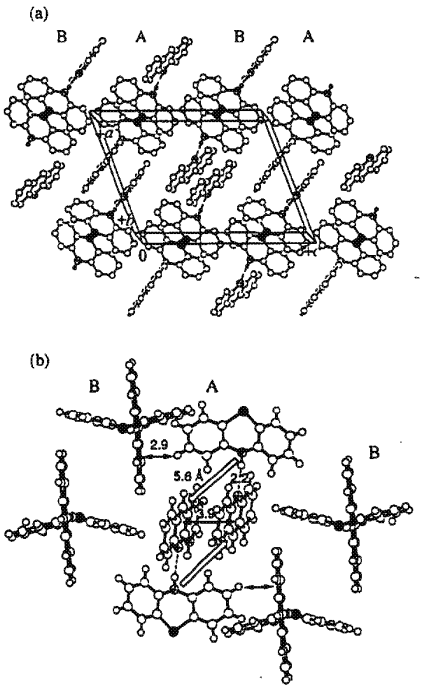


Fig. 3 (*a*) Molecular packing and (*b*) the radical coupling path in **4**. In (*a*), the hydrogens are omitted except for the NH hydrogens for clarity. Sulfur (●) and nitrogen ⊕. (A) and (B) are the independent molecular stacking columns.

by X-ray structure analysis (Fig. 4). However, **4** showed much lower photoreactivity and afforded no isolated product. The difference in photoreactivities between **3** and **4** can be attributed to the difference in crystal structures because both crystals consist of the same components **1** and **2**. For a comparison, irradiation of a solution of **1** and **2** in acetonitrile produced **5** and biacridine **6** in 64 and 35% yield, respectively.

The transient absorption spectra of the yellow microcrystals **3** are shown in Fig. 5. The absorption bands with maximum wavelengths at around 600 and 520 nm were observed immedi-

Table 2 Photoreaction of acridine and phenothiazine in bimolecular crystals and in solution

State on irradiation	Conversion (%)		Yield[a] (%)	
	1	2	5	6
Yellow crystal **3**	8	15	14	0
Red crystal **4**	3	7	0	0
MeCN soln	16	50	64	35

[a] Yield based on consumed **1**.

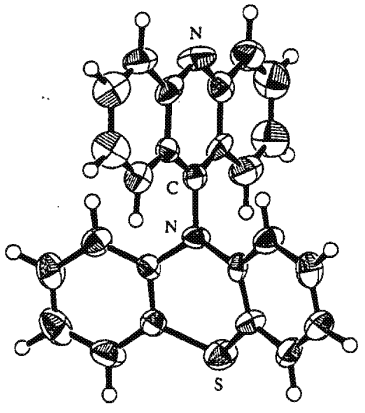


Fig. 4 Molecular structure of product **5**

ately after excitation with a 390 nm laser pulse. They could be assigned to the absorption spectrum of acridine anion radical and that of the phenothiazine cation radical, respectively, on the basis of the similarity to those in solution.[16] This result provides direct evidence for the generation of ionic species in a photoreactive two-component crystal. The decay of transient absorption in Fig. 6 shows non-exponential behaviour, and it can be approximated to by a double-exponential function with lifetimes of 2 and about 50 ps. Since almost the same decay was observed even at a half the excitation intensity, the observed decay may be mainly ascribed to geminate recombination of charge-separated species but not bulk recombination of them. Most probably it reflects the uncommon molecular arrangement in the crystal lattice of **3**, for instance disordered

UM00013951
NOVARTIS EXHIBIT 1017
Novartis v. Regents, IPR2023-01346
Page 2697 of 4460

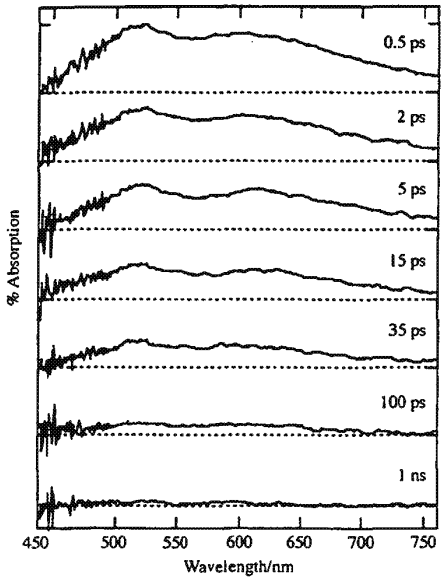


Fig. 5 Transient absorption spectra of **3** excited at 390 nm

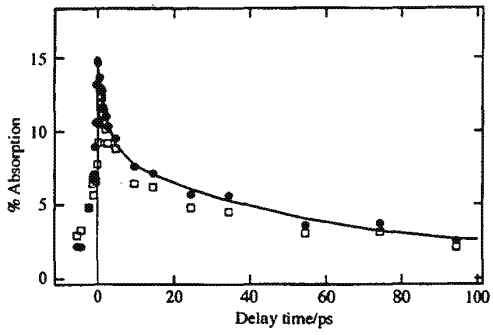
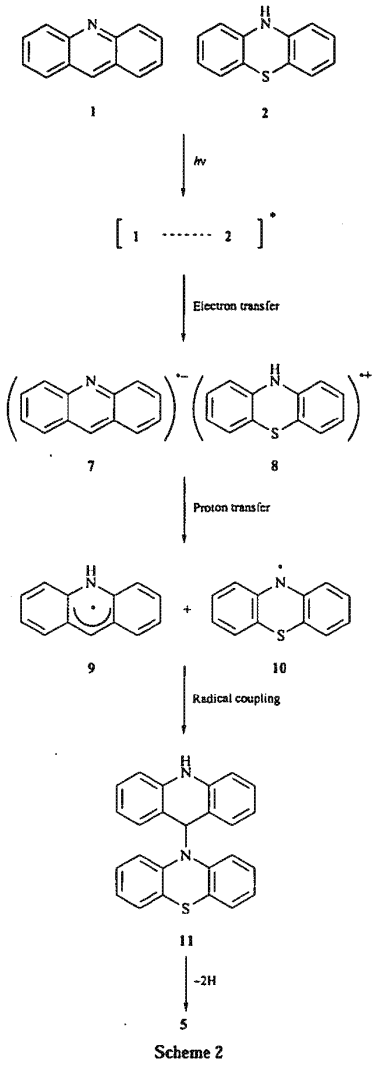


Fig. 6 Observed time profiles of the transient absorption of **3**. Probe wavelengths are at 524 nm (●) and 613 nm (□). Solid lines are calculated curves by eqn. (2) in ref. 14: $n(t) = 5.8\exp(-t/2.5\ \text{ps}) + 7.5\exp(-t/50\ \text{ps}) + 1.4$.



Scheme 2

acridine molecules and the coexistence of hydrogen bonding and non-hydrogen bonding pairs.

In the case of red microcrystals of **4**, similar transient absorption spectra to those of the yellow crystals were observed, but the decay was approximated to by a single exponential decay with a lifetime of about 2 ps and no transient absorption was observed after several tens of picoseconds. The fast decay components observed for the two crystals are probably due to the charge-transfer (CT) excited state of the hydrogen bonding pair. Compared with the CT excited state of some typical crystals of weak CT complexes,[14] this lifetime is very short. It is suggested that hydrogen-bonding is the key role in the ultrafast deactivation of the excited state. The details of the dynamics and the mechanisms will be discussed elsewhere. On the other hand, a slow deactivation observed only for the yellow crystals corresponds to a charge separated species formed between the non-hydrogen bonding pairs. If we consider that a part of them results in the formation of photoproduct **5** then the above results for transient absorption measurements are quite consistent with the different photoreactivities of the yellow and red crystals.

Scheme 2 shows the possible reaction mechanism based on the transient absorption spectra and the photoproduct **5**. Upon irradiation, PET from **2** to **1** occurs to give the acridine anion radical **7** and the phenothiazine cation radical **8**. Then proton transfer produces the hydroacridine radical **9** and the dehydrophenothiazine radical species **10**. In the case of the crystalline **3** [Fig. 2(*b*)], radical coupling between **9** and **10**, which originates from the disordered acridine and non-hydrogen bonding phenothiazine, can occur over the shortest distance of 4.14 Å most effectively and is followed by dehydrogenation to give product **5**. Occurrence of radical coupling between the hydrogen bonding pair is difficult because a half rotation of **9** is needed in the crystal lattice. The low yield of **5** (Table 2) is most probably due to the existence of only four disordered acridine molecules out of twelve in the unit cell.

On the other hand, the lack of production of **5** on irradiation of **4** should be attributed not only to the short lifetimes of the radical species but also to the molecular arrangement in the crystal lattice. The distance of 5.58 Å for the radical coupling of **9** and **10** in Fig. 3(*b*) can be said to be short enough for radical coupling because an even longer distance of 6.8 Å causes

UM00013952
NOVARTIS EXHIBIT 1017
Novartis v. Regents, IPR2023-01346
Page 2698 of 4460

radical coupling in other bimolecular crystals.[9] Steric hindrance may also be a reason for the non-occurrence of radical coupling. In Fig. 3(*a*), the plane distance between two acridine molecules in column (A) is 3.9 Å. On the other hand, the phenothiazine molecule of the stacking column (A) is close to the acridine molecule of the next stacking column (B) with the shortest distance (2.9 Å) between the H atom of phenothiazine and the acridine plane. Therefore, radical **10** cannot move to radical **9** in the crystal lattice. Such a rigid molecular packing arrangement leads to no production of **5**. The reason for the lower conversion of **1** compared to **2** is the regeneration of **1** by dehydrogenation of the radical **9** (Table 2).

Conclusions

Spontaneous crystallization of two kinds of bimolecular crystals occurs from the acetonitrile solution of acridine phenothiazine. Irradiation of **3** gives the photoadduct **5** as the sole product. On the other hand, **4** has a much lower photoreactivity. Transient absorption spectra of the microcrystals could be measured by femtosecond diffuse reflectance spectroscopy and provide the first evidence for a photoinduced electron transfer reaction in a bimolecular crystal. The difference in reactivities between the two crystals could be explained by their molecular arrangements in the crystal lattice.

Experimental

Instrumentation

^{1}H NMR spectra were measured on a 60 MHz JEOL spectrometer with tetramethylsilane as an internal standard. IR spectra were recorded on a JASCO FTIR-8300 spectrophotometer. UV spectra were measured on Shimadzu UV-3100 and MPS 2000 spectrophotometers. Powder X-ray diffractograms (PXD) were taken on a Rigaku Geigerflex by using Cu-target X-ray tube equipped with a RAD-C system. Differential scanning calorimetry (DSC) was done on a Rigaku Thermoflex TAS-200 DSC8230D and melting points were uncorrected. Elemental analysis was carried out with a Yanaco CHN Corder MT-5. HPLC with a photodiode-array detector was used to determine the products on a Waters HPLC system.

Preparation of bimolecular crystals 3 and 4

Acridine **1** (GR grade, Tokyo Kasei) was recrystallized from ethanol. Phenothiazine **2** (GR grade, Tokyo Kasei) was used as received. Yellow crystals of **3** and red crystals of **4** were prepared by slow evaporation of a 1:1 solution of **1** and **2** in acetonitrile at room temp. by seeding.

Crystals of **3**; mp 133–135 °C [Found: C, 79.74; H, 5.05; N, 7.39. Calc. for $C_{87}H_{63}N_7S_4$ (3:4): C, 78.29; H, 4.76; N, 7.35%]; ν_{max}(KBr)/cm^{-1} 3342 (NH of **2**), 3391, 3237 and 3164 (N···HN); λ(solid state)/nm 190–550.

Crystals of **4**; transition point about 90 °C; mp 133–135 °C [Found: C, 79.30; H, 4.93; N, 7.42. Calc. for $C_{25}H_{18}N_2S_1$ (1:1): C, 79.34; H, 4.79; N, 7.40%]; ν_{max}(KBr)/cm^{-1} 3395, 3240 and 3179 (N···HN); λ(solid state)/nm 190–600.

Preparative photoreaction of 1 and 2 in MeCN

A solution containing **1** (0.895 g, 5 mmol) and **2** (0.996 g, 5 mmol) in acetonitrile (100 cm^3) was irradiated internally with a 100 W high-pressure mercury lamp under argon for 45 h at room temp. followed by filtration to give biacridane **6** (0.052 g, 5.6%) as a solid, mp 211–212 °C (from tetrahydrofuran) (Found: C, 86.76; H, 5.76; N, 7.85. Calc. for $C_{26}H_{20}N_2$: C, 86.64; H, 5.59; N, 7.77%); ν_{max}(KBr)/cm^{-1} 3370 (NH), consistent with an authentic sample. After evaporation of the filtrate, the residue was chromatographed using a silica gel plate (5% ethyl acetate–hexane) to give the condensation product **5** (0.195 g, 10.3%), mp 289–291 °C (from MeCN) (Found: C, 79.80, H, 4.41; N, 7.46. Calc. for $C_{25}H_{16}N_2S$: C, 79.76; H, 4.28; N, 7.44%); ν_{max}(KBr)/cm^{-1} no NH; δ_H(60 MHz, [$^2H_8$]THF) 5.82–5.67 (2H, m, Ph), 7.14–6.44 (6H, m, Ph), 7.96–7.41 (4H, m, Ph) and 8.39–8.20 (4H, m, Ph); λ_{max}/nm (10% THF in MeCN) 384 (log ε, 3.79), 362 (4.11), 345 (3.97) and 252 (5.16). The molecular structure was confirmed by X-ray crystallographic analysis (Fig. 4).

Solid-state photoreaction of 3 and 4

Crystals of **3** and **4** (20 mg) were pulverized in a mortar and placed between two Pyrex glass plates and irradiated with a 400 W high-pressure mercury lamp (>290 nm irradiation) under argon at 15 °C for 24 h followed by HPLC analysis using a C_{18} column (methanol–water). The results are shown in Scheme 1 and Table 2.

X-Ray crystallography

Experimental details of the structure determination of **3**, **4** and **5** are presented in Table 1. Data collections were performed on a Rigaku AFC7R automatic four-circle X-ray diffractometer with graphite monochromated Cu-Kα (λ = 1.541 78 Å) Mo-Kα (λ = 0.710 69 Å) radiation and a rotating anode.† The structure was solved by direct method (SHELXS-86) and refined by full-matrix least squares analysis. The non-hydrogen atoms were refined anisotropically. All the calculations were carried out on the teXsan crystallographic software package from Molecular Structure Corporation.

Measurement of transient absorption spectra

The details of a femtosecond diffuse reflectance spectroscopic system have been reported.[13] Briefly, an excitation light source consisting of a continuous wave self-mode-locked Ti:sapphire laser (Mira 900 Basic, Coherent), pumped by an Ar$^+$ laser (Innova 310, Coherent), and a Ti:sapphire regenerative amplifier system (TR70, Continuum) with a Q-switched regenerative amplifier (780 nm, 3–4 mJ/pulse, 170 fs fwhm, 10 Hz) was frequency doubled (390 nm) and used as an excitation light source. The residual of the fundamental output was focused into a quartz cell (1 cm path length) containing H_2O to generate a white-light continuum as a probe beam.

Acknowledgements

This work was partly supported by a Grant-in-Aid for scientific research from the Ministry of Education, Science, Sports and Culture, Japan. Y. W. is a guest researcher from Zhengzhou University, China.

† Atomic co-ordinates, thermal parameters, and bond lengths and angles have been deposited at the Cambridge Crystallographic Data Centre (CCDC). See 'Instructions for Authors', *J. Chem. Soc., Perkin Trans. 2*, 1997, Issue 1. Any request to the CCDC for this material should quote the full literature citation and the reference number 188/87.

References

1 M. D. Cohen and G. M. Schmidt, *J. Chem. Soc.*, 1964, 1996.
2 *Reactivity in Molecular Crystals*, ed. Y. Ohashi, VCH, Weinheim, 1993.
3 *Organic Solid State Chemistry*, ed. G. R. Desiraju, Elsevier, Amsterdam, 1987.
4 H. Koshima and T. Masuura, *Kokagaku*, 1995, **19**, 10.
5 H. Koshima, Y. Chisaka, Y. Wang, X. Yao, H. Wang, R. Wang, A. Maeda and T. Matsuura, *Tetrahedron*, 1994, **50**, 13 617.
6 H. Koshima, K. Ding and T. Matsuura, *J. Chem. Soc., Chem. Commun.*, 1994, 2053.
7 H. Koshima, K. Ding, Y. Chisaka and T. Matsuura, *Tetrahedron Asymmetry*, 1995, **6**, 101.
8 H. Koshima, K. Ding, Y. Chisaka, T. Matsuura, Y. Ohashi and M. Mukasa, *J. Org. Chem.*, 1996, **61**, 2352.
9 H. Koshima, K. Ding, Y. Chisaka and T. Matsuura, *J. Am. Chem. Soc.*, 1996, **18**, 12 059.

UM00013953
NOVARTIS EXHIBIT 1017
Novartis v. Regents, IPR2023-01346
Page 2699 of 4460

10 *Photoinduced Electron Transfer, Part C*, ed. M. A. Fox and M. Chanon, Elsevier, Amsterdam, 1988.
11 J. A. Elgavi, B. S. Green and G. M. J. Schmidt, *J. Am. Chem. Soc.*, 1973, **95**, 2058.
12 T. Suzuki, T. Fukushima, Y. Yamashita and T. Miyashi, *J. Am. Chem. Soc.*, 1994, **116**, 2793.
13 T. Asahi, Y. Matsuo and H. Masuhara, *Chem. Phys. Lett.*, 1996, **256**, 525.
14 T. Asahi, Y. Matsuo, H. Masuhara and H. Koshima, *J. Phys. Chem.*, 1997, **101**, 612.
15 J. D. Bell, J. F. Blout, O. V. Briscoe and H. C. Freeman, *Chem. Commun.*, 1968, 1656.
16 T. Shida, in *Electronic Spectra of Radical Ions*, Elsevier, Amsterdam, 1988.

Paper 7/01221G
Received 21*st February* 1997
Accepted 21*st May* 1997

UM00013954
NOVARTIS EXHIBIT 1017
Novartis v. Regents, IPR2023-01346
Page 2700 of 4460

CRYSTAL GROWTH & DESIGN
2001
VOL. 1, NO. 5
355–357

Polymorphs of a Cocrystal with Achiral and Chiral Structures Prepared by Pseudoseeding: Tryptamine/Hydrocinnamic Acid

Hideko Koshima* and Masashi Miyauchi

Department of Applied Chemistry, Faculty of Engineering, Ehime University, Matsuyama 790-8577, Japan

Received April 12, 2001; Revised Manuscript Received July 5, 2001

ABSTRACT: Helical-type of chiral cocrystal of tryptamine and hydrocinnamic acid was prepared by crystallization in the presence of different chiral crystals having similar crystal structures, despite spontaneous crystallization itself giving only achiral crystal.

Chiral crystals formed from achiral molecules are utilized as reactants for absolute asymmetric synthesis by means of solid-state reactions.[1–3] Such chiral crystals are also important for the development of new functional materials such as those used in nonlinear optics.[4] Although chiral crystallization of achiral molecules occurs statistically with a low probability of around 5%,[5–7] we have already succeeded in preparing various chiral two-component crystals through self-assembly of flexible molecules.[3,8,9] In particular, a series of helical-type crystals formed from tryptamine and achiral carboxylic acids were obtained with a probability of around 50%.[9] Furthermore, their enantiomorphous control could be achieved by "pseudoseeding" based on utilizing these various helical-type crystals as seeds for each other.[10,11] This was significant because chiral crystallization of achiral molecules by itself always gives both enantiomorphous (left and right) crystals. Polymorphism, whereby a compound can crystallize in more than one different crystal structure, often occurs for organic molecules. However, it is sometimes difficult to obtain all such possible polymorphs due to the different crystallization variables required. Herein, we found that pseudoseeding could be successfully utilized to prepare chiral crystals, which is one of the polymorph forms, despite achiral crystals being usually formed by spontaneous crystallization.

Crystals incorporating tryptamine (**1**) and hydrocinnamic acid (3-phenylpropionic acid) (**2**) were first prepared by spontaneous crystallization from a solution of both components in methanol (Chart 1). Achiral crystals **1·2A** in space group $P2_1/n$ were the product obtained (Table 1). Our previous success in helicity control of a series of helical-type crystals by pseudoseeding[10,11] reminded us that this method might be applicable in producing the chiral crystals **1·2C**, if these exist as one of the stable polymorphs.

Chiral crystal **1·3**[11] formed from **1** and *trans*-cinnamic acid (**3**) was selected from a series of available helical-type crystals as a pseudo-seed crystal, because the molecular structures of **2** and **3** are similar (Chart 1). The space group of **1·3** belongs to $P2_12_12_1$, and the absolute structures of *P*-**1·3** (clockwise helix) and *M*-**1·3** (counterclockwise helix) are also known.[11]

Chart 1

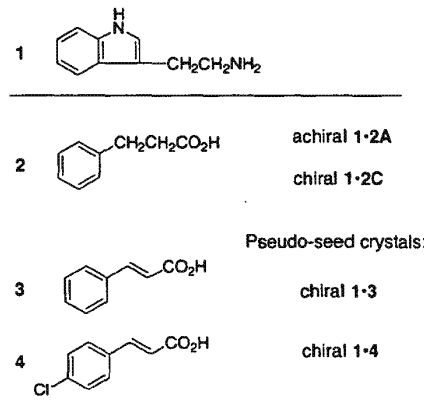


Table 1. Crystal Data for Achiral 1·2A and Chiral 1·2C of the Tryptamine/Hydrocinnamic Acid Cocrystal

	1·2A	1·2C
cryst syst	monoclinic	orthorhombic
cryst size/mm	0.3 × 0.4 × 0.2	0.3 × 0.1 × 0.03
temp/K	293	293
a/Å	15.658(5)	9.616(2)
b/Å	6.599(1)	26.251(8)
d/Å	16.411(2)	6.816(1)
space group	$P2_1/n$	$P2_12_12_1$
cell vol/Å^3	1679.1(7)	1720.6(7)
calcd density/g cm^{-3}	1.228	1.198
Z	4	4
data/params	2547/221	1516/209
R	0.045	0.130
R_w	0.062	0.103

A piece of a small single crystal of *P*-**1·3** was added to a slightly supersaturated solution of **1** and **2** in methanol and acetonitrile (1:1). The covered vessel was allowed to stand at room temperature, and fine needle crystals formed in a radial manner on the surface of the pseudo-seed crystal. These crystals were collected to afford around 10% yield, of which the amount of seed crystal was less than 0.1%. Next, measurement of solid-state CD spectra as Nujol mulls gave curve a in Figure 1, showing the formation of one-handed crystals of **1·2C** which are most probably the *P*-form on the analogy of successful enantiocontrol by pseudoseeding.[10,11] Conversely, seeding using *M*-**1·3** in the same solution gave opposite handed crystals, most probably *M*-**1·2C**, cor-

* To whom correspondence should be addressed. Fax: +81-89-927-8523. E-mail: koshima@en3.ehime-u.ac.jp.

10.1021/cg0155189 CCC: $20.00 © 2001 American Chemical Society
Published on Web 08/14/2001

UM00013955
NOVARTIS EXHIBIT 1017
Novartis v. Regents, IPR2023-01346

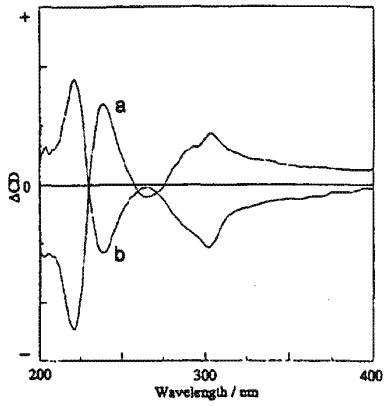


Figure 1. Solid-state CD spectra of (a) *P*-**1**·**2C** and (b) *M*-**1**·**2C**.

responding to the CD curve b with a mirror image relationship to the curve a. The X-ray crystallographic analysis of **1**·**2C** confirmed its chiral nature, the space group being the same $P2_12_12_1$ (Table 1) as that of seed crystal **1**·**3**, but with different unit cell dimensions from those of **1**·**3** (a = 9.681(3) Å, b = 29.00(1) Å, c = 5.931(4) Å). Thus, the effectiveness of pseudoseeding was confirmed for the chiralilty induction as well as the enantiocontrol. In addition, the chiral crystal **1**·**4**[11] formed from **1** and 4-chlorocinnamic acid (**4**) (Chart 1) also acts as a seed crystal for the formation of **1**·**2C**.

The melting point of **1**·**2A** (146−148 °C) is slightly lower than **1**·**2C** (150−152 °C), but its density (1.228 g cm^{-3}) is slightly larger than that of **1**·**2C** (1.198 g cm^{-3}). The IR (KBr) absorptions are similar: 3226, 2446−3058 (broad), and 1537 cm^{-1} for **1**·**2A** and 3219, 2456−3059 (broad), and 1536 cm^{-1} for **1**·**2C**. These small differences in physical properties suggest the similarity of the molecular arrangements in the lattices of both crystals. In fact, $NH_3^+\cdots CO_2^-$ quaternary ammonium salt bridge and In-NH···O−C hydrogen bonding are commonly formed between the molecules of **1** and **2**, both of which distances obtained from the X-ray crystallographic analyses are very similar. The $NH_3^+\cdots CO_2^-$ distances are 1.86, 1.86, and 2.01 Å in **1**·**2A** and 1.88, 1.89, 1.98 Å in **1**·**2C**, and the In-NH···O−C distances are 1.92 Å in **1**·**2A** and 1.95 Å in **1**·**2C**.

In the lattice of achiral **1**·**2A**, a symmetrical molecular unit is formed between the two molecules of each component through the two kinds of intermolecular bonding (Figure 2a). The two pairs of symmetrical units are centrosymmetrically arranged in the unit cell (Z = 4). On the other hand, a 2-fold helix is formed in chiral **1**·**2C** between the two components through the two types of intermolecular bonding (Figure 2b), and it is the existence of two pairs of unidirectional helices in the unit cell that induces the crystal chirality of **1**·**2C**.

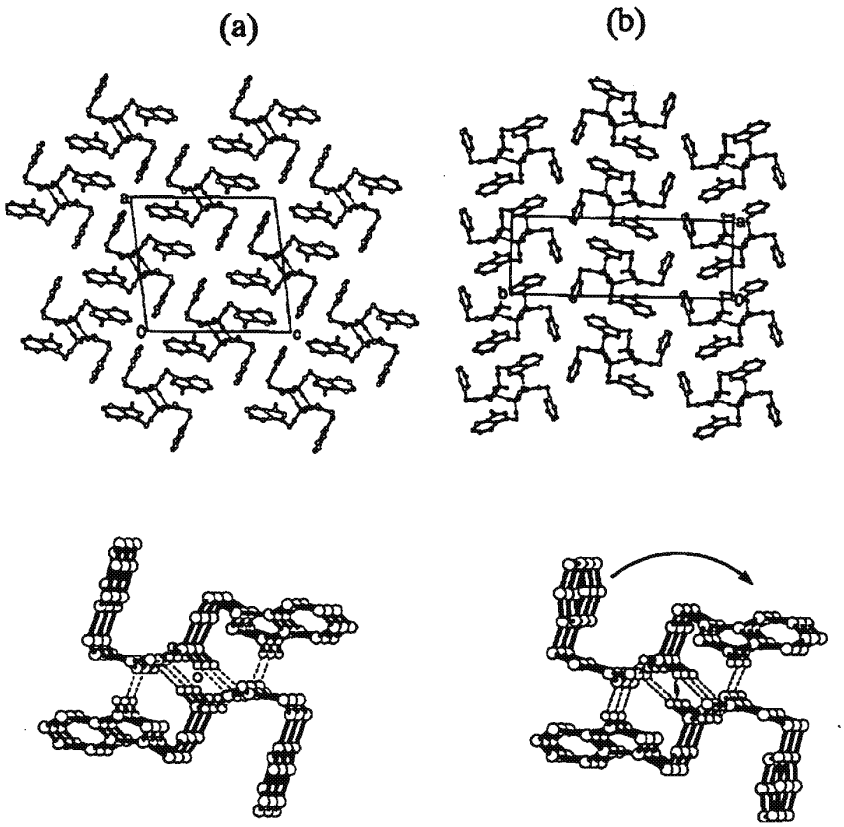


Figure 2. Molecular arrangements of (a) symmetrical unit in the achiral crystal **1**·**2A** and (b) clockwise 2-fold helix in the chiral crystal *P*-**1**·**2C**.

UM00013956
NOVARTIS EXHIBIT 1017
Novartis v. Regents, IPR2023-01346
Page 2702 of 4460

The InC−C−C−N torsion angles (62.2° and 63.1°) of the tryptamine aminoethyl group as well as the dihedral angles (86.7° and 96.8°) of the indole plane of **1** and phenyl plane of **2** are similar between the symmetrical unit (**1·2A**) and the helix (**1·2C**). The PhC−C−C−CO torsion angles of propionic acid group of **1** are, however, almost opposite at 66.2° and −68.7°, respectively. Thus, whether the molecules of **1** and **2** are arranged into the symmetrical unit or the helical structure depends on the conformation of the propionic acid group of **1**.

The following explanation may explain these successful chirality inductions. Strong intermolecular bondings of the $NH_3^+\cdots CO_2^-$ salt bridge and the In-NH···O−C hydrogen bond are common among all of the achiral and chiral crystals. The similar melting points as well as the similar crystal densities between **1·2A** and **1·2C** suggest their small energy differences in crystallization. Therefore, at the initial crystallization process from solution, the amino and imino groups of the tryptamine molecule and the carboxyl group of the acid molecule in solution are abstracted with highest priority to the helical binding sites on the surface of the seed crystals followed by continuing assembly in the same manner as the seed crystals, to form the corresponding chiral crystals. In other words, the seed helical binding sites act as templating growth points for crystal growth.

Acknowledgment. We thank Dr. Motoo Shiro in Rigaku Corp. for the help of X-ray data analysis. This work was supported by a Grant-in-Aid from the Ministry of Education, Culture, Sports, Science, and Technology in Japan.

Supporting Information Available: X-ray crystallographic information files (CIF) are available for **1·2A** and **1·2C**. This material is available free of charge via the Internet at http://pubs.acs. org.

References

(1) (a) Green, B. S.; Lahav, M.; Ravinovich, D. *Acc. Chem. Res.* **1979**, *12*, 191. (b) Sakamoto, M. *Chem. Eur. J.* **1997**, *3*, 684. (c) Feringa, B. L.; van Delden, R. A. *Angew. Chem., Int. Ed.* **1999**, *39*, 3418.

(2) (a) Elgavi, J. A.; Green, B. S.; Schmidt, G. M. J. *J. Am. Chem. Soc.* **1973**, *95*, 2059. (b) Suzuki, T.; Fukushima, T.; Yamashita Y.; Miyashi, T. *J. Am. Chem. Soc.* **1994**, *116*, 2793.

(3) (a) Koshima, H.; Ding, K.; Chisaka, Y.; Matsuura, T. *J. Am. Chem. Soc.* **1996**, *118*, 12059. (b) Koshima, H.; Nakagawa, T.; Matsuura, T.; Miyamoto, H.; Toda, F. *J. Org. Chem.* **1997**, *62*, 6322.

(4) (a) Koshima, H.; Wang, Y.; Matsuura, T.; Mibuka, N.; Imahashi, S. *Mol. Cryst. Liq. Cryst.* **1996**, *175*, 233. (b) Koshima, H.; Wang, Y.; Matsuura, T. *Mol. Cryst. Liq. Cryst.* **1996**, *177*, 63.

(5) Jacques, J.; Collet, A.; Wilen, S. H. In *Enantiomers, Racemates, and Resolutions*, Wiley: New York, 1981; pp 14−23.

(6) (a) Koshima, H.; Matsuura, T. *J. Synth. Org. Chem.* **1998**, *56*, 268 (Japanese). (b) Koshima, H.; Matsuura, T. *J. Synth. Org. Chem.* **1998**, *56*, 466 (Japanese).

(7) Cambridge Structure Database System V5.20, 2000.

(8) (a) Koshima, H.; Hayashi, E.; Matsuura, T.; Tanaka, K.; Toda, F.; Kato, M.; Kiguchi, M. *Tetrahedron Lett.* **1997**, *38*, 5009. (b) Koshima, H.; Hayashi, E.; Matsuura, T. *Supramol. Chem.* **1999**, *11*, 57.

(9) (a) Koshima, H.; Khan, S. I.; Garcia-Garibay, M. A. *Tetrahedron: Asymmetry* **1998**, *9*, 1851. (b) Koshima, H.; Honke, S. *J. Org. Chem.* **1999**, *64*, 790. (c) Koshima, H.; Honke, S.; Fujita, J. *J. Org. Chem.* **1999**, *64*, 3916.

(10) Koshima, H.; Honke, S.; Miyauchi, M. *Enantiomer* **2000**, *5*, 125.

(11) Koshima, H.; Miyauchi, M.; Shiro, M. *Supramol. Chem.* **2001**, *13*, 137.

CG0155189

UM00013957
NOVARTIS EXHIBIT 1017
Novartis v. Regents, IPR2023-01346
Page 2703 of 4460

X-Ray crystal structure of $C_6H_3(CO_2H)_3$·1,3,5·1.5(4,4′-bipy): a 'super trimesic acid' chicken-wire grid

C. V. Krishnamohan Sharma and Michael J. Zaworotko*

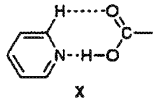
Department of Chemistry, Saint Mary's University, Halifax, Nova Scotia, Canada B3H 3C3

Trimesic acid cocrystallizes with 1.5 equivalents of 4,4′-bipyridine to generate a large distorted hexagonal network with *ca.* 35 × 26 Å internal dimensions: three independent networks interweave to afford a novel threefold two-dimensional corrugated sheet.

Hydrogen-bonded supramolecular synthons represent a primary tool for crystal engineering.[1,2] In such a context, trimesic acid (benzene-1,3,5-tricarboxylic acid, TMA) is a molecule which predictably forms honeycomb networks with interesting supramolecular properties (catenation or interpenetration, polymorphism and inclusion) as a consequence of its molecular symmetry and complementary hydrogen-bonding capabilities.[1] Early work focused upon TMA itself and generated a large number of inclusion compounds, both with and without catenation.[3] That carboxylic acids can form homo- or heterodimers with a variety of complementary functional groups (*e.g.* pyridines, 2-aminopyridines and pyrimidines) has allowed functionalized TMA,[4] its deprotonated forms[5] or its metal complexes[6] to be exploited as templates in crystal engineering studies. In this contribution we report the remarkable networking and interweaving[7] in a cocrystal of TMA, TMA·1.5(4,4′-bipy) **1**, the supramolecular structure of which is effectively an enlarged analogue of TMA that exhibits a novel mode of interpenetration.

The pyridine–carboxylic acid motif, **X**, has previously been exploited to design liquid-crystalline materials and two-dimensional β networks.[8,9] It occurred to us that it should be possible to use simple bifunctional spacer moieties based upon pyridine moieties (*e.g.* pyrazine, 4,4′-bipyridine) to afford fine-tunable chicken-wire motifs with large cavities. A hot solution of propan-2-ol and benzene (3 : 1 ratio) containing 1 and 1.5 equiv. of TMA and 4,4′-bipyridine, respectively, afforded the desired cocrystals of **1** (mp > 300 °C) upon cooling and slow evaporation of the solvent at room temperature over a period of two days.

The crystal structure exhibits the desired architecture.† An expanded form of the infinite two-dimensional honeycomb grid seen in TMA is sustained by supramolecular synthon[10] **X**: strong N–H···O hydrogen bonds coupled with complementary C–H···O hydrogen bonds [graph set[11] = $R^2_2(7)$, N···O, H···O, N–H···O, C···O, H···O, C–H···O: 2.604(4), 1.470(5) Å, 178.5°, 3.182(5), 2.419(5) Å, 125.2°; 2.719(4), 1.798(4) Å, 157.1°, 3.401(5), 2.683(5) Å, 122.3°; 2.660(4), 1.695(4) Å, 165.3°, 3.116(5), 2.255(5) Å, 133.34°; Fig. 1]. The internal dimensions of the distorted hexagons are 35 × 26 Å compared to just 14 × 14 Å in TMA itself. Self-inclusion is facilitated by the chair conformation of the large hexagon that intercalates and engages in π stacking with two other independent networks. Nevertheless, the other two networks only partially fill these cavities and empty space remains within the layer of interpenetrated networks, Fig. 2. Interpenetrated chicken-wire frameworks have also been seen for coordination polymers but the nature of the interpenetration is somewhat different.[12] This void space is effectively filled in a cog-like manner because of the way adjacent layers stack. To our knowledge, such an architecture (a threefold interpenetrated chicken-wire layer) has not yet been



X

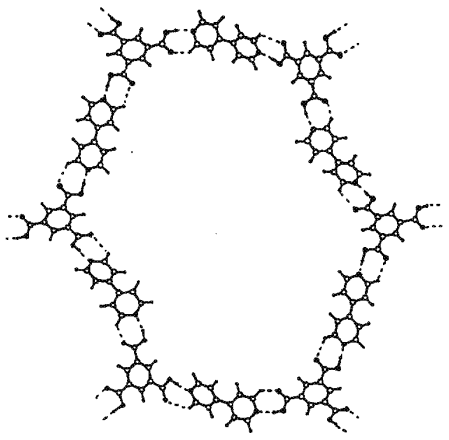


Fig. 1 The non-planar hexagonal unit formed *via* motif **X** in cocrystal **1**. N–H···O and C–H···O hydrogen bonds are illustrated by dashed lines; (⊕) N, ● (O).

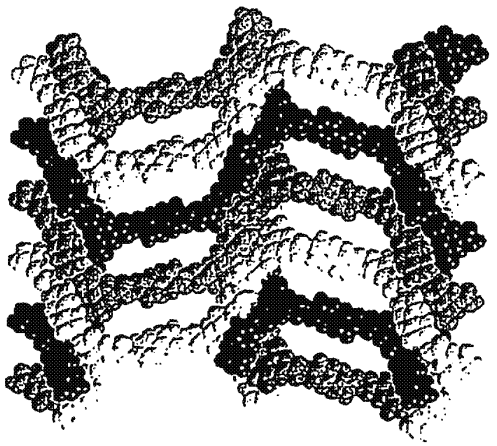


Fig. 2 The threefold two-dimensional chicken-wire networks of **1**. The independent networks are shaded for clarity. Note that void space remains even after catenation of the networks.

UM00013958
NOVARTIS EXHIBIT 1017
Novartis v. Regents, IPR2023-01346
Page 2704 of 4460

observed. However, interpenetrated 'supramolecular carpets' based upon twofold interweaving of square grids have been encountered and twofold layered coordination polymers have also been observed.[13]

The significance of C–H···O hydrogen bonds in supramolecular synthon **X** has been analysed using the Cambridge Structural Database[14] (version 5.11) and has been exploited very recently in a similar context.[15] A total of 60 compounds containing pyridine with at least one *ortho*-H atom and a carboxylic acid moiety (N···O < 3.0 Å) were considered. Of these, 29 compounds were found to exhibit C–H···O interactions (C···O < 3.7 Å, C–H···O 100–180°) with mean C···O distances and C–H···O angles of 3.27 Å and 125.4°, respectively.[16] The majority of the compounds that do not exhibit these interactions are engaged in other strong hydrogen bonds (O–H···O, N–H···O) which compete with the C–H···O hydrogen-bond formation or motif **X**. This observation suggests that C–H···O interactions afford additional stability and rigidity to motif **X** and the generality of this interaction is further supported by the existence of a 3 : 1 cocrystal of TMA with pyridine.‡

In conclusion, the large open networks (Fig. 1) of **1** are built by the strong yet flexible supramolecular synthon **X** and achieve close packing ingeniously in the absence of guest molecule(s) by adopting: (*i*) a chair conformation hexagonal architecture that facilitates two-dimensional interpenetration, (*ii*) staggered stacking of corrugated layers so as to eliminate continuous channels. Although **1** is the first crystal structure to be reported that simultaneously exploits the preceding two features in order to avoid vacuum in its crystal structure, it seems likely that there will be numerous simple analogues with supramolecular synthon **X** and related synthons.

We acknowledge the generous financial support of the NSERC (Canada) in the form of a research grant (M. J. Z.).

Footnotes

† *Crystal data* for **1**: $C_{24}H_{18}N_3O_6$, monoclinic, space group $P2_1/c$, a = 11.105(4), b = 10.132(4), c = 18.889(7) Å, β = 99.95(6), U = 2093.30(12) Å^3, Z = 4, D_c = 1.41 Mg m^{-3}, λ = 0.709 30 Å, $F(000)$ = 924. 2582 reflections out of 3671 unique reflections with $I_{net} > 3\sigma(I)$ measured at 290 K for a crystal of dimensions 0.6 × 0.2 × 0.4 mm on an Enraf-Nonius CAD4 diffractometer using the ω scan mode (4 < 2θ < 50°) afforded on convergence final R-factors of R_f = 0.057 and R_w = 0.055. The H atoms of the OH groups were found *via* difference Fourier map inspection. Other H atoms were placed in calculated positions (C–H = 1.00 Å). All non-hydrogen atoms were anisotropically refined. The crystallographic calculations were carried out using the NRCVAX program package. Atomic coordinates, bond lengths and angles, and thermal parameters have been deposited at the Cambridge Crystallographic Data Centre (CCDC). See Information for Authors, Issue No. 1. Any request to the CCDC for this material should quote the full literature citation and the reference number 182/240.

‡ The crystal structure of the cocrystal TMA·3py has been determined in space group $C2/c$, a = 24.587(4), b = 13.994(2), c = 13.610(2) Å, β = 100.75°, U = 4600.2(12) Å^3, Z = 8, W. S. Furey and M. J. Zaworotko, unpublished work.

References

1 G. R. Desiraju and C. V. K. Sharma, in *Perspectives in Supramolecular Chemistry, The Crystal as a Supramolecular Entity*, ed. G. R. Desiraju, Wiley, Chichester, 1996.
2 M. C. Etter, *Acc. Chem. Res.*, 1990, 23, 120; C. B. Aakeroy and K. R. Seddon, *Chem. Soc. Rev.*, 1993, 22, 397.
3 F. H. Herbstein, *Top. Curr. Chem.*, 1987, 140, 107; F. H. Herbstein, M. Kapon and G. M. Reisner, *J. Inclusion Phenom.*, 1987, 5, 211.
4 S. V. Kolotuchin, E. E. Fenlon, S. R. Wilson, C. J. Loweth and S. C. Zimmerman, *Angew. Chem., Int. Ed. Engl.*, 1995, 34, 2654.
5 R. E. Melendez, C. V. K. Sharma, C. Bauer, R. D. Rogers and M. J. Zaworotko, *Angew. Chem., Int. Ed. Engl.*, 1996, 35, 2213.
6 O. M. Yaghi, G. Li and H. Li, *Nature*, 1995, 378, 703; S. O. H. Gutschke, M. Molinier, A. K. Powell, R. E. P. Winpenny and P. T. Wood, *Chem. Commun.*, 1996, 823.
7 D. B. Amabilino and J. F. Stoddart, *Chem. Rev.*, 1995, 95, 2725.
8 C. M. Paleos and D. Tsiourvas, *Angew. Chem., Int. Ed. Engl.*, 1995, 34, 1696.
9 J. J. Kane, R. Liao, J. W. Lauher and F. W. Fowler, *J. Am. Chem. Soc.*, 1995, 117, 12 003.
10 G. R. Desiraju, *Angew. Chem., Int. Ed. Engl.*, 1995, 34, 2311.
11 J. Bernstein, R. E. Davis, L. Shimoni and N. Chang, *Angew. Chem., Int. Ed. Engl.*, 1995, 34, 1555.
12 L. R. MacGillivray, S. Subramanian and M. J. Zaworotko, *J. Chem. Soc., Chem. Commun.*, 1994, 1325; G. B. Gardner, D. Venkataraman, J. S. Moore and S. Lee, *Nature*, 1995, 374, 792.
13 S. B. Copp, S. Subramanian and M. J. Zaworotko, *Angew. Chem., Int. Ed. Engl.*, 1993, 32, 706; D. M. L. Goodgame, S. Menzer, A. M. Smith and D. J. Williams, *Angew. Chem., Int. Ed. Engl.*, 1995, 34, 574.
14 F. H. Allen, J. E. Davies, J. J. Galloy, O. Johnson, O. Kennard, C. F. Macrae and D. G. Watson, *J. Chem. Inf. Comput. Sci.*, 1991, 31, 187.
15 V. R. Pedireddi, W. Jones, A. P. Chorlton and R. Docherty, *Chem. Commun.*, 1996, 997.
16 R. Raylor and O. Kennard, *J. Am. Chem. Soc.*, 1982, 104, 5063.

Received, 9th July 1996; Com. 6/04843I

UM00013959
NOVARTIS EXHIBIT 1017
Novartis v. Regents, IPR2023-01346
Page 2705 of 4460

This Page is Inserted by IFW Indexing and Scanning Operations and is not part of the Official Record

BEST AVAILABLE IMAGES

Defective images within this document are accurate representations of the original documents submitted by the applicant.

Defects in the images include but are not limited to the items checked:

- ☐ BLACK BORDERS
- ☐ IMAGE CUT OFF AT TOP, BOTTOM OR SIDES
- ☐ FADED TEXT OR DRAWING
- ☐ BLURRED OR ILLEGIBLE TEXT OR DRAWING
- ☐ SKEWED/SLANTED IMAGES
- ☐ COLOR OR BLACK AND WHITE PHOTOGRAPHS
- ☐ GRAY SCALE DOCUMENTS
- ☐ LINES OR MARKS ON ORIGINAL DOCUMENT
- ☐ REFERENCE(S) OR EXHIBIT(S) SUBMITTED ARE POOR QUALITY
- ☐ OTHER: _____

IMAGES ARE BEST AVAILABLE COPY.

As rescanning these documents will not correct the image problems checked, please do not report these problems to the IFW Image Problem Mailbox.

COMMUNICATION

ChemComm
www.rsc.org/chemcomm

Generation of a co-crystal phase with novel coloristic properties *via* solid state grinding procedures

Reiko Kuroda,*[ab] Yoshitane Imai[b] and Nobuo Tajima[b]

[a] *Department of Life Sciences, Graduate School of Arts and Sciences, The University of Tokyo, Komaba, Meguro-ku, Tokyo 153-8902, Japan. E-mail: ckuroda@mail.ecc.u-tokyo.ac.jp*

[b] *Japan Science and Technology Corporation, ERATO, Kuroda Chiromorphology Project, 4-7-6 Komaba, Meguro-ku, Tokyo 153-0041, Japan*

Received (in Cambridge, UK) 29th July 2002, Accepted 19th September 2002
First published as an Advance Article on the web 30th October 2002

Co-grinding of crystals of racemic-bis-β-naphthol (*rac*-BN) and benzoquinone (BQ) produces a novel crystal adduct through crystal sheering and molecular diffusion processes in the solid state, which is structurally distinct from adducts obtained from solution or melt.

In contrast to crystallization from solution, crystallization in the solid state is rare and its mechanism has hardly been studied. We have found that co-grinding of crystals of *rac*-BN and BQ crystals, in the total absence of liquid, produces adduct crystals which are different from those obtained from solution or melt. To understand the mechanism of the adduct crystal formation, the crystallization conditions and the structures of crystals obtained from solid and solution phases have been studied.

On grinding white racemic crystals of *rac*-BN and yellow BQ in an agate mortar in a ratio of 1:2.5, the colour of the powder changes progressively with time from very pale yellow to pink and eventually to strong red (Fig. 1). The process was monitored by X-ray powder diffractometry. The powder diffraction pattern recorded after 20 min of grinding exhibits a new set of peaks in addition to the peaks corresponding to pure *rac*-BN and pure BQ crystals (Fig. 2a). After 45 min of grinding, the *rac*-BN and BQ peaks disappear completely and the new set of peaks becomes stronger (Fig. 2b). It should be noted that no intermediate phase is observed.

Recrystallization of the red powder crystals produced by grinding was carried out from ether/hexane (1:1) solution. Crystallization of a 1:1 mixture of BQ and *rac*-BN component crystals was also carried out from the same solvent. Both crystallization experiments produced chunky dark-red crystals (**II**) from a yellow/orange-coloured saturated solution. In a very rare case, a small amount of long thin plate-like crystals of red colour (**I**) emerged before the appearance of **II**. The structures of both **I** and **II** were determined by single crystal X-ray diffractometry.† The composition of the two crystals is different: **I** contains 1:1.5 *rac*-BN:BQ (*i.e.*, 1:1:3 in terms of *R*-BN: *S*-BN:BQ), whereas **II** exhibits a 1:1 ratio (1:1:2 in terms of *R*-BN:*S*-BN:BQ). Comparison of the observed X-ray powder diffraction pattern in Fig. 2b with that of crystal **II** (Fig. 2d) and calculated ones of **I** (Fig. 2c) and **II** (data not shown) based on the single-crystal structure unambiguously established that the red materials obtained by mixing/grinding have the same crystal structure as **I**. A measurement of the powder X-ray diffraction on **I** was not practical, as the yield of the single-crystals was very small.

The experimental results have shown clearly that simple co-grinding of crystals of component chemicals formed a new crystal. Several such cases have been reported previously by various researchers,[1] but the detailed formation process is unknown. A lubricant was used to accelerate the process in one case.[1d] Our experiments were carried out in the absence of any liquid phase. We have investigated foreseeable factors affecting the formation process. Given the low melting point of BQ (113–115 °C), it might be suggested that grinding results in a local melting of the crystals and that the adduct then crystallizes from the melt. However, grinding at low temperature did not inhibit adduct formation. Furthermore, when a mixture of BQ and *rac*-BN crystals was melted completely at *ca.* 110 °C, red material was also formed and this was shown by X-ray powder diffraction to be a new adduct crystal, **III** (Fig. 2e). We have checked by TLC that the compounds were not decomposed in the melting experiment. Together these results indicate that the grinding produced co-crystals by a mechanism that is different from crystallization from what we normally call the 'melt'.

To help understand the mechanism of adduct crystal formation by solid grinding, we have carried out various crystallization experiments, noting that **II** has a higher BN:BQ ratio than **I**. The use of higher mixing ratios than the original

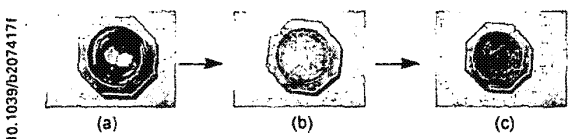


Fig. 1 Colour change of the co-ground crystals of *rac*-BN and BQ, (a) before grinding, (b) during the grinding and (c) the final product.

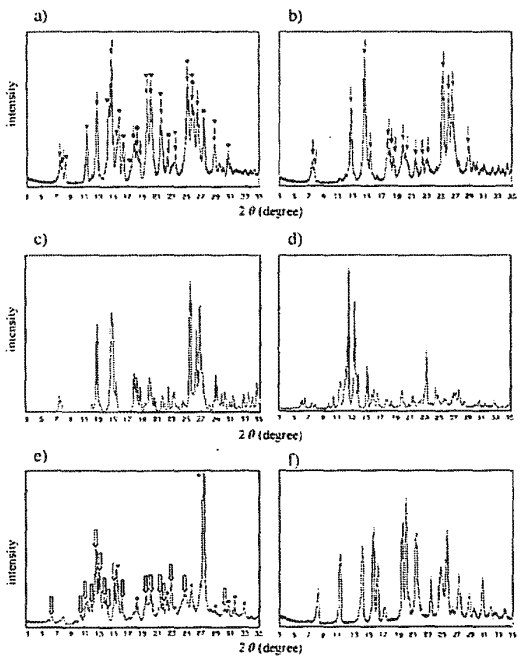


Fig. 2 X-ray powder diffraction patterns of mixtures of BQ and *rac*-BN crystals after grinding together for 20 min (a) and 45 min (b). Peaks belonging to BQ (●), BN (▼) and new crystals (↓) are indicated. (c) Calculated pattern of **I**, (d) and (e) are measured diffraction patterns of **II** and **III**. Peaks corresponding to **III** are indicated by open arrows (⇩). (f) The pattern of **I** after extended exposure to air.

DOI: 10.1039/b207417f

This journal is © The Royal Society of Chemistry 2002

UM00013961
NOVARTIS EXHIBIT 1017
Novartis v. Regents, IPR2023-01346
Page 2707 of 4460

1 : 2.5 or a longer sample grinding time (as BQ easily sublimes) did not produce **II**. Co-grinding of **I** and *rac*-BN crystals did not produce **II**. Grinding **II** with BQ did not produce **I**. Grinding was carried out in the dark, under a dry Ar atmosphere, or in a metal container placed on a wet tissue in order to rule out the involvement of photons, oxygen, and static charge, respectively. None of these procedures slowed formation of the adduct. Placing *rac*-BN crystals under BQ vapour, or simply mixing crystals of *rac*-BN and BQ without grinding did not form an adduct. All these issues were judged unambiguously by colour change and X-ray powder diffraction patterns. These observations demonstrate unequivocally the necessity for direct contact between the two solids followed by mixing of the two components at the molecular level *via* appropriate sheering and diffusion processes.

The crystal structures of **I** and **II** are compared in Fig. 3. It is fortuitous that the structure of **I** was revealed, as it would otherwise require difficult determination from the powder diffraction pattern. The molecular geometries are similar in the two crystals, with only a slight difference in the central C–C torsion angles of BN (81° for crystal **I**, 75, 86 and 100° for the three independent molecules in crystal **II**).

Crystal **I**: (Fig. 3a). The asymmetric unit comprises one independent BN molecule and two independent BQ molecules, of which one resides at the centre of symmetry. A semi-column structure runs along the c axis where the aromatic planes of naphthol and BQ stack alternately. BQ is sandwiched by the naphthol rings of the *R*-BN and *S*-BN molecules, which are related by the c-glide. Only one of the carbonyl groups of BQ forms a hydrogen bond to the hydroxy group of a naphthol (O···O = 2.733 Å). The BQ on the centre of inversion forms a triplet structure sandwiched by the inversion-related *R*- and *S*-naphthol rings. Two symmetry-related hydrogen bonds are formed between the BQ carbonyl and the hydroxy group of the nearly perpendicular naphthol ring of a BN molecule (O···O = 2.703 Å).

Crystal **II**: (Fig. 3b). There are three independent molecules of BN and BQ in the asymmetric unit. The three independent BQ molecules are always sandwiched by the roughly parallel naphthol rings of two BN molecules. All possible hydrogen bonds are exploited between the carbonyl oxygen of BQ and the hydroxy group of the nearly perpendicular naphthol ring of BN molecules (O···O distance varies from 2.707 to 2.789 Å).

Theoretical calculations using the ZINDO method[2] indicated that the strong red colour of **I** and **II** which appear only in the crystal phase is due to charge transfer essentially from the 1 : 1 BN : BQ complex. The details will be reported elsewhere.

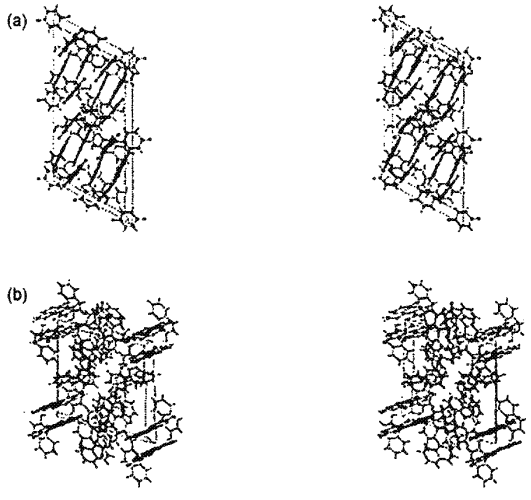


Fig. 3 Stereo views of the crystal structures of **I** (a) and **II** (b).

The local geometry of the BN···BQ···BN triplets in **I** and **II** appears similar, although the chirality is in sharp contrast. BQ is sandwiched by a racemic pair in **I**, but by a homochiral pair in **II**. In the crystal structure of pure racemic BN (space group *Iba*2), hydrogen bonds are formed between the hydroxy groups of BN molecules related by a 2_1 screw axis, thus forming a homochiral column.[1i,3] The crystal structure of pure BQ (space group $P2_1/a$) has no hydrogen bonds.[4,5] On co-grinding, BQ molecules may be inserted between the neighbouring opposite-handed homochiral BN columns of a *rac*-BN, which may encourage the formation of a hetero-chiral sandwich found in **I**. Chiral BN crystals do not form a new phase with BQ by either solid or solution crystallization. Upon complexation in the solid state, BN and BQ molecules change their crystal packing critically and form new hydrogen bonds between the two component molecules.

When adduct crystals **I** or **II** were exposed to air, the strong red colour was lost with time and, after 23 h, the crystals eventually became white. It might be expected that the crystals would deteriorate and become amorphous, but instead, they reverted to the starting *rac*-BN crystals, as unambiguously demonstrated by the X-ray powder diffraction (Fig. 2f for **I**). When the adduct crystals were placed in the vicinity of BQ crystals, no decomposition of the adducts was observed.

Crystallization by solid mixing/grinding and spontaneous crystal-to-crystal transformation both demonstrate that diffusion of molecules in the solid state can be substantial and can lead to new phases that are sometimes different from those prepared by crystallization of the same components from solution. The solid-state chemistry of these materials and the mechanisms governing their formation are clearly an exciting area for future investigation.

Notes and references

† *Crystal data.* For **I**: red crystal (0.15 × 0.33 × 0.38 mm). $C_{20}H_{14}O_2 1.5[C_6H_4O_2]$, M = 448.45, monoclinic, space group $C2/c$, a = 26.132(2), b = 13.7800(9), c = 13.9782(9) Å, β = 118.932(1)°, U = 4405.3(5) Å^3, Z = 8, D_c = 1.352 Mg m^{-3}, μ(Mo-Kα) = 0.092 mm^{-1}, 16286 measured, 5469 unique (R_{int} = 0.0308), final $R(F^2)$ = 0.046 using 3254 reflections with $I > 2\sigma(I)$, R(all data) = 0.0740. CCDC 170478. For **II**: red crystal (0.23 × 0.40 × 0.53 mm). $C_{20}H_{14}O_2[C_6H_4O_2]$, M = 394.40, triclinic, space group $P\bar{1}$, a = 14.479(2), b = 15.671(2), c = 15.725(2) Å, α = 69.792(2), β = 66.635(2), γ = 71.762(2)°, U = 3009.1(6) Å^3, Z = 6, D_c = 1.306 Mg m^{-3}, μ(Mo-Kα) = 0.088 mm^{-1}, 23185 measured, 14710 unique (R_{int} = 0.0364), final $R(F^2)$ = 0.054 using 6020 reflections with $I > 2\sigma(I)$, R(all data) = 0.140. CCDC 170479. See http://www.rsc.org/suppdata/cc/b2/b207417f/ for crystallographic files in CIF or other electronic format.

Data were collected on a Bruker APEX CCD diffractometer at 133 K and the structures were solved by the direct method using SHELX. We gratefully acknowledge Dr K. Yoza and Mr S. Igarashi of Bruker Japan for the crystallographic data collection.

1 (*a*) A. R. Ling and J. L. Baker, *J. Chem. Soc.*, 1893, **63**, 1314–1327; (*b*) A. O. Patil, D. Y. Curtin and I. C. Paul, *J. Am. Chem. Soc.*, 1984, **106**, 348–353; (*c*) W. T. Pennington, A. O. Patil, I. C. Paul and D. Y. Curtin, *J. Chem. Soc., Perkin Trans 2*, 1986, 557–563; (*d*) F. Toda, K. Tanaka and A. Sekikawa, *J. Chem. Soc., Chem. Commun.*, 1987, 279–280; (*e*) M. C. Etter and G. M. Frankenbach, *Chem. Mater.*, 1989, **1**, 10–12; (*f*) M. D. Hollingsworth, M. E. Brown, B. D. Santarsiero, J. C. Huffman and C. R. Goss, *Chem. Mater.*, 1994, **6**, 1227–1244; (*g*) F. Toda and H. Miyamoto, *Chem. Lett.*, 1995, 861; (*h*) M. R. Caira, L. R. Nassimbeni and A. F. Wildervanck, *J. Chem. Soc., Perkin Trans. 2*, 1995, 2213–2216; (*i*) F. Toda, K. Tanaka, H. Miyamoto, H. Koshima, I. Miyahata and K. Hirotus, *J. Chem. Soc., Perkin Trans. 2*, 1997, 1877–1885.
2 J. E. Ridley and M. C. Zerner, *Theor. Chem. Acta*, 1973, **32**, 111–134.
3 K. Mori, Y. Masuda and S. Kashino, *Acta Crystallogr., Sect. C*, 1993, **49**, 1224–1227.
4 J. Trotter, *Acta Crystallogr.*, 1960, **13**, 86–95.
5 F. van Bolhuis and C. Th. Kiers, *Acta Crystallogr., Sect. B*, 1978, **34**, 1015–1016.

UM00013962
NOVARTIS EXHIBIT 1017
Novartis v. Regents, IPR2023-01346
Page 2708 of 4460

Tableau 4. *Distances cation–oxygène* (Å) *dans les polyèdres de coordination des cations associés*

Ba–O(*E*21)	2,714 (5)	Ba–O(*W*4)	2,772 (7)
Ba–O(*E*22)	2,749 (7)	Ba–O(*W*3)	2,809 (8)
Ba–O(*E*11)	2,796 (6)	Ba–O(*W*2)	2,877 (7)
Ba–O(*E*32)	2,821 (4)	Ba–O(*W*2)	2,987 (6)
Ba–O(*E*12)	2,922 (6)		
Ag–O(*E*32)	2,445 (5)	Ag–O(*E*32)	2,629 (7)
Ag–O(*E*11)	2,531 (6)	Ag–O(*E*12)	2,706 (5)
Ag–O(*E*22)	2,624 (5)	Ag–O(*W*1)	2,370 (9)

des cations associés qui se développe en une chaîne de direction moyenne **a** − **b**.

Références

DURIF, A. & AVERBUCH-POUCHOT, M. T. (1976). *J. Appl. Cryst.* **9**, 247.

MARTIN, C. & DURIF, A. (1972). *Bull. Soc. Fr. Minér. Crist.* **95**, 149–153.

PREWITT, C. T. (1966). *SFLS-5. A Fortran* IV *Full-Matrix Crystallographic Least-Squares Program.*

Acta Cryst. (1977). B33, 2719–2733

The Molecular Packing Modes and the Hydrogen-Bonding Properties of Amide : Dicarboxylic Acid Complexes

BY L. LEISEROWITZ

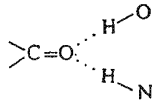
Department of Structural Chemistry, The Weizmann Institute of Science, Rehovot, Israel

AND F. NADER

Organisches Chemisches Institut der Universität Heidelberg, 69 Heidelberg, Im Neunheimer Feld 270, Federal Republic of Germany

(*Received* 18 *January* 1977; *accepted* 26 *February* 1977)

The various possible modes of forming H-bonded complexes of primary and secondary amides with dicarboxylic acids in the crystalline phase have been constructed in terms of: (*a*) O–H···O and N–H···O hydrogen-bond geometry, (*b*) the nature of the residues attached to the amide and carboxyl groups, and (*c*) the commonly occurring crystallographic symmetry elements required to generate hydrogen-bonding arrangements. The existence of these packing modes was corroborated by crystal structure analyses of model compounds. The various observed hydrogen-bonding motifs are compared to determine preferred hydrogen-bond geometries. There is a tendency for a carbonyl O atom which participates in both an N–H···O and O–H···O bond to adopt, the residues permitting, an arrangement where the system



is coplanar with linear hydrogen bonds and C=O···H angles ≃120°. The angular geometry of the complexing O–H···O(amide) bond invariably displays an O(H)···O=C angle ≃120°. The N–H···O (carboxyl) bond shows much greater variation in the N(H)···O=C angle. The O–H···O(amide) distance between amide and carboxyl groups linked by a single hydrogen bond is 2·50 ± 0·02 Å, which is shorter than the average length of the corresponding O–H···O(carboxyl) bond of 2·64 Å. A similar comparison of N–H···O(amide) and N–H···O(carboxyl) bonds shows no systematic differences. The C=O length is, on average, 0·04 Å longer in amides than in carboxylic acids.

1. Introduction

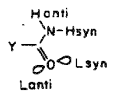
A systematic study of crystalline molecular complexes formed by a large variety of amides and dicarboxylic acids was undertaken as part of an analysis of the packing modes of H-bonded functional groups. The rationale behind these studies is that much information of chemical interest is imbedded in crystal structures because they represent minimum-energy arrangements and, whereas little can be extracted from a single structure, certain trends become apparent if enough structures are available. Our principal purpose lay in the detection of the primary hydrogen-bonding motifs of the amide : acid complexes as governed by the

UM00013963
NOVARTIS EXHIBIT 1017
Novartis v. Regents, IPR2023-01346
Page 2709 of 4460

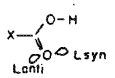
residues attached to the carboxyl and amide groups, and consequently in gaining a deeper understanding of the hydrogen bonds in amides and carboxylic acids and the factors responsible for complexation. This approach is reflected in the general outlay of the paper; first we describe the various packing arrangements in amide : acid complexes, followed by an analysis of their hydrogen-bonding properties.

2. Primary point motifs of amide : acid complexes

The forces responsible for molecular complexation between an amide (1) and a carboxylic acid (2) are mainly due to hydrogen bonds (to be referred to as H-bonds) involving both the N–H and O–H proton donor groups. Possible proton acceptors are the electron lone-pair lobes L of the carbonyl O atoms as depicted in (1) and (2). We shall specify the presumed locations of the two lone-pair lobes L^* of the carbonyl O atom as well as the locations of the H atoms by the symbols *syn* and *anti* adopting the following convention: the H atom, or lone-pair lobe, closer to the other hetero-atom of the functional group is designated as H_{syn}, or L_{syn}, while that which is further is labelled H_{anti} or L_{anti}.



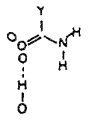
(1)

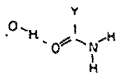


(2)

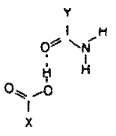
Complexation must be associated with the fact that the amide and carboxyl groups together have an excess of proton acceptors: three proton donors *versus* four proton acceptors. While the H-bond requirements of the amide group are completely satisfied, H_{syn} and H_{anti} are complemented by L_{syn} and L_{anti}, the carboxyl group lacks one proton donor (H_{syn} *versus* L_{syn} and L_{anti}). This deficiency is a necessary but not sufficient requirement for complexation since there are several amide : acid combinations (*e.g.* formamide : succinic acid, and various amides with, for example, fumaric acid) which do not seem to yield complexes. Consequently, it would seem necessary that the lattice energy of the crystalline complex must override that of the individual components.

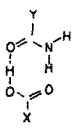
Since the O–H···O bond is significantly shorter and stronger than the N–H···O bond (Pimentel & McClellan, 1960), we shall first consider the possible ways in which O–H···$OCNH_2$ bonds, rather than N–H···OCOH bonds, are formed between the carboxyl and amide groups leading to a set of basic packing motifs. This may be accomplished on the assumption that the O–H proton donor is directed at the acceptor carbonyl O atom along the line of its lone-pair lobe. Since either the L_{syn} or the L_{anti} lobes of (1) may serve as proton acceptors, the O–H group may form two distinct H-bond geometries shown in (3) and (4).

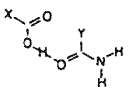

(3)

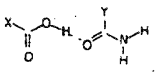

(4)

The relative orientations between the carboxyl and amide groups in (3) and (4) may be varied by rotation about the interlinking O–H···O(amide) bond. We confine ourselves to orientations which lead to coplanar arrangements. Therefore (3) and (4) each yield two motifs, (3*a*) and (3*b*), and (4*a*) and (4*b*) respectively.

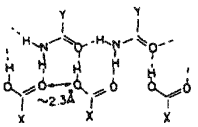

(3*a*)


(3*b*)

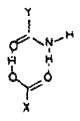

(4*a*)


(4*b*)

The H-bonding schemes in these motifs may be further extended utilizing first the N–H_{syn} proton donor and the available lone-pair lobes of the carbonyl O atoms to form linear N–H···O bonds. This extension precludes the motif (3*a*) since the resulting arrangement (5), which also incorporates a N–H_{anti}···$OCNH_2$ bond, would contain too close a contact of ~2·3 Å between carbonyl and hydroxyl O atoms of neighbouring carboxyl groups. In a similar arrangement (Huang, Leiserowitz & Schmidt, 1973) (see § 3.3.2.1) an O···O contact of not less than 3·6 Å was found. Inserting this distance into motif (5) would induce a pronounced distortion in the whole H-bonding geometry. Motif (3*b*), on the other hand, is satisfactory since it already embodies the N–H_{syn}···O bond yielding the cyclic dimer (6).



(5)

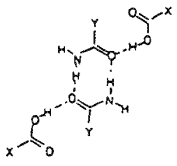

(6)

Both motifs (4*a*) and (4*b*) may be extended *via* N–H_{syn}···O bonds by associating the amide groups to form the commonly observed centrosymmetric H-bonded pair, resulting in motifs (7) and (8) respectively.

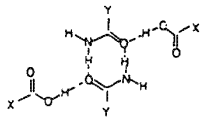
While it is possible to generate additional H-bonding arrangements from (4*a*) and (4*b*) in which the N–H_{syn} bond interacts with the available L_{anti} lobe of the carboxyl group as shown in (9*a*), (9*b*) and (9*c*), these schemes inhibit the formation of further N–H···O

* The lone-pair lobes are assumed to lie in the plane of the carbonyl system >C=O and make angles of 120° with C=O: *i.e.* the O atom is sp^2 hybridized.

UM00013964
NOVARTIS EXHIBIT 1017
Novartis v. Regents, IPR2023-01346
Page 2710 of 4460

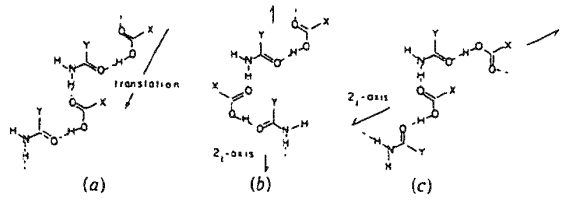


(7)



(8)

bonds since all available lone-pair lobes of the carbonyl O atoms are blocked. Thus motifs (9) may be discarded.



(a) (b) (c)

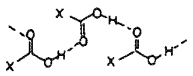
(9) Three unfavourable chain motifs constructed from point motifs (7) and (8).

The remaining primary motifs (6), (7) and (8) may be regarded as *point* motifs, analogous to crystallographic point groups, from which we may develop *space* motifs, analogous to space groups, by interlinking the *point* motifs by H-bonds. In constructing these space motifs use will be made only of the commonly occurring space symmetry elements in organic molecular crystals, *i.e.* translation, glide plane, and twofold screw axis. The existence of these point motifs, and their resulting space motifs, are critically dependent on the steric nature of the amide and acid residues *Y* and *X*. This dependence will now be examined in detail for motifs (7), (8) and (6) in turn.

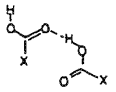
3. Space motifs of the amide : acid complexes

3.1. *Point motif* (7)

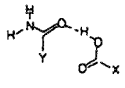
The planar arrangement in point motif (7) induces a close contact between the amide residue *Y* and the carbonyl O atom of the carboxyl group. Therefore the question arises as to the size of the residue *Y* which may be incorporated into motif (7). The answer is provided by the H-bond motif (10) common to formic acid (Holtzberg, Post & Fankuchen, 1953), acetic acid (Nahringbauer, 1970; Jönsson, 1971) and β-tetrolic acid (Benghiat & Leiserowitz, 1972).



(10) Polymeric motif of H-bonded carboxyl groups.



(11*a*)

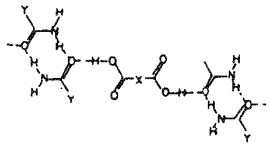


(11*b*)

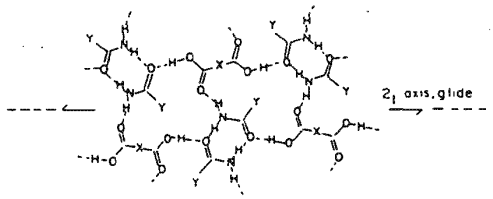
These molecules, $X-CO_2H$, are interlinked by *single* O–H···O bonds in a geometry which strongly resembles that of the O–H···$OCNH_2$ bond in (7). The common features are obvious from (11*a*) and (11*b*). Only these three monocarboxylic acids have been observed incorporating point motif (11), this having been accounted for by the close van der Waals contact *X*···O (Leiserowitz, 1976). By analogy, formamide, acetamide and tetrolamide might be expected to fit into motif (7).

3.1.1. *Twofold screw axis and translation packing*

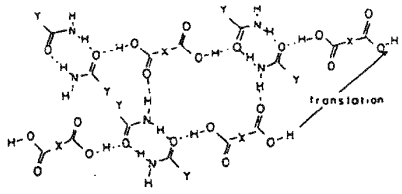
Translation of the point motif (7) generates a one-dimensional space motif (12) in which the two carboxyl groups are linked by C–*X*–C where *X* represents either a chemical bond or a van der Waals contact. These chains (12) may be interlinked only by $N-H_{anti}\cdots OCOH$ bonds *via* the L_{anti} lobes of the carboxyl O atoms, in fact the only acceptor lobes available. This may be achieved by a 2_1 axis or a glide, both running parallel to the chain axis or alternatively by translation, yielding space motifs (13) and (14) respectively. An essential difference between (13) and (14) lies in the geometry of their interchain N–H···O bonds.



(12) Chain motif derived from translation linkage of point motifs (7).



(13) Space motif containing chain motifs (12) linked by a 2_1 axis, or glide.



(14) Space motif containing chain motifs (12) linked by translation.

In the 2_1 axis, or glide, space motif (13) the distance between the two carboxyl groups, C–*X*–C, affects the geometry of the interchain N–H···O bond, since its length depends on the length of the 2_1 axis, or glide axis.

UM00013965
NOVARTIS EXHIBIT 1017
Novartis v. Regents, IPR2023-01346
Page 2711 of 4460

which varies with the C–*X*–C distance. Therefore the C–*X*–C distance cannot be longer than 2 Å to accommodate an interchain N–H···O bond of 2·9–3·0 Å. Only oxalic acid satisfies this condition. Furthermore, of the three amides which may fit into the chain (12) only formamide and acetamide may be accommodated into the two-dimensional motif (13); tetrolamide is precluded because of molecular overcrowding.

The C–*X*–C distance imposes no obvious restrictions on the translation space motif (14). However, the short interchain contact between the *Y* groups, determined by the interchain N–H···O distance, probably does not permit the residue *Y* to be bulkier than a H atom, so it would seem that only formamide complexes could pack in this motif.

The 2:1 complex of formamide with oxalic acid (Leiserowitz & Nader, 1977), whose cell constants are listed in Table 1, does not crystallize in the translation space motif (14); rather it appears in the space motif (13) in which the chains (12) are interlinked by a 2_1 axis. The H-bonded system (Fig. 1) contains two striking features: a short O–H···OCNH$_2$ bond of 2·5 Å and a H-bonded network which is not coplanar, but crosslinked by virtue of a tilt of 19° between the chain axis of (12) and the 2_1 axis. Such a crosslinked network cannot be achieved in the glide space motif (13) because the axes of the glide-related chains (12) are parallel, and so would yield a layer structure.

The molecular complex of formamide with formic acid (Nahringbauer & Larsson, 1969), which of course cannot pack in the 2_1 axis motif (13) (the distance C–*X*–C – C–H···H–C > 2 Å), contains two different H-bonded networks, (I) and (II), shown in Fig. 2, both of which resemble the translation motif (14). In (I), the point motifs (7) are interlinked by N–H···O bonds generated by a shallow glide which is almost akin to translation. In (II) the amide groups do not comprise ring dimers as in (I); rather they form H-bonds along a 3·6 Å axis about a twofold screw, an arrangement which is not unique; it appears in the

Table 1. *Cell constants and* H*-bonding motifs of amide:carboxylic acid complexes*

Amide	Carboxylic acid	Amide:acid ratio	Space group	*Z*	*a* (Å)	*b* (Å)	*c* (Å)	*β* (°)	Point motif/space motif
Formamide	Oxalic acid	2:1	$P2_1/c$	2	3·669	11·066	10·314	99·40	(7)/(13)
Acetamide		1:1	*A*2/*a*	16	20·542	9·079	13·931	112·09	(8)/(16)
α-F-acetamide		2:1	$P2_1/c$	2	4·72	4·83	22·96	108	(17)/(23*c*)
α-Cl-acetamide		2:1	$P2_1/c$	2	4·27	5·20	26·77	108	(17)/(23*c*)
Crotonamide		2:1	$P2_1/c$	4	5·203	12·896	9·310	90·64 92·19	(17)/(18)
Furamide		2:1	$P\bar{1}$	1	7·459	6·578	8·064	95·59 120·29	(17)/(23*c*)
Benzamide		2:1	$P2_1/c$	2	5·13	5·27	30·97	108·6	(17)/(23*a*)
N-Me-formamide		2:1	*P*2/*c*	4	13·817	3·838	19·860	110·8	(25*b*)/(26)*
N-Me-acetamide		2:1	$P2_1/c$	4	15·23	4·02	19·94	93·2	(25*b*)/(26)*
Crotonamide	Succinic acid	2:1	$P2_1/c$	2	5·14	16·60	9·55	98·5 129·7	(17)/(18)
Furamide		2:1	$P\bar{1}$	1	7·23	9·66	11·81	71·6 111·0	(17)/(23*b*)
Benzamide		2:1	$P2_1/c$	2	9·194	5·116	19·480	105·66	(17)/(23*a*)
Acrylamide	*meso*-DiCl-succinic acid	2:1	$P2_1$	2	5·22	21·65	6·85	109	(17)/(23*a*)
Crotonamide		2:1	*Pbca*	8	20·40	8·69	9·88		
Acrylamide	(±)-DiBr-succinic acid	2:1	$P2_1/c$	4	12·80	13·96	9·33	104	
Acetamide	Maleic acid	1:1	$P2_1$	2	6·09	6·45	10·48	92	
Formamide	Allenedicarboxylic acid	2:1	*Cc* or *C*2/*c*	4	11·78	7·93	10·90	93	
Acetamide		1:1	*C*2/*c*	8	19·017	4·829	21·838	118·69	(8)/(16)
Crotonamide		2:1	$P2_1/c$	4	18·80	18·20	4·52	93·5	
Acetamide	Acetylenedicarboxylic acid	2:1	*Aba*2 or *Acam*	4	13·64	12·86	6·50		
Acrylamide		2:1	*C*2 or *C*2/*m*	4	14·85	6·38	13·40	91	
Tetrolamide		2:1	*C*2/*c*	4	22·279	9·139	6·944	98·51 96·8	(17)/(18)†
Crotonamide	Adipic acid	2:1	$P\bar{1}$	1	8·58	7·96	7·07	116·5 88·0	(17)/(23*b*)
Furamide		2:1	$P2_1/c$	4	6·96	14·36	20·98	123	(17)
Benzamide		2:1	$P2_1/c$	2	5·04	5·34	37·22	91·9	(17)/(23*a*)

* The observed motif in *N*-methylformamide:oxalic acid is very similar to that given in the table (see § 4). The crystal structure of *N*-methylacetamide:oxalic acid has not been solved, yet its H-bonding motif must be almost isostructural with *N*-methylformamide:oxalic acid (see § 4).

† The observed motif in tetrolamide:acetylenedicarboxylic acid is analogous to that given (see § 3.3.1).

UM00013966
NOVARTIS EXHIBIT 1017
Novartis v. Regents, IPR2023-01346
Page 2712 of 4460

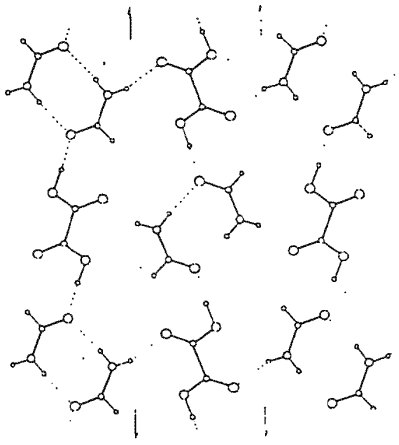


Fig. 1. Formamide:oxalic acid. H-bonding network viewed along a.

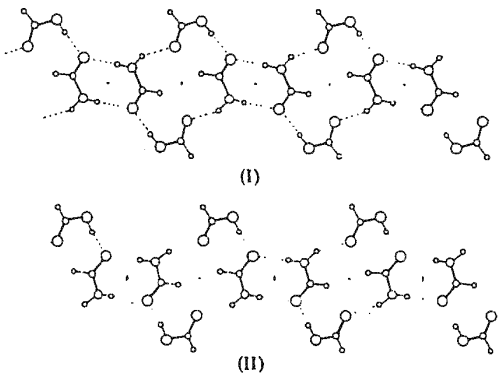


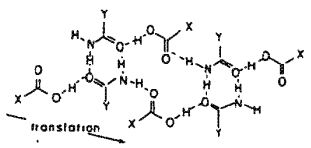
Fig. 2. Formamide:formic acid (Nahringbauer & Larsson, 1969). H-bonding networks (I) and (II) viewed along b. In (I) the amide groups form H-bonded rings; in (II) the amide groups are related by a 2_1 axis to form a helical H-bonded system along the short b axis of 3·6 Å.

crystal structures of hydroxyurea (Larsen & Jerslev, 1966), isohydroxyurea (Larsen, 1968), and a number of secondary *cis* amides (Leiserowitz & Tuval, 1977).

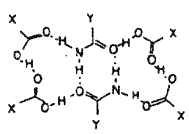
It was argued above that acetamide:oxalic acid could pack in point motif (7) as part of the 2_1 axis space motif (13). The actual structure is quite different displaying the point motif (8). The advantage reaped by acetamide:oxalic acid appearing in point motif (8) is discussed below.

3.2. *Point motif* (8)

A space motif derived from point motif (8) by interlinking the free $N-H_{anti}$ donor with the only available L_{anti} lobe of the carboxyl group would induce close contacts between the residues X and Y as shown in (15). Nevertheless point motif (8) is incorporated into the crystal structures of the 1:1 complexes of acetamide with oxalic acid (Leiserowitz & Nader, 1972) and with allenedicarboxylic acid (Nader, 1977) through an additional carboxyl function, as shown in (16), which bridges the $N-H_{anti}$ proton donor and the available L_{anti} acceptor lobe of the carboxyl group by N—H···OCOH and O—H···OCOH bonds. Characteristic of this point motif in the two complexes are very short O—H···$OCNH_2$ bonds of 2·48 and 2·52 Å.



(15) Space motif containing point motifs (8) linked by translation.



(16) Point motif observed in acetamide:oxalic acid and acetamide:allenedicarboxylic acid.

To accommodate point motif (16) into the crystal structure of acetamide:oxalic acid the less favoured synplanar O=C—C=O conformation of oxalic acid (*i.e.* the torsion angle of O=C—C=O is 0°) is adopted. The structure (Fig. 3) contains acetamide dimers H-bonded to infinite chains of the synplanar oxalic acid molecules linked to each other by *single* O—H···O bonds along a pseudo 2_1 axis* forming a layer. Application of the pseudo 2_1 axis provides the bond linkage between the two 'independent' carboxyl groups in point motif (16) to form the synplanar oxalic acid conformer; indeed it is impossible to construct a H-bond network incorporating (16) with oxalic acid in its stable antiplanar conformation. The question then arises why the acetamide complex does not appear in space motif (13), as does formamide:oxalic acid, in which the oxalic acid is antiplanar. Were acetamide:oxalic acid to pack in motif (13) this postulated arrangement would bear a disadvantage in that the O—H···$OCNH_2$ bond could not be as short as in the observed structure (2·48 Å) because of a close methyl···O(carbonyl) contact [*i.e.* the Y···O contact in (7)]. In the observed structure the length of the O—H···$OCNH_2$ bond, which is part of point motif (8), is not at all affected by the bulkiness of the amide residue Y.

* The structure contains two crystallographically independent oxalic acid molecules related by a pseudo 2_1 axis and two independent acetamide molecules forming the ring dimer.

UM00013967
NOVARTIS EXHIBIT 1017
Novartis v. Regents, IPR2023-01346
Page 2713 of 4460

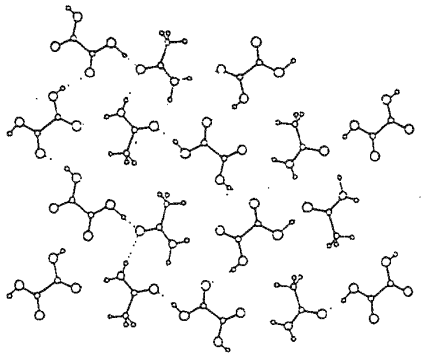
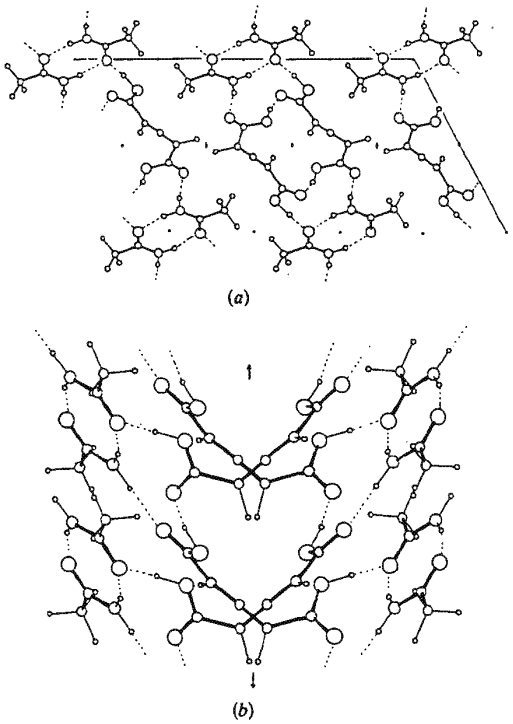


Fig. 3. Acetamide:oxalic acid. H-bonding sheet structure in the *ab* plane.



(*a*)

(*b*)

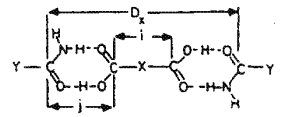
Fig. 4. Acetamide:allenedicarboxylic acid (Nader, 1977). (*a*) Packing arrangement in the *ac* projection. (*b*) The H-bonding layer structure seen perpendicular to the *bc* plane.

Point motif (16) is evident in the H-bond network of acetamide:allenedicarboxylic acid which is a layer structure (Fig. 4*a*). In a manner similar to acetamide:oxalic acid, the allenedicarboxylic acid molecules form infinite chains (Fig. 4*b*) by *single* O–H···O bonds along the 4·5 Å *b* axis. Such chains are made of double-stranded helices. The molecules in each H-bonded strand are related by a twofold screw of repeat **2b** (*i.e.* a combination of the twofold axis and a repeat unit), while the two interwoven strands are related to each other by the twofold axis (Fig. 4*a*). The double-stranded helices are connected to centrosymmetric acetamide pairs by the N–H···OCOH and O–H···$OCNH_2$ bonds inherent in point motif (16). The allenedicarboxylic acid molecule in the complex maintains an overall conformation* similar to that of its parent compound (Leiserowitz & Nader, 1973), in contrast to the oxalic acid complex.

The question arises whether the point motif (16) may be encountered in other systems. It is obvious from the sheet structure of acetamide:oxalic acid (Fig. 3) that an increase in size of the amide residue *Y* will lead to molecular overcrowding. Indeed, F or Cl substitution of one of the methyl H atoms of acetamide leads to a change in packing type. Nevertheless, we envisage molecular complexes with arrangements similar to acetamide:oxalic acid by choosing appropriate *X* and *Y* residues. This may be achieved, for example, by increasing the intramolecular separation between the two carboxyl groups from C–C (oxalic acid) to C–C≡C–C (acetylenedicarboxylic acid).

3.3. *Point motif* (6)

The point motifs (7) and (8), and their corresponding space motifs, impose strict limitations on the sizes of the residues *X* and *Y*. In contrast, point motif (6) obviously has no such restrictions and thus should be commonly observed. Indeed, in the reported monoamides of dicarboxylic acids, *e.g.* fumaramic acid (Benghiat, Kaufman, Leiserowitz & Schmidt, 1972), bromosuccinamic acid (Murakami & Iitaka, 1969), succinamic acid and muconamic acid (Leiserowitz, 1976), the molecules are linked by the carboxyl:amide pair (6). Since this analysis is focused on centrosymmetric dicarboxylic acids point motif (6) develops into a molecular complex (17) with a 2:1 amide:acid composition.



(17) 2:1 amide:acid complex incorporating point motif (6).

The point motif (17) can be interlinked into a space motif either by an N–H···$OCNH_2$ bond or by an N–H···OCOH bond. This may be accomplished either by translation or by a glide (or 2_1 axis). The latter

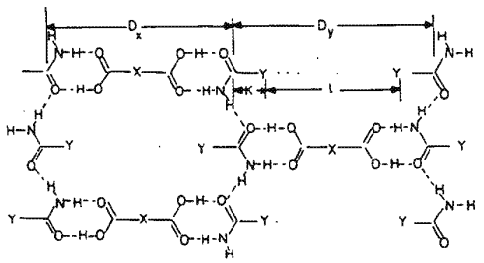
* The torsion angle of C–C=C=C–C in allenedicarboxylic acid is ≃90° in both the acetamide complex and the parent compound. The O=C–C=C conformation is antiplanar ($\tau \simeq 180°$) in the parent compound, whereas in the complex τ = 178 and 163° (Nader, 1977).

UM00013968
NOVARTIS EXHIBIT 1017
Novartis v. Regents, IPR2023-01346
Page 2714 of 4460

symmetry, however, permits formation of an extended structure by N–H···OCNH$_2$ bonds only;* translation symmetry imposes no such restrictions.

3.3.1. *Glide packing*

The extended H-bonded system achieved by joining the point motifs (17) by a glide, or 2_1 axis, is shown in (18). This mode of linking amide groups is analogous to that observed in primary amides (Leiserowitz & Schmidt, 1969) where it was shown that, to obtain a sufficiently short, linear, interpair N–H···O bond, the glide plane has to pass close to the amide C atom at an angle approximately perpendicular to the Y–CONH$_2$ bond, and in a direction parallel to the plane of the amide group. This glide† has an axial component of 9·6 ± 0·3 Å.



(18) Space motif generated by linking point motifs (17) by a glide or 2_1 axis.

An examination of space motif (18) reveals a relation between the sizes of the residues X and Y. Firstly, steric contacts arising from the length of the interpair N–H···O bond hardly permit X and Y to extend along the interpair direction and thus X and Y are limited to non-bulky chains (*e.g.* the phenyl ring is most likely excluded). Secondly, the residues X and Y must be of appropriate lengths along the chain direction. This geometric relation between X and Y may be described by two distances D_x and D_y shown in (17) and (18). D_x is the separation between the two amide C atoms in the 2:1 molecular complex, given by $i + 2j$ where i is the intramolecular distance between the two carboxyl C atoms and j is the distance between the amide and carboxyl C atoms of the H-bonded carboxyl:amide pair and thus a constant (= 4·0 Å). D_y is the separation between the two amide C atoms across the residues Y equal to $2k + l$, where k is the length of the residue Y and l is the intermolecular distance between the two Y groups. $D_x + D_y$ is the translation repeat normal to the glide plane in space motif (18). As mentioned above, a linear N–H···O bond of the proper length of 2·9 Å is possible only if the glide plane passes close to the amide C atom, achievable only if $D_x = D_y$.

Such a situation arises for the 2:1 complex of tetrolamide:acetylenedicarboxylic acid (Nader, 1977). Here $D_x \simeq 12{\cdot}1$ Å and $D_y \simeq 12{\cdot}2$ Å ($D_x \simeq i + 8$ Å, $i \simeq 4{\cdot}1$ Å for C–C≡C–C; $D_y = 2k + l$, $k \simeq 4{\cdot}1$ Å for H_3C–C≡C–C and $l \simeq 4$ Å for a $CH_3\cdots H_3C$ contact). The actual structure (Fig. 5) is analogous to the planar space motif (18), the primary difference being that the acetylenedicarboxylic acid does not lie on a centre of inversion but on a twofold axis, so that the acid molecule adopts a synplanar O=C–C≡C–C=O conformation.

The condition $D_x \simeq D_y$ is also satisfied for the 2:1 complex crotonamide:succinic acid ($D_x \sim 3{\cdot}7 + 8{\cdot}0 = 11{\cdot}7$ Å; $D_y \simeq 2 \times 3{\cdot}8 + 4{\cdot}0 = 11{\cdot}6$ Å). The structure exhibits a packing scheme analogous to space motif (18) as indicated by the characteristic glide axis of 9·5 Å (Table 1). Were the complex to adopt the motif (18) in its planar form the translation repeat normal to the glide plane would be $D_x + D_y = 23{\cdot}3$ Å. The actual length of the appropriate b axis, however, is 16·6 Å (Table 1), implying that the plane of the complex unit (17) is not perpendicular to the glide plane, but rather inclined to it at an angle of $\arcsin(b/D_x + D_y) \sim 45°$. Thus the H-bonding scheme of crotonamide:succinic acid is not planar although the spatial relations between the residues X and Y seem to be satisfied. This type of H-bonding arrangement, as viewed along the 9·5 Å glide, is depicted in (19). Were crotonamide:succinic acid to appear in a planar arrangement of (18), the crotonamide molecules interlinked by N–H···O bonds along the glide would be involved in prohibitively short contacts between the NH_2 group and the β-H atom as indicated in (20). A very similar situation has been encountered in the structure of crotonamide itself (Leiserowitz & Schmidt, 1969).

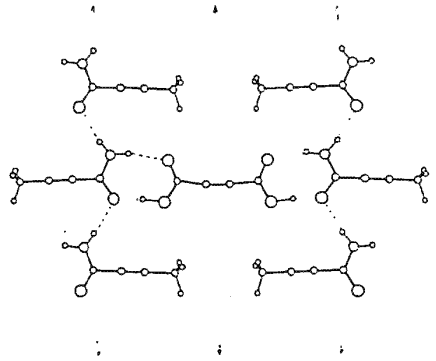
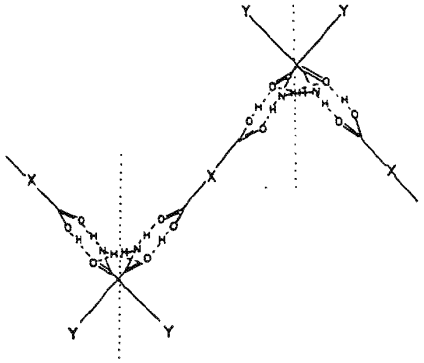


Fig. 5. Tetrolamide:acetylenedicarboxylic acid (Nader, 1977). H-bonding sheet structure.

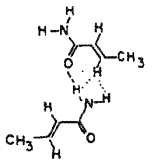
* An extended arrangement wherein interpair N–H···OCOH bonds are interlinked by glide symmetry cannot be achieved. This may be seen by constructing hypothetical models.

† This N–H···O bond may also be achieved *via* a 2_1 axis, imposing requirements similar to that of the glide: the 2_1 axis must pass through the Y–CONH$_2$ bond and be in the plane of the amide group.

UM00013969
NOVARTIS EXHIBIT 1017
Novartis v. Regents, IPR2023-01346
Page 2715 of 4460



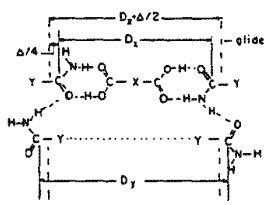
(19) View of space motif (18) along the glide axis in which the amide plane makes a shallow tilt of ~45° with the glide plane.



(20)

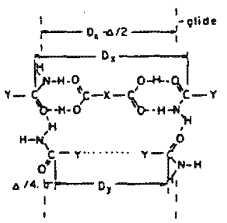
In general the condition $D_x = D_y$ is rarely satisfied, leaving the two alternatives $D_x < D_y$ and $D_x > D_y$ to be considered.

Given $D_x < D_y$, $= \Delta$ say, the separation between the adjacent glide planes in (18) $= D_x + \Delta/2$, so that the glide plane would pass through the H_2NOC-Y bond at a distance of $\Delta/4$ from the amide C atom as shown in (21). An appreciable deviation Δ would induce too long an interpair N—H···O bond. This situation exists for the 2:1 complex of crotonamide:oxalic acid (Leiserowitz & Nader, 1977). Here the estimated mismatch between D_x and D_y (9·5 *versus* 11·6 Å) is 2 Å. Yet this complex crystallizes in the glide motif (18) (Fig. 6*a*). The packing scheme in Fig. 6(*b*), viewed along the H-bonding glide axis, shows how the mismatch Δ is compensated. The complex unit (17) is not inclined at a steep angle to the glide plane but at a shallow angle of 40° which serves to bring the glide-related amide groups into close proximity, yielding a normal N—H···O bond of 2·95 Å.

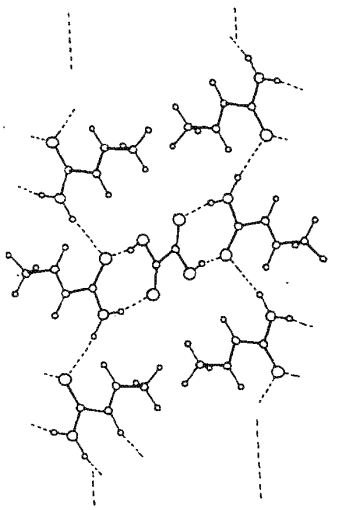


(21) Space motif (18) in which $D_y > D_x$.

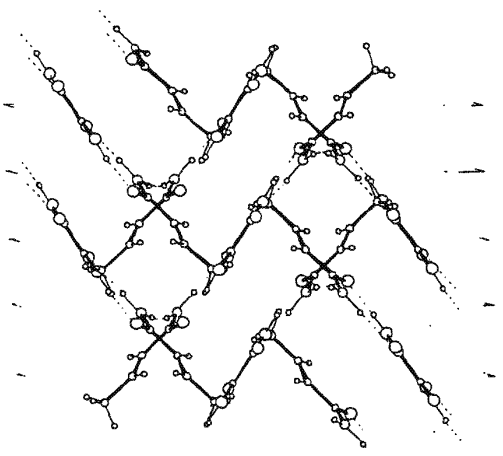
In the event where $D_x > D_y = \Delta$ the glide planes in (18) pass through the C=O and C—N amide bonds at a distance of $\Delta/4$ from the C atom as shown in (22). The glide operation yields a geometrically unsatisfactory interpair N—H···O bond if $\Delta/4$ is of appreciable length (*i.e.* 0·5 Å). This N—H···O bond geometry cannot be improved by varying the tilt of the complex unit with respect to the glide plane, unlike the prior condition D_x



(22) Space motif (18) in which $D_x > D_y$.



(*a*)



(*b*)

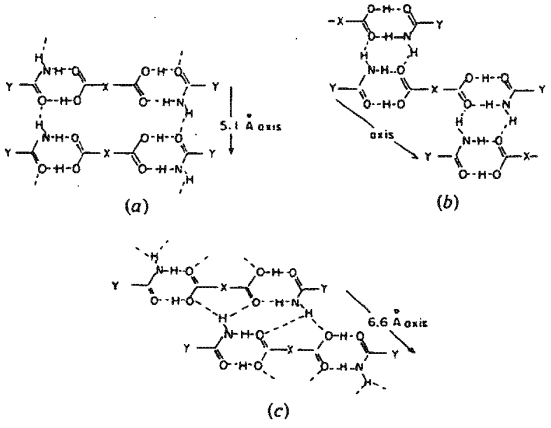
Fig. 6. Crotonamide:oxalic acid. (*a*) H-bonding network viewed along a. (*b*) Packing arrangement in the *ab* projection.

UM00013970
NOVARTIS EXHIBIT 1017
Novartis v. Regents, IPR2023-01346
Page 2716 of 4460

$< D_y$. This point is illustrated by the example of the 2:1 complex crotonamide:adipic acid ($D_x \simeq 14{\cdot}6$, $D_y \simeq 11{\cdot}6$ Å) for which $\Delta \simeq 3$ Å, too large a mismatch to permit the glide space motif (18). This is indeed supported by the cell constants (Table 1). Applying the same arguments we rule out packing motif (18) for a number of 2:1 complexes such as fluoro- and chloroacetamide with oxalic acid, supported again by their cell constants (Table 1).

3.3.2. *Translation packing*

All the previously discussed space motifs impose rather severe constraints on the sizes of residues X and Y. These restrictions may be partially overcome by interlinking the complex units (17) by translation in three distinct ways, shown in (23*a*), (23*b*) and (23*c*).



(23) Three modes of interlinking point motifs (17) by translation.

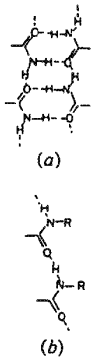
The packing mode (23*a*) exhibits an interpair N—H···$OCNH_2$ bond between amide groups along a 5·1 Å axis. The same type of linkage is frequently encountered in both primary and secondary amides, as shown in (24*a*) and (24*b*). In space motif (23*b*) an interpair N—H···OCOH linkage occurs between amide and carboxyl groups. The interpair N—H···O geometries in (23*a*) and (23*b*) resemble one another; their overall packing structures, however, differ completely and thus their relative merits should depend on the sizes of X and Y. A significant crystallographic distinction between the two space motifs is provided by the translation axis; in (23*a*) it is of constant value (5·1 Å), whereas in (23*b*) it varies according to the length of C—X—C and must always be appreciably longer than in (23*a*).

The packing mode (23*c*) contains interpair N—H··· O(carboxyl) bonds which are bifurcated; both the carbonyl and the hydroxyl O atoms act as proton acceptors. Such a H-bond is possible if the intramolecular separation C—X—C between the two carboxyl groups is sufficiently short, which is satisfied only in oxalic acid. The length of the translation axis in these oxalic acid complexes is a constant ≃6·6 Å.

3.3.2.1. *Space motif* (23*a*). The space motif (23*a*) is strongly indicated for the three molecular complexes of benzamide with oxalic, succinic, and adipic acid (Huang, 1969) since all exhibit 5·1 Å axes (Table 1). Indeed, this mode has been proved for benzamide:succinic acid (Huang, Leiserowitz & Schmidt, 1973) (Fig. 7). For the two remaining complexes the alternative modes (23*b*) and (23*c*) are ruled out by their cell constants since none of their translation axes, and combinations thereof, are compatible with the axial lengths required by (23*b*) and (23*c*).*

A unique feature of the benzamide:succinic acid structure is the non-planarity of its H-bonded carboxyl:amide pair (6). The distortion comprises a twist of 20° between the planes of the amide and carboxyl groups about the N—H···OCOH bond. Such a pronounced distortion is not evident in other structures which contain the carboxyl:amide pair (6). The angle between the planes of the amide and carboxyl groups in the structures of fumaramic acid (Benghiat, Kaufman, Leiserowitz & Schmidt, 1972), furamide:oxalic acid (Huang, Leiserowitz & Schmidt,

* Motif (23*b*) would demand interpair repeat distances ~8·2 and 11·8 Å for the oxalic and adipic acid complexes respectively; (23*c*), which is possible only for the oxalic acid complex, requires a 6·6 Å axis.



(24*a*) Primary amide dimers H-bonded by translation.

(24*b*) Secondary amides H-bonded by translation.

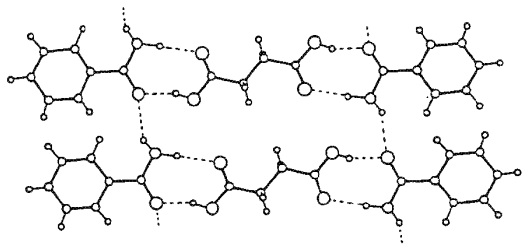


Fig. 7. Benzamide:succinic acid (Huang, Leiserowitz & Schmidt, 1973). H-bonding along the 5·2 Å translation axis.

UM00013971
NOVARTIS EXHIBIT 1017
Novartis v. Regents, IPR2023-01346
Page 2717 of 4460

1973), and tetrolamide:acetylenedicarboxylic acid (Nader, 1977) are 0·5, 3 and 10·0° respectively. As a result of this distortion in benzamide:succinic acid a separation of 3·6 Å is achieved between the carbonyl and hydroxyl O atoms of the carboxyl groups related by the 5·2 Å axis. Were the carboxyl:amide pair (6) coplanar, this O···O separation would be ≃3·0 Å. Thus it was deduced (Huang *et al.*, 1973) that O···O lone-pair repulsions do not permit an approach less than 3·6 Å between two O atoms of neighbouring carboxyl groups arranged in such a way that their lone-pair lobes are partially directed towards each other.

3.3.2.2. *Space motif* (23*b*). No detailed crystal structure analysis of a molecular complex embodying space motif (23*b*) has yet been undertaken. Nevertheless, the evidence for the existence of this motif in the crystal structures of furamide:succinic acid and crotonamide:apidic acid (Huang, 1969) is indisputable. Both are triclinic ($P\bar{1}$) containing one complex unit (17) per unit cell (Table 1). Therefore interpair N—H···O bonds can be formed only *via* translation. Space motif (23*a*) is ruled out by the absence of 5·1 Å axes. Incorporating furamide:succinic acid and crotonamide:adipic acid into motif (23*b*) with reasonable distances and angles (Fig. 8*a* and *b*) yields axial repeats of 9·6 and 10·9 Å respectively, in excellent agreement with the corresponding axial lengths b = 9·7 Å and $|b + c|$ = 11·2 Å (Table 1).

3.3.2.3. *Space motif* (23*c*). The precise packing of motif (23*c*), with its characteristic 6·6 Å axis, follows from the crystal structure of furamide:oxalic acid (Huang, Leiserowitz & Schmidt, 1973) (Fig. 9). The interpair N—H···O bond is bifurcated, since the N—H group straddles the carbonyl and hydroxyl O atoms of oxalic acid with distances N···O(hydroxyl) 3·10 Å and N···O(carbonyl) 2·94 Å. This H-bond system is similar to that observed in azodicarbonamide (Bryden, 1961), which is bifurcated with N—H···N and N—H···O bonds.

The motif (23*c*) in all likelihood appears in the isomorphous crystal structures of fluoroacetamide:oxalic acid and chloroacetamide:oxalic acid although their crystal structures have not yet been determined and their cell dimensions (Table 1) do not unambiguously identify their H-bond space motifs. While the vectors **a** + **b** for both compounds are of the proper length of 6·7 Å for space motif (23*c*) the 4·80 Å axis of the fluoro derivative, and particularly the 5·20 Å axis of the chloro derivative, imply that these two structures might, however, belong to space motif (23*a*). On scrutiny the 4·8 Å axis of the fluoro compound seems too short for an interpair N—H···O bond. Fluoroacetamide itself (Hughes & Small, 1962) exhibits a 5·15 Å axis motif (24*a*) with an interpair N—H···O distance of 2·88 Å. Were the fluoroacetamide complex to form the interpair N—H···O bond along the 4·8 Å axis, the resulting N···O distance would be appreciably shorter than 2·88 Å. Moreover, the average value of this H-bond translation axis in (24*a*) for 23 primary amide structures (Leiserowitz & Schmidt, 1969) is 5·12 Å with a scatter $|= (\Sigma \Delta^2/23 - 1)|$ of 0·07 Å and thus is significantly longer than 4·8 Å. Consequently fluoroacetamide:oxalic acid undoubtedly does not appear in the motif (23*a*), but crystallizes in motif (23*c*) forming the bifurcated N—H···O bond along the 6·7 Å axis. Since both the F and Cl complexes appear to be isomorphous we conclude that chloroacetamide:oxalic acid features the same H-bond scheme, despite its 5·2 Å axis.

3.3.2.4. *Comparison of the three translational modes.* The existence of the three translation modes of N—H···O bonding between complex units (17) raises the question of their relative merits. The packing mode (23*a*) suffers from the disadvantage of a non-planar carboxyl:amide pair (6) apparently induced by O···O lone-pair repulsions. These O···O contacts are absent in space motif (23*b*), and therefore one may query why the benzamide complexes with oxalic, succinic,

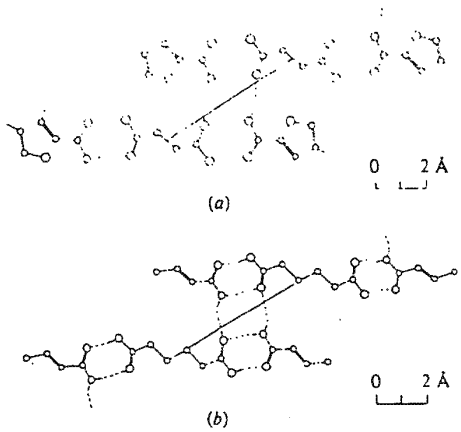


Fig. 8. H-bonding translation motif (23*b*) postulated for (*a*) furamide:succinic acid, (*b*) crotonamide:adipic acid, yields axial repeats of 9·6 and 10·9 Å respectively.

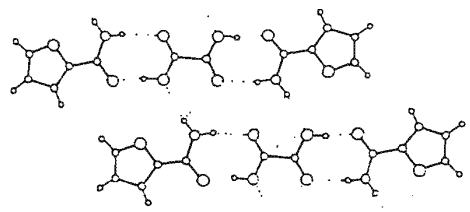


Fig. 9. Furamide:oxalic acid (Huang, Leiserowitz & Schmidt, 1973). H-bonding arrangement along the 6·6 Å axis.

UM00013972
NOVARTIS EXHIBIT 1017
Novartis v. Regents, IPR2023-01346
Page 2718 of 4460

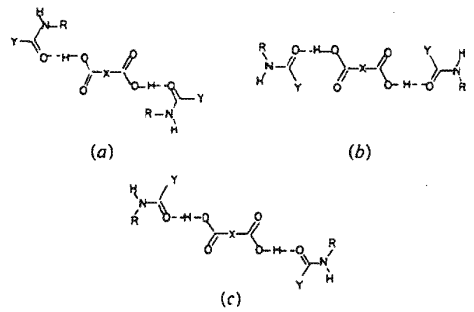
and adipic acid do not adopt this motif instead of (23*a*). It is obvious that such hypothetical arrangements would induce very short intermolecular contacts between the benzamide ring and the carboxylic acid molecule along the H-bond axis. However, we are not certain of the distortions the amide and acid molecules would undergo to relieve the repulsive contacts and how the energy of such a motif would compare with that of the alternative motif (23*a*). Perhaps a more satisfactory approach to this question lies in examining the effect of substituting the bulky phenyl residue by a smaller group, *e.g.* furan or allyl. Indeed furamide:succinic acid and crotonamide: adipic acid both appear in space motif (23*b*) rather than (23*a*) implying that of the two packing arrangements the former is probably preferred, steric factors permitting.

The preference of space motif (23*c*) over that of (23*a*) and (23*b*) in oxalic acid complexes is probably due to the bifurcated N—H···O bonds in (23*c*).

4. Point and space motifs of secondary amide:dicarboxylic acid complexes

The principles applied in constructing the possible modes of H-bonding between secondary amides *Y*—CONH*R* and dicarboxylic acids are similar to those adopted in generating the point and space motifs involving the primary amides.

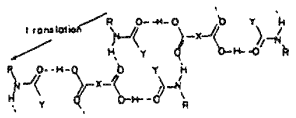
Three cardinal modes (25*a*), (25*b*) and (25*c*) of forming O—H···OCNH*R* bonds may be envisaged.* It is evident that motif (25*a*) may be discarded in view of the too short contact between the OH group and the residue *R*. Motif (25*b*), which is analogous to (7) in the primary amide series, obviously cannot accommodate a bulky *Y* residue. Motif (25*c*), which is analogous to (8) in the primary amides, has no such restrictions.



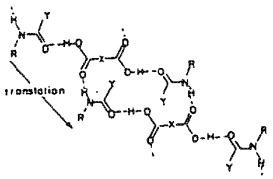
(25) Three possible point motifs linking secondary amides with dicarboxylic acids.

* Only the synplanar O=C—N—*R* conformation is considered in deriving the motifs since this is the conformer invariably found in crystalline secondary amides.

The point motifs (25*b*) and (25*c*) may each be interlinked by N—H···OCOH bonds, *via* translation to generate the one-dimensional space motifs (26) and (27). As planar arrangements these two motifs suffer from the shortcoming of very close contacts.

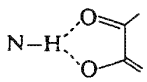


(26) Space motif containing point motifs (25*b*) linked by translation.



(27) Space motif containing point motifs (25*c*) linked by translation.

The H-bond arrangement in *N*-methylformamide: oxalic acid (Leiserowitz & Nader, 1977) (Fig. 10) mostly resembles (26). Its geometry is characterized by a linear and short O—H···OCNH bond of 2·475 Å and a bifurcated H-bonded system



which is approximately coplanar with N···O distances of 2·96 and 3·09 Å. The *N*-methylformamide and carboxyl groups, linked by the O—H···OCNH bond into a point motif akin to (25*b*), are not coplanar, the angle between them being 57°. It is by virtue of this non-planarity that repulsive contacts are avoided between the point motifs (25*b*), which are interlinked by the bifurcated N—H···O bonds *via* a shallow glide, which may be regarded as a pseudo translation in view of the short *b* axis of 3·8 Å (Table 1). The shallow glide performs the role of bringing the N—H bond, which is not coplanar with the oxalic acid molecule in point motif (25*b*), into approximate coplanarity with the oxalic acid molecule to which it is linked by a bifurcated H-bond.

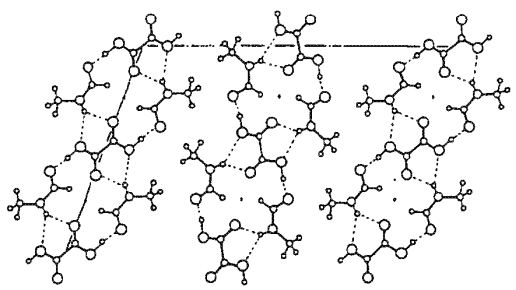


Fig. 10. *N*-Methylformamide:oxalic acid. H-bonding arrangement in the *ac* projection.

UM00013973
NOVARTIS EXHIBIT 1017
Novartis v. Regents, IPR2023-01346
Page 2719 of 4460

Table 2. H-*bonding parameters of amide:carboxylic acid complexes*

d is the *X*–(H)···O distance (Å); α is the *X*–H···O angle (°); β is the C=O···(H)*X* angle (°).

	O–H···O bonds				N–H···O bonds					
	single O–H···OCNH	ring O–H···OCNH	single O–H···OCOH	ring $N–H_{syn}$···OCNH	ring $N–H_{syn}$···OCOH	$N–H_{anti}$···OCNH	$N–H_{anti}$···OCOH	Bifurcated N–H (O_1 carbonyl, O_2 hydroxyl)		References
	d α β	*d* α β	*d* α β	*d* α β	*d* α β	*d* α β	*d* α β	d_1 α_1 β_1	d_2 α_2 β_2	
Formamide: oxalic acid	2·52 173 116·5	—	—	2·99 173 119·4	—	—	2·95 162 133·1	—	—	
Acetamide: oxalic acid*	2·48 167 128·5	—	2·71 168 129·6	2·93 161 124·8	—	—	2·96 173 139·6	—	—	
Acetamide: allenedicarboxylic acid	2·52 169 127·0	—	2·66 157 121·2	3·01 171 127·4	—	—	3·05 177 133·0	—	—	Nader (1977)
Crotonamide: oxalic acid	—	2·61 170 126·7	—	—	3·00 170 115·5	2·95 171 129·0	—	—	—	
Tetrolamide: acetylenedicarboxylic acid	—	2·56 168 116·8	—	—	2·93 163 116·1	2·87 168 112·2	—	—	—	Nader (1977)
Furamide: oxalic acid	—	2·53 170 126·1	—	—	2·92 172 119·2		—	2·91 104 127·2	3·10 172 123·0	Huang, Leiserowitz & Schmidt (1973)
Benzamide: succinic acid	—	2·60 173 126·4	—	— —	2·98 160 117·6	3·02 142 150·1	—	—	—	Huang, Leiserowitz & Schmidt (1973)
N-Methylformamide: oxalic acid*	2·48 174 115·3	—	—	—	—	—	—	2·96 144 129	3·09 143 125	
Formamide: formic acid†	2·60 2·58 174 172 113·0 114·5	—	—	2·99 2·93 176 177 116·8 122·7	—	—	2·95 2·87 151 140 136·0 138·7	—	—	Nahringbauer & Larsson (1969)
Fumaramic acid‡	—	2·66 180 125·6	—	—	2·84 171 120·9	2·94 163 113·6	—	—	—	Benghiat *et al.* (1972)
2,5-Pyridinedicarboxylic acid: dimethylformamide $+H_2O$	2·52	—	—							Ito, Kashino & Haisa (1976)

* Average values of two independent parameters for acetamide:oxalic acid and *N*-methylformamide:oxalic acid.
† Values are given for the two different H-bonding networks (I) and (II) shown in Fig. 2.
‡ Fumaramic acid is not a molecular complex yet it is relevant since it contains the carboxyl:amide ring (6).

UM00013974

NOVARTIS EXHIBIT 1017
Novartis v. Regents, IPR2023-01346
Page 2720 of 4460

N-Methylacetamide:oxalic acid is almost isostructural with the *N*-methylformamide analogue as is evident from their cell constants (Table 1). This is in contradiction with what is found in the analogous primary amide series because acetamide:oxalic acid is not isostructural with formamide:oxalic acid, as discussed in § 3.2.2. The latter complex has a point motif (7) which is analogous to (25*b*), but in a planar arrangement. Since in the secondary amide series the amide group is not coplanar with the oxalic acid molecule in (25*b*), *N*-methylacetamide may easily be inserted into motif (25*b*) without incurring a close $C-CH_3\cdots O{=}COH$ contact and thus a short O—H···O(amide) bond may be formed.

5. H-bonding properties

The systematics of the packing of the amide:acid complexes, and their H-bond lengths and angles (Table 2) may provide a fuller understanding of the H-bonding properties of amides and acids and of the factors responsible for their complexation.

According to a study on the packing modes of primary amides $Y-CONH_2$ (Leiserowitz & Schmidt, 1969), a carbonyl O atom which participates in *two* N—H···O bonds tends to adopt, the residue *Y* permitting, the motif (28) which is coplanar and contains two linear N—H···O bonds symmetrically disposed about the carbonyl bond with C=O···N angles ≃120°.



(28)

Electron density maps about the carbonyl O atom, as determined from the diffraction analyses of a number of carbonyl systems such as cyanuric acid (Verschoor & Keulen, 1971) (combined X-ray and neutron study at −170 °C) and diketopiperazine (Harel & Hirshfeld, 1977) (X-ray study at −150 °C) display, fairly convincingly, two lone-pair lobes of the O atom in the plane of the carbonyl system C=O at approximately 0·6 Å from the O atom and making an angle of about 110° with the C=O bond. Combining these findings with the favoured geometry of motif (28) suggests that in the preferred H-bonded system the *two* N—H proton donors are directed towards the acceptor O atom approximately along the line of its lone-pair lobes.

The same angular properties as deduced for the N—H···O bonded motif (28) also seem to prevail for the O—H···OCOH bond present in carboxylic acids. Here the carbonyl O atom participates in only *one* H-bond.* A study of the packing modes of carboxylic acids (Leiserowitz, 1976) appears to have provided ample evidence that the $O-H\cdots O{=}C\lesssim$ system is coplanar with an angle $C{=}O\cdots(H)O \simeq 120°$.

5.1 *Preferred geometry of the* H-*bonded* $C{=}O\begin{matrix}\cdot^{H-O}\\ \cdot_{H-N}\end{matrix}$ *system*

The amide:acid complexes follow a trend similar to the primary amides insofar as a carbonyl O atom which participates in *two* H-bonds N—H···O and O—H···O, tends to adopt, the residues *Y* and *X* permitting, a motif (29) whose geometry is analogous to the N—H···O bonded system (28). The justification of the preferences for motif (29) is based primarily on the observation that those complexes which tend to incorporate (29) [namely, formamide:formic acid, formamide:oxalic acid, acetamide:oxalic acid, acetamide:allenedicarboxylic acid, tetrolamide:acetylenedicarboxylic acid, crotonamide:oxalic acid, crotonamide:succinic acid] appearing in space motifs (13), (16) and (18) could as well exist in a translation space motif, *e.g.* (23*b*). In the translation packing the N—H···O bond along the translation axis is non-linear with a C=O···N angle ≃150°. Thus the translation modes (23*a*), (23*b*) are inferior to (13), (16) or (18). It is noteworthy that most of the complexes which appear in the translation modes (23) cannot, on steric grounds, fit into any of the preferred motifs. As to the relative merits of the preferred motifs (13), (16), and (18), their H-bonding geometries do not permit a clear distinction.



(29)

5.2. H-*bonding lengths*

The O—H···OCNH bond has proved to be surprisingly short in most of the complexes (Table 2), particularly where the amide and carboxyl groups are linked by a *single* H-bond as in point motifs (7), (8), and (25*b*). Its length is 2·50 ± 0·02 Å for formamide:oxalic acid, acetamide:oxalic acid, acetamide:allenedicarboxylic acid, and 2,5-pyridine dicarboxylic acid:dimethylformamide + H_2O (Ito, Kashino & Haisa, 1976), and *N*-methylformamide:oxalic acid. Only in formamide:formic acid were relatively long O—H···O bonds of 2·58 and 2·60 Å found (Table 2).

* It does not necessarily follow that the preferred geometry of a *single* H-bond about a carbonyl O atom is the same as for a double H-bonded carbonyl group, *i.e.* the angle $C{=}O\cdots H{-}X$ for single O—H···O or N—H···O bonds may not preferentially be ~120°.

UM00013975
NOVARTIS EXHIBIT 1017
Novartis v. Regents, IPR2023-01346
Page 2721 of 4460

The O—H···$OCNH_2$ bond shows much greater variation in length when it forms part of the cyclic carboxyl:amide pair (6). Furamide:oxalic acid and tetrolamide:acetylenedicarboxylic acid form short O—H···O bonds of 2·53 and 2·56 Å whereas in crotonamide:oxalic acid and benzamide:succinic acid these distances are 2·61 and 2·60 Å. Moreover, the structures of fumaramic acid (Benghiat, Kaufman, Leiserowitz & Schmidt, 1972) and of 2-bromosuccinamic acid (Murakami & Iitaka, 1969) both contain the carboxyl:amide pair (6) with O—H···$OCNH_2$ bonds of 2·66 and 2·57 Å respectively. Thus it may be concluded that only those motifs containing a single O—H···OCNH bond, namely point motifs (7), (8) and (25*b*), lead, with only one exception, to the formation of exceptionally short (and therefore strong) O—H···O bonds. Therefore a preference of these motifs over the cyclic structure (6) seems to exist.

There appears to be no obvious distinction in length between dimeric and single O—H···O bonds of carboxylic acids. The average length of the single O—H···O bond of 2·65 Å (Table 3) matches the O—H···O distance of 2·64 Å of a large variety of cyclic dimers (Leiserowitz, 1976). Consequently, there seems to be little doubt that the single O—H···OCNH bond is distinctly shorter than the single or dimeric O—H···OCOH bond. An analogous comparison of N—H···$OCNH_2$ and N—H···OCOH lengths, both for intra- and interpair motifs, does not appear to display any significant pattern (Table 2).

5.3. *The* C=O *length in amides and acids*

In the context of the findings on O—H···OCOH and O—H···OCNH lengths it is significant that the C=O

Table 3. O—H···O *distances* (Å) *between carboxyl groups linked by single* O—H···O *bonds*

Compound	O—H···O distance	Reference
Formic acid	2·58	Holtzberg, Post & Fankuchen (1953)
Acetic acid	2·631	Jönsson (1971)
β-Tetrolic acid	2·655	Benghiat & Leiserowitz (1972)
Maleic acid	2·643	James & Williams (1974)
Cyclopropane-1,1-dicarboxylic acid	2·641	Meester, Schenk & MacGillavry (1971)
Bicyclo[2.2.2]octa-2,5-diene-2,3-dicarboxylic acid	2·590 2·585	Hechtfischer, Steigemann & Hoppe (1970)
D-Tartaric acid	2·707	Okaya, Stemple & Kay (1966)
α-Oxalic acid	2·702	Derissen & Smit (1974)
Acetamide:oxalic acid	2·71	
Acetamide:allenedicarboxylic acid	2·66	Nader (1977)

Table 4. *Bond lengths* (Å) *and angles* (°) *of amide and carboxyl groups*

	Amide group			Carboxyl group			
Compound	C=O	C—N	O=C—N	C=O	C—OH	O=C—O	References
Formamide:formic acid	1·251*	1·312	124·6	1·202*	1·320	125·4	Nahringbauer & Larsson (1969)
Formamide:oxalic acid	1·246	1·298	123·9	1·203	1·302	125·8	
N-Methylformamide:oxalic acid	1·234*	1·296	124·7	1·194*	1·295	125·9	
Acetamide:oxalic acid	1·251*	1·301	120·0	1·212†	1·298	126·2	
Acetamide:allenedicarboxylic acid	1·255	1·305	120·8	1·222*	1·294	124·2	Nader (1977)
Tetrolamide:acetylenedicarboxylic acid	1·248	1·313	123·2	1·204	1·297	126·4	Nader (1977)
Crotonamide:oxalic acid	1·255	1·324	121·7	1·201	1·307	126·1	
Furamide:oxalic acid	1·250	1·322	123·6	1·201	1·310	126·2	Huang, Leiserowitz & Schmidt (1973)
Benzamide:succinic acid	1·230	1·335	122·0	1·194	1·318	123·1	Huang, Leiserowitz & Schmidt (1973)
Fumaramic acid	1·247	1·323	122·6	1·209	1·310	124·0	Benghiat *et al.* (1972)
Acetamide (orthorhombic)	1·260*	1·334	123·1				Hamilton (1965)
Acetamide (rhombohedral)	1·241	1·324	122·6				Denne & Small (1971)
Benzamide	1·249	1·342	122·1				Blake & Small (1972)
α- and *β*-oxalic acid				1·214*	1·298	126·8	Derissen & Smit (1974)
Allenedicarboxylic acid				1·222*	1·293	124·3	Leiserowitz & Nader (1973)

* Mean values of two independent groups.
† Mean values of four independent groups.

UM00013976
NOVARTIS EXHIBIT 1017
Novartis v. Regents, IPR2023-01346
Page 2722 of 4460

length is, on average, 0·04 Å longer in amides than in acids (1·25 *versus* 1·21 Å) (Table 4). This implies that the carbonyl O atoms of the two groups have different electron density distributions and therefore different proton acceptor properties, the amide carbonyl group probably being the stronger acceptor. This statement is also borne out by the fact that in the complexes it is the amide O atom which participates in two H-bonds rather than the carboxyl O atom. The only exception is space motif (23*b*).

5.4. *The bifurcated* N–H···O *bond*

A bifurcated N–H···O bond occurs in the oxalic acid complexes which appear in space motifs (23*c*) and (26). On inspection it would seem that the bifurcated N–H···O system could have been avoided by formation of a single N–H···O(carbonyl) bond. Thus we conclude, tentatively, that the bifurcated N–H···O bond is preferred over the single N–H···O(carbonyl) bond.

Partial support by a Minerva Grant is acknowledged. One of us, F. Nader, is indebted to 'Stiftung Volkswagenwerk' for a fellowship (1969–1972) within the framework of an Israel–Germany scientific exchange program, as well as to the Deutsche Forschungsgemeinschaft (1972–1974) for financial support. We thank Mrs K. Reich for technical assistance.

References

BENGHIAT, V., KAUFMAN, H. W., LEISEROWITZ, L. & SCHMIDT, G. M. J. (1972). *J. Chem. Soc. Perkin* II, pp. 1758–1763.
BENGHIAT, V. & LEISEROWITZ, L. (1972). *J. Chem. Soc. Perkin* II, pp. 1763–1768.
BLAKE, C. C. F. & SMALL, R. W. H. (1972). *Acta Cryst.* B28, 2201–2206.
BRYDEN, J. H. (1961). *Acta Cryst.* **14**, 61–63.
DENNE, W. A. & SMALL, R. W. H. (1971). *Acta Cryst.* B27, 1094–1098.
DERISSEN, J. L. & SMIT, P. H. (1974). *Acta Cryst.* B30, 2240–2242.
HAMILTON, W. C. (1965). *Acta Cryst.* **18**, 866–870.
HAREL, M. & HIRSHFELD, F. L. (1977). To be published.
HECHTFISCHER, S., STEIGEMANN, W. & HOPPE, W. (1970). *Acta Cryst.* B26, 1713–1722.
HOLTZBERG, F., POST, B. & FANKUCHEN, I. (1953). *Acta Cryst.* **6**, 127–130.
HUANG, C.-M. (1969). MSc Thesis, The Weizmann Institute of Science, Rehovot, Israel.
HUANG, C.-M., LEISEROWITZ, L. & SCHMIDT, G. M. J. (1973). *J. Chem. Soc. Perkin* II, pp. 503–508.
HUGHES, D. O. & SMALL, R. W. H. (1962). *Acta Cryst.* **15**, 933–940.
ITO, K., KASHINO, S. & HAISA, M. (1976). *Acta Cryst.* B32, 511–515.
JAMES, M. N. G. & WILLIAMS, G. J. B. (1974). *Acta Cryst.* B30, 1249–1257.
JÖNSSON, P.-G. (1971). *Acta Cryst.* B27, 893–898.
LARSEN, I. K. (1968). *Acta Chem. Scand.* **22**, 843–853.
LARSEN, I. K. & JERSLEV, B. (1966). *Acta Chem. Scand.* **20**, 983–991.
LEISEROWITZ, L. (1976). *Acta Cryst.* B32, 775–802.
LEISEROWITZ, L. & NADER, F. (1972). *Angew. Chem. Int. Ed.* **11**, 514–515.
LEISEROWITZ, L. & NADER, F. (1973). *Angew. Chem. Int. Ed.* **12**, 158–159.
LEISEROWITZ, L. & NADER, F. (1977). To be published.
LEISEROWITZ, L. & SCHMIDT, G. M. J. (1969). *J. Chem. Soc.* (*A*), pp. 2372–2382.
LEISEROWITZ, L. & TUVAL, M. (1977). *Acta Cryst.* Submitted.
MEESTER, M. A. M., SCHENK, H. & MACGILLAVRY, C. H. (1971). *Acta Cryst.* B27, 630–634.
MURAKAMI, Y. & ITTAKA, Y. (1969). *Chem. Pharm. Bull. Japan*, **17**, 2397–2404.
NADER, F. (1977). *Liebigs Ann.* Submitted.
NAHRINGBAUER, I. (1970). *Acta Chem. Scand.* **24**, 453–462.
NAHRINGBAUER, I. & LARSSON, G. (1969). *Ark. Kem.* **30**, 91–102.
OKAYA, Y., STEMPLE, N. R. & KAY, M. I. (1966). *Acta Cryst.* **21**, 237–243.
PIMENTEL, G. C. & MCCLELLAN, A. L. (1960). *The Hydrogen Bond*, p. 224. San Francisco: Freeman.
VERSCHOOR, G. C. & KEULEN, E. (1971). *Acta Cryst.* B27, 134–145.

UM00013977
NOVARTIS EXHIBIT 1017
Novartis v. Regents, IPR2023-01346
Page 2723 of 4460